

NASA/CP-2002-210002

International VLBI Service for Geodesy and Astrometry

# General Meeting Proceedings

Nancy R. Vandenberg and Karen D. Baver, Editors



February 4-7, 2002  
Tsukuba, Japan



## The NASA STI Program Office ... in Profile

Since its founding, NASA has been dedicated to the advancement of aeronautics and space science. The NASA Scientific and Technical Information (STI) Program Office plays a key part in helping NASA maintain this important role.

The NASA STI Program Office is operated by Langley Research Center, the lead center for NASA's scientific and technical information. The NASA STI Program Office provides access to the NASA STI Database, the largest collection of aeronautical and space science STI in the world. The Program Office is also NASA's institutional mechanism for disseminating the results of its research and development activities. These results are published by NASA in the NASA STI Report Series, which includes the following report types:

- **TECHNICAL PUBLICATION.** Reports of completed research or a major significant phase of research that present the results of NASA programs and include extensive data or theoretical analysis. Includes compilations of significant scientific and technical data and information deemed to be of continuing reference value. NASA's counterpart of peer-reviewed formal professional papers but has less stringent limitations on manuscript length and extent of graphic presentations.
- **TECHNICAL MEMORANDUM.** Scientific and technical findings that are preliminary or of specialized interest, e.g., quick release reports, working papers, and bibliographies that contain minimal annotation. Does not contain extensive analysis.
- **CONTRACTOR REPORT.** Scientific and technical findings by NASA-sponsored contractors and grantees.

- **CONFERENCE PUBLICATION.** Collected papers from scientific and technical conferences, symposia, seminars, or other meetings sponsored or cosponsored by NASA.
- **SPECIAL PUBLICATION.** Scientific, technical, or historical information from NASA programs, projects, and mission, often concerned with subjects having substantial public interest.
- **TECHNICAL TRANSLATION.** English-language translations of foreign scientific and technical material pertinent to NASA's mission.

Specialized services that complement the STI Program Office's diverse offerings include creating custom thesauri, building customized databases, organizing and publishing research results . . . even providing videos.

For more information about the NASA STI Program Office, see the following:

- Access the NASA STI Program Home Page at <http://www.sti.nasa.gov/STI-homepage.html>
- E-mail your question via the Internet to [help@sti.nasa.gov](mailto:help@sti.nasa.gov)
- Fax your question to the NASA Access Help Desk at (301) 621-0134
- Telephone the NASA Access Help Desk at (301) 621-0390
- Write to:  
NASA Access Help Desk  
NASA Center for AeroSpace Information  
7121 Standard Drive  
Hanover, MD 21076-1320

# General Meeting Proceedings

Nancy R. Vandenberg and Karen D. Baver, Editors



February 4-7, 2002

Tsukuba, Japan



Available from:

NASA Center for Aerospace Information  
7121 Standard Drive  
Hanover, MD 21076-1320  
Price Code: A17

National Technical Information Service  
5285 Port Royal Road  
Springfield, VA 22161  
Price Code: A10

## Preface

This volume is the proceedings of the second General Meeting of the International VLBI Service for Geodesy and Astrometry (IVS), held in Tsukuba, Japan, February 4–7, 2002. The contents of this volume also appear on the IVS web site at

<http://ivscc.gsfc.nasa.gov/publications/gm2002>

The second General Meeting was held at Tsukuba International Congress Center (Epochal Tsukuba) in Tsukuba City, Ibaraki, Japan. The meeting was hosted by the Geographical Survey Institute (GSI) and Communications Research Laboratory (CRL), both IVS member organizations. Supporting organizations for the meeting were the National Committee for Geodesy, Science Council of Japan, the Geodetic Society of Japan and the Japanese VLBI Consortium.

The keynote of the second GM was prospectives for the future, in keeping with the re-organization of the IAG around the motivation of geodesy as “an old science with a dynamic future” and noting that providing reference frames for Earth system science that are consistent over decades on the highest accuracy level will provide a challenging role for IVS. The goal of the meeting was to provide an interesting and informative program for a wide cross section of IVS members, including station operators, program managers, and analysts.

Photographs taken during the meeting are available on the web at

<http://ivscc.gsfc.nasa.gov/meetings/gm2002/pictures>

The April 2002 issue of the IVS Newsletter has a feature article about the meeting. The Newsletter is available at

<http://ivscc.gsfc.nasa.gov/newsletter/issue2.pdf>

This volume contains the following:

- **General information about the meeting.** This section includes the welcome addresses from the sponsoring organizations, the group photograph of all participants, and the resolution adopted at the meeting.
- **The papers presented at the meeting.** There are six major sections of this volume, each corresponding to a meeting session. Poster and oral papers are mixed. This volume includes 71 papers; abstracts only are printed for five papers for which a paper was not provided for publication. Poster papers about IVS component status are not included in this volume; they have been published in the 2001 Annual Report and are available on the IVS web site.
- **Reports from splinter meetings.** Included are reports about the mini-TOW (Technical Operations Workshop) held at Tsukuba station, the meeting of the analysis working group on geophysical modeling, and the third IVS Analysis Workshop.
- **A list of registered participants.**
- **The meeting program.**
- **An author index.**



## Table of Contents

Preface .....	iii
About the Meeting .....	1
Group Photo .....	3
Welcome Address from GSI .....	4
Welcome Address from CRL .....	5
Resolution .....	6
Session 1. VLBI: Precise and Consistent for Decades .....	7
<i>Wolfgang Schlüter</i> : Chair's Report at 2nd IVS General Meeting .....	9
<i>Nicole Capitaine</i> : The Essential Contribution of VLBI to Fundamental Astronomy .....	14
<i>Hermann Drewes, Gerhard Beutler, Reiner Rummel</i> : Challenges for VLBI Within an Integrated Global Geodetic Observing System .....	24
<i>Markus Rothacher</i> : Combination of Space-Geodetic Techniques .....	33
Session 2. Improving the Performance and Products of IVS .....	45
<i>Harald Schuh</i> : IVS Working Group 2 for Product Specification and Observing Programs .....	47
<i>Nancy R. Vandenberg</i> : IVS Observing Programs 2002–2005 .....	49
<i>Daniel MacMillan, Leonid Petrov, Chopo Ma</i> : Geodetic Results from Mark 4 VLBI .....	50
<i>Yasuhiro Koyama</i> : Expected Contributions of the K-4 and its Next-Generation Systems .....	55
<i>Calvin Klatt, Mario Bérubé, Wayne Cannon, W.T. Petrachenko, Anthony Searle</i> : Geodetic S2 VLBI: International Plans .....	60
Session 3. Network Stations, Operation Centers, Correlators .....	65
<i>Brian Corey</i> : Fundamentals of Phase Calibration in Geodetic VLBI .....	67
<i>Y. C. Minh, D. -G. Roh</i> : Construction of the Korean VLBI Network (KVN) .....	68
<i>Hideo Hanada, Takahiro Iwata, Yusuke Kono, Koji Matsumoto, Seiitsu Tsuruta, Toshiaki Ishikawa, Kazuyoshi Asari, Jinsong Ping, Kosuke Heki, Nobuyuki Kawano</i> : VRAD Mission: Precise Observation of Orbits of Sub-Satellites in SELENE with International VLBI Network .....	72

<i>Calvin Klatt, Mario Bérubé, Anthony Searle, Jason Silliker: A Next Generation Geodetic Experiment Scheduling Tool? (SKED++)</i> .....	<b>77</b>
<i>Hiroshi Takaba, Minoru Yoshida, Ken-ichi Wakamatsu, Tetsuro Kondo, Yasuhiro Koyama, Jun-ichi Nakajima, Mamoru Sekido, Ryuichi Ichikawa, Eiji Kawai, Hiroshi Okubo, Hiro Osaki, Jun Amagai, Noriyuki Kurihara, Yukio Takahashi, Yoshihiro Fukuzaki, Noriyuki Akiyama, Kouhei Shiba, Kazuhiro Takashima, Michiko Onogaki, Shinobu Kurihara, Kohhei Miyagawa, Kyoko Kobayashi, Hiroshi Hori, Shigeru Matsuzaka: Geodesy with the World's Smallest (3-m) VLBI Telescope</i> .....	<b>81</b>
<i>Gino Tuccari: A Multiband Primary Focus Receiver for Noto Antenna</i> .....	<b>84</b>
<i>Halfdan P. Kierulf, Lars Bockmann, Oddgeir Kristiansen, Hans-Peter Plag: Foot-Print of the Space-Geodetic Observatory, Ny-Ålesund, Svalbard</i> .....	<b>86</b>
<i>Martin Lidberg, Rüdiger Haas, Sten Bergstrand, Jan Johansson, Gunnar Elgered: Local Ties Between the Space Geodetic Techniques at the Onsala Space Observatory</i> .....	<b>91</b>
<i>Shigeru Matsuzaka, Yuki Hatanaka, Keizo Nemoto, Yoshihiro Fukuzaki, Kyoko Kobayashi, Kaoru Abe, Tadayuki Akiyama: VLBI-GPS Collocation Method at Geographical Survey Institute</i> .....	<b>96</b>
<i>Roger Cappallo: Mark 4 Correlator Software: Status and Plans</i> .....	<b>101</b>
<i>A. Müskens, I. Rottmann, H. Rottmann, A. Höfer, I. Benndorf: The Mark IV Correlator - Faster, Better, Optimal??</i> .....	<b>102</b>
<i>A. Nothnagel, O. Bromorzki, J. Campbell, A. Müskens, H. Rottmann, I. Rottmann: Comparison of the Output of Repeated Mark III and Mark IV Correlation Results</i> .....	<b>107</b>
<i>Brian Corey, Michael Titus: Comparison of the VLBI Observables from Mk3 and Mk4 Correlation of a 24-hour Geodetic Experiment</i> .....	<b>112</b>
<i>Jun Amagai, Hitoshi Kiuchi, Yasuhiro Koyama, Mamoru Sekido, Ryuichi Ichikawa, Tetsuro Kondo, Taizoh Yoshino, Koichi Sebata: Status of the KSP VLBI Stations and IMT-2000 Interference</i> .....	<b>117</b>
<i>Matti Paunonen: Metsähovi Geodetic VLBI Station: Status Report</i> .....	<b>120</b>
<b>Session 4. New Technology Developments in VLBI</b> .....	<b>121</b>
<i>Junichi Nakajima, Yasuhiro Koyama, Tetsuro Kondo, Mamoru Sekido, Moritaka Kimura, Hiroshi Okubo, Hiroo Osaki: VSI Interface Implementation, Performance Enhancement of Gbps VLBI Instruments</i> ..	<b>123</b>
<i>Jouko Ritakari, Ari Mujunen: A VSI-H Compatible Recording System for VLBI and e-VLBI</i> .....	<b>128</b>
<i>Alan R. Whitney: Mark 5 Disc-Based Gbps VLBI Data System</i> .....	<b>132</b>
<i>Alan R. Whitney: High-Speed e-VLBI Demonstration: Haystack Observatory to NASA/GSFC</i> .....	<b>137</b>
<i>Tetsuro Kondo, Yasuhiro Koyama, Junichi Nakajima, Mamoru Sekido, Ryuichi Ichikawa, Eiji Kawai, Hiroshi Okubo, Hiro Osaki, Moritaka Kimura, Yuichi Ichikawa, GALAXY Team: Real-time Gigabit VLBI System and Internet VLBI System</i> .....	<b>142</b>

<i>Qinghui Liu, Masanori Nishio, Kunihiro Yamamura, Tomoyuki Miyazaki: Observation of Atmospheric Disturbances Using a Real-Time VLBI System</i> .....	147
<i>Sotetsu Iwamura, Hisao Uose, Tetsuro Kondo, Shin-ichi Nakagawa, Kenta Fujisawa: IP Data Transfer System for Real-time VLBI</i> .....	152
<i>Hitoshi Kiuchi: Parallel Data Processing System</i> .....	157
<i>W.T. Petrachenko, Calvin Klatt, Vincent Ward: Multi-Beam VLBI</i> .....	162
<i>Yoshiaki Tamura, VERA Group: Geodetic Observation System in VERA</i> .....	167
<i>Hisashi Hirabayashi, Yasuhiro Murata, David W. Murphy: The VSOP-2 Space VLBI Mission</i> .....	171
<i>Yasuhiro Murata, Hisashi Hirabayashi: Wide-band Data Transmission System Expected in the Next Generation Space VLBI Mission: VSOP-2</i> .....	175
<i>Yusuke Kono, Hideo Hanada, Kenzaburo Iwadate, Yasuhiro Koyama, Yoshihiro Fukuzaki, Nobuyuki Kawano: Precise Positioning of Spacecrafts by Multi-frequency VLBI</i> .....	179
<i>Yoshihiro Fukuzaki, Kazuo Shibuya, Koichiro Doi, Takaaki Jike, David L. Jauncey, George D. Nicolson: Processing of the Data of Syowa VLBI Experiment by Copying Between the Different Recording Systems and the Result of the Analysis</i> .....	184
<i>Kenichiro Takahei, Hirohiko Suga, Yuji Ohuchi, Hiroshi Sutoh, Masaharu Uchino, Shigenori Mattori, Masahiro Tsuda, Yoshikazu Saburi, Yasuki Koga, Ken Hagimoto, Takashi Ikegami: Laser-Pumped Cs Gas-Cell Type Atomic Clock for VLBI</i> .....	189
<i>Charles J. Naudet, Steve Keihm, Gabor Lanyi, Roger Linfield, George Resch, Lance Riley, Hans Rosenberger, Alan Tanner: Media Calibration in The Deep Space Network - A Status Report</i> .....	194
<i>Makoto Miyoshi, Seiji Kameno: A Proposal for Constructing a New Sub-mm VLBI Array, Horizon Telescope - Imaging Black Hole Vicinity</i> .....	199
<b>Session 5. Data, Models, and Software</b> .....	<b>203</b>
<i>Hans-Georg Scherneck, Machiel S. Bos: Ocean Tide and Atmospheric Loading</i> .....	205
<i>Arthur Niell, Jennifer Tang: Gradient Mapping Functions for VLBI and GPS</i> .....	215
<i>Johannes Boehm, Harald Schuh, Robert Weber: Tropospheric Zenith Path Delays Derived from GPS Used for the Determination of VLBI Station Heights</i> .....	219
<i>Ryuichi Ichikawa, Yasuhiro Koyama, Junichi Nakajima, Mamoru Sekido, Eiji Kawai, Hiroshi Ohkubo, Hiro Ohsaki, Tetsuro Kondo, Jun Amagai, Hitoshi Kiuchi, Taizoh Yoshino, Fujinobu Takahashi, Kazumasa Aonashi, Yoshinori Shoji, Hiromu Seko, Tetsuya Iwabuchi, Ryu Ohtani, Kazuhiro Takashima, Shinobu Kurihara, Yoshihiro Fukuzaki, Yuki Hatanaka: Comparison of Atmospheric Parameters from VLBI, GPS and WVR</i> .....	223
<i>Jinling Li, Bo Zhang, Guangli Wang: A Discussion on the Modeling of the Residual Clock Behavior and</i>	

Atmosphere Effects in the Astrometric and Geodetic VLBI Data Analysis .....	228
<i>Patrick Charlot</i> : Modeling Radio Source Structure for Improved VLBI Data Analysis .....	233
<i>Ojars J. Sovers, Patrick Charlot, Alan L. Fey, David Gordon</i> : Structure Corrections in Modeling VLBI Delays for RDV Data .....	243
<i>Anne-Marie Gontier, Martine Feissel</i> : PIVEX: a Proposal for a Platform Independant VLBI Exchange Format .....	248
<i>Chopo Ma, Daniel MacMillan, Leonid Petrov</i> : Integrating Analysis Goals for EOP, CRF and TRF ..	255
<i>Axel Nothnagel, Markus Vennebusch, James Campbell</i> : On Correlations Between Parameters in Geodetic VLBI Data Analysis .....	260
<i>Christoph Steinforth, Axel Nothnagel</i> : Outlier Detection in the Combination of VLBI EOP .....	265
<i>Hansjörg Kutterer, Volker Tesmer</i> : Statistical Assessment of Subdiurnal Earth Orientation Parameters from VLBI .....	272
<i>David Gordon</i> : RDV Analysis and Mark 4/VLBA Comparison Results .....	277
<i>Alan L. Fey, David A. Boboltz</i> : USNO Analysis of VLBA RDV Data .....	282
<i>The SBL Team</i> : The New IERS Special Bureau for Loading (SBL) .....	287
<b>Session 6. Analysis and Geodetic/Geophysical/Astrometric Interpretation .....</b>	<b>293</b>
<i>Volker Tesmer</i> : VLBI Solution DGFI01R01 Based on Least-Squares Estimation Using OCCAM 5.0 and DOGS-CS .....	295
<i>Toshimichi Otsubo, Tadahiro Gotoh</i> : SLR-based TRF Contributing to the ITRF2000 project .....	300
<i>Tetsuro Imakiire, Masaki Murakami</i> : Establishment of the New Geodetic Reference Frame of Japan (JGD2000) .....	304
<i>Zinovy Malkin, Natalia Panafidina, Elena Skurikhina</i> : Variations of European Baseline Lengths from VLBI and GPS Data .....	309
<i>Elena Skurikhina</i> : Influence of Antenna Thermal Deformations on Estimation of Seasonal Variations in Baseline Length .....	310
<i>Oleg Titov</i> : Spectral Analysis of the Baseline Length Time Series from VLBI Data .....	315
<i>Taizoh Yoshino, Hiroo Kunimori, Futaba Katsuo, Jun Amagai, Hitoshi Kiuchi, Toshimichi Otsubo, Tetsuro Kondo, Yasuhiro Koyama, Ryuichi Ichikawa, Fujinobu Takahashi</i> : Comparison of the Baseline Length Between the Keystone Sites by Different Space Geodetic Techniques .....	320
<i>Takaaki Jike, Seiji Manabe, Yoshiaki Tamura, Kazuo Shibuya, Koichiro Doi, Teruhito Tanaka, Peter McCulloch, Marco Costa, George Nicolson, Jonathan F. H. Quick, Katsuhisa Sato, Katsunori M. Shibata, Yoshihiro Fukuzaki, David L. Jauncey, John Reynolds</i> : The Antarctic VLBI Experiments During JARE39	

and Geodetic Analysis by the Mitaka FX Correlator .....	<b>324</b>
<i>Kurt Lambeck, Anthony Purcell, Oleg Titov, David Jauncey</i> : VLBI Evidence for Glacial Rebound in Europe .....	<b>329</b>
<i>D. Gambis, Ch. Bizouard, T. Carlucci, D. Jean-Alexis</i> : Comparative Study of the EOP Series Derived for the Second IVS Pilot Project .....	<b>330</b>
<i>Zinovy Malkin</i> : A Comparison of the VLBI Nutation Series with IAU2000 Model .....	<b>335</b>
<i>Johannes Boehm, Eva Messerer, Harald Schuh</i> : Comparison of Tropospheric Parameters Submitted to the 2nd IVS Analysis Pilot Project .....	<b>340</b>
<i>Thomas Hobiger, Johannes Boehm, Harald Schuh</i> : Determination of Ionospheric Parameters by Geodetic VLBI .....	<b>345</b>
<i>C. S. Jacobs, D. L. Jones, G. E. Lanyi, S. T. Lowe, C. J. Naudet, G. M. Resch, J. A. Steppe, L. D. Zhang, J. S. Ulvestad, G. B. Taylor, O. J. Sovers, C. Ma, D. Gordon, A. L. Fey, D. A. Boboltz, P. Charlot</i> : Extending the ICRF to Higher Radio Frequencies .....	<b>350</b>
<i>Chopo Ma, David Gordon, Daniel MacMillan, Leonid Petrov</i> : Towards a Future ICRF Realization ..	<b>355</b>
<i>Edward Fomalont, Tony Beasley, Alison Peck, Colleen Gino</i> : Searching for High Quality VLBI Calibrators .....	<b>360</b>
<i>Alan L. Fey, David A. Boboltz, Ralph A. Gaume, T. Marshall Eubanks, Kenneth J. Johnston</i> : Extragalactic Radio Source Selection for Radio/Optical Frame Ties .....	<b>363</b>
<i>Martine Feissel, Chopo Ma</i> : Radio Source Stability and the Observation of Precession-Nutation .....	<b>367</b>
<i>Seiji Manabe, Hiroshi Imai, Takaaki Jike, VERA Group</i> : Astrometric and Geodetic Analysis System of VERA .....	<b>372</b>
<i>Takahiro Iwata, Takeshi Sasaki, Yusuke Kono, Hideo Hanada, Nobuyuki Kawano, Noriyuki Namiki</i> : Results of the Critical Design for the Selenodetic Mission using Differential VLBI Methods by SELENE	<b>377</b>
<i>Koji Matsumoto, Kosuke Heki, Hideo Hanada</i> : Global Lunar Gravity Field Recovery from SELENE	<b>381</b>
<b>Splinter Meeting Reports .....</b>	<b>387</b>
<i>Rich Strand, Brian Corey</i> : Mini-TOW (Technical Operations Workshop) .....	<b>389</b>
<i>Axel Nothnagel</i> : Summary of the Third IVS Analysis Workshop .....	<b>394</b>
<i>Hans-Georg Scherneck</i> : IVS Analysis Working Group for Geophysical Models in VLBI Software: Splinter Meeting .....	<b>398</b>
<b>Registered Participants .....</b>	<b>403</b>

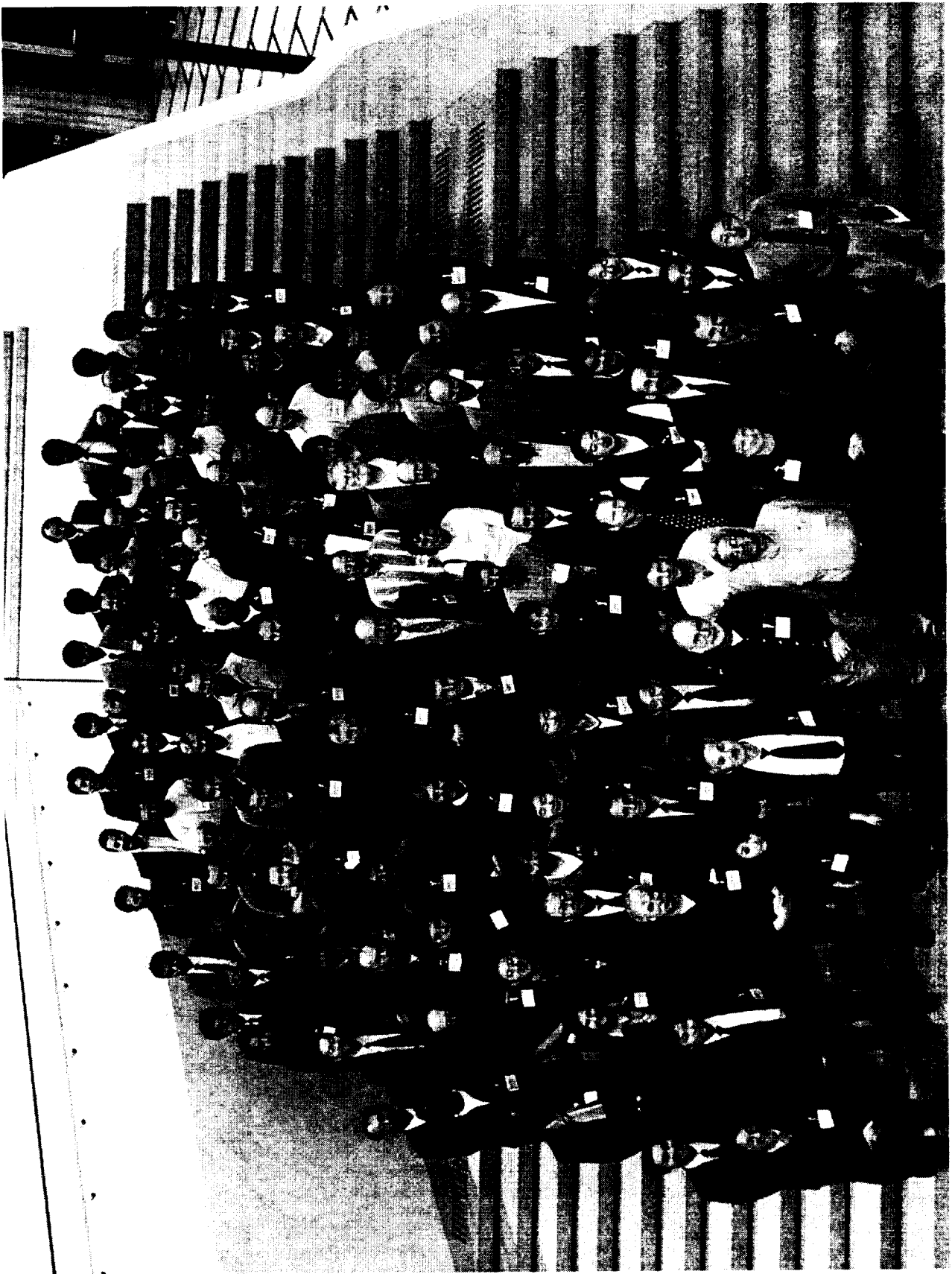
Program ..... 411

Index of Authors ..... 427

# About the Meeting







## Welcome Address of Geographical Survey Institute



Ladies and Gentlemen,

Good morning. My name is Aoyama, Vice-Minister for Engineering Affairs, Ministry of Land, Infrastructure and Transport. It is a great pleasure to be given an opportunity to say a few words on the occasion of the opening ceremony of the second General Meeting of International VLBI Service.

First of all I would like to extend my sincere thanks to Professor Wolfgang Schlüter, chairman of IVS, and all other attendants, for taking time and effort to come a long way to take part in this meeting. I am most delighted to be able to wel-

come you here in Japan to the second meeting of IVS, which is steadily moving forward since its establishment in 1999, followed by the first meeting in 2000 in Germany.

In Japan, the Survey Act and other related laws and ordinances were revised last year and accordingly our geodetic reference system is to be changed to an international one this April. We greatly owe to the knowledge from the space geodetic technologies, VLBI for instance, in establishing this kind of highly precise global reference frame. I find it very fortunate for us to host the second general meeting of IVS in Japan at this time of most critical change for our geodetic activities.

The world is getting increasingly smaller in this "IT era." VLBI technology is based on internationally collaborative observations of radio sources in outer space, far beyond the Galaxy, by two stations several thousand kilometers apart.

I believe that the international scientific collaboration as VLBI promoted at this scale is an eloquent symbol of peace and harmony of the whole humanity.

Such efforts would be even more significant if we could better understand the phenomena of the earth and thus contribute to the environment-friendly sustainable development of the globe.

It is my sincere desire that study and application of VLBI further progresses as a result of active information exchanges and discussions at this second general meeting of IVS.

Incidentally today, February 4th is the very beginning of spring according to the old Japanese calendar. I hope you will enjoy a pleasant change of the seasons, from winter to spring during your stay in Japan.

Finally I wish you a success of the meeting as well as in your personal careers.

Thank you for your attention.

Toshiki Aoyama  
Vice-Minister for Engineering Affairs,  
Ministry of Land, Infrastructure and Transport

## Welcome Address of Communications Research Laboratory

Ladies and Gentlemen,

It is a great pleasure and a privilege for me to participate in the opening ceremony of the Second General Meeting of International VLBI Service for Geodesy and Astrometry. As the President of Communications Research Laboratory, I am proud to have been given the responsibility on this important occasion held in Tsukuba, Japan.

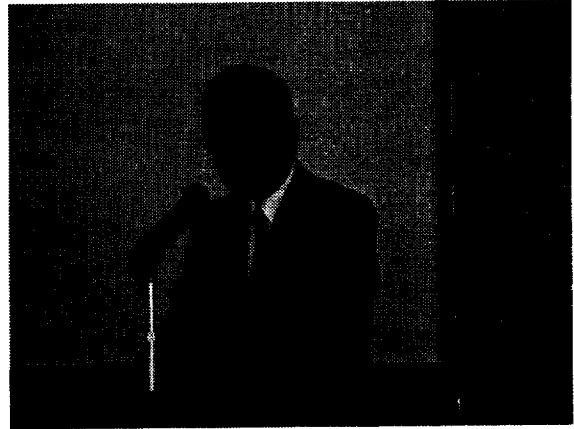
I would like to thank all participants for their interest and efforts in helping us make this General Meeting possible, especially those who traveled great distance and taken valuable time from their very busy schedules to attend the conference.

Since the September Eleven tragedy last year, we Japanese people have also reconfirmed the importance of the national security. For Japanese, the earthquake hazards are also very urgent subject of national security. For the measures of earthquake hazards, GPS satellites play very important roles on Japanese Islands. The cooperation between VLBI and GPS is very important to confirm the accuracy of geodetic measurements. The real-time VLBI using the global high-speed network will be important to improve the accuracy and analyzing speed of GPS geodesy. As the only national institute regarding info-communication research in Japan, CRL is interested in realizing the global real-time VLBI experiments and the rapid determination of earth-orientation parameters.

I heard that on the Ice-breaker ceremony last evening you enjoyed the Japanese historical early-spring events "Setsubun Mamemaki" scattering parched beans to drive out evil spirits and summon good luck. I wish all participants of this General Meeting have a pleasant stay in Japan and enriching experience both personal and professional.

Thank you very much for your kind attention.

Takashi Iida  
President, Communications Research Laboratory



## Resolution of the Second IVS General Meeting

Tsukuba, February 6, 2002

### The International VLBI Service for Geodesy and Astrometry

#### recognizing

1. that geodetic and astrometric VLBI is fundamental for the establishment and maintenance of the ICRF and contributes extensively to the generation of the ITRF, and
2. that geodetic VLBI plays an essential role in geodesy and astrometry due to its uniqueness in observing the complete set of Earth orientation parameters (EOPs) which describes the transformation between the ICRF and ITRF stable over a time span longer than a few days, and
3. that providing the reference frames and EOPs consistent over decades on the highest accuracy level will be a challenging role for IVS,

#### noting

the final report of the IVS Working Group 2 for Product Specification and Observing Programs,

#### recommends

that all IVS components should concentrate their efforts and resources to accomplish the following objectives :

- significant improvement of the accuracy of VLBI products
- shorter time delay from observation to availability of results
- continuous temporal coverage by VLBI sessions.

# Session 1. VLBI: Precise and Consistent for Decades





## Chair's Report at 2nd IVS General Meeting

*Wolfgang Schlüter*

*Bundesamt für Kartographie und Geodäsie*

*e-mail: [schlueter@wetzell.ifag.de](mailto:schlueter@wetzell.ifag.de)*

### Abstract

This report presents the status of the IVS and gives some prospects for the future.

### 1. Welcome and Introduction

With great pleasure I welcome you to our 2nd General Meeting in Tsukuba. I thank our hosts,

- Geographical Survey Institute
- Communications Research Laboratory

for the support both agencies supplied to IVS, both jointly organized our Conference. My special thanks to:

- Director General of GSI Hoshino and to
- Director General Dr. Takashi from CRL.

I would like to express my gratitude to the local Organizing Committee (LOC):

- Fujinobu Takahashi, chair of the LOC
- Shigeru Matsuzaka
- Tetsuro Kondo
- Tetsuro Imakiire
- Yoshihiro Fukuzaki
- Kazuhiro Takashima
- Yasuhiro Koyama
- Junichi Nakajima

for the excellent organization of the meeting. I would like to emphasize, that our hosts have also given us strong support by providing travel funds for some of the participants.

The scientific program of the meeting has been organized by the Program Committee. The Members are:

- Nancy Vandenberg
- Ed Himwich
- Axel Nothnagel

- Alan Whitney
- Shigeru Matsuzaka
- Yasuhiro Koyama
- Harald Schuh
- Calvin Klatt
- Arno Müskens
- Rüdiger Haas
- Zinovy Malkin
- Chopo Ma
- Seiji Manabe

The Program is ambitious and balanced concerning the areas of interests. I thank the program committee members for the excellent work, in particular Nancy Vandenberg for helping to keep the PC on track. We have more than 120 papers, 60 presented orally and 60 as posters. I thank the authors for the contributions and the chairpersons for their support during the meeting. We have more than 140 participants, coming from 15 nations.

I sincerely welcome all of you and thank you for coming to the 2nd IVS General Meeting.

## 2. Progress Report

IVS is in its third year of existence; the last General Meeting was two years ago in Kötzing.

To maintain the strong requirement for consistency, which is the basis for realizing and maintaining global reference frames such as the CRF and TRF, IVS initially employed and accepted existing infrastructure, observing programs, and related data handling. In the year 2001, a review of existing products and observing programs was performed in order to improve the official IVS products.

A Working Group (WG2) for product specification and observing programs was established at the 5th Directing Board Meeting in February 2001. Harald Schuh was appointed as chair of WG2. The assignment of WG2 was to

- review the usefulness and appropriateness of the current definition of IVS products and suggest modifications,
- recommend guidelines for accuracy, timeliness, and redundancy of products,
- review the quality and appropriateness of existing observing programs with respect to the desired products,
- suggest a realistic set of observing programs which should result in achieving the desired products taking into account existing agency programs,
- set goals for improvements in IVS products and
- suggest how these may possibly be achieved in the future.

A written report was presented in November 2001, and printed in the 2001 Annual Report.

As result of the Working Group 2 Report, the evolution of IVS's own observing programs has started in order to improve our products over the next few years. The programs will include for 2002:

**Earth Orientation Parameter:** Two rapid turnaround sessions each week, designed to have comparable Xp and Yp results. One-baseline 1-hr INTENSIVE sessions four times per week, with at least one parallel session.

**Terrestrial Reference Frame (TRF):** Monthly TRF sessions with 8 stations including a core network of 4 to 5 stations and using all other stations three to four times per year.

**Celestial Reference Frame (CRF):** Bi-monthly RDV sessions using the VLBA and 10 geodetic stations, plus quarterly astrometric sessions to observe mostly southern sky sources.

**CONT2002:** a 14-day continuous sessions to demonstrate the best results that VLBI can offer, aiming for the highest sustained accuracy.

**Monthly R&D sessions:** to investigate instrumental effects, research the network offset problem, and study ways for technique and product improvement.

## 2.1. Data Analysis

With respect to data analysis, emphasis was placed towards reliable and robust products, coordinated by the Analysis Coordinator, Axel Nothnagel:

- Today six analysis centers provide a timely, reliable, continuous solution for the entire set of EOPs.
- The Analysis Coordinator makes a combined solution as timely input for the International Earth Rotation Service (IERS) and its combination with the GPS and DORIS solutions.

It turns out that the IVS combined solution gains more than 20% in accuracy over the single solutions. Under the reorganization of the IERS, IVS is one of the IERS Product Centers. To improve the analysis results more Analysis Centers are encouraged to contribute and have been invited to participate in Pilot Projects. Their solutions were compared, discussed and improved as all Analysis Centers reach for high standards. The 2nd Analysis Workshop was held in February, 2001 at Goddard Space Flight Center.

## 2.2. Technology Developments

Under the leadership of the IVS Technology Coordinator, Alan Whitney,

- The VLBI Standard Interface (VSI) was developed and the experts internationally agreed upon the specifications for the hardware interface. In 2001 the work for the software specifications was proceeding with similar promise of success. The international collaboration was regarded as very important, which resulted in the IVS Directing Board receiving an award from Japanese Ministry of Public Management, Home Affairs, Post and Telecommunication on "Radio Day," June 1, 2001. I sincerely thank Alan Whitney and Testuro Kondo for their strong effort.
- The development of the MK5 Data Recording System was promoted which is important for reducing operation cost and improving data recording towards real time developments.

### 2.3. Network Developments

A major goal of the Network Coordinator, Ed Himwich, was improving the quality of the observations and the network:

- Continuous investigations and statistics were maintained to find weak points especially in the performance of network stations.
- On the international level some additional stations will soon support IVS, such as the new station TIGO, and some additional stations will become involved which are equipped with data acquisition, recording or transmission systems developed by Canada (S2) and Japan (K4).

A first Technical Operations Workshop was organized in March 2001 at the Haystack Observatory.

### 2.4. WG 1

Working Group 1 (WG1), for mapping the GPS antenna phase center, chaired by Brian Corey, evaluated an error budget for possible VLBI contributions. The goal was to map the phase centers of the transmitting antennas of GPS satellites with respect to quasars. The WG 1 reports indicated the limits of current VLBI support. One result has been not to propose an observing campaign as any gain would be very difficult to accomplish. A final report is being prepared.

## 3. IAU and FAGS Membership

As IVS is responsible for maintaining the Celestial Reference Frame, IVS applied in early 2000 for being recognized as a service of the International Astronomical Union (IAU). After its General Assembly in Summer 2000 in Birmingham IAU accepted IVS as an IAU service too, and requested IVS officially to maintain the CRF.

In 2001 IVS applied for membership in the Federation of Astronomical and Geophysical Data Analysis Services (FAGS). In summer 2001 IVS was approved as a member of FAGS which supports IVS with some funds. Thanks to the IAG and IAU representatives, in particular Nicole Capitaine, who supported us in obtaining the FAGS membership.

## 4. Newsletters

The first IVS Newsletter was released December 1, 2001. The Newsletter is a very good medium to inform all of us about events. It is of importance that contributions are made by the members. I would like to encourage all members to take these opportunities and participate more actively in the IVS life. Thanks to the editors, Nancy Vandenberg, Hayo Hase and Heidi Johnson, who will spend a lot of time informing us with IVS news every four months.

## 5. Prospective Developments

Improvements are required in the availability and reliability of the network stations and the network configuration:

- Automation for unattended observing will help to overcome the weekend gaps.
- More capacity is required in data transmission media, which will be solved by the development of a modern disc based recording system (Mk5) and by the ability to transfer data via the Internet (e-VLBI). These new systems will reduce the time delay and reduce expenses currently needed to for tapes and tape drives.
- The global network configuration has to be improved, especially in the southern hemisphere
- More observing time is required overall.

Encouraging additional related institutions and including the S2 and K4 technologies will improve the situation. High priority has to be placed on rapid turnaround sessions at the correlator. More analysis centers with different software are required to improve the analysis and to increase the robustness of the products.

Very promising was the fact that for the observing program of 2002 the international contributions will be increased by about 20%.

To meet the ambitious goals, proposed by the WG2 and set up by the IVS Directing Board, I kindly ask all responsible members of the contributing agencies to support IVS as fully as possible and to be prepared for the requirements we have to meet in the future. Let us do our best for meeting the requirements for maintaining consistent and precise reference frames and related products, which will become a very strong request from IAG towards the establishment of the International Global Geodetic Observing System (IGGOS).

Thank you.

# The Essential Contribution of VLBI to Fundamental Astronomy

*Nicole Capitaine*

*Observatoire de Paris/SYRTE-CNRS*

*e-mail: capitaine@obspm.fr*

## Abstract

The adoption of the International Celestial Reference System ICRS based on VLBI observations of extragalactic radiosources, by the International Astronomical Union (IAU), since 1st January 1998, has open a new era for astronomy. The ICRS and the corresponding frame ICRF replaced the FK5 based on positions and proper motions of bright stars. According to its definition, the ICRS is such that the barycentric directions of distant extragalactic objects show no global rotation with respect to these objects. The old dream of astronomers of an absolute reference for measuring the angular motion of celestial bodies has thus become reality. This results in an historical abandonment of the link of the celestial reference system with the motion of the Earth. This has to be taken into account by revising the current concepts of fundamental astronomy; IAU 2000 Resolutions provided new definitions for the celestial pole, Universal Time and parameters to be used in the transformation between celestial and terrestrial frames, in consistency with the properties of the ICRS. VLBI observations of Earth orientation referred to the ICRS provide very accurate determination of the actual celestial position of the pole and of the Earth's angle of rotation. This has led to significant improvements in the models for variations of Earth's angular velocity as well as for precession and nutation. Such models are very useful for astrometry and provide a better knowledge of the dynamics of the Earth's interior.

## 1. Introduction

Fundamental astronomy is concerned by the determination of positions and motions of celestial objects. Therefore, it requires definition and realization of reference systems, maintenance of the reference frames which realise the systems, improvement of the models for the observables, and determination of Earth orientation on a regular basis.

This paper emphasizes the essential contribution of VLBI for defining and realizing the fundamental quasi-inertial celestial reference system, for making possible the definition of more basic concepts in fundamental astronomy and for providing accurate Earth orientation parameters.

## 2. Essential Contribution of VLBI for the Celestial Reference System

### 2.1. The Availability of an Absolute Celestial Reference System

The availability of an absolute reference system is required for celestial dynamics. A catalogue of stars, even it is constructed in order to realize a dynamical reference system, as is the FK5 [11], cannot be realized without any rotation, due to the inaccuracies in the estimation of proper motions of stars. This is actually a critical problem and only extragalactic objects, which do not participate in the rotation of the Galaxy, can provide convenient fiducial points. This had already been discussed by Hershel [14] as well as by Laplace [16] in the 18th century, but extragalactic objects have only been discovered in 20th century and compact radio sources as quasars in the 1960s. The hypothesis that the Universe as a whole does not rotate is necessary and seems to

be confirmed by observations. VLBI is, at present, the only technique which can provide the measurement of the directions of quasars with a sufficient accuracy such that it is the unique technique which can realize an absolute celestial reference system.

These issues have been largely discussed by Ma [18], [19] and by Walter & Sovers [31].

## 2.2. The IAU Fundamental Celestial Reference System

The FK5 (Fundamental catalogue) ([11] [12]) has been the IAU celestial reference system from 1976 to 1997. It was based on a concept of dynamical reference system in order to be an “absolute system” and it was realized by positions and proper motions of nearby bright stars. It was oriented so that at a given date, the positions are referred to the best estimate of the location of the mean pole and mean equinox of epoch. The proper motions were evaluated so that, for a given model of precession, they provide the best access to the mean pole and mean equinox of epoch (J2000) at any other date. Its precision is of the order of 0.02” for positions and 1 mas/c for proper motions (see Table 1). The so-called “FK5 System” refers to the FK5 catalogue and to the associated IAU 1976 model for precession [17], the IAU 1980 theory of nutation [27] and GMST/UT1 relationship [1]. Since 1988, there have been successive IAU Resolutions for the adoption of a new celestial reference system based on extragalactic radiosources :

- the IAU General Assembly in 1988 called for the use of extragalactic objects to define the celestial reference frame,
- the IAU GA 1991 adopted General Relativity as the fundamental theory, confirmed 1988 Resolution and specified the continuity with existing stellar and dynamic realisations,
- the IAU GA 1994 adopted a list of some 600 extragalactic radio sources and formed a Working group to define the positions,
- the IAU GA 1997 resolves : (a) that, as from 1 January 1998, the IAU celestial reference system shall be the International Celestial Reference System (ICRS) as specified in the 1991 IAU Resolution on reference frames and as defined by the International Earth Rotation Service (IERS) [2] ; (IERS Technical Note 1997), (b) that the corresponding fundamental reference frame shall be the International Celestial Reference Frame (ICRF) constructed by the IAU Working Group on Reference Frames [18],
- the IAU GA 2000 provides a clarification of IAU’s 1991 definition of the coordinate systems in the framework of General Relativity, making a distinction between the system of space-time coordinates (a) for Solar System (BCRS) which can be considered to be a “global coordinate system” that contain all the “far away regions” [28] and (b) for the Earth (GCRS) which can only be considered as a “local coordinate system”.

## 2.3. The Significant Change from FK5 to ICRF

The International Celestial Reference System ICRS adopted by the IAU to replace the FK5 since the 1st January 1998 as the fundamental celestial reference system is such that the barycentric directions of distant extragalactic objects show no global rotation with respect to these objects. It was specified that the orientation of the GCRS follows the kinematical condition of absence of global rotation of geocentric directions w.r.t. the objects defining the ICRS [2]. The maintenance of the axes is obtained by a statistical condition that the coordinates of selected “defining sources” (see Figure 1) show no global rotation when improving positions. The ICRF [20] was aligned with the FK5 at J2000 but no attempt is made to refer the positions of the sources to the mean

pole and mean equinox at J2000. It is no longer dependent on the Earth's motion and further improvement of the ICRF will be accomplished without introducing any global rotation. The ICRF is therefore independent from precession-nutation models. This actually corresponds to an historical abandonment of the link of the celestial reference system with the motion of the Earth.

#### **2.4. The Fundamental Role of VLBI and IVS for the ICRF**

In 2000, the IAU adopted the Resolution B1.1 untitled "Maintenance and establishment of Reference frames and Systems" which recognizes :

1. the importance of continuing operational observations made with VLBI to maintain the ICRF,
2. the importance of VLBI observations to the operational determination of the parameters needed to specify the time-variable transformation between the International Celestial and Terrestrial Reference Frames.

The IAU 2000 Resolution B1.1 also recommends the following role for IVS :

1. that IAU Division I maintain the WG on Celestial Reference Systems formed from Division I members to consult with the IERS regarding the maintenance of the ICRS,
2. that the IAU recognise the International VLBI Service (IVS) for Geodesy and Astrometry as an IAU Service Organization,
3. that an official representative of the IVS be invited to participate in the IAU Working Group on Celestial Reference Systems,
4. that the IAU continue to provide an official representative to the IVS Directing Board.

#### **2.5. The International Reference Frame, ICRF and its Extension**

The ICRF has been provided by the IAU WG which was formed in 1994. It is realized [21] by the coordinates of 608 extragalactic radiosources with an accuracy from 0.4 mas to 1 mas (see Table 1 and Figure 1). These sources are divided in three categories according to quality criteria. It includes 212 defining sources, corresponding to the best observed set of sources, 294 candidate sources and 102 others sources; the stability of the axes is ensured by the defining sources at the 20 microarcsecond level. The coordinates of the sources result from the analysis of 1.6 million observations of dual frequency delays and rates during the period 1979-1995.5 using 24-hr VLBI sessions. The abandonment of the link of the CRS with the motion of the Earth requires that an offset at epoch be introduced in the description of the precession-nutation of the Earth's pole, this offset being experimentally determined and being revisable in conventionally adopted models of precession-nutation.

The maintenance and extension of the ICRF, which is one of the tasks of the IAU Working Group ICRS with IERS and IVS, is based on geodetic and astrometric observing VLBI and VLBA programs such as CORE, NEOS, RDV (VLBA). The ICRF-Ext.1 is the first extension of the ICRF [20] adding 59 new sources (see Figure 2) and improving positions and errors for the candidate sources, but with unchanged positions and errors for the defining sources in order to realize the ICRF as defined previously. It results from the re-analyzing of the 1979-1999 data set adding 600,000 observations in 461 sessions and refining the analysis. Further extensions of the ICRF would represent a valuable contribution to fundamental astronomy.

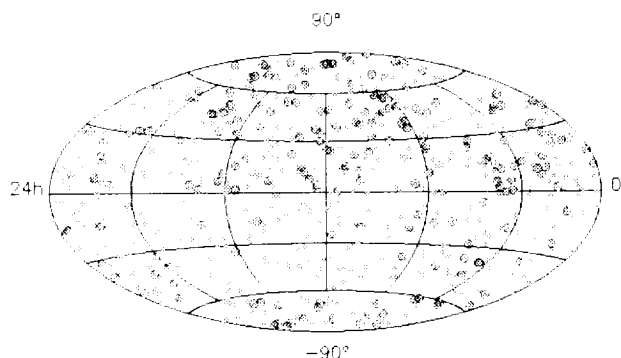


Figure 1. The catalogue ICRF (Ma *et al.* 1998), defining sources: filled circles.

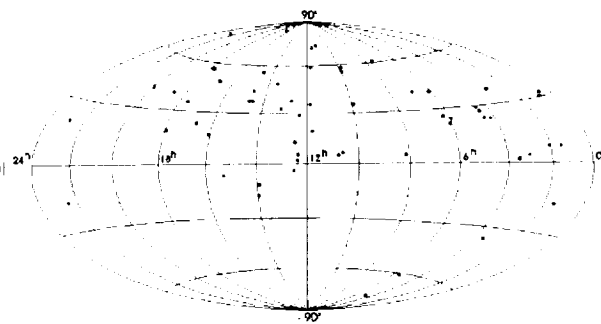


Figure 2. The ICRF-Ext1 catalogue (IERS 1999, Ma 2000).

## 2.6. The ICRS as the Primary Reference System for Astrometry

The ICRS, as the fundamental celestial reference system, constitutes the primary reference system for astrometry to which all global catalogues and surveys have to be tied. The FK5 has been tied to the ICRF [23] and Hipparcos Catalogue (ESA 1997) was adopted by the IAU in 1997 as the optical realisation of the ICRS. It had been tied to ICRF with a positional accuracy of 0.60 mas at  $1991.25 \pm 0.25$  mas /yr [15]. Such a realization through the 100,000 good sources of the observed stars of the Hipparcos mission has been labelled HCRF for “Hipparcos Celestial Frame”. At the mean epoch, 1991.25, of the space mission, the positional accuracy is of the order of 1 mas, but this accuracy degrades quickly with time (see Table 1) due to the inaccuracies in proper motions of stars. HCRF also suffers from a too low density on the sky as well as to the fact that the core of the HCRF is made of sources usually too bright to be used as reference stars for high accurate astrometric measurements of faint celestial objects [24].

The densification of the HCRF, the optical counterpart of the ICRF, as well as the extension of the ICRF in other wavelengths are major tasks of the IAU Working Group ICRS with IERS and IVS. First densifications in the optical wavelengths have already been achieved (e.g. Tycho-1, ACT, TRC, Tycho-2) and other are under realization (e.g. US Naval CCD Astrograph Catalogue) and IR surveys such as 2MASS and DENIS will lead to an extension of the ICRF in the near IR. The future space astrometric missions such as DIVA, FAME, SIM and GAIA will open new perspectives within the next twenty years.

## 2.7. The ICRF as the Primary Reference Frame for Celestial Dynamics

Until recent years, celestial dynamics referred to various “dynamical” celestial reference systems which were linked together in a very complex way [10], [8].

New ephemerides in the Solar System now refer to the ICRS. Recent numerical JPL ephemerides DE405 and LE405 have been referred to the ICRF using adjustments to VLBI observations of spacecraft around Venus and Mars, providing the orientation w.r.t. ICRS with an accuracy of the order of 1 mas [30]. Recent analytical ephemerides of the planets [25] or the Moon [8] also referred to the ICRF, which has now become the primary reference systems for celestial dynamics.

In addition, the orientation of the equator and ecliptic have been recently referred to the ICRF

at a submilliarsecond accuracy thanks to the joint use of lunar laser ranging and VLBI observations for the location of the dynamical ecliptic in the ICRF [8] and thanks to VLBI observations for the position of the mean pole at J2000 in the ICRF [21].

It has to be noticed that such an evolution of the celestial reference frames from a dynamical concept to a “natural” concept is very similar to the evolution of the reference time scales during the 20th century from the concept of Universal Time as realized by Earth rotation, to the International Atomic Time, TAI [5] (see Table 2).

Table 1. Evolution of celestial reference frames

Name	Fiducial objects	Number	Limit of magnitude	Mean time of observations	Observation Technique	Uncertainties: pos., proper motion	Status
FK5	stars	1535 3117	< 7 < 9.5	1940 - 1950	Optical astrometry	0.02" 0.0008"/y 0.08" 0.002"/y	Fundamental catalog from 1976 to 1997
ICRF	Extra galactic radio sources	212 defining 398 others		1987	VLBI	0.0004" 0.001"	Celestial reference frame from 1998
Hipparcos catalogue	stars	118 218	< 12	1991.25	Astrometric satellite Hipparcos	$10^{-3}$ " $10^{-3}$ " /y	HCRF: Optical counterpart of ICRF

Table 2. Evolution of reference time scales

Time scale	Physical phenomenon	Irregularity	Uncertainty of reading	Use for celestial dynamics
Universal time (UT1)	Earth rotation	$10^{-7}$	$5 \cdot 10^{-5}$ s	Until 1950
Ephemeris time (ET)	Earth orbital motion	$10^{-9}$	0.1 s	Until 1995
Internat. atomic time (TAI)	Hyperfine atomic transition	$10^{-14}$	$5 \cdot 10^{-9}$ s	Since 1955

### 3. Essential Contribution of VLBI for Concepts in Fundamental Astronomy

#### 3.1. Improvement in the Concepts of Earth's Orientation

The new concept of the celestial reference system based on a kinematical definition of no global rotation, on which relies the definition of ICRS, must be associated with the revision and the improvement of concepts regarding the Earth's orientation in space. This is necessary in order that the stability of the ICRS is maintained and that the accuracy of the estimated parameters to which VLBI is sensitive is not perturbed. Actual pole and UT1 are estimated by VLBI in the ICRF through a very simple geometric principle which has not to be damaged by the use of old and complicated concepts which are no more adequate [4]. Concerning the classical reference to the equinox, which is the intersection between the ecliptic and the equator, it is important to note that VLBI observations of quasars are not sensitive to its position and that moreover, in General Relativity, the ecliptic is a BCRS coordinate object related with the Earth's ephemerides, whereas the equator is defined in the GCRS only [28].

The relationship between GST and UT1, referring to the equinox, contains the accumulated precession and nutation in right ascension as well as the accumulated coupling between precession and nutation [7]. New parameters are therefore necessary to replace the classical parameters for precession [17], nutation [27] and sidereal angle [1], which are referred to the FK5 (i.e. to the ecliptic and the equinox, see Figure 3). A new definition of the pole is also required to be in agreement with the submilliarsecond accuracy as provided by VLBI estimation of the celestial pole offsets.

Several resolutions were adopted by the IAU in 2000 regarding transformation between the celestial and terrestrial reference systems to be implemented in the IERS procedures beginning on 1 January 2003.

Resolution B1.7 recommends that the Celestial Intermediate Pole (CIP) be implemented in place of the Celestial Ephemeris Pole (CEP) in order to extend the definition in the high frequency domain and coincides with that of the CEP in the low frequency domain [5].

Resolution B1.8 recognizes the need for a rigorous definition of sidereal rotation of the Earth and the desirability of describing the rotation of the Earth independently from its orbital motion and therefore recommends the use of the “non-rotating origin” [13] both in the GCRS and the ITRS. These origins are designated as the Celestial Ephemeris Origin (CEO) and the Terrestrial Ephemeris Origin (TEO). The “Earth Rotation Angle” is defined as the angle measured along the equator of the CIP between the CEO and the TEO. This Resolution recommends that UT1 be linearly proportional to the Earth Rotation Angle and that the transformation between the ITRS and GCRS be specified by the position of the CIP in the GCRS, the position the CIP in the ITRS, and the Earth Rotation Angle [6].

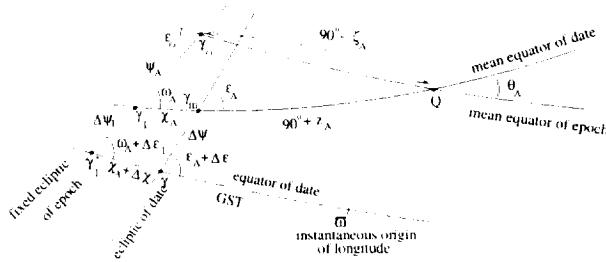


Figure 3. Earth orientation parameters (precession, nutation, GST) in the FK5

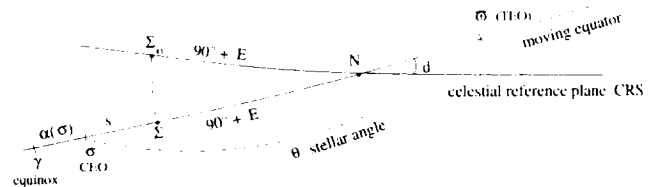


Figure 4. Earth orientation parameters (E, d,  $\theta$ ) referred to the ICRS

### 3.2. The Earth Orientation Parameters Referred to the ICRS

The new concepts for the EOP referred to the ICRS, as adopted by the IAU in consistency with the ICRS, are such that they abandon the current parameters in the FK5 System and they abandon the current formulation which combines the motions of the equator and the ecliptic w.r.t. the ICRS. The Earth's angle of rotation is no more reckoned from the true equinox in order to clearly separate precession-nutation from Earth rotation and to include both precession and nutation in the new parameters X and Y. It must be noticed that the new adopted reference

for UT1, the NRO [13], is actually an unavoidable origin to express a rotation along the moving equator.

The new parameters as adopted by the IAU allow the parameters to clearly separate high frequency and low frequency motions. This reduces to five the parameters for transformation between ITRF and GCRF [3]: two (E, d) for the position of the CIP in the GCRS, two (F, g) for the position of the CIP in the ITRS and one for the Earth's angle of rotation; this provides a symmetric representation for the celestial and terrestrial parts of the motion :  $PN(t) = R3(-E).R2(d).R3(E)$  for precession-nutation and  $W(t) = R3(-F).R2(g).R3(F)$  for polar motion.

The position of the CEO in the GCRS is given by the quantity  $s$ , which can be expressed by a development as function of time [6]. The relationship between the Earth's rotation angle and UT1 is linear [6] and ensures the continuity in phase and rate of UT1 with the value obtained by the conventional relationship between Greenwich Mean Sidereal Time (GMST) and UT1 [1]. Such a linearity represents a significant improvement in the definition of UT1.

#### 4. Essential Contribution of VLBI for Earth Orientation

##### 4.1. The Accurate Determination of UT1

Improvement in precision and time resolution of the estimation of UT1 has been from 1 mas with a resolution of one day in 1980 to 0.1 mas with a resolution to one hour in 2002. There have been, moreover, improvement in strategy and procedures and the combined use of several high precision techniques (VLBI, GPS, ...).

Among these techniques, VLBI is the only one which provides the determination of the actual angle of Earth's rotation in the GCRF (see Figure 5) as well as of the actual position of the pole at the date of the observation in the GCRF (see Figure 6). This is of major importance for the knowledge of the variations in length of day (l.o.d.) which include variations from secular to sub-daily periods.

The determination of UT1 by VLBI provides the reference of this angle for all other techniques (GPS, SLR, LLR,...), with an accuracy of  $5 \mu s$  for UT1 as estimated during 1d-session and  $20 \mu s$  for UT1 estimated for 1h intensive sessions [26].

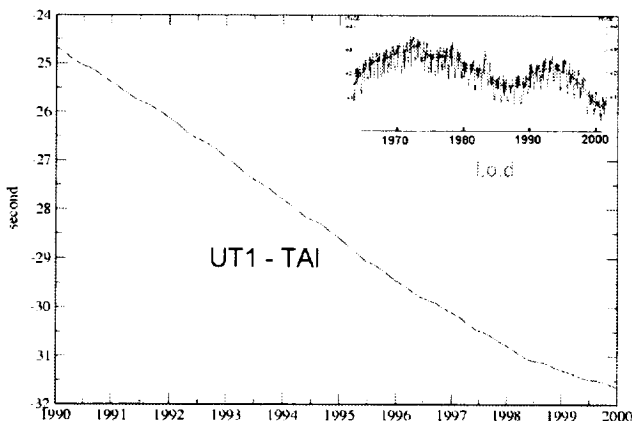


Figure 5. Estimation of UT1-TAI from VLBI (GSFC) observations from 1990 to 2000

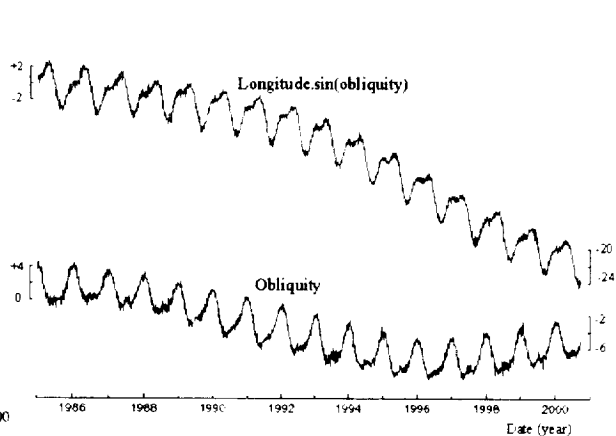


Figure 6. Celestial pole offsets estimated from VLBI observations (1982-2001).

## 4.2. The Accurate Determination of Precession and Nutation

Large improvements have been obtained recently in the nutation theory as well as in the estimation of the precession-nutation motion from VLBI observations [9]. Resolution B1.6 of the 2000 IAU GA recommended that the IAU 1976 precession model [17] and IAU 1980 theory of nutation [27] are replaced by the IAU 2000 precession-nutation model. This model is based on a new rigid Earth nutation model [29] and a new transfer function of Mathews *et al.* [22] whose coefficients are adjusted on VLBI observations.

The IAU 2000A (for 0.2 mas level) and IAU 2000B (its shorter version, for 1 mas level) with the associated precession and obliquity rates and celestial pole offsets at J2000 adjusted on VLBI observations, will replace the previous IAU models beginning on 1 January 2003.

The transfer function from the rigid to the non-rigid Earth model is based on improved geophysical parameters estimated from VLBI (see Table 3) and improved precession rates in longitude and obliquity. Due to the definition of the CIP, the prograde diurnal and semi-diurnal terms in nutation (with amplitudes of the order of 15 microarseconds) are considered as variations of polar motion [4]. Comparisons of the models with VLBI observations show an agreement of the order of 200 microarseconds [9].

Table 3. Estimates of Basic Earth Parameters from least squares fit by Mathews *et al.* (2001)

Basic Earth Parameters	Estimate	Adjustment
$e_f$	$0.0026456 \pm 20$	0.0000973
$\kappa$	$0.0010340 \pm 92$	- 0.0000043
$\gamma$	$0.0019662 \pm 14$	0.0000007
$e$	$0.0032845479 \pm 12$	0.000037
$\text{Im } K^{(CMB)}$	$-0.0000185 \pm 14$	..
$\text{Re } K^{(ICB)}$	$0.00111 \pm 10$	..
$\text{Im } K^{(ICB)}$	$-0.00078 \pm 13$	..
rms $(sd)_{input}$	0.0039	..
rms residuals	0.0132	..

Improvement in the model for nutation corresponds to a better knowledge of the dynamics of the Earth's interior. One illustration is the period of the Free Core nutation (FCN) [22], which is closely linked to the dynamical flattening of the outer core,  $e_f$  (see Table 3). Geophysical model PREM gives a period of 458 days, whereas VLBI estimate is  $430.20 \pm 0.28$  d (see Figure 8) which corresponds to a difference of 350 m in  $e_f$  resulting from the non-hydrostatic effect plus electromagnetic coupling.

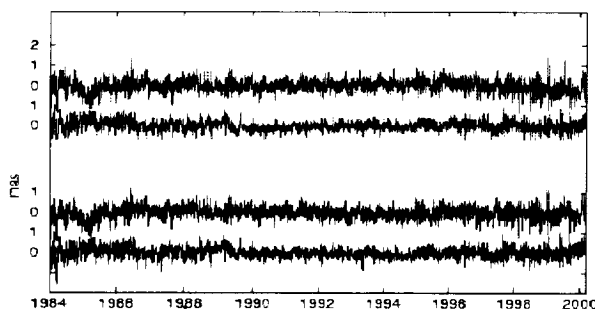


Figure 7. Comparison between models (top: MHB2000, bottom: IERS1996) and VLBI observations (from Dehant *et al.* 1999).

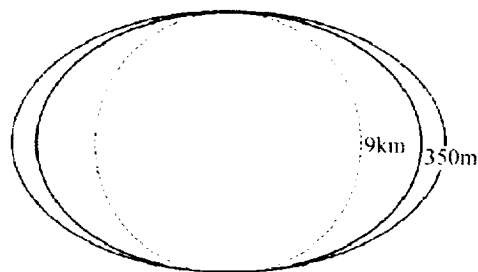


Figure 8. Comparison between the geophysical model (PREM) and VLBI estimate of the fluid core flattening (from Dehant *et al.* 1999).

## 5. Conclusion

Thanks to VLBI, a new celestial reference system is available based on directions of extragalactic radiosources. This new system, ICRS, which is a quasi-inertial system, opens a new era in astronomy. Positions and proper motions of stars are now expressed in the corresponding frame, the ICRF, as well as positions of celestial objects observed at other wavelengths and solar system ephemerides. Earth rotation being observed with respect to the ICRS, the concepts regarding this motion will benefit from its property which leads to a potential improvement in accuracy of the EOP.

## References

- [1] Aoki, S., Guinot, B., Kaplan, G. H., Kinoshita, H., McCarthy, D. D., and Seidelmann, P. K., 1982, "The New Definition of Universal Time," *Astron. Astrophys.*, **105**, pp. 359–361.
- [2] Arias, E.F., Charlot, P., Feissel, M. and Lestrade, J.-F., 1995, *Astron. & Astrophys.*, **303**, pp. 604–608
- [3] Capitaine, N., 1990, "The Celestial Pole Coordinates," *Celest. Mech. Dyn. Astr.*, **48**, pp. 127–143.
- [4] Capitaine, N., 2000, "Definition of the Celestial Ephemeris Pole and the Celestial Ephemeris Origin," in "Towards Models and Constants for Sub-Microsecond astrometry", K.J. Johnston, D.D. McCarthy, B. Luzum, G. Kaplan (eds), USNO.
- [5] Capitaine, N., Guinot, B., 1997, "Les Systèmes de référence en astronomie", CRAS, 725–738.
- [6] Capitaine, N., Guinot, B., McCarthy, D.D., 2000, "Definition of the Celestial Ephemeris origin and of UT1 in the international Reference Frame", *Astron. & Astrophys.*, **335**, pp. 398–405.
- [7] Capitaine, N. and Gontier A.-M., 1993, "Accurate procedure for deriving UT1 at a submilliarcsecond accuracy from Greenwich Sidereal Time or from stellar angle," *Astron. Astrophys.*, **275**, pp. 645–650.
- [8] Chapront, J., Chapront-Touzé, M., and Francou, G., 1999, "Determination of the lunar orbital and rotational parameters and of the ecliptic reference system orientation from LLR measurements and IERS data.", *Astron. & Astrophys.*, **343**, pp. 624–633.
- [9] Dehant, V. *et al.*, 1999, *Celest. Mech. and Dyn. Astr.* **72**, pp. 245–310.

- [10] Folkner, W.M. *et al.*, 1994, "Determination of the extragalactic-planetary tie from joint analysis of radio interferometric and lunar laser ranging measurements", *Astron. & Astrophys.*, **287**, pp. 279–289.
- [11] Fricke, W., Schwan H., Lederle T. Et al., 1988, "Fifth Fundamental Catalog (FK5)", Part I, Verffent. Astron. Rechen-Institut, Heeidelberg, NB0 32.
- [12] Fricke, W., Schwan H., Corbin, T. Et al., 1991, "Fifth Fundamental Catalog (FK5)", Part II, Verffent. Astron. Rechen-Institut, Heeidelberg, NB0 33.
- [13] Guinot B., 1979, "Basic problems in the kinematics of the roation of the Earth", in *Time and the Earth's Rotation*, IAU Symposium N 82, McCarthy D.D, Pilkington D.H., eds, D. Reidel, pp. 7–18.
- [14] Hershel W., 1785, *Phil. Trans. Royal Soc. London*, 75, p. 213.
- [15] Kovalevsky, J. *et al.* 1997, "The Hipparcos Catalogue as a realization of the extragalactic reference system", *Astron. Astrophys.*, **323**, pp. 620–633.
- [16] Laplace S., 1796, "Exposition du Système du Monde".
- [17] Lieske, J. H., Lederle, T., Fricke, W., and Morando, B., 1977, "Expressions for the Precession Quantities Based upon the IAU (1976) System of Astronomical Constants," *Astron. Astrophys.*, **58**, pp. 1–16.
- [18] Ma, C., 1999, "The Celestial Reference Frame", in 1999 IVS Annual Report, pp. 18–22.
- [19] Ma, C., 2000, "The ICRF and the relationship between frames", in IVS 2000 General Meeting Proceedings.
- [20] Ma,C., 2000, "The ICRF: Construction, Maintenance and interaction with EOP and nutation", in *Journées Systèmes de référence spatio-temporels*, N. Capitaine (ed), Observatoire de Paris, pp. 3–7.
- [21] Ma, C., Arias, E.F., Eubanks, T.M., Fey, A., Gontier, A.-M., Jacobs, C.S., Sovers, O. J., Archinal, B.A., Charlot, P., 1998, "The International Celestial Reference Frame as realized By Very Long Baseline Interferometry", *Astron. Astrophys.*, **116**, pp. 516–546.
- [22] Mathews P.M., Herring, T.A., Buffett B.A., 2001, "Modeling of nutation-precession: New nutation series for nonrigid Earth, and insights into the Earth's Interior," *J. Geophys. Res.*, in press.
- [23] Mignard, F. and Froeschle, M., 2000, "Global and local bias in the FK5 from the Hipparcos data", *Astron. Astrophys.*, **354**, pp. 732–739.
- [24] Mignard, F., 2000, "Densification of the ICRF in the visible and IR", in *Journées Systèmes de référence spatio-temporels*, N. Capitaine (ed), Observatoire de Paris, pp. 8–15.
- [25] Moisson, X., "Solar System planetary motion to third order of the masses", *Astron. Astrophys.*, **341**, pp. 318–327.
- [26] Schuh, H., *et al.* 2001, "Final Report of the IVS Working Group 2 for Product specification and observing programs."
- [27] Seidelmann, P. K., 1982, "1980 IAU Nutation: The Final Report of the IAU Working Group on Nutation," *Celest. Mech.*, **27**, pp. 79–106.
- [28] Soffel, M., 2000, "Practical aspects of the new conventions for astrometry and celestial mechanics in the relativistic framework", in *Journées Systèmes de référence spatio-temporels*, N. Capitaine (ed), Observatoire de Paris, pp. 67–69.
- [29] Souchay, J., Loysel, B., Kinoshita, H., Folgeira, M., 1999, "Corrections and new developments in rigid Earth nutation theory : III. Final tables REN-2000 ," *Astron. Astrophys. Supp. Ser.*, **135**, pp. 111-131.
- [30] Standish, E.M., Newhall, XX, Williams, J.G., Folkner, W.M., 1995, "JPL Planetary ephemerides", JPL IOM 314.10-127.
- [31] Walter., H.G., Sovers, O.J., 2000, "Astrometry of Fundamental Catalogues", Springer -Verlag.

# Challenges for VLBI Within an Integrated Global Geodetic Observing System

Hermann Drewes<sup>1</sup>, Gerhard Beutler<sup>2</sup>, Reiner Rummel<sup>3</sup>

<sup>1</sup>) *Deutsches Geodätisches Forschungsinstitut*

<sup>2</sup>) *Astronomisches Institut, Universität Bern*

<sup>3</sup>) *Institut für Astronomische und Physikalische Geodäsie, Technische Universität München*

Contact author: Hermann Drewes, e-mail: [drewes@dgfi.badw-muenchen.de](mailto:drewes@dgfi.badw-muenchen.de)

## Abstract

The Integrated Global Geodetic Observing System (IGGOS), proposed as a Project in the new structure of the International Association of Geodesy (IAG), is viewed as the essential contribution of geodesy to the interdisciplinary research of the System Earth. It will provide the basis for precise, reliable point positioning, the orientation of Earth in space, and the determination of the Earth's gravity field within a consistent reference system. All space geodetic techniques and their services have to be integrated into the IGGOS, and they shall take over their specific role according to their strengths and preferences. VLBI has some extraordinary capabilities which cannot be accomplished by other techniques. These are, in particular, the direct connection to the inertial celestial reference system, its high precision, and the independence from the Earth's gravity field. In addition, there is a very long VLBI time series for geodetic parameters (Earth rotation, station positions and velocities) which is not available from other techniques. Therefore, VLBI has to take a prominent role in the establishment of the Integrated Global Geodetic Observing System.

## 1. Introduction

Geodesy, as the science of the measurement and the mapping of the Earth's surface, provides precise information on the state and the temporal variations of the Earth's orientation in space, its geometric figure and shape, and its outer gravity field. The parameters describing the variations with time reflect the effects of mass displacements due to dynamic processes in the system Earth. They include the processes in the solid geosphere (motions of the core, mantle convection, plate tectonics, etc.), in the hydrosphere (ice mass exchange, ocean currents, sea level changes, etc.) and in the atmosphere (winds, pressure variations, global warming, etc.). By these means, geodetic observations and products contribute directly to Earth system research. To do this contribution efficiently, i.e., to provide unequivocal information, the efforts have to be strictly coordinated and to be integrated into one unique observing system with consistent constants, standards, reference frames, models and parameters.

At present, the geodetic observation systems providing the data for estimation of the geometric and gravimetric parameters are mainly based on space techniques (very long baseline interferometry, satellite positioning systems, satellite altimetry and satellite gravity missions). They are globally oriented and are subject to the same kind of environmental and physical influences. The evaluation and analysis of the data, however, is often done independently using different standards and models. The individual geodetic techniques have their particular strengths and weaknesses. To take maximum benefit of the advantages and to compensate the shortcomings as far as possible, they have to be combined in a proper way using one and the same fundamental reference system.

Both the generation of consistent products for Earth system research and the optimum use of the geodetic observations require thus the unification of all fundamentals (constants, standards, reference frames, models) underlying the geodetic techniques and methods. This leads to the establishment of an Integrated Global Geodetic Observing System (IGGOS).

## 2. Decisions of the IAG Concerning the Establishment of an IGGOS

During its Scientific Assembly in Budapest, Hungary, September 2001, the International Association of Geodesy (IAG) decided to install a new structure for the next legislature period starting in 2003. The basic scientific components of the new structure are the Commissions, the Services, the IAG Project(s), the Inter-Commission Committee(s) and the Communication and Outreach Branch.

The *Commissions* shall promote the advancement of science, technology and international cooperation in their fields. Four Commissions will be established to cover the entire field of geodesy:

1. Reference Frames,
2. Gravity Field,
3. Earth Rotation and Geodynamics,
4. Positioning and Applications.

The *Services* are part of the Association's work and generate products, using their own observations and/or observations of other services, relevant for geodesy and for other sciences and applications. At present the services of IAG are:

- International GPS Service,
- International VLBI Service,
- International Laser Ranging Service,
- International Earth Rotation Service,
- International Bureau of Weights and Measures (Time Section),
- International Gravimetric Bureau,
- International Geoid Service,
- International Center for Earth Tides,
- Permanent Service for Mean Sea Level,

*Inter-Commission Committees* shall handle well defined, important and permanent tasks involving all commissions. An example might be a committee for geodetic theory and methodology.

The *Communication and Outreach Branch* provides the Association with communication, educational/public information and outreach links to the membership, to other scientific associations and to the world as a whole.

*IAG Projects* are of a broad scope and of highest importance for the entire field of geodesy. These projects serve as the flagships of the Association for a long time period (decade or longer). To establish IAG Projects, the IAG Executive Committee (EC) shall appoint a planning group for the creation of each project. Each IAG Project shall have a Steering Committee consisting of the Project Chair, one member from each Commission, two members-at-large, and the chairs of the Project sub-groups (if any).

During the IAG Scientific Assembly, Budapest 2001, a candidate IAG Project "Integrated Global Geodetic Observing System (IGGOS)" was proposed by R. Rummel et al. (2002). It was discussed and approved by the "IAG Committee for the Realization of the New IAG Structure" on September 6, 2001. A planning committee for the project consisting of about ten persons will be installed soon. This committee has to take into account all the work performed by IAG in

this area in order to design the objectives, the charter, and the structure of the project. It has to include a close cooperation with the IAG Services, relevant Commissions and Sub-Commissions.

### 3. Requirements and Interdisciplinary Position of IGGOS

The Integrated Global Geodetic Observing System (IGGOS) should be seen as geodesy's contribution to the study of the System Earth composed of the solid geosphere, the hydrosphere and the atmosphere. It will provide its findings to interdisciplinary research, governmental agencies and private sectors. In this context one has to consider the existing initiatives in this field.

In 1998, the *United Nations (UN)* released an Integrated Global Observing Strategy (IGOS: <http://ioc.unesco.org/igospartners>). The development and implementation of this IGOS is supported by a partnership of several groups of agencies, international research programs and other sponsors. The two major groups of agencies are the Committee on Earth Observation Satellites (CEOS) created in 1984 by the Economic Summit of Industrialized Nations (G-7) including some 20 national space agencies, and the International Group of Funding Agencies for Global Change Research (IGFA) grouping national research funding agencies. The major international research programs involved are the International Geosphere-Biosphere Programme (IGBP) and the World Climate Research Programme (WCRP). Both programs are mainly driven by the International Council for Science (ICSU) and the United Nations Educational, Scientific and Cultural Organization (UNESCO).

The Global Observing Strategy comprises three Global Observing Systems (G3OS):

- The *Global Climate Observing System (GCOS)* signed on September 29, 1998 by the World Meteorological Organization (WMO), the Intergovernmental Oceanographic Commission (ICO) of UNESCO, the United Nations Environment Programme (UNEP), and ICSU;
- The *Global Ocean Observing System (GOOS)* agreed upon by a new Memorandum of Understanding between IOC, WMO, UNEP and ICSU at the end of 1998;
- The *Global Terrestrial Observing System (GTOS)* established in January 1996 by the Food and Agriculture Organization (FAO) of the UN, ICSU, UNEP, WMO and UNESCO.

The purpose of these observing systems is mainly policy oriented rather than dealing with scientific objectives. Their "mission is to provide policy-makers, .... , with data they need to detect, locate, understand and warn of changes in the terrestrial ecosystems".

Geodesy, and in particular IAG, is very active in some of the interdisciplinary committees of ICSU. We just mention the

- Scientific Committee on Antarctic Research (SCAR),
- Committee on Space Research (COSPAR),
- Scientific Committee on the Lithosphere (SCL) with the International Lithosphere Programme (ILP),

where IAG has its representatives and common projects, commissions and other activities.

Thus we may summarize the IAG Project IGGOS being the interface between the IAG Commissions and Services and the ICSU, WMO and UN initiatives (Fig. 1).

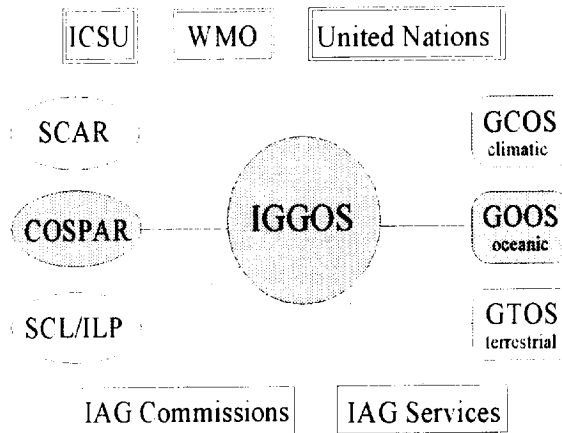


Figure 1. Interdisciplinary position of the IAG Project IGGOS

#### 4. Requirements of IGGOS and Its Position in Geodetic Science

The Integrated Global Geodetic Observing System (IGGOS) shall provide a consistent reference system for all groups of fundamental geodetic parameters (Fig. 2):

- Earth rotation parameters (precession, nutation, rotational velocity, pole position),
- Terrestrial position parameters (point coordinates and velocities, surface models - DTM's - and deformations),
- Gravity field parameters (gravity anomalies, height anomalies, geoid, deflections of the vertical, "mean" sea level).

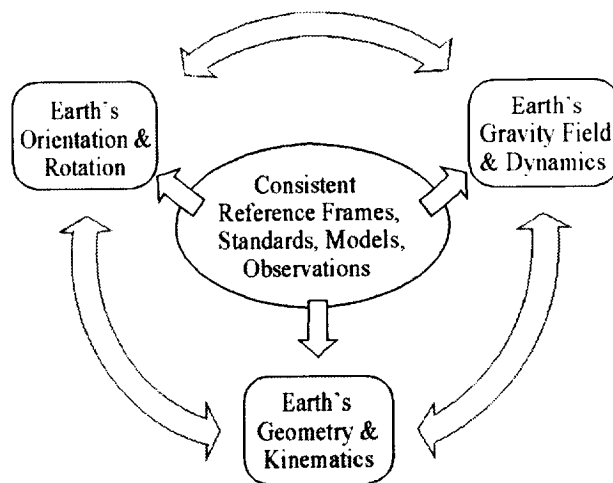


Figure 2. The IGGOS within geodetic science

Reference system in this sense means the definition of a set of geometric and physical parameters necessary for the measurement and the description of the geometry and physical processes

within the Earth's system. It shall use hereby consistent standards in geometry (origins, orientations, scales, ...), in physics (speed of light in the media, geocentric gravitational constant, ...), and in dynamics (geopotential and other forces). It shall use consistent, coordinated observation techniques (e.g., within an Integrated Space Geodetic Network, ISGN) and unique data exchange formats (e.g., SINEX).

The accomplishment of these requirements will be the primary duty of the Services of the IAG. The interaction and coordination of the services' activities is the basic concept of the IGGOS. The three pillars of geodesy — geometry & kinematics, Earth orientation & rotation, gravity field & dynamics — shall be combined to a consistent, unified observing system. From this combination a series of new products for Earth sciences shall emerge, such as the feasibility of establishing a global mass balance.

While the scientific foundations will mainly come from the relevant IAG Commissions, the products to be given to the interdisciplinary community will be provided by the Services. However, IGGOS is not seen as a new "Super-Service" that generates the products or the scientific results, but it is to coordinate the scientific work and to serve as an interface to the non-geodetic scientific community and to society. It shall strive for the fulfillment of the requirements mentioned above. IGGOS will not be able to operate without the Services of IAG (Fig. 3).

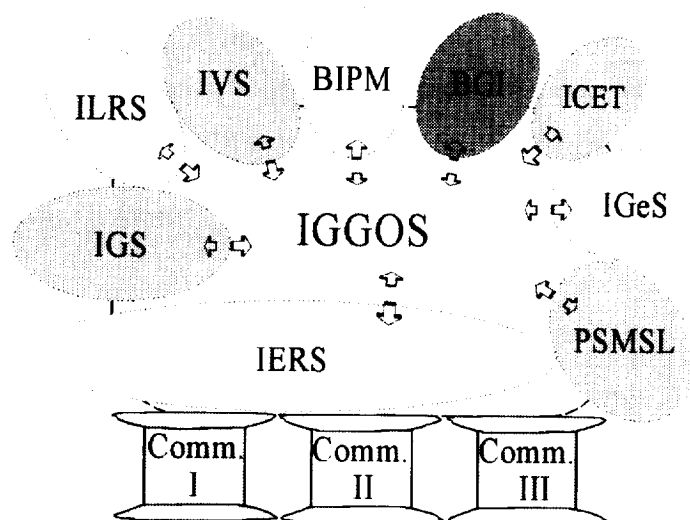


Figure 3. Interaction of IAG Commissions and Services with IGGOS (IERS: International Earth Rotation Service, IGS: International GPS Service, ILRS: International Laser Ranging Service, IVS: International VLBI Service for Geodesy and Astrometry, BIPM: Bureau International de Poids et Mesure (Time Section), BGI: Bureau Gravimétrique International, ICET: International Center of Earth Tides, IGeS: International Geoid Service, PSMSL: Permanent Service of Mean Sea Level).

## 5. Contribution of VLBI to IGGOS

Very Long Baseline Interferometry (VLBI) will contribute to two basic parameter groups of the IGGOS, the Earth Orientation Parameters (EOP) and parameters related to the Terrestrial Reference System (TRS). Both are of fundamental importance for the establishment of the Integrated

Global Geodetic Observing System.

### 5.1. Earth Orientation Parameters

Dynamic processes in the Earth's system cannot be observed directly but they have to be modeled from the observation of particular effects caused by those processes. Examples are the variations of the Earth's rotation or the deformation of the Earth's surface due to mass displacements in the solid, liquid or gaseous part of the Earth. To model the dynamic processes by adequate physical approaches we need an inertial reference system where the corresponding basic equations hold. In the case of modeling the Earth's motion in space we refer to the inertial system defined and realized by the Celestial Reference System (CRS). The connection between CRS and TRS is given by the EOP, i.e., precession, nutation, rotational velocity (UT1-UTC), and pole coordinates ( $X_p$ ,  $Y_p$ ). This chain of parameters can be provided completely only by VLBI because it is the only technique that has direct observational access to the CRS. The other space techniques are only able to refer to quasi-inertial systems. We just mention the problem of separating the variation of the longitude of the node of the satellites' orbits from the variations in UT1-UTC.

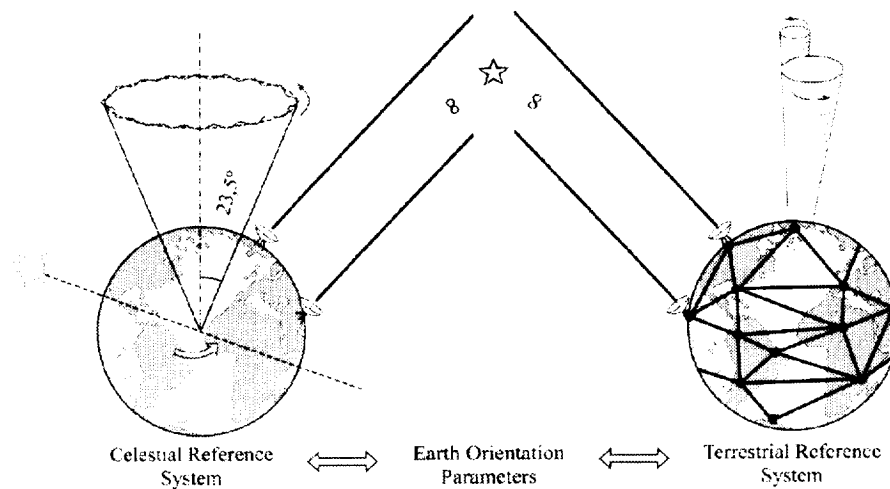


Figure 4. Connection of the Celestial System and the Terrestrial System can only be provided by VLBI.

The knowledge of the EOP and their variations with time is very important for many practical applications. Extraterrestrial space missions have to refer to the exact orientation of Earth in space to get the correct trace. Long period navigation of artificial spatial bodies has to consider the variation of Earth's orientation for its continuous positioning. Astronomical and astrometric research need the precise relation of the TRS with respect to the CRS given by the EOP.

The change of EOP, i.e., the variation of the Earth's rotation, is a fundamental tool for the interdisciplinary study of several processes in the Earth's system. Geology uses the methods of historical geology, paleo-climatology and paleo-magnetometry which refer directly or indirectly to the time dependent rotation axis of the Earth. In geophysics the parameters of the magnetic field and of core-dynamics are affected by the Earth's rotation. Global change research (atmospheric and oceanographic) gets important information from Earth rotation variations which reflect mass displacements in the atmosphere (pressure and winds) and in the oceans (currents, pressure, tem-

perature).

How precisely do we need to know the variations of Earth orientation parameters? The answer depends on the application. The most evident requirements are certainly given by the realization of the celestial and terrestrial reference frames. If we ask for millimeter precision of terrestrial coordinates, then we need the pole coordinates better than  $\pm 0.1$  mas and the rotational velocity (UT1-UTC) better than  $\pm 0.01$  msec. This precision of pole coordinates can probably be provided by several space geodetic techniques (VLBI, SLR, GPS, DORIS). The corresponding precision of UT1-UTC, however, may hardly be provided by techniques other than VLBI. Figure 5 shows the comparison of the (formal) precision of VLBI (solution of Goddard Space Flight Center, GSFC) and GPS (IGS) from January 1994 to December 2000. VLBI is in general below  $\pm 0.01$  msec, with lower precision where only poorly configured observation sessions are available, while GPS varies around  $\pm 0.02$  msec.

Besides the internal precision we shall compare directly the estimated values of UT1-UTC. Here we find significant systematic and random differences. In 2000 there exists an offset of 0.26 msec between the solutions, and after its reduction there is a w.r.m.s. difference of  $\pm 0.17$  msec (Fig. 6). As GPS has no direct access to the inertial celestial reference system, it has to adjust its time series frequently to the VLBI data, i.e., it is only able to estimate relative values or rates of UT1-UTC.

This example proves again the need for VLBI for the determination of the Earth rotation parameters. Without any doubt, the long-term stability can only be achieved by VLBI observations with its direct connection between CRS and TRS.

## 5.2. Station Positions and Velocities for Realization of the Terrestrial Reference Frame

VLBI contributes essentially to the realization of the terrestrial reference frame (TRF) by providing precise station coordinates and velocities. In the latest realization of the IERS TRF (ITRF2000, <http://lareg.ensg.ign.fr/ITRF/ITRF2000/>) the individual VLBI solutions showed w.r.m.s. errors in position of about  $\pm 4$  mm and in velocity of about  $\pm 0.6$  mm/a. The other techniques' solutions were significantly less precise (SLR about  $\pm 10$  mm and  $\pm 2.0$  mm/a; GPS about  $\pm 4$  mm and  $\pm 1.4$  mm/a, respectively).

Comparing the velocities of the combined VLBI solution, which entered into the ITRF2000 with the combined solutions of the other techniques, we see the best relative adaptation of VLBI results (Table 1). In particular for the height component (Up) this may be surprising, because the satellite techniques (GPS, SLR) refer to the geocenter by means of the gravity field models used for orbit determination and provide herewith "absolute" heights. The scale of the ITRF2000, however, is derived with high weight from VLBI due to its extreme stability (see ITRF2000). As the scale affects mainly the radial component of the station coordinates, the VLBI heights are obviously more reliable than those derived from satellite techniques.

An accurate terrestrial reference frame is essential for an Integrated Global Geodetic Observing System (IGGOS) in its interdisciplinary role and for many practical application:

- Geo-referencing for geographic information systems;
- Precise positioning in engineering, cadastre, rural and urban planning, etc.;
- Navigation in air, on land and sea;

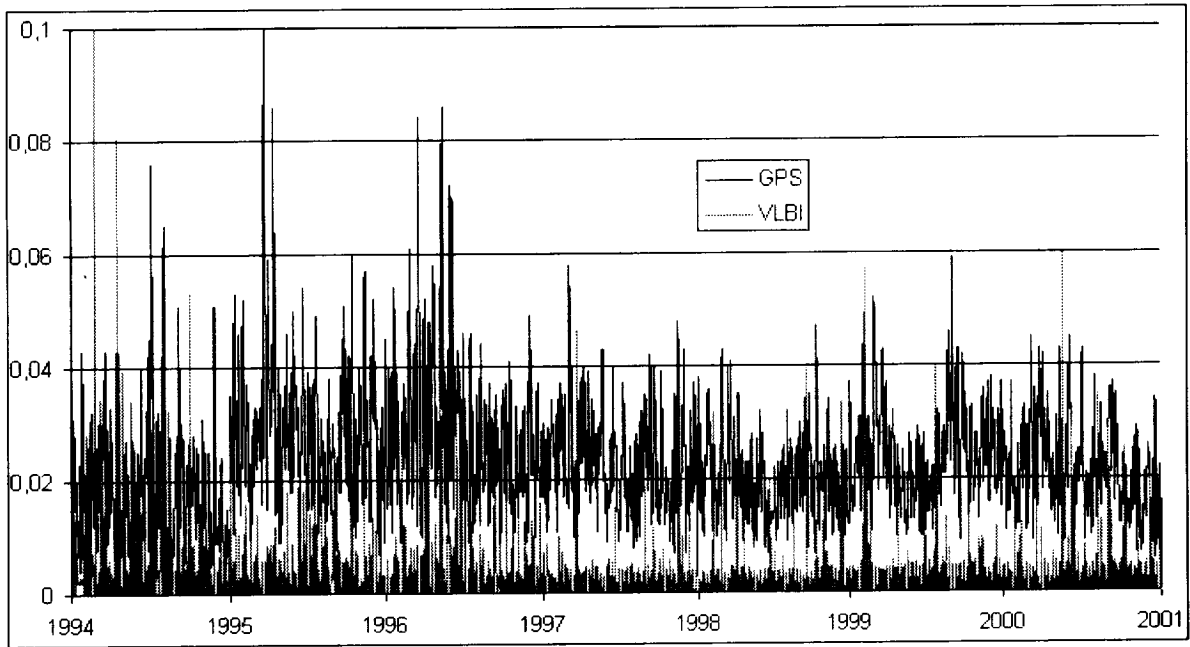


Figure 5. Comparison of UT1-UTC precision estimated from VLBI and GPS [msec]

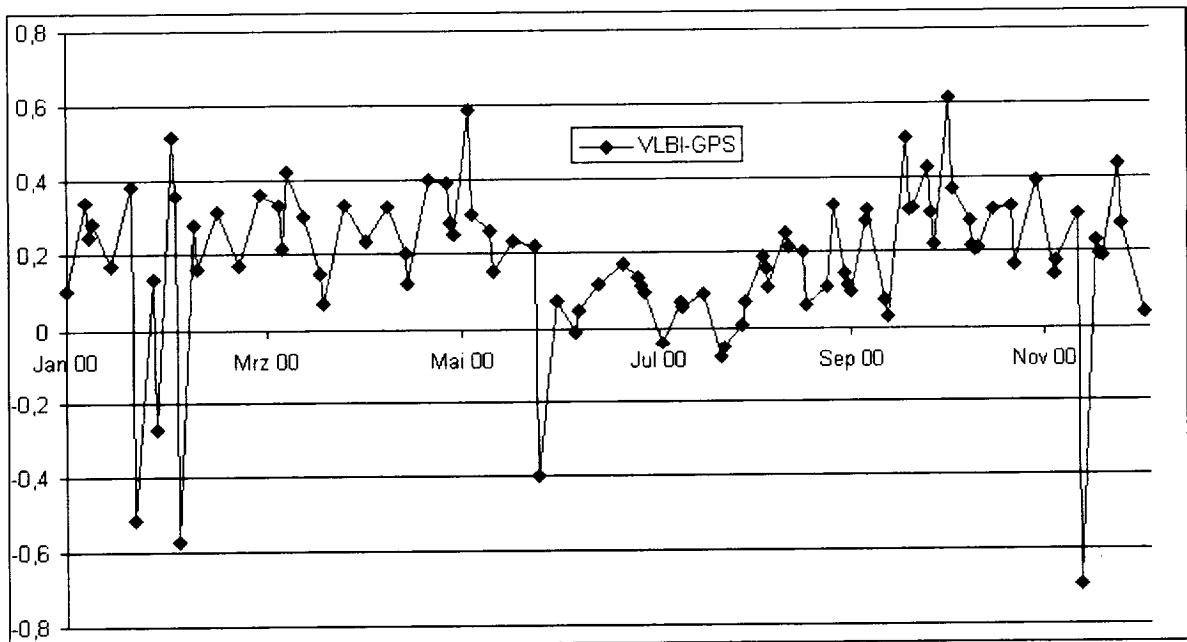


Figure 6. Differences of UT1-UTC in 2000 estimated from VLBI and GPS [msec]

- Disaster research: earthquakes, inundations, volcanoes, etc.;
- Geophysics: geodynamics, plate tectonics, geocenter variations, etc.;
- Oceanography: currents (buoys positioning), tide gauge control, ice surface control, etc.

The various needs and uses of terrestrial reference frames in practice and in society seem not to be sufficiently well known in geodesy. On the other hand, the role of geodesy for the definition, establishment and maintenance of terrestrial reference frames seems not to be sufficiently well known and appreciated in practice and in society.

Table 1. Comparison of station velocities derived from different techniques (combined solutions) and w.r.t. ITRF2000 (w.r.m.s. deviations in mm/a)

		vs. SLR	vs. GPS	vs. ITRF
VLBI	No. of sites	13	29	69
	North	$\pm 2.4$	$\pm 1.0$	$\pm 1.4$
	East	$\pm 1.0$	$\pm 2.1$	$\pm 0.8$
	Up	$\pm 2.6$	$\pm 3.7$	$\pm 1.1$
SLR	No. of sites		24	64
	North		$\pm 2.7$	$\pm 1.8$
	East		$\pm 2.5$	$\pm 1.2$
	Up		$\pm 3.2$	$\pm 3.5$
GPS	No. of sites			151
	North			$\pm 1.5$
	East			$\pm 0.9$
	Up			$\pm 2.7$

## 6. Conclusions

The Integrated Global Geodetic Observing System (IGGOS) is a fundamental requirement for geodesy, for the other Earth sciences, for interdisciplinary research, and for many practical applications. The Services of the International Association of Geodesy (IAG) play an important role in the realization of the IGGOS in its geometrical and gravimetric components. Only the cooperation between Services and Commissions of the IAG will guarantee the success of IGGOS.

The International VLBI Service for Geodesy and Astrometry (IVS) is an indispensable partner in the establishment of the IGGOS because it provides unique and fundamental parameters to realize and maintain the global reference frames (celestial and terrestrial) and gives important information for monitoring the System Earth.

## References

- [1] Rummel, R., H. Drewes, G. Beutler: Integrated Global Geodetic Observing System - A candidate IAG project. Proc. of the IAG Scientific Assembly, Budapest 2001, Springer-Verlag, 2002.

# Combination of Space-Geodetic Techniques

*Markus Rothacher*

*Forschungseinrichtung Satellitengeodäsie, TU Munich*

*e-mail: rothacher@bv.tum.de*

## Abstract

The combination of all major space-geodetic techniques — Very Long Baseline Interferometry (VLBI), Satellite Laser Ranging (SLR), Lunar Laser Ranging (LLR), Global Positioning System (GPS), and Doppler Orbitography and Radiopositioning Integrated by Satellite (DORIS) — into an “Integrated Global Geodetic Observing System” (IGGOS) must be a primary goal in geodesy in the next years. Such an integrated system should also include observation techniques such as satellite altimetry, Synthetic Aperture Radar (SAR) and the various measurements that become or will become available through the new satellite gravity missions CHAMP, GRACE, and GOCE. In this article we will mainly focus on the combination of the observation techniques VLBI, SLR, LLR, GPS, and DORIS, that form the basis for the realization of the International Terrestrial Reference Frame (ITRF), the International Celestial Reference Frame (ICRF), and the Earth orientation parameters (EOPs) that describe the transformation between the ICRF and ITRF. A combination of these techniques is beneficial in many ways, especially to distinguish genuine geodetic/geophysical signals from technique-specific systematic biases and to ensure the consistency of the resulting geodetic products. The integration effort should finally lead to a more detailed view and understanding of the complexity of the “System Earth” and its geophysical processes.

The variety of combination aspects resulting from a rigorous integration will be discussed and illustrated.

## 1. General Combination Aspects

The idea to compare and combine the results of the major space-geodetic techniques is not new. For a long time groups involved in the processing of data of one space-geodetic technique have compared their results with those of groups working on other observation techniques. But in most cases these comparisons were limited so far to one specific parameter type, e.g., the station coordinates of collocated sites, the troposphere zenith delays at collocated sites or the Earth Rotation Parameters determined by different techniques. The only product that is presently based on a rigorous combination of the results of the individual techniques is the ITRF, where the full variance-covariance information of the individual solutions is included in the combination algorithms to obtain site coordinates and velocities. The EOP series of the International Earth Rotation Service (IERS) are still generated with rather simple procedures (typically a weighted mean of the individual series) and independent of the ICRF and ITRF. It is clear, however, that there are considerable benefits to be expected from a rigorous combination and integration of the space-geodetic observation techniques. The most important aspects are:

- It helps to distinguish technique-specific systematic biases from real geodetic or geophysical signals, a crucial aspect in view of the fact that the results of the individual techniques are primarily limited by systematic biases today.
- The complementarity, strengths and weaknesses of the individual techniques may be used to obtain an optimum solution for the geodetic and geophysical parameters concerning not

only the precision and accuracy, but also time resolution and availability of the results.

- We can benefit from the collocation of different observing instruments at the same site. The data of these instruments have to yield identical results for site-specific parameters common to more than one technique.
- There is only one orientation of the Earth's rotation axis for all techniques, only one rotation velocity of the Earth, only one tropospheric and ionospheric refraction for VLBI, GPS, and other microwave techniques, and only one set of coordinates and velocities should result for collocated sites.
- Observing satellites with different techniques (e.g. GPS, SLR, and DORIS) should yield identical orbits, independent of the technique used.
- The rigorous combination is a prerequisite to ensure the consistency of the geodetic results obtained, in particular the consistency of the ITRF, ICRF, and EOP products of the International Earth Rotation Service (IERS).

The final goal of such an integration process would be the combination of all observing techniques into an "Integrated Global Geodetic Observing System" (IGGOS). This should also include observation techniques like satellite altimetry, Synthetic Aperture Radar (SAR), and the measurements of the new gravity satellite missions CHAMP, GRACE, and GOCE, and thus embrace all the three pillars of geodesy: the site positions (displacement fields), Earth orientation and the gravity field.

### 1.1. Links Between the Space-Geodetic Techniques

Let us now consider the two principal types of links that exist between the individual observation techniques: (1) links at individual stations or satellites and (2) links through common parameters. The first type of link concerns the connection between the techniques that can be established on the Earth's surface (stations) and in space (satellites):

- *Stations as link*: Different observation techniques present at the same location — typically at sites called fundamental stations (e.g. Wettzell, Onsala, Fairbanks, ...) — may be linked using accurate information about the local ties between the reference points of the individual techniques.
- *Satellites as link*: Tracking of a satellite with several observation techniques (e.g. SLR, GPS, DORIS, altimetry) allows for a link at the satellite, if the offsets between the various instruments on the satellite (GPS antenna phase center, SLR reflector, ...) are accurately known.

These two types of links will be discussed in more detail in Sections 2 and 3.

The second type of link is realized by all parameters that are common to more than one space-geodetic technique. This link based on common parameters can be performed on two different levels, namely, the combination of the common parameters on the normal equation level (stacking of normal equation matrices) or on the observation level.

The second approach is certainly more demanding and only one or two software packages are available today capable of treating all the major techniques in a consistent way. In principle, both methods (normal equation and observation level) are mathematically equivalent and give identical results. In practice, however, it is much more difficult to ensure the consistency of all the models involved in the processing of the space-geodetic data, if independent computer programs are used to generate the normal equations (or variance-covariance matrices) and the parameterization

might not be identical, which inevitably leads to problems in the combination. In addition, the combination on the observation level has the advantage that parameters that have to be estimated with a high temporal resolution can easily be treated (e.g. using pre-elimination schemes or filter algorithms) without having to deal with extremely large and bulky normal equation systems.

It should be pointed out that — independent of the method chosen to combine the results — consistent standards (IERS Conventions and more) and parameterizations are a necessity for a correct and rigorous combination procedure.

Let us have a closer look now at the observation equations of the individual techniques to get more insight into the various parameter types involved.

## 1.2. Basic Observation Equations and Parameter Space

It is not our intention and goal here to come up with an elaborate and complex observation model including, e.g., a fully relativistic formulation and going into the subtleties of the individual techniques. Detailed observation equations may be found in [7] (GPS), [1] (SLR), [6] (VLBI), and many text books on space geodesy (see e.g. [5]). The simplified observation equations for GPS, SLR, and VLBI given here — similar equations exist for GLONASS, DORIS, altimetry — should primarily demonstrate the similarities between the techniques and show where the various parameter types turn up in the individual observation equations:

$$c \Delta\tau_R^{S,GPS} = |\mathbf{r}_i^S - \mathbf{R} \cdot \mathbf{r}_{e,R}| - c \delta t^S + c \delta t_R + \delta\rho_{trp,R}^S + \delta\rho_{ion,R}^S + \delta\rho_{rel,R}^S + \dots + \epsilon \quad (1)$$

$$\frac{1}{2} c \Delta\tau_R^{S,SLR} = |\mathbf{r}_i^S - \mathbf{R} \cdot \mathbf{r}_{e,R}| + \delta\rho_{trp,R}^S + \delta\rho_{rel,R}^S + \dots + \epsilon \quad (2)$$

$$c \Delta\tau_{R_1,R_2}^{S,VLBI} = -\mathbf{R} \cdot \mathbf{r}_{e,R_1} \cdot \mathbf{e}_i^S - c \cdot \delta t_{R_1} - \delta\rho_{trp,R_1}^S - \delta\rho_{ion,R_1}^S - \delta\rho_{rel,R_1}^S \\ + \mathbf{R} \cdot \mathbf{r}_{e,R_2} \cdot \mathbf{e}_i^S + c \cdot \delta t_{R_2} + \delta\rho_{trp,R_2}^S + \delta\rho_{ion,R_2}^S + \delta\rho_{rel,R_2}^S + \dots + \epsilon \quad (3)$$

with the following quantities and parameters (parameter types are given in italics):

$\Delta\tau_R^{S,GPS}$	Code or phase observation between satellite $S$ and station $R$ (pseudo light travel time)
$\Delta\tau_R^{S,SLR}$	Light travel time (station $R \rightarrow$ satellite $S \rightarrow$ station $R$ )
$\Delta\tau_{R_1,R_2}^{S,VLBI}$	Light travel time difference between stations $R_1$ and $R_2$ for radio source $S$
$c$	Speed of light in vacuum
$\mathbf{r}_i^S$	Position of satellite $S$ in inertial frame: <i>orbit parameters, coefficients of the gravity field</i>
$\mathbf{e}_i^S$	Direction of radio source $S$ in inertial frame: <i>radio source coordinates</i>
$\mathbf{r}_{e,R}$	Position of station $R$ in the Earth-fixed frame: <i>station coordinates</i>
$\mathbf{R}$	Rotation matrix of Earth rotation: <i>Earth orientation parameters (<math>x, y, UT1, \Delta\epsilon, \Delta\psi</math>)</i>
$\delta t^S$	Clock error of satellite $S$ : <i>satellite clock parameters</i>
$\delta t_R$	Clock error of station $R$ : <i>station clock parameters</i>
$\delta\rho_{trp,R}^S$	Tropospheric delay: <i>troposphere parameters</i>
$\delta\rho_{ion,R}^S$	Ionospheric delay: <i>ionosphere parameters</i>

$\delta\rho_{rel,R}^S$	Relativistic corrections: <i>parameters of relativity theories</i>
$\epsilon$	Measurement error

Let us briefly mention some essential shortcomings present in these three equations:

- The satellite as well as the station positions ( $\mathbf{r}_i^S$  and  $\mathbf{r}_{e,R}$ , respectively) differ from observation technique to observation technique by the local ties or sensor eccentricities. The local ties (at the ground) and the eccentricities between the center of mass of the satellite and the individual sensors are therefore extremely important elements to connect the techniques.
- The tropospheric and ionospheric delays are not identical for all techniques. They depend on the frequency of the signals used.
- Different time arguments (e.g. for signal emission and reception; for the two rotation matrices  $\mathbf{R}$  included in (3); ...) have to be used for the various quantities.
- The “...” in (1), (2) and (3) indicate that additional, technique-specific correction terms and parameters (initial phase ambiguities and phase center variations in GPS, range biases and system delays in SLR, telescope deformation and radio source variability in VLBI, to name just a few) have to be taken into account.

From the observation equations (1), (2) and (3) we immediately see that only VLBI is capable of realizing the ICRF (radio source positions), that all techniques including the satellite position  $\mathbf{r}_i^S$  may in principle be used for gravity field determination, and that all the three equations contain station coordinates  $\mathbf{r}_{e,R}$  and Earth orientation parameters (rotation matrix  $\mathbf{R}$ ) and can thus contribute to the realization of the ITRF and to the EOP series. The terms  $\delta\rho_{trp,R}^S$  and  $\delta\rho_{ion,R}^S$  indicate that information about the atmosphere also may be derived from the various observation techniques, although with varying precision.

We conclude this section with Table 1, which gives a summary of the connections between the techniques in the parameter space. It has to be the goal to rigorously combine all the parameters common to more than one technique in order to obtain the most consistent and accurate geodetic products (ITRF, ICRF, EOPs, gravity field, atmosphere, ...).

## 2. Stations as Link Between Techniques

Stations may only serve as link between techniques if they are so-called fundamental sites i.e., sites where more than one observation technique is collocated. For collocated sites two different types of links may be established:

- Link between site coordinates ( $\mathbf{r}_{e,R}$ ) of the individual techniques through local ties.
- Link between parameters describing the atmospheric delays ( $\delta\rho_{trp,R}^S$ ,  $\delta\rho_{ion,R}^S$ ) of the individual techniques.

Let us have a closer look at these two types of links (Sections 2.1 and 2.2).

### 2.1. Site Coordinates and Velocities

The links established through fundamental stations with accurate local ties are the most important connections between the individual techniques and are, at present, the only links between the terrestrial reference frame realizations of the individual technique. Without these links, the

Table 1. Parameter space for the combination of space-geodetic techniques.

Parameter Type	VLBI	GPS/GLO.	DORIS	SLR	LLR	Altimetry
Quasar Coord. (ICRF)	X					
Nutation $\Delta\epsilon, \Delta\psi$	X	(X)			X	
Pole $x, y$	X	X	X	X	X	
UT1	X					
Length of Day		X	X	X	X	
Sub-daily ERPs	X	X				
ERP-Ampl. (Ocean tides)	X	X		X		X
Coord.+Veloc.(ITRF)	X	X	X	X	X	(X)
Geocenter		X	X	X		X
Gravity Field		X	X	X	(X)	X
Orbits		X	X	X	X	X
LEO-POD		X	X	X		X
Troposphere	X	X	X	(X)		X
Ionosphere	X	X	X			X
Clocks (time transfer)	X	X		(X)		

reference frames of the individual techniques would be arbitrarily translated and rotated with respect to each other. It has to be emphasized that today fundamental stations will only contribute significantly to the global link budget -- given by a weighted mean of all known local ties -- if the local ties between the reference points of the observing instruments are accurately known. In view of the precision achieved nowadays by each of the individual techniques, the local ties have to be known with an accuracy of 1-2 mm or better. Local ties are one of the major if not the major error source in the realization of a common terrestrial reference frame.

For quite some time multi-year solutions of the individual techniques have been combined by the ITRF Product Center including all local ties and the full variance-covariance matrices of the individual solutions to obtain a consistent terrestrial reference frame: ITRF station coordinates and velocities. Time series of coordinates from fundamental stations, however, have not been routinely compared between techniques and combined into consistent time series so far. Such comparisons are crucial for the separation of technique-specific effects and real signals (geodynamics, geophysics). The two GPS coordinate time series from the CODE analysis center of the IGS shown in Figures 1(a) and (b) may illustrate this point. It is not really clear whether the annual signal seen in the Onsala time series (Figure 1(a)) after mid 1997 is genuine or a systematic bias produced by the processing strategy or the modeling (e.g., the troposphere mapping function). Especially the circumstance that the annual period only starts to be visible around mid of 1997 should make us suspicious and hold us back from geophysical interpretation, unless a similar signal is also visible in the VLBI time series. (Even then it might still be an artifact coming from a modeling error common to both the VLBI and GPS processing strategy.)

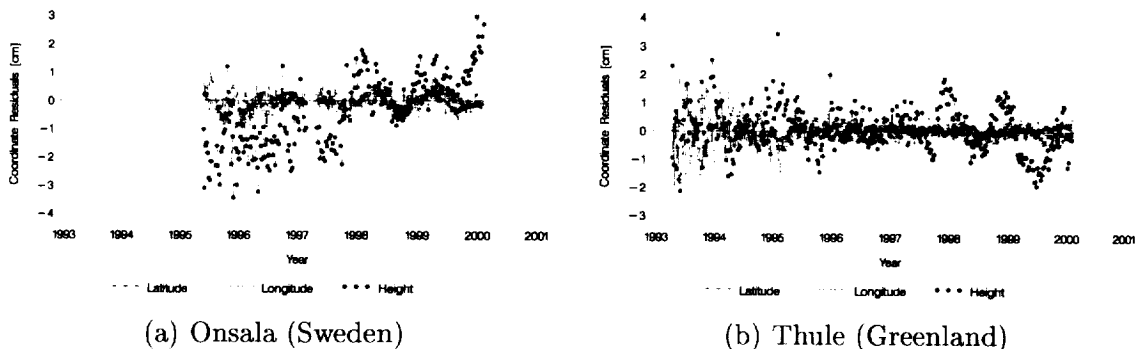


Figure 1. GPS site coordinate time series from the CODE analysis center.

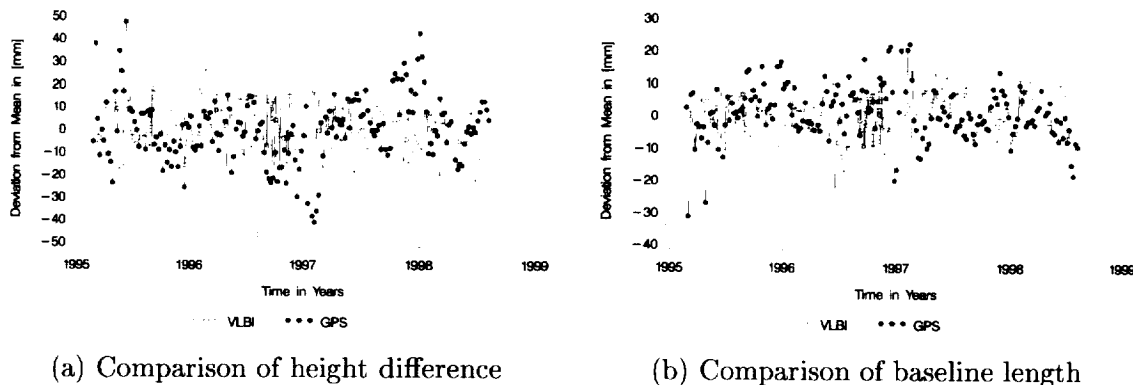


Figure 2. Baseline length and height difference between Fairbanks (Alaska) and Wettzell (Germany) from GPS and VLBI time series.

Similarly, we should be cautious to interpret the height change in Thule, which looks very much like a post-glacial rebound signal (Figure 1(b)), without having an additional independent check.

That a lot of work still has to be done in this area can be seen in Figure 2, where the height difference and the baseline length of a GPS (CODE: Center for Orbit Determination in Europe) and a VLBI (GSFC: Goddard Space Flight Center) time series are compared. Common signals cannot be detected so far and the series seem to be dominated by noise. Conclusive comparisons of this kind are made difficult by the fact that only very few fundamental stations exist with long and accurate coordinate time series of more than one technique. Activities initiated by the IERS Analysis Coordinator (see <http://alpha.fesg.tu-muenchen.de/iers/>, e.g., the SINEX Campaign to combine weekly/monthly SINEX files from all major techniques) will hopefully lead to deeper insights into the behavior of coordinate time series.

The local ties at fundamental sites also have an impact on the consistency of the EOP series from different techniques. An analysis campaign of the IERS is presently studying remaining systematic biases (offsets, rates) between EOP series from different techniques after careful alignment of the series to the ITRF2000 reference frame. The IERS is now starting to look into the rigorous combination of ITRF, EOPs and ICRF using the time series of these parameters (SINEX files) from all contributing space-geodetic techniques. A lot of problems will still have to be overcome

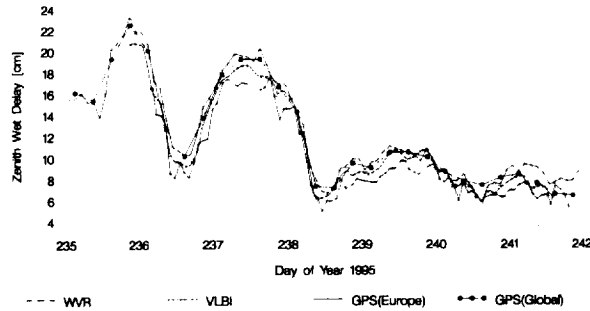


Figure 3. Comparison of troposphere zenith wet delays from VLBI, GPS (global and European solutions) and from the water vapor radiometer (WVR) at the Onsala site in Sweden during the CONT95 campaign.

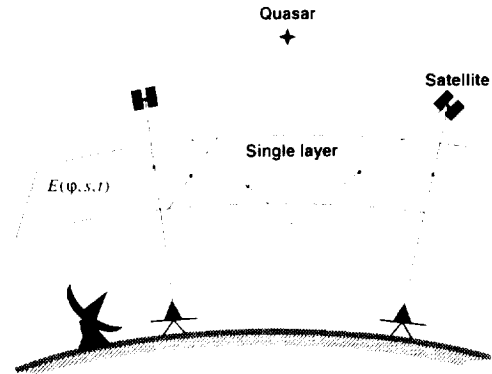


Figure 4. Validation of global GPS ionosphere models by VLBI.

on the way to such a consistent set of IERS products (e.g. the combination of UT1 from VLBI and LOD from satellite techniques).

## 2.2. Troposphere and Ionosphere

So far the fact that the tropospheric zenith delays have to be identical for GPS and VLBI observations made at a collocation site has not been used in any combination of solutions. It is clear from comparison studies, however, that especially the height component should benefit from such a combination. At some of the fundamental stations a lot of different information on the atmosphere is available and should be exploited:

- GPS and VLBI estimates of tropospheric zenith delays
- Water vapor radiometer (WVR) measurements
- 2-color SLR measurements
- Meteorological data (pressure, temperature, humidity)

Because of the complementarity of some of these measurements (optical pulses of SLR are much less affected by water vapor than the radiowaves of VLBI and GPS; meteorological data and WVR data can be used to compute the dry and wet zenith delay, respectively), we may expect to obtain better height estimates from a combination of all these data. A comparison of the wet zenith delays computed from VLBI, GPS (global and European) and water vapor radiometer (WVR) data is depicted in Figure 3 and shows the good and encouraging agreement between the estimates of the independent techniques.

The VLBI station network will probably never be dense enough to compute global ionosphere models similar to those obtained from the global IGS network. But VLBI observations could very well be used to validate the GPS-derived global ionosphere models (see Figure 4). Interesting results on how VLBI might be used to obtain information about the ionosphere have recently been presented by [2] (this volume).

### 3. Satellites as Link Between Techniques

Apart from the obvious links at fundamental stations we may also make use of the links that exist at a satellite if the satellite is tracked by more than one technique. A typical example is the TOPEX/Poseidon mission, where four different techniques, namely, SLR, DORIS, GPS, and altimetry, could be used for precise orbit determination (POD). The possibility to inter-compare all these different orbit types led to a considerable improvement in POD strategies and insight into the suitability of different tracking systems for POD.

Another example are the GPS (SVN35 and SVN36) and GLONASS satellites that carry SLR retro-reflectors. Using SLR data to these satellites the accuracy of the GPS and GLONASS microwave orbits could be confirmed with an independent technique and a systematic bias between the SLR observations and the orbit determined using the GPS/GLONASS microwave data could be detected. The origin of this bias of about 5 cm — SLR ranges are too short compared to the microwave orbits — is not yet clear and needs further investigation.

In the future an additional interesting link might be established at the satellite level: the observation of GPS or GLONASS L-band signals with VLBI. Differential VLBI observations between quasars and GPS/GLONASS satellites could tie the satellite orbits directly into the inertial reference frame of the quasars and give interesting information on UT1-UTC and on the non-conservative forces acting on GPS/GLONASS satellites (e.g. systematic orbit errors).

### 4. Earth Orientation Parameters

According to observation equations (1), (2), and (3) Earth orientation parameters may be estimated from the data of all the major space-geodetic techniques. Due to the one-to-one correspondence between orbital elements on one side and UT1-UTC and nutation offsets on the other side, satellite techniques may only determine polar motion (PM), the rate of change of UT1-UTC, i.e., the length of day (LOD), and nutation rates (see [3] for details). With these limitations, the EOP series of all techniques should agree on the level of precision of the individual techniques. There are still considerable systematic biases that are not yet properly understood, however, between the polar motion series of the individual techniques. Much work is still required in this field to come up with a combined consistent EOP product from all techniques.

In this paper we will focus on two examples to illustrate the benefits of a combination of the techniques: sub-daily Earth rotation parameters (Section 4.1) and nutation amplitudes derived from nutation offsets and rates (Section 4.2).

#### 4.1. Sub-daily Earth Rotation Parameters

Sub-daily Earth Rotation Parameters (ERPs) are available nowadays from both GPS and VLBI solutions. The GPS series analyzed here were computed by the CODE analysis center in Berne, the VLBI series by the group at GSFC. The GPS and VLBI series cover a period of 6.5 and 20 years and have a time resolution of 2 hours and 1 hour, respectively. These two series were used to estimate the amplitudes of all the major diurnal and semi-diurnal terms due to ocean tides (57 tides in PM, 41 in UT1; see also [4] for details). Apart from the estimation of amplitudes based on the individual series a combined estimation from the GPS and VLBI series was also performed. The amplitude differences (RMS difference) over all these diurnal and semi-diurnal terms between different solutions are given in Table 2. In addition, the GPS and VLBI results were compared to



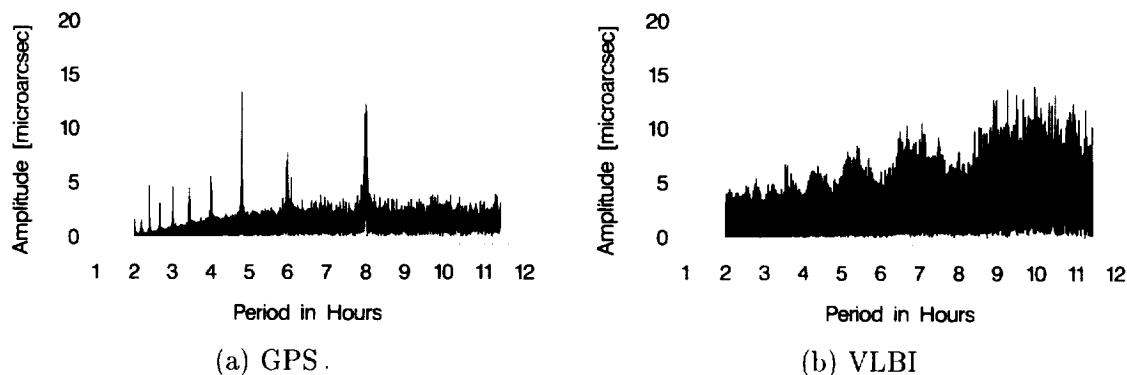


Figure 6. Comparison of the prograde polar motion spectrum below periods of 11 hours derived from sub-daily GPS and VLBI ERP estimates, respectively.

A similar situation may be seen when comparing the high-frequency prograde polar motion spectrum obtained from GPS and VLBI, as depicted in Figure 6. Whereas significant amplitudes are visible in the GPS spectrum at frequencies of 2, 3, 4, . . . cycles per day, no such signals can be detected in the corresponding VLBI spectrum. There is even a decrease in the VLBI amplitudes at these frequencies. A closer inspection of the GPS ERP time series suggests that a very small systematic bias in the daily polar motion rate of only a few tens of microarcseconds is sufficient to produce such a spectrum. Due to the fact that the GPS results can be compared to those of VLBI, we are able to conclude that most (if not all) of the signals seen at periods below 11 hours should be considered as artifacts resulting from the GPS processing strategies (e.g. small systematic biases in the orbit modeling over each daily solution).

#### 4.2. Nutation Offsets and Rates

Complementary information is available from VLBI and GPS for the estimation of nutation amplitudes. Whereas nutation offsets ( $\Delta\epsilon$  in obliquity and  $\Delta\psi$  in longitude) are routinely estimated once per day from the VLBI data, only nutation rates  $\Delta\dot{\epsilon}$ ,  $\Delta\dot{\psi}$  may be derived from GPS measurements (typically estimated over 1–3 days). The VLBI nutation estimates are free of orbit errors and allow the long-term monitoring of the Earth's rotation axis in space (nutation and precession). The GPS nutation rate estimates in contrast are very sensitive to orbit modeling errors but may provide dense information on the short-term variations (periods smaller than about 20–30 days).

In view of these strengths and weaknesses, a comparison and combination of the techniques will help to check the results obtained by an individual technique and to gain more confidence in the results in general. The sine and cosine amplitudes of the 13.66-day period of nutation derived from different techniques are shown in Figure 7 as an example. The nutation amplitudes at this period are essential to test different non-rigid Earth models and the elasticity of the Earth. The agreement between VLBI and GPS amplitudes establishes a solid basis for the geophysical interpretation of the results.

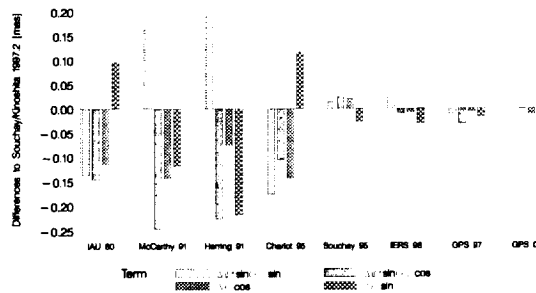


Figure 7. Comparison of the amplitudes of the 13.66-day nutation period derived from different techniques with the Souchay/Kinoshita model 1997.2.

## 5. Conclusions

We have seen that the integration and combination of the space-geodetic techniques is essential to improve the consistency of the results, to realize optimum reference frames (ITRF, ICRF, and EOPs) for future missions and challenges (e.g. global change), and to distinguish between technique-specific biases and geophysical signals.

All links between the techniques — be it on the station or satellite level — should be determined as accurately as possible (local ties, satellite antenna offsets, ...) to allow for an optimum integration of the techniques.

All parameter types common to more than one technique should be compared in detail and combined as rigorously as possible. This will eventually lead to a set of consistent combined products for all major geodetic parameter types, an important step towards an “Integrated Global Geodetic Observing Systems” (IGGOS). Such an IGGOS is crucial to get a more detailed view and understanding of the complexity of the “System Earth” and its geophysical processes.

## References

- [1] Degnan, J.J., Millimeter Accuracy Satellite Laser Ranging: A Review, In: Contributions of Space Geodesy to Geodynamics: Earth Dynamics, Geodyn. Ser., vol. 25, edited by D.E. Smith and D. L. Turcott, pp. 133–162, AGU, Washington, D.C., 1993.
- [2] Hobiger, T., J. Boehm, and H. Schuh, Determination of Ionospheric Parameters by Geodetic VLBI, this volume, 2002.
- [3] Rothacher, M., G. Beutler, T.A. Herring, and R. Weber, Estimation of nutation using the Global Positioning System, *J. Geophys. Res.*, 104, 4835–4859, 1999.
- [4] Rothacher, M., G. Beutler, R. Weber, and J. Hefty, High-Frequency Variation of Earth Rotation from Global Positioning System Data, *J. Geophys. Res.*, 106(B7), 13,711–13,738, 2001.
- [5] Seeber, G., *Satellite Geodesy*, Walter de Gruyter, Berlin, New York, ISBN 3-11-012753-9, 1993.
- [6] Sovers, O.J., J.L. Fanelow, and C.S. Jacobs, Astrometry and geodesy with radio interferometry: experiments, models, results, *Reviews of Modern Physics*, 70(4), 1393–1454, 1998.
- [7] Teunissen, P. J. G., and A. Kleusberg (Eds.), *GPS for Geodesy*, Lecture Notes in Earth Sciences, Springer Verlag, 2nd edition, 1998.



# Session 2. Improving the Performance and Products of IVS





## IVS Working Group 2 for Product Specification and Observing Programs

*Harald Schuh*

*Institute of Geodesy and Geophysics IGG, University of Technology, Vienna*

*e-mail: [hschuh@luna.tuwien.ac.at](mailto:hschuh@luna.tuwien.ac.at)*

### Abstract

An important part of the IVS efforts is to provide the best products for the user community and to optimize the use of available global resources. During the 5th IVS Directing Board meeting on February 15th, 2001 the IVS products and related programs were discussed with respect to the general goals described above. It was decided to set up an IVS Working Group (WG2) for Product Specification and Observing Programs. Members of WG2 were chosen among experts in the field of geodetic/astrometric VLBI. The Terms of Reference (ToR) of WG2 were to

- review the usefulness and appropriateness of the current definition of IVS products and suggest modifications,
- recommend guidelines for accuracy, timeliness, and redundancy of products,
- review the quality and appropriateness of existing observing programs with respect to the desired products,
- suggest a realistic set of observing programs which should result in achieving the desired products, taking into account existing agency programs,
- set goals for improvements in IVS products and suggest how these may possibly be achieved in the future,
- present a written report to the IVS Directing Board (DB).

The WG2 report was approved by the IVS DB on November 7th, 2001. The introduction of the report contains the scientific rationale. Then the present status and future goals of all international activities within IVS are described. In particular the current products of IVS are described in terms of accuracy, reliability and frequency of observing sessions. The temporal resolution of the parameters estimated by VLBI data analysis, the time delay from observing to product, i.e. time which has passed after the end of the last session included in the VLBI solution till availability of the final products, and the frequency of solution (in the case of "global solutions", when all existing or a high number of VLBI sessions are used to determine so-called global parameters) are also important aspects. All IVS products and their potential users are covered in the report. This includes the Earth orientation parameters (EOP), the reference frames (TRF and CRF), geodynamical and geophysical parameters and physical parameters such as tropospheric zenith delays. Measures which should be taken within IVS to meet the goals defined in the first steps are presented. As most of the measures are related to the observing programs, these are the main focus for improving the current status of IVS products. The report shows that due to various requirements of the different users of IVS products the following aspects must be accomplished:

- significant improvement of the accuracy of VLBI products,
- shorter time delay from observation to availability of results,
- almost continuous temporal coverage by VLBI sessions.

A first scenario of the IVS observing program for 2002 and 2003 considers an increase of observing time by about 30%-40% and includes sessions carried out by S2 and K4 technology. The midterm observing program for the next 4-5 years seems to be rather ambitious. However, it appears feasible if all efforts are concentrated and the necessary resources are made available. The full WG2 report was published in the IVS Annual Report 2001 (Schuh, 2002 [1]) and can be downloaded from the IVS homepage (<http://ivscc.gsfc.nasa.gov/WG/wg2/>).

## References

- [1] Schuh, H. and 12 co-authors: IVS Working Group 2 for Product Specification and Observing Programs - Final Report (Feb. 13, 2002). In: IVS Annual Report 2001 ed. by N.R. Vandenberg and K.D. Baver, NASA, 2002.

## IVS Observing Programs 2002–2005

*Nancy R. Vandenberg*

*NVI, Inc./NASA Goddard Space Flight Center*

*e-mail: nrv@gemini.gsfc.nasa.gov*

### Abstract

This paper reports on section 6 of the Working Group 2 report. The other sections of the WG2 report are covered in the paper by Harald Schuh (see previous paper).

At its inception IVS had no observing programs of its own and yet it is responsible for generating products. Through 2001 IVS used existing programs including NEOS, CORE, Europe, Intensive. For 2002 the IVS community is implementing its own observing program with the goals to:

- combine requirements of various users for TRF and EOP,
- include all recording technologies,
- include R&D sessions for technique improvement,
- include CRF sessions for monitoring,
- maintain continuity with previous programs,
- improve global coverage with more stations.

Targeted areas of improvement via the observing programs are: improved accuracy of results, reduced time delay from observing to availability of results, and frequency of sessions.

There are three types of resources available for observing programs: station time, correlator time, and recording media. It is expected that station time will become most precious resource in the next few years.

The highlights of the IVS observing program in future years include:

- 2002: two rapid-turnaround sessions per week (replacing NEOS and CORE), monthly 8-station TRF session, monthly session using S2, monthly R&D sessions, CONT02 campaign
- 2003: increase rapid sessions to eight stations, begin a bi-weekly weekend session, increase S2 sessions to bi-weekly
- 2004: begin weekly weekend observing
- 2005: full 7-day program

Please refer to the full WG2 report at Schuh, H. and 12 co-authors: IVS Working Group 2 for Product Specification and Observing Programs - Final Report (Feb. 13, 2002). In: IVS Annual Report 2001 ed. by N.R. Vandenberg and K.D. Bayer, NASA, 2002.

## Geodetic Results from Mark 4 VLBI

*Daniel MacMillan*<sup>1</sup>, *Leonid Petrov*<sup>1</sup>, *Chopo Ma*<sup>2</sup>

<sup>1</sup>) *NVI, Inc./NASA Goddard Space Flight Center*

<sup>2</sup>) *NASA Goddard Space Flight Center*

*Contact author: Daniel MacMillan, e-mail: [dsm@leo.gsfc.nasa.gov](mailto:dsm@leo.gsfc.nasa.gov)*

### Abstract

We present geodetic results of a series of 30 VLBI experiments recorded in Mark 4 mode at rates of 128 and 256 Mbps. The formal uncertainties of UT1, polar motion, and nutation offsets derived from these experiments are better than the corresponding uncertainties from NEOS-A experiments by a factor of 1.3-2. Baseline length repeatability for the series of 32 experiments over a period of one year is about 0.9 ppb. For comparison, NEOS-A length repeatability is about 1.4 ppb. We will discuss optimal use of Mark 4 in the design of future observing networks.

### 1. Introduction

In 1990, the first demonstration of 1 Gbps recording was accomplished with a modified Mark 3 system. About a decade later, in June 2001, the first series of standard Mark 4 experiment sessions were correlated. In this paper, we will discuss results from the first 30 of the Mark 4 sessions. The milestones in Mark 4 development since 1990 are summarized below.

- 1990 - First lab demonstration of 1 Gbps recording with modified Mark 3A system
- 1992 - Start of Mark 4 correlator development at MIT Haystack Observatory
- 1993 - Formation of joint U.S.-European International Advanced Correlator Consortium for Mark 4 correlator development
- 1993 - Demonstration of first prototype Mark 4 data acquisition system
- 1995 - Commercial availability of upgrade of Mark 3A system to Mark 4
- 1995 - First prototype of Mark 4 ASIC correlator chip produced
- 1997 - First fringes with Mark 4 correlator
- 1999 - Four Mark 4 correlators put on line: USNO, Haystack Observatory, MPI (Germany) and JIVE (Netherlands)
- 2001 - Mark 4 correlator used to obtain first fringes with new disc-based Mark 5 data system
- 2001 - Correlated first series of standard Mark 4 experiment sessions

The Mark 4 VLBI hardware provides much more precise measurements due to an increase in recorded bandwidth by up to a factor of 16 from the standard Mark 3 data rate of 56 Mbps. This will be possible through a combination of the improved Mark 4 data acquisition system and the higher playback efficiency of the Mark 4 correlator. The Mark 4 correlator will be capable of supporting continuous data acquisition and simultaneously processing all 120 baselines from 16

stations at 1 Gbps/station. Currently the correlators are set up to process a maximum of eight stations.

The full data rate capability of 1 Gbps is not yet possible due to limitations of currently installed tape recording hardware at some VLBI stations and the cost of the increased number of required VLBI tapes. The full data rate will be possible once the Mark 5 system is implemented at VLBI sites in late 2002 or early 2003. Mark 5 is a magnetic disc-based data system that uses commercial off-the-shelf components. This type of system is possible because of the steady decrease in the cost of magnetic disc drives relative to the standard VLBI recording tapes.

We have analyzed the first 30 Mark 4 experiments that were observed during the period July 2000 to November 2001. These experiments were recorded in Mark 4 mode at rates of 128 Mbps or 256 Mbps. They were run with 2 different networks, CORE-1 (most at 256 Mbps) and CORE-3 (at 128 Mbps) shown in Figure 1. Generally, the increased Mark 4 data rate has allowed more observations to be made than with Mark 3. For example, the CORE-1 network stations observe at an average rate of 16 observations per hour compared with 10-12 observations per hour for the operational NEOS network.

In the following we discuss the quality of these experiments including the baseline length precision and the formal Earth orientation parameter (EOP) uncertainties. We then discuss possibilities for future observing with Mark 4.

## 2. Baseline Length Repeatability

We have computed the baseline length repeatabilities for several series of experiments: the Mark 4 experiments, the NEOS-A experiments from 1997 to 2001, and the CORE experiments (A and B series) from 1997 to 2000. Repeatabilities are generally better for the Mark 4 experiments. As function of baseline length, the length repeatabilities for baselines with at least 10 observations are shown above and were fit as:

$$wrms(Mark4) = [(2.0mm)^2 + (0.90ppb)^2]^{1/2}$$

$$wrms(NEOS) = [(1.7mm)^2 + (1.45ppb)^2]^{1/2}$$

$$wrms(CORE) = [(1.8mm)^2 + (1.50ppb)^2]^{1/2}$$

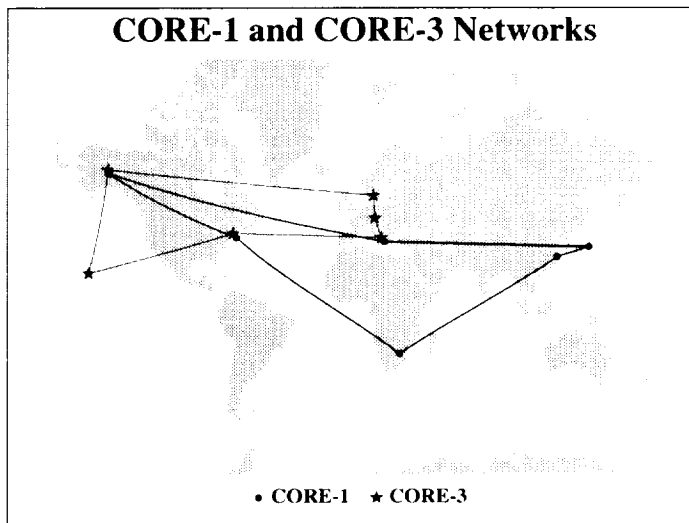


Figure 1. The CORE-1 network used Fairbanks, Hartbeestock, Matera, Tsukuba, Westford, and Seshan. CORE-3 used Kokee, Gilcreek, Matera, Westford, Wettzell, and Onsala.

One can derive approximate values for the site position precision by decomposing the baseline length error into average local station vertical and horizontal errors,

$$\sigma_L^2 = (2 - f_L)\sigma_H^2 + f_L\sigma_V^2,$$

where  $\sigma_L$  is the baseline length error,  $\sigma_V$  is the average site vertical error,  $\sigma_H$  is the average site horizontal error,  $f_L = L^2/2R^2$ , L is the baseline length, and R is the Earth's radius. The average station vertical error is  $\sim 8$  mm for the Mark 4 series and  $\sim 13$  mm for both the NEOS and CORE series.

### 3. Earth Orientation Parameter Uncertainties

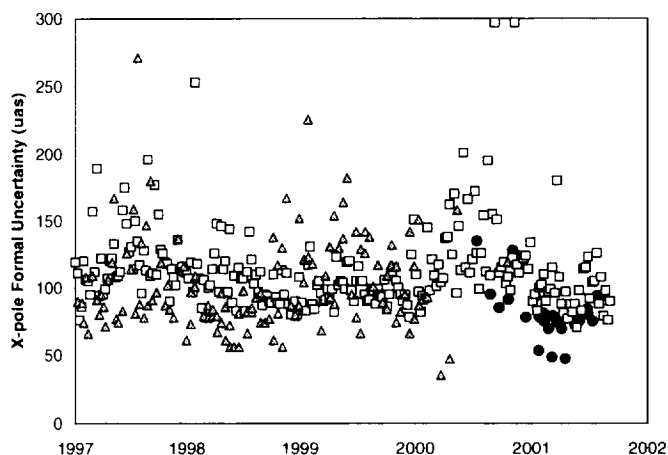


Figure 2. X-pole formal uncertainties for Mark 4 (black circles), NEOS (open squares), and CORE A+B (triangles).

The formal uncertainties of polar motion, UT1, and nutation offsets from the Mark 4 experiments are generally better than uncertainties from the NEOS-A or CORE-A and CORE-B series of VLBI experiments. Figure 2 compares the X-pole formal uncertainties for these series of experiments from 1997 to 2001. Plots for the other EOP components are similar. One can see that the Mark 4 points (clearly for the sessions in 2002) are mostly at the lower edge of the envelope of all the values plotted. The lowest three Mark 4 points are for the CORE-1 network, which

has better geometry from global coverage than the CORE-3 network.

The median formal uncertainties given in Table 1 give a measure of the average performance of any given session. Larger values of the uncertainties for a given network session are usually caused by loss of data, either from specific station problems or not being able to schedule a station.

Table 1. Median EOP Formal Uncertainties

Session Type	X ( $\mu\text{as}$ )	Y ( $\mu\text{as}$ )	UT1 ( $\mu\text{s}$ )	$\psi \sin\epsilon$ ( $\mu\text{as}$ )	$\epsilon$ ( $\mu\text{as}$ )
Mark 4	80	66	2.6	65	67
CORE A+B (1997-2000)	91	79	3.2	70	72
NEOS-A (1997-2001)	107	86	4.4	81	78

#### 4. Future Observing with Mark 4

We have been investigating different strategies of observing to take advantage of the increased data rate of Mark 4. An obvious way of improving the precision and accuracy of EOP measurements is to increase the number of stations in the observing network. The global coverage of the stations must of course also be optimized within the practical limitation of the actual locations of VLBI telescopes. Increasing the number of antennas provides better observing geometry and better local sky coverage of observations. To study this, we made simulations for observing schedules with different sized networks from 6 to 16 stations. For observed sessions, the simulation uncertainties are usually within 10-30% of observed formal uncertainties, depending on the performance of a session.

Figure 3 shows the X-pole formal uncertainties from simulations of experiment sessions varying the network size and experiment data rate. Generally, one can see that EOP uncertainties decrease with the number of antennas. The series of networks starts with the NEOS-A 6-station network (Algonquin, Kokee, Fortaleza, Fairbanks, Nyalesund, and Wettzell) and then stations are added to make larger networks. The improvement with more than 10 sites is limited. Points are shown for these networks observing at data rates of 128 Mbps, 256 Mbps, and 1 Gbps. Formal precision improvement beyond 256 Mbps diminishes rapidly because of antenna slewing time. For instance, at 1 Gbps, observing time is only 15-20%. Several additional points are shown. The precision for the 6-station NEOS network improved by about 30% in going from 56 Mbps to 256 Mbps. Network dependence can be seen from the difference between the 6-station NEOS and CORE-1 networks, where CORE-1 is a significantly larger network than NEOS-A.

In Figure 4, we have plotted on the left side the number of observations as a function of data rate for the 6-station NEOS network and for the 10-station network. The number of observations does not increase much beyond 256 Mbps. Despite this, the right-hand plot in Figure 4 shows that the median SNR of the observations nearly doubles in going from 128 Mbps to 1 Gbps.

It is not clear how to best use Mark 4. One possibility is to use the increased sensitivity of Mark 4 to observe weaker sources and exploit larger source catalogs (for example, the new VLBA Calibrator Survey of  $\sim 1400$  sources). This would improve sky coverage and increase the number of observations and would provide more information about the spatial and temporal variation of tropospheric delay. Alternatively, experiments could be scheduled to get much higher SNR observations, which would allow phase delay solutions to be done so that one could take advantage of the much more precise phase delays to possibly determine and correct instrumental errors. The

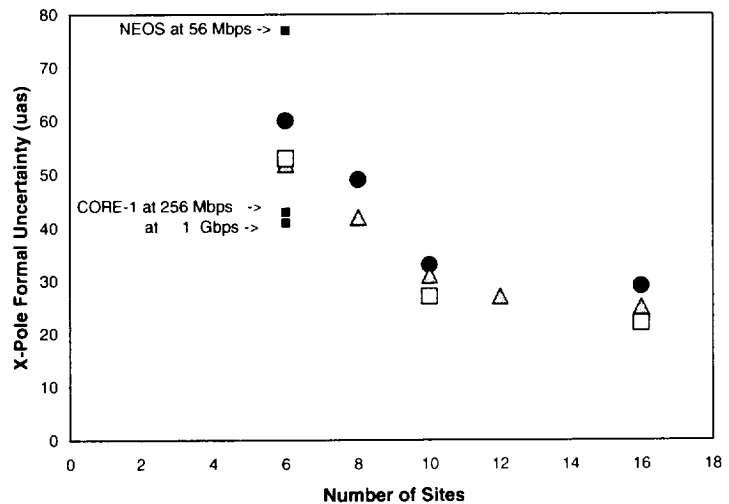
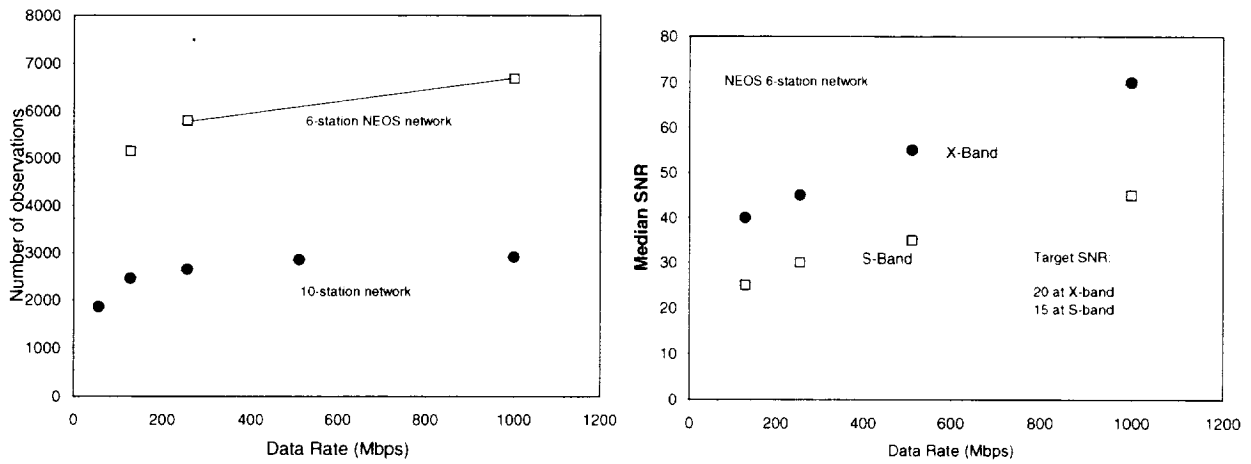


Figure 3. Simulated X-pole formal uncertainties for Mark 4 at data rates of 128 Mbps (black circles), 256 Mbps (triangles), and 1 Gbps (open squares).

R&D experiment series for 2002 will include this type of experiment to investigate this.



Observations in 24 hour session at different data rates.

Median session SNR at different data rates.

Figure 4. Dependence of number of observations and SNR on data rate.

## 5. Acknowledgements

We thank Nancy Vandenberg for running many Mark 4 simulation schedules and Alan Whitney for providing information regarding the Mark 4 development history.

## Expected Contributions of the K-4 and its Next-Generation Systems

Yasuhiro Koyama

*Kashima Space Research Center, Communications Research Laboratory*

*e-mail: koyama@crl.go.jp*

### Abstract

Unattended observations at observing stations and automated data processing were realized under the Key Stone Project by utilizing the capabilities of the K-4 VLBI observation and data processing system in 1995. The data recording to the magnetic media were replaced later with the high speed data transmission system in 1997, which enabled the almost continuous observations at the total data rate of 256 Mbps and real time data processing. Current developments of the Communications Research Laboratory are in the directions to enhance the sensitivities of the VLBI observations by using the higher data rate and the use of Internet Protocol to realize real time VLBI observations with many VLBI observing sites in the world. Expected contributions of these system developments for the IVS products will be discussed in this paper.

### 1. K-4 VLBI System

The main concept of the developments of the K-4 VLBI observation and data analysis system was to minimize required human operations and to maximize operational reliability and durability. The second generation set of the K-4 VLBI system was completed through the developments of the Key Stone Project (KSP) VLBI system which started in 1994. The KSP VLBI network can be considered as an integration of the researches and developments at CRL. For the KSP VLBI Network system, a lot of technological challenges were made and realized. Figure 1 shows pictures of the K-4 observation system at observing stations and K-4 correlator system at Kashima Space Research Center.



Figure 1. K-4 VLBI observation system at observing stations (left) and K-4 correlator system at Kashima Space Research Center (right).

The K-4 data recording system does not require frequent maintenance procedures and can record and reproduce observation data at the total data rates of 64 Mbps, 128 Mbps, and 256 Mbps with the bit error rate of less than  $1 \times 10^{-10}$  because of its robust error correction capability. The D-1 standard cassette tapes used to record the data are easy to handle and to transport. Using the tape changer unit with the K-4 data recorder unit, data recording can be continued up to 24 tapes which are equivalent to 20 continuous hours at the data rate of 256 Mbps. The correlation processing and the following data analysis procedures were also automated. Once all the observation tapes recorded during a VLBI session are set in the tape changer units of the correlator system, data correlation processing and data analysis are performed automatically without any human operations. With these systems, routine VLBI sessions were performed every day and the results of data analysis were placed on the WWW server within two days. Later in 1997, the data recording system was replaced with the high speed data transmission system using the high speed network and the real-time VLBI observations were realized ([1]). With the real-time VLBI system, almost continuous observations at the data rate of 256 Mbps became possible and the analysis results were actually produced immediately after each observing session ([2]), since all procedures from the observation at the observing stations through the data analysis processing are completely automated ([3]).

The usefulness and the power of the automated real-time VLBI system was demonstrated by the frequent measurements during the dynamic crustal deformation event associated with activities of the Miyake-jima volcano started in June 2000. Figure 2 shows the horizontal site coordinates of the Tateyama station measured by the KSP VLBI network. As clearly seen in the figure, the north-eastward motion of the site which started at the end of June 2000 was observed. The motion continued for a few months and the accumulated motion reached about 5 cm. Such irregular site motion was studied in detail by the VLBI technique for the first time and it was made possible by the real-time and automated features of the KSP VLBI Network.

In addition, the data obtained by the frequent real-time VLBI sessions were used to estimate Earth Orientation Parameters and flux densities of the observed radio sources with almost no time lag from observations ([4], [5]). Figure 3 shows the X and Y wobble parameters and UT1-UTC estimated from the KSP VLBI sessions. In the estimation of these parameters, no *a-priori* information was used and these estimates were obtained independently only from the KSP VLBI data. The uncertainties of the estimated parameters were large because the lengths of the baselines are very short (between 35 km and 135 km) to precisely estimate these parameters. However, the important point is that the capabilities to estimate daily values of these parameters within one day from each data point were technically demonstrated. If the same real-time VLBI technology becomes possible with longer baselines, there will be no technical difficulties to achieve precise estimations of these parameters.

## 2. Current System Developments and Future Plans in CRL

After the realization of the KSP VLBI systems, CRL has been concentrating its efforts in two major directions. One of the directions is to enhance the sensitivity of the VLBI system by increasing the data rate of the data acquisition system. The other direction is to realize real-time VLBI system over the Internet by using Internet Protocol (IP).

The developments of the giga-bit VLBI system began in 1996 and the first successful observations were performed on October 19, 1999 ([6]). The system consists of a sampler system, a data

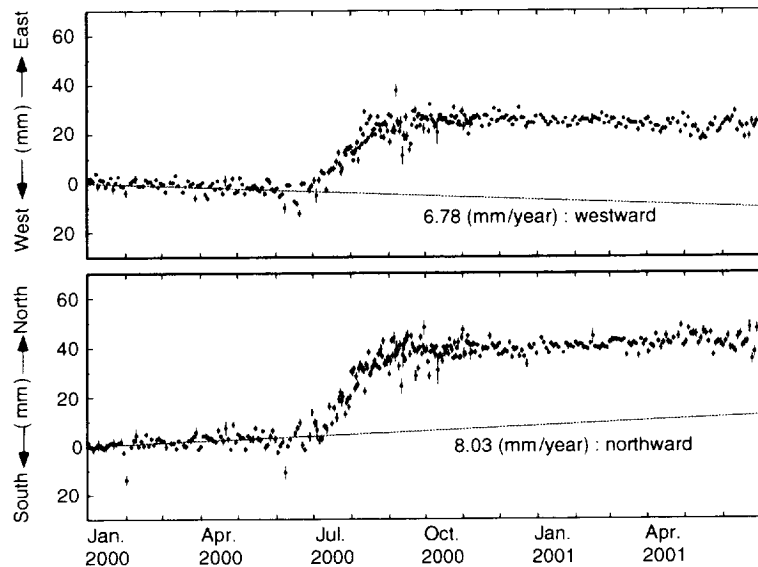


Figure 2. Horizontal site coordinates of Tateyama determined from KSP VLBI observations. Error bars are the estimated one-sigma formal error uncertainties of the coordinates. In each plot, a least square fit for the data before June 2000 is shown by a slanted line.

recording system, and a data correlation system. The sampler system was initially developed by modifying a commercially available digital oscilloscope unit so that the observed data are sampled at the data rate of 1024 Mps and only one bit data stream out of 4 sampling bits is extracted. The data recording system was developed by modifying commercially available high definition broadcasting recorder system so that it can record at the data rate of 1024 Mbps. The correlator system was initially developed as the real-time correlator for the Nobeyama Millimeter Array of National Astronomical Observatory. These systems constitute the initial version of the Giga-bit VLBI system and were used in a series of geodetic and astronomical VLBI sessions since the year 1999.

The developments of the second generation Giga-bit VLBI system began to adapt the hardware specifications of the VLBI Standard Interface (VSI) of which the first version was agreed in August 2000. All the systems were re-designed to meet the specifications. The new data correlator unit is capable to correlate two data streams at the data rate of 1024 Mbps. The unit can be used to correlate two data channels for single baseline or one data channel for two baselines simultaneously by synchronizing the data recorder units. All these new systems are interfaced with each other based on the VSI specifications. Therefore, these systems can be connected with other VLBI systems as long as the other systems are also based on the VSI specifications.

On the other hand, CRL started developments of the new real-time VLBI system using IP in late 1999 expecting to reduce the cost of the network and to expand connected sites for the real-time VLBI observations. In the KSP real-time VLBI system, data were transmitted through the high-speed ATM (Asynchronous Transfer Mode) network. However, the cost of the ATM network is still expensive and connection sites are extremely limited. At present, high speed IP connection is already available at many observing sites and the real-time VLBI system based on the IP is considered as the most promising to realize real-time VLBI observations with global baselines.

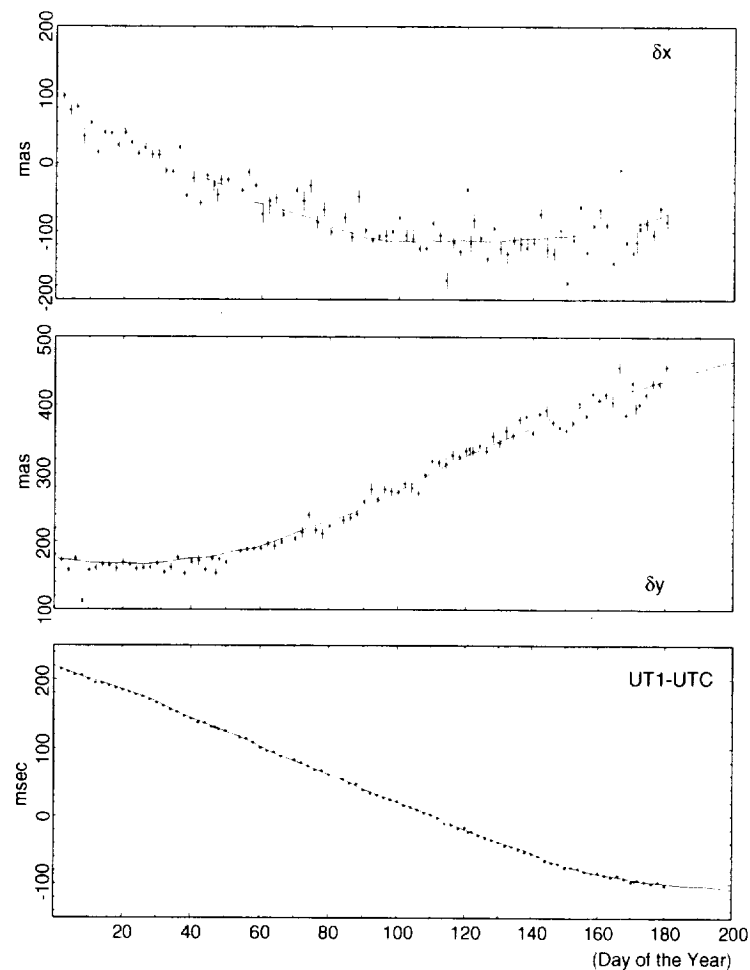


Figure 3. Two wobble parameters ( $\delta x$  and  $\delta y$ ) and  $UT1 - UTC$  estimated from the KSP VLBI sessions. Solid lines are the EOP97C04 data series of these parameters provided by the International Earth Rotation Service.

The PC-based Internet VLBI system consisting of a sampler board for the usual PC extension bus and software to make real-time data transmission and reception is currently under development. With the system, the data received by a PC are correlated by the correlation processing software which runs on the PC. One sampler board can have four video signal inputs and is designed to be able to sample analog signal with a frequency of up to 16 MHz for one bit sampling level. The sampler board has been evaluated by using actual signals from radio sources. Real-time characteristics have been evaluated by using the Local Area Network at Kashima Space Research Center. So far, it was confirmed that the board has a sufficient performance of coherent sampling up to 16 MHz. The preliminary results indicated that the real-time correlation on a PC system is possible up to 4 MHz data rate. Improvements in the software algorithm to make correlation processing faster are in progress.

### 3. Concluding Remarks

To realize continuous high quality VLBI observations to produce continuous series of Earth Orientation Parameters, it is essential to utilize all available resources for the IVS. The K-4 VLBI observation and correlation systems will contribute to IVS products not only by increasing the data correlation processing capacity but also by minimizing operational costs at observing stations. If the automated observations become possible, it will enable the observing station to increase the frequency of participation in the observing sessions. The automated feature of the K-4 correlator will also contribute to minimize the time delay to obtain IVS products after each observing session. Since the predetermined term of the KSP mission is completed, discussions about the possibility to utilize existing resources of the KSP systems to perform regular international VLBI sessions began in the Communications Research Laboratory and IVS community.

In the CRL, further technology developments are continuing to enhance the capabilities of the K-4 system. Especially, the development of the real-time VLBI system over the IP network and VSI (VLBI Standard Interface) based VLBI system will enable us to improve the IVS program in the sense of timeliness, robustness, and reduction of human resources. On the other hand, enhancement of the observation sensitivity using the Giga-bit VLBI system will enable us to use smaller antenna system which has in general faster slewing speed and smaller structure deformation. The Internet VLBI system will enable us to perform real-time VLBI observations with more sites other than the currently connected sites. In the future, our vision is to establish variety of the VLBI data acquisition systems based on the VSI specifications so that users can select the system according to the necessity of the observations.

### References

- [1] Kiuchi, H., Imae, M., Kondo, T., Sekido, M., Hama, S. Hoshino, T., Uose, H., and Yamamoto, T.: Real-time VLBI system using ATM network, *IEEE Trans. Geosci. Remote Sensing*, Vol.38, No.3, pp.1290-1297, 2000.
- [2] Kondo, T., Kurihara, N., Koyama, Y., Sekido, M., and Ichikawa, R.: Evaluation of repeatability of baseline lengths in the VLBI network around the Tokyo metropolitan area, *Geophys. Res. Lett.*, Vol.25, No.7, pp.1047-1050, 1998.
- [3] Koyama, Y., Kurihara, N., Kondo, T., Sekido, M., Takahashi, Y., Kiuchi, H., and Heki, K.: Automated geodetic Very Long Baseline Interferometry observation and data analysis system, *Earth, Planets, and Space*, Vol.50, pp.709-722, 1998.
- [4] Koyama, Y., Ichikawa, R., Otsubo, T., Amagai, J., Sebata, K., Kondo, T., and Kurihara, N.: Recent activities in Very Long Baseline Interferometry, *J. Comm. Res. Lab.*, Vol.46, No.2, pp.253-258, 1999.
- [5] Koyama, Y., Kondo, T., and Kurihara, N.: Microwave flux density variations of compact radio sources monitored by real-time Very Long Baseline Interferometry, *Radio Science*, Vol.36, No.2, pp.223-235, 2001.
- [6] Nakajima, J., Koyama, Y., Sekido, M., Kurihara, N., Kondo, T., Kimura, M., and Kawaguchi, N.: 1-Gbps VLBI, The first detection of fringes, *Experimental Astronomy*, Vol.11, pp.57-69, 2001.

## Geodetic S2 VLBI: International Plans

Calvin Klatt<sup>1</sup>, Mario Bérubé<sup>1</sup>, Wayne Cannon<sup>2</sup>, W.T. Petrachenko<sup>1</sup>, Anthony Searle<sup>1</sup>

<sup>1)</sup> *Geodetic Survey Division, Natural Resources Canada*

<sup>2)</sup> *York University, Department of Physics and Astronomy and Space Geodynamics*

*Laboratory/CRESTech*

*Contact author: Calvin Klatt, e-mail: cklatt@nrcan.gc.ca*

### Abstract

International use of the S2 geodetic system is beginning in 2002 after a successful series of experiments in Canada that began in 1999. The S2 Recording Terminal (RT), which utilizes commercial VCR tape transports, has been used internationally for several years. The S2 Data Acquisition System (DAS) is designed for geodetic usage and differs from the Mk3/Mk4 mainly through its use of rapid frequency-switching to achieve the necessary delay resolution. Correlation is performed at the 6-station Canadian Correlator, which has been used extensively for many years by the Space-VLBI community.

We review the geodetic experiments that have been performed in Canada using the Algonquin, Yellowknife and CTVA antennas. In 2002 a network of stations equipped with S2 systems will be included in the IVS observation program. The goals of this international series of experiments will be discussed as well as our future plans.

## 1. S2 Overview

### 1.1. Hardware Status

The Canadian S2 VLBI system includes the recording terminal, the frequency switched VLBI data acquisition system, and the S2 correlator.

The record terminal is a 128 Mbit/sec, Mostly-Off-The-Shelf (MOTS) system based on an array of eight video tape transports. The extensive use of MOTS hardware in the S2 design resulted in a low cost, high performance, VLBI data record/playback system of which more than 50 have been fabricated and are now in use in a variety of radio astronomy and VLBI applications in more than a dozen countries around the world.

The S2 DAS, when configured for geodetic applications, includes two baseband converters, each with a frequency agile local oscillator (LO). The baseband channelization modes of the S2 DAS BBCs are completely compatible with those of the VLBA/Mk-IV. The frequency agile LO was incorporated to enable high sensitivity group delay measurements without appealing to a more costly parallel IF/baseband sub-system.

The Canadian correlator is an (expandable) six station correlator using S2 playback terminals and is designed to handle S2 frequency switched bandwidth synthesis data.

All of these components are necessary for geodetic S2 VLBI to take place. Many stations have an S2 RT which is not paired with an S2 DAS and hence these stations are not equipped to operate in an S2 geodetic network. Furthermore, it should be noted that the S2 DAS frequency switched geodetic mode and the usual Mk-III/Mk-IV DAS geodetic mode are not compatible with each other.

Given the availability of a large number of recording terminals and a correlator, the main limitation to the expansion of geodetic S2 operations is the availability of the S2 DAS.

At this time seven DASs have been manufactured. Three are located at the Canadian stations (ARO, YELO, CTVA) and one is owned by BKG and will be used at TIGO. One will remain in Toronto for development/user-support and two can be deployed elsewhere. Three of these DASs are currently in final operational testing, two for GSD and one for BKG. We intend to update all of the DASs during 2002 with hardware modifications and improvements that have occurred as a result of recent usage.

## 1.2. Experiment Scheduling and Operations

The standard geodetic VLBI scheduling tools, SKED/DRUDG, now support the S2 RT but not the DAS.

The use of the S2 RT is quite simple and it is fully supported by the PCFS. 128 Mbits/sec are recorded onto 8 parallel VCR transports. Cassette motion is continuous (making recovery from failures very simple) and tape changes occur every six hours. For the S2 RT and DAS status monitoring and control is available via a console (or ethernet).

The DAS is similarly easy to operate. While formal PCFS support is still being discussed we have implemented the capability for mode setup and loading of frequency sequence from the PCFS at the Canadian stations. The DAS has a power on self test and system testing via phase cal extraction/monitoring is available.

We currently operate the DASs with two BBCs. The frequency sequence we have typically used involves 12 steps with a 1 sec dwell time, giving 24 “virtual frequencies”.

## 1.3. Correlation

The Canadian correlator is located at the Dominion Radio Astrophysical Observatory near Penticton, B.C. A large tape library is available for Space-VLBI which we have access to. The correlator has six playback terminals (PTs) and is easily expandable to ten. The correlator was designed for geodesy and space-VLBI projects (Japanese VSOP/MUSES-B) and has been in production mode (astronomy) for approximately five years.

Support for geodetic data switching schemes are complete and efforts continue to enhance the tools used for examining data quality.

## 1.4. Analysis

The official S2 correlator export output is in the UVFITS format, which is then “fringe’d” and output in the “CGLBI” format. A software program called “CGLBIDB” converts this to a Mk-III database for further analysis in CALC/SOLVE. Analysis in CALC/SOLVE is virtually identical to that for Mk-III/IV data.

Because of the wide single band channel (16 MHz), the wide ambiguity spacing (200ns) and the use of all 16 of the PCAL tones in each band, we do not see any group delay ambiguities. In our standard small network analysis, ALGO is held fixed and apriori EOPs and Nutation are used. Typical group delay residuals after analysis are 25-50ps, consistent with the SNR obtained and the delay resolution function.

Software for data quality analysis is available and further developments are underway.

## 1.5. Further Developments

The areas of most active development include:

- S2 DAS cleanup (updating early production systems, documentation, etc.)
- S2 DAS support in PCFS
- Frequency-switching sequence optimization (S-band interference / 1 BBC operations)
- Interpretation of geodetic results

## 2. Experiments Performed

The experiments conducted to date utilized the Algonquin Radio Observatory, the Yellowknife Geophysical Observatory, and the Canadian Transportable VLBI Antenna - CTVA (see Table 1).

Table 1. Canadian VLBI Stations

Station Name	Antenna Diameter (m)	X SEFD	S SEFD	Equipment
Algonquin	46	200	250	VLBA4, Mk-III, S2
Yellowknife	9	7600	6500	Mk-III, S2
CTVA	3.6	~ 70,000	~ 70,000	S2

Note that at 128 Mbits/sec, the ALGO-CTVA baseline is approximately as sensitive as two 16m antennas at 56 Mbits/sec. The YELO-CTVA baseline is very weak, producing very few scans. 44 experiments have been performed but many were system tests and some geodetic experiments failed to produce results of sufficient quality for geodetic interpretation.

### 2.1. Results: “PENTICTN”

From June 1999 to June 2001 the CTVA was located near Penticton, B.C., near the location used by the NASA transportable in the 1980s. See Figure 1 for baseline results of S2 experiments involving the CTVA at Penticton.

Table 2 compares the results from the Goddard Solution 2001c (third week of May, 2001), which includes Mk-III data only, and the GSD Global solution performed on May 7, 2001 which includes Mk-III data supplemented by the S2 data. The large difference in the results is due to the additional data used in the GSD analysis.

### 2.2. Mk-III and S2 Results: “YELO7296”

Figure 1 gives baseline length results of ten years of Mk-III and S2 experiments involving YELO7296. The S2 experiments begin in late 1999. There appears to be little to distinguish the Mk-III from the S2 data. A line giving the ITRF2000 position (determined by GPS and VLBI) is also shown.

### 2.3. Summary

Given the results obtained using the S2 system, we can conclude that the S2 system performance meets expectations. The system’s capability is, therefore, largely determined by the data rate,

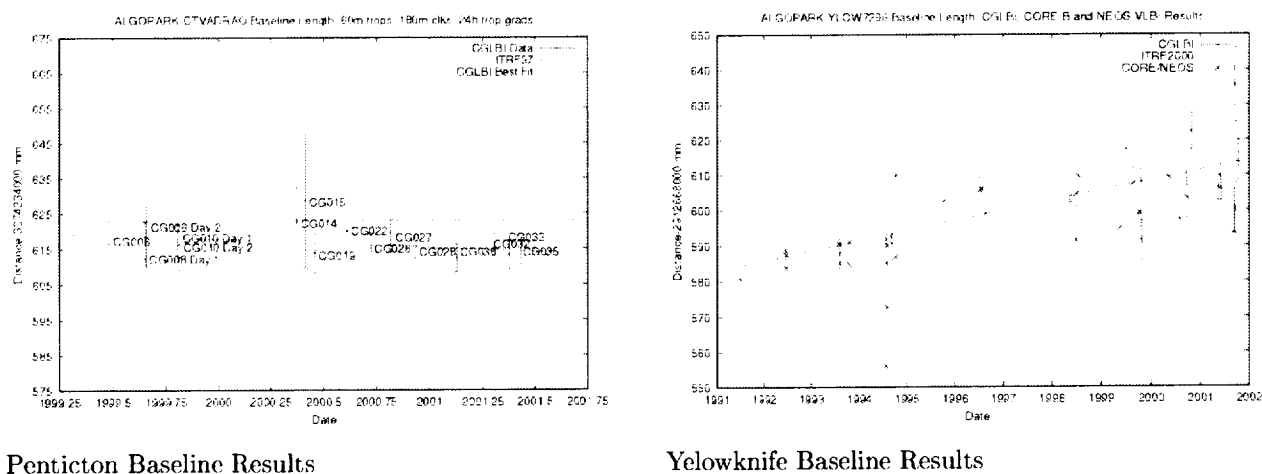


Figure 1. Results

Table 2. Global Solution Results: PENTICTN

Solution	X mm Sigma	Y mm Sigma	Z mm Sigma	Vx mm/yr Sigma	Vy mm/yr Sigma	Vz mm/yr Sigma
<b>GSFC</b>	-2058840546.1 28.0	-3621286535.2 44.8	4814420846.0 58.5	-22.8 3.4	-12.4 5.6	8.7 7.1
<b>GSD</b>	-2058840505.6 2.50	-3621286723.1 4.4	4814420723.1 5.4	-19.2 0.6	-3.1 1.0	-3.0 1.3

128 Mbits/sec. The Mk-III system operates at 56 Mbits/sec and the Mk-IV has recently begun operations at 256 Mbits/sec. Each factor of 2 increase in data rate allows scan lengths to be halved or gives an SNR increase of root 2. There is some debate how much increases in data rate (either number of scans or SNR) help us do geodesy. Refer to the paper by Dan Macmillan (NVI/GSFC), this volume, on simulations performed using higher data rates.

### 3. The Future of S2-based Geodesy

“Deployment of geodetic S2 and K4 systems at more stations is encouraged so that good geodetic networks can be designed that use these systems and be integrated into the international geodetic observing program.”

#### Recommendation of IVS WG2

##### 3.1. The E3 Network in 2002

The S2-based IVS E3 network will begin operations in March 2002. For 2002 the network will operate monthly, with weekly operations in future years being discussed. In addition to the three S2 equipped stations in Canada (See Table 1), the Canadian contributions to this effort include:

- Tape Supply
- Correlation
- Scheduling/Analysis Support
- Loans of S2 DASs to up to two partners and possible RT loans

Current partners in this effort include BKG which has purchased both an S2 RT and a DAS for use at TIGO which will be operated in Chile. NASA will be operating Kokee in this network this year with an RT borrowed from an Australian group and a DAS on loan from NRCan. There has been some discussion of adding NOTO to the network in the autumn. Additional stations could participate in this network using equipment on loan from NRCan.

Since the E3 network will initially be very small (three stations), and will include two stations whose position is poorly determined, we cannot reasonably expect high precision EOP results in 2002. In the medium term the goals of the E3 network are to provide EOP results with accuracies comparable to similar Mk-IV networks. This effort will be delayed by the need to obtain position information for the TIGO and CTVA stations. The fundamental limitations of the E3 network are the same as those for any Mk-IV network: network design, data rate, etc.

### 3.2. Future Opportunities

We hope to add additional stations to the E3 network starting in the summer of 2002. A number of stations are already equipped with S2 RTs and would require DASs on loan from NRCan. The number of available S2 RTs is expected to increase as the VSOP space-VLBI mission winds down. These RTs are expected to become the property of NRCan or CRESTech and could be loaned out.

In loaning S2 equipment NRCan hopes to strike an optimum balance between working with stations that strengthen the network (e.g. Kokee), working with partners that have or will purchase equipment (e.g. TIGO) and assisting interested partners that have difficulty purchasing equipment. We feel that additional purchases of S2 DAS equipment are necessary for the continuation of the IVS E3 network.

Stations that have S2 RTs (through purchase or loan) need only purchase the DAS component (about 130K USD) to contribute. Ideally, we would like stations to obtain a complete set of S2 RT, DAS and Playback Terminal (PT) (at a cost of 200K USD if free RTs are available). The PT would be used at the correlator to increase its capacity. Each S2 RT/DAS/PT added to the S2 World increases the network size.

With four such additions we could operate a ten-station S2 network, significantly enhancing the VLBI product through greater network strength.

# Session 3. Network Stations, Operation Centers, Correlators





## Fundamentals of Phase Calibration in Geodetic VLBI

*Brian Corey*

*MIT Haystack Observatory*

*e-mail:* `bcorey@haystack.mit.edu`

### **Abstract**

An integral part of the RF hardware at a geodetic VLBI station is the pulse, or phase, calibration system, in which a train of short pulses generated coherently with respect to the station frequency standard is injected into the signal path in the receiver. By measuring the phases of different frequency tones of the calibration signal at baseband, the instrumental phase and group delays from the injection point to the VLBI recorder can be estimated. After a brief introduction to how the pulse train is generated, this paper focuses on (1) applications of the calibration data to correcting VLBI data for instrumental effects, and (2) pitfalls in the application of calibration data, including the ubiquitous spurious signals. A few illustrative case histories will be presented.

## Construction of the Korean VLBI Network (KVN)

Y. C. Minh, D. -G. Roh

*KVN Headquarters, Korea Astronomy Observatory*

*Contact author: Y. C. Minh, e-mail: [minh@trao.re.kr](mailto:minh@trao.re.kr)*

### Abstract

Korea's new VLBI project has been started at 2001 as a 5 year project. We plan to build three new radio telescopes of 20-m diameters in three places in Korea, Yonsei University at Seoul, Ulsan University at Ulsan, and Tamna University at Jeju island. This KVN is the first VLBI facility in Korea and these telescopes will be used for VLBI observations exclusively. We plan to focus on the 100 and 150 GHz millimeter-wave VLBI observations, but the 2/8, 22, and 43 GHz HEMT receivers will be installed first for astronomical, geodetic, and earth science researches. The new hard-disk type recorder Mk 5 will be KVN's main recorder and the KVN correlator will also be developed.

The KVN research center is also planned to be built at Seoul, which will be a center for exchanges of manpower, research activities, and technical developments. It must be essential to collaborate with the leading institutes in VLBI activities in the world for the success of this project. After the completion of our project, we will be actively involved in the international VLBI activities.

### 1. Background

The first radio astronomical project of Korea Astronomy Observatory (KAO) was the construction of the radome enclosed 14-m millimeter wave radio telescope, which was completed about 15 years ago. This radio telescope is the main observing facility of Taeduk Radio Astronomy Observatory (TRAO) of KAO. After this 14-m radio telescope project, KAO has concentrated its power mainly to the construction of several optical telescopes, including a 1.8-m reflector of Bohyunsan Optical Astronomy Observatory of KAO, for last 10 years. By the completion of the optical telescope constructions, the KVN project was submitted to our government a few years ago and finally this project has been accepted. We will be carrying forward this project as a national facility in the basic science field.

At present the 14-m radio telescope has the dual channel SiS receivers, working at the frequencies of 100 and 150 GHz. An autocorrelator and filter banks are being used as spectrometers. This telescope has been used mostly for interstellar molecular line observations, such as the transitions from CO, CS, HCN, HCO<sup>+</sup>, etc. Our research activities using this radio telescope have been concentrated mainly to the studies of Galactic molecular clouds and their structures and chemistry.

To improve the mapping efficiency of our 14-m radio telescope, we plan to install a multi-beam receiver, QUARRY, made by Five College Radio Astronomy Observatory at Massachusetts, USA. This focal plane array receiver has 15 Schottky mixers working at 100 GHz band, and, as the backend, the 15 auto-correlators are planned to be ready this year. This focal plane array and our present dual-channel receiver will be the two main receivers for the common use of the 14-m telescope from the fall of 2003.

From the year 2001, we are carrying out VLBI experiments with the Nobeyama VLBI group at Japan and detected fringes successfully at 86 GHz of the SiO maser line toward several well known

maser sources, such as Orion KL, VY CMa, etc., in the last two observing sessions. We used Japan's VSOP terminal and the data from our 14-m telescope at Taeduk and 45-m telescope at Nobeyama have been successfully correlated at Mitaka, Japan. We are making the 43 GHz HEMT receiver for more frequent VLBI test experiments and for KVN receiver constructions. Our radio group's main power will be concentrated to the construction of the KVN system for next 5 years at least.

## 2. Outline of the Project

Our KVN project is to build three new radio telescopes of 20-m diameters and latest VLBI systems inside Korea. These antenna's main dish will be made of carbon-fiber coated with aluminium and we expect high efficiency observations even at 300 GHz. Our main target will be 100 and/or 150 GHz millimeter-wave VLBI observations, but we plan to install HEMT receivers of the 2/8 GHz for geodesic observations, and the 22 and 43 GHz for interstellar maser line observations first. And as a recorder we plan to use the new hard-disk type Mk 5 and participated in the consortium to develop the final version of Mk 5 being developed at Haystack. But we are still discussing with many VLBI researchers in the world to decide the details of our system configurations to have the best and latest systems available. We also plan to develop the KVN correlator.

In constructing the KVN we are not configuring a special system to unveil *unknown* or

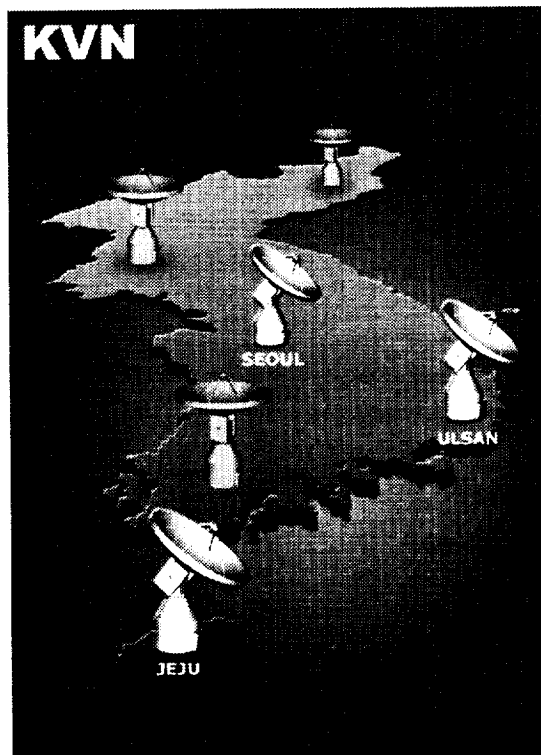


Figure 1. The three sites in south Korea to build KVN antennas: Seoul, Ulsan, and Jeju locations are indicated. The other three antennas (shaded) are the plan for future.

*totally unexplored* cosmic phenomena, or to overcome the present limits in technologies. This KVN is the first VLBI facility in Korea and will be used for all VLBI activities in Korea in the fields of Astronomy, Geodesy, Earth Science, etc. So, generally speaking, KVN will be a *conventional* VLBI system, but we will make the KVN as one of the most efficient and productive VLBI networks in the world.

Last year we chose the three places in Korea as our KVN observatory sites. Many candidate places have been reviewed and judged depending on the scientific merits, accessibility, convenience facilities, etc. and finally three universities have been chosen: Yonsei University at Seoul, Ulsan University at Ulsan, and Tamna University at Jeju island. The rough position of the sites are shown in Fig. 1. The actual construction of the site will be started at the end of 2002. When this KVN project goes alright for next couple of years as the 3-site project, we plan to submit the second expansion project to put 2-3 antennas more in north and south Korea in the places shown in Fig. 1, and will make the KVN as a 6-antenna network.

In Table 1 and 2 we summarize the positions and baseline lengths of our three selected sites. These three sites are located in the big cities and their altitudes are not high and the baseline lengths between them are less than 500 km. Since the sites are located in big cities, the radio interference by commercial telecommunications appears to be serious in 2 GHz band. We think that the proper selection of the frequency band and using protecting filters may be necessary at 2 GHz band. In Fig. 2 we show a sample UV coverage and the synthesized beam shape for these three sites combined with the 14-m telescope at Taeduk.

### 3. Domestic and International Collaborations

Since this KVN is the first VLBI system in Korea, we plan to make a consortium consisting of several VLBI-related institutes in Korea, and to construct KVN as a national facility for the basic science research. The construction and operation of KVN are being discussed by the nationwide KVN steering committee. After the completion of this project we will participate actively in various international VLBI research programs. We hope that VLBI research activities and international

Table 1. Location of the KVN Observatories

	Site	Longitude	Latitude	Altitude
1	Yonsei U. (Seoul)	126° 56' 35" E	37 33 44 N	260 m
2	Ulsan U. (Ulsan)	129 15 04 E	35 32 33 N	120 m
3	Tamna U. (Jeju)	126 27 43 E	33 17 18 N	320 m
4	TRAO (Taeduk)	127 22 19 E	36 23 53 N	110 m

Table 2. Baseline Lengths between KVN Sites

	Site	Seoul	Ulsan	Jeju	TRAO
1	Yonsei U. (Seoul)	-	305.2 km	477.7 km	135.1 km
2	Ulsan U. (Ulsan)	305.2 km	-	358.5 km	194.2 km
3	Tamna U. (Jeju)	477.7 km	358.5 km	-	356.0 km
4	TRAO (Taeduk)	135.1 km	194.2 km	356.0 km	-

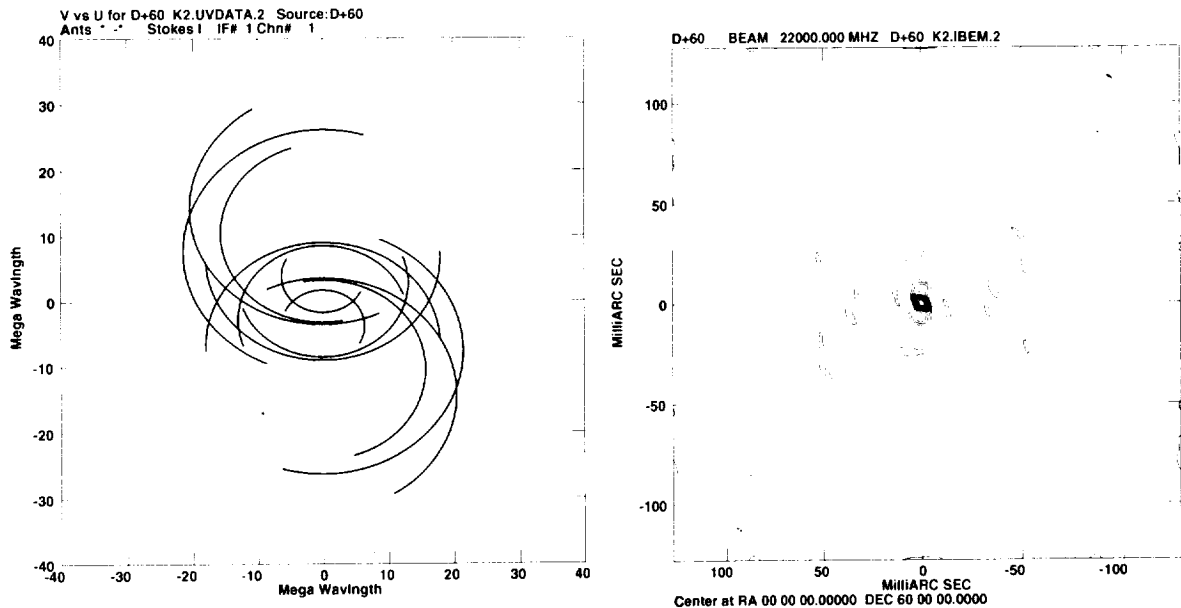


Figure 2. The UV coverage(*left*) and the synthesized beam shape (*right*) for the Seoul-Ulsan-Jeju-Taeduk baselines for the source of  $\delta = 60^\circ$ .

collaborations by Korean researchers can be greatly promoted through KVN. Various support programs to stimulate the VLBI activities in Korea will be prepared with the construction of KVN.

We think that we will face many difficulties in constructing the KVN because of our lack of VLBI experience and manpower. Therefore, for the success of this project, it must be essential for us to collaborate with and get many suggestions and consultations from the leading institutes in VLBI in the world. We are having discussion on Mk 5 and the development of the correlator with Haystack, and on antenna systems with German institutes. Especially the Japan-Korea collaboration in VLBI has been started in very good shape. At present the possible collaborations between VERA of Japan and our KVN have also been discussed very positively in both sides. The compatibility between two systems could be very exciting in future VLBI measurements. It is very fortunate that the international VLBI society is very open and cooperative. We are already having many productive discussion with many VLBI research institutes in the world, which will lead to the success of our KVN.

## VRAD Mission: Precise Observation of Orbits of Sub-Satellites in SELENE with International VLBI Network

Hideo Hanada<sup>1</sup>, Takahiro Iwata<sup>2</sup>, Yusuke Kono<sup>3</sup>, Koji Matsumoto<sup>1</sup>, Seiitsu Tsuruta<sup>1</sup>,  
Toshiaki Ishikawa<sup>1</sup>, Kazuyoshi Asari<sup>1</sup>, Jinsong Ping<sup>1</sup>, Kosuke Heki<sup>1</sup>,  
Nobuyuki Kawano<sup>1</sup>

<sup>1</sup>) *National Astronomical Observatory*

<sup>2</sup>) *National Space Development Agency of Japan*

<sup>3</sup>) *Graduate University for Advanced Studies*

Contact author: Hideo Hanada, e-mail: hanada@miz.nao.ac.jp

### Abstract

VRAD (VLBI radio source on the Moon) mission is one of selenodetic missions in SELENE project and we measure angular distance between radio transmitters on board two sub-satellites around the Moon and quasars by differential VLBI. VRAD can contribute to establish a lunar gravity field model and a lunar ephemeris of higher accuracy and higher reliability by measuring components of the orbits perpendicular to line-of-sight direction. The radio transmitters emit three carrier waves in S-band and one wave in X-band and special recording systems as well as conventional ones such as K-4 receive the waves through VLBI antennas and determine phase differences between them within 10 degrees. Combination of Japanese VERA and International VLBI network will observe the radio sources for one year including intensive observation periods of one month. The intensive observation will need more than 200 hour machine time. It is under way to establish an International VLBI network for VRAD mission.

### 1. Introduction

VLBI (Very Long Baseline Interferometer) has a potential to find new phenomena not only on the Earth but also on the Moon and the planets. Some attempts have already been made in order to apply VLBI to selenodesy, for example positioning of landers and spacecrafts on and around the Moon based on positions of quasars [1] [2]. It is, however, not necessarily to be said that ability of VLBI has fully been shown on the observations made until now, partly because they did not obtain a phase delay of carrier waves or they did not solve cycle ambiguities even if they used the phase delay. A multi-frequency VLBI has been proposed for the purpose of precise positioning using the phase delay and the optimum frequency spacing has been obtained [3] [4]. This method uses carrier waves of lower power consumption instead of noise and is appropriate for positioning of a spacecraft. It has been shown by VLBI experiments using carrier waves from Lunar Prospector that measurement error of phase delay of the carrier waves was possible to be less than 10 degrees which was equivalent to positioning error of about 20 cm on the Moon [5].

In SELENE project, which is Japanese lunar exploration using H-2A rocket with the launch in 2005, we plan to apply the multi-frequency VLBI to measurements of angular distances between two radio sources by using an international VLBI network in order to improve the lunar gravity field Model (VRAD mission) [6]. We receive four carrier waves in S and X-bands emitted from the two radio sources in order to resolve the cycle ambiguity. VRAD mission will improve the accuracy of the spherical harmonics of the lunar gravitational field and the lunar ephemeris by one

or two orders higher than before in cooperation with 4-way Doppler measurements and two-way Doppler and ranging measurements by using the main orbiter and Rstar (RSAT mission) [7]. This will advance a study of origin and evolution of the Moon since stronger constraint on the bulk composition of the Moon will be imposed.

In this paper we introduce outline of VRAD mission, and show condition of VLBI stations which can participate in the mission and a data policy imposed on co-investigators of VLBI observations of VRAD.

## 2. VRAD Mission

In VRAD mission, two radio sources VRAD-1 and VRAD-2 on board Rstar and Vstar continuously emit four carrier waves with different frequencies in S and X bands for differential VLBI as shown in Table 1. No special X-band carrier wave is produced in Rstar for VLBI observations but down link signal for Doppler measurements is shared, and only noise with 120 kHz bandwidth will be transmitted when Doppler measurements are not carried out. Rstar and Vstar is on the orbits as shown in Table 2 and angular distance between them is in the range from 0 to at most 1 degree. It is possible to discriminate between a signal from Rstar and that from Vstar by frequencies since they vary independently according to respective orbital motions even if they are received by an antenna in the same attitude.

Table 1. Specification of Transmitted Waves from Sub-Satellites

Wave Name in SELENE	S7	S8	S9	X2
Frequency Band	S	S	S	X
Center Frequency	2212 MHz	2218 MHz	2287 MHz	8456 MHz
Band Width	CW	CW	CW	120 kHz (Rstar) CW (Vstar)
EIRP	> 24 mW	> 24 mW	> 24 mW	> 250 mW(Rstar) > 38 mW(Vstar)

Table 2. Orbits of Two Sub-Satellites, Rstar and Vstar

	Perilune	Apolune	Inclination	Period
Rstar	100 km	2,400 km	90 deg.	240 min.
Vstar	100 km	800 km	90 deg.	153 min.

Fringe phases of the X2 wave at frequency  $f_{x2}$  are the final products for determination of angular distances between Rstar and Vstar. Group delays measured at S-band are used for resolution of cycle ambiguity of X2. It is necessary to obtain a group delay with an error smaller than the period of X2 in order to resolve the cycle ambiguity. This relation is expressed as

$$\sigma_p / 2\pi f_{s7} = \sigma_{g1} < 1 / f_{x2}, \quad (1)$$

where  $\sigma_p$  is measurement error (standard deviation) of fringe phase at S7 and  $\sigma_g$  error of the group delay. Next we need to resolve cycle ambiguity of S7 by using the group delay obtained from S7

and another wave  $S9$ . This condition is shown in the relation

$$f_{s9} - f_{s7} > \sigma_p f_{s7} / 2\pi. \quad (2)$$

Then we use the third wave  $S8$  in order to resolve cycle ambiguity of  $S9$  and the relation

$$f_{s8} - f_{s7} > \sigma_p (f_{s9} - f_{s7}) / 2\pi \quad (3)$$

is necessary. Although cycle ambiguity of  $S8$  is not resolved yet, it can be resolved if a group delay with an error smaller than 170 ns is obtained. The group delay will be easily obtained by conventional VLBI between quasars and Rstar/Vstar or delay rate measurements of Rstar/Vstar since the error of 170 ns corresponds to 9.5km on the lunar surface. The frequencies of  $S7$ ,  $S8$ ,  $S9$  and  $X2$  shown in Table 1 satisfy the relations (1), (2) and (3).

A VLBI network with 2,000 km baselines and measurements of phases with an accuracy of 0.17 radians (10 degrees) in X-band bring about the accuracy of the angular distance or the distance between Rstar and Vstar of  $5.3 \times 10^{-10}$  ( $1.1 \times 10^{-4}$  arcsec) or 20 cm, since there is the relation

$$\Delta d = c\sigma_\phi l / (2\pi f D), \quad (4)$$

where  $\Delta d$  is the positioning error of Rstar and Vstar,  $c$  the light velocity,  $\sigma_\phi$  the error in the phase delay measurements,  $l$  the distance between the Earth and the Moon,  $f$  frequency of  $X2$  and  $D$  baseline length.

### 3. Ground System for VRAD Mission

Carrier waves in S and X bands received by a VLBI antenna are converted to video signals by a video converter in the K-4/Mark-III system and they are recorded either by the K-4/Mark-III system like conventional VLBI experiments or by a narrow band recorder especially developed for VRAD experiments [5]. The narrow band recorder (S-RTP Station, System Design Service Corp.), consisting of four channels for the video signals and one for a reference clock signal, samples and digitizes the video signals at 200 kHz intervals with 6 bit resolution. The digital data are stored in a 8 mm tape with the maximum capacity of 20 Gbytes which corresponds to the data for 7.4 hours. The bandwidth of each channel is restricted to 60 kHz by a low pass filter so that effects of aliasing are not included in the digitized data. We need to adjust frequencies of the video signals by 10 kHz steps by using the video converter in order to put them into the narrow band channel since they change according to Doppler shift which amounts to 40 kHz in S-band and 120 kHz in X-band. Cross-correlation procedures for determination of phase differences between corresponding video signals recorded at two VLBI stations are carried out with a computer, and a special correlator is not necessary.

Seven narrow band recorders will be prepared for VRAD mission and three of them will be distributed to domestic stations belonging to VERA [8] and the others for foreign stations which will participate in VRAD mission. Needless to say, stations which are not equipped with the narrow band recorder can observe the carrier waves from Rstar and Vstar and quasars by the conventional VLBI system. VLBI stations for VRAD mission need to have a performance equivalent to that shown in Table 3 since the power of carrier waves emitted from Rstar/Vstar are not very strong.

The domestic network VERA will take part in VRAD mission for the whole mission period of one year and we make a plan to twice conduct intensive observations each of which consists

of one month period under participation of foreign stations. A tentative plan of two kind of observations are shown in Table 4. Anyone who is interested in VRAD mission and is permitted by the principle investigator (PI) of VRAD mission can be a co-investigator. A co-investigator can participate in observations of VRAD mission by using his/her antenna, receiver and VLBI system. Information which is necessary for observations such as observation schedules, orbits and status of the satellites will be provided to the co-investigator by the PI. The Data recorded by the K-4/Mark-III system, however, will not be processed for correlation at an analysis center of VRAD mission due to restriction of facilities but the data recorded by S-RTP Station will be processed there. The co-investigator of VRAD mission can access to the scientific data related to VRAD under any agreed data policy and can read or write papers making use of the data with a permission of the PI of VRAD mission before their official release to the public

We are developing an international network for VRAD mission from the points view of baseline length in north-south and east-west directions, and BKG Wettzell, Shanghai Astronomical Observatory, Urumqi Astronomical Observatory and Hobart Observatory are expected to constitute the international network. It is necessary to make adjustments of machine time and data policy between the international stations including VERA either by direct negotiations or by negotiations with mediation of IVS Coordinating Center.

Table 3. Condition of Typical Ground Stations

	Gain	Antenna Diameter	Aperture Efficiency	System Temperature
S-band	> 45 dB	> 20 m	> 0.14	< 150 K
X-band	> 60 dB	> 20 m	> 0.35	< 150 K

Table 4. Tentative Plan of the VLBI Observations

	Regular	Intensive
Network	Domestic (VERA)	International
Period	1 year	1 month $\times$ 2
Frequency	3 days a week	>3 days a week
Observation Time a Day	8 hours	8 hours
Cumulative Observation Time	About 1300 hours	About 200 hours

## References

- [1] Slade, M. A., R. A. Preston, A. W. Harris, L. J. Skjerve, D. J. Spitzmesser, ALSEP-Quasar Differential VLBI, *Moon*, 133–147, 1977.
- [2] Sagdeyev, R. Z., V. V. Kerzhanovitch, L. R. Kogan, V. I. Kostenko, V. M. Linkin, L. I. Matveyenko, R. R. Nazirov, S. V. Pogrebenko, I. A. Struckov, R. A. Preston, J. Purcel, C. E. Hildebrand, V. A. Grishmanovskiy, A. N. Kozlov, E. P. Molotov, J. E. Blamont, L. Boloh, G. Laurans, P. Kaufmann, J. Galt, F. Biraud, A. Boisshot, A. Ortega-Molina, C. Rosolen, G. Petit, P. G. Mezger, R. Schwartz, B. O. Rönnäng, R. E. Spencer, G. Nicolson, A. E. E. Rogers, M. H. Cohen, R. M. Martirosyan, I. G. Moiseyev, J. S. Jatskiv, Differential VLBI Measurements of the Venus Atmosphere Dynamics by Balloons: VEGA Project, *Astron. Astrophys.*, 254, 387–392, 1992.

- [3] Kawano, N., S. Kuji, S. Tsuruta, K. Sato, K. Iwadate, H. Hanada, M. Ooe, N. Kawaguchi, H. Mizutani, A. Fujimura, Development of a Radio Transmitter on the Moon, *J. Jap. Soc. Planet. Sci.*, 3, 159-169, 1994. (in Japanese)
- [4] Hanada, H., T. Iwata, N. Kawano, K. Heki, S. Tsuruta, T. Ishikawa, H. Araki, K. Matsumoto, Y. Kono, Y. Kaneko, M. Ogawa, Y. Iijima, Y. Koyama, M. Hosokawa, T. Miyazaki, N. Namiki, A. Sengoku, Y. Fukuzaki, T. Ikeda, F. Fuke, RISE group, Observation System of radio sources on the Moon by VLBI in SELENE project, *Proc. Int. Workshop on Geodetic Measurements by the collocation of Space Techniques on Earth (GEMSTONE)*, 126-130, 1999.
- [5] Kono, Y., H. Hanada, N. Kawano, K. Iwadate, Y. Koyama, Y. Fukuzaki, Precise positioning of spacecrafts by multi-frequency VLBI, *Proc. IVS2002*, this issue.
- [6] Iwata, T., T. Sasaki, Y. Kono, H. Hanada, N. Kawano, N. Namiki, Results of the critical design for the selenodetic mission using differential VLBI methods by SELENE, *Proc. IVS2002*, this issue.
- [7] Matsumoto, K., K. Heki and H. Hanada, Global lunar gravity field recovery from SELENE, *Proc. IVS2002*, this issue.
- [8] Sasao, T and VERA Project Team, Scientific objective and present status of VERA Project *Proc. IVS2002*, this issue.

# A Next Generation Geodetic Experiment Scheduling Tool? (SKED++)

*Calvin Klatt, Mario Bérubé, Anthony Searle, Jason Silliker*

*Geodetic Survey Division, Natural Resources Canada*

*Contact author: Calvin Klatt, e-mail: [cklatt@nrcan.gc.ca](mailto:cklatt@nrcan.gc.ca)*

## Abstract

A number of the software tools used in geodetic VLBI were designed twenty years ago and written in FORTRAN. Despite their good performance, the software requires maintenance and new features are desirable. This presentation is a proposal to the geodetic VLBI community to think about re-writing one of the essential utilities, namely SKED. A new version of SKED could take advantage of new programming techniques, such as object-oriented (OO) programming to ease the maintenance of the software. Such a new OO software design would enable the optimization routines to be improved by a variety of users, with the best features of SKED remaining. This presentation is intended to get feedback on this proposal and generate further discussion about the status of crucial VLBI operational software.

## 1. Essential Software

SKED plays an important role in all VLBI experiments and in the vast majority of experiments the schedules are very well optimized.

### 1.1. Why Change?

1) SKED is aging. The core was written many years ago and has been repeatedly modified as VLBI technology has evolved. As new hardware appears, more *if* statements are added - in many places - making changes and debugging difficult. The distribution of SKED/DRUDG now contains hundreds of FORTRAN files plus C and Java. The user-interface is a mix of text menus plus a Java GUI.

2) A dynamic future involves changes. The formation of the IVS was intended to further involve the entire VLBI community in how VLBI is performed. Open-source flexible software tools could be part of this effort. Small antennas (CTVA, Mizusgsi) are currently difficult to schedule with other antennas that are significantly more sensitive. Some new systems' features are not fully utilized (e.g. continuous tape motion). In the near future much greater data recording rates, shorter scans and real-time VLBI will come into practice. Finally, we should use real-time/adaptive scheduling to make the most of the huge investments at the antennas.

### 1.2. Why Bother?

There are a number of arguments against fixing a tool that isn't broken. SKED could be patched indefinitely, and, given this, the community's resources may be better spent elsewhere. Some of the new features, such as adaptive scheduling may not be realistic in the next few years. Another concern is who will maintain a new version of SKED (over the long term)?

## 2. A Dynamic Future

### 2.1. Programming Languages

Continued reliance on aging FORTRAN tools cannot continue forever, and the longer we avoid this change the higher the price we pay. We will have difficulties attracting new staff when programmers are not being trained in the FORTRAN language. Furthermore, we have an obligation to students to give them up-to-date and marketable skills: Both students and new employees need training that is useful to their careers.

New software development could take advantage of modern software development environments and could take advantage of Object Oriented Programming. The VLBI scheduling task lends itself to OO programming extremely well: New equipment would only require the creation of a new derived class and the addition of necessary virtual functions. The existing OO code would remain untouched.

If the VLBI community wants to have a dynamic future it must respond to changes and be up to date.

### 2.2. Design Goals

The following are the design goals we feel are most important in re-writing SKED:

- Learn from the past: copy or improve on the existing features. Separate the source-selection algorithm from the detailed construction of the objects involved.
- Open source optimization: enable anyone to write optimization software without extensive interaction with the basic equipment functionality (antenna slewing, tape status, frequency, modes, etc.).
- Take advantage of available software development tools on the most common hardware platform (PC).
- Ease the maintenance of the software by utilizing existing software tools such as Excel.
- Use an up-to-date, friendly user interface.
- Maximize flexibility of the antennas and data systems (e.g. allow for multi-beam, real-time systems).
- Enable real-time or adaptive scheduling. The schedule should respond if one antenna fails mid-way through an experiment.

## 3. A Preliminary Version

In the initial stages of the software development we have two main deliverables, the first being software suitable for one VLBI system (S2) but not including the optimization routine. The architecture is designed for all VLBI systems, obviously. The second deliverable is a stand alone optimization routine that will try to duplicate as closely as possible the existing routine in SKED.

We feel that future developments in schedule optimization should be separated from the basic station operations, such as antenna slewing, horizon masks, tape control, etc. The project is designed such that the scientific aspects that are embodied in the optimization routine can be addressed by a maximum number of people (including students).

### 3.1. Assumptions Made

- Bill Gates' dream of a PC on every desktop has nearly come to pass.
- These PCs run Windows with MS Excel installed.

### 3.2. Decisions Taken

- The software is written in the C++ language within Borland Development Environment, Builder C++ 5.0. Further developments would not be dependent on this choice.
- Data (catalogs of station characteristics, source flux, etc.) are stored in an MS Excel file. The software accesses data from the Excel file through an Excel Com server.

### 3.3. Objects

Figure 1 illustrates the objects in our design and their interrelationship.

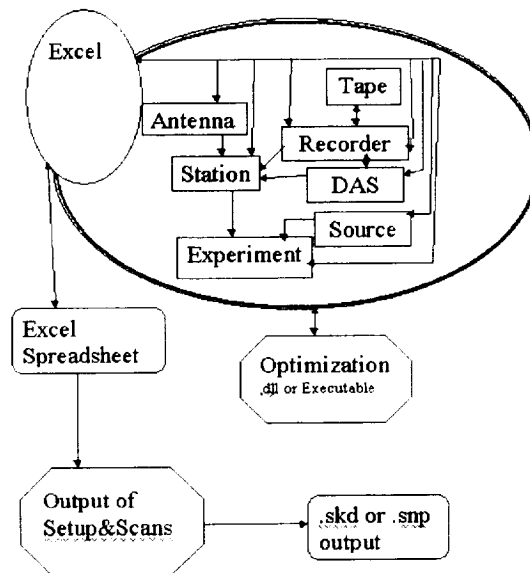


Figure 1. Objects

- **Experiment** A list of stations and sources at a defined epoch. Uses a baseline approach with two antennas and a source.
- **Station** Pointers to Antenna, DAS, Recorder.
- **Antenna** Different classes for axis, slewing rates, sensitivities.
- **Data Acquisition System (DAS)**
- **Recorder** Pointer to the Tape object.
- **Tape**
- **Source**

### 3.4. Program Flow:

At this time our design involves a program flow as follows:

- The user chooses stations, sources, DAS setup, recorder and optimization scheme. An alternative is to load a saved list of selections. These are used to create an experiment class.
- The user defines the start epoch and length, the optimization or autosked++ routine, and starts the creation of a schedule.
- The optimization routine queries the experiment class of the main program for available baselines, plus other parameters.
- The optimization routine generates instructions for each station that are time stamped.

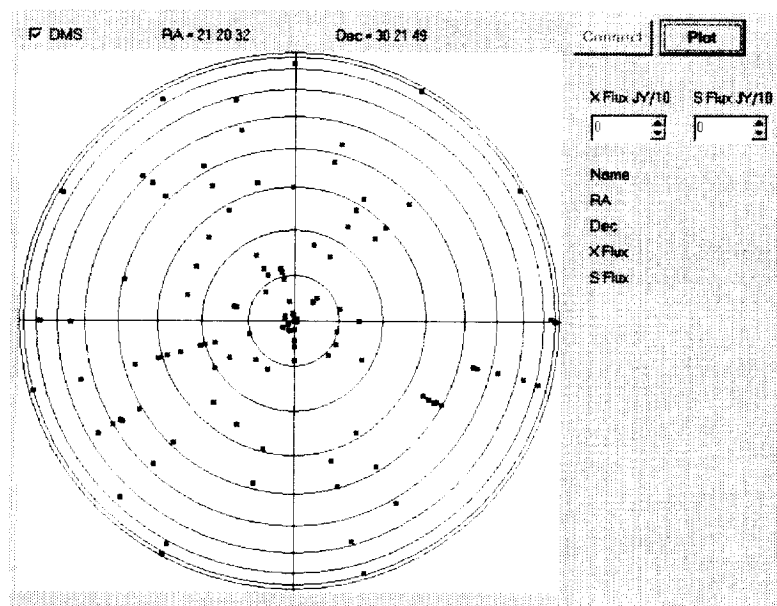


Figure 2. Source Selection Screen Capture

## Geodesy with the World's Smallest (3-m) VLBI Telescope

Hiroshi Takaba<sup>1</sup>, Minoru Yoshida<sup>1</sup>, Ken-ichi Wakamatsu<sup>1</sup>, Tetsuro Kondo<sup>2</sup>,  
Yasuhiro Koyama<sup>2</sup>, Jun-ichi Nakajima<sup>2</sup>, Mamoru Sekido<sup>2</sup>, Ryuichi Ichikawa<sup>2</sup>,  
Eiji Kawai<sup>2</sup>, Hiroshi Okubo<sup>2</sup>, Hiro Osaki<sup>2</sup>, Jun Amagai<sup>2</sup>, Noriyuki Kurihara<sup>2</sup>,  
Yukio Takahashi<sup>2</sup>, Yoshihiro Fukuzaki<sup>3</sup>, Noriyuki Akiyama<sup>3</sup>, Kouhei Shiba<sup>3</sup>,  
Kazuhiro Takashima<sup>3</sup>, Michiko Onogaki<sup>3</sup>, Shinobu Kurihara<sup>3</sup>, Kohhei Miyagawa<sup>3</sup>,  
Kyoko Kobayashi<sup>3</sup>, Hiroshi Hori<sup>3</sup>, Shigeru Matsuzaka<sup>3</sup>

1) *Gifu University, Faculty of Engineering*

2) *Communications Research Laboratory*

3) *Geographical Survey Institute*

Contact author: Hiroshi Takaba, e-mail: [takaba@cc.gifu-u.ac.jp](mailto:takaba@cc.gifu-u.ac.jp)

### Abstract

We show results of geodetic VLBI with the world's smallest 3-m VLBI telescope at Gifu University (Figure 1). This telescope was originally made for mobile VLBI experiments in 1984 by the Communications Research Laboratory, and was moved to Okinawa, Wakanai, Minami-Daitoh Island, and Koganei [1]. In 1999, the telescope was moved to Gifu University, which lies at the central part in Japan. Geodesy VLBI experiments by using the Giga-bit Recorder System succeeded and the baseline between Kashima 34m telescope and Gifu 3m telescope was obtained.



Figure 1. Gifu University 3m Radiotelescope.

Table 1. Specification of the 3-m radio telescope of Gifu University.

Parameter	Gifu Univ. 3-m telescope
X-band (standard $\nu = 8.230GHz$ , $\lambda = 0.0365m$ )	7.860 – 8.600 GHz
$T_{sys}$	135 K
Efficiency	0.43
HPBW	0.8°
Az and El Drive speed	10° /sec.

## 1. Merits of the Small Telescope

Small VLBI telescopes are good at geodesy because

- 1) very little thermal and gravity deformation
- 2) large slew rates (10°/sec. both in azimuth and elevation axes for our 3m telescope)
- 3) low costs for building and maintenance
- 4) simple collocation with GPS.

## 2. Results of Giga-bit Recorder Experiments

The most serious problem for the small telescope is its low sensitivity. By using the most advanced Giga-bit Recorder (GBR: 1Gbps) system developed by CRL [2], the sensitivity grows up to 4 times compared to the normal K-4 VLBI system (64Mbps). Then we tried to conduct Giga-bit recorder experiments between Kashima 34-m telescope and Gifu 3-m telescope (GIFT01 and GIFT02), the K-4 system (64Mbps) was also used for comparison. Results are shown in Table 2. Because of a problem in the sampler, errors were larger for GBR than K-4, but we could obtain the geodesy solution. The baseline length repeatability and accuracy were good within errors for GBR and K-4, respectively. New Giga-bit VLBI samplers are now being developed by CRL and we will try again to obtain more accurate geodesy solution.

Table 2. Results of the VLBI experiments by using K-4 (64 Mbps) and GBR (1 Gbps) between Gifu 3-m and Kashima 34-m telescopes.

Exp. Code	X (mm)	Y (mm)	Z (mm)	Baseline (mm)
GIFT01(K-4)	- 3787518271.5 ± 10.6	3564247195.4 ± 9.2	3679797149.1 ± 8.9	358918278.6 ± 3.5
GIFT02(K-4)	- 3787518246.6 ± 11.8	3564247170.2 ± 10.0	3679797146.6 ± 10.3	358918279.1 ± 3.7
GIFT01(GBR)	- 3787518255.2 ± 37.3	3564247235.5 ± 29.7	3679797178.3 ± 30.3	358918316.6 ± 11.9
GIFT02(K-4)	- 3787518248.7 ± 17.3	3564247131.9 ± 15.5	3679797135.2 ± 14.6	358918248.5 ± 6.1

### 3. Collocation of The VLBI and GPS

Before construction of the 3-m radio telescope, we set the GPS antenna at the telescope base and made GPS observations for 6 days. Figure 2 and 3 shows results of the horizontal and vertical position of the 3-m telescope obtained by VLBI (GIFT: Gifu 3-m - Kashima 34-m, JADE: Gifu 3-m - Tsukuba 32-m) and GPS. The horizontal positions of the VLBI and GPS coincide within several centimeters. The vertical positions of the GPS differ from VLBI by about 10 centimeters.

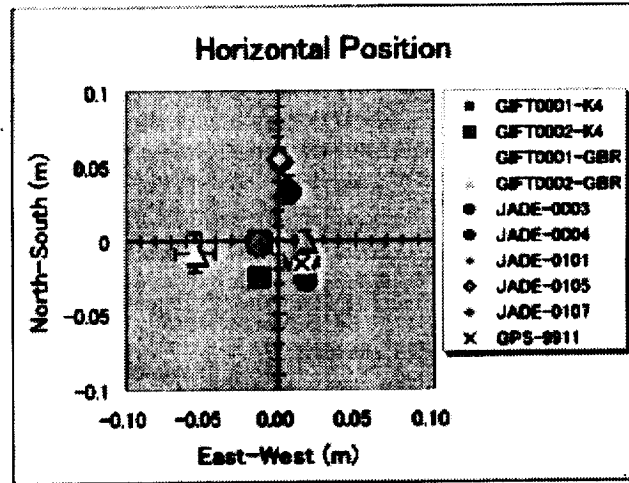


Figure 2. Horizontal Position of the 3-m telescope obtained by VLBI and GPS,

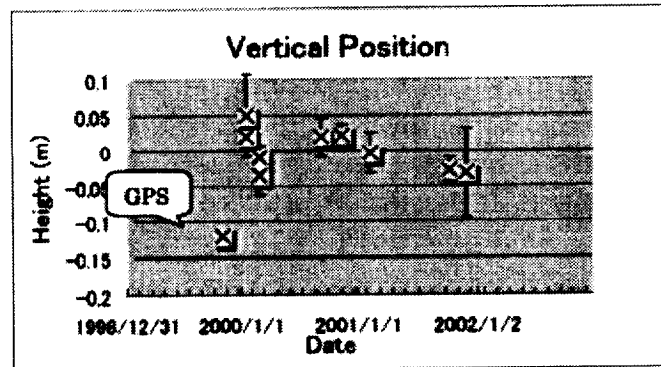


Figure 3. Vertical Position of the 3-m telescope obtained by VLBI and GPS,

### References

- [1] Amagai, J., et al., Journal of the Communications Research Laboratory, Vol. 37, 63, 1990
- [2] Koyama, Y., et al., Proceedings of the IVS 2000 General meeting, p98, 2000

# A Multiband Primary Focus Receiver for Noto Antenna

*Gino Tuccari*

*Radioastronomy Institute of the Italian National Research Council*

*e-mail: tuccari@ira.noto.cnr.it*

## Abstract

A new multiband receiver has been completed to be used in the primary focus of the 32m Noto parabola. The included frequency bands in double circular polarisation are: 3.6/13 coaxial, 21, 18, 2.5 cm. The range 250-1000 MHz is also covered with the addition of external dedicated antennas. Main features are described along with the architecture adopted to integrate in the entire new system also receivers placed in the secondary focus. Cooled front-end and feeds for both L and S/X bands allow to achieve interesting performance.

## 1. Description

The multiband receiver developed in Noto is in the final stages of mounting and testing before being installed in the primary focus of the 32 m Noto parabola. It will replace the old uncooled S/X and L band receivers, the former being placed in the primary, the latter in secondary focus. The system presents several improvements with respect to the old one and adds new functionality. Moreover a full range between 250 and 1000 MHz is added, that includes the 92 and 49 cm VLBI bands. An holographic set of receivers is mounted allowing to check with the phase reference method the surface accuracy.

Receivers for secondary focus are integrated in the new system, allowing the entire set of receivers to be seen as a unique multifunctional block. Indeed three blocks are present, defined as "primary", "vertex" and "VLBA" box. The first is included in the receiver box placed in the primary focus and contains all the electronics. Moreover the receiver box contains the great dewar, and the noise-cal module. The S/X coaxial feed and the L band one are cooled at 77 K to reduce the noise contribution, while the six LNAs are cooled at 20 K. Appropriate thermal gaps are placed between the orthomode transducer and the waveguide-coaxial conversion to properly take into account the temperature difference.

The "vertex" box is placed in the secondary focus room and is fed by the signals at sky frequency transferred through appropriate cables, as selected by the primary box switch matrix, remotely controlled. IFs produced by the other receivers placed even in the vertex room are selected along with the new receiver bands to be sent to the control room through two channels 1 GHz bandwidth analog fibre optic connection.

Finally the "VLBA" box is responsible for reconstructing from the fibres two IFs, to adjust the power levels with 0.5 dB of accuracy and to send to a double channel up-converter, from where is sent back again to this box and selected to feed the four IFD channels of the VLBA terminal.

The three sections are remotely controlled by a dedicated addressable serial/optical interface, and a Windows based program is used to set and control the entire functionality.

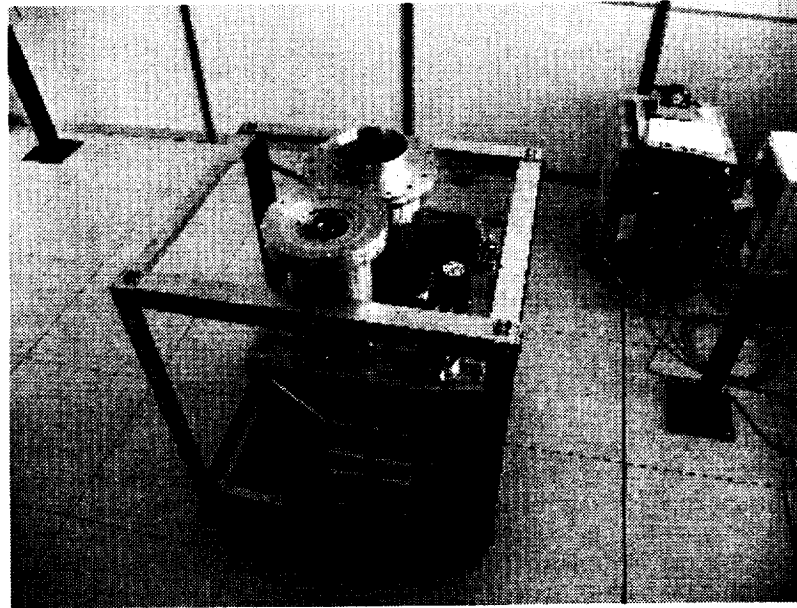


Figure 1. Receiver Box View with Dewar and Feeds

## 2. Main Receiver Features

In the following list, the main difference with respect to the old system are shown:

- Wide X band for geodesy (8100-8900 MHz);
- New design for the both cooled (77 K) feeds, the coaxial S/X and L band;
- Cooled (20 K) low noise cryogenic front-end amplifiers;
- Centralized synthesizer used as local oscillator for the full set of receiver (including the secondary focus receiver system);
- Double Up-Converter for the VLBA terminal;
- Four IFs usage with remote feeding selection;
- Two IFs coarse-fine power level control;
- Entire set of receivers controlled and checked by Windows based software (dialogue with FS in development).

Temperature performance showed in laboratory satisfactory values, with a total noise contribution including feed and amplifiers of about 15-20 K in L and S band, while 20-25 K in X band. The actual final system temperature will be determined when the receiver will be mounted on top of the antenna, during 2002.

## Foot-Print of the Space-Geodetic Observatory, Ny-Ålesund, Svalbard

*Halfdan P. Kierulf, Lars Bockmann, Oddgeir Kristiansen, Hans-Peter Plag*

*Norwegian Mapping Authority*

*Contact author: Halfdan P. Kierulf, e-mail: [halfdan.kierulf@statkart.no](mailto:halfdan.kierulf@statkart.no)*

### Abstract

The Space-Geodetic Observatory at Ny-Ålesund, Svalbard, which is operated by the Norwegian Mapping Authority, has developed over recent years into a fundamental geodetic station. At such fundamental sites, detailed knowledge of the stability of the station, both locally and with respect to the region, is essential for geodetic and geophysical applications of the observations. The extensive foot-print study for the observatory includes repeated GPS campaigns on a 50 km by 30 km control network and repeated classical surveys of the inner control network extending 400 m by 40 m. The results from the GPS campaigns indicate neo-tectonic movements in the vicinity of the observatory.

### 1. Introduction

The geodetic observatory in Ny-Ålesund is a fundamental geodetic station located at 78.9°N and 11.9°E on the southern coast of the Kings Bay (Fig. 1). The geodetic infrastructure includes a 20-m VLBI-antenna, several GPS and GPS/GLONASS receivers, a tide gauge, a superconducting gravimeter and a co-located DORIS station (see e.g. [4] and [5] for a detailed description of the station).

The space-geodetic techniques provide point measurements with the baseline of the monument having typically a dimension of a few metres. In order to be able to interpret the observations in terms of geophysical signals, the actual foot-print size of the measured point needs to be known. The foot-print is determined by the stability of the monument with respect to the surrounding ground but also by how representative the location is with respect to the surrounding area and even region. This again is a consequence of the geophysical processes relevant at a given location.

The Western Svalbard fold-and-thrust belt has a complex tectonic history linked to the opening of the Northern Atlantic Ocean. The last recognised important tectonic event in this area is dated from the Tertiary [1] when the Ny-Ålesund tertiary basin was overthrust by carboniferous rocks. Today, Western Svalbard is located only 150 km away from the Knipovich Ridge, which is an active segment of the Mid-Atlantic Ridge system. High heat flow anomalies and considerable seismic activity have been recorded offshore western Svalbard [3]. In the Kings Bay area, minor seismicity may indicate some neotectonic activity. Some faults are relatively close to the observatory. This setting warrants a careful study of the actual foot-print size for the fundamental station in Ny-Ålesund.

Local monument stability has been studied in detail based on classical measurements on a local inner control network (see e.g. [2], [6]). For studies of the larger foot-print of the observatory, campaign type GPS measurements are applied.

## 2. The GPS Control Network and Observations



Figure 1. Location of the GPS control network

The numbers 1-8 denote the GPS markers established in 1998; those with number 9-11 were established in 1995, while number 12 is close to the tide gauge and was established in 2000. Colours denoted different geological units, with dark grey: Proterozoic; light grey: tertiary, intermediate grey (on Brøggerhalvøya): cretaceous-permian. Note the fault and the small tertiary unit close to the geodetic observatory. From [5].

In order to study the stability of the Kings Bay area, a GPS control network was established in 1998 extending in east-west and north-south directions approximately 50 km by 30 km (see Fig. 1 and [5]). The points were selected in order to cover most of the different geological units in the surrounding of the observatory. Other criteria were the GPS horizon and the presence of bedrock. At high latitudes, GPS satellites are always seen at low elevations while satellites are also seen over the pole. A unperturbed horizon in all directions is an asset. Due to the steep topography and the effect of permafrost on rocks, both criteria are difficult to meet. Accessibility of the points also had to be taken into account. However, most of the outer points are only accessible by helicopter, depending on weather conditions.

At points outside the inner control network with its elaborated pillars (see [6]), the GPS markers are brass screw bolts drilled and cemented into solid rock. Elevation of the top of the bolt above ground is of the order of 5 cm.

In Fig. 2, the surroundings of selected points are illustrated. The points at Kap Mitra (1 on Fig. 1, upper right in Fig. 2) and Kapp Guissez (2) on the northern coast of Kings Bay are located on bedrock exposed due to extreme high waves keeping the bedrock free from debris. For both sites, the horizon is almost unperturbed with some mountains towards north with maximum elevation angles of 5-6°. Engelsbukta (6, upper right on Fig. 2) is located on the lower part of the southern side of a mountain, with no view to satellites in the north. Bedrock is very scarce in that area and therefore the trade-off between site stability and horizon was decided in favour



Figure 2. Selected points of the Control network.

Upper left: Kap Mitra, view towards south-east; upper right: Engelsbukta, view to north-west; middle: Kvadehuken, view to south-west; lower: Knochttjørna, view to south. All photos by Plag, 1998.

of the former. Other areas where stable bedrock is scarcely found are Sarsfjellet (4) at the inner end of Kings Bay and the vicinity of the observatory itself. The marker in the outcrop within Kronebreen (5) has been abandoned since even with a helicopter accessibility is too difficult due to weather conditions. The points across Kings Bay from Ny-Ålesund (3 and 9) are placed in bedrock but their northern horizon is obscured by mountains with elevation angles of more than  $10^\circ$ . Kvadehuken (7, lower left on Fig. 2) and Knochttjørna (8, lower right on Fig. 2) are in flat areas covered by broken-up permafrost material. At Kvadehuken, the marker is placed in an outcrop of bedrock of more than 20 m extension, while at Knochttjørna it is not clear whether the marker is in an outcrop or a larger block.

GPS campaigns were carried out in September 1998 (1 campaign), August 1999 (2 consecutive campaigns), and 2000 (3 consecutive campaigns). In 1998, seven points established in 1998 were measured. In both, 1999 and 2000, all points suitable for GPS measurements were occupied in two consecutive campaigns (see [5] for more details). A new campaign is planned for 2002.

In each campaign, the points were occupied for at least 4 complete days and in most cases for five full days. Care was taken to occupy, wherever possible, a given point each year with the same receiver and antenna pair. All campaigns were carried out by the same observer (LB).

Table 1. Movements for the markers in the control network.  
 Site velocities:

No.	ID	East mm/yr	North mm/yr	Height mm/yr
6	ENGL	9.6 +/- 1.0	14.5 +/- 0.8	4.9 +/- 1.5
2	KAPG	10.9 +/- 0.5	15.0 +/- 0.6	2.8 +/- 0.9
1	KAPM	9.4 +/- 0.5	14.9 +/- 0.6	3.6 +/- 1.2
8	KNOC	11.0 +/- 0.6	12.6 +/- 0.6	2.8 +/- 1.0
7	KVAD	10.0 +/- 0.6	14.2 +/- 0.6	-2.5 +/- 1.3
4	SARS	11.2 +/- 0.7	13.4 +/- 0.6	6.6 +/- 1.5
12	NYAL	12.4 +/- 0.5	15.1 +/- 0.5	-2.0 +/- 1.5
	NUVEL	12.95	13.60	
	NYAL	10.8 +/- 0.1	15.2 +/- 0.1	4.0 +/- 0.3
	NYA1	9.2 +/- 0.1	14.7 +/- 0.1	3.5 +/- 0.3

### 3. GPS Analysis and Results

Analyses were carried out with GIPSY, using a free network analysis (FNW) as well as a precise point positioning (PPP, see [7]). JPL precise satellite orbits and clocks and EOPs were used. Cut-off elevation angle for both solutions was set to 7°. For transformation to ITRF97, JPL's global transformation parameters were used. In the analysis, no ambiguity resolution was made. For identical data sets, no significant difference were found between the FNW and PPP solutions. The PPP has the advantage that the reference frame is realised by the satellite orbits, only, and therefore is independent of the actual sites measured. Thus, data gaps do not affect the reference frame. Moreover, for PPP consecutive campaigns on disjoint sets are in the same reference frame.

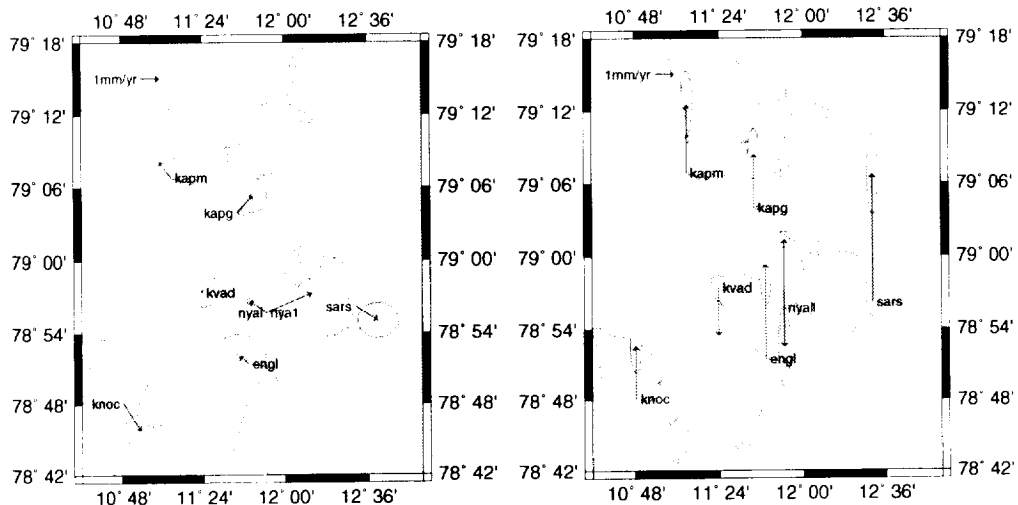


Figure 3. GPS determined motion of the control network.

Left: horizontal movement relative to ITRF97 velocity for Ny-Ålesund; right: vertical movement.

In order to account for long-period variations in the GPS time series, the day to day movements for the permanent station NYA1 are subtracted from the individual day to day results for the campaign stations. This reduces common variations at all stations due to orbit errors and unmodelled atmospheric and loading effects.

The resulting linear velocities are given in Table 1. For the horizontal components, all points show the same north-east movement with respect to ITRF. However, differences are of the order 2 mm/yr, and there is a systematic difference to the NUVEL-1A-NNR predictions. In order to elaborate the geographical pattern of the differences, the ITRF97 velocity for Ny-Ålesund has been subtracted (Fig. 3). The resulting spatial pattern appears to be somewhat correlated with the fault structure. NYA1 shows a large difference to NYAL, and instability of the NYA1 is suspected.

Vertically, all points show uplift except for KVAD and NYAL (Table 1). NYAL and NYA1 show the same long-term trend (lower lines in Table 1), and the negative trend for NYAL in the campaign may be due to gaps in NYAL during one campaign. For KVAD, no data problems can explain the negative trend, and a tectonic origin cannot be excluded (Fig. 3).

#### 4. Conclusions

The secular horizontal velocities determined from three repeated GPS campaigns indicate a possible small scale tectonic movement. More GPS campaigns in conjunction with classical surveys are needed to exactly determine the foot-print of the observatory with respect to horizontal and vertical movements

#### References

- [1] Blythe and Kleinspehn. Tectonically versus climatically driven Cenozoic exhumation of the Eurasian plate margin, Svalbard: Fission track analyses. *Tectonics*, 17:4 621–4 639, 1998.
- [2] L. Grimstveit and S. Rekkedal. Geodetic control of permanent sites in Tromsø and Ny-Ålesund. In H.-P. Plag, editor, *Book of Extended Abstracts for the Ninth General Assembly of the Working group of European Geoscientists for the Establishment of Networks for Earth-science Research. Second Edition*, pages 25–28. Norwegian Mapping Authority, 1998.
- [3] S. Høgden. *Seismotectonics and crustal structure of the Svalbard Region*. PhD thesis, Department of Geology, University of Oslo, 1999.
- [4] H.-P. Plag. Space-geodetic contributions to global-change research at Ny-Ålesund. In *Proceedings for the 27-th Int. Symp. on Remote Sensing of Environment: Information for Sustainability, June 8-12, 1998, Tromsø, Norway*, pages 227–231. Norwegian Space Centre, 1998.
- [5] H.-P. Plag, L. Bockmann, H. P. Kierulf, and O. Kristiansen. Foot-print study at the space-geodetic observatory, ny-ålesund, svalbard. In P. Tomasi, F. Mantovani, and M.-A. Perez-Torres, editors, *Proceedings of the 14th Working Meeting on European VLBI for Geodesy and Astrometry, Castel San Pietro Terme, Sept. 8 - Sept. 9, 2000*, pages 49–54. Consiglio Nazionale Delle Ricerche, Istituto di Radioastronomia, 2000.
- [6] P. Tomasi, P. Sarti, and M. Rioja. The determination of the reference point of the VLBI antenna in Ny Ålesund. *Memoirs of National Institute of Polar Research, Japan*, 54, 2001. 319-330.
- [7] J. F. Zumberge, M. B. Heflin, D. C. Jefferson, and M. M. Watkins. Precise point positioning for the efficient and robust analysis of GPS data from large networks. *J. Geophys. Res.*, 102:5005–50017, 1997.

# Local Ties Between the Space Geodetic Techniques at the Onsala Space Observatory

*Martin Lidberg, Rüdiger Haas, Sten Bergstrand, Jan Johansson, Gunnar Elgered*

*Onsala Space Observatory (OSO)*

*Contact author: Martin Lidberg, e-mail: [lidberg@oso.chalmers.se](mailto:lidberg@oso.chalmers.se)*

## Abstract

We describe the local tie measurements between the collocated space geodetic techniques at the Onsala Space Observatory. Several classical geodetic measurement campaigns have been performed since the beginning of the 70s. Later also short baseline VLBI measurements and GPS campaigns have been performed. So far all realizations of local tie measurements had to use some information from construction drawings of the 20 m telescope. Thus, the local tie between the IVS reference point, i.e. the intersection of the azimuth and elevation axes of the 20 m radio telescope, and the IGS reference point, i.e. the phase center of the GPS antenna, has an uncertainty at a level of several millimeters. Footprint GPS-campaigns indicate that the observatory site is more stable than the uncertainty of these measurements which is 1–3 mm. Currently a small network of new observation pillars is installed to allow a new classical geodetic determination of the local tie between the IGS and the IVS reference points. We expect this new realisation of the tie to reach sub-millimeter uncertainties.

## 1. Introduction

The Onsala Space Observatory (OSO) is a network station for the International VLBI service for Geodesy and Astrometry (IVS) as well as a global station for the International GPS Service (IGS). IVS and IGS are the major contributors to the International Terrestrial Reference Frame (ITRF) [1]. In order to maintain the ITRF with high accuracy, the knowledge of the local ties at sites with collocated space geodetic techniques is required. This includes an accurate determination of the tie between the reference points and the monitoring of its temporal stability.

## 2. History of Local-tie Efforts at Onsala

The first space geodetic instrument used at the Onsala Space Observatory was the 25 m radio telescope erected in 1964 [2]. Already in 1968 Onsala participated in the first Mark-I geodetic VLBI experiment [3]. A classical geodetic measurement campaign was performed in 1973 to connect the reference point of the 25 m telescope to the triangulation reference point of the Swedish national geodetic system situated on the observatory estate [4]. In 1976 the 20 m radio telescope was constructed. Its reference point was connected by classical geodetic observations to the triangulation reference point in 1978. Since 1979 the 20 m telescope has been used for geodetic VLBI observations. In order to connect the reference points of the 25 m telescope and the 20 m telescope, a classical campaign was performed in 1981, and the earlier measurements of 1973 and 1978 were re-adjusted at the same instance [5]. Short baseline X-band VLBI experiments between the two telescopes were performed in 1980 and 1981 [6]. Precise levelling between the different geodetic markers at the observatory was performed in 1986 [7].

The Global Positioning System (GPS) was introduced at the observatory in 1987 and a few geodetic markers were established in the bedrock surrounding the GPS site. In connection to that, classical geodetic measurements and several GPS campaigns were performed around 1990 to connect the new GPS monument with the existing VLBI reference points [8], [9]. Some distances in the 20 m telescope were taken from construction drawings, since its reference point is not accessible as a real physical marker.

A short baseline VLBI campaign was performed when the mobile telescope MV-2 was at Onsala in 1992 [10]. In 1993 the coordinate differences of the geodetic markers at Onsala were transformed to WGS84 [11]. In order to monitor the vertical height changes of the 20 m telescope, an invar-rod based measurement system was installed in the telescope tower in 1996 [12], see Figure 1.

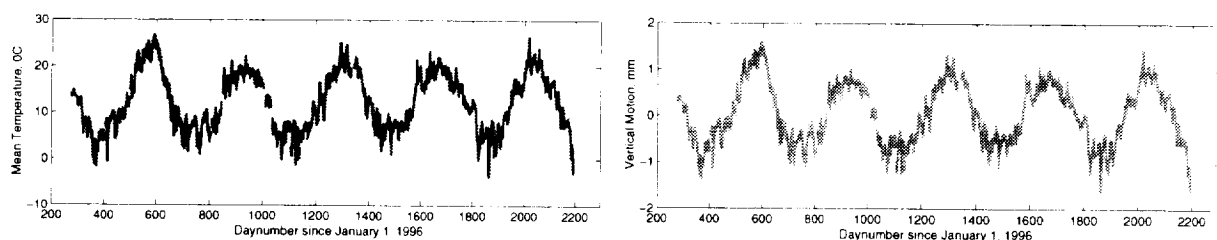


Figure 1. Left: Mean temperature of 16 temperature sensors in the concrete telescope tower. Right: Relative vertical height of the telescope tower as measured by the invar rod.

### 3. A GPS-VLBI Tie Using GPS-antennas on the 20 m Telescope

In the summer of 1999, a Dorne Margolin GPS antenna was installed permanently on top of the VLBI telescope behind the sub-reflector close to its Apex position [13]. Sporadically, an additional GPS antenna has been mounted close to the vertex position of the main reflector. The idea is to monitor the local tie between the IVS and the IGS reference monuments on regular intervals. During breaks in the ordinary observing schedule the telescope is oriented to its zenith position and GPS observations are performed. Analysis of the GPS data using the Bernese GPS-software yields daily solutions for the position of the APEX and VTEX antennas with respect to the IGS station. Figure 2 shows the residuals of the daily solutions compared to a combined solution. The deviation in north component of the APEX antenna between the 1999/2000 and the 2001/2002 experiments is not yet fully understood. However, the usage of different telescope pointing models over time is one possibility.

### 4. Local and Regional Footprint Campaigns

A local and regional GPS footprint campaign was performed in 2001 [14]. Geodetic markers at the observatory (inner-network of size  $\sim 1$  km) and its surrounding region (outer-network of size  $\sim 30$  km) were equipped with choke-ring antennas and Turbo Rogue or Ashtech-Z12 receivers for several weeks. The GPS-data were analysed together with data from the IGS permanent station at Onsala and three SWEPOS sites surrounding the observatory using the Bernese software Version 4.2 [15]. For nearly all stations the repeatabilities are at the level of 1-2 mm for the

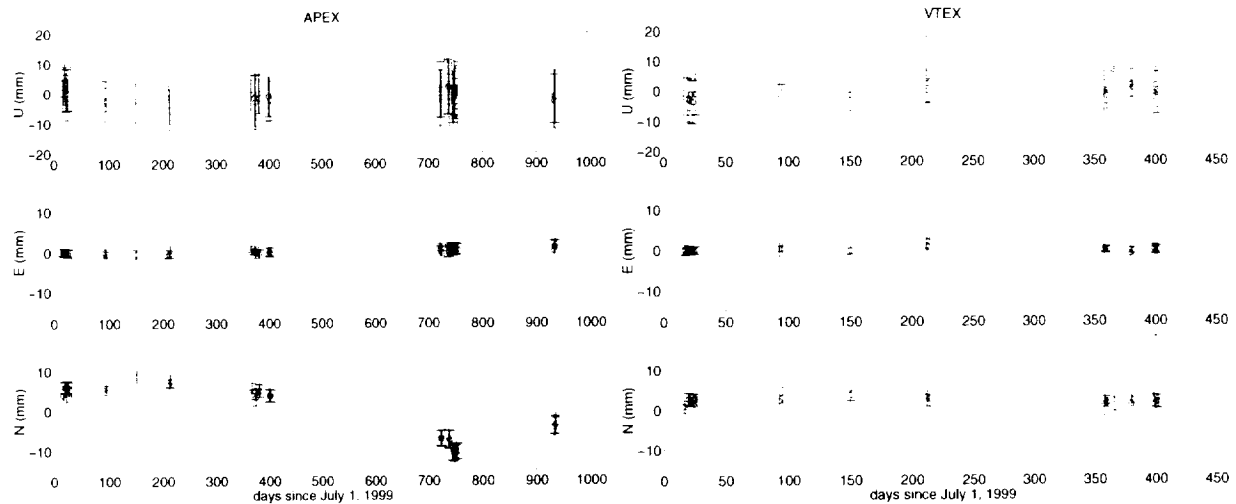


Figure 2. Left: Time series between July 1999 and February 2002 for the up, east and north components of the GPS antenna APEX atop of the 20 m telescope. Right: Time series between July 1999 and mid 2000 for the up, east and north components of the GPS antenna VTEX atop of the 20 m telescope.

horizontal components and 2–3 mm for the vertical component. Two stations with less data due to failing equipment and severe interference from a relay station for cellular telephony, respectively, performed worse. The estimated coordinates were compared to earlier GPS results from 1990 [9]. We performed a seven parameter Helmert transformation using both coordinate sets as random variables [16] and determined the transformation parameters. Given the observed repeatabilities during the campaign, none of the markers has been significantly displaced between 1990 and 2001.

## 5. A New Classical Geodetic Tie

A new classical geodetic tie between the GPS and the VLBI reference points of the 20 m telescope will be performed in 2002. For this purpose five new observation pillars will be installed on the concrete foundation of the radome. Survey targets will be mounted on both sides of the telescope cabin close to the elevation axis. These survey targets will be observed from the new observation pillars with two theodolites simultaneously, thus allowing accurate determination of their position. The procedure will be similar to the one described in [17]. The 20 m telescope is going to be positioned at several different elevation and azimuth directions, so that the positions of the survey targets describe circles around the telescope's azimuth and elevation axes. Thus, the telescope's geodetic reference point, which should be the intersection of the azimuth and elevation axes, can be determined. The new observation pillars will be connected by angular and distance measurements to the geodetic markers in the bedrock around the IGS permanent station and the IGS reference point itself. We expect to derive the local tie between the IGS and IVS reference points by this method with a sub-millimetre uncertainty.

Figure 3 shows a topview of the telescope inside the radome and the new survey pillars and supporting points (left picture), and a crossview of the observation of survey targets on the telescope cabine (right picture).

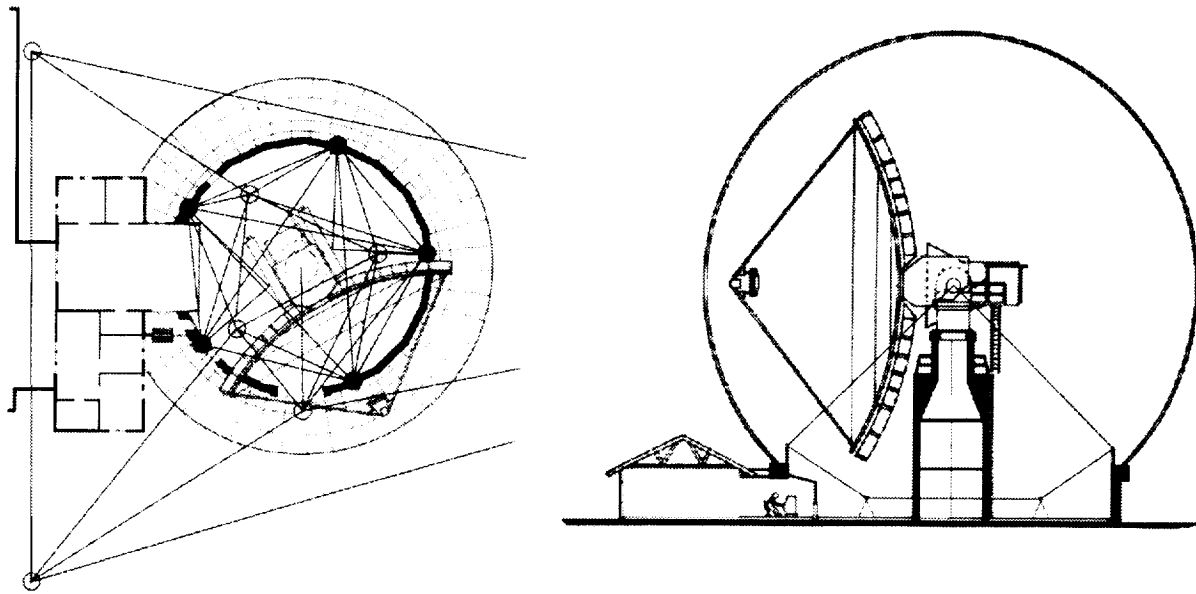


Figure 3. Left: Topview of the local network for the tie to be performed in 2002. Five observation pillars on the radome foundation and are going to be tied by classical geodetic observations and additional temporary supporting markers to the IGS reference marker. Right: Crossview through the radome showing the geometry of observation pillars and the survey targets mounted on the telescope cabin close to the elevation axis of the telescope.

## 6. Conclusions and Outlook

Several efforts concerning the local ties at the Onsala Space Observatory have been performed through the years. However, since some distances have been taken from construction drawings, the local tie between the IVS and the IGS reference points currently has an uncertainty of a few millimetres. Since the tie is of interest for the maintenance of the ITRF, the efforts will continue to monitor the vertical height changes of the telescope foundation using the invar rod measurement system and to carry out repeated GPS campaigns involving GPS antennas on the VLBI telescope. The new determination of the tie by classical geodetic techniques to be performed in 2002 has the potential to reach an uncertainty at the sub-millimetre level.

## References

- [1] Altamini, Z., Angermann, D., Argus, D., Blewitt, G., Boucher, C., Chao, B., Drewes, H., Eanes, R., Feissel, M., Ferland, R., Herring, T., Holt, B., Johansson, J., Larson, K., Ma, C., Manning, J., Meertens, C., Nothnagel, A., Pavlis, E., Petit, G., Ray, J., Ries, J., Scherneck, H.-G., Sillard, P., and Watkins, M.: The Terrestrial Reference Frame and the Dynamic Earth. *EOS Transactions*, **82(25)**, 273, 278–279, Americal Geophysical Union, 2001.
- [2] Scherneck, H.-G., Elgered, G., Johansson, J. M., and Rönnäng, B. O.: Space Geodetic Activities at the Onsala Space Observatory: 25 years in Service of Plate Tectonics. *Phys. Chem. Earth*, **23(7–9)**, 811–823, 1998.

- [3] Whitney, A.R., Precision Geodesy and Astrometry via Very Long Baseline Interferometry. Ph.D. thesis, Dept. of Electrical Engineering, MIT, Cambridge, MA, 1974.
- [4] Handlingar rörande inmätning av parabolantenn vid Råöobservatoriet utförda i oktober 1973 av VIAK AB. Kartavdelningen, 1973.
- [5] Eliasson, L.: Redogörelse för nyberäkning. file G 7331 of the Geodetic Archive, Lantmäteriverket, 1981.
- [6] Lundqvist, G.: Precision surveying at the 1-mm level using radio interferometry. In: Lundqvist, G.: Radio interferometry as a probe of tectonic plate motion. Ph.D. Thesis, appendix 1, 64–71, Chalmers University of Technology, *Techn. Rep. 150*, 1984.
- [7] Lindström, J.: Redogörelse för mätning och beräkning av höjdnät inom Kungsbacka kommun (Anslutning av Onsala rymdobservatorium till nya riksnätet i höjd). Lantmäteriverket, 1986.
- [8] Peterson, I.: Nymätning och nyberäkning av punkter vid Onsala rymdobservatorium på Råö. Lantmäteriverket, 1991.
- [9] Johansson, J. M., Elgered, G., and Rönnäng, B. O.: The Space Geodetic Laboratory at the Onsala Observatory: Site Information. In: Johansson, J. M.: A Study of Precise Position Measurements Using Space Geodetic Systems, Ph.D. Thesis, paper A, A1–A16, Chalmers University of Technology, *Techn. Rep. 229*, 1992.
- [10] Potash, R.: Accurate VLBI Geodetic Tie from Onsala VLBI Reference Point to Ground. Report, Interferometrics/GSFC, Nov. 31, 1992.
- [11] Reit, B.-G.: Beräkning av WGS 84 koordinatdifferenser på Onsala. Lantmäteriverket, 1993.
- [12] Johansson, L.-Å, Stodne, F., and Wolf, S.: The PISA project: Variations in the height of the foundation of the 20 meter radio telescope. *Research Report 178*, Onsala Space Observatory, Chalmers University of Technology, 1996.
- [13] Bergstrand, S., Haas, R., and Johansson, J. M.: A new GPS-VLBI Tie at the Onsala Space Observatory. In: N.R. Vandenberg and K.D. Baver (eds.): *Proc. of the First IVS General Meeting*, 128–132, NASA/CP-2000-209893, Goddard Space Flight Center, Greenbelt, MD 20771 USA, 2000.
- [14] Haas, R., and Kirchner, M.: Local survey activities at the Onsala Space Observatory 1999–2001. In: D. Behrend and A. Rius (Eds.): *Proc. of the 15<sup>th</sup> Working Meeting on European VLBI for Geodesy and Astrometry*, Institut d’Estudis Espacials de Catalunya, Consejo Superior de Investigaciones Científicas, Barcelona, Spain, 177–184, 2001.
- [15] Hugentobler, U., Schaer, S., Fridez, P., (Eds.): Bernese GPS Software Version 4.2. 515 pp., Astronomical Institute University of Berne, 2001.
- [16] Koch, K. R., Fröhlich, H., and Böker, G.: Transformation räumlicher variabler Koordinaten. *Allgemeine Vermessungs-Nachrichten*, **107**, 293–295, 2000.
- [17] Nothnagel, A., Steinforth, Ch., Binnenbruck, B., Bockmann, L., and Grimstveit, L.: Results of the 2000 Ny-Ålesund Local Survey. In: D. Behrend and A. Rius (Eds.): *Proc. of the 15<sup>th</sup> Working Meeting on European VLBI for Geodesy and Astrometry*, Institut d’Estudis Espacials de Catalunya, Consejo Superior de Investigaciones Científicas, Barcelona, Spain, 168–176, 2001.

## VLBI-GPS Collocation Method at Geographical Survey Institute

Shigeru Matsuzaka, Yuki Hatanaka, Keizo Nemoto, Yoshihiro Fukuzaki, Kyoko Kobayashi,  
Kaoru Abe, Tadayuki Akiyama

*Geographical Survey Institute*

Contact author: Shigeru Matsuzaka, e-mail: shigeru@gsi.go.jp

### Abstract

We report our effort to establish a precise tie between VLBI and GPS. For local-tie survey, we employed conventional survey method using total-stations and leveling, and to pursue the precision, introduced permanent observation monuments for ground survey and Cateye reflector for the target on the VLBI antenna. With these instruments and careful measurements, 3D coordinates of antenna reference point were determined with sub-mm error at GSI-Tsukuba and Aira stations.

### 1. Introduction

Geographical Survey Institute (GSI) now operates and maintains five VLBI stations for international and domestic experiments: Shintotsukawa, Tsukuba, Kashima26, Aira and Chichijima. The results of these experiments were utilized in establishing Japan's new geodetic datum compatible with ITRF and provided a fundamental set of coordinates in the reference frame. Densification was accomplished by connecting nationwide GPS (GEONET) solution to the VLBI results [3]. Although their relationship was compared and assured within a few cm, to further utilize the space-geodetic networks and detect smaller signals for the study of geodesy, geophysics and astrometry, millimeter-level collocation and inter-comparison of different techniques are required. In our earlier study [2], we tried to establish the tie using GPS measurements permanently attached to the 32 m dish. The accuracy of vertical component was not satisfactory due probably to GPS antenna's phase effect. In this paper, we adopted a conventional survey method to improve the accuracy of local-tie and the reliability of observations (see, e.g. [1]).

### 2. Method and Instrumentation

Conventional terrestrial surveying method was chosen for the local-tie survey: electro-optical measurements for distance and angle and leveling for height. Introduction of a specially designed ground monument and Cateye reflector must be highlighted in the improvement of accuracy and efficiency of the survey (see below). Although high precision surveying instruments are recommended, we used commercially available instruments, which are good enough but not the very best of all.

### 3. Procedures

Procedures for the VLBI-GPS tie would be as follows;

- Determine the relations between ground monuments and GPS reference points by distance and angle measurements and/or leveling.

- Determine from the monuments around the VLBI antenna the positions of Cateye reflector on the dish when the antenna points to various directions.
- Assume the trace of the target is a sphere and estimate the position of its center. If necessary, make corrections for VLBI antenna deformations due to temperature change and gravity.
- Calibrate the GPS antenna's phase variation.
- Make GPS measurements with a point in the local network and a point outside of it for orientation of the network.
- Transform the local network to align with a global reference system by rotating it using the direction obtained above and deflection of the vertical.

## 4. Local Survey

### 4.1. Construction of Ground Monuments

Our newly designed monument is a hollow stainless steel pillar with outer stainless steel cover sandwiching styrofoam sheet. On top of it are an adaptor for survey instruments and metal plates to hold them down (see Figure 1).

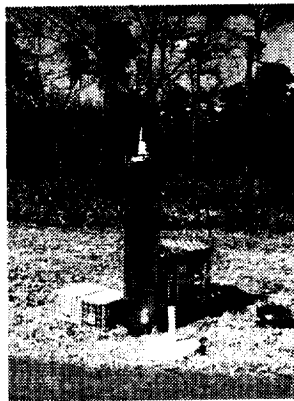
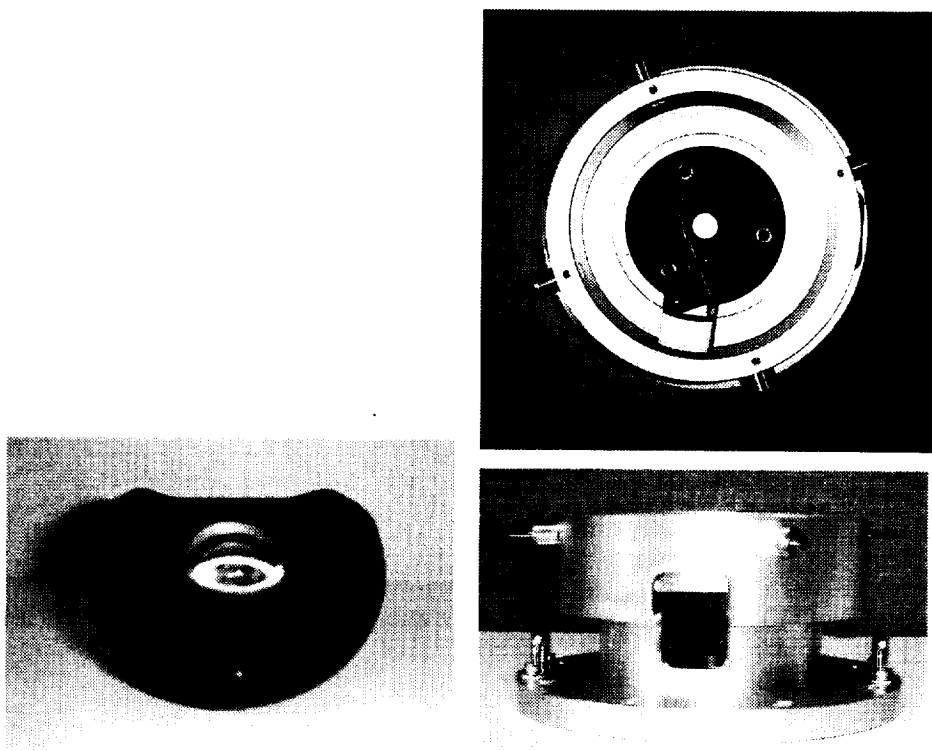


Figure 1. GSI Ground Monument

### 4.2. Introduction of Cateye Reflector as a Target on the Antenna

The Cateye is a half-sphere reflector with much wider range of entry angle ( $120^\circ$ ) than a conventional plane mirror reflector ( $< 60^\circ$ ), which helps the measurements from fixed ground monuments. It is held in a magnet support remodeled for angle measurements as well as distances to serve as a target on the VLBI antenna (see Figure 2).



**Leica Cateye Reflector.** Entry angle:  $\pm 60^\circ$ , centering error of housing and reflector:  $< 0.01\text{mm}$ , dimension of hemispherical housing:  $75 \pm 0.05\text{mm}$ .

**Magnet Support for Cateye, pins for angle measurement.** Diameter:  $170\text{mm}$ , height:  $79\text{mm}$ , weight:  $1.55\text{kg}$

Figure 2. Cateye and its Support

## 5. Observations and Data Reduction

A survey was performed with total stations to measure distances, horizontal and vertical angles to tie the ground monuments and target positions. Leveling was also carried out for precise height measurements. The Cateye was mounted on the supporting structure of the dish. The location of the Cateye must be at rigid part of the antenna and simultaneously visible from at least two ground monuments at various positions of the antenna. Observations were made at around 20 antenna positions (4-6 azimuths and 4-5 elevations). List of instruments we used are in Table 1.

Table 1. Instruments and Accuracy

Instrument and Type	Accuracy(distance)	Accuracy(angle: seconds)
SOKKIA NET2B: Total Station	$2.0\text{mm} + 2\text{ppm} * D$	2.0
TOPCON GTS-700: Total Station	$2.0\text{mm} + 2\text{ppm} * D$	1.0
WILD T2: Theodolite		
WILD N3: Tilting Level		

Network solution and the position of VLBI antenna reference point are obtained in an arbitrarily chosen 3D Cartesian coordinate system,  $(u, v, w)$ . In this paper, 3D positions of ground monuments and antenna targets were calculated by a (plane coordinate) network adjustment program of triangulation and vertical angles, which is standard survey reduction software in GSI. One of the ground monuments was chosen as the origin of  $w$  is tangent to the local vertical, and the direction from the origin to another monument is contained in  $uw$  or  $vw$  plane. A least squares fit program was used to determine the center of a sphere on which the target must be positioned. Here, we employed the following method.

Let  $\vec{u}_c = (u_c, v_c, w_c)^T$  be the position vector of the center of the sphere and  $\vec{u}_0 = (u_0, v_0, w_0)^T$  be the vector from the center to the antenna target when the antenna is at  $(az, el) = (0^\circ, 90^\circ)$ ,  $\omega_x, \omega_y, \omega_z$  are small rotation angles of antenna frame with respect to the topocentric frame (east, north, up) and  $\phi_0$  is the angle between  $v$ -direction of  $uvw$  frame and the north of antenna frame. The mathematical model is

$$\vec{u}_i = \vec{u}_c + R_3(\omega_z)R_2(\omega_y)R_1(\omega_x)R_3(-(\phi_i + \phi_0))^{-1}R_1(-90 - \theta_i)^{-1}\vec{u}_0 \quad (1)$$

where  $\vec{u}_i = (u_i, v_i, w_i)^T$  is the  $i$ th position of the target when the antenna points to  $(\phi_i, \theta_i)$ , and

$$R_1(\alpha) = \begin{pmatrix} 1 & 0 & 0 \\ 0 & \cos\alpha & \sin\alpha \\ 0 & -\sin\alpha & \cos\alpha \end{pmatrix}, R_2(\alpha) = \begin{pmatrix} \cos\alpha & 0 & -\sin\alpha \\ 0 & 1 & 0 \\ \sin\alpha & 0 & \cos\alpha \end{pmatrix}, R_3(\alpha) = \begin{pmatrix} \cos\alpha & \sin\alpha & 0 \\ -\sin\alpha & \cos\alpha & 0 \\ 0 & 0 & 1 \end{pmatrix}$$

are rotation matrices. We took nine independent parameters as, for example,  $\vec{u}_c = (u_c, v_c, w_c)^T$ ,  $u_0, d_0 = (v_0^2 + w_0^2)^{1/2}$ ,  $\theta_0 = \arctan(v_0/w_0)$ ,  $\phi_0 - \omega_z, \omega_x$  and  $\omega_y$ .

As equation (1) is nonlinear in some of the parameters, it was linearized to get the observation equation and solved with iteration.

## 6. Results

### 6.1. Aira

The survey was performed in February - March 2001. The network is shown in Figure 3 left. Three new monuments were used along with a temporary monument. The network includes 2 points for orientation and 1 benchmark. There were 18 target positions on the 10m dish for antenna survey. For network adjustment, 1 set of horizontal angle was used with distance measurements to strengthen the network because Point 2 and 3 were not mutually visible. Point 3 was chosen as origin and 3 to 1 direction as  $v$ -axis. Leveling data was not used in the calculation. The position of VLBI reference point was determined as (6.5431, 41.1339, 9.0602) with s.e. of (0.0007, 0.0006, 0.0011)(unit : m).

### 6.2. Tsukuba

The survey was performed in March 2001. Network is shown in Figure 3 right. Four new monuments around VLBI (32m) and one near GPS (TSKB) were used along with four existing monuments used for instrument calibration. The network includes one triangulation point for orientation (Mt. Tsukuba) and one benchmark. There were 20 target positions on the 32 m dish

for antenna survey. Point 4 was chosen as origin and 4 to 6 direction as u-axis. Leveling was not yet performed. The position of VLBI reference point was determined as  $(35.9808, -51.3111, 18.3028)$  with s.e. of  $(0.0005, 0.0005, 0.0010)$ (unit : m).

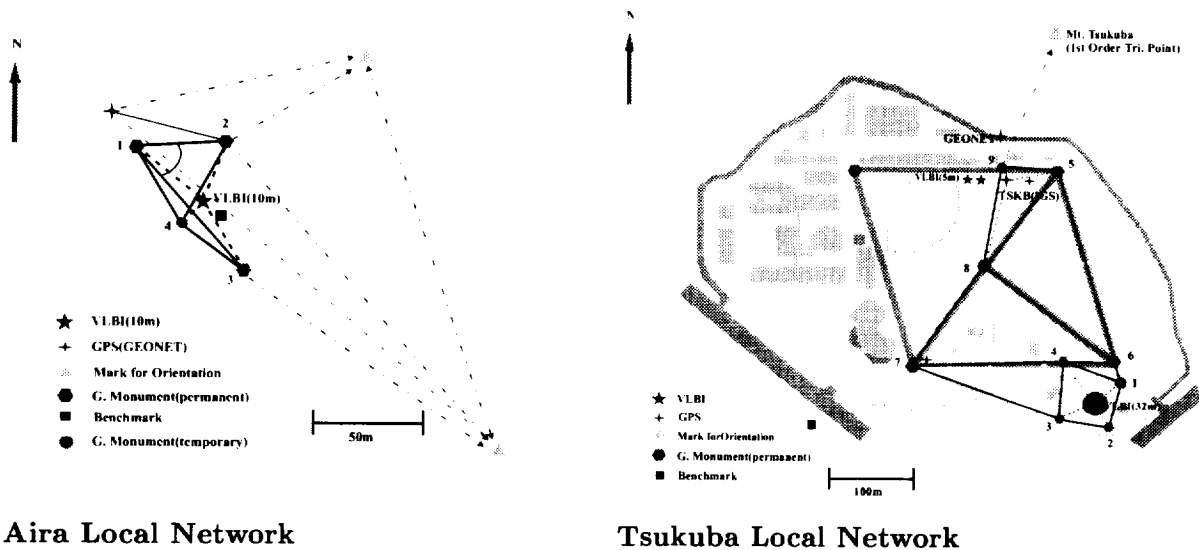


Figure 3. Local Networks

## 7. Conclusions and Future Works

By introducing the Cateye reflector and new ground monuments, we realized the local tie between VLBI and GPS with sub-mm level at two of our VLBI sites and established our standard procedures for it. Future work will include completion of survey at Tsukuba and other VLBI stations, actual comparison of space-geodetic data, annually or seasonally repeated observations to reveal any periodic/systematic variations, and expanding our measurements to collocate with other space-geodetic techniques.

## References

- [1] Long, J. and J. Bosworth, The importance of local surveys for tying techniques together, In: IVS2000 General Meeting Proceedings, NASA/CP-2000-209893, N. R. Vandenberg and K. D. Baver (eds.), 113-117, 2000.
- [2] Matsuzaka, S., M. Ishihara, K. Nemoto, K. Kobayashi, Local tie between VLBI and GPS at Geographical Survey Institute, In: Proceedings of the International Workshop on Geodetic Measurements by the collocation of Space Techniques on Earth, GEMSTONE, CRL, Koganei, Tokyo, Japan, 68-72, 1999.
- [3] Murakami, M., Establishment of the new reference frame of Japan using space geodetic techniques, In: Proceedings of the International Workshop on Geodetic Measurements by the collocation of Space Techniques on Earth, GEMSTONE, CRL, Koganei, Tokyo, Japan, 179-183, 1999.

## Mark 4 Correlator Software: Status and Plans

*Roger Cappallo*

*MIT Haystack Observatory*

*e-mail: rjc@haystack.mit.edu*

### **Abstract**

The Mark 4 Correlator has been operational now for over two years, yet it is still evolving as new features are added. The current capability of the software and its recent enhancements will be discussed, as well as our plans for future improvements.

# The Mark IV Correlator - Faster, Better, Optimal??

A. Mueskens, I. Rottmann, H. Rottmann, A. Höfer, I. Benndorf

Geodetic Institute of the University of Bonn

Contact author: A. Mueskens, e-mail: [geodesy@mpifr-bonn.mpg.de](mailto:geodesy@mpifr-bonn.mpg.de)

## Abstract

We present a detailed efficiency analysis of the various processing stages of an experiment, from the tape shipment phase up to the final release of the correlated datasets. We summarize and evaluate the statistics accumulated for all geodetic experiments processed at the Bonn Correlator during 2001. These statistical data are used to identify “bottlenecks” and weak spots in the processing chain. We propose possible ways of further improving the efficiency of the Bonn correlator in order to match the IVS goals of fast and routine processing of geodetic experiments.

## 1. Introduction

The Bonn correlator is operated jointly by the BKG and the MPIfR and is available for processing of geodetic experiments for 50% of the total available time. In 2001 around 50 geodetic experiments of type IRIS-S, CORE-3, CORE-OHIG, CORE-C, and EUROPE were correlated in Bonn.

Starting in 2001 we have begun to statistically analyze all experiments in terms of how much time was spent in each of the various processing stages. Our goal is to identify the “bottlenecks” in the correlation process and propose ways of minimizing the time needed from observation to final data release.

## 2. Processing at the Bonn Correlator

The processing chain can be divided into the following stages:

- *shipment* - time between shipping the tape from the station and arrival at the Bonn correlator (see Section 3).
- *waiting queue* - time spent on checking the tapes into the local tape library, finding clock delays and waiting for free correlator time.
- *correlation* - time spent on processing, including overhead for tape positioning, synchronization, SU wait states etc.
- *post-correlation* - time spent on fourfitting the data, analysis, preparation of recorrelation files and waiting for free correlator time.
- *recorrelation* - time spent on reprocessing (including overhead).
- *database* - time spent on fourfitting the recorrelated data, analysis, refourfitting, creating a correlator report and submitting the data to the Data Center.

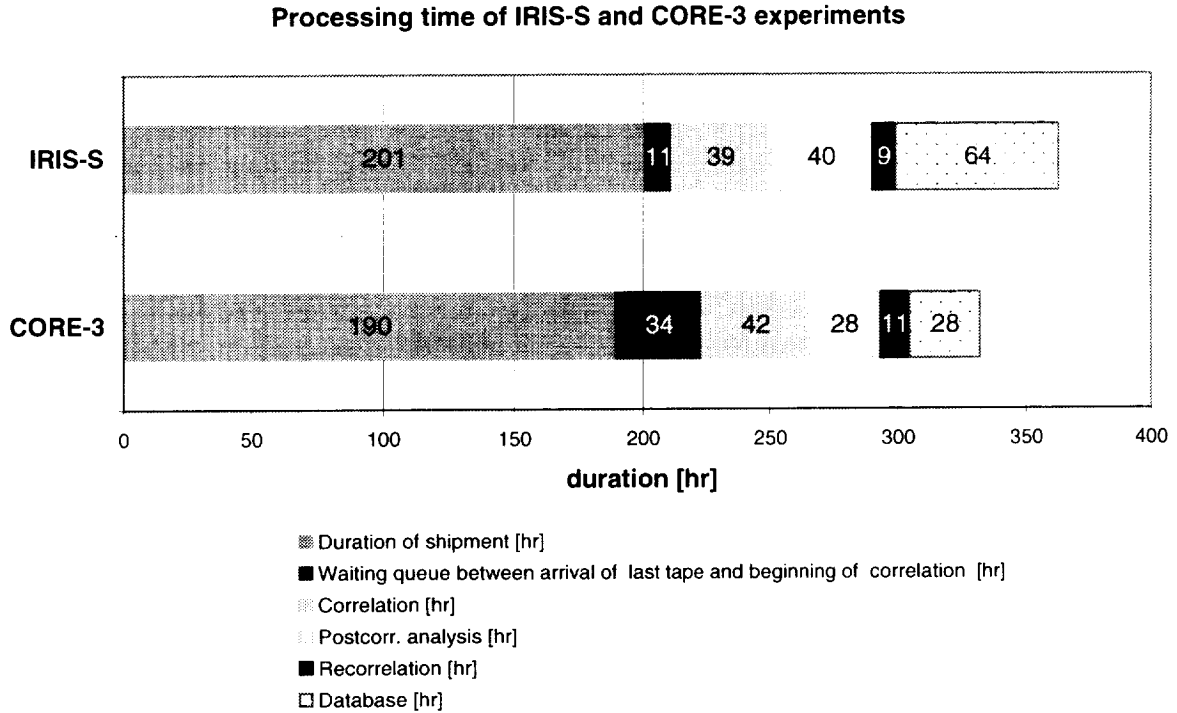


Figure 1. Time spent in the various stages of the processing chain for IRIS-S (top) and CORE-3 (bottom) experiments. Note that the average time for the database release was calculated excluding the C3007 to C3009 experiments. These experiments could not be released after completion due to a delay for a necessary software patch.

The results of the statistical analysis for CORE-3 and IRIS-S experiments are presented in Fig.1. As can be seen, the largest amount of time is spent on tape shipment ( $\approx 200$  hrs) which accounts for  $\approx 50\%$  of the total processing time. We will discuss the tape shipment in greater detail in Section 3. Other time-consuming stages are the correlation and recorrelation. Combined, these steps require  $\approx 50$  hrs which is about a factor of 2 larger than the total duration of the observation (24 hrs). During correlation and recorrelation a considerable amount of time is spent on head positioning, tape changing, synchronization, SU wait states, etc.. These overhead tasks can amount to around 30% of the total correlation/recorrelation duration. The time required to release the database strongly depends on the quality of the observation and correlation. Before the database is released, data problems which have arisen have to be analyzed and solved (if possible). In the case of IRIS-S experiments the post-correlation analysis has resulted in release times of up to 60 hours.

### 3. Tape Shipment

The duration of tape shipment has been calculated separately for each experiment type and station. Note that due to the low number of CORE-C, CORE-OHIG and EUROPE experiments in 2001, we have excluded them from further analysis at this point. These experiment types will be statistically analyzed on a multi-year basis once more data becomes available. Remotely placed network stations like O'Higgins and Syowa naturally take a long time for tape shipment and consequently were not included in the analysis. For the calculation we have taken the day after the observations were finished as the first day of shipment. The day of arrival of the tapes at the Bonn Correlator was taken to be the last day of shipment. Furthermore, we have excluded Saturdays, Sundays and holidays, because usually no pick-up or delivery of the tapes is possible on these days. In the following we will refer to these as *shipment days*.

The results for IRIS-S and CORE-3 experiments can be found in Fig. 2. In the case of IRIS-S we have found that tapes from Hobart (Hh) take the longest (7 shipment days) to get to us. For CORE-3 setups including Medicina (Mc) and Onsala (On) these stations typically take the longest (9 and 6 shipment days respectively) to deliver the tapes to Bonn. CORE-3 setups including Ny Alesund (Ny) instead of Mc and On, result in an average shipment delay of 10 shipment days for Ny tapes.

### 4. Recorrelation - Is It Necessary?

After the initial correlation the fraction of "good" data is typically 80% - 90%. The most common data problems that require recorrelation of a particular scan are:

- the scan duration is too short for unknown reasons
- the scan was not correlated at all
- the scan has a quality code  $FQ = 0$  for unknown reasons
- the scan has quality codes  $FQ = 1-5, A-H$

Looking at the correlation phases outlined in Section 2 it is obvious that recorrelation can significantly decrease the efficiency of data processing. The data have to be inspected in detail prior to recorrelation. Setup files have to be produced and depending on the correlator load the waiting time until recorrelation can be long. Also the involved processing overhead due to tape changing, head positioning etc. is immense for recorrelation as compared to the initial correlation. If recorrelation has to be performed it is therefore desirable to reduce the number of recorrelated scans to a minimum. In order to achieve this goal we have developed a post-correlation analysis tool (*fifi*) that aids the analysts in attributing a particular data problem either to the observing station or the correlation process. By excluding bad station data from the recorrelation a considerable amount of processing time can be saved. On average about half of all "bad" scans are scheduled for recorrelation (around 10 – 20% of the total number of scans). From these about 60% result in good data after reprocessing (see Fig.3 right). We can see that the fraction of bad scans that can be improved due to recorrelation is of the order of a few percent. Taking into account that the time needed for recorrelation is about 25% of the total correlation time (see Fig.3 left), we can conclude that recorrelation is highly inefficient. The processing factor (PF = processing time divided by observing time) of the recorrelation is about a factor of 3 higher than that of the correlation (see Fig. 4). We therefore seriously question the need for recorrelation.

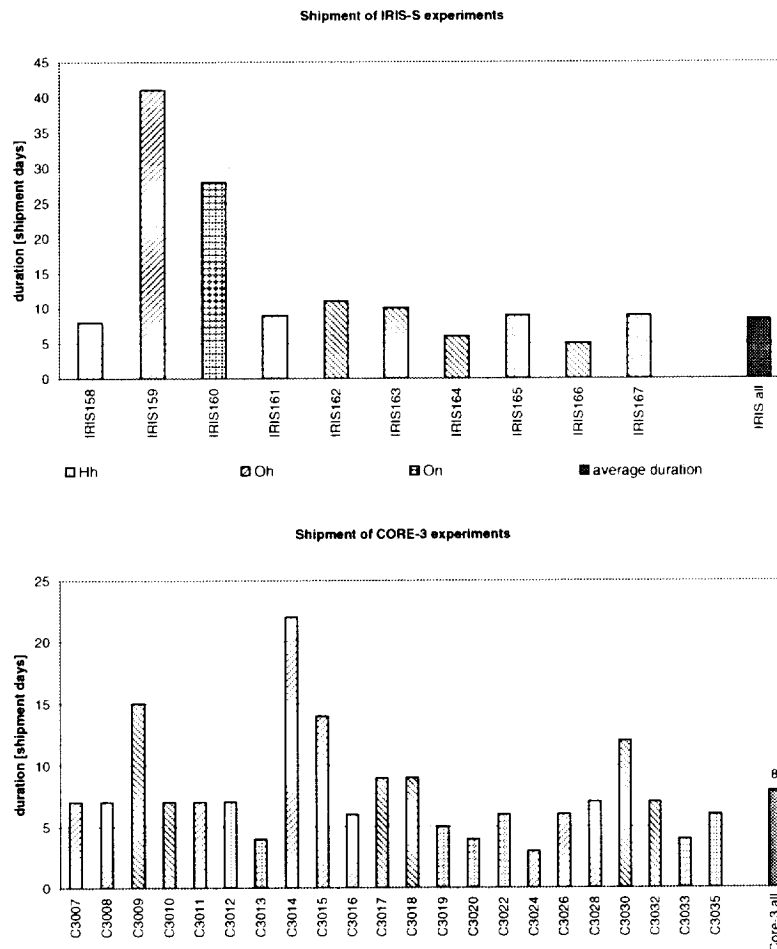


Figure 2. Shipment time for IRIS-S (top) and CORE-3 (bottom) experiments. Each bar corresponds to an individual station with the longest deliver duration. The solid bar at the far right represents the average over all stations.

## 5. Conclusions

Based on the detailed analysis of the processing stages of all IRIS-S and CORE-3 experiments correlated in the year 2001 at the Bonn Correlator the following conclusions can be made:

- The tape shipment requires by far the largest amount of time in the processing chain. Network stations should commit to shipping tapes more efficiently, in order to reduce the delays to a minimum. This is very important and we strongly recommended that all network station strive for a speedy forwarding of recorded media.
- Recorrelation is inefficient. The amount of good data gained by recorrelation is small compared to the considerable amount of time spent on the recorrelation. We therefore seriously question whether recorrelation should be performed routinely in the future. Correlators should decide on the basis of the actual experiment whether recorrelation is reasonable or

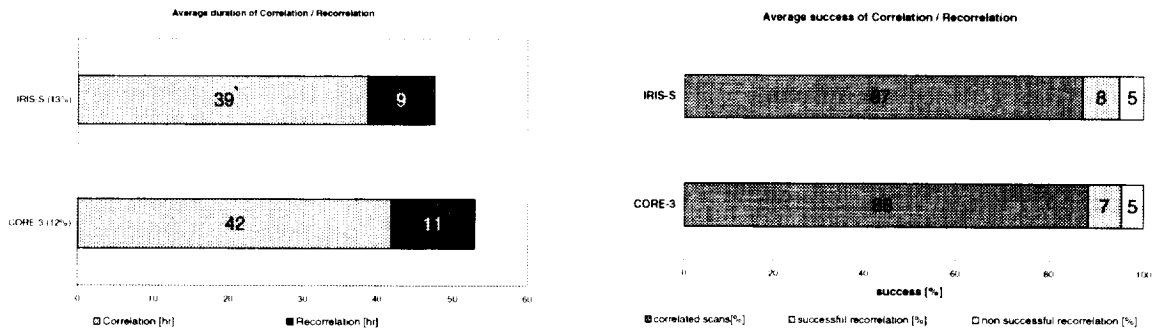


Figure 3. **left:** Total time [hrs] spent on the correlation and recorrelation of IRIS-S and CORE-3 experiments (the percentage corresponds to the fraction of re-correlated scans compared to the total number of scans); **right:** Amount of the good and bad data after correlation and recorrelation (as percentage of the total number of scans);

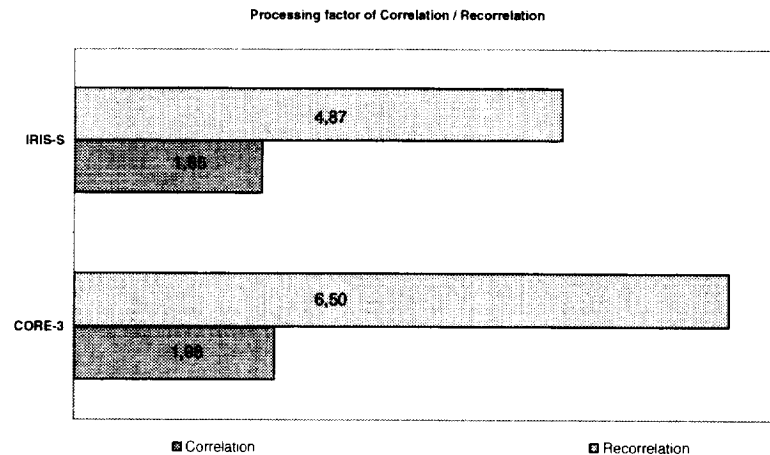


Figure 4. A comparison of processing factors of the correlation and the recorrelation. As can be seen the recorrelation results in processing factor that are worse by a factor of around 3. *Note: recorrelation PF in relation to the initial processing*

essential for further analysis.

- We hope to further speed-up the post-correlation data analysis by developing and improving software tools that aid the analyst in identifying and fixing data problems.
- The IVS recommendations for their products are clear and well constructed. We have to support these goals by challenging our (possibly well-established) procedures and rules.
- Bonn and possibly also other IVS Correlators should routinely collect and analyze efficiency information in the future. We propose to present similar analyzes at the next IVS meeting, to discuss our conclusions, and to possibly make recommendations in order to better meet the requirements of a rapid VLBI service.

## Comparison of the Output of Repeated Mark III and Mark IV Correlation Results

A. Nothnagel, O. Bromorzki, J. Campbell, A. Müskens, H. Rottmann, I. Rottmann

*Geodetic Institute of the University of Bonn*

Contact author: A. Nothnagel, e-mail: [nothnagel@uni-bonn.de](mailto:nothnagel@uni-bonn.de)

### Abstract

During the transition phase from the Mark IIIA to the Mark IV correlator but also at later stages of the maturing Mark IV correlator a number of correlations of the same session was carried out at the MPIFR/BKG Correlator Center in Bonn. Comparisons of the results provide a good insight into the repeatability of the correlation process. It is found that at the latest stage the repeatability of Mark IV correlations in terms of WRMS differences between two correlations is on average on the order of 6 picoseconds (ps) for the X band delay observables and 50 ps for S band. On the other hand, the larger scatter of differences between the results from the “old” and the “new” correlator persists.

### 1. Introduction

The transition from the Mark IIIA to the Mark IV correlator at the MPIFR/BKG Correlator Center (Max Planck Institute for Radio Astronomy/Bundesamt für Kartographie und Geodäsie) in Bonn early in the year 2000 has significantly improved the efficiency and the capacity of routine correlation processes (ALEF ET AL. 2000; ALEF AND MÜSKENS 2001). During the time of the change-over the tapes of an IRIS-S session (IS148, 2000.03.27) with four stations (Wetzell, Westford, Fortaleza and HartRAO) had been ear-marked for multiple correlations with the Mark IIIA and the Mark IV correlator. The purpose of re-correlations was and still is to carry out a quality assessment of the correlators in various stages of their development and maturing. By investigating the repeatability of the correlation results, the accuracy of the correlation process can be characterized.

Following a previous publication of a first comparison of correlation results with the two correlators (MÜSKENS ET AL. 2000) we now present a refined analysis of the correlation results concentrating on the group delay observables. In the meantime four different correlations with different correlator and fringe fitting software for the determination of the delay observables have been carried out (Table 1).

Correlation Label	Correlator and software version	Fringe fitting program and version
A	Mark IIIA	FRNGE
B	Mark IV (2000.06.15)	fourfit V0 (2000.08.02)
C	Mark IV (2000.12.15)	fourfit V3 (2001.08.01)
D	Mark IV (2001.04.19)	fourfit V3 (2001.08.01)

Table 1. Correlation and fringe fitting dates and versions

In the following comparisons all observations with signal-to-noise ratios (SNR) of less than 10 are excluded in order to free the intercompared data from erroneous fringe fitting results due to marginal detection levels and their more arbitrary consequences.

## 2. Mark IIIA (A) versus Mark IV (B)

The first comparison is carried out between the correlation with the Mark IIIA correlator and a correlation with the Mark IV correlator in an early stage of development. Due to different algorithms for the acceptance of accumulation periods, the fringe fitting programs (FRNGE and fourfit) were found to end up with different reference epochs for the individual observations of the Mark IIIA and the Mark IV correlations. Epoch differences could be as large as 3 seconds. It was therefore necessary to apply a suitable interpolation routine in order to determine the delay differences at the median epoch. Here, we used a linear interpolation applying the corresponding delay rates for the transformations to the median epoch before forming the differences. This method worked quite reliably since the scatter in the delay differences did not increase with increasing epoch differences.

Table 2. Group delay differences (Mark IV (B) minus Mark III (A))

Baseline		X band		S band	
		delay bias ps	WRMS ps	delay bias ps	WRMS ps
Fortaleza	- HartRAO	2.5	20.9	38.3	112.2
Fortaleza	- Westford	-2.3	22.7	-1.7	91.2
Fortaleza	- Wettzell	3.3	24.7	-3.4	121.2
HartRAO	- Westford	-7.4	31.5	-16.8	116.4
HartRAO	- Wettzell	-1.1	23.4	12.2	78.7
Westford	- Wettzell	-0.2	16.7	18.7	96.1

Forming the weighted RMS differences of identical scans and excluding observations with SNRs < 10 yielded biases for each baseline for X-band on the order of a few picoseconds (ps) and an average WRMS difference of 23 ps (Tab. 2). At S-band the biases were one order of magnitude larger and the WRMS differences are 103 ps.

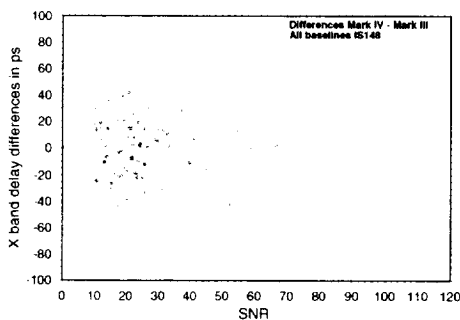


Figure 1. X band delay differences versus SNR

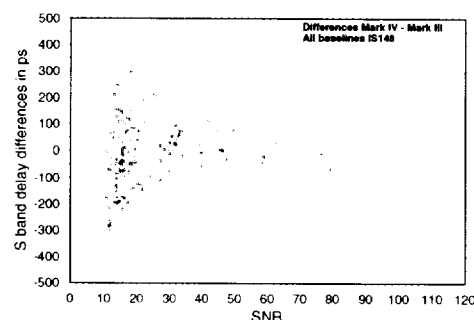


Figure 2. S band delay differences versus SNR

More interesting than the sheer numbers are graphical representations of the differences. While delay differences versus time only show a random scatter, delay differences versus SNR are more informative. Figures 1 and 2 show the X-band and S-band differences versus SNR for all baselines

of the network together.

It is immediately obvious that the scatter is largest at low SNRs with a progressive reduction at higher SNRs. This effect appears in both, X- and S- band, with maximum differences of 100 ps at X-band and of up to 350 ps at S-band. If the same plots are produced for individual baselines, they show identical characteristics though with less data. No baseline dependent effects are seen.

### 3. Mark IV (C) versus Mark IV (D)

The second comparison is carried out for two Mark IV correlations at a very stable stage of the correlator development. The only difference in terms of the procedures used for the Mark IV versus Mark IV comparisons is the fact that here all reference epochs are identical and interpolation is not required. The weighted RMS scatter in the differences amounts on average to 6 ps at X-band and 50 ps at S-band.

Table 3. Group delay differences (Mark IV (D) minus Mark IV (C))

Baseline	X band		S band	
	delay bias	WRMS	delay bias	WRMS
	ps	ps	ps	ps
Fortaleza – HartRAO	0.26	7.1	-8.3	53.7
Fortaleza – Westford	-0.30	5.3	1.7	48.5
Fortaleza – Wettzell	0.49	7.7	-9.0	60.3
HartRAO – Westford	0.93	6.1	4.5	37.0
HartRAO – Wettzell	0.65	6.9	9.4	59.6
Westford – Wettzell	0.39	4.9	-3.0	41.8

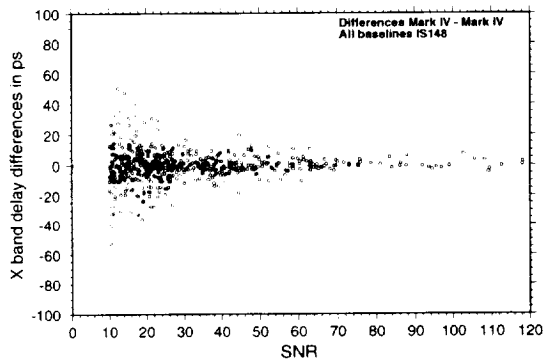


Figure 3. X band delay differences versus SNR for all baselines.

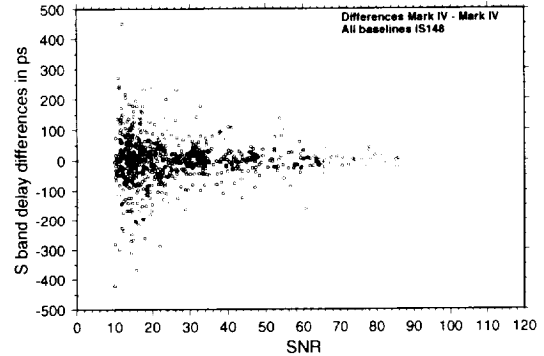


Figure 4. S band delay differences versus SNR for all baselines

We see that the scatter in the differences is much smaller than in the case of the Mark IIIA – Mark IV comparison. Looking at the graphical representation of the differences we see a similar pattern as in the previous case. From a correlator/fringe fitting point of view it should be expected that the reliability of the delay determination increases with higher SNR. In addition, the lower the SNR the higher the formal error and, thus, the smaller the impact on the geodetic parameter estimation process. To test this, the delay differences were normalized with their formal errors. Figures 5 and 6 show the corresponding distributions for X- and S-band which show only slightly hyperbolic envelopes. This is a good indication that there are no remaining systematic effects beyond the random variations in the delay observables which depend only on the SNR.

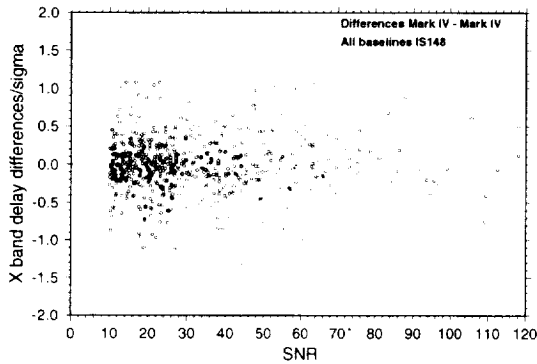


Figure 5. Normalized X band delay differences versus SNR

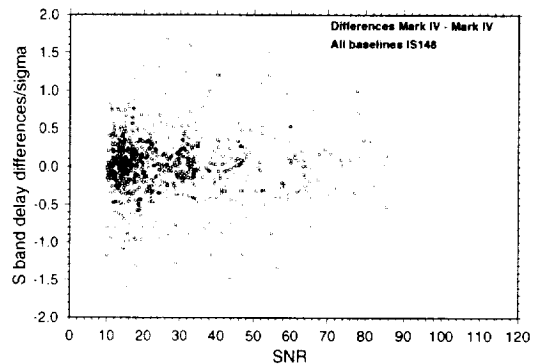


Figure 6. Normalized S band delay differences versus SNR

#### 4. Mark III (A) versus Mark IV (D)

In April 2001 when the last one of this series of Mark IV correlations (D) was carried out, the Mark IV correlator had reached a certain level of maturity as compared to the time of the first Mark III – Mark IV comparison. It is, therefore, quite interesting to see whether the improvements in the correlator software in the years 2000 and 2001 have brought the Mark IV results closer to the original Mark IIIA correlator output. Table 4 lists the results of the comparisons.

Table 4. Group delay differences (Mark IV (D) minus Mark III (A))

Baseline	X band		S band	
	delay bias	WRMS	delay bias	WRMS
	ps	ps	ps	ps
Fortaleza – HartRAO	1.5	20.3	9.1	130.9
Fortaleza – Westford	-0.6	21.9	-3.5	105.5
Fortaleza – Wettzell	0.8	22.9	-26.3	101.0
HartRAO – Westford	-4.5	27.7	-17.4	113.3
HartRAO – Wettzell	-2.5	20.2	20.8	93.5
Westford – Wettzell	-0.6	13.4	0.6	95.1

These numbers do not differ very much from the comparison of the Mark IIIA correlation with the early Mark IV correlation as listed in table 2, although for S-band the WRMS scatter is even a bit larger here. The same holds true for the graphical representations as depicted in figures 7 and 8.

#### 5. Conclusion

In conclusion it can be stated that none of the comparisons showed any systematic differences between any two correlations carried out in this project. The biases found are not significant considering the corresponding WRMS noise and, hence, do not degrade the quality of the correlations.

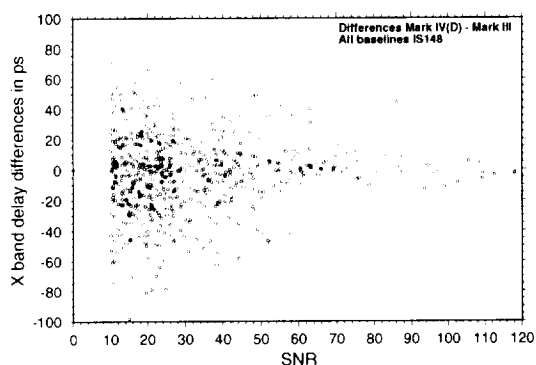


Figure 7. X band delay differences versus SNR for all baselines.

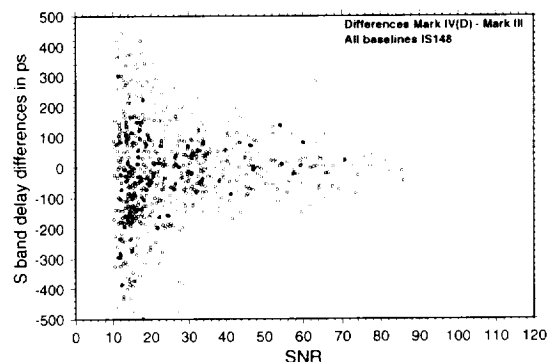


Figure 8. S band delay differences versus SNR for all baselines

If we assume that the hard- and software of the Mark III and the Mark IV correlators are of equal quality the correlations with the two correlators may be seen as repeated processes and the differences can be considered as representing an external repeatability of two different correlators. The comparison of the original Mark IIIA correlation with two Mark IV correlations at different development stages has shown that all of the software improvements between June 2000 and April 2001 have not reduced the level of the noise in the differences. The WRMS scatter of the differences of about 21 ps at X-band and about 100 ps at S-band persists even after all initial flaws of the Mark IV correlator software have been eliminated.

With the comparison of two Mark IV correlations which were carried out at a relatively stable period of correlator hard- and software, we are able to quantify an internal repeatability induced by one and the same correlator. The WRMS scatter is only 6 ps at X-band and 50 ps at S-band with the typical reciprocal dependency on the SNR level.

Low SNR observations are always affected by higher uncertainties, but although the reduced weights of the observations in the geodetic parameter estimation process take care of this deficit, the measured delays may still be off by several tens of picoseconds or more. Therefore, we strongly suggest that in the design of observing schedules more emphasis is placed on higher SNR rather than to have as many observations as possible with short duration and low SNR.

## References

- Alef W., D.A. Graham, J.A. Zensus, A. Müskens, W. Schlüter (2000): The New MPIfR-BKG MkIV Correlator, *Proceedings of the 14th Working Meeting on European VLBI for Geodesy and Astrometry*, Castel San Pietro Terme, Istituto di Radioastronomia, Bologna, 111–118
- Alef A., A. Müskens (2001): Status of the MPIfR-BKG MKIV Correlator, *Proceedings of the 15th Working Meeting on European VLBI for Geodesy and Astrometry*, Barcelona, IEEC
- Müskens A., K. Börger, M. Sorgente, J. Campbell (2000): Comparisons of MkIII and MkIV Correlation using a 4-Station IRIS-S Experiment *Proceedings of the 14th Working Meeting on European VLBI for Geodesy and Astrometry*, Castel San Pietro Terme, Istituto di Radioastronomia, Bologna, 125–136

## Comparison of the VLBI Observables from Mk3 and Mk4 Correlation of a 24-hour Geodetic Experiment

*Brian Corey, Michael Titus*

*MIT Haystack Observatory*

*Contact author: Brian Corey, e-mail: [bcorey@haystack.mit.edu](mailto:bcorey@haystack.mit.edu)*

### Abstract

Data from geodetic experiment CORE-B605 were processed on a Mk3A and a Mk4 correlator, and the resulting X-band delays, rates, and fringe amplitudes were compared. The scatter in multiband delay differences is larger than expected. Time series of phase delay differences exhibit geometry-dependent systematic variations of a few ps. The singleband delay differences have baseline-dependent biases as large as 5-8 ns. Mk4 fringe amplitudes are generally 2-5% lower than Mk3.

### 1. Introduction

This report presents the preliminary results of a comparison of the primary geodetic VLBI observables generated from correlation of a 24-hour geodetic experiment on a Mk3 and a Mk4 correlator. A similar study is reported by Nothnagel *et al.* [2] in these proceedings.

### 2. Geodetic Session

The geodetic experiment selected for multiple correlation is CORE-B605 (CB605), which was recorded on 4-5 October 1999. Fourteen frequency channels, each 2 MHz wide, were 1-bit sampled and recorded on tape. The “narrowband” geodetic frequency sequence was used, with eight X-band channels spanning 360 MHz and six S-band channels spanning 85 MHz. Seven stations participated, but one station (Yellowknife) was not included in the Mk4 correlation. The six stations that were processed on both correlators are: Algonquin Park 46m, Canada; DSS65 34m, Spain; Fortaleza 14m, Brazil; Kashima 26m, Japan; Kokee Park 20m, Hawaii, U.S.; and Onsala 20m, Sweden.

### 3. Correlation and Fringe-fitting

Correlation of CB605 was done on the Mk3A and Mk4 correlators at Haystack Observatory in November 1999 and July 2000, respectively. The Mk3A [3] has a baseline-based XF architecture, and the Mk4 [4] has a station-based XF design. CB605 was correlated with 8 lags on the Mk3A and 32 lags on the Mk4. The time tags associated with the accumulated Mk3 correlator data are the wavefront arrival times at the reference station, which is the first station in the baseline name; the Mk4 time tags are the hypothetical wavefront arrival times at the center of the Earth.

The Mk3 and Mk4 correlator data were fringe-fit with programs `mk3fit` and `fourfit` in November 1999 and January 2002, respectively. Fringe phases were aligned across frequency channels using the 10 kHz phase cal tones, except for Kokee S- and X-band and DSS65 X-band, which were fringed with manual phases due to phase cal instabilities. The same manual phases and additive

phase cal corrections were used in Mk3 and Mk4 fringing. In order to allow geodetic analysis programs designed for Mk3 data to work with Mk4 data, `fourfit` converts the total delay and rate observables from the geocentric frame of the Mk4 correlator to a Mk3-style reference station frame. The Mk4 data for each scan were fringe-fit with the fringe reference time (FRT) forced to be the same as the Mk3 FRT.

#### 4. Comparison of Observables

Differences in the Mk3 and Mk4 results can be expected if the time spans of the data read from the VLBI tapes in the two correlations are not identical due to, *e.g.*, differing playback quality or tape synchronization times. In order to minimize this effect, only scans for which the total amounts of Mk3 and Mk4 correlator data differed by  $<10\%$  were included in the comparisons.

Analysis to date of the results has concentrated on the Mk4-Mk3 differences in the total (correlator model + residual to model) X-band multiband delay (MBD), singleband delay (SBD), phase delay, and delay rate, and on the X-band fringe amplitude ratios. Figure 1 shows the time series of the differences and ratios of the five observables for two representative baselines that have significantly different sensitivities. It is obvious from figure 1 that, for all the observables except phase delay, the larger the error in the undifferenced data, the larger the scatter in the differences.

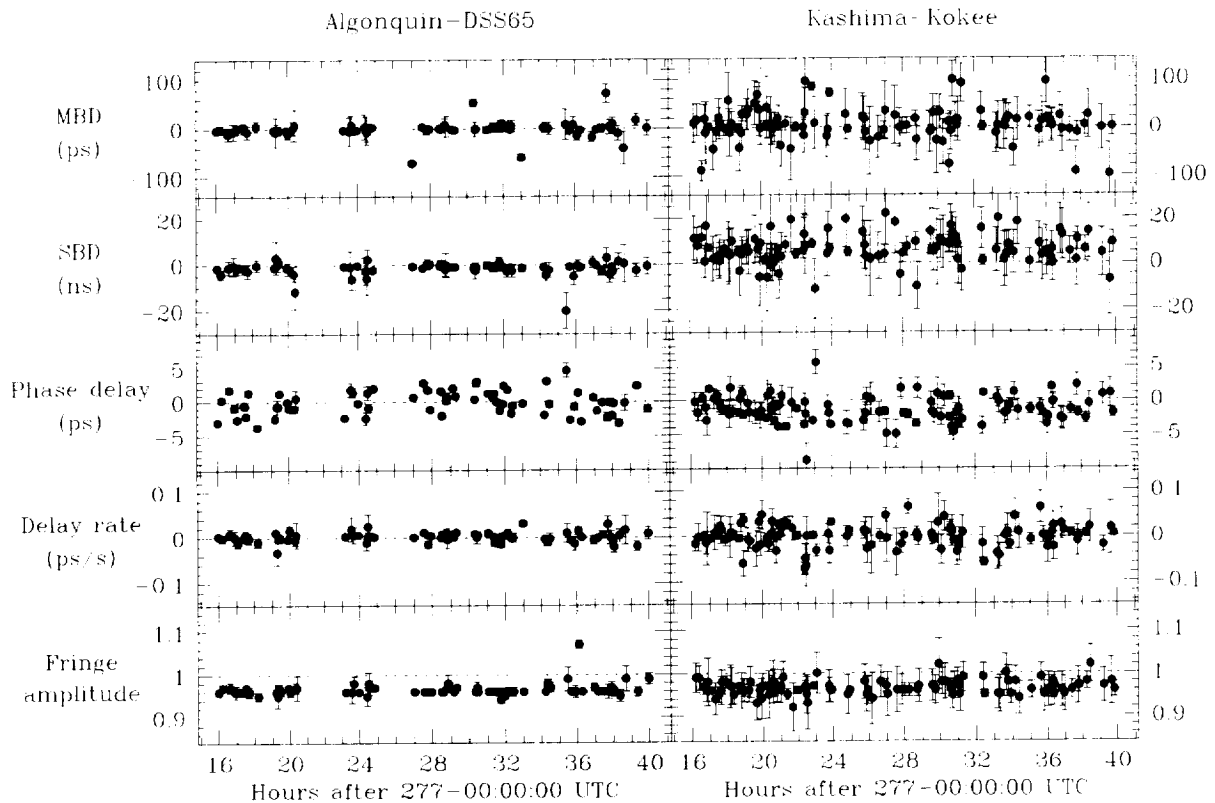


Figure 1. Mk4-Mk3 X-band delay and rate differences and Mk4/Mk3 X-band fringe amplitude ratios for the Algonquin-DSS65 (left) and Kashima-Kokee (right) baselines. Only data with  $\text{SNR} > 15$  are shown. Error bar =  $\sigma_u$  (see text for definition).

In the remainder of this paper,  $\sigma_u$  refers to the smaller of the two standard errors for the *undifferenced* Mk3 and Mk4 observables that go into each difference or ratio.

#### 4.1. Multiband Delay

The relationship between MBD difference and SNR is shown in the lefthand panel of figure 2. (For the CB605 X-band sequence, SNR is related to the standard error  $\sigma_{MBD}$  of the undifferenced MBD by  $\sigma_{MBD} = 1135 \text{ ps/SNR}$ .) There appear to be two fairly distinct populations: (1) the majority of points, which lie between, or close to, the  $\pm 1\sigma_u$  curves and whose scatter scales inversely with SNR, and (2) outliers whose magnitude of 50-100 ps is nearly independent of SNR. The distribution of the majority, after scaling by  $\sigma_u$ , is well described by a normal distribution. A useful statistic, suggested by A. Niell, for estimating the scatter relative to  $\sigma_u$  in a manner less sensitive to outliers than the  $\chi^2$  statistic is the value of  $S$  for which  $|\Delta\text{MBD}/\sigma_u| < S$  for 68% of the points. This is the percentage of points in a normal distribution that lie within  $1\sigma$  of the mean, so if  $\Delta\text{MBD}$  were distributed normally with standard deviation  $\sigma_u$ ,  $S$  would be unity. The actual value of  $S$  is 0.64.

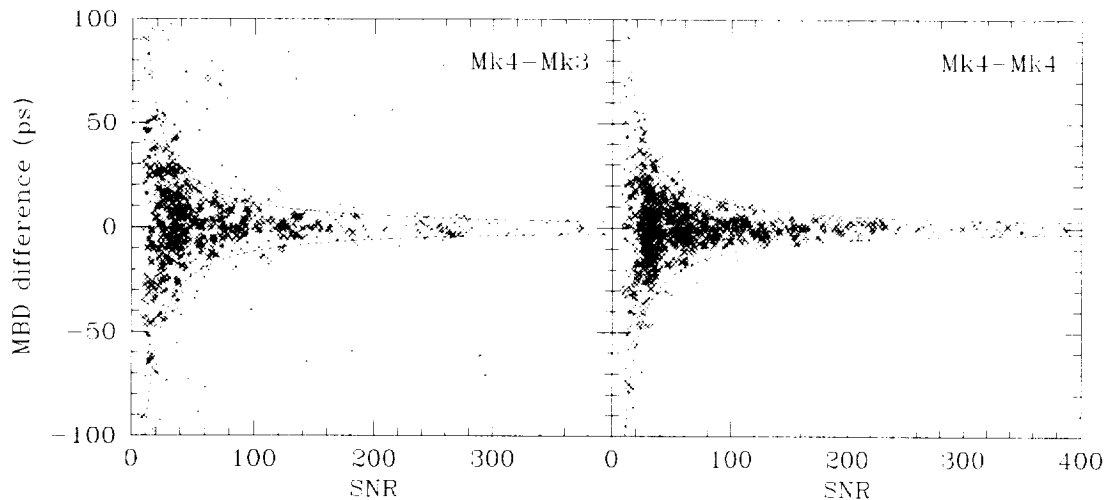


Figure 2. X-band MBD difference *vs.* SNR for all baselines. SNR shown is lesser of two SNRs of undifferenced data. Dotted curves are  $\pm 1\sigma_u$ . *Left:* Mk4-Mk3 differences. *Right:* Differences from fringing each set of Mk4 correlator data twice, once with central 60 seconds of data and once with central 48 seconds.

A dependence of the observable differences on SNR is to be expected if the time spans of the correlator data differ. In order to simulate the effects of disjoint input data, 907 Mk4 scans were fringed using first the central 60 seconds of data and then just the central 48 seconds. The Mk4-Mk4 differences are shown in the righthand panel of figure 2. Their scatter is smaller than for Mk4-Mk3:  $S = 0.49$ , which is close to the value of 0.45 calculated under some simple but reasonable assumptions for the case of two input data sets differing by 20% (12 seconds out of 60). But the disparity in integration time is larger, not smaller, for Mk4-Mk4 (20%) than for Mk4-Mk3 (a maximum of 10%). So the Mk4-Mk3 scatter is greater than can be explained simply by differences in the input data sets.

The outliers, which can also be seen in the top panels of figure 1, are distinctive for their large  $|\Delta\text{MBD}/\sigma_u|$  ratio. Nine scans from four baselines with  $|\Delta\text{MBD}/\sigma_u| > 8$  and  $|\Delta\text{MBD}| > 50$  ps were investigated by examining the two sets of fringe plots and by refringing portions of the data. We were unable to identify the cause for any of the large discrepancies. Mk4 recorrelation of the scans in February 2002 yielded MBDs that agreed to within 2 ps with the original values. One of the scans happened to have been correlated three times on the Mk3 processor; even though the integration time ranged from 45 to 65 seconds in the three tries, the total spread in MBD was only 12 ps, which is much less than the Mk4-Mk3 difference. The S-band MBDs are too imprecise to provide a complementary comparison. In sum, the outliers remain a mystery.

For all 15 baselines that were processed, the bias in the MBD differences is small compared with the rms scatter, with bias typically  $<10\%$  the rms scatter.

## 4.2. Singleband Delay

Unlike the MBD, the SBD differences exhibit significant biases on some baselines, particularly those involving Kokee (see figure 1), for which the biases are 5-8 ns. Of all six stations, Kokee happened to have the largest residual SBD ( $\sim 50$  ns) relative to the correlator model in both correlations. Large SBD residuals can lead to systematic errors in the SBD, phase delay, and fringe amplitude due to the limited number of correlator lags available [1]. A 50-ns correlator residual is too small to cause a 5-ns SBD error on either the Mk3 or Mk4 correlator, however.

The rms scatter in SBD differences about the baseline means is 5 ns. A normal distribution agrees very well with the distribution of SBD differences adjusted by the baseline means and scaled by  $\sigma_u$ . As a fraction of  $\sigma_u$ , the SBD scatter about zero on non-Kokee baselines is given by  $S = 1.0$ .

## 4.3. Phase Delay

Unlike the other four observables considered here, the scatter in the phase delay differences is approximately the same on all baselines and is independent of SNR. Displaying all the data for a baseline together in one plot, as in figure 1, obscures the fact that there are systematic trends for individual sources. In figure 3, attention is restricted to two sources, 0552+398 and 4C39.25, on two independent baselines. The declinations for these sources differ by  $<1^\circ$ . In the bottom two panels of figure 3, the 0552+398 points have been shifted 3.53 hours to the right from their correct position, to simulate moving 0552+398 across the sky to the same right ascension as 4C39.25. Note how closely the two sources, now forced to be in nearly the same location on the sky, track each other. Similar behavior is observed on other baselines and with other sources. Clearly the delay differences are related to the source/baseline geometry, as reflected in the correlator model. This is most surprising, as total quantities should be insensitive to the model. The magnitude of the delay differences is generally  $<5$  ps, or  $<15^\circ$  in phase. If such systematic variations are present at the same level in the MBD, they are too small to be detected there, as least with this data set.

## 4.4. Delay Rate

The delay rate differences have small biases relative to the scatter, with mean values of only a few fs/s on most baselines. There is no evidence of systematic trends with source. The scatter increases with  $\sigma_u$ , but the distribution of  $\Delta\text{rate}/\sigma_u$  deviates from a normal distribution in the excessive number of points in the tails of the distribution. The same is true of Mk4-Mk4 rate differ-

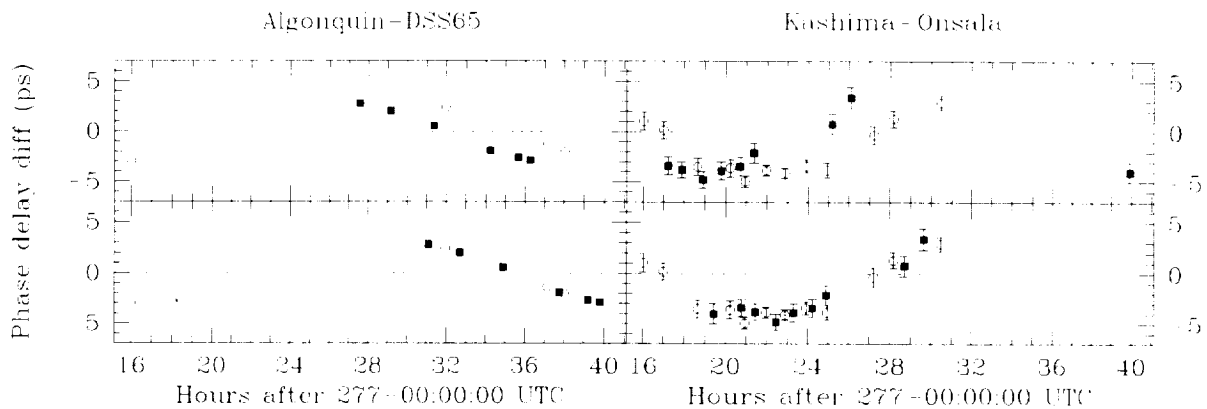


Figure 3. Time series of Mk4-Mk3 phase delay differences for 0552+398 (solid squares) and 4C39.25 (open circles) on the Algonquin-DSS65 (left) and Kashima-Onsala (right) baselines. 1 ps delay  $\Leftrightarrow$   $3.0^\circ$  fringe phase. Error bar =  $\sigma_u$ . Error bars for Algonquin-DSS65 are smaller than plot symbols. *Top*: Original data. *Bottom*: Epochs of the 0552+398 points have been shifted by the RA difference for the two sources.

ences created in the same manner as the Mk4-Mk4 MBD differences. The cause is almost certainly temporal phase variations induced by propagation media effects with a red noise spectrum; small differences in the data span analyzed can lead to relatively large changes in the estimated rate. The value of  $S$  for the Mk4-Mk3 differences is 1.0.

#### 4.5. Fringe Amplitude

On almost all baselines, the Mk4 fringe amplitudes are systematically biased 2-5% lower than the Mk3 (see figure 1). The only definite exception is Fortaleza-Kokee, for which the mean Mk4/Mk3 ratio is  $0.996 \pm 0.005$ . With correlator residual delays smaller than 100 ns, biases in the Mk3 amplitudes due to the finite number of lags should be  $<1\%$  [1]; Mk4 biases should be even smaller.

#### References

- [1] Herring, T.A., Precision and Accuracy of Intercontinental Distance Determinations Using Radio Interferometry, Ph.D. thesis, M.I.T., 1983.
- [2] Nothnagel, A., O. Bromorzki, J. Campbell, A. Müskens, H. Rottmann, and I. Rottmann, Comparisons of the Output of Repeated Mark III/IV Correlations, in IVS 2002 General Meeting Proceedings, NASA/CP-2002-210002, N. R. Vandenberg and K. D. Baver (eds.), xx-yy, 2002.
- [3] Whitney, A.R., Capabilities and Performance of the Upgraded Mark III Correlator System, in The Earth's Rotation and Reference Frames for Geodesy and Geodynamics, A.K. Babcock and G.A. Wilkins (eds.), 429-437, 1988.
- [4] Whitney, A.R., R. Cappallo, W. Aldrich, B. Anderson, A. Bos, J. Casse, J. Goodman, S. Pogrebenko, R. Schilizzi, and D. Smythe, The Mark 4 VLBI Correlator: Architecture and Algorithms, in preparation.

## Status of the KSP VLBI Stations and IMT-2000 Interference

Jun Amagai<sup>1</sup>, Hitoshi Kiuchi<sup>1</sup>, Yasuhiro Koyama<sup>2</sup>, Mamoru Sekido<sup>2</sup>,  
Ryuichi Ichikawa<sup>2</sup>, Tetsuro Kondo<sup>2</sup>, Taizoh Yoshino<sup>2</sup>, Koichi Sebata<sup>1</sup>

<sup>1</sup>) *Communications Research Laboratory*

<sup>2</sup>) *Kashima Space Research Center/Communications Research Laboratory*

Contact author: Jun Amagai, e-mail: amagai@crl.go.jp

### Abstract

Two Keystone project (KSP) VLBI stations operated by the Communications Research Laboratory (CRL) have been closed, and the antennas and facilities have been moved to Hokkaido and Gifu Universities. VLBI observation at the Koganei station revealed radio interference at 2.14 GHz. The source of the interference was found to be IMT-2000 signal.

### 1. KSP/VLBI Closed

Since 1996, the Communications Research Laboratory has conducted the Keystone Project to monitor crustal deformation around the Tokyo metropolitan area using three space geodetic techniques, VLBI, SLR, and GPS. We made real-time VLBI observations every other day using a high-speed ATM network since June 1997. A remarkable crustal deformation caused by the volcanic activity on Miyake-jima Island was detected by the KSP-VLBI network in July 2000.

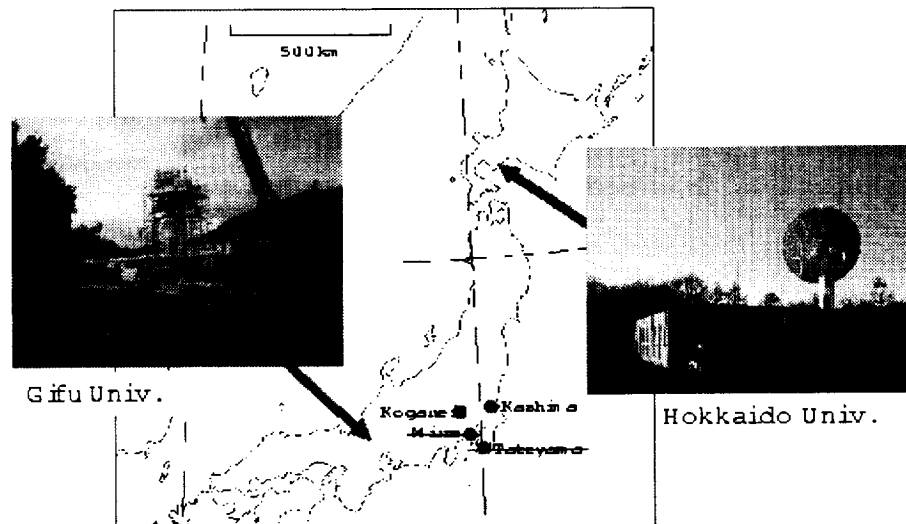


Figure 1. Locations of the stations.

Though CRL had planned to close the project by the end of 2000, we closed only the Miura station as scheduled, and continued routine VLBI observation using the Koganei, Kashima and Tateyama stations until the end of November 2001 to monitor crustal deformation after the event.

After closing stations, 11 m antennas and VLBI facilities used in the Miura and Tateyama stations were moved to Hokkaido University and Gifu University respectively and will be used for astronomical observations (Figure 1). The Koganei and Kashima stations are continuously maintained by CRL and used for R & D experiments.

## 2. IMT-2000 interference

Recently, VLBI observation at the KSP Koganei station experienced quite heavy radio interference in the S-band. Figures 2 (a) and (b) show the spectra of the RF and IF signals received at the Koganei station. We can see heavy interference at 2.14 GHz. The RF low noise amplifier (LNA)

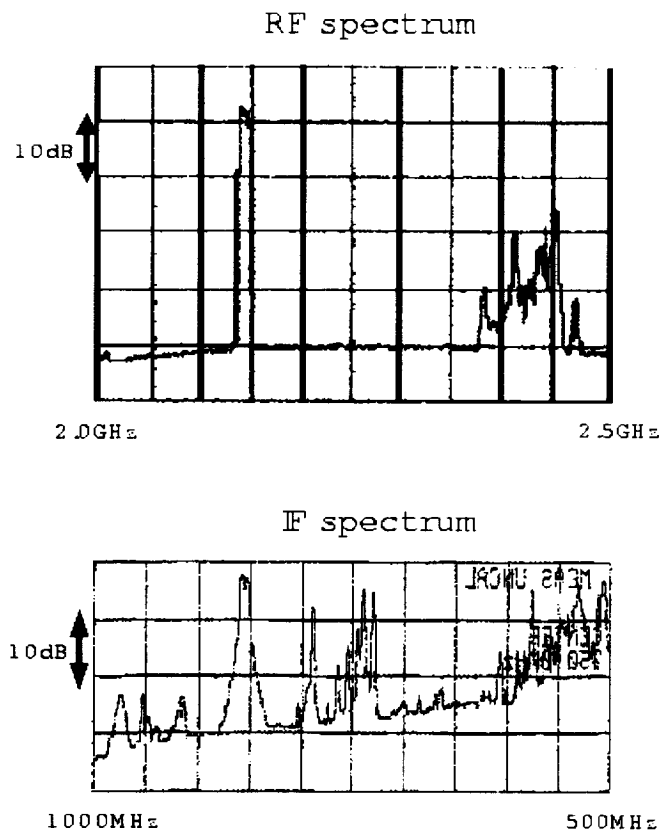


Figure 2. (a) Spectrum of RF signals obtained when the antenna was directed toward the zenith at a maximum hold integration of 30 minutes. (b) Spectrum of IF signals obtained using maximum hold integration during 24 hours of VLBI observation.

was not saturated, while the IF amplifier was saturated and the noise floor level of the amplifier was suppressed. We were forced to change the frequency arrangement to avoid this interference. Though a filter is needed after the LNA to avoid IF saturation, we have not yet found a suitable one.

We investigated the source of the interference and found that it was a signal that came from

Table 1. Specifications of IMT-2000 station near KSP Koganei station

Frequency	2137.6 - 2147.4 MHz (50 bands with 200 kHz spacing)
Modulation	G7W
Transmit power	16 W max
Antenna gain	21 dB
Antenna height	57.8 m

the antenna of a telecommunication company, 900 m from the Koganei station. On July 2, 2001, the company started transmitting IMT-2000 test signals, and since then the interfering signal has jammed our observation signal. The specifications of the transmission station are listed in Table 1. The incident power flux of the signal at our antenna is estimated to be very high. It is expected the IMT-2000 network will be extended to every major city in Japan before April 2002. Since other countries will face a similar situation, VLBI stations in many countries will likely be jammed by IMT-2000 signals and be forced to take measures to deal with the interference. We need to investigate the frequency band suitable for geodetic VLBI.

## References

- [1] IMT-2000: The global-standard for third generation wireless communications (<http://www.imt-2000.org/portal/index.asp>).

## Metsähovi Geodetic VLBI Station: Status Report

*Matti Paunonen*

*Finnish Geodetic Institute*

*e-mail:* `Matti.Paunonen@fgi.fi`

### Abstract

The astronomical VLBI system of the Metsähovi Radio Observatory of the Helsinki University of Technology is being upgraded also for geodetic work by adding five baseband converters, a cooled S/X receiver, a removable subreflector and the cable delay and phase calibration units. The station is situated 40 km west from Helsinki.

The Cassegrain telescope with a radome has a primary paraboloid dish with a diameter of 13.7 m and a focal length of 5.08 m, and a removable secondary mirror (a hyperboloid with a diameter of 1.7 m, an eccentricity of 1.5562, and an interfocal distance of 3.17 m) to be constructed from carbon fiber reinforced plastic. The cooled, axially positioned and removable, S/X receiver (15 K) and feed will be constructed by a Spanish company TTINorte. The cable delay calibrator will be of own design and the existing antenna unit for phase calibration is from Istituto di Radioastronomia, Italia. The existing data acquisition terminal is of type VLBA4. The estimated position of the antenna in ITRF2000 (Epoch 1997.0) is according to the survey in 1994:  $x = 2892585.59$ ,  $y = 1311715.33$ ,  $z = 5512639.81$ . The name METS 7601 in the IERS ITRF2000 VLBI catalog refers to the site named Sjökölla about 3 km North, where a mobile MV-3 instrument took five one-day-long observations in 1989.

The geodetic VLBI system will be an important addition to the existing space geodetic and related instrumentation at the Metsähovi Geodetic Observatory of the Finnish Geodetic Institute (GPS, GLONASS, SLR, DORIS, a superconducting gravimeter, an absolute gravimeter, and a seismometer). Initial test measurements are expected within this year.

# Session 4. New Technology Developments in VLBI





# VSI Interface Implementation, Performance Enhancement of Gbps VLBI Instruments

*Junichi Nakajima, Yasuhiro Koyama, Tetsuro Kondo, Mamoru Sekido, Moritaka Kimura, Hiroshi Okubo, Hiroo Osaki*

*Kashima Space Research Center, Communications Research Laboratory*

*Contact author: Junichi Nakajima, e-mail: nakaji@crl.go.jp*

## Abstract

Communications Research Laboratory had intensively performed implementation of the VSI (VLBI Standard Interface) and popularization. As a Technology Development Center of the IVS (International VLBI Service), this is the first attempt to adapt the VSI to existing VLBI system. The VSI modifications of the former CRL VLBI system proved the Gbps performance both in tape based observation and real-time observation. The VSI functional block concept also enabled flexible system integration and future enhancement to PC-based VLBI. Realization of the VSI compatibility in telescopes will bring further strength to the worldwide VLBI observation network which used in astrometry and geodesy. As well as several astronomy dedicated VLBI systems, the VSI-based VLBI will increase the network potential. In other words, Gbps compatibility between different systems will be difficult without VSI.

## 1. Introduction

After the endorsement of VSI-H (VLBI Standard Interface - Hardware) [8] in August 2001 by the International VLBI Service, VLBI is promised further evolution in this decade through the VSI interface. In former VLBI systems, the hardware is almost isolated from each other since each VLBI system had been designed for its own scientific objective and technology prepared by the each group. Thus the interface specification is satisfied internally. However, to realize the VLBI observation using a different system, the whole particular system installation at the telescope is required. This strongly limits the flexibility of VLBI telescope resources. The first step to solve this inconvenience, VSI-H allows researchers to connect multi-national and multi-vendor instruments. Second step VSI-S (VLBI Standard Interface- Software) which will control DAS (Data Acquisition System), DIM (Data Input Module), DOM (Data Output Module) and DPS (Data Processing System), and DTS (Data Transmission System; kind of media or fiber) in same manner. Here the DAS, DIM, DOM, DPS and DTS are the abstracted system in the VSI. The researcher can make the best use of VSI instruments in the target station and minimum effort is needed in preparation. For example, if the target VLBI station is using different VLBI acquisition system and recorder. VSI based media conversion will enable correlation between the stations playback. If a special sampling mode is needed in a planned observation only the DAS part sent to the target station will satisfy the VLBI objective.

## 2. VSI Popularization

VSI popularization is one important role of the Technology Development Center (TDC) [2] and contribution of VLBI development to the scientific communities. Since VLBI has been thought

of as a technology which uses specially designed high speed hardware and original software to process data, the promotion of the VSI concept and simple introduction are important to increase the popularity of VSI. Otherwise, it is difficult to let other researchers use VSI as a convenient interface. CRL has prepared short presentations and education material introducing the VSI trends to domestic engineers, scientists and graduate students. Distribution of sample VSI cables and brochures about VSI have attracted attentions [6]. Since VSI is becoming the de-facto standard, we also aim for formal standardization in the JIS (Japan Industrial Standardization) as a step to ISO standard.

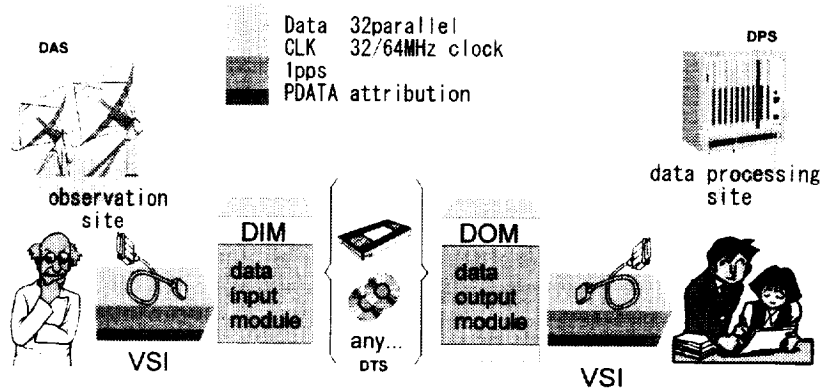


Figure 1. Pictorial drawing to introduce VSI-H to beginners



Figure 2. GBR-1000 (right) VSI adapted Gbps recorder and GBR2000D(left), the VSI native data recorder and related VSI components (AD sampler, Burst memory and Switcher) are shown.

### 3. Development

In developments through 2001, all present Gbps VLBI system had adapted to VSI interfaces. Most of the Gbps VLBI system interfaces designed in 1990s are using ECL interfaces [4] [5]. Simple VSI level converters between the ECL and LVDS (Low Voltage Differential Signal) were developed. For convenience, a VSI switcher is produced too. New 1 Gbps (1ch, 2bit) VSI AD samplers are fully operational. A brand new VSI native Gbps data recorder GBR-2000D in Figure 2 has started operation too. These VSI functional units are summarized in Table 1 and 2. Although the slow speed IP-VLBI board is not VSI-compatible, the onboard AD PCI card, which becomes popular, is

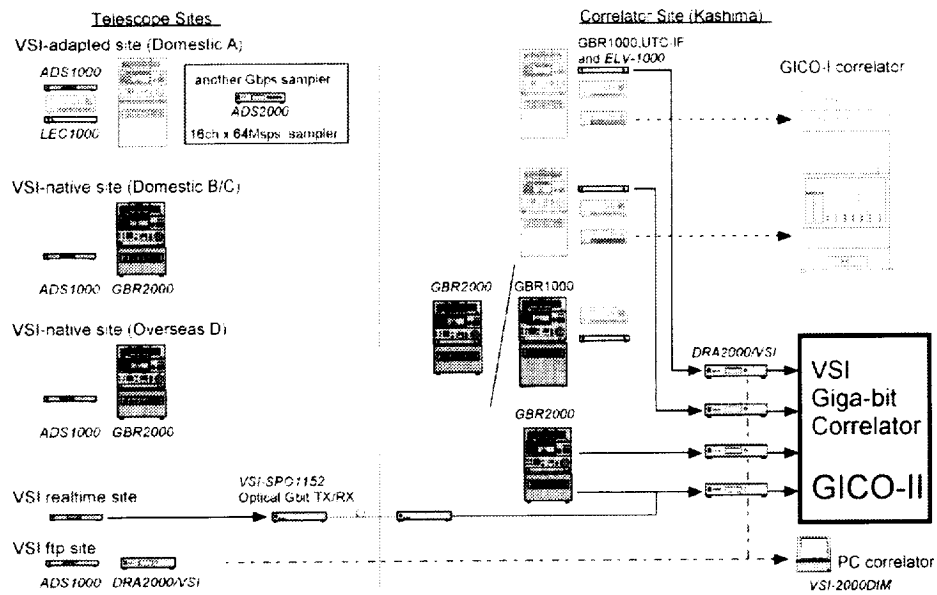


Figure 3. Integrated VSI Gbps VLBI system, including VSI adaptation of ECL interfaces. A new VSI correlator GICO-II (GIgabit CORrelator-2) is being produced. VSI instruments are indicated by slanted fonts

presented as an exception. As for the 256 Mbps conventional system, an S2-to-VSI converter and VSI-to-K4 converter were developed to achieve data conversion from S2 to K4 VLBI systems. In Table 2, PC-VSI2000-DIM will be a tool to confirm multi-national compatibility of VSI interface. The VSI-bench system with high performance PC can receive and inspect conformity of VSI Gbps data directly.

A new VSI correlator of four stations are in the final stage of hardware completion. A Gbps VLBI system in 2002 will be completed as shown in Figure 3. Without BBC (Base Band Converters) the simple Gbps VLBI system is easily adapted to any telescope's IF and enable high sensitivity observation. VLBI survey of faint sources as an expansion of previous VLBI source monitoring technique [3] is planned with a related institute. In the future, PC based VLBI system will also handle Gbps data with emerging high density media (holographic storage device for example).

#### 4. Recent Achievement

A Gbps system installation on the Japanese domestic network [7] had been carried out three times. Astronomical results focusing on survey and Hi-z quasars are processed.

On July 23, 2001, the first Gbps real-time VLBI between Usuda 64 m and Kashima 34 m was successfully performed by collaboration of National Astronomical Observatory, Institute of Space and Astronautic Science, Nippon Telegraph and Telecommunications, and CRL. Between the telescopes, the 208 km baseline was connected by NTT's ATM network and an ATM-to-parallel VLBI interface developed by NAO. These telescopes are connected by fibers and the telescope network is named GALAXY (Gigabit Astronomical Large Array Xross connected) [1]. In the

Table 1. Recent VSI compliant (conventional speed) instruments developed by CRL. Contributing Manufacturers are N:Nittsuki Co. Ltd., D:digitallink Co. Ltd., Y:YEM Co. Ltd., C: Cosmo Research.

Mbps	Instrument Name	Function	Purpose, Research Objective	Product
128	IP-VLBI board, Model 9820	Real-time IP VLBI PCI interface board. 32 Msps, 4 ch on-board AD converter (Non-VSI)	Initial network VLBI as moderate speed. Parallel operation will replace ATM or tape-based 256 Mbps system	N
256	VSI-K4-DIM	Data Protocol Converter, VSI to K4	S2 to K4 copier, K4 adaptation to VSI sampler	C
256	VSI-S2-DOM	Data Protocol Converter, S2 to VSI	S2 to K4 copier, S2 to other VSI instruments	C
256-2048	LEC-1000	Level converter, LVDS (VSI) to ECL (conventional)	Simple level converter for the predecessor ECL system	D
256-2048	ELV-1000	Level converter, ECL (old system) to LVDS (VSI)	Simple level converter. Receive data from ECL system	D
256-2048	VSI-SW-22	VSI switcher	2 input, 2 output data selector distributor	D
256-2048	DRA-2000VSI	1 Gbps (128 MB) FIFO Data memory unit, remote observing data ftp extraction tool	Portable VLBI w/o standard signal. Data freezing and ftp access from remote site.	Y
256-2048	MCG-2000	Master VSI clock for off-line environment (ex. Correlator).	Multi port LVDS, ECL, 1PPS, DPS source and test TVG generator.	Y
-	VSI cables	High reliable VSI connection	0.5, 1, 2, 5, 10m length	D

observation, VSI Gbps samplers and a Gbps correlator (GICO-I) adapted to VSI were used. In the first real-time observation, data of Usuda 64 m telescope data was recorded in front of the GICO correlator at Kashima in case of no fringe analysis. This complex configuration is enabled by the transparent VSI concept and identical interface.

Another achievement was the first-ever 2 Gbps VLBI between Koganei 11 m and Kashima 11 m telescopes. On December 22, 2001, 1-Gbps 2-bit sampling observation were carried out between the telescopes and 1.4 times sensitivity was confirmed by 2-bit correlation.

## 5. Conclusion

VSI-based VLBI development and achievements were reported. VSI provides easy integration environment of VLBI system by functional treatment of units. As the first trial of the VSI-H adaptation, the system worked perfectly both in real-time VLBI and tape-based VLBI up to 2 Gbps. Further effort will be needed after the endorsement of VSI-S is finalized in the IVS discussion.

In CRL, the development fund for the VSI standardization is partially supported by Telecommunications Advancement Organization (TAO).

Table 2. Gbps VSI compliant (high speed) instruments developed by CRL. Manufactures are N:Nittsuki Co. Ltd., D:digitallink Co. Ltd., T: Toshiba Corporation, Y:YEM Co. Ltd.

Mbps	Instrument Name	Function	Purpose, Research Objective	stat.
1024-2048	ADS-1000	AD sampler, 1 ch, 1024 M sample, 2 bit	High-speed AD sampler up to 2 GHz analog input. 0.3 ps jitter. Bit distribution monitoring.	D
256-2048	ADS-2000	AD sampler, 16 ch, 64 Msample, 2 bit	Wide-band enhancement of multi-channel conventional VLBI. AGC control and module channel expansion.	N
2048-4096	ADS-4000	AD sampler, 1 ch, 2048 Msample, 2 bit	Ultimate high-speed AD sampler for VLBI sensitivity.	2002
1024-2048	VSI-SPO1152-TX/RX	VSI optical digital serial transmitter and receiver	Optical fiber VSI connection. For interferometer and telescope VLBI avoid analog transmission	Y+D
1024-2048	GBR-2000D	New Generation Data Recorder, Skip-back (No start-up time) and direct data access by ftp	Gbps VLBI observation with a cart robot. Data transfer with out tape shipping. Production	T
2048-8096	PC-VSI2000-DIM	VSI data analyzer, Burst VLBI (PC-VSI perspective)	Inspect VSI data and burst storage with emerging IT media.	2001-2002
2048-8096	PC-VSI2000-DOM	VSI data generator	Generate complex VLBI data with delay and rate with a PC	2002-2003

## References

- [1] Fujisawa, K., et al. [2001], "GALAXY- Real-time VLBI for Radio Astronomy Observations", Journal of the Communications Research Laboratory, vol.48, No.1, pp.47-58.
- [2] Kondo, T. [2000], "Technology Development Center at CRL", IVS Annual Report, Ed by N.R. Vandenberg and K.D. Baver, NASA/TP-2001-209979. pp.263-266.
- [3] Koyama, Y., T. Kondo, and N. Kurihara [2001], "Microwave flux density variations of compact radio sources monitored by real-time Very Long Baseline Interferometry", Radio Science, vol.36, No.2, pp.223-235.
- [4] Nakajima, J., Y. Koyama, M. Sekido, H. Kiuchi, S. Hama, T. Kondo and Y. Takahashi [1998], "Gigabit VLBI Data Recorder, New Concept of Formatter Independent", Proc. IAU Colloq. 164, Radio Emission from Galactic and Extragalactic Radio Sources, ASP Conf. Ser. vol 144, p p395-396.
- [5] Nakajima, J., Y. Koyama, M. Sekido, N. Kurihara, and M. Kimura [2001], "1-Gbps VLBI The First Detection of Fringes", Experimental Astronomy, vol.11 pp.57-69.
- [6] Nakajima, J. [2001], "Gigabit Versatile Scientific Interfaces", New Breeze, ITU-J, Sep. pp.26-27.
- [7] Omodaka, T., et al. [2001], "Operation Result of J-Net (Japanese Domestic VLBI Network)", Journal of the Communications Research Laboratory, vol.48, No.1, pp.23-30.
- [8] Whitney A.R. [2000], "VLBI Standard Interface Hardware Specification", International VLBI Service <http://ivscc.nasa.gov>.

# A VSI-H Compatible Recording System for VLBI and e-VLBI

*Jouko Ritakari, Ari Mujunen*

*Metsähovi Radio Observatory*

*Contact author: Jouko Ritakari, e-mail: Jouko.Ritakari@hut.fi*

## Abstract

Metsähovi is developing a scalable disk-based recording system. The system uses standard PC hardware and standard Linux operating system. VLBI data is stored in normal Linux files and can be transported via Internet using normal Linux networking programs. This makes the system especially suitable for short-term storage of data for near-realtime VLBI. We have estimated that it is possible to replace an existing VLBI recorder with only one office PC and that the system is scalable to at least 2048 Mbit/s just by adding a few more PCs.

## 1. Introduction

The PC-based recording system we are developing at Metsähovi is one of the half a dozen projects that attempt to use off-the-shelf PC technology and Internet in VLBI.

Our project differs from the others in the respect that we do not try to re-design the technology to fit VLBI, we are using it with minimal modifications.

## 2. Underlying Philosophy

At this moment it is possible to use inexpensive office PCs and achieve 256 Mbit/s recording speed and 480 GB recording density in one machine. For comparison, the recording speed of a Honeywell 96-based recorder is 256 Mbit/s with one headstack and the capacity of a thin tape is 600 GB.

If we want to double the speed or the capacity of an office PC, it is possible but difficult. An order of magnitude improvement is almost impossible.

We think that it is better to stay with the mainstream technology and let the computer industry take care of improving the speeds and capacities.

## 3. Things We Have Tried to Avoid

The most common mistake in VLBI is to think that the data is somehow special, it must be formatted and transported in real-time data streams that must be synchronized.

Well.

The commercial PCs are very good in storing data in files but they are terrible in synchronizing data streams.

Internet is very good in transferring data, but terrible if real-time transfer is required.

In our opinion it is better to think that the data is normal data. It can be stored on hard disks in normal file formats and the files can be transported with FTP or other commonly used Internet protocols.

## 4. System Architecture

The system is built using normal PCs with Linux operating system. The data is stored into files in Linux file system according to the well-known FITS format, widely used elsewhere in VLBI.

No formatting of data is required because the 1PPS marker in the VSI data stream is used to divide the data into slices that contain an integer number of seconds.

If expansion beyond the capabilities of a single PC is required, time-multiplexing the data into several PCs is the preferred method. That means that each PC captures several seconds worth of data synchronized by the 1PPS pulse, then the next one starts the data acquisition.

## 5. VSI Input/Output Board

The VSI input/output board is a simple standard-size PCI board with the following features:

- Two bidirectional VSI-H ports.
- Data acquisition at VSI clock rate or VSI clock rate divided by an integer.
- Normally one VSI port is used as input, second port as output.
- Facilitates chaining of PCs, which eliminates the need for a separate VSI data distributor. The 1PPS marker in the VSI port is used to synchronize the computers.
- 512 Mbit/s sustained I/O capability to/from main memory.
- Uses PLXtech PCI9054 and Xilinx Spartan II chips.
- 1024 \* 32-bit internal FIFO to overcome PCI bus latencies.
- Can either record the data in parallel or separate four 1-bit or 2-bit channels in different files.
- The same board can be used to play the data back to correlator.
- The board supports scatter/gather DMA and can be used to format the data during playback.

The board can be connected directly to the Japanese Giga-Bit VLBI sampler or with a simple adapter to the existing VLBA or Mark IV systems, either directly to samplers or to the formatter outputs.

The programming interface of board is very simple, it really has only two commands. The first command is “reset everything” and the second command is “wait for the next 1PPS pulse and capture X seconds worth of data in computer main memory”. These commands facilitate easy time-multiplexing of the data acquisition. The control of the board is not time-critical, the computer has one whole second to start the capturing even in time-multiplexed mode.

A picture of the layout is in Figure 1 at the end of this paper.

## 6. VLBA to VSI converter

The VLBA sampler to VSI converter is a stand-alone module that converts the data from VLBA samplers to the VSI format. It is really only a level converter, but a Xilinx Spartan II chip has been added for expandability reasons.

- Two VLBA sampler 40-pin inputs (differential ECL).
- Two VSI-H compatible LVDS outputs.
- The VSI ports are identical, both output all the sampler signals.

Similar converters can be easily designed for Mark IV sampler to VSI conversion or Mark IV formatter to VSI conversion.

However, we think that the best approach is to connect directly to the sampler outputs. There are two reasons for this: first, the function of the formatter is to change the data into a form that can be recorded on a tape recorder. There is no tape recorder in our system. The second reason is that the formatter fans out the data to lots and lots of tracks, one 32 Mbit/s signal goes to four tracks. If we use formatter outputs, we must have another device to multiplex the data back to one track. Nothing is really accomplished, but a lot of electronics is needed.

## 7. Performance

At this moment the performance of the system is limited by the speed of the hard disks. One PC can sustain a speed of 256 Mbit/s to disks.

We expect the sustained recording speed to increase to 512 Mbit/s later this year as the speeds of the hard disks and the architectures of PC motherboard chipsets improve.

## 8. Expandability

The system is designed to be scalable.

If we need 256 Mbit/s sustained speed, we need only one PC.

If we need 512 Mbit/s sustained speed, we chain two PCs together and time-multiplex the recording.

If we need 1024 Mbit/s sustained speed, we use two chains of two PCs.

When new PC bus architectures (64-bit 66 MHz PCI or some totally different architecture) emerge, the design can be easily modified. The bus interface chips have simple interfaces to the local bus on the board and the Xilinx is programmed in VHDL language.

## 9. Future

The PC technology keeps improving. We expect that later this year we can achieve 512 Mbit/s throughput using only one PC.

When the 64-bit 66 MHz PCI chips arrive later this year, the PCI bus speed quadruples and we can achieve up 2048 Mbit/s speed from the VSI port to computer main memory.

When the serial ATA disks arrive, hopefully the disk cabling inconveniences will be solved.

In this system the data is already organized into normal files in the Linux file system, migration into the use of Internet is easy.

The data in the files is error-free sampler data with no formatting, migration into distributed correlation is easy.

Anyway, the beauty of this design is that it adapts very easily to evolving standards. There are no expensive black boxes anywhere.

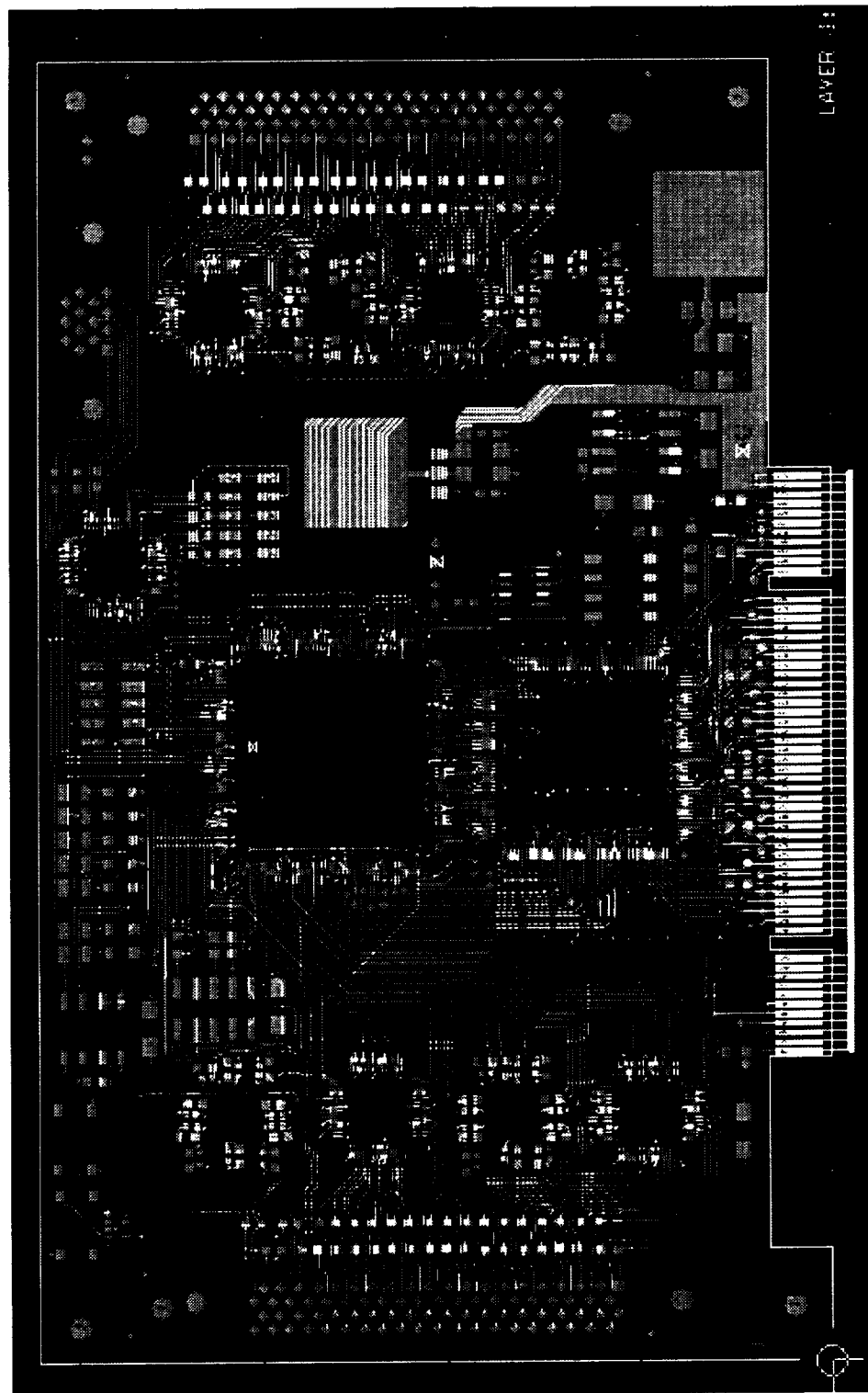


Figure 1. VSI Input/Output board layout.

# Mark 5 Disc-Based Gbps VLBI Data System

*Alan R. Whitney*

*MIT Haystack Observatory*

*e-mail: [awhitney@haystack.mit.edu](mailto:awhitney@haystack.mit.edu)*

## Abstract

The Mark 5 system is being developed as the first high-data-rate VLBI data system based on magnetic-disc technology. Incorporating primarily low-cost PC-based components, the Mark 5 system will support data rates up to 1024 Mbps recording to an array of up to 16 inexpensive removable IDE discs. An initial demonstration system was used in March 2001 to record data at 576 Mbps, with correlation on the Mark 4 correlator at Haystack Observatory.

With the continuing fall in disc prices, IDE discs are already becoming competitive with the cost of Mark 4/VLBA/K4 tape, with the expectation that prices will continue to fall to a level below ~\$1/GB with capacities of hundreds of GB per disc.

The Mark 5A system, which is a direct replacement for a Mark4 or VLBA tape transport, will deploy ~12 prototype units in mid-2002 to stations and correlators around the world, at a cost of ~\$20K/unit. A fully VSI-compliant Mark 5 system, dubbed Mark 5B, will be available in late 2003, along with the necessary adapter interface required to utilize the system with existing Mark 4 and VLBA data-acquisition and correlator systems.

The Mark 5 development effort at Haystack Observatory is supported by BKG, EVN/JIVE, KVN, MPI, NASA, NRAO and USNO.

## 1. Introduction

The Mark 5 system is being developed as the first high-data-rate VLBI data system based on magnetic-disc technology. Incorporating primarily low-cost PC-based components, the Mark 5 system will support data rates up to 1024 Mbps, recording to an array of up to 16 inexpensive removable IDE discs. An initial demonstration system has been used to record data at 576 Mbps, with correlation on a Mark 4 correlator at Haystack Observatory. A program is now in place for the development of an operational Mark 5 system.

The goals of the Mark 5 system are:

- Low cost
- Based primarily on unmodified COTS components
- Modular, easily upgradeable
- Robust operation, low maintenance cost
- Easy transportability
- Conformance to VSI specification
- Compatibility with existing VLBI systems during transition
- Flexibility to support e-VLBI
- Minimum of 1 Gbps data rate

- 24-hour unattended operation at 1 Gbps

All but the last are clearly achievable with today's technology; 24-hour unattended operation at 1 Gbps is expected to arrive naturally within ~2-3 years with continued development in disc technology. The first Gbps Mark 5 systems will be put into operations in 2002.

## 2. Why Discs?

Though both magnetic-disc technology and magnetic-tape technology have made great strides over the past few years, the pace of magnetic-disc development has been so great that it is very likely that disc storage will become cheaper than magnetic tape storage by ~2004. Figure 1 shows the comparison of disc and tape prices since 1980. Current consumer IDE disc costs are ~\$2/GB and falling; current Mark4/VLBA tape prices are ~\$2/GB and remaining steady. By ~2005-2006, industry projections suggest the price of discs will fall to ~\$0.5/GB. Similarly, current single-disc capacities are ~160 GB and rising; by ~2004-2005, single-disc capacities are expected to rise to 500-1000 GB! A Mark 5 system with sixteen 700 GB disc drives will record 1024 Mbps continuously for 24-hours unattended.

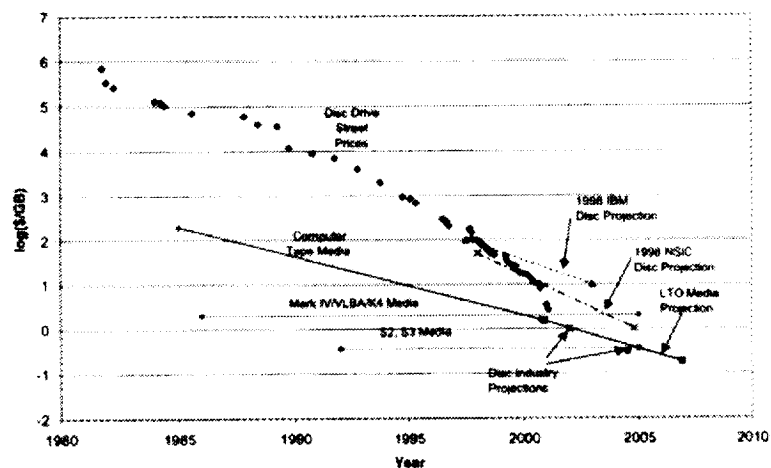


Figure 1. Disc/Tape Price Comparisons

In addition to falling prices and increasing capacity, discs have several other advantages:

- Readily available inexpensive consumer product
- continually improving in price/performance with standard electrical interface
- Self contained; do not have to buy expensive tape drives, so host system can be inexpensive
- Technology improvements independent of electrical interface
- Rapid random access to any data
- Essentially instant synchronization on playback to correlator (no media-wasting early starts needed)
- No headstacks to wear out or replace - ever!

### 3. Mark 5 Development Program

Based on the success of the 512 Mbps Mark 5 demonstration unit in early 2001 (developed and demonstrated in 3 months time, shown in Figure 2), Haystack Observatory is now undertaking the development of an operational 1 Gbps Mark 5 system with support from BKG, KVN, MPI, NASA, JIVE, NRAO and USNO.

The Mark 5 system is being developed in two stages:

1. Mark 5A: Records 8, 16, 32 or 64 tracks from a Mark4/VLBA formatter, up to 1024 Mbps, and plays back in the same Mark4/VLBA format. As such, the Mark 5A is a direct replacement for a Mark4/VLBA tape drive. We anticipate deployment of ~20 systems mid-2002.
2. Mark 5B: VSI-compliant system, up to 1024 Mbps; no external formatter necessary. Will be backwards compatible to existing Mark4/VLBA correlator systems. We anticipate deployment in 2003.

A Mark 5A system may be upgraded to a Mark 5B system simply by replacing PCI boards in the host PC.

The cost of either the 1 Gbps Mark 5A or Mark 5B recording or playback system (without discs) is expected to be  $< \sim \$15K$  with a do-it-yourself kit. These costs are more than an order-of-magnitude below current costs of available tape-based Gbps systems. With currently available disc drives of  $\sim 160$  GB each, a Mark 5 system will record 1024 Mbps of user data for  $\sim 5.5$  hours using 16 discs. Normally, the 16 discs will be divided into two 8-disc sets. The Mark 5 will automatically and seamlessly ping-pong between the two 8-disc sets. Disc drives are mounted in carriers made for multiple insertion/removal cycles. When modern disc drives are powered down, they are quite robust to external handling forces and can be shipped easily in padded containers. Including the carriers, the shipping weight per disc is  $< \sim 0.9\text{kg}$ , so that the shipping weight of 8 discs plus shipping container is  $\sim 9\text{kg}$ .

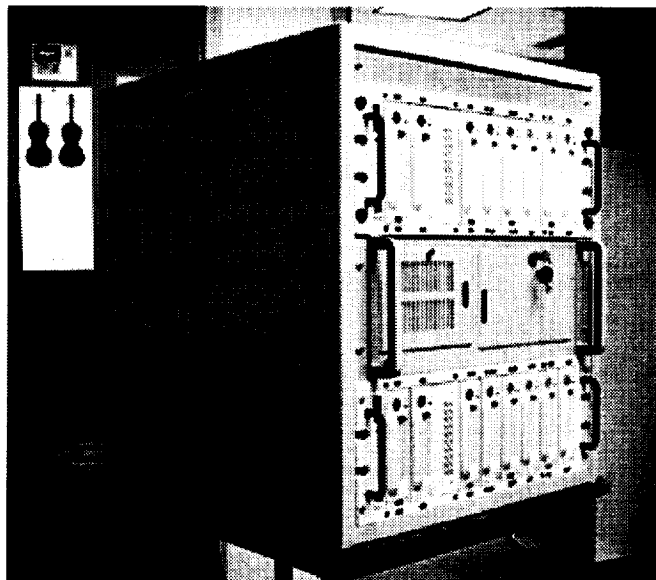


Figure 2. Photograph of demonstration Mark 5 System

Figure 3 shows a simplified block diagram of the Mark 5 system. The heart of the system is a streaming disc interface which supports 16 disc drives at data rates in excess of 1024 Mbps. For recording, external data from a Mark 4 or VLBA formatter is transformed to 32 parallel bit streams to be accepted by the disc interface for recording. On playback, the 32 bit streams played back from the discs are re-transformed to re-create the formatter input. The VSI version of the Mark 5, called Mark 5B, will operate in a similar manner.

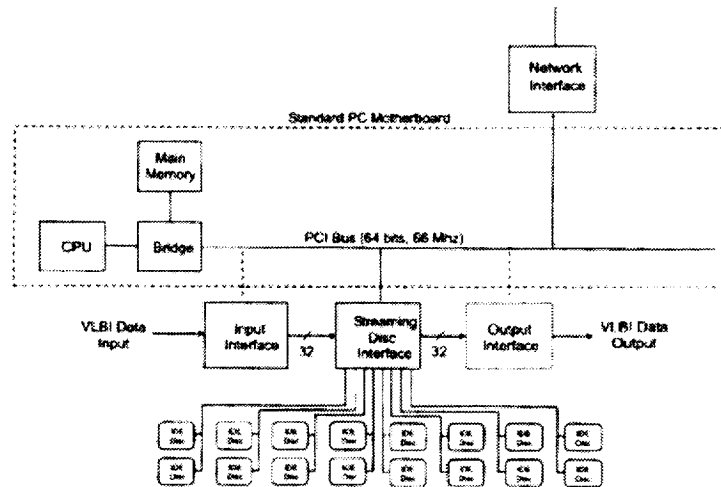


Figure 3. Simplified block diagram of Mark 5 system

Figure 4 shows the anticipated packaging of the operational Mark 5 system, which will be housed in a single 7"-high chassis.

#### 4. Compatibility Considerations

The Mark 5 system is being designed for extensive forward and backwards compatibility with existing VLBI systems. For example, data may be recorded with a VSI-compatible interface and re-played into a Mark4/VLBA correlator. Conversely, data may be recorded from a Mark4/VLBA system and re-played into any VSI-compatible correlator.

In addition, it is expected that existing interfaces to S2 recorders can be easily adapted to record on Mark 5B, which can then be re-played into either a VSI-compatible or Mark4/VLBA correlator.

This inter-compatibility among various systems will allow a much broader and flexible use of existing VLBI facilities throughout the world.

#### 5. e-VLBI Support

The Mark 5 system allows easy connection of a VLBI data system to a high-speed network connection. Because the Mark 5 system is based on a standard PC platform, any standard network connection is supported.

Depending on the availability of high-speed network connections, this can be accomplished in at least two ways:

1. Direct Station to Correlator: If network connections allow, data may be transferred in real-time at up to 1 Gbps from Station to Correlator, either for immediate real-time correlation or buffering to disc at the Correlator.
2. Station Disc to Correlator Disc: If network connections are not sufficient to allow real-time transmission of data to the Correlator for processing, data may be recorded locally to disc at the Station, then transferred to disc at the Correlator at leisure for later correlation.

Depending on the available network facilities, either entire experiments or small portions of experiments may be transmitted electronically. The latter may be particularly useful for verifying fringes in advance of important experiments.

Haystack Observatory is being supported by DARPA to demonstrate Gbps e-VLBI data transmission between Haystack Observatory and NASA/GSFC (~700 km) using the Mark 5 system. Data will be collected at the Westford antenna at Haystack Observatory and the GGAO antenna at NASA/GSFC and transmitted in real-time to the Mark 4 correlator at Haystack Observatory.

## 6. Summary

The Mark 5 system promises to move VLBI data systems to dramatic new levels of high-performance and low-cost by leveraging the enormous investments of the computer industry in high-speed data technology. Within only a very short time, the possibilities to economically expand VLBI observing programs by large factors appear to be within reach.

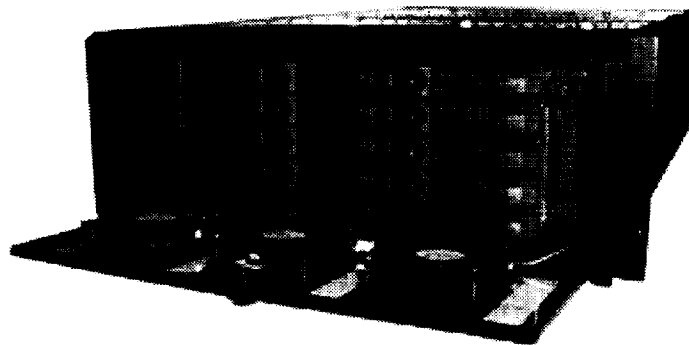


Figure 4. Mark 5 prototype system

# High-Speed e-VLBI Demonstration: Haystack Observatory to NASA/GSFC

*Alan R. Whitney*

*MIT Haystack Observatory*

*e-mail: awhitney@haystack.mit.edu*

## Abstract

Haystack Observatory, with support of a grant from DARPA, is preparing a high-speed e-VLBI demonstration using antennas at Westford, MA and NASA/GSFC in Maryland, with correlation at Haystack Observatory. The link between Haystack and GSFC includes a number of both private and public network facilities, including the Bossnet, Glownet, Supernet and GSFC/HECN networks. The Mark 5 system will be used at both stations and at the Haystack Mark 4 correlator to interface VLBI data through a standard TCP/IP Gigabit Ethernet connection at a sustained rate of  $\sim 900$  Mbps. Due to the many different networks involved, much effort is being undertaken to examine every link in the path and to optimize and upgrade components as necessary in order to achieve the desired speed. Expansion of this effort to include stations in Europe and Japan is being explored.

## 1. Goals of the e-VLBI Experiment with Haystack and NASA/GSFC

Under the sponsorship of DARPA, Haystack is preparing a high-speed e-VLBI demonstration between Haystack Observatory in Westford, Massachusetts and NASA/GSFC in Greenbelt, Maryland, a direct-path distance of  $\sim 650$  km, as illustrated in Figure 1. The significant features of this demonstration are:

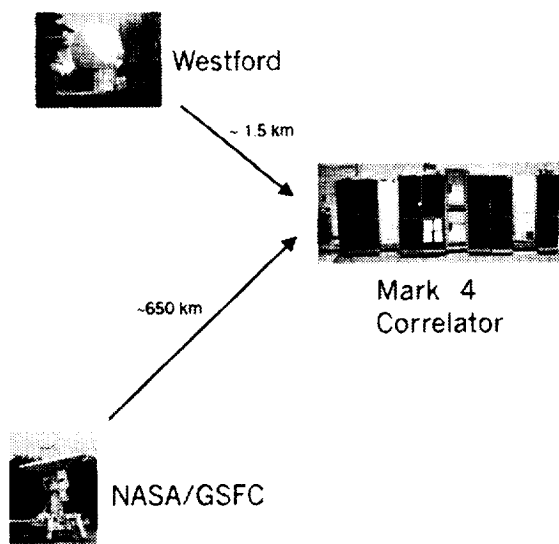


Figure 1. Gbps e-VLBI demonstration

- To demonstrate ~1 Gbps near-real-time and real-time VLBI data transmission from Westford antenna at Haystack Observatory and GGAO antenna at NASA/GSFC to the Mark 4 correlator at Haystack Observatory.
- Utilize Mark 5 systems for data transmission and reception.
- Use standard Gigabit Ethernet connections at all sites

This experiment is not the first e-VLBI at Gbps speed, as at least one network in Japan has already operated at this speed. However, it may be the first Gbps e-VLBI experiment to operate over ordinary shared networks with many users.

## 2. The Mark 5 System and e-VLBI Connectivity

The Mark 5 system is being built to support e-VLBI requirements up to ~1 Gbps. It supports a “triangle of connectivity” between the VLBI data port (source or sink), a disc array, and a high-speed network connection attached to a standard PCI bus, as shown in Figure 2. The path between any of these three nodes of the “triangle of connectivity” may be exercised at up to 1 Gbps.

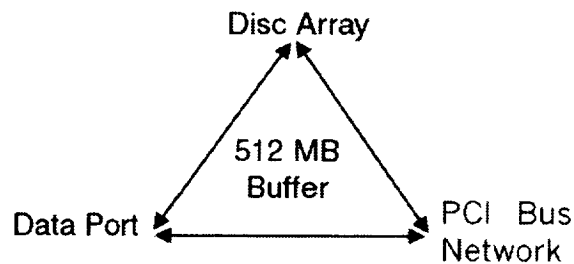


Figure 2. Mark 5 'triangle of connectivity'

As a result of this 'triangle of connectivity', the Mark 5 can support several practical e-VLBI data-transfer modes:

1. VLBI data may be recorded on disc, then transferred at a later time to a correlator, where it can either be processed in real time or re-recorded onto disc for later processing.
2. VLBI data may be transferred directly to a correlator, where it may either be processed in real time or re-recorded onto disc for later processing.

In addition, the Mark 5 allows data to be simultaneously recorded to disc and transferred to the network at data rates up to ~800 Mbps in cases where it may be desirable to keep a “backup” copy of data being transmitted in real time to a correlator. Initially we plan to use Gigabit Ethernet for the network connection, though any standard network connection can be supported, with 10 Gigabit Ethernet on the near horizon.

## 3. Network Details

The network connection between the Westford antenna and Haystack correlator is dedicated. However, the connection from the GGAO antenna to Haystack is a combination of dedicated and

shared networks, as illustrated in Figures 3a and 3b. Starting at Haystack Observatory, a dedicated fiber network called GlowNet links to another dedicated network called Bossnet, which carries data from Washington, D.C. At Washington, D.C., the link connects over several segments of both dedicated and shared network links to the GGAO antenna. Use of some shared segments of the path must be coordinated with other users in order to achieve the necessary data throughput rate.

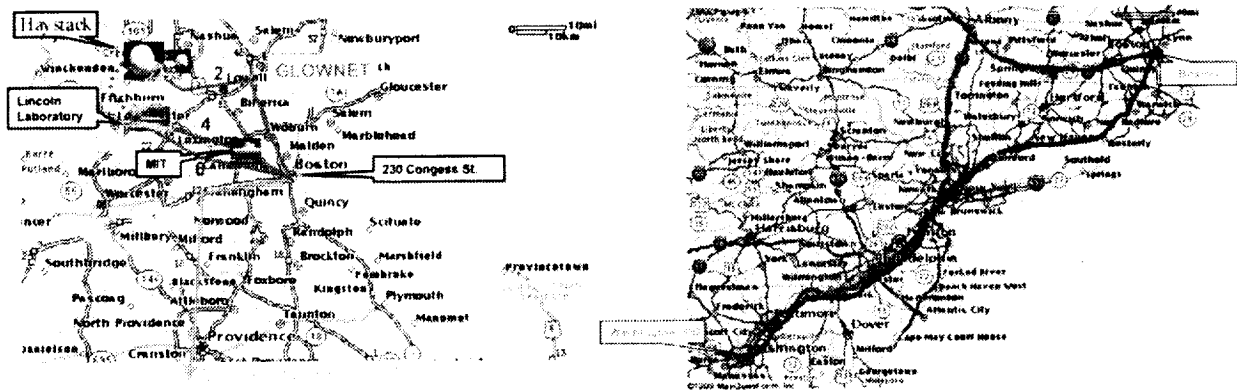


Figure 3. a:Connection of Haystack to GlowNet, b:Bossnet route from Boston to Washington, D.C.

Figures 4 and 5 show the details of the path between Haystack Observatory and GGAO, including more than a dozen routers and switches along the way. Each piece of equipment in this path must be carefully examined for suitability to operate at 1 Gbps and upgraded or replaced as necessary.

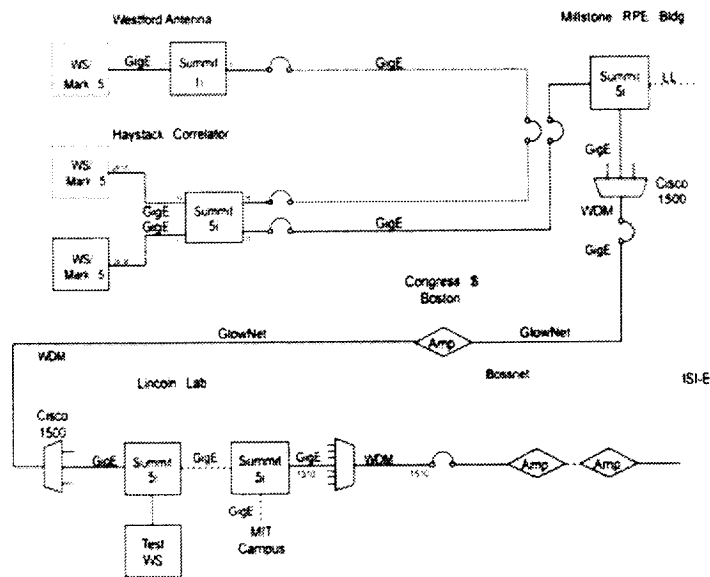


Figure 4. Detailed connection diagram part 1

Test workstations are placed at several points along the route in order to facilitate network testing. To date, the segment between Haystack Observatory and the beginning of Bossnet have



1. The daily UT1 Intensive measurements between Wettzell in Germany and Kokee Park in Hawaii are an obvious early target for conversion to e-VLBI. Each daily observation collects  $\sim 100$  GB of data, easily manageable with the Mark 5 system. Because there are no direct high-speed network connections to either site, the discs will be transported to a nearby high-speed node where they will be re-played through the network and re-recorded on disc at the correlator. When the transfers are complete, the data will be correlated in the normal way. This mode of operation should reduce the interval from observation to results from several days to several hours and significantly improve important UT1 predictions.
2. Several high-speed international science links exist which might be used for e-VLBI, particularly to Europe and Japan. The Surfnet link is jointly supported by the U.S. and Europe and provides a  $>1$  Gbps link between Amsterdam and Chicago. We are currently investigating possible high-speed connections from Haystack to Chicago; the European VLBI community is planning high-speed connections to Surfnet in Amsterdam in the near future. Similarly, the TransPAC link connects Chicago and Tokyo with a high-speed connection (currently OC-12, but with anticipated upgrades). Efforts are currently underway in Japan to connect telescopes to TransPAC, which will allow real-time and near-real-time experiments between the U.S. and Japan.

## 6. Summary

Though currently in its infancy, e-VLBI is expected to develop rapidly to provide connectivity unimagined only a few years ago. For many telescopes, the “last mile” problem is still a severe impediment to full real-time operation. However, interim operation of buffered data (on discs) transported to nearby high-speed nodes is an attractive step in the right direction. Eventually, it is likely that full global e-VLBI operation will not only become possible, but will extend VLBI observations to new levels of sensitivity and timeliness.

## Real-time Gigabit VLBI System and Internet VLBI System

Tetsuro Kondo <sup>1</sup>, Yasuhiro Koyama <sup>1</sup>, Junichi Nakajima <sup>1</sup>, Mamoru Sekido <sup>1</sup>,  
Ryuichi Ichikawa <sup>1</sup>, Eiji Kawai <sup>1</sup>, Hiroshi Okubo <sup>1</sup>, Hiro Osaki <sup>1</sup>, Moritaka Kimura <sup>1</sup>,  
Yuichi Ichikawa <sup>2</sup>, GALAXY Team <sup>3</sup>

<sup>1</sup>) *Kashima Space Research Center, Communications Research Laboratory*

<sup>2</sup>) *Nihon Tsushinki Co.Ltd.*

<sup>3</sup>) *CRL, NAOJ, ISAS, and NTT joint project team*

Contact author: Tetsuro Kondo, e-mail: [kondo@crl.go.jp](mailto:kondo@crl.go.jp)

### Abstract

The development of a gigabit VLBI system and an Internet VLBI system at CRL is carried out as one of the subjects to promote “research on key technologies to establish the space-time infrastructure in the space”, a new project started two years ago. First we have developed a tape-based gigabit VLBI system. Some geodetic VLBI experiments were performed using this system. In parallel with the development of the tape-based system, a real-time gigabit VLBI system has been developed in collaboration with National Astronomical Observatory Japan (NAOJ), Institute of Space and Astronautical Science (ISAS) and Nippon Telegraph and Telephone Corp.(NTT). In the real-time system, VLBI data are transmitted through the high speed ATM network to a correlator. We successfully carried out the first real-time 1 Gbps VLBI experiment using Kashima 34m antenna and Usuda 64m antenna on June 23, 2001, and first real-time fringes were successfully detected. In addition to the success in 1 Gbps real-time VLBI, we also succeeded in 2 Gbps tape-based VLBI on December 12, 2001.

On the other hand a new real-time VLBI system using IP (Internet protocol) technology called “IP-VLBI” or “Internet VLBI” has been developed since 1999 to reduce network cost and to expand connection sites. We have been developing the IP-VLBI system as a PC-based system consisting of a PCI-bus sampler board and PC software to make real-time data transmission, reception and correlation.

### 1. Introduction

“Research on key technologies to establish the space-time infrastructure in the space” is a project started in FY2000, and shares research subjects with Time and Frequency Measurements Group, Atomic Frequency Standards Group, and Radio Astronomy Applications Group (VLBI group) at Communications Research Laboratory.

With the advent of GPS known as a “Car-Navi: car navigation system”, wherever we might be on the earth, we could know our position correctly. The space version of this positioning system is a “Space-Navi: space navigation system” which offers precise time and position information to spacecrafts in space. “Research on key technologies to establish the space-time infrastructure in the space” is the project to investigate key technologies to realize the Space-Navi. A system assumed at present is schematically depicted in Fig.1. This project consists of four research subjects, that is, (1) highly stable space-borne Hydrogen maser frequency standard, (2) time keeping of satellite group, (3) establishment of a space-time standard coordinate system, and (4) research on spacecraft positioning technology. VLBI group takes charge of the subjects (3) and (4). “Establishment of a space-time standard coordinate system” is subdivided into real-time precise measurement of the earth orientation parameters (EOP) and precise positioning of a space-time fiducial point (space lighthouse) in space. To achieve real-time and high-time resolution EOP monitoring (Fig.2), we

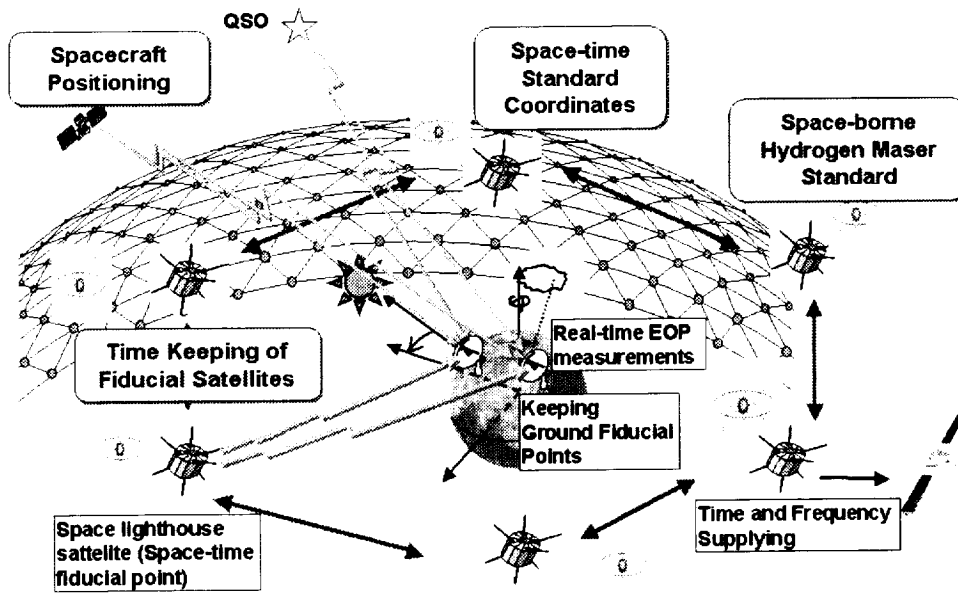


Figure 1. Research on key technologies to establish the space-time infrastructure in the space.

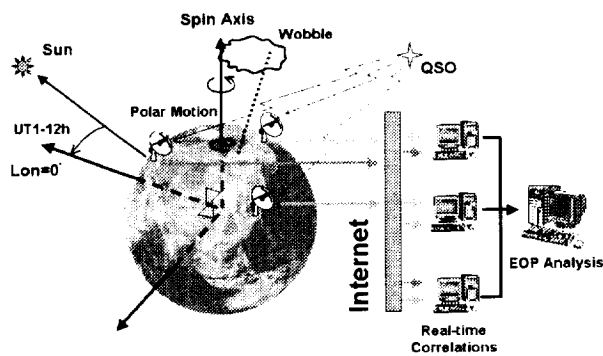


Figure 2. Real-time EOP monitoring system.

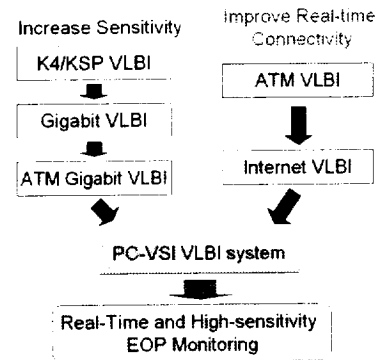


Figure 3. A plan of system development.

started the development of a gigabit and Internet VLBI system. A plan of our development is shown in Fig.3. Current status of the development of the system will be reported here.

## 2. Gigabit VLBI system

In order to increase time resolution of EOP measurement, it becomes important how many sources (quasars) can be observed in a short time period. Thus it is required to shorten observation time per one source, i.e., increasing system sensitivity is essential. Two approaches can be considered to realize this requirement. One is to use a larger antenna; the other is to make the receiving bandwidth larger. Generally, since drive speed becomes slow for a larger antenna, a source change comes to take time, and it is disadvantageous for the increase in the number of observation per unit time. We hence take an approach of receiving bandwidth expansion, i.e., we

started the development of a gigabit VLBI system.



Figure 4. A gigabit VSI recorder.

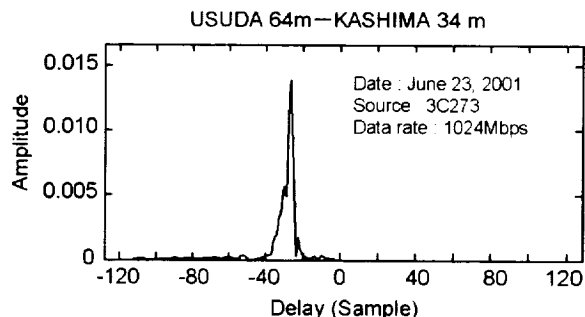


Figure 5. First real-time 1 Gbps VLBI fringes observed on June 23, 2001 on Kashima-Usuda baseline.

First system was developed as a tape-based system. Now the system evolution is continued as a VSI compliant system (Fig. 4) [1], and real-time capability has been taken into the system. Since we already have ATM real-time VLBI technique developed under the Key Stone Project (e.g., see [2]), a real-time gigabit VLBI experiment became possible soon in collaboration with the Institute of Space and Astronautical Science (ISAS), National Astronomical Observatory (NAO), and Nippon Telegraph and Telephone Corporation (NTT). Challenge to get real-time fringes using gigabit VLBI system was carried out between Usuda 64-m antenna and Kashima 34-m antenna on June 23, 2001, and first real-time fringes with a data rate of 1 Gbps were successfully detected (Fig.5). Now it is possible to carry out 1 Gbps real-time VLBI stably.

In addition to the success in 1 Gbps real-time VLBI, we also succeeded in 2 Gbps VLBI using ADS-1000 on December 12, 2001 but in tape-based VLBI (not real-time VLBI). Two 1 Gbps recorders were used at each station. Sampling frequency was 1 GHz and we adopted 2 bit Analog to Digital conversion, so the data rate became 2 Gbps. We could confirm the increase of signal to noise ratio corresponding to the theoretical expectation compared with the case of 1 bit A/D conversion.

### 3. Internet VLBI system

Regarding the real-time VLBI system, we have already developed real-time VLBI system using the ATM high speed network. However connection site is still limited and network cost is still expensive. In order to reduce network cost and to improve interconnectivity with other sites, we have been developing new real-time VLBI system using IP (Internet protocol) technology that has already spread widely. We call this system "IP-VLBI". Two kinds of IP-VLBI system are under development by NTT and CRL.

One is the substitution of protocol from ATM to IP. In this system, serial high-speed data stream is directly sent by using IP instead of ATM. Although the data consist of several physical channels of data, no channel distinction is made in the transmission process. However, not only VLBI data but also any kind of data stream can be transmitted by this system. NTT has been

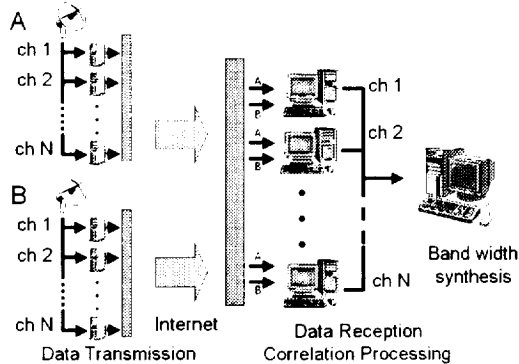


Figure 6. Internet VLBI system for geodetic use.

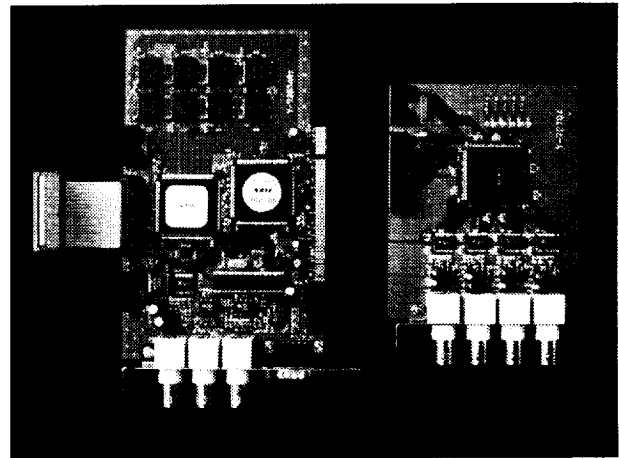


Figure 7. A PCI sampler board for the IP-VLBI system (left) and an auxiliary board for 4ch inputs (right).

developing this type.

The other kind of system is on the basis of channel data. A geodetic VLBI system usually receives 14 to 16 frequency channels at S and X bands. Each channel's data are transmitted independently by using the IP. We refer to this system as "Multi-channel IP-VLBI", because only establishing the system for one channel, we can easily expand it to the multi-channel system (Fig.6). Only the network speed limits the number of channels and sampling frequency. CRL has been developing this type to take over current geodetic VLBI system. We have been developing a PC-based IP-VLBI system consisting of a PCI-bus sampler board (Fig.7) and PC software to make real-time data transmission and reception. We also intend to carry out the real-time correlation by PC software. One sampler board can have 4 video signal inputs by adopting an auxiliary board and is designed to be able to sample each signal with a sampling frequency of up to 16 MHz with an A/D conversion resolution of from 1 bit to 8 bits. The sampler board has been evaluated and confirms sufficient performance of both "coherent sampling" and "real-time transmission" with a sampling frequency of up to 16 MHz.

Regarding real-time software correlation processing, we can process 8 MHz sampling data in real-time at present time. An improvement in the algorithm to make correlation processing faster is in progress [3]. It is under consideration also about distributed correlation processing.

#### 4. Conclusion

We are developing the gigabit VLBI system and the Internet VLBI system to give a proof of the possibility of the real-time precise EOP-measurement system. At present the development of both systems is proceeding independently, but both will be unified to a PC-VSI system in the near future. PC-VSI is a personal computer based VSI and we just start the development of PC-VSI.

## 5. Acknowledgements

The gigabit VLBI system has been developed under a cooperative effort by Communications Research Laboratory, NAOJ, Tokyo University, and Nippon Telegraph and Telephone Corp. We would like to express deep appreciations to colleagues in these organizations.

## References

- [1] Nakajima, J., Y. Koyama, M. Sekido, R. Ichikawa, and T. Kondo, Approved upgrade of the Gbit VLBI system expansion, *Technical Development Center News CRL*, No.17, 25, 2000.
- [2] Koyama, Y., N. Kurihara, T. Kondo, M. Sekido, Y. Takahashi, H. Kiuchi, and K. Heki, Automated geodetic Very Long Baseline Interferometry observation and data analysis system, *Earth, Planets and Space*, 50, 709-722, 1998.
- [3] Kondo, T., Y. Koyama, M. Sekido, J. Nakajima, H. Okubo, H. Osaki, S. Nakagawa, and Y. Ichikawa, Development of the new real-time VLBI technique using the Internet Protocol, *Technical Development Center News CRL*, No.17, 22-24, 2000.

## Observation of Atmospheric Disturbances Using a Real-Time VLBI System

Qinghui Liu<sup>1</sup>, Masanori Nishio<sup>2</sup>, Kunihiro Yamamura<sup>1</sup>, Tomoyuki Miyazaki<sup>1</sup>

<sup>1)</sup> Department of Electrical and Electronics Engineering, Kagoshima University

<sup>2)</sup> Department of Physics, Kagoshima University

Contact author: Qinghui Liu, e-mail: eem0338@elib.eee.kagoshima-u.ac.jp

### Abstract

This paper reports observation results of atmospheric disturbances on a very long baseline. Using a real-time VLBI system, the observation was performed by the Kagoshima 6-m and the Mizusawa 10-m radio telescopes, which are 1,284 km apart. Beacon waves from geostationary satellites were received and data were sent via public communication lines. The time variation of the correlation phase obtained was analyzed by calculating the Allan standard deviation,  $\sigma_y(\tau)$  and the time structure function,  $D_\phi(\tau)$ , as a function of a time interval  $\tau$ . It is found that the time variations of the correlation phase were mainly caused by atmospheric disturbances, and that for  $1 \text{ s} < \tau < 200 \text{ s}$ , the Allan standard deviation of atmospheric disturbances  $\sigma_y(\tau) \propto \tau^{-0.2}$  and the time structure function  $D_\phi(\tau) \propto \tau^{5/3}$ .

### 1. Introduction

Atmospheric disturbances, which are mainly caused by fluctuations of water vapor distribution in the troposphere, bring about phase fluctuations of radio waves passing through the troposphere. In VLBI, the phase fluctuations not only decrease the angular resolution, but also cause coherence loss.

Observations of atmospheric disturbances were made with a real-time VLBI system developed for diagnosis of VLBI observation facilities [1]. In this paper, observation results are reported.

### 2. Real-time VLBI System

The block diagram of the real-time VLBI system is shown in Fig.1. The system consists of two remotely located antennas connected with data transmission lines using ISDN and a PC-based cross-correlator. In the system, beacon waves of 19 GHz emitted from geostationary satellites are received by the two antennas. The signals received are recorded into PCs after down-conversion and 2-bit A-D conversion. Bandwidth of the signals is ten-odd kilohertz. Local signals for the down-conversion and clocks for the A-D conversion are supplied by hydrogen maser oscillators. The time synchronization is made by recording 1-pps signals together with the A-D converted signals. In addition, start of the A-D conversion is synchronized with the 1-pps signals. An accuracy of an order of  $1 \mu\text{s}$  is achieved in the time synchronization between two recorded signals.

The signal received by the antenna located at a remote station (Y-Station in Fig. 1) is transmitted to a personal computer PC<sub>Z</sub> located at another station (X-Station in Fig. 1) at a rate of 128 kbps by FTP. On the other hand, the signal received by the antenna located at X-station is transmitted to PC<sub>Z</sub> via Ethernet. Cross-correlation between the two signals is calculated with PC<sub>Z</sub>.

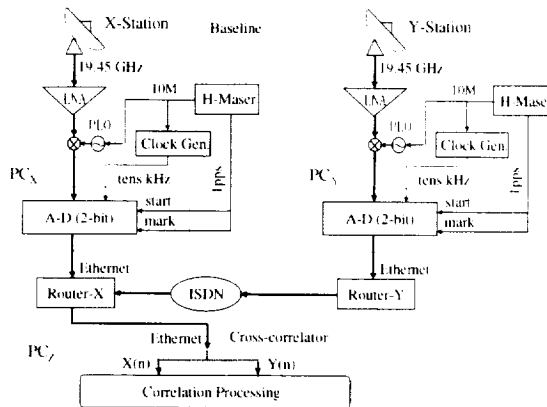


Figure 1. Block diagram of the real-time VLBI system.

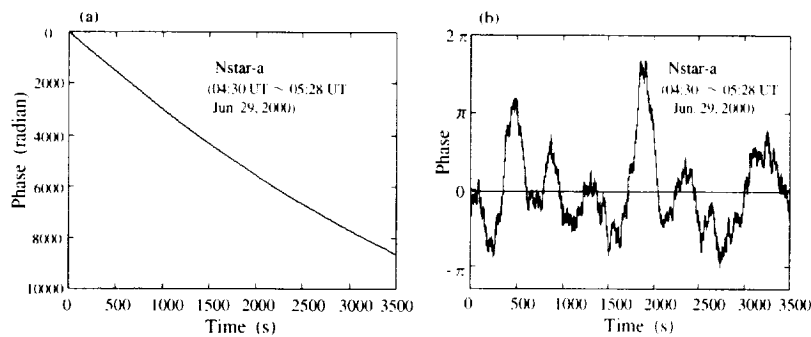


Figure 2. Correlation phase. (a) before fringe stopping and (b) after fringe stopping.

The correlation phase shows temporal variations caused by atmospheric disturbances overlaid on a gradual variation by the orbital motion of the satellite. The latter component,  $\phi_s(t)$  is calculated from the observed phase variations by the method of least squares with a period,  $T_p$ . In the next step, the fringe stopping was carried out by which the component,  $\phi_s(t)$  is subtracted from the time variations of the correlation phase observed.

### 3. Observations and Results

Observations of atmospheric disturbances were made using the Kagoshima 6-m and the Mizusawa 10-m radio telescopes. The baseline length is 1,284 km. Two geostationary satellites, Nstar-a and Nstar-b, are used for the observations. The frequencies of the beacon waves are 19.45 GHz. Nstar-a was observed twice from 04:30 to 05:28 UT on June 29, 2000 and from 00:00 to 00:57 UT on June 30, 2000. Furthermore, Nstar-b was observed three times: 05:40–06:17 UT on June 29, 2000, 07:30–08:15 UT on June 29, 2000, and 01:10–02:07 UT on June 30, 2000.

The received bandwidth was 12.5 kHz, and the sampling frequency was set at 25 kHz. The data

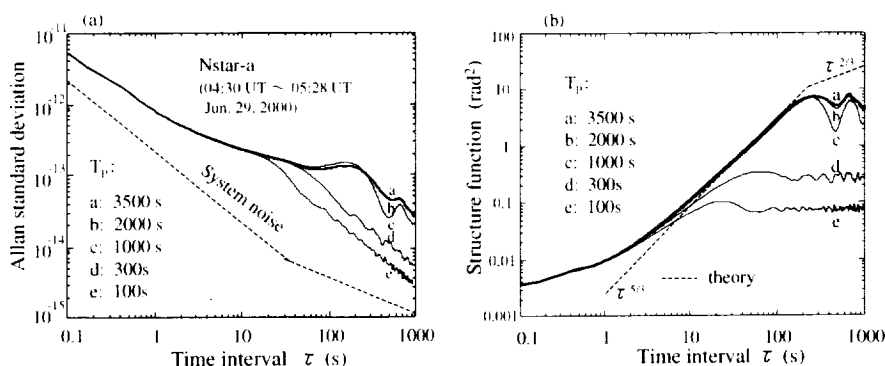


Figure 3. (a) Allan standard deviation and (b) time structure function with different values of  $T_p$ .

at the Mizusawa station were transmitted to the Kagoshima station via ISDN. At the Kagoshima station, the correlation phase was calculated with an integration time of 82 ms.

Figure 2(a) shows the correlation phase before fringe stopping for the data from 04:30 UT to 05:28 UT on June 29, 2000. As shown in Fig. 2(a), the correlation phase decreased monotonically. By the method of least squares with  $T_p=3,500$  s, the following expression for the component of long period of the correlation phase was obtained:

$$\phi_s(t) = 2.0181 \times 10^{-4} t^2 - 3.1684t, \quad (1)$$

where  $t$  is measured in second. It was confirmed that the coefficients of each term in  $\phi_s$  agreed with those calculated from the orbital data of the satellite. The correlation phase after fringe stopping using Eq. (1) is shown in Fig. 2(b).

#### 4. Analysis

In order to analyze the time variation of the correlation phase  $\phi(t)$ , the Allan standard deviation,  $\sigma_y(\tau)$  [2], and the time structure function,  $D_\phi(\tau)$  [3], were calculated;

$$\sigma_y(\tau) = \frac{1}{\sqrt{2\omega\tau}} \langle [\phi(t+2\tau) - 2\phi(t+\tau) + \phi(t)]^2 \rangle^{1/2} \quad (2)$$

$$D_\phi(\tau) = \langle [\phi(t+\tau) - \phi(t)]^2 \rangle \quad (3)$$

Here,  $\omega$  is the observation angular frequency,  $\tau$  is a time interval, and  $\langle \cdot \rangle$  means time averaging.

Figures 3(a) and 3(b) show the Allan standard deviations and the time structure functions of the correlation phase variation for different values of  $T_p$ , respectively. The dashed line in Fig. 3(a) is the calculated result of  $\sigma_y(\tau)$  of the system noise including the instability of hydrogen maser oscillators, thermal noise, and so on. The dashed line in Fig. 3(b) is the theoretical curve of  $D_\phi(\tau)$  of atmospheric disturbances [3]. As seen in Fig. 3(a), the magnitude of  $\sigma_y(\tau)$  of the time variations of the correlation phase observed was three times larger than that of the system noise. Thus, the main cause of the time variation of the correlation phase observed is considered to be atmospheric disturbances.

For  $T_p > 1,000$  s, the curves of  $\sigma_y(\tau)$  almost did not depend on  $T_p$  for the entire region of  $\tau$ , and showed a flat region for  $\tau < 200$  s. On the other hand, the time structure functions showed the

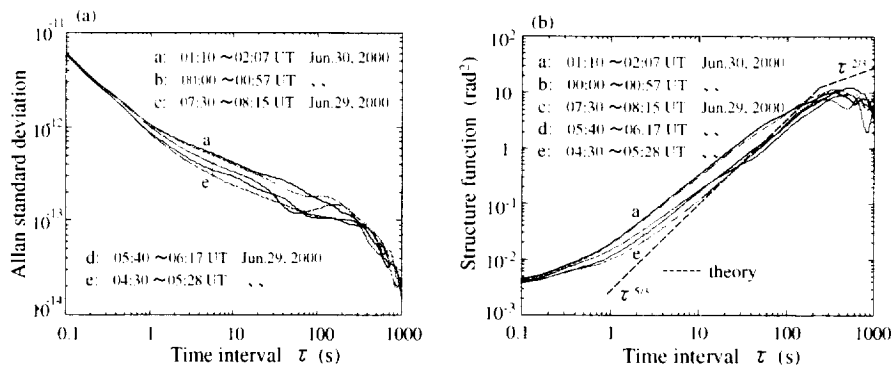


Figure 4. (a) Allan standard deviation and (b) time structure function of the 5 observations.

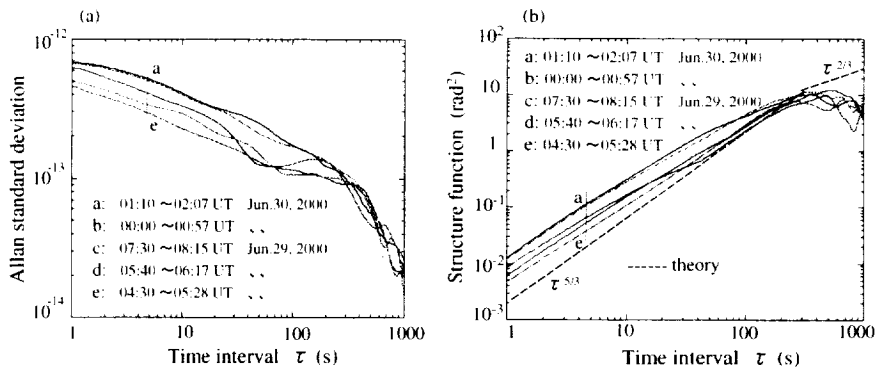


Figure 5. (a) Allan standard deviation and (b) time structure function of the 5 observations after moving-averaging with  $T_a=1$  s.

independence of  $T_p$ , and approached the theoretical curve,  $D_\phi(\tau) \propto \tau^{5/3}$  in the region of  $\tau < 200$  s [3]. That is to say, to get the information of atmospheric disturbances with long period,  $T_p$  is required to be longer than 1,000 s.

Figure 4(a) shows the Allan standard deviations and Figure 4(b) shows the time structure functions of the time variations of the correlation phase observed in this work. The values of  $T_p$  were different for different observations, but larger than 2,000 s. As seen in Fig. 4(a) and 4(b), for  $\tau < 1$  s, the curves of the five observations coincide with each other for either  $\sigma_y(\tau)$  or  $D_\phi(\tau)$ . In this region,  $\sigma_y(\tau) \propto \tau^{-0.8}$  and  $D_\phi(\tau)$  does not change so much compared with that in other regions except for  $\tau > 200$  s. These facts suggest that the dominant factor of the correlation phase variations in the region is white phase noise.

In the next step, the component of high frequency in the time variations of the correlation phase was subtracted by the moving average method with an interval  $T_a=1$  s. Figures 5(a) and 5(b) show the results for the moving-averaged time variations of the correlation phase. As seen in Fig. 5, in the region of  $1 \text{ s} < \tau < 200$  s, the curves are almost parallel to each other and  $\sigma_y(\tau) \propto \tau^{-0.2}$ , and  $D_\phi(\tau) \propto \tau^{5/3}$ . These facts suggest that the dominant factor of the correlation phase variations in the region is flicker frequency noise. On the other hand, in the region of  $\tau > 200$  s, where

$\sigma_y(\tau) \propto \tau^{-1}$ , the main factor of the correlation phase variations seems to be white phase noise.

## 5. Discussion

The explanation of the results obtained in this work was made with a frozen-screen model of atmospheric disturbances [4]. In the model, water vapor is contained in tropospheric screens of various sizes, which move horizontally over the antennas at an average velocity. In each screen, the distribution of water vapor is given by Kolmogorov's turbulence theory. The motion of the screens and the turbulence inside the screens cause random variations in the phase of radio waves passing through the screens.

The quick variation of the correlation phase in the region of  $\tau < 1$  s may be mainly caused by turbulence inside the screens. The coincidence of the curves of the five observations suggests that the strength of the turbulence inside the screens varied slightly during the observation time.

The correlation phase variation in the region of  $1 \text{ s} < \tau < 200 \text{ s}$  may be mainly caused by the motion of the screens. The variations of  $\sigma_y(\tau)$  and  $D_\phi(\tau)$  in this region reflect the strength of atmospheric disturbances.

The profile of  $\sigma_y(\tau)$  and  $D_\phi(\tau)$  for  $\tau > 200$  s mainly reflects to the phase variations with large amplitude and period longer than several hundred seconds, which may be mainly caused by the motion of large screens. Since the observation periods in this work were less than 1 hour, we could not exactly confirm the properties of  $\sigma_y(\tau)$  and  $D_\phi(\tau)$  for  $\tau > 200$  s. We will get data for longer observation time to study the properties of  $\sigma_y(\tau)$  and  $D_\phi(\tau)$  for  $\tau$  larger than several hundred seconds.

## 6. Conclusions

For real-time observations of atmospheric disturbances on a very long baseline, the beacon waves of the geostationary satellites were received using the Kagoshima 6-m and the Mizusawa 10-m radio telescopes. From the Allan standard deviation and the time structure function, it is found that the time variations of the correlation phase were mainly caused by atmospheric disturbances, and that for  $1 \text{ s} < \tau < 200 \text{ s}$ , the Allan standard deviation of atmospheric disturbances  $\sigma_y(\tau) \propto \tau^{-0.2}$  and the time structure function  $D_\phi(\tau) \propto \tau^{5/3}$ . The profiles of  $\sigma_y(\tau)$  and  $D_\phi(\tau)$  were explained with a frozen-screen model of atmospheric disturbances.

## References

- [1] M. Nishio, Q. Liu, T. Miyazaki, N. Kawaguchi, T. Sasao, T. Omadaka, and M. Morimoto, "Development of real-time diagnostic system for VLBI using public communication lines," *IEICE Trans.B*(in Japanese), vol.J83-B, no.8, pp.1195-1202, 2000; *Electronics and Communications in Japan*, John Wiley & Sons, part 2, vol.84, no.6, pp.1-9, 2001.
- [2] A.E.E Rogers and J.M. Moran, "Coherence limits for very long baseline interferometry," *IEEE trans., Instrum. & Meas.*, IM-30, no.4, pp.283-286, 1981.
- [3] A.F. Dravskikh and A.M. Finkelstein, "Tropospheric limitations in phase and frequency coordinate measurement in astronomy," *Astrophys. Space Sci.*, vol.60, pp.251-265, 1979.
- [4] C.R. Masson, "Atmospheric effects and calibration in astronomy with millimeter and submillimeter wave interferometry," M. Ishiguro and W.J. Welch, Eds., *Astron. Soc. Pacific Conf. Series* 59, pp.87-95, 1994.

## IP Data Transfer System for Real-time VLBI

Sotetsu Iwamura<sup>1</sup>, Hisao Uose<sup>1</sup>, Tetsuro Kondo<sup>2</sup>, Shin-ichi Nakagawa<sup>3</sup>, Kenta Fujisawa<sup>4</sup>

<sup>1</sup>) *NTT Information Sharing Platform Laboratories*

<sup>2</sup>) *Kashima Space Research Center, Communications Research Laboratory*

<sup>3</sup>) *Communications Research Laboratory*

<sup>4</sup>) *National Astronomical Observatory of Japan*

Contact author: Sotetsu Iwamura, e-mail: [iwamura.sotetsu@lab.ntt.co.jp](mailto:iwamura.sotetsu@lab.ntt.co.jp)

### Abstract

We constructed a data transfer system for real-time very long baseline interferometry (VLBI) using Internet protocol (IP) in GALAXY project. The system achieves maximum transfer rate of 256 Mb/s based on parallel transfer using multiple IP streams. This system features bandwidth scalability by increasing the number of PCs for transmitting and receiving IP data. Using the system, we conducted experiments transmitting VLBI observation data at 128 Mb/s and successfully detected a fringe. This is the first IP-based real-time VLBI in the world.

### 1. Introduction

This paper presents our data transfer system for very long baseline interferometry (VLBI) using Internet protocol (IP) in GALAXY project.

Since 1998, GALAXY project, which is composed of Communications Research Laboratory, National Astronomical Observatory of Japan, The Institute of Space and Astronautical Science and NTT, has been conducting experiments on real-time VLBI. In the experiments, observation data is transmitted over NTT's 2.4 Mbps asynchronous transfer mode (ATM) network; therefore, we can catch up with real-time phenomena as well as improve observation efficiency.

In addition to the experiments based on ATM, we have been focusing on IP transfer for VLBI data delivery. Adopting IP technique into real-time VLBI brings the following advantages that are essential to our goal.

- Improvement of interconnectivity with other observation sites far apart
- Easiness to introduce distributed processing schemes
- Utilization of low-cost but high-performance equipment

### 2. IP Transfer Architecture for Real-time VLBI

As policies in constructing an IP transfer system, we focused on the following points:

- Making the most use of the existing equipment such as samplers and cross correlators,
- Achievement of transparency in data transfer,
- Examining performance of multi-purpose PC in IP transfer for real-time VLBI.

A configuration of our IP transfer system is shown in Figure 1. The system consists of an ID1 parallelizer, an ID1 serializer, IP-transmitting PCs, and IP-receiving PCs.

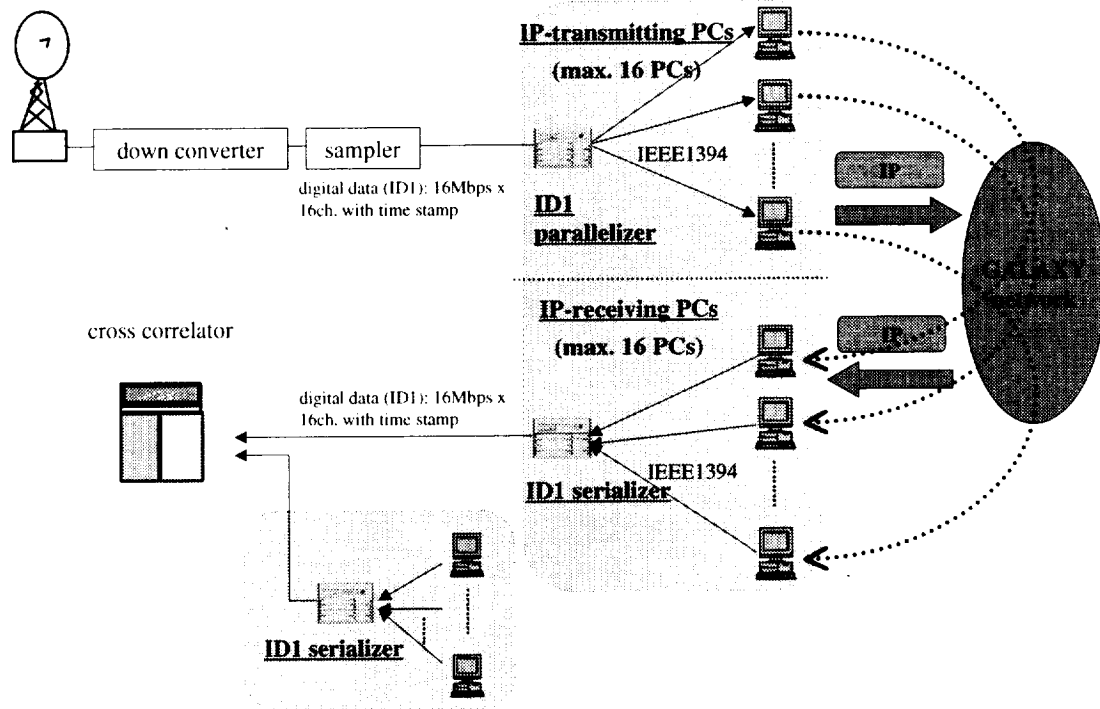


Figure 1. Configuration of IP transfer system for real-time VLBI

In order to achieve high transfer-rate required for real-time VLBI observation, we adopted a parallel IP transfer schemes, using multi-purpose PCs. In the system, the ID1 parallelizer receives the data stream from the sampler through the ID1 interface, and divides it into multiple IEEE1394 streams. Each IP-transmitting PC receives the IEEE 1394 stream, extracts observation data, and transmits it in IP packets.

On receiving the IP packets, each IP-receiving PC extracts observed data and transfers it to the ID1 serializer in an IEEE 1394 stream. Upon receiving the IEEE 1394 data streams from the IP-receiving PCs, the ID1 serializer constructs the observation data and sends it to the cross correlator.

Thus the cross correlator can process cross-correlating calculation, also by receiving other observation data from the other IP transfer system.

### 3. ID1 Parallelizer and ID1 Serializer

Internal action of ID1 parallelizer and ID1 serializer is shown in Figure 2.

An ID1 parallelizer divides received data into multiple blocks of a fixed length and stores each of them in the internal queues, by a round robin manner. Accordingly, the top data blocks of each queue are transmitted in parallel IEEE 1394 streams.

An ID1 serializer collects data blocks of fixed length via IEEE 1394 interfaces. After receiving enough numbers of the data blocks, the ID1 serializer constructs observation data, also by adopting the same round robin scheme as the ID1 parallelizers, and outputs it through the ID1 interface.

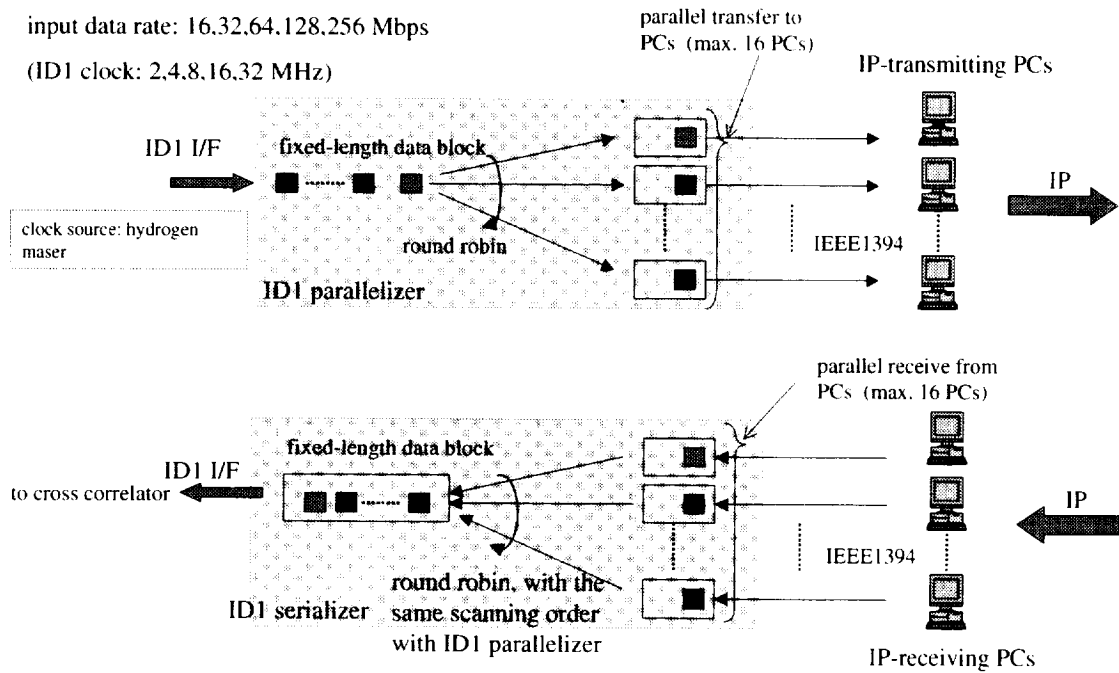


Figure 2. Internal action of ID1 parallelizer/serializer.

#### 4. IP-transmitting PC and IP-receiving PC

Each IP-transmitting PC receives data in an IEEE 1394 data stream, and transmits it in UDP/IP packets to the corresponding IP-receiving PC. The IP-receiving PC extracts data from received UDP/IP packets, and sends it in an IEEE 1394 stream. Accordingly, multiple UDP sessions are set up between the IP-transmitting PCs and the IP-receiving PCs.

The reason we use UDP instead of TCP is to reduce the PC's CPU load and not to be influenced by round trip time.

Generally, a parallel transfer scheme must guarantee data to correctly be ordered. In this system, by the round robin manner common both in the ID1 parallelizer and the ID1 serializer, the same data can be obtained from the ID1 serializer as the input data to the ID1 parallelizer.

Another important issue to consider is possibility of packet loss, caused by lacking of retransmission mechanism on UDP. This can disturb the construction of correct data in ID1 serializer. In order to solve this problem, we decided to generate random data of the same size on the IP-receiving PC when packet loss is detected. Detection of packet loss on receipt can be easily achieved by adding a sequence number at the top of each payload of UDP packets before transfer. This

simple handling causes no problem for cross correlation because result of cross correlation will be influenced little by inserting up to 0.1% of dummy data.

## 5. Implementation

We implemented the ID1 parallelizers and ID1 serializers as specific equipment. Major specifications of ID1 serializer and ID1 parallelizer are described in Table 1.

Table 1. Specifications of ID1 parallelizer/serializer

	ID1 parallelizer	ID1 serializer
input I/F	ID1 x1 port	IEEE1394 x16 port
output I/F	IEEE1394 x16 port	ID1 x1 port
maximum PCs to connect	16	16
internal data-block size [KB]	32,64,128,256,512,1024	←
ID1 clock [MHz]	synchronization to input ID1 I/F	2,4,8,16,32
maximum throughput [Mbits/sec]	256	256

For IP-transmitting and IP-receiving PCs, we use Pentium2/400 PCs, on which Linux 2.4.6 is running. On these PCs, we implemented application software in C language to send and receive IEEE1394 packets and IP packets.

## 6. Experiment

We conducted IP-based real-time VLBI observation, using our IP transfer system. The configuration is shown in Figure 3.

Important information is as follows.

- date: Jan. 17, 2002
- antenna: 64 m (Usuda site) and 34 m (Kashima site)
- baseline: 200 km
- observation band: C band
- observed object: J0136+47
- data rate: 128 Mbps
- network: GALAXY experimental network (based on 2.4 Gbits/sec SDH)
- data transfer protocol: IP (Usuda - Musashino, 115km), ATM (Kashima - Musahino, 100km)
- PCs: four PCs (two PCs for each sending and receiving IP)
- IP streams: 32 Mbps x4 streams (each pair of PCs to handle two IP streams)

In the experiment, observed data at Usuda 64 m antenna was transmitted to Musashino (NTT R&D Center) by the IP transfer system at the rate of 128 Mbps. At the same time, another observation data was sent from Kashima 34 m antenna also to Musashino by ATM. By conducting cross-correlation processing at Musashino, we confirmed fringes. We are convinced that this is the first successful experiment in the world on real-time VLBI observation based on high-speed IP transfer.

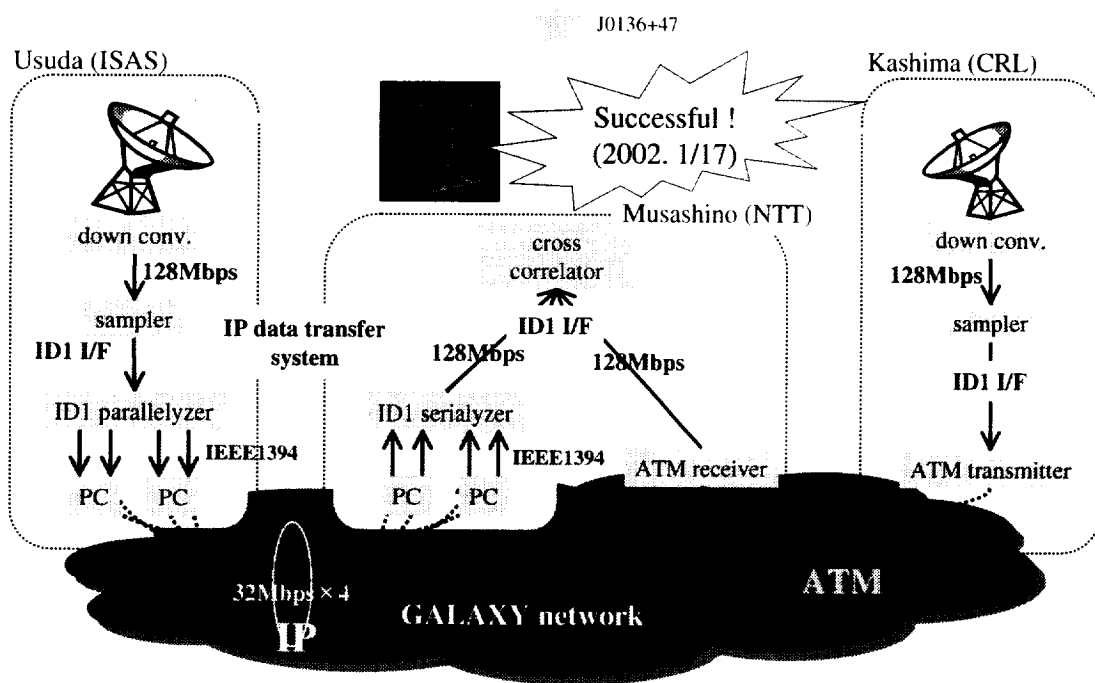


Figure 3. IP-based real-time VLBI experiment

## 7. Future Plans

We are currently working on the following issues.

- Implementing appropriate protocol between IP-transmitting PC and IP-receiving PC, which can adapt to dynamic change of network quality,
- Increasing transfer rate up to order Gbits/sec,
- Application to other scientific fields that require high speed data transfer.

# Parallel Data Processing System

*Hitoshi Kiuchi*

*Communications Research Laboratory, H.Q.*

*e-mail: kiuchi@crl.go.jp*

## Abstract

Signal processing in the current correlation processing algorithm is bit-serial. The speed of correlation is limited by the speed of the correlation device, and, as a result, the device speed limits observing bandwidth. The algorithm is thus not effective for astronomical applications. To overcome this problem, I have developed a new correlation-processing algorithm for parallel data. We focus on the derivation of serial data-processing algorithms for parallel data.

## 1. The Current Parallel-data Processing System

The improvement of sampling and recording technologies to achieve higher speeds of data processing is required. The data-processing speed, however, is restricted by the correlation device-clock in serial data processing. In recent technologies, we can obtain the data rate to several gigabits per second. New 1024-Mbps recorders including GBR-1000, Mark-IV, S3, and DIR-2000U, will become available.

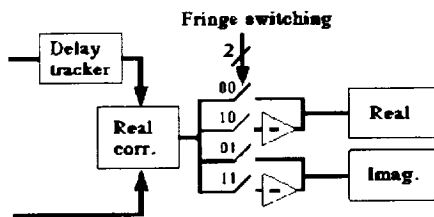


Figure 1. Block diagram of a current giga-bit correlation system GICO.

The GICO (giga-bit correlator) is the first parallel data processing system. GICO's correlation processing algorithm operates on parallel data (Fig. 1). However, because fringe stopping is carried out in parallel data steps rather than in bit steps, there is some loss of coherence. The continuous delay tracking range is limited to 8064 bits.

## 2. New Parallel Data Processing System

When designing a correlation processor, we must take into account delay tracking, fringe stopping, and 90-degree phase jumps. We focus on how to derive processing serial data algorithms for parallel unit of data. The serial data processing algorithm of the Mark III is sophisticated, so I wished to convert it to operate on unit of parallel data.

### 2.1. Delay Tracking Based on Parallel Data

We consider the operation of the parallel delay tracking algorithm in one-bit steps. We assume that there are  $n$  parallel data bits. The circuit consists of parallel shift registers A and B (Fig. 2).

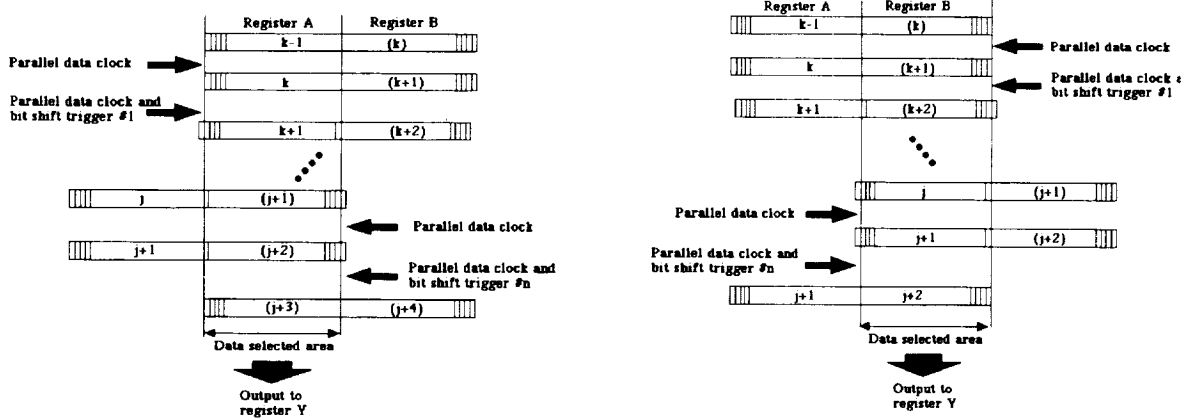
Initially, the  $(k - 1^{th})$  datum is loaded into parallel shift register B from the parallel data buffers for Station-Y data; these buffer memories work in a pipeline sequence.

The  $k^{th}$  data bit is then loaded into parallel shift register B from the buffer memory. At the time at which the data in shift register B are shifted to shift register A. The data output to register Y for correlation with Station X data, displayed as the data selected area between two lines in the figure, is selected by a parallel data selector which is controlled by a control counter. When a bit shift occurs, the control counter is incremented/decremented. All of the circuits are driven by a parallel data clock. The shifting of bits is thus performed with this parallel data clock's timing.

Next, we consider the timing of bit shifts in more detail. We can detect a bit shift in the following way. We performed *a priori* calculations of the Earth's rotational parameters including wobble, diurnal polar motion, diurnal rotation, nutation, precession, aberration, time difference, etc..  $\tau_g$  was calculated and approximated as a fourth-order polynomial in the built-in controller which was adopted from the KSP correlator [1]. Comparing the delay of the current parallel clock cycle with that of the previous cycle, we find that the difference in time is  $n$  (parallel number) of the sampling period when the delay difference is more than 1 bit, fractional delay in the parallel bits was occurred. Usually, the values of all bits of the bit-select control register are "0". If there is a fractional delay in the parallel bits, "0" and "1" are sent to the bit-select control register. The fractional bit shift timing is indicated by the boundary between the "0" and "1" bits (Fig. 3). Parallel data can be bit-shifted in one-bit steps.

When the control counter's value reaches its maximum (left-hand side: Fig. 2), the next data bit is loaded into the parallel shift registers from the parallel data buffers and the conditions of registers are simultaneously set to "zero" on the next data-clock cycle.

When the control counter reaches zero (right-hand side: Fig. 2), the next data bit is unloaded into the parallel shift registers from the parallel data buffer, and the conditions of the registers are simultaneously set to "full" on the next data-clock cycle.



Memory control sequence (positive delay rate).  
Data numbers in brackets are loaded data from  
buffer memory.

Memory control sequence (negative delay rate).  
Data numbers in brackets are loaded data from  
buffer memory.

Figure 2. Delay tracking.

## 2.2. Parallel Fringe Rotation

We performed *a priori* calculations in the built-in controller for every cycle of the parallel data clock.

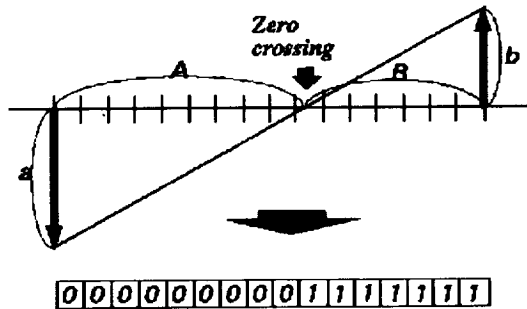


Figure 3. Zero cross decision.

Usually, the bits of the phase control register are all "0". Comparing the fringe phases at time  $k$  with those at time  $(k+1)$ , we find that the difference in time is  $n$  (parallel width) sampling periods when the phase difference is more than  $\pi/8$ , and "0" and "1" are set in the phase control register. The boundary between "0" and "1" bit indicates the fractional bit shift timing, and the fringe phase must be changed by  $\pm\pi/8$  radian. The position of the boundary is determined (Fig. 3) by the division circuits.

## 2.3. Parallel 90-degree Phase Jump

Fringe stopping is performed on the band center frequency; a 90-degree phase jump and a bit shift are done simultaneously. The bit select control register (for delay tracking based on the parallel data but in one-bit steps) also controls the 90-degree phase jump. The timing of the 90-degree phase jump is indicated by the boundary between the "0" and "1" bits of the bit select control register (Fig. 3).

## 2.4. Data Synchronization

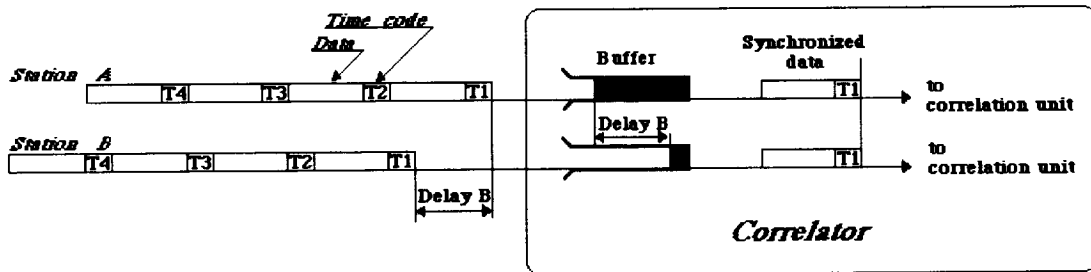


Figure 4. Data synchronization sequence in case of real-time VLBI.

In real-time correlation [1], the correlator is equipped with a function for automatic data synchronization so there is no need for external units. Time stamps composed of indicators of year, day, hour, minute, second, and the SYNC code used in time code recognition are inserted

in the data at regular intervals. To absorb the transmission path delay, signals are stored in the buffer memory at the same time as the time stamp is received. This time stamp is generated by the ATM interface unit. Readout starts immediately after the time stamps from all observation stations have arrived, and this allows synchronization of timing. The data are only output to the correlation part after the timing has been synchronized, so the output data for each station are correct up to the time at which the time stamp is applied. The size of the buffer memory is 64 Mbits/ch. The same data synchronization function is used in tape-based correlation.

### 3. System Evaluation

The giga-bit system consists of a giga-bit sampler, an ATM interface unit, and a giga-bit correlator.

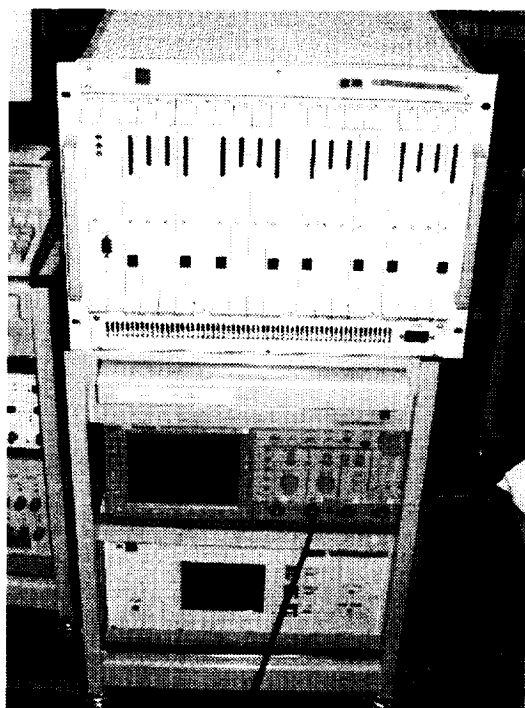


Figure 5. Picture of giga-bit system (Upper: giga-bit correlator, middle: sampler (TDS-784), lower: ATM interface).

The giga-bit sampler is based on a commercially available digital oscilloscope (Tektronix TDS784). The development of this radio astronomical A/D sampler began in 1995. The oscilloscope has four analog-to-digital sampler chips, each of which operates at a maximum speed of 1 Gbps with a quantization level of eight bits for each sample. The two MSBs quantized bits of each sample (ch.) are extracted from the digital oscilloscope and sent connected to the ATM-interface unit. The sampling rate was increased by 25.6/25, to make the original 1-Gsps sampler operated as a 1.024-Gsps sampler. This modification was applied in the A/D sampled signal pick-up daughter board in the oscilloscope. The output signal is sent via high-speed parallel coax and the (4-channel) \* (256 or 512 or 1024 Msps) \* (2-bit sampling) data are output from the pick-up daughter board. The oscilloscope is able to calibrate itself by signal path compensation. A self-calibration function is also used to calibrate the DC offsets of the A/D converters according to changes in the ambient temperature. This function is useful in multi-bit sampling.

The ATM interface has a real-time clock that is phase-locked to the data clock of the giga-bit sampler. The data input from the giga-bit sampler are formatted and a time code is inserted. Channel selection (1/2/4 ch) and quantization-bit selection (1 or 2 bit) are performed in the formatting section. The rate of the output of data to the recorder or ATM line is selected from among four rates, ranging from 256 to 2048 Mbps.

Fig. 5 is a photograph of the correlation system. The number of parallel data bits is 64. The

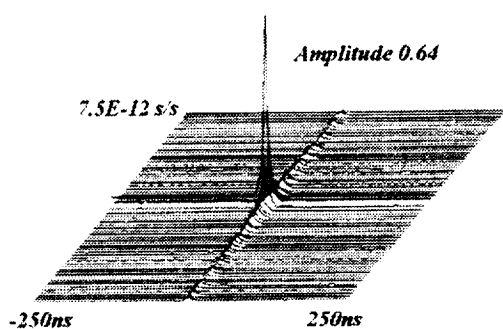
maximum speed of processing is 2048 bps/ch, and the correlator is four-channel. Each channel has 1024 complex lags.

### 3.1. Correlation by Using a Wavefront-clock Fringe-simulator

White noise from a noise diode is converted to simulate a signal received from a star as if it were being observed at the target station by using a wavefront clock system. If the RF noise signal is divided with one branch acquired by using a normal VLBI system and the other branch acquired by a wavefront clock system, we are able to obtain a simulation of VLBI data at two different stations, that is, a VLBI fringe data simulator. The simulator-generated virtual VLBI station data was used to check the operation of the giga-bit correlator. One set of the results of this simulation is shown in Fig. 6.

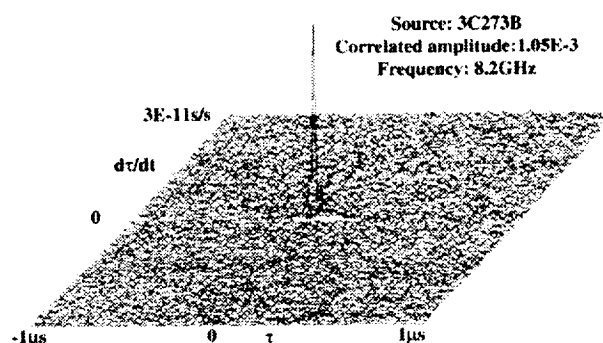
### 3.2. Real-time Fringe Detection using an ATM Network

A real-time experiment between the Koganei and Kashima KSP stations was carried out. The IF signal was down-converted to a wide bandwidth video signal by using a KSP local oscillator. The wide bandwidth video signal was sampled by the giga-bit sampler, and then formatted by the ATM interface unit. The formatted signal was transmitted from Kashima to Koganei via the ATM line. After that, correlation processing was performed. The experimental result is shown in Fig. 7, displayed 512 lags around the fringe. The result shows that we had been able to obtain fringes with high SNR.



Simulated result (1024 Mbps) by using a wavefront clock simulator. Correlated amplitude is 0.64.

Figure 6. System check.



Result of this system (Koganei-Kashima baseline experiment).

Figure 7. Real-time experiment.

## References

- [1] Kiuchi H., M. Imae, T. Kondo, M. Sekido, S. Hama, T. Hoshino, H. Uose, and T. Yamamoto, In: Real-time VLBI system using ATM network, IEEE Trans. Geosci. and Remote Sensing, Vol.38, No.3, pp.1290-1297, 2000.

## Multi-Beam VLBI

*W.T. Petrachenko, Calvin Klatt, Vincent Ward*

*Geodetic Survey Division, Natural Resources Canada*

*Contact author: W.T. Petrachenko, e-mail: [bill.petrachenko@hia.nrc.ca](mailto:bill.petrachenko@hia.nrc.ca)*

### Abstract

In comparison to GPS, VLBI, as it is typically practised today, suffers from the fact that at any location only one source can be observed at a time. In this paper, we ask the audience to consider a world in which each VLBI reference location is equipped with a cluster of small antennas. Fringe detection limitations experienced by the small antenna pairs can be overcome by using large antennas for SNR enhancement and then mathematically forming the cluster-cluster observables after the fact. The resulting network, if the co-located antennas are carefully tied together, could perform multi-beam VLBI. By having multiple beams in different directions, parameter correlations could be reduced and parameters of interest could be determined more quickly and accurately. Taking advantage of new developments in the astronomical community, inexpensive antennas may be available to make this dream a reality. Advantages and limitations of this approach will be considered. The resulting advancement in geodetic VLBI science may be significantly more cost-effective than simply increasing the recording bandwidth. This presentation is intended to generate further discussion and lateral thinking about the future of geodetic VLBI.

### 1. Introduction

Ever since the first successful demonstration of VLBI, recording technology has been a dominant focus of VLBI development. However, with the advent of low cost high capacity off the shelf discs and the anticipation of low cost global fiber/optic connections, simple economical solutions to VLBI's data transmission problem can at long last be envisioned. With the data transmission problem in principle solved, now is an opportune time for IVS Technology Development Centers to turn their focus to the many other factors that limit VLBI and to work out a comprehensive technological vision for the future that addresses as many of these factors as possible.

It is in this spirit that we embarked on the present investigation. It eventually led us to consider an innovative implementation of the concept of "multi-beam" VLBI. "Multi-beam" VLBI refers to the ability of an interferometer baseline to observe more than one source at a time. Technologically this can be achieved a number of different ways such as with multi-beam phased arrays or Lunenberg lenses. However, the most obvious approach, the one considered here, is to use multiple antennas at each station. Although the concept is not new [1], and its benefits are widely understood, it has never been implemented due to the excessive cost of clusters of large antennas. The challenge of this paper will be to show that there is in fact an affordable solution to the problem that uses clusters of small low cost antennas in conjunction with a few large antennas for sensitivity enhancement. In fact, it will be shown that the cost of each cluster can be reduced to the extent that significantly larger geodetic VLBI networks can be considered.

## 2. Search for a Low Cost Geodetic VLBI Antenna

Although geodetic VLBI has a potential performance advantage over other space geodetic techniques due to its use of the stable quasar reference frame it is not currently fulfilling this promise. This results at least partially from the high capital and operating costs associated with the large antennas used to collect the weak quasar signals. These high costs, in turn, result in VLBI networks that are undersized and observations that are comparatively infrequent. This investigation began with a desire to see whether the “commercial off the shelf” (COTS) principle, already used to such good advantage in recording technology, could be extended to the design of a complete low cost geodetic VLBI station. In particular, a solution was considered involving widely available commercial satellite technology. News of progress being made on the Allen Telescope Array (ATA) to apply this principle to the development of a low cost radio antenna with large collecting area provided further encouragement.

The ATA is a joint project of the SETI Institute and the University of California, Berkeley. The purpose of the project is to design and build a one-hectare microwave collecting area for less than \$26,000,000 US. First light for the instrument is expected some time around 2005. It is one of five competing technologies for the Square Kilometer Array.

Loosely speaking, the ATA can be described as a field of phased satellite antennas, with the current design employing 350 6.1m antennas. Although the antennas take their inspiration from the satellite industry, their projected performance far exceeds that of a typical backyard satellite dish as can be seen in the specifications summary in Table 1. The projected cost for an antenna including pier, pedestal, positioner, reflector, feed, LNA, fiber optic transmission system and RF-to-IF converter is about \$50,000 when produced in large quantities.

Table 1. Projected ATA Antenna Specifications

Diameter	6.1m
Focus	Offset Gregorian
F/D	0.4
Efficiency	63%
Positioner	Alt-Az
Feed	Pyramidal log periodic
Polarization	Dual linear
Tsys goal	35K
RF Band	0.5 to 11 GHz

One interesting characteristic of the ATA antenna that is worth mention in the context of geodetic VLBI is that the antenna, feed, LNA and RF-to-IF electronics can all handle the full continuous frequency band from 0.5 to 11 GHz. This is an essential specification for the ATA to avoid the need to change 350 “front-ends” every time a new frequency band is selected. For geodetic VLBI, it has the benefit of enabling phase connection across more than 10 GHz. This, in turn, enables the use of the phase delay observable even for modest SNR observations. This is important since it represents more than an order of magnitude improvement in delay measurement precision; and to make matters even better, this is coupled with a proportional decrease in the effect of systematic phase biases on the delay observable. Furthermore, continuous frequency coverage from 0.5 to 11 GHz provides access to the higher order ionospheric terms.

### 3. Baseline Sensitivity with an ATA Antenna

Whenever considering the effectiveness of a small antenna, the most obvious issue is one of sensitivity. Fortunately, the sensitivity of an interferometer baseline is proportional to the geometric mean of the diameters of its two antennas. Hence, a small antenna can achieve adequate baseline sensitivity provided that its partner antenna is sufficiently large.

In geodetic VLBI, the question of sensitivity has two facets. First, is the signal strong enough to determine delay and delay rate with sufficient accuracy; and second, can enough sources be detected at that SNR to provide the geometric strength to produce a well-conditioned parameter inversion? Based on these two considerations, a reasonable sensitivity criterion for an ATA-style antenna could be stated as follows: *A large fraction of the usual geodetic VLBI candidate sources must be detectable, with  $SNR > 20$ , when the ATA antenna forms baselines with other IVS network antennas.* To see whether the ATA antenna meets this criterion, a list of 18 IVS antennas with SEFD < 3500 and a list of 92 typical geodetic candidate sources were considered. A record rate of 1 Gbit/s and a scan length of 300s were assumed. For all 18 antennas, at least 95% of the sources achieve SNR=20 or better.

It is clear that an ATA-style antenna has more than adequate sensitivity when it observes along with any of the above 18 IVS antennas. However, using the same assumptions as above, it is also interesting to note that for a baseline that has ATA antennas at both ends, 71% of the 92 candidate sources are detectable at SNR=20. In short, a network, made up entirely of ATA-style antennas, is useable but probably not optimum until data rates beyond 1 Gbit/s become affordable.

### 4. A New Low Cost Geodetic VLBI Station

So far, we have been considering the antenna subsystems in isolation. However, there is more to a geodetic VLBI station than the antenna, e.g. hydrogen maser, data acquisition system (DAS), data recorder, monitor/control and ancillary data systems, and infrastructure such as power and shelter. Given that the maser and DAS are themselves costly items, it is not likely that a complete station can be constructed for less than \$500,000 if traditional VLBI solutions are assumed. However, the application of a combination of innovation, modern technology and the COTS/MOTS principle to the design of these subsystems promises to greatly reduce their cost. In the case of the DAS, some examples of applying these approaches might include the use of low cost commercial satellite components, the use of high speed samplers coupled with a completely digital back-end, or perhaps the use of a single wide-bandwidth baseband channel along with a frequency switched local oscillator. In the case of the maser, it might be possible to replace it entirely with a lower performance clock and then achieve coherence through, for example, VLBI phase referencing to geostationary satellites.

### 5. "Multi-beam" VLBI

A small antenna paired with a large antenna for sensitivity enhancement is not a new idea in geodetic VLBI. In fact, it was this principle that made the use of the small mobile MV antennas practical during the Crustal Dynamics Project (CDP). However, in the CDP, a single small antenna was used in an array of large antennas. Here we consider the opposite, a network with a single large antenna and numerous small antennas. The main attraction of this network architecture is

that the incremental cost of adding new VLBI stations is greatly reduced, making larger networks affordable. Although the performance of the new low cost geodetic VLBI stations and the proposed network architecture is promising, with an additional twist to the configuration, the potential for performance improvement is even more impressive.

Since antenna cost is low, the idea is to equip each station with more than one antenna, each observing a different source, i.e. multi-beam VLBI. This mode of operation has two important benefits. First, because of the multiple antennas used, significantly more scans can be acquired per day. This is an important figure-of-merit with respect to improving the conditioning of VLBI parameter inversions. Second, since the hydrogen maser reference oscillator is common to all antennas in the cluster, its corrupting effect disappears when data is differenced between antennas. Removal of clock terms from the parameter list also greatly improves the conditioning of the parameter inversion.

The procedure that enables the use of clusters of *small* antennas is simple. For sensitivity enhancement, each of the small antennas in a cluster observes along with one large antenna. In other words, if there are four antennas in each cluster, then a total of four large antennas will be required. Antenna number 1 in each cluster will observe with the first large antenna; antenna number 2 in each cluster will observe with the second large antenna; and so on. Fringes are only detected on baselines that include one small and one large antenna. Observables on the baselines between pairs of small antennas, although often too weak to be detected, are determined mathematically after the fact through differencing.

## 6. A Vision for the Future of Geodetic VLBI

In this final section, we challenge the reader to consider the following list of performance benefits of a new IVS reality that includes a network of identical low-cost multi-beam VLBI stations.

1. **Larger networks.** With the greatly reduced incremental cost of adding VLBI stations, much larger networks become affordable. A larger network has the potential of adding accuracy and robustness to VLBI solutions.
2. **Improved site selection.** For practical reasons, early VLBI stations were often acquired on an “as is, where is” basis. Assuming that a new large VLBI network is being planned, station locations can be selected according to merit, based on, for example: achieving uniform global coverage; occurrence of benign tropospheric conditions; accessibility to infrastructure such as power, advanced communications networks and personnel; geological stability; accessibility of bedrock; lack of interference; nearness to other fundamental geodetic measurements; etc.
3. **More scans per day.** Obviously, if several antennas are observing simultaneously at each station, more scans can be acquired per day. This tendency is further augmented by the fact that, with multiple antennas, each antenna can be assigned a different region of the sky, which significantly reduces slew distances. Finally, it is also easier to implement high slew rates on small antennas. This will have a more significant impact when data rates become high enough that the large antennas will not be required for SNR enhancement and can be eliminated entirely.
4. **Simultaneous scans and the removal of clock terms.** With a multi-beam VLBI station, scans on different antennas can be arranged to be simultaneous. Since the H maser clock is common to each antenna, its effect then disappears when observables are differenced between

antennas. The ability to remove clock terms from parameter adjustments may have a profound effect on performance. A simulation of a typical NEOS observation, with and without the inclusion of clock terms in the adjustment, showed that a factor of 3-4 improvement in EOP precision could be achieved when the clock terms were removed.

5. **Increased Data Rate.** Current trends indicate that disc capacities and fiber/optic data rates and costs, with their huge commercial drivers, will continue to improve at a rapid and exponential rate into the foreseeable future. Geodetic VLBI as it is currently practised does not stand to reap significant benefits from these industry advances since typical schedules are already slew time dominated. The multi-beam proposal, with its bias towards low sensitivity, stands to benefit from increased data rates well into the future. If data rates continue to increase, the obvious next step for multi-beam VLBI is to operate without the assistance of the large antennas used for sensitivity enhancement.
6. **Unattended operation.** The current state of communication systems, antenna controllers and record systems is such that automatic operation of a modern VLBI site is an attainable goal. In fact, it is probably a necessary goal if regular operations with a large network are to be practical. With the exception of trouble-shooting, routine maintenance, and shipping of record media, it should be possible to design stations to be robust and to operate completely unattended.
7. **Spanned bandwidth enhancement.** With the technologies used in the ATA antenna system, continuous bandwidth coverage in the range 0.5 to 11 GHz can be achieved. This opens up the possibility of using phase delay observables even for modest SNR observations. This will result in more than an order of magnitude improvement in delay observable precision and a proportional reduction in contributions of phase biases. The wide continuous frequency coverage also opens up the possibility of a higher order ionospheric correction.
8. **Stiffer antennas.** Small antennas tend to be stiffer than large antennas. This eases the requirements for modeling gravitational deformation. Thermal deformations are also smaller.
9. **Better survey ties.** It is assumed that it would be easier with a small antenna to implement a design for efficient and accurate survey ties to local networks.
10. **Efficient station development.** Assuming that a new large VLBI network is being planned, the opportunity exists to deploy identical stations at each site. This would allow funds to be focused on the design of an optimized station, with development costs being amortized among all the network stations. A coherent station design would also improve maintenance efficiency.

## References

- [1] Sasao, T., M. Morimoto, Antennacluster-Antennacluster VLBI for Geodesy and Astrometry, In: Proceedings of the AGU Chapman Conference on Geodetic VLBI: Monitoring Global Change, NOAA Technical Report NOS 137 NGS 49, 48-92, 1991.

## Geodetic Observation System in VERA

Yoshiaki Tamura <sup>1</sup>, VERA Group <sup>2</sup>

<sup>1)</sup> National Astronomical Observatory, Mizusawa

<sup>2)</sup> National Astronomical Observatory, Kagoshima University and Hosei University

Contact author: Yoshiaki Tamura, e-mail: tamura@miz.nao.ac.jp

### Abstract

VERA (VLBI Exploration of Radio Astrometry) consists of four VLBI stations. Each Station has a 20 m diameter antenna and is capable of observing at the frequencies of 2, 8, 22 and 43 GHz bands. The baseline length of VERA network is 1000–2270 km. The first VLBI fringe test in 22 GHz band was carried out in February 2002 between two stations. The geodetic observation system is under preparation to carry out the first observation in middle of 2002. Several observation modes are expected in the geodetic VLBI observations in VERA. One is VERA original mode which has a recording rate of 1 Gbps at the maximum. Another is so called K4 system whose recording rate is 128 Mbps. The latter system will be used for principally domestic compatible observations. The aimed accuracy of geodetic observation is 1–2 mm in 3 dimensions in VERA internal network, and 10 mm in the ITRF. This accuracy is required to obtain 10 micro arcsecond order astrometry purposes.

### 1. Introduction

VERA (VLBI Exploration of Radio Astrometry) is a new Japanese VLBI system dedicated to differential VLBI to measure the position and proper motion of maser sources in the Galaxy with 10 micro arcsecond level accuracy. VERA also aims at the Earth and planetary science such as studies on the tectonic motions around Japan, lunar geodetics by observing artificial radio sources loaded in satellites around the Moon (SELENE mission, launch in 2005). VERA project is being promoted by National Astronomical Observatory of Japan in collaboration with several domestic universities.

VERA network consists of four 20 m-diameter antennas. They are located at Mizusawa, Iriki, Ogasawara, and Ishigaki-jima. The range of the baseline length in the network is 1000 km to 2270 km. The provisional coordinates of VERA stations are listed in table 1.

In each station, dual receiver system of 22 GHz and 43 GHz bands are equipped to do differential VLBI observations for astrometry purpose. The dual receiver system is introduced in details by Kawaguchi et al. [1]. For the geodetic observations at 2 GHz and 8 GHz bands (S/X bands), ordinal single receiver system is adopted.

Table 1. Provisional coordinates of VERA stations.

Station	X	Y	Z	in meter
Mizusawa	-3857241.8	3108784.8	4003900.5	
Iriki	-3521719.4	4132174.6	3336994.3	
Ogasawara	-4491068.8	3481544.7	2887399.5	
Ishigaki-jima	-3263810.	4808265.	2619784.	(rough value)

## 2. Requirements in Geodetic Observations

The objective of geodetic observations is to attain as high precision as possible introducing wide band observation system which uses 1 Gbps recording system (SONY DIR2000 recorder). Construction of high precision coordinates is required not only for the studies of Earth science, but also for astrometric purpose. In astrometry, VERA is aiming to measure 10 micro arcsecond order annual parallax of radio sources by differential VLBI observation. In the case that the angular distance of two radio sources is 2 degree (maximum distance in VERA dual receiver system), the baseline accuracy of  $10^{-9}$  is required. That is, to measure 10 micro arcsecond order annual parallax of radio sources, the VERA internal network should be constrained 1–2mm precision in 3 dimensions. Also, VERA network should be connected with global reference frame (ITRF) with the precision of 10 mm.

To obtain such precision, VERA internal geodetic observations are planed to carry out once a week at the maximum when the system is ready for regular operation. The observations to connect VERA network to ITRF will be carried out several times per year in collaboration with the Geographical Survey Institute (GSI), Japan.

In the early phase of VERA design, the measurements of the Earth orientation parameters (EOP) was one of the main targets. However, regular EOP observation is not intended to carry out at present. EOP will not regularly be estimated by VERA network itself. EOP produced by IERS will be used in the regular astrometric observation in VERA. It is estimated that the precision of IERS products is enough for astrometric purpose at present.

## 3. Geodetic Observation System

### 3.1. Specifications of S/X receivers

The specification of S/X band receivers are summarized in table 2. S/X bands are single receiver system, while dual system is equipped in 22GHz and 43GHz. The band width of down converter and intermediate frequency (IF) is limited within 400 MHz while that of radio frequency (RF) amplifier in X band is 900 MHz. This wide band extension is reserved for future reformation.

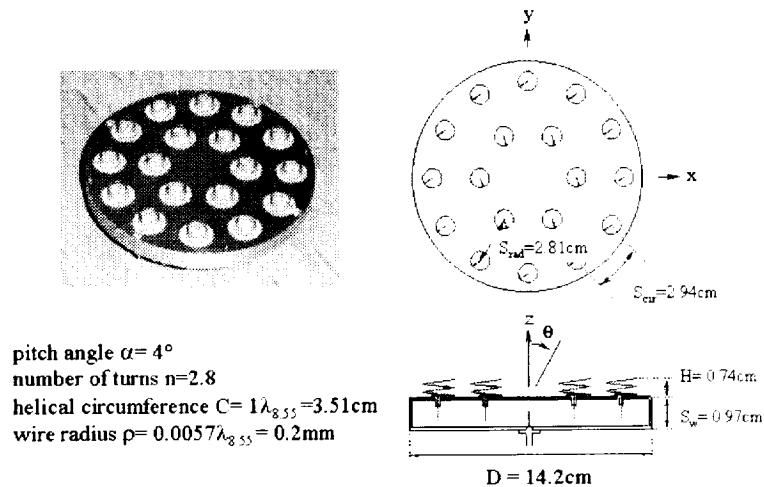
Table 2. Specification of S/X band front end.

1) S band	band width	2.2 GHz – 2.4 GHz
	system noise temp.	less than 150 K (considering radome loss)
	aperture efficiency	about 30 %
2) X band	band width	8.1 GHz – 9.0 GHz (within 400 MHz for one channel)
	system noise temp.	150 K – 170 K at present
	aperture efficiency	more than 40 %

### 3.2. Antenna Feeds

If we adopt a horn feed for S band, it becomes difficult to design cassegrainian focus area to share the space with other bands system, because of its large size. Moreover, it is difficult to obtain high aperture efficiency in S band. A micro strip antenna was designed at first, but it could

obtain only 20% aperture efficiency in S band. To avoid such problems in antenna feeds, helical array antenna of S and X bands are developed by a group in Hosei University. We obtained better aperture efficiency in S band, and wide band characteristic in X band. In each band, 6 helical antenna elements are arranged on an inner circle and 12 elements are arranged on outer circle (Figure 1). The diameter of array sizes are 60cm and 15cm in S and X bands respectively. The array of both bands are placed in co-axial.



X-band helical array antenna

Figure 1. Design of X band feed by Hosei University group.

### 3.3. Digital and Analogue IFs

In S/X bands, RF amplifiers of room temperature type are used. The RF signals are converted to IF bands. The IF bands are 200-300MHz and 100-500MHz in S and X bands respectively. These bandwidths are traditional ones. Those IF signals are digitized at the front end (i.e. in the antenna focus room), and transmitted to the observation room using optical fibers. This digital IF system is used for VERA internal observations. The IF signals are applied to a digital band-pass filter in the observation room, and then they are stored in the 1 Gbps recorder.

The analogue IF signals are also transmitted to the observation room at the same time using co-axial cables or optical fibers. This analogue IF system is designed to keep compatibility in the observations with VERA external stations. In this case, recording system of 64 Mbps or 128 Mbps will be used.

### 3.4. Supposed Observation Modes

Many observation modes are equipped in VERA system. Typical observation modes which are available in geodetic observations are listed in table 3. In VERA original modes, the system of Giga bit sampler, digital filter and 1Gbps recorder are used. The observation modes can be

changed by selecting digital filter characters in VERA original mode. In VLBA applied mode, it has only logical compatibility at present. The recoding media differs from Mark III and Mark IV system, and bandwidth is limited to 512 MHz. Media conversion is required in practice.

Table 3. Typical observation modes in geodetic use. Modes for astrometric use are not listed here.

Mode	band	band width (MHz)	sampling (bit)	channels	data rate Mbps
VERA original mode A	S	64	2	1	
	X	64	2	3	1024
VERA original mode B	S	32	2	1	
	X	32	2	7	1024
K4 system	S	4	1	6	
	X	4	1	8	128
VLBA applied	any	8	1	16	256

### 3.5. Correlation, Analysis

The VSOP correlator (Mitaka FX correlator) will be used for the correlation processes. This correlator has the capacity to process 10 stations with 512 Mbps rate, and now upgraded to be able to process 5 stations with 1 Gbps rate at the maximum. The status of analysis software development is mentioned by Manabe et al. [2] in this proceedings.

### 4. Associated Observations

Colocated GPS observations are already started at Mizusawa and Iriki stations. It will start soon at remaining two stations. Trimble 4000SSE and 4000SSi receivers are used at those observations. GPS observation data in all stations is corrected in Mizusawa via network. The baseline change observed by GPS in the network will be compared with the results of VLBI observations.

Each station has a general purpose observation basement. It size is 1m×2m. Gravity tide observations using spring type gravimeters are planed. Absolute gravity measurements are also planed. The gravity changes will also compared with the vertical movements measured by VLBI and/or GPS.

### References

- [1] Kawaguchi, N., T. Sasao, S. Manabe, H. Kobayashi, O. Kameya, 10 micro-arcsecond Astrometry with Two Beam System of VERA, In: this proceedings, 2002.
- [2] Manabe, S., H. Imai, T. Jike, Astrometric and Geodetic Analysis System of VERA, In: this proceedings, 2002.

## The VSOP-2 Space VLBI Mission

Hisashi Hirabayashi <sup>1</sup>, Yasuhiro Murata <sup>1</sup>, David W. Murphy <sup>2</sup>

<sup>1</sup>) *The Institute of Space and Astronautical Science*

<sup>2</sup>) *Jet Propulsion Laboratory*

Contact author: Hisashi Hirabayashi, e-mail: [hirax@vsop.isas.ac.jp](mailto:hirax@vsop.isas.ac.jp)

### Abstract

Following the success of the VLBI Space Observatory Programme (VSOP), a next generation space VLBI mission, VSOP-2, is currently being planned. Higher observing frequencies, cooled receivers, increased bandwidths and larger telescope diameters will result in gains in resolution and interferometer sensitivity by factors of  $\sim 10$  over the VSOP mission. The use of phase-referencing by fast switching between a calibrator source and the target source is now being studied as this technique allows sources 50–150 times weaker to be observed depending on the frequency band. Such a capability would greatly enhance the VSOP-2 mission. Several other enhancements to the VSOP-2 mission are also presently under investigation including the VSOP-2 spacecraft operating at the same time as a U.S. spacecraft to form what has come to be known as the iARISE (international ARISE) mission.



Figure 1. Artist's conception of the VSOP-2 mission illustrating how a spacecraft in orbit can create a synthetic aperture several Earth diameters in size.

### 1. Introduction to Next Generation Space-VLBI Mission VSOP-2

Space VLBI synthesizes a telescope larger than the Earth as illustrated in Figure 1 for the case of the VSOP-2 mission. ISAS's launch of the HALCA satellite in 1997, as part of the VLBI Space Observatory Programme (VSOP), has allowed sub-milli-arcsecond-scale imaging at 1.6 GHz and 5 GHz ([1],[2]). In addition, successful detection of space-ground fringes at 22 GHz confirmed that there will be no major problems extending space VLBI to shorter wavelengths in the future. Planning for a next generation space VLBI mission, currently designated as VSOP-2, is well underway ([3]). The VSOP-2 spacecraft will have a 10m-class antenna with cryogenically cooled low-noise receivers and a downlink data rate of at least 1 Gbps, resulting in an improvement of

an order of magnitude in interferometer sensitivity over the VSOP mission. Observing frequencies up to 43 GHz will allow high angular resolution observations of the optically thin emission in many AGN cores. An angular resolution of  $\sim 25$  micro-arcseconds at 43 GHz will be achievable, corresponding to  $\sim 10$  Schwarzschild radii at the distance of M87.

The international cooperation and coordination required for VSOP observations make it one of the most complex space science missions undertaken, and a lot has been learned for future space VLBI missions. A similar level of collaboration will be essential for the success of VSOP-2. Submission of the VSOP-2 proposal to ISAS will take place within the next year and consequently launch on an ISAS M-V rocket could be as early as 2009.

## 2. VSOP-2 Science Goals

The VSOP-2 science goals include: study of emission mechanisms in conjunction with the next generation of X-ray and gamma-ray satellites; full polarization studies of magnetic field orientation and evolution in jets, and measurements of Faraday rotation towards AGN cores; high linear resolution observations of nearby AGN to probe the formation and collimation of jets and the environment around supermassive black holes; and the highest resolution studies of spectral line masers and mega-masers, and circum-nuclear disks.

## 3. VSOP-2 Phase-Referencing Capability

Phase-referencing observations remove atmospheric phase fluctuations and consequently can increase the coherence time and hence allow weaker sources to be detected. Although this capability was not considered in the ordinal VSOP mission design nevertheless successful ‘in-beam’ phase-referencing observations have been carried out with the quasar pair 1342+662/1342+663 separated by  $4.8'$  ([4],[5]). Furthermore the VERA array of the National Astronomical Observatory of Japan, which consists of four 20 m antennas with dual beam systems will enable phase-referencing technique to be explored in great depth. It is therefore very desirable that the VSOP-2 spacecraft have such a capability at all observing bands as this will greatly enhance the science return from the mission and make it more exciting to the wider astronomical community as it will allow a wider range of astrophysical phenomena to be observed and for astrometric experiments to be undertaken.

Table 1. Comparison of VSOP-2 Detection Limits with and without Phase-Referencing

Frequency (GHz)	Coherence Time ( $\tau_c$ ) (min)	No Phase-Referencing 5- $\sigma$ Detection Limit (mJy)	Phase-Referencing 3- $\sigma$ Image Noise Level (mJy/beam)
5	10	2.8	0.06
8	6	4.7	0.08
22	2	19.0	0.18
43	1	47.0	0.31

A rough estimate of the atmospheric coherence times and the VSOP-2 detection thresholds (without phase-referencing) are shown in the second and third columns of Table 1. The use of

water vapor radiometers to measure directly the short term changes in the tropospheric path length may help extend the coherence time considerably and hence lower the detection thresholds. Combining radio source count data and information from the VSOP 5 GHz survey on the source visibility function on ground-space baselines, we have estimated, as shown in the fourth column of Table 1, the image noise level in a 12-hour phase-referencing observation with the VLBA. By using phase-referencing techniques we not only increase the effective coherence time but we coherently use data from all baselines to detect the target source. These two effects combined reduce the detection threshold by the factor  $\approx 150/\sqrt{\tau_c}(\text{min})$  compared to non phase-referencing observations. Phase-referencing is easier at lower frequencies because the separation between target and calibrator sources are typically only a few primary beam widths or a few degrees. With the nominal VSOP-2 parameters, phase-referencing is feasible at 22 GHz and below but becomes challenging at 43 GHz.

#### 4. Current VSOP-2 Spacecraft Design Parameters

The VSOP-2 spacecraft will be three-axis stabilized, and will probably employ a 10–12 m diameter off-axis paraboloid antenna. The observing bands will be 5 or 8, 22, and 43 GHz, with the highest frequency placing stringent requirements on the surface accuracy on the mesh surface of the antenna ( $\approx 0.3$  mm RMS). The VSOP-2 satellite will be placed in an elliptical orbit with an apogee height of  $\sim 30,000$  km and a perigee height of  $\sim 1,000$  km, resulting in a period of  $\sim 8$  hours. Unlike HALCA, the VSOP-2 satellite will detect both LCP and RCP, and use cryogenic coolers to reduce the system temperature. Observing requires a two-way link between the satellite and a tracking station. The link frequency bands that will be used are the 37–38 GHz band for the wideband down link at 1 Gbps or more, and 40 GHz for the uplink used to transfer a ground-generated ultra-stable reference signal. Currently studies are being undertaken into the antenna design and the high speed backend digital electronics ([6]).

One method of implementing phase-referencing observations is the nodding of the whole spacecraft quickly between the calibrator and target sources. Such fast slewing of the spacecraft may be possible with the use of 4 large momentum reaction wheels (RWs), and the addition of two Control Moment Gyroscopes (CMGs). This configuration does not impose too much of a penalty on the mass and power budgets but does require more complicated attitude control logic.

#### 5. Current Ground Support System Design Parameters

VSOP observations are supported by a network of five tracking stations ([1]), however as only one of these is located in the southern hemisphere, significantly less tracking coverage was available when HALCA's apogee is in the south. Potential solutions for VSOP-2 include the addition of an ESA tracking station in Malindi, Kenya, or a tracking station near the ALMA site in Chile.

Over 25 ground telescopes and arrays from over 12 countries have participated in VSOP observations ([2]). By the time of the launch of the VSOP-2 spacecraft a number of new arrays and telescopes will also be in operation, with 1 Gbps and higher recording widely available. VSOP data is being correlated at the VSOP correlator (Japan), the VLBA correlator (USA) and the S2 correlator (Canada). Upgrades to all three will be required for the correlation of VSOP-2 data. In addition, the JIVE MkIV correlator (the Netherlands) may also be upgraded to handle space VLBI data.

## 6. Orbit Accuracy Requirements

For phase-referencing observations orbit accuracies of  $\approx 120$  cm (5 GHz), 50 cm (8 GHz), 6.5 cm (22 GHz) and 1.8 cm (43 GHz) are required, and to detect H<sub>2</sub>O maser proper motions in AGN requires a 2 cm accuracy. With HALCA, using 2-way Doppler tracking, 3–10 m orbit accuracy has been achieved but this may be the limit of this technique. However, better orbit determination accuracy can be achieved by adding GPS receivers and a high precision accelerometer, even though the GPS coverage is limited for the VSOP-2 orbit. Simulations performed at JPL for the VSOP-2 orbit show that a  $\approx 2$  cm orbit accuracy can be realized by installing a JPL-developed GPS receiver package (2.5 kg, 20 W) which includes a 3-dimensional accelerometer (20 kg, 8 W) with 0.1 mm s<sup>-2</sup> accuracy.

## 7. A Two Spacecraft Mission?

Apart from phase-referencing another way to greatly enhance any space VLBI mission is to use more than one spacecraft. A 2-spacecraft mission (named iARISE) has recently been studied in the U.S. ([6]) and offers several advantages over a single spacecraft mission. The primary advantage being that high resolution observations over the whole sky can be obtained at all epochs. One realization of the iARISE 2-spacecraft concept is that the VSOP-2 spacecraft would be one spacecraft of the i-ARISE pair with the other being provided by non-Japanese space agency such as NASA. Alternatively, VSOP-2 might be a precursor which fully demonstrates the techniques, such a phase-referencing, which the iARISE mission needs.

## 8. Acknowledgments

VSOP-2 is a collaborative project led by ISAS involving many institutions in many countries and the authors gratefully acknowledge the work undertaken by many people in preparing for the VSOP-2 mission.

## References

- [1] Hirabayashi, H. et al. 1998, *Science*, 281, 1825 and erratum 282, 1995.
- [2] Hirabayashi, H. et al., *PASJ*, 52, 955, 2000.
- [3] Hirabayashi, H. et al., in *Astrophysical Phenomena Revealed by Space VLBI*, ed. H. Hirabayashi, P.G. Edwards, & D.W. Murphy (ISAS), 277, 2000.
- [4] Porcas, R.W., Rioja, M.J., Machalski J., and Hirabayashi, H., in *Astrophysical Phenomena Revealed by Space VLBI*, ed. H. Hirabayashi, P.G. Edwards, & D.W. Murphy (ISAS), 245, 2000.
- [5] Guirado, J.C., Ros, E., Jones, D.L., Lestrade, J.F., Marcaide, J.M., Perez-Torres, M.A., and Preston, R.A., *Astronomy and Astrophysics*, 371, 766-770, 2001.
- [6] Murata Y., Hirabayashi, H., this volume, 2002.
- [7] Fomalont, E. et al. Whitepaper submitted to NASA's SEU roadmap team, 2002. <http://universe.gsfc.nasa.gov/docs/roadmap/iarise.whitepaper.pdf>

## Wide-band Data Transmission System Expected in the Next Generation Space VLBI Mission: VSOP-2

Yasuhiro Murata, Hisashi Hirabayashi

The Institute of Space and Astronautical Science

Contact author: Yasuhiro Murata, e-mail: [murata@vsop.isas.ac.jp](mailto:murata@vsop.isas.ac.jp)

### Abstract

Following the success of the VLBI Space Observatory Programme (VSOP), a next generation space VLBI mission (VSOP-2) is currently being planned. We expect the data rate of more than 1 Gbps to get more sensitivity. Here we will present: 1) How to sample the data (on board), including the radiation test results which show we can have the 10 Gbps sampler LSI which can use in space. 2) Possibility of the bit rate more than 1 Gbps to downlink the VLBI data. We studied the link budget for the wide band data transmission, and discussed the various ideas which can get more than 1 Gbps. 3) What kind of VLBI tracking station and recording system will be expected for the VSOP-2 mission? We will present the idea of using normal radio telescopes as a tracking station, and also review the possibility of recording and processing at the tracking stations and correlators.

### 1. VSOP-2 Mission

The overview of the VSOP-2 mission has been shown by Hirabayashi et al. (2002) [1] in this symposium. Here is the summary of the VSOP-2 mission and the comparison with the VSOP mission [2].

Table 1. Comparison of the VSOP, VSOP-2 and the options.

	VSOP	VSOP-2	(options)
Antenna Diameter	8m	10m	10 ? 15 m
Apogee Height	21,500 km	30,000 km	40,000 km
Period	6.3 hours	8.9 hours	12.2 hours
Polarization	LCP	LCP/RCP	
Downlink bit rate	128 Mbps	1 Gbps	1 - 4 Gbps
Observing Bands (GHz)	1.6, 5, (22)	5 or 8, 22, 43	5 to 8, 86
Maximum Resolution	0.3 mas	0.025 mas	
Typical Sensitivity	140 mJy	12 mJy (5 GHz, 25m GRT)	
Launch	1997 February	2009	

We studied the mission based on so-called *basic* design. It is also useful to study the possibility of the various extension of the mission, shown in the (options) column. Main target of the data transmission rate in the *basic* design is 1 Gbps, but now we try to find the possibility of the link more than 1 Gbps. We also try to find the possibility of the options.

## 2. On-board Data Sampling

When we design the space VLBI mission, we select the ellipsoidal orbit, which is more severe environment than that in LEO, or geo-stationary orbit. We must consider carefully about the radiation effect of the space environment. We can use space-qualified parts for the units/parts of the spacecraft.

When we design the on-board observing system of the satellite one of the problems is whether we can have a space-qualified high speed sampler to get the digital data adequate to the high bit rate link. If we assume the bit rate of 1 Gbps, and 2 bit sampling mode, the maximum total IF bandwidth will be 256 MHz (cf. HALCA, 32 MHz @ 128 Mbps downlink rate). It is difficult to make a video converter with more than 50 MHz bandwidth. The solutions to sample a 256 MHz bandwidth are to split into 8 - 16 IF channels, or to use the over-sampling technique to get the wider bandwidth sampling, which is used for the VSOP terminal A/D converter [3]. Many IF channels are not good for the satellite to make the smaller and lighter circuit. We need more than three times faster sampling speed than for the normal bandwidth. Because we will make the polarization observation, we will have the two IF channels. This means we need the sampler to work at more than 768 Mbps. This number will be 1536 Mbps in case we can do 2 Gbps downlink. We do not know of a space-qualified sampling LSI with such a high speed in this time.

We tested the sampler LSI and 1:16 demultiplexer LSI (figure 1), which work with 10 Gbps speed maximum, in the simulated space radiation environment [4]. We simulate the total dose environment up to 1000 k rad, which corresponds to a total dose of about 30 years with HALCA orbit. We also made a heavy ion radiation test to simulate the single event phenomena in space (figure 2). We can know that as least those LSI's are possible to use the future space VLBI mission.

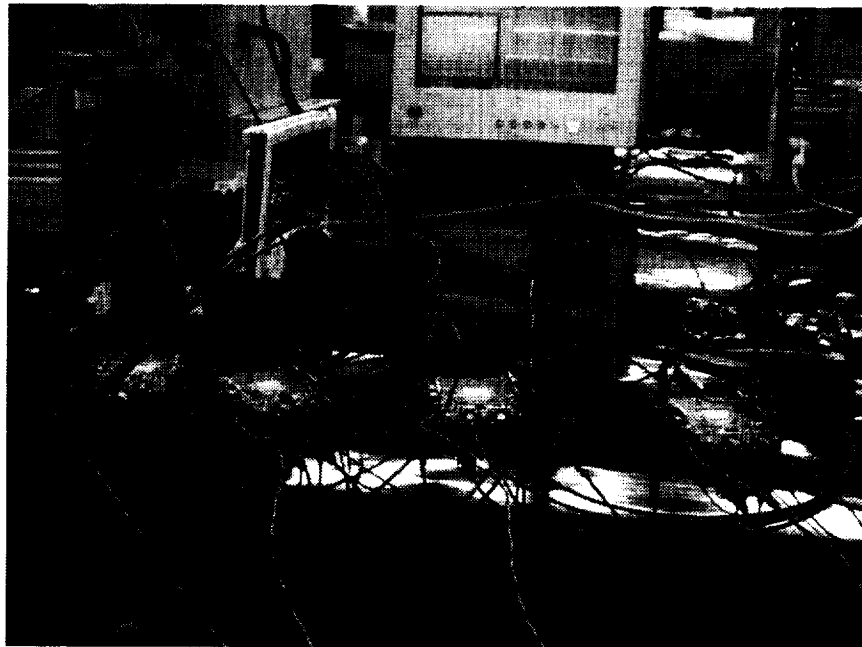


Figure 1. 10 Gbps 1 bit A/D LSI and 1:16 demultiplex LSI, configured for the radiation test

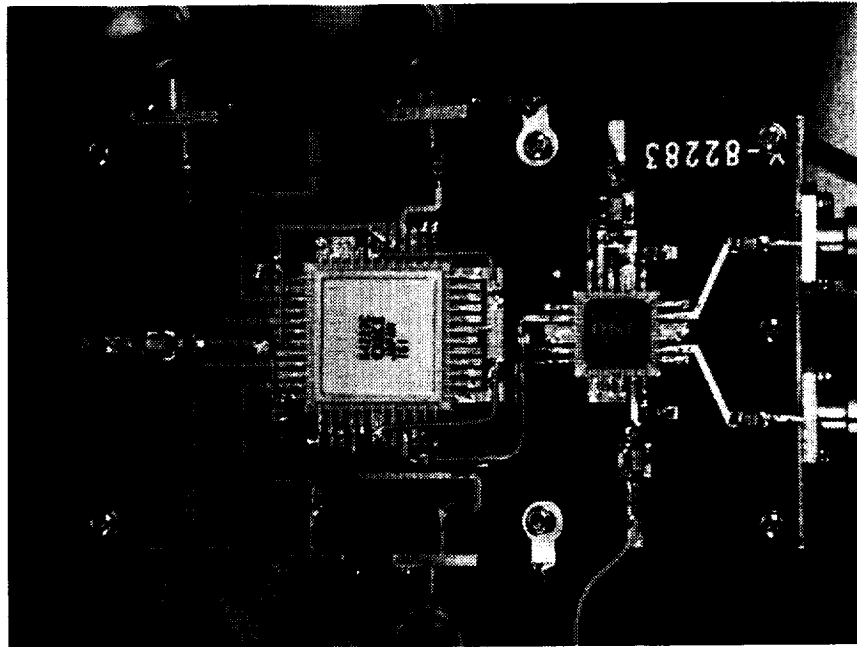


Figure 2. The single-event radiation test configuration. The tested LSI is set in the vacuum chamber, and the heavy ion beam is radiated.

Based on these tests, we think we can design the larger bandwidth IF channels, at least 256 MHz, which have the benefit to make the onboard wideband digital system simpler. Currently, we designed to have two IFs with the total data rate of 1 Gbps, total bandwidth of 128 MHz per IF, which will be sampled with 2-bit mode. If the downlink of the spacecraft allow us to have 2 Gbps, we will make the IF bandwidth twice.

### 3. The High Data Rate Link

One of the technical problems for the VSOP-2 mission is the high speed data link between the spacecraft and ground stations. We realized the bandwidth of 128 Mbps with HALCA. Uplink signal to the VLBI spacecraft is a tone signal locked to the hydrogen maser reference. We also have the round trip frequency offset change information to measure the time offset between the ground tracking station and the spacecraft.

Downlink requires a wideband signal. HALCA was allocated  $14.2 \text{ GHz} \pm 64 \text{ MHz}$  for the 128 Mbps downlink. When we make the target of more than 1 Gbps data transmission, it is difficult to use Ku band. This is because we have no uplink frequency allocation for space research use at Ku band, and downlink allocation bandwidth is not enough for the wider bandwidth.

Possible frequency for the  $> 1 \text{ Gbps}$  downlink will be the band of 37 - 38 GHz with selecting current frequency allocation table for the telecommunication and the radio observation. Uplink will be 40 GHz. Though the antenna gain will be larger with the higher frequency, wider bandwidth transmission requires more signal to noise ratio, and the rain attenuation of the signal is estimated to be 15 - 25 dB (based on various conditions) maximum. We need larger transmission power

(about 20 W) in onboard transmitter, and the larger ground station antenna (larger than 15 - 20 m class antennas).

Springett and Smith (2001) [5] proposed the idea that we use the radio telescopes for receiving the wideband data. We can separate the functions of the time-keeping and the data transmission of the spacecraft. The time-keeping needs the uplink and the round trip timing measurement functions at the tracking station. This is a narrow band system and 3-5 m antenna is enough to establish the timing link. On the other hand, the data transmission needs only the receiving function. If we replace the VLBI sampler with the demodulator of the downlink signal at the VLBI station, we can use the telescope as the downlink station of the space VLBI spacecraft. We need to add the tone signal for the timing link to the wideband signal transmitted from the spacecraft.

We assume QPSK modulation (same as HALCA modulation) for the 1 Gbps data transmission. If we want to have wider bandwidth, we need to have n-PSK (or n-QAM, n-QASK) modulation, where integer  $n > 4$ . When we try to get 2 Gbps data transmission, we need to have 6-7 dB more link budget to get enough signal to noise ratio for the demodulation.

Current target data rate of the VSOP-2 mission is 1 - 2 Gbps. We have already had the experimental VLBI system recording and correlating with this bandwidth. We think it is easier to have the wideband recording/correlating functions at the time of VSOP-2 launch. There is the possibility to use the disk and the optical link for the next mission.

#### 4. Concluding Remarks

We are investigating the many possibilities to the backend of the VSOP-2 mission. We have many technical issues to confirm, but we think we do not have the major difficulty to realise the VSOP-2 data transmission, except for the budget cap for the mission.

#### 5. Acknowledgements

This paper includes many results for the mission design of VSOP-2. Authors thank many contributors in ISAS, NAOJ, JPL, NRAO, ATNF, JIVE, DRAO, and SGL.

#### References

- [1] Hirabayashi H., Murata Y., and Murphy, D.W., The VSOP-2 Space VLBI mission, 2002, this volume.
- [2] Hirabayashi H., et al. Overview and Initial Results of the Very Long Baseline Interferometry Space Observatory Programme, 1998, *Science*, 281, 1825.
- [3] Iguchi, S., Kawaguchi, N., Kameno, S., Kobayashi, H., and Kiuchi, H. 2000 , Development and Performance of the Terminal System for VLBI Space Observatory Programme (VSOP), *IEICE Trans. Commun.*, vol.E83-B, no.2, pp.406-413.
- [4] Wajima, K., Kawaguchi N., and Murata, Y., The radiation test of the high speed sampling LSI for the space VLBI use, 2002, in preparation.
- [5] Springett, C.J., Smith J.G., Achieving Future SVLBI Gbps Data Rate, 2002, in private communications.

## Precise Positioning of Spacecrafts by Multi-frequency VLBI

Yusuke Kono <sup>1</sup>, Hideo Hanada <sup>2</sup>, Kenzaburo Iwadate <sup>2</sup>, Yasuhiro Koyama <sup>3</sup>,  
Yoshihiro Fukuzaki <sup>4</sup>, Nobuyuki Kawano <sup>2</sup>

<sup>1</sup>) *The Graduate University for Advanced Studies*

<sup>2</sup>) *National Astronomical Observatory, Japan*

<sup>3</sup>) *Communications Research Laboratory*

<sup>4</sup>) *Geographical Survey Institute*

Contact author: Yusuke Kono, e-mail: [kono@miz.nao.ac.jp](mailto:kono@miz.nao.ac.jp)

### Abstract

Multi-Frequency VLBI (MFV) is one of the most powerful methods for precise positioning of spacecraft. Radio sources for MFV transmit three carrier waves at S-band and one wave at X-band. These frequencies are set to resolve the cycle ambiguity of the carrier wave at X-band from the two group delays between carrier waves at S-band. A procedure to resolve the cycle ambiguity is proposed. Some conditions about frequency variation and prediction of position and the ionosphere are also summarized for resolving cycle ambiguities. The dedicated recording system for MFV is also developed. A preliminary observation of MFV is carried out with this system by using Lunar Prospector. As a result of the experiment, residual phases from predicted ones are within about 1000 degrees, and the RMS of the residual for the period of several seconds is about 4 degrees, which corresponds to 1.5 m in the positioning error around the Moon. It is confirmed that the hardware and software system have enough availability to achieve the expected accuracy in MFV.

### 1. Introduction

The study of orbital motion and the interior structure of the Moon and planets is one of the methods to approach for the revolution as a dynamical system and the origin of the solar system. It is a powerful method to measure the gravity fields obtained by the orbital motion of a spacecraft in order to estimate the inner layer and the density structure of the Moon and the planets. Orbits or positions of a lunar or planetary spacecraft have mainly been determined by range and Doppler measurements. These measurements provide only one-dimensional information about the position along the line of sight. On the other hand, differential VLBI (Very Long Baseline Interferometry) has the sensitivity of positioning in direction perpendicular to the line of sight, so that combining both range and Doppler measurements with differential VLBI enables us to measure three-dimensional position of a spacecraft.

VLBI methods have been used for positioning of spacecraft since 1960s. In these methods, carrier waves were transmitted from a spacecraft because of saving its transmitting power and obtaining high SNR. Unfortunately, the phase delay of a carrier wave, however, has cycle ambiguities, therefore only phase delay changes have been mainly used so far [1]. A new method, multi-frequency VLBI (MFV) was proposed [2, 3]. Radio sources for MFV transmits three frequency signals in S-band and one signal in X-band. These frequencies are set to resolve the cycle ambiguity of carrier wave at X-band from three group delays between carrier waves at S-band. A procedure to resolve the cycle ambiguity is proposed in this article. Some conditions about frequency variation and prediction of position and the ionosphere are summarized for resolving

the cycle ambiguity. The dedicated recording system for MFV is also developed. A preliminary observation of MFV is carried out with this system by using Lunar Prospector as a test of the whole system.

## 2. Cycle Ambiguity Resolving by MFV

In MFV method, two radio sources emit three carrier waves  $s_1, s_2, s_3$  in S-band and one wave  $x$  in X-band. Cross correlation between the two received signals of the respective carrier waves at two ground stations produces four  $\times$  two fringe phases for each unit integration time. By differencing the fringe phases between two radio sources, four differenced fringe phase  $\phi_i$  are obtained for the carrier wave  $i$  ( $=s_1, s_2, s_3$  and  $x$ ). Our final observable is the phase delay of the wave  $x$  without cycle ambiguity from the four phases. The phase delay  $\tau_{pd,x}$  of the wave  $x$  is expressed as follows,

$$\tau_{pd,x} = \frac{\phi_x}{2\pi f_x} + \frac{kd}{f_x^2} + \frac{\sigma_x}{2\pi f_x} + \frac{N_x}{f_x}, \quad (1)$$

where  $f_i, \sigma_i, N_i$  is the frequency, the phase noise, the integer ambiguity of the wave  $i$ , respectively, and  $k$  is the ionospheric constant ( $= 1.34 \times 10^{-7} [m^2 el.^{-1} s^{-1}]$ ),  $d$  is the differenced total electron content (TEC) [ $el.m^{-2}$ ] in the ionosphere. In order to resolve the cycle ambiguity  $N_x$ , uncertainty of the left side  $\tau_{pd,x}$  and the second and third term in Equation (1) must be less than  $1/2f_x$ . Conditions for the second and third term are summarized in the next section. The term  $\tau_{pd,x}$  should be predicted within the accuracy of  $1/2f_x$  by the phase delay  $\tau_{pd,s_1}$  of the carrier wave  $s_1$  as follows,

$$\tau_{pd,s_1} = \frac{\phi_{s_1}}{2\pi f_{s_1}} + \frac{kd}{f_{s_1}^2} + \frac{\sigma_{s_1}}{2\pi f_{s_1}} + \frac{N_{s_1}}{f_{s_1}}. \quad (2)$$

Because the delay ambiguity interval  $1/f_{s_1}$  of carrier wave  $s_1$  in Equation (2) is wider than that of wave  $x$  in Equation (1), it is easier to resolve the delay ambiguity of  $s_1$  than that of  $x$ . In order to resolve the cycle ambiguity  $N_s$ , uncertainty of the left side  $\tau_{pd,s_1}$  and the second and third term in Equation (2) must be less than  $1/2f_{s_1}$ . Conditions for the second and third term are summarized in the next section. The term  $\tau_{pd,s_1}$  should be predicted within the accuracy of  $1/2f_{s_1}$  by the group delay  $\tau_{gd,s_3s_1}$  of  $s_3-s_1$  as follows,

$$\tau_{gd,s_3s_1} = \frac{\phi_{s_3} - \phi_{s_1}}{f_{s_3} - f_{s_1}} + \frac{kd}{f_{s_3}f_{s_1}} + \frac{\sigma_{s_3} - \sigma_{s_1}}{f_{s_3} - f_{s_1}} + \frac{N_{s_3} - N_{s_1}}{f_{s_3} - f_{s_1}}. \quad (3)$$

It is easier to resolve the delay ambiguity of  $s_1-s_3$  than that of  $s_1$ . In order to resolve the cycle ambiguity  $N_{s_1}-N_{s_3}$ , uncertainty of the left side  $\tau_{gd,s_3s_1}$  and the second and third term in Equation (2) must be less than  $1/2(f_{s_3}-f_{s_1})$ . Conditions for the second and third term are summarized in the next section. The term  $\tau_{gd,s_3s_1}$  should be predicted within the accuracy of  $1/2(f_{s_3}-f_{s_1})$  by group delay  $\tau_{gd,s_2s_1}$  of  $s_2-s_1$  as follows,

$$\tau_{gd,s_2s_1} = \frac{\phi_{s_2} - \phi_{s_1}}{f_{s_2} - f_{s_1}} + \frac{kd}{f_{s_2}f_{s_1}} + \frac{\sigma_{s_2} - \sigma_{s_1}}{f_{s_2} - f_{s_1}} + \frac{N_{s_2} - N_{s_1}}{f_{s_2} - f_{s_1}}. \quad (4)$$

It is easier to resolve the delay ambiguity of  $s_1-s_2$  than that of  $s_1-s_3$ . In order to resolve the cycle ambiguity  $N_{s_2}-N_{s_1}$ , uncertainty of the left side  $\tau_{gd,s_2s_1}$  and the second and third term in Equation (2) must be less than  $1/2(f_{s_2}-f_{s_1})$ . Conditions for the second and third term are summarized in the next section. The term  $\tau_{gd,s_2s_1}$  should be predicted within the accuracy of  $1/2(f_{s_2}-f_{s_1})$  by another tracking method. The condition of the accuracy is summarized in the next section.

## 2.1. Conditions for Resolving Cycle Ambiguities

In order to resolve the cycle ambiguity  $N_x$  mentioned above, the frequencies are selected as,  $f_{s_1}=2212\text{MHz}$ ,  $f_{s_2}=2218\text{MHz}$ ,  $f_{s_3}=2287\text{MHz}$  and  $f_x=8456\text{MHz}$ . The condition of the phase noise, the delay accuracy of the prediction, the TEC, the frequency difference, frequency stability are summarized in Table 1. Radio transmitters on spacecraft should be designed to satisfy also these conditions. These conditions are discussed in more detail by some works [4, 5].

Table 1. Conditions for resolving cycle ambiguities

Phase noise, $\sigma_{\phi_i}$	less than 4.2	degrees
Accuracy of the predicted delay	better than $8.3 \times 10^{-8}$	second
TEC, d	less than $2.3 \times 10^{15}$	el./m <sup>2</sup>
Frequency difference between two radio sources	less than $1.7 \times 10^5$	Hz
Frequency stability $y(\tau)$ $10 < \tau < 100$ sec.	better than $2.8 \times 10^{-5}$	Hz/Hz

## 3. Ground System for MFV

MFV method will be realized under the Japanese lunar exploring program, SELENE. The radio sources will be installed in the relay satellite and the vrad satellite [6]. We developed a new ground VLBI system, which consists of hardware to sample and record the carrier waves and software to estimate phase delays. The hardware samples and digitizes the video signals at sampling rate of 200 sps and records them on an 8 mm tape. The narrow bandwidth sampler and recorder is shown in Figure 1. The new software cross-correlates the recorded signals and produces the phase delay. The product is input to software to estimate orbits and gravity fields [7].

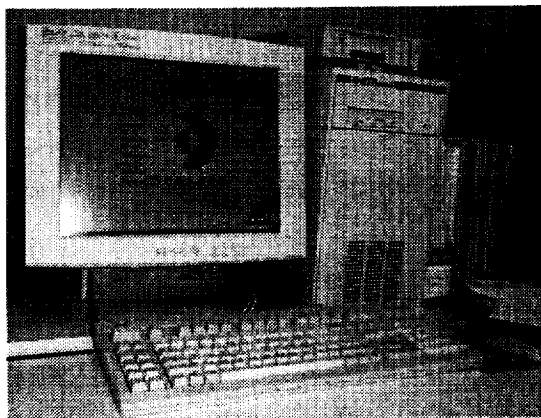


Figure 1. Narrow bandwidth sampler for MFV

#### 4. Preliminary Experiment of MFV by Using Lunar Prospector

As a preliminary test of the whole system, an experiment of Lunar Prospector was carried out from 08:00 to 17:00 in Sep. 21, 1998. The antennas involved in the observation were the Kashima 34m-diameter antenna of CRL, the Mizusawa 10m-diameter antenna of NAO and the Tsukuba 3.8m-diameter antenna of GSI. The developed ground system was used to record and estimate the fringe phases. Unfortunately it transmitted only one carrier wave, so that the test for resolving the ambiguity of the fringe phase could not be achieved. The residual fringe phases after the correction for the ionospheric delay have systematic variations of about 1000 degrees with period of about one hour (Figure 2). These variations are supposed to be caused by the errors in the initial orbital elements and model errors of the lunar gravity fields used. Although these long period variations cannot be estimated in this experiment, they will be estimated in SELENE mission by MFV. The short period variations of the residual fringe phases will remain even if the two variations are estimated. The rms of the residual for the period of several tens of seconds is about 4.4 degrees (Figure 3). The rms residual for several seconds means that we can determine the position of Lunar Prospector within the error of 1.5 m around the Moon if we can correct the variations with long period by using the MFV.

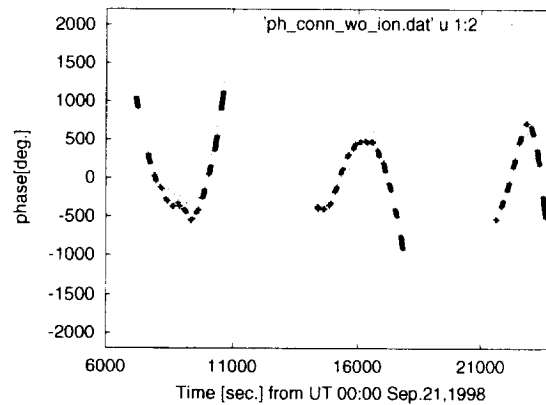


Figure 2. Residual fringe phases. Linear components are removed.

#### 4.1. Conclusion

MFV method, which enables us to obtain the phase delay of RF signals at S- and X-band without cycle ambiguity, is proposed. The several conditions of the realization of this method are summarized. The new ground VLBI system, which consists of hardware to sample and record the received signals and software to estimate the phase delay, has been developed.

The preliminary experiment was carried out by using Lunar Prospector. Unfortunately it transmitted only one carrier wave, so that the test for resolving the ambiguity of the fringe phase could not be achieved. The residual fringe phases after the correction for the ionospheric delay have systematic variations of about 1000 degrees with period of about one hour. These variations are supposed to be caused by the errors in the initial orbital elements and model errors of the lunar gravity fields used. The rms of the residual fringe phases averaged for several tens of seconds

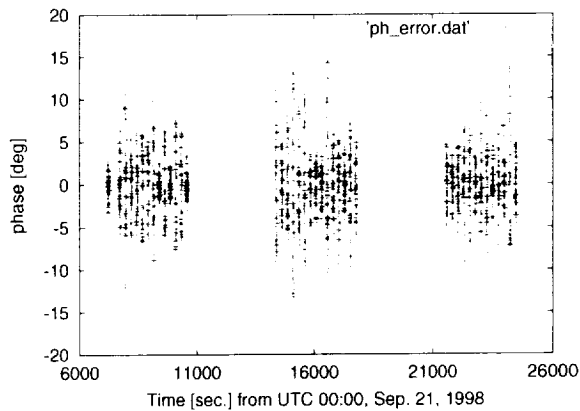


Figure 3. The short period variation of the residual fringe phase

reaches about 4 degrees, which corresponds to 1.5 m in the positioning error around the Moon. It is confirmed that the hardware and software system have enough availability to achieve the expected accuracy in MFV.

## References

- [1] Border, J. S., W. M. Folkner, R. D. Kahn, and K. S. Zukor, "Precise Tracking of the Magellan and Pioneer Venus Orbiters by Same-Beam Interferometry, Part I: Data Accuracy Analysis", TDA progress report, 42-110, Aug. 15, 1992.
- [2] Kawano, N., S. Kuji, S. Tsuruta, K-H. Sato, K. Iwadate, H. Hanada, M. Ooe, N. Kawaguchi, H. Mizutani and A. Fujimura, "Development of the artificial radio source on the Moon", J. Jap. Soc. Planet. Sci., 3, 159-169, 1994 (in Japanese).
- [3] Hanada, H., T. Iwata, N. Kawano, K. Heki, S. Tsuruta, T. Ishikawa, H. Araki, K. Matsumoto, Y. Kono, Y. Kaneko, M. Ogawa, Y. Iijima, Y. Koyama, M. Hosokawa, T. Miyazaki, N. Namiki, A. Sengoku, Y. Fukuzaki, T. Ikeda, F. Fuke and RISE group, "Observation system of radio sources on the Moon by VLBI in SELENE project", Proceedings of the International Workshop on GEMSTONE, jun. 25-28, 126-130, 1999.
- [4] Hanada, H., T. Iwata, Y. Kono, K. Matsumoto, "VRAD Mission: Precise Observation of Orbits of Sub-satellites in SELENE", IVS 2002 General Meeting Proceedings, edited by N. R. Vandenberg and K. D. Baver, NASA/CP-2002-210002.
- [5] Kono, Yusuke, "Precise Three-dimensional Positioning of Spacecrafts by Multi-frequency VLBI and Doppler Measurements", Doctor thesis at The Graduate University for Advanced Studies, 2002.
- [6] Iwata, T. T. Sasaki, Y. Kono, H. Hanada, N. Kawano and N. Namiki, "Results of the critical design for the selenodetic mission using the differential VLBI methods by SELENE", IVS 2002 General Meeting Proceedings, edited by N. R. Vandenberg and K. D. Baver, NASA/CP-2002-210002.
- [7] Matsumoto, K, K. Heki and H. Hanada, "Global lunar gravity field recovery from SELENE", IVS 2002 General Meeting Proceedings, edited by N. R. Vandenberg and K. D. Baver, NASA/CP-2002-210002.

# Processing of the Data of Syowa VLBI Experiment by Copying Between the Different Recording Systems and the Result of the Analysis

Yoshihiro Fukuzaki <sup>1</sup>, Kazuo Shibuya <sup>2</sup>, Koichiro Doi <sup>2</sup>, Takaaki Jike <sup>3</sup>,  
David L. Jauncey <sup>4</sup>, George D. Nicolson <sup>5</sup>

<sup>1</sup>) *Geographical Survey Institute*

<sup>2</sup>) *National Institute of Polar Research*

<sup>3</sup>) *National Astronomical Observatory of Japan*

<sup>4</sup>) *Hartebeesthoek Radio Astronomy observatory*

<sup>5</sup>) *Australia Telescope National Facility, CSIRO*

Contact author: Yoshihiro Fukuzaki, e-mail: [fukuzaki@gsi.go.jp](mailto:fukuzaki@gsi.go.jp)

## Abstract

At the Syowa Station on Antarctica, regular VLBI experiments have been undertaken since 1998. In this experiment different recording systems were employed. Development of copy system, however, enabled us to process the data. Meanwhile, since 1992, the O'Higgins Station on Antarctic Peninsula has participated in VLBI experiment with most of the VLBI stations in the southern hemisphere. The Syowa station has been taking part in this experiment since 1999 by developing another copy system. This is the first VLBI observation of the intra-Antarctic plate baseline.

## 1. Introduction

The Japanese Antarctic Research Expedition (JARE), which is coordinated by the National Institute of Polar Research (NIPR), started regular VLBI experiments at the Syowa station in 1998. The Syowa station is located at 69.0 deg S and 39.6 deg E on East Ongul Island, Antarctica, and has 11-m antenna. This experiment is called "Syowa VLBI experiment" or "SYW session." Three stations in the southern hemisphere, Syowa, Hobart and HartRAO, have participated in SYW sessions. In addition, the Syowa Station has been taking part in CORE-OHIG experiment, which is the largest network in the southern hemisphere, since 1999. But there was a serious problem concerning the data-recording format. The Syowa station has only K4 recorder, but there is no other station that has K4 recorder in the southern hemisphere. To solve this problem two types of copy system were developed. By using the copy systems, we have processed the data of SYW and CORE-OHIG sessions including Syowa station. In this article, I will report on the copy systems and results of the analysis, and the results of the first-ever observation of the baseline in Antarctic plate undertaken in collaboration with the O'Higgins station.

## 2. Copy System

In SYW session, the Syowa station has only K4 recording system, and Hobart and HartRAO adopted S2 recording system. In order to process the data of this session, we developed the copy system from the S2 data into K4. A conversion device from the S2 format into the K4 was already

developed by the Mitaka Correlator of the National Astronomical Observatory of Japan (NAOJ) for the VLBI Space Observatory Programme. On the assumption that this device converts the format, the Hobart and the HartRAO stations adopted the S2 format in the SYW session. Nevertheless, we were faced by the challenge that the time stamps recorded at a normal geodetic session were not embedded on the data copied by the conversion device, since it was designed for the correlation of astronomical observation data.

In order to overcome this issue, Jike et al. (2000) [1] developed software to obtain the geodetic solution from the SYW session data processed by the Mitaka Correlator (FX Correlator). At the same time, Fukuzaki et al. (2001) [2] developed a method to embed the time stamps on data converted from the S2 into the K4 format so that an ordinary correlator for geodetic session could be used for processing. For embedding the time stamps on the data, a time stamp generator developed by the NAOJ was utilized. The S2 playback recorder reproduces and reads out the time stamps written on the observation tape every second. Concurrently a pulse (1PPS) synchronized to the time stamp is also generated. Entry of this 1PPS into the time stamp generator, which synchronizes with the time stamp, enabled us to process the data as if the time stamps were embedded at the time of observation. The flow of data is shown in Fig. 1. This method allowed the correlators owned by the Geographical Survey Institute (GSI) or the Communications Research Laboratory to process data in the SYW session.

On the other hand, the CORE-OHIG session adopted the Mark III format, interfering with the participation of the Syowa Station that employed nothing other than the K4 format. The GSI, nonetheless, completed the development of a copy system for converting the K4 data into the Mark III format by 1999, which opened the door for the Syowa station to join the CORE-OHIG session. The correlation process for this session is performed at the Bonn Correlator.

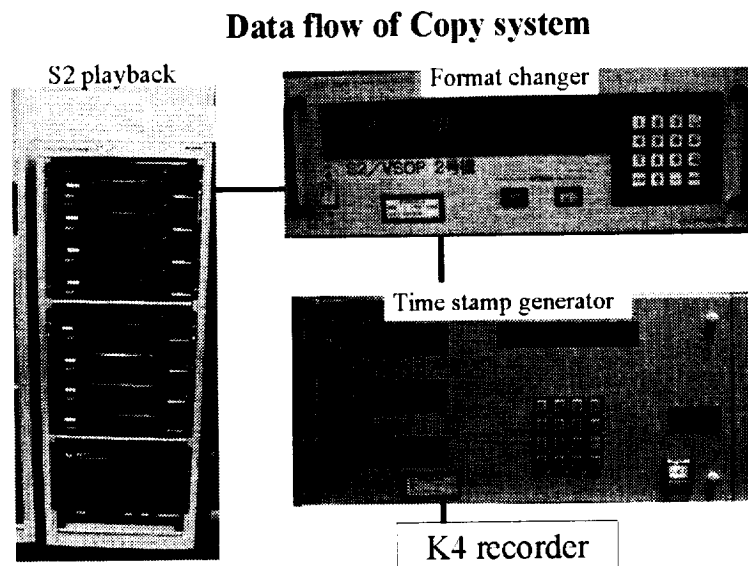


Figure 1. Data Flow of Copy System

### 3. Result of the Analysis

The analysis has so far been completed of the data of the SYW and the CORE-OHIG sessions conducted in 1999 and 2000. Since the SYW and the CORE-OHIG sessions use different copy systems and correlators, comparison of the results of the analysis provides a tool to verify the proper operation of the systems. Tables 1 and 2 show the Syowa-Hobart and Syowa-HartRAO baseline lengths, respectively. A comparison of the sessions recorded on approximately the same date revealed that they agreed with each other within the acceptable margin of error, confirming that this method could determine the baseline solution as intended. The baseline lengths in the time series are shown in Figs. 2 (between Syowa and Hobart) and 3 (between Syowa and HartRAO). The trends of the change of baseline length approximately agree in both cases with the geophysical plate kinematic model, NNR-NuvellA.

The CORE-OHIG session marked the first VLBI experiment of the intra-Antarctic plate baseline (between Syowa and O'Higgins). Table 3 lists its analyses, each of which was determined with a precision of about 10 mm. These were analysed by Dr. Leonid Petrov of GSFC/NASA. The time series data are shown in Fig. 4. Although having too few samples to produce a clear idea regarding change in the baseline length between Syowa and O'Higgins, this multinational session is expected to offer crucial information as to whether or not the plate motion in east Antarctica is different from that in west Antarctica.

Table 1. Baseline Length of Syowa-Hobart

CODE	Date	Baseline Length (mm)	Sigma (mm)
SYW995	99/Sep/09	6035892342.49	12.54
SYW996	99/Oct/07	6035892345.31	9.45
COHIG7	99/Nov/08	6035892355.70	10.55
COHIG8	99/Nov/10	6035892333.17	12.20
COHIG9	99/Nov/11	6035892336.18	11.41
SYW997	99/Nov/18	6035892340.52	10.35
SYW008	00/Feb/02	6035892371.66	11.33
COHG12	00/Feb/10	6035892360.42	10.52
SYW015	00/Dec/07	6035892419.63	19.52

### 4. Summary

At the Syowa station, regular VLBI experiment has been undertaken with Hobart and HartRAO since 1998. In this SYW session different recording systems were employed. Development of copy system, however, enabled us to process the data of SYW session. The goal of SYW session is to strengthen the reference frame in the southern hemisphere and to detect the motion of Antarctic plate.

Meanwhile, the Syowa station has been taking part in CORE-OHIG sessions since 1999 by developing another copy system for converting from the K4 data into the Mark III format. This is the first VLBI experiment of the intra-Antarctic plate baseline, so the results obtained by future

Table 2. Baseline Length of Syowa-HartRAO

CODE	Date	Baseline Length (mm)	Sigma (mm)
SYW995	99/Sep/09	4741786031.16	10.24
SYW996	99/Oct/07	4741786037.32	11.91
COHIG7	99/Nov/08	4741786026.64	7.55
COHIG8	99/Nov/10	4741786056.07	6.80
COHIG9	99/Nov/11	4741786030.17	7.67
SYW997	99/Nov/18	4741786008.05	12.46
SYW008	00/Feb/02	4741786032.37	16.76
COHG12	00/Feb/10	4741786024.55	9.75
SYW015	00/Dec/07	4741786044.69	9.56

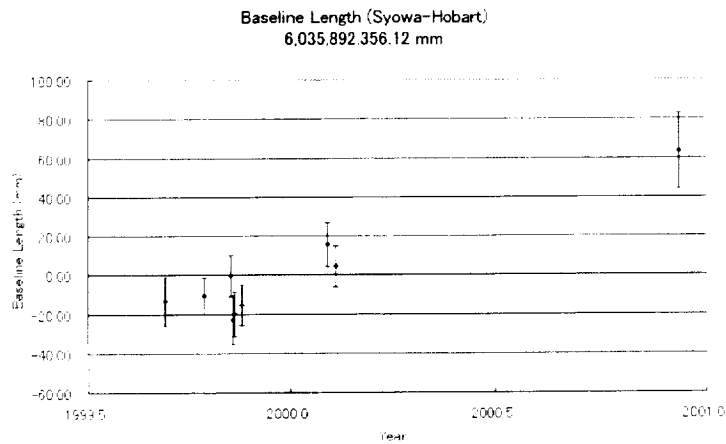


Figure 2. Baseline Length of Syowa-Hobart

Table 3. Baseline Length of Syowa-O'Higgins

CODE	Date	Baseline Length (mm)	Sigma (mm)
COHIG7	99/Nov/08	3908686827.72	9.03
COHIG8	99/Nov/10	3908686803.40	10.77
COHIG9	99/Nov/11	3908686814.17	8.66
COHG12	00/Feb/10	3908686813.38	10.87

sessions should provide data that can greatly contribute to the investigation of the motion of Antarctic plate.

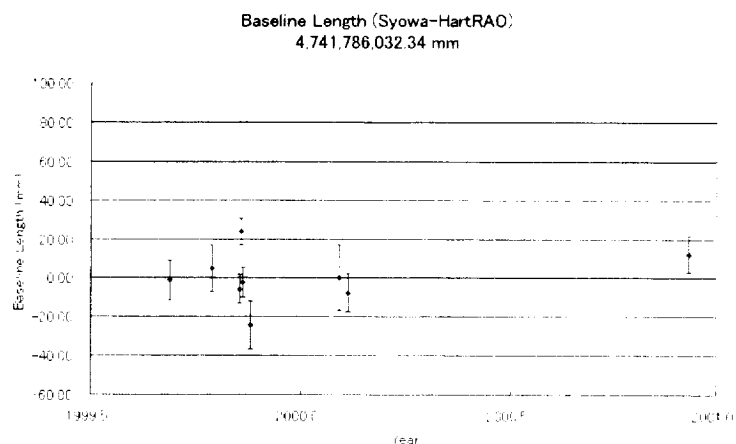


Figure 3. Baseline Length of Syowa-HartRAO

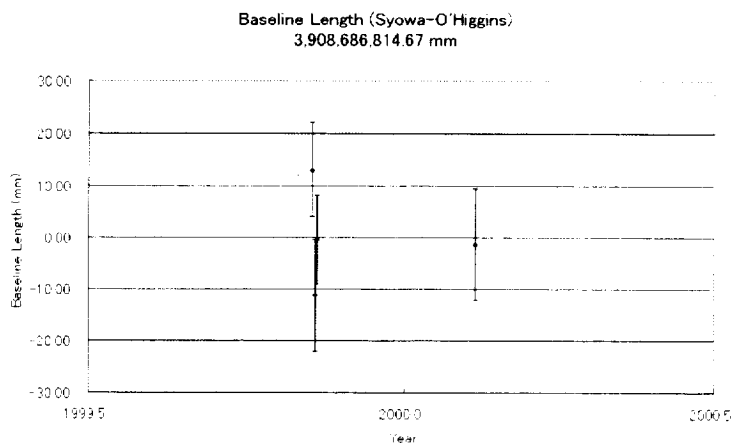


Figure 4. Baseline Length of Syowa-O'Higgins

## References

- [1] Jike, T., S. Manabe, Y. Tamura, and K. Shibuya (2000): Development of geodetic analysis software for FX Correlator and its application to the Antarctic VLBI experiments, presented at the 20th Symposium on Antarctic Geosciences 12-13 October 2000, Program and Abstracts, p155.
- [2] Fukuzaki, Y., K. Shibuya, K. Doi, and T. Jike (2001): Processing of the data of Syowa VLBI experiment by dubbing S2 into K4, presented at the 21st Symposium on Antarctic Geosciences 18-19 October 2001, Program and Abstracts, p109.

## Laser-Pumped Cs Gas-Cell Type Atomic Clock for VLBI

Kenichiro Takahei<sup>1</sup>, Hirohiko Suga<sup>1</sup>, Yuji Ohuchi<sup>1</sup>, Hiroshi Sutoh<sup>1</sup>, Masaharu Uchino<sup>1</sup>,  
Shigenori Mattori<sup>1</sup>, Masahiro Tsuda<sup>1</sup>, Yoshikazu Saburi<sup>1</sup>, Yasuki Koga<sup>2</sup>,  
Ken Hagimoto<sup>2</sup>, Takashi Ikegami<sup>2</sup>

<sup>1</sup>) *Anritsu Corporation*

<sup>2</sup>) *National Institute of Advanced Industrial Science and Technology*

Contact author: Kenichiro Takahei, e-mail: [takahei.kenichiro@jj.anritsu.co.jp](mailto:takahei.kenichiro@jj.anritsu.co.jp)

### Abstract

A hydrogen maser is generally used as a local clock of a VLBI system, where very high frequency stability is required. No other atomic clocks such as Cs beam type and Rb gas-cell type clocks were sufficiently stable in the short- and medium-term time scale, which is used in VLBI measurements. Recently, we have developed a gas-cell type atomic clock using Cs gas and a semiconductor laser as a light source. It is desktop size and much smaller than conventional hydrogen masers, but it has a stability of  $7 \times 10^{-13}$  at 1 second reaching a flicker floor of  $2.5 \times 10^{-14}$  at 1000 seconds. When fluctuation due to the atmosphere in actual VLBI measurements is considered, this stability is good enough for most of the VLBI measurements using S-band and X-band. A preliminary results of VLBI experiments at X-band (8 GHz) using the atomic clock developed in this study is discussed.

### 1. Introduction

Atomic clocks are often used when a high frequency stability is required in measurements such as VLBI. Among commercially available various types of atomic clocks, a hydrogen maser is commonly used in VLBI, but it is large and expensive compared to other types of atomic clocks. A Cs beam-type atomic clock with a magnetic state selector has a high stability when averaged for a long time, but its stability in the time range generally used in VLBI is about two orders of magnitude less stable than that of the hydrogen maser. A Rb gas-cell type atomic clock is small and inexpensive, but its stability is not better than that of a high-performance Cs beam type atomic clock, and it shows a drift in frequency in a long term. Thus, only the hydrogen maser could be used in VLBI measurements.

There have been a number of studies on the gas-cell type atomic clock with laser pumping. It is theoretically known that the stability of this type of atomic clock becomes better if the Rb plasma lamp of the Rb gas-cell type atomic clock is replaced by a laser light source [1, 2, 3, 4]. We have been studying this type of atomic clock using Cs instead of Rb, and developed a desk-top size laser-pumped Cs gas-cell type atomic clock having a stability between that of the hydrogen maser and that of the conventional Rb gas-cell type atomic clock [5]. In this paper, this new type of atomic clock is briefly introduced and a preliminary application of this atomic clock to VLBI measurements is discussed.

### 2. LD-pumped Cs gas-cell type atomic clock

Figure 1 is a block diagram of the developed atomic clock. Light from the frequency-stabilized LD is put into the physics unit containing a Cs gas-cell in a TE011-mode 9.192-GHz resonance

cavity. The light passing through the Cs gas-cell is detected by the photodetector 1 (PD1). Part of the LD light reflected by a beam splitter is put through a reference cell without microwave resonance cavity and detected by the photodetector 2 (PD2). The output of the PD2 is subtracted from that of the PD1 to reduce noise caused by LD amplitude and frequency fluctuations [4]. Cesium absorbs the maximum amount of light when the microwave injected from the synthesizer resonates at the frequency corresponding to the hyperfine transition within the Cs ground state. The microwave synthesizer output frequency is locked to the Cs transition frequency using a voltage-controlled quartz oscillator (VCXO).

Figure 2 is the photograph of the atomic clock developed in this study. Since some components are not designed for this specific equipment, it is still contained in two cabinets; one contains the

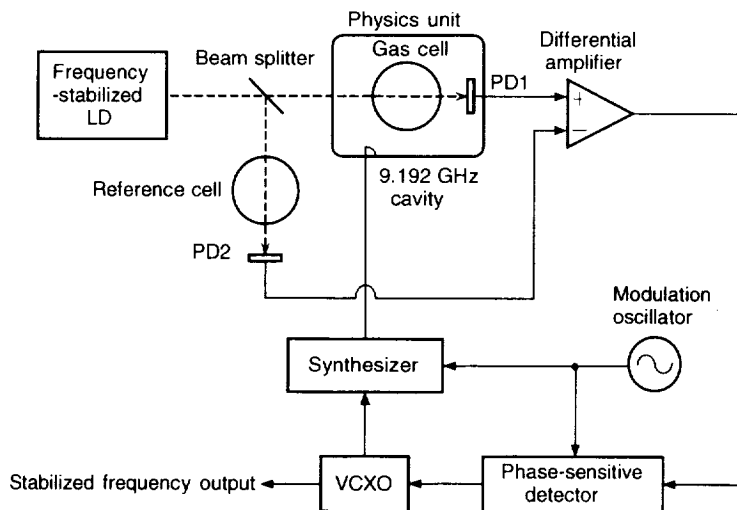


Figure 1. Block diagram of the developed atomic clock. Electrical connections and optical paths are indicated by solid and broken lines, respectively.



Figure 2. Photograph of the developed atomic clock. The 1-MW 7"-high module on the bottom contains the physics unit coupled with the light frequency-stabilized LD and most of the electronic circuits. The 1-MW 5"-high module on the top contains the frequency-adjustment digital switch, a CPU, and power supplies.

physics unit coupled with the light frequency-stabilized LD, a microwave synthesizer and electronic circuits, and the other contains a frequency adjustment digital switch, a CPU, and power supplies. The laser frequency is automatically locked to a specific saturated-absorption line of Cs and the gas-cell is heated up to the temperature that gives the best frequency stability.

The stability of the atomic clock was measured in comparison to a hydrogen maser (Anritsu RH401A). The dual mixer time difference method was used for an averaging time of 100 sec or less, and the phase comparison method was used for an averaging time longer than 100 sec. The results are shown in Fig. 3 along with the characteristics of some commercially available atomic clocks. It shows that this atomic clock has unique characteristics between the hydrogen maser and the Cs beam type atomic clock. Up to  $3 \times 10^3$  sec, it has at least one order of magnitude better stability than a commercial high-performance Cs beam type atomic clock with a magnetic state selector (Agilent 5071A, Op. 001). The stability of the atomic clock developed in this study reaches the flicker floor of  $2.5 \times 10^{-14}$  at about 1,000 sec. A study is in progress to clarify what determines the short-term stability and flicker floor of this atomic clock. We have not yet been able to obtain a reliable data of stability for an averaging time longer than  $1 \times 10^4$  sec, but since there seems to be no obvious drift of the frequency, we believe that the flicker floor at low  $10^{-14}$  will be extended to a longer averaging time by a future study.

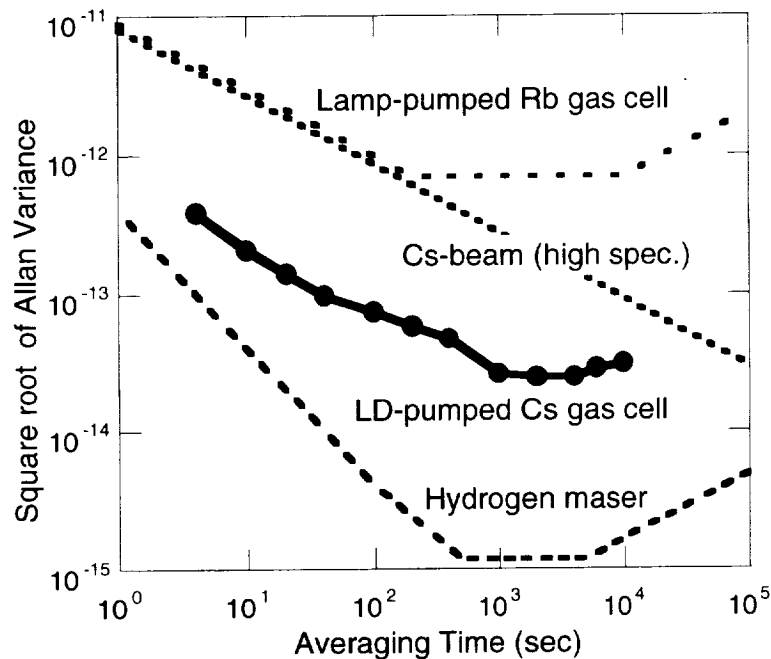


Figure 3. Measured stability of developed atomic clock and characteristics of various commercially available atomic clocks (typical Rb gas-cell type, high-performance Cs beam type (Agilent 5071A Option 001), and hydrogen maser (Anritsu RH401A)). The developed atomic clock was evaluated with reference to the hydrogen maser.

### 3. Application to VLBI Measurements

In VLBI measurements, local clocks must have a sufficiently high stability that gives satisfactory coherence at the measurement frequency for an averaging time of a specific measurement [6]. Figure 4 shows the calculated coherence assuming the stability of the clock developed in this study as shown in Fig. 3. The coherence was calculated for the measurements frequency of 2, 8 and 22 GHz. If the coherence better than 0.8 is assumed to be required for the VLBI measurements, the stability of the clock developed in this study is good enough for measurements at 2 and 8 GHz in the calculated averaging time range, and at 22 GHz, the averaging time would be limited to up to 300 sec.

Another factor that frequently limits the actual accuracy of VLBI measurements is the fluctuation due to water vapor in the atmosphere. It has been observed that the magnitude of such fluctuation changes depending on weather. The atmospheric fluctuation was measured, and the square root of Allan variance was deduced [7]. It shows that, for the averaging time between 10 and 100 sec, the square root of Allan variance is mostly in the range of  $1 \times 10^{-13}$  to  $5 \times 10^{-13}$  depending on the weather conditions. In the averaging time range longer than 100 sec, the fluctuation is white noise and the square root of Allan variance decreases as the averaging time increases. Therefore, if the clock developed in this study is used in VLBI measurements at the frequencies and the averaging time range shown in Fig. 3, the limiting factor of the VLBI measurement accuracy is likely to be the fluctuation due to the atmosphere. That is to say, the stability of the clock developed in this study is good enough and does not affect the accuracy in most of the VLBI measurement.

In February 2001, a preliminary VLBI measurements was carried out using the atomic clock under study at Aira site of the Geographical Survey Institute, Japan. The results of analyses are shown at the following web site, <http://vlbldb.gsi.go.jp/sokuchi/vlbi/english/main.html>. It indicates that each independent measurement was carried out with a reasonable accuracy. However, there was a slow variation of atomic clock frequency which was later found to be due to temperature variation of the room where the atomic clock was installed. This lead to some additional errors in the analyses, as the final result of geodetic measurements is obtained by averaging many observation using different sources. So the experimental results showed that the atomic clock developed in this study could be used in place of a hydrogen maser either by a further suppression of the temperature dependence of the output frequency or by stabilizing the ambient temperature of the atomic clock.

### 4. Conclusions

A laser-pumped Cs gas-cell type atomic clock with a high stability has been developed. It has a stability of  $7 \times 10^{-14}$  at 100 sec with a flicker floor of  $2.5 \times 10^{-14}$  at around 1000 sec. This stability is better than those of conventional commercial Rb gas-cell type atomic clocks and Cs beam type atomic clocks with a magnetic state selector in the averaging time range measured in this study (from 4 sec to 10,000 sec). A VLBI measurement was carried out using the atomic clock developed in this study, and it became clear that this clock could be used in place of a hydrogen maser if output frequency variation due to ambient temperature is suppressed.

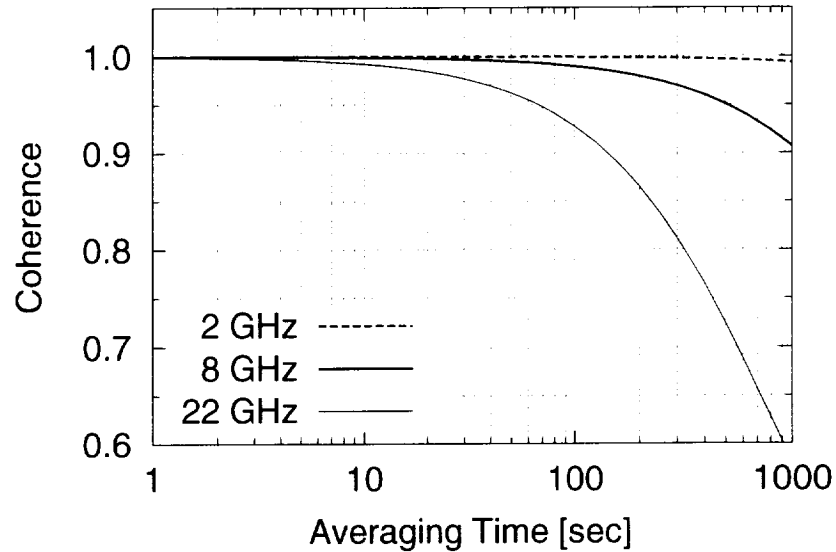


Figure 4. Coherence calculated by assuming the stability obtained for the atomic clock developed in this study.

## 5. Acknowledgements

The authors are grateful to Prof. N. Kawaguchi (National Astronomical Observatory of Japan) for suggesting the use of the laser-pumped Cs gas-cell type atomic clock in VLBI. We would also like to thank Mr. Y. Fukuzaki (Geographical Survey Institute, Tsukuba, Japan) for the preliminary VLBI experiment carried out using the atomic clock developed in this study.

## References

- [1] Lewis, L.L., M. Feldman, In: Proc. 35th Annu. Symp. Frequency Control, 612–624, 1981.
- [2] Saburi, Y., Y. Koga, S. Kinugawa, T. Imamura, H. Suga, Y. Ohuchi, In: Electronics Lett. 30 (8), 633–635, 1994.
- [3] Camparo, J., In: Proc. International Freq. Cont. Symp., 988–992, 1996.
- [4] Mileti, G., J. Deng, F.L. Walls, D.A. Jennings, R.E. Drullinger, In: IEEE J. Quant. Elect., 233–237, 1998.
- [5] Ohuchi, Y., H. Suga, M. Fujita, T. Suzuki, M. Uchino, K. Takahei, M. Tsuda, Y. Saburi, In: Proc. International Freq. Cont. Symp., 651–655, 2000.
- [6] Thompson, A.R., J.M. Moran, G.W. Swenson, Jr., In: Interferometry and Synthesis in Radio Astronomy, (John Wiley & Sons, New York), 277–280, 1986.
- [7] Kawaguchi, N., M. Oho, H. Hirose, Z. Yamamoto, In: Adv. Space Res., 617–623, 2000.

# Media Calibration in The Deep Space Network - A Status Report

*Charles J. Naudet, Steve Keihm, Gabor Lanyi, Roger Linfield, George Resch, Lance Riley,  
Hans Rosenberger, Alan Tanner*

*Jet Propulsion Laboratory, California Institute of Technology*

*Contact author: Charles J. Naudet, e-mail: [Charles.J.Naudet@jpl.nasa.gov](mailto:Charles.J.Naudet@jpl.nasa.gov)*

## Abstract

A new media calibration system (MCS) has been implemented at the Goldstone complex of the DSN. It is intended to calibrate the delay of radio signals imposed by the neutral atmosphere. The system provides periodic measurements of both the static dry and fluctuating wet components of this delay. In particular, the system will calibrate the fluctuations in line of sight path delay due to atmospheric water vapor that we believe will dominate the error budget for several radio science and radio astronomy experiments. We have compared two of these media calibration systems with a connected element interferometer on a 21 km baseline. In this report we describe a total of 30 observations in which a radio source was tracked for an hour or more and the delay residuals then calibrated using the MCS. The accuracy of the comparison appears to be limited by systematic errors in the interferometer, which are under investigation. However, our results do indicate that the MCS can meet or exceed the two-way Allan standard deviation specification of  $1.5 \times 10^{-15}$  on time scales of 2,000 - 10,000 sec, as required by the Cassini GWE for two way Doppler tracking.

## 1. Introduction

Over the last few years we have been developing a troposphere calibration system, in support of the Cassini radio science experiments. The Cassini spacecraft was launched in 1997, will arrive at Saturn in 2004, and started radio science experiments during its cruise phase (late 2001). The Cassini gravitational wave experiment (GWE) has been described in detail by Armstrong, [1] and Tinto and Armstrong [2]. Detailed studies of the GWE error budget [3] [4] point to atmospheric delay fluctuations as the dominant error component on time scales greater than 100 seconds. Thus the sensitivity of the GWE is limited, unless these atmospheric delays are calibrated. Since almost all the power in the atmospheric delay fluctuations at frequencies less than 0.01 Hz is due to the wet troposphere, the principle instrumentation used for calibration is a water vapor radiometer.

An advanced water vapor radiometer (WVR), shown in Figure 1, was developed at JPL and is described in detail by Tanner [5]. The WVR has an off-axis reflector, giving a one degree beamwidth with very low sidelobes. The pointing accuracy is 0.1 degree. The WVR measures the brightness temperature at 22.2, 23.8, and 31.4 GHz, with long term stability of 10 mK on time scales of 10,000 seconds. The path delay along the line-of-sight depends on the integrated columnar density of water vapor, and may be estimated by measuring the strength of the 22.2 GHz spectral line of water. In order to reduce the sensitivity to the variable height distribution of the water vapor, and to the presence of clouds, we use two additional frequency channels at 23.8 and 31.4 GHz [4]. The WVR acquires data in subsecond intervals and produces a time-series of line-of-sight brightness temperatures. Off to the right in the background of the picture one can see the microwave temperature profiler (MTP). The microwave temperature profiler retrieves the vertical distribution of atmospheric temperature. The data from the WVR, MTP, and surface

meteorological stations are then post-processed with two retrieval algorithms [8] [9] to extract the line-of-sight delay

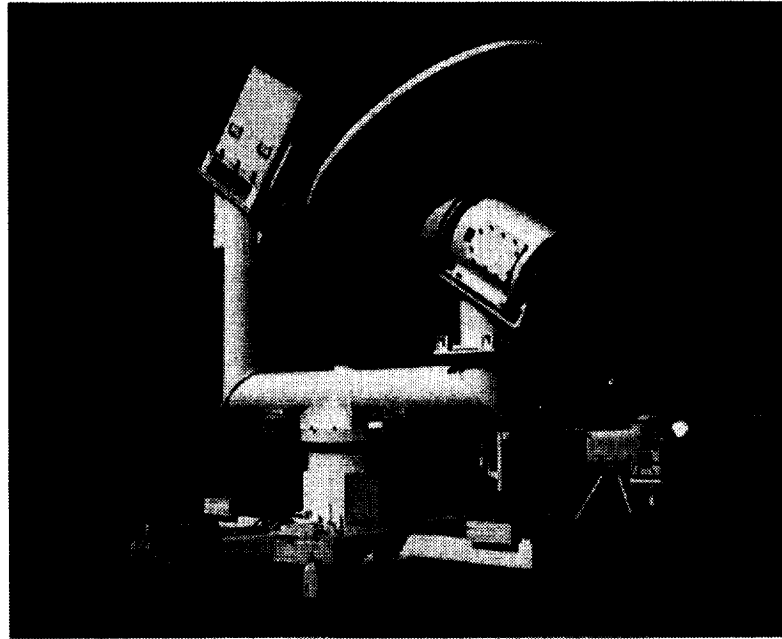


Figure 1. A photo of the Cassini calibration subsystem taken at DSS-13 in Goldstone CA. The new advanced WVR is seen in the center and the MTP and J-series WVR are shown in the background to the right.

## 2. Performance Testing

The objective of the Cassini media calibration system is to measure the atmospheric path delay fluctuation of signals transmitted between the Cassini spacecraft and the Goldstone DSS-25 antenna. Two advanced WVRs have been built to support Cassini radio science experiments. Dual WVRs allows for operational reliability and robustness in the case of equipment failure, and allow cross-checks between the units. A detailed inter-comparison between the two units has been made [9], and the Allan standard deviation (ASD) [10] was shown to be significantly better than the GWE requirements for all interval times greater than 100 seconds. However, this side-by-side comparison reflects only the stability of the WVR. In order to demonstrate a WVR's accuracy it is necessary to compare it to results from another measurement technique. Following earlier successful comparison experiments utilizing older model WVRs [6] [7] a connected element interferometer (CEI) was used to independently measure the line-of-sight path delay fluctuations. Additional details of the experimental setup can be found in reference 10.

From Aug, 1999 until May, 2001 we conducted a series of dual frequency (2.3 and 8.4 GHz) CEI observations on the 21 km baseline between the Deep Space Network's (DSN) high efficiency 34 m diameter antenna at DSS15 and a 34 m diameter beam waveguide antenna at DSS13. Since the effective wind speed is typically between 5 and 10 m/s, the tropospheric fluctuations at each site will be nearly independent for time scales less than  $\sim 4000$  seconds making this baseline well-suited

for a WVR comparison experiment. Strong, point-like radio quasar sources (flux density  $\geq 1$  Jy) with accurately known positions were chosen to minimize CEI errors. The data from each antenna were cross-correlated and the interferometric delay (difference in arrival times at the two antennas) was extracted. After subtraction of an a priori model, the residual phase delay (phase divided by the observing frequency) and delay rate (time rate of change of phase delay) were obtained. In addition, a linear clock model was fitted to the data and removed.

Each WVR was positioned  $\sim 50$  meters from the base of the 34 m antenna. This offset was chosen to maximize the sky coverage, while minimizing the magnitude of beam-offset errors. The WVR was co-pointed with the DSN antennas during sidereal tracking of distant natural radio sources. The WVRs were monitored in real time and derived path-delay time series were produced during post-processing at JPL. After the WVR path delay time series were smoothed over 6 seconds, the WVR data from each site (DSS15, DSS13) were subtracted to create a site-differenced delay time-series. Finally, the data was fitted for clock-like effects, resulting in a differenced WVR data type which could be directly compared with the CEI residual phase delays.

The comparison experiments conducted in 1999 were limited in scan duration to less than 26 minutes (the duration of a single pass on the CEI tape recorder). Several experiments produced little data, due to an assortment of instrumental problems and operator errors. In addition, instrumental problems at DSS13 caused uncalibrated delay errors on long ( $\geq 1000$ s) time scales [11]. By May, 2000 we were able to correct long-term CEI instrumental stability problems enabling WVR-CEI comparison over very long time scales ( $\geq 1000$  seconds). A detailed discussion of the entire data set may be found in references 11 and 12. In this report we will discuss two representative experiments, DOY137 and DOY138, that were conducted after these long term stability problems were corrected. The CEI and WVR delay time-series data from DOY138 is shown in Figure 2. For ease of comparison between data sets at different elevations, both the CEI and WVR data sets have been converted (mapped) to the equivalent delays in the zenith direction. It is clear that the correlation between the two data sets is strong. The CEI data can be corrected for phase delay fluctuations by subtracting the corresponding WVR data. The CEI data has a RMS of  $\sim 4.3$  mm. After WVR calibration this is reduced to  $\sim 1$  mm, a factor of four improvement. On DOY137 an improvement factor of 1.7 was measured, however the surface winds were measured to be greater than 40 km/hour. For a full discussion of all the experimental results see references 11, 12 and 13. Figure 3 shows a histogram of CEI residuals both before and after the WVR calibration for the entire data set acquired after May 2000. The CEI residual RMS is seen to improve (decrease) by almost a factor of four after calibration by the WVR data.

Figure 4 plots the Allan standard deviation (ASD) of the site-differenced delays as a function of the sampling time for DOY138. The CEI data and WVR data have ASD values that track one another very closely over almost the entire range of sampling times. After the WVR data is used to calibrate the CEI data, the ASD decreases by a factor of six at time intervals greater than 1000 seconds. The calibrated CEI data shows improvement for all sampling times down to  $\sim 15$  seconds, below which the 50 m WVR-DSN offset precludes useful calibration.

### 3. Discussion

We have described an atmospheric media calibration system which was shown to calibrate out the atmospheric delay fluctuations down to a Allan standard deviation level of  $1.5 \times 10^{-15}$  for sampling times greater than 2000 seconds. This system meets the GWE requirements for time

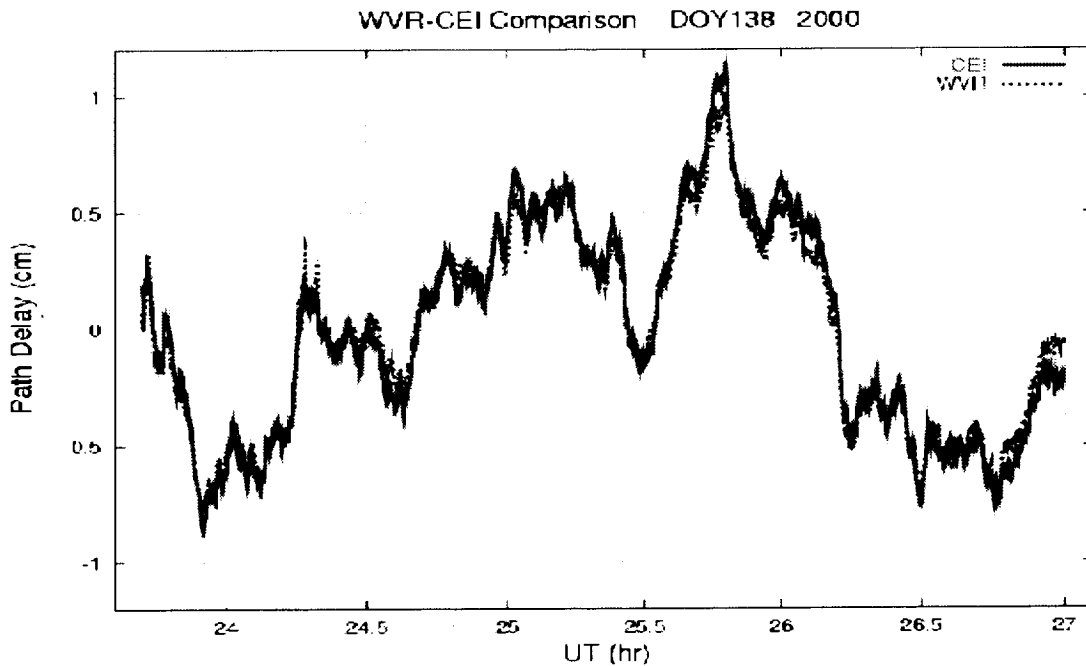


Figure 2. The site differenced, zenith mapped residual delay data from the CEI and WVR for DOY 138, 2000.

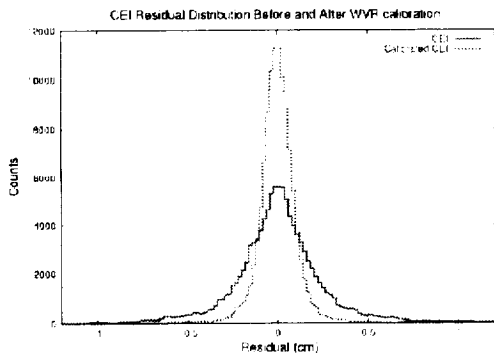


Figure 3. The Histograms of the residual CEI before and after WVR calibration

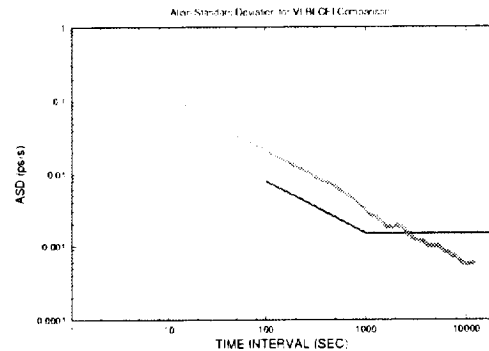


Figure 4. The Allan standard deviation plotted for DOY 138, 2000. The figure shows the calibrated CEI residual data and the requirements for the Cassini GWE.

scales greater than 2000 seconds. Calibration of the CEI data reduced the measured delay residuals by a factor of  $\sim 4$ .

The level of the CEI residual delay error is composed of the quadrature sum of the CEI errors and the WVR errors. Hence, the Allan standard deviation values in Figure 4 really are an

upper estimate of the WVR residual delay errors. To improve upon our assessment of the WVR performance, the error budget of each measurement technique must be independently examined in greater detail. Work is now under way to critically reevaluate the WVR error budget (precision, stability, beam size, beam offset, beam mismatch, retrieval accuracy) and the CEI error budget (electronic stability, instrumental delay mis-modelling, baseline accuracy).

#### 4. Acknowledgements

We would like to thank Larry Teitelbaum, John Eric Clark, Charles Snedeker, Lyle Skjerve, Leroy Tanida, the staff of DSS-13, and the Operations crews at the Goldstone Signal Processing Center for the invaluable assistance provided during these operations. The research described in this paper was carried out by the Jet Propulsion Laboratory, California Institute of Technology, under a contract with the National Aeronautics and Space Administration.

#### References

- [1] Armstrong, J.W., and R.A. Sramek, Observations of tropospheric phase scintillations at 5 GHz on vertical paths, *Radio Science*, 17, pp. 1579 - 1586, Nov. 1982.
- [2] Tinto, M., and J.W. Armstrong, Spacecraft Doppler tracking as a narrow-band detector of Gravitational Radiation, *Phys. Rev. D*, 58, 042002, 1998.
- [3] Armstrong, J.W, B. Bertotti, F.B. Estabrook, L. Iess, and H.D. Wahlquist, The Galileo/Mars Observer/Ulysses Coincidence Experiment, Proc. of the Second Edoardo Amaldi Conf. on Gravitational Waves, Ed., E. Cocchia, G. Pizzella, and G. Veneziano, Edoardo Amaldi Foundation Series, Vol. 4, World Scientific, 1998.
- [4] Keihm, S.J. Water Vapor Radiometer Measurements of the Tropospheric Delay Fluctuations at Goldstone Over a Full Year, TDA Prog. Report, 42-122, p 1-11, 1995.
- [5] Tanner, A.B., Development of a high-stability water vapor radiometer, *Radio Sci.*, 33, pp. 449-462, Mar. 1998.
- [6] Resch, G.M., D.E. Hogg, and P.J. Napier, Radiometric correction of atmospheric path length fluctuations in interferometric experiments, *Radio Sci.*, 19, pp. 411-422, Jan. 1984
- [7] Teitelbaum, L.P, R.P. Linfield, G.M. Resch, S.J. Keihm, and M.J. Mahoney, A Demonstration of Precise Calibration of Tropospheric Delay Fluctuations With Water Vapor Radiometers, TDA Prog. Report 42-126, pp. 1-8, 1996.
- [8] Resch, G.M., Inversion Algorithms for Water Vapor Radiometers Operating at 20.7 and 31.4 GHz, TDA Prog. Report 42-76, pp. 12-26, Oct. 1983.
- [9] Keihm, S.J. and S. Marsh, Advanced algorithm and system development for Cassini radio science tropospheric calibration, TDA Prog. Report 42-127, pp. 1-19, 1996.
- [10] Allan, D.W., Statistics of Atomic Frequency Standards, *Proc. IEEE*, 54.
- [11] C. Naudet, C. Jacobs, S. Keihm, G. Lanyi, R. Linfield, G. Resch, L. Riley, H. Rosenberger, and A. Tanner, The Media Calibration System for Cassini Radio Science: Part I, TMO Progress Report 42-143, pp 1-8, 2000.
- [12] G. Resch, J.E. Clark, S. Keihm, G. Lanyi, C. Naudet, L. Riley, H. Rosenberger, and A. Tanner, The Media Calibration System for Cassini Radio Science: Part II, TMO Progress Report 42-145, pp 1-21, 2001.

# A Proposal for Constructing a New Sub-mm VLBI Array, Horizon Telescope – Imaging Black Hole Vicinity

*Makoto Miyoshi, Seiji Kamenno*

*National Astronomical Observatory, Japan*

*Contact author: Makoto Miyoshi, e-mail: [miyoshi@miz.nao.ac.jp](mailto:miyoshi@miz.nao.ac.jp)*

## Abstract

The existence of a black hole in the universe has become very clear and is now one of our common sense in astronomy. But the direct image of a black hole showing relativistic phenomena around the event horizon was still beyond our reach at the previous century because the sizes of black holes are too small to observe. Sagittarius A\* (SgrA\*) is the closest massive black hole at our galactic center. The Schwarzschild radius of SgrA\* is about  $6 \mu\text{arcseconds}$ . Early in the 21st century developments of VLBI techniques and millimeter and sub-millimeter radio astronomy will soon reach the point to make such observations of black hole possible. We here propose to construct a new VLBI array that should be named as (Event) Horizon Telescope.

## 1. The Existence of Black Holes Are Confirmed Last Century

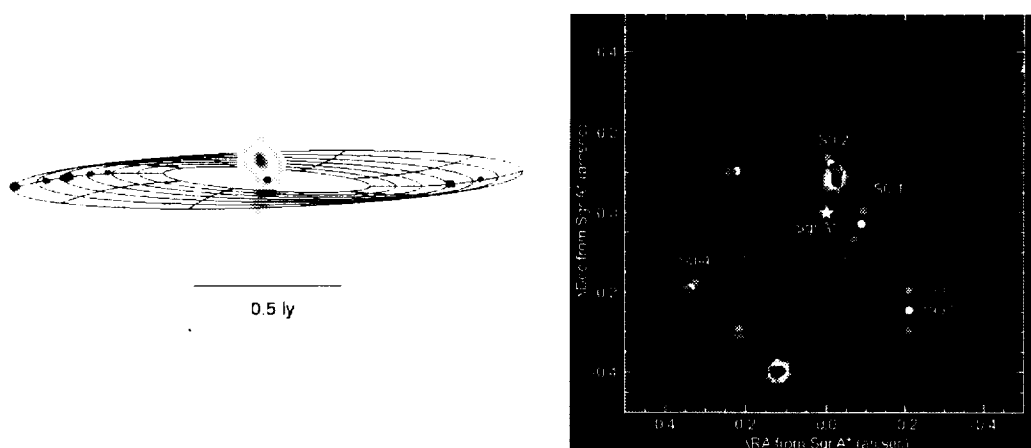
The existence of a black hole in the universe is now really confirmed from observations using the Hubble Space Telescope and the VLBA and ground based IR telescopes [1][2][3][4]. One of best examples is NGC4258 that has a massive black hole with mass of  $3.9 \times 10^7 M_{sun}$  at its center, another best case is the SgrA\* at our galactic center whose mass is measured to be  $2.6 \times 10^6 M_{sun}$ . In the both case, the masses are measured from dynamical motion around the black holes, namely from proper motions of rotating molecular gas disk and orbiting stars with velocity more than 1000 km/sec respectively. It is too difficult to deny the existence of black holes in the universe today.

## 2. Can We Watch Black Holes?

Though some observations suggest the existence of surrounding disk or matter at parsec scale around central black holes [6][5], the vicinities of black holes are still veiled observationally. We now know the existence of them but nothing about their real faces. Only theorists have investigated how black holes look at several Schwarzschild radii scale [11][9][10].

### 2.1. Apparent Sizes of Black Holes

Once we get a new telescope with higher resolution, which object is the best candidate that we can observe black hole vicinity? From the mass and distance of black holes we can calculate the apparent angular size of Schwarzschild radii and the diameter of the shadow. The Schwarzschild radius of stellar black hole with 1 solar mass at 1 pc is only  $0.02 \mu\text{arcseconds}$  (20 nano! arcseconds), then the stellar black hole would be too small to observe even in 21-st century. Most of massive black holes at several Mega parsec also show very small apparent sizes less than  $1 \mu\text{arcseconds}$ .



Disk around black hole in NGC4258[3]

The Orbital Motions of high velocity stars around the SgrA\*[4]

Figure 1. The NGC 4258 and SgrA\* the best confirmed case of existing black holes [2][4].

**Mass of Black Holes and the sizes**

object	mass of BH in solar mass	Distance ( kpc )	Schwarzschild radius Rs in km	Rs in Astronomical Unit (au)	apparent angular size ( $\mu$ as)	diameter of the shadow ( $\mu$ as)
Stellar BH	1	<b>0.001</b>	$295 \times 10^3$	$1.97 \times 10^{-8}$	$1.97 \times 10^{-2}$	<b>0.10</b>
M82 medium size BH (max)	$1 \times 10^6$	<b>3700</b>	$295 \times 10^9$	$1.97 \times 10^{-2}$	$5.32 \times 10^{-3}$	<b>0.03</b>
Galactic Center Sgr A*	$2.6 \times 10^6$	<b>8</b>	$7.67 \times 10^9$	$5.11 \times 10^{-2}$	6.39	<b>31.97</b>
<b>M31</b>	$3.5 \times 10^7$	<b>800</b>	$1.03 \times 10^{11}$	$6.89 \times 10^{-1}$	$8.61 \times 10^{-1}$	<b>4.30</b>
mega maser galaxy NGC4258	$3.9 \times 10^7$	<b>7200</b>	$1.15 \times 10^{11}$	$7.67 \times 10^{-1}$	$1.07 \times 10^{-1}$	<b>0.53</b>
<b>M87</b>	$3.2 \times 10^9$	<b>16100</b>	$9.44 \times 10^{12}$	$6.30 \times 10^{-1}$	3.91	<b>19.55</b>

Figure 2. Mass of Black Holes and their apparent Diameter.

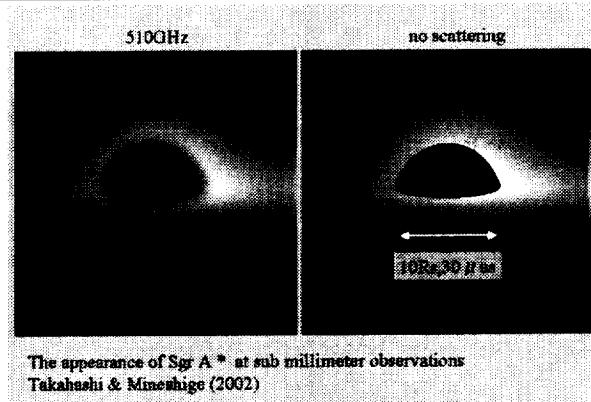


Figure 3. A View Model of SgrA\* at sub millimeter observations [10].

## 2.2. Best Candidate, SgrA\*

The black hole of SgrA\* at our galactic center has the largest apparent size ( $R_s = 6 \mu\text{arcsec}$ ,  $D_{\text{shadow}} = 30 \mu\text{arcsec}$ ), then the SgrA\* is the best candidate we can observe black hole vicinity.

Previous VLBI observations at centimeter to millimeter region were already performed to watch the face of SgrA\* but in vain. Because of plasma gas surrounding the SgrA\* washed away the true image of the black hole [8]. At sub millimeter wavelength, however, the effect of plasma is reduced by  $\lambda^{-2}$  and the true face of the black hole can be seen [7][10]. Let's construct a sub-mm VLBI array and observe the black hole vicinity. Such observations will testify to general relativity at strong gravity, and at the same time make a new field of observational black hole astronomy.

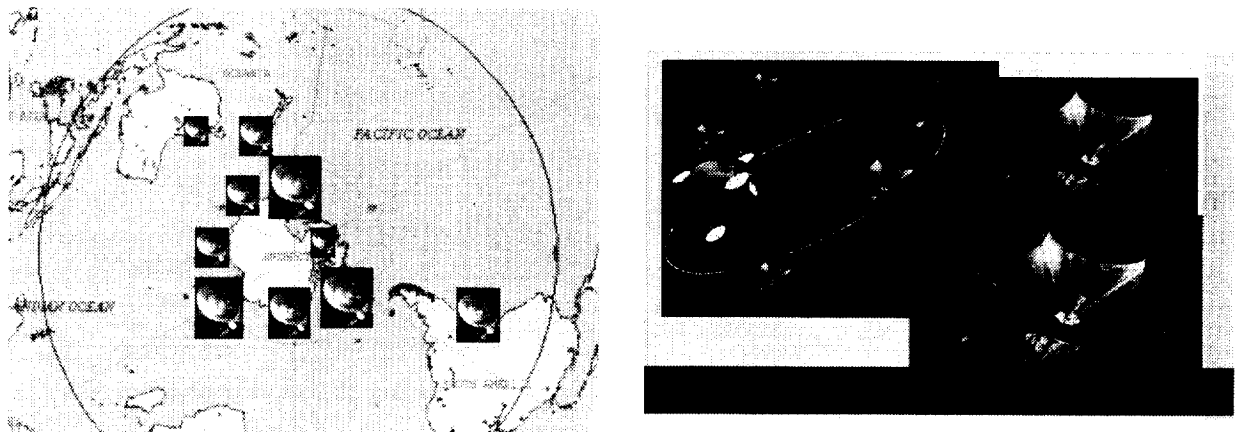
## 3. Horizon Telescope for Monitoring the Black Hole at SgrA\*

In order to obtain the black hole image of SgrA\*, the Horizon Telescope must be sub-millimeter VLBI system. Below we show the least specifications of the Horizon Telescope.

- Observing Frequency: 350 GHz to 800 GHz (sub millimeter) - to escape from the scattering effect of circumnuclear plasma
- Observing Site:(1) Space, or (2) Southern Hemisphere highlands or the Antarctic - to receive sub-mm radio emission from SgrA\* (low declination)
- Stations: More than 10 like VLBA - for getting sufficient uv coverage to obtain high dynamic range in image
- Array Size: More than 8000 km at 500 GHz - to attain less than  $10 \mu\text{ arc seconds}$  resolutions

## 4. Acknowledgements

The authors thank Dr. Hachisuka and Mr. Oyama for their helpful discussions.



Antarctic Sub-MM VLBI Array

Space to Space Sub-MM VLBI Array

Figure 4. Two Examples of Horizon Telescope - Ground or Space

## References

- [1] Macchetto, F., Marconi, A., Axon, D. J., Capetti, A., Sparks, W., Crane, P., 1997, *Astrophys. J.* 489, 579
- [2] M.Miyoshi, J.Moran, J.Herrnstein, L.Greenhill, N.Nakai, P.Diamond and M.Inoue, *Nature* Vol. 373, pp.127-129, 1995.
- [3] J.R.Herrnstein, J.M.Moran, L.J.Greenhill, P.Diamond, M.Inoue, N.Nakai, M.Miyoshi, C.Henkel, A. Riess *Nature*, 400, 539-541(1999)
- [4] Ghez, A.M., Morris, M., Becklin, E.E., Tanner, A.& T. Kremenek, 2000, *Nature*, 407, 349
- [5] Kamenno, Seiji, Sawada-Satoh, Satoko, Inoue, Makoto, Shen, Zhi-Qiang, Wajima, Kiyooki, *Publications of the Astronomical Society of Japan*, vol.53, no. 2, p. 169-178.
- [6] Jones, Dayton L., Wehrle, Ann E., Piner, B. Glenn, Meier, David L., *The Astrophysical Journal*, Volume 553, Issue 2, pp. 968-977.
- [7] Falcke, Heino, Melia, Fulvio, Agol, Eric, *The Astrophysical Journal*, Volume 528, Issue 1, pp. L13-L16.
- [8] Lo, K. Y., Shen, Z., Zhao, J.-H., Ho, P. T. P., *The Central Parsecs of the Galaxy*, ASP Conference Series, Vol. 186. Edited by Heino Falcke, Angela Cotera, Wolfgang J. Duschl, Fulvio Melia, and Marcia J. Rieke. ISBN: 1-58381-012-9, 1999, p. 72
- [9] Usui, Fumihiko, Nishida, Shogo, Eriguchi, Yoshiharu, *Monthly Notices of the Royal Astronomical Society*, Volume 301, Issue 3, pp. 721-728.
- [10] R. Takahashi, S. Mineshige, 2002 in preparation
- [11] Fukue, J., Yokoyama, T., 1988, *Publ. Astron. Soc. Japan*, 40, 15-24

# Session 5. Data, Models, and Software





# Ocean Tide and Atmospheric Loading

Hans-Georg Scherneck <sup>1</sup>, Machiel S. Bos <sup>2</sup>

<sup>1</sup>) *Chalmers/Radio and Space Science*

<sup>2</sup>) *Delft Institute for Earth-Oriented Space Research (DEOS)*

Contact author: Hans-Georg Scherneck, e-mail: [hgs@oso.chalmers.se](mailto:hgs@oso.chalmers.se)

## Abstract

We describe the ingredients of an automatic service for the dissemination of ocean tide loading coefficients and the considerations that led to the solution employed. The paper reviews the surface loading problem, methods for computation and especially the improvement of coastline resolution for accurate representation of coastal loads. We finally compare the loading results based on several ocean tide models with coefficients estimated from VLBI observations.

## 1. Introduction

Loading processes are still gaining increasing attention in space geodesy. The resolution of VLBI, using the data bases collected since the late 70s, makes estimation of tidal parameters feasible at the sub-millimeter level. The loading process affects in the first case the station position. This parameter, however, would average out the loading effect in the long-term average. Actually more relevant in this context are the major products of VLBI, Earth Orientation Parameters and, with increasing importance, atmosphere parameters. VLBI is heading towards near-real-time and high-rate applications, like EOP on the ten-minute basis, and atmospheres in a similar pace. On the sub-diurnal time scale, tide processes do generally not average out. Also, one of the findings of GPS in applications to atmospheres is that the zenith delay is sensitive to unmodeled vertical motion. The two processes, loading displacement and wave propagation, can be separated [5], but the correlation of the estimated parameters remains high. In relation to EOP's from small VLBI networks, an ocean-loading induced bias due to horizontal parameters may occur. A study using the VLBI observations from the CONT-94 experiment showed that the admittance of local, incoherent horizontal motion may be several times larger in the case of real data compared to the orientation changes that would be obtained on theoretical grounds using Helmert rotations [24].

The purpose of this paper is to respond to the demands of the analysts in space geodesy to retrieve high-accuracy coefficients for an ocean tide loading model in a convenient way. We describe an automatic ocean loading provider that we have made available on the Internet. We motivate the specific methods of computation that are employed. In the section on VLBI data analysis we show that the different ocean tide models that can be employed to compute the loading coefficients are uncritical at present given the accuracy of the observations.

The process of atmospheric loading is similar as far as the physical effects of load induced deformations of the solid earth body and subsequent displacement of points on the surface are concerned. There is one important difference though. Tidal processes are described to a very high order of approximation by sinusoidal variations in time. It turns out that only a few coefficients need to be imported into fairly unsophisticated formulas in order to describe tidal motion during extensive time periods. The atmospheric pressure, however, is aperiodic in most of its signal power.

Therefore, time series of loading displacements must be computed for each station at subdiurnal intervals. Generally, ocean loading tide and atmospheric pressure induced deformations are similar in size. The former is of course more pronounced in oceanic and coastal areas, whereas atmospheric loading is more efficient in the interior of continents, where there is no ocean to yield and equilibrate the surface pressure. In the ocean, the inverse barometer response is widely efficient, but limitations have recently been pointed out [15].

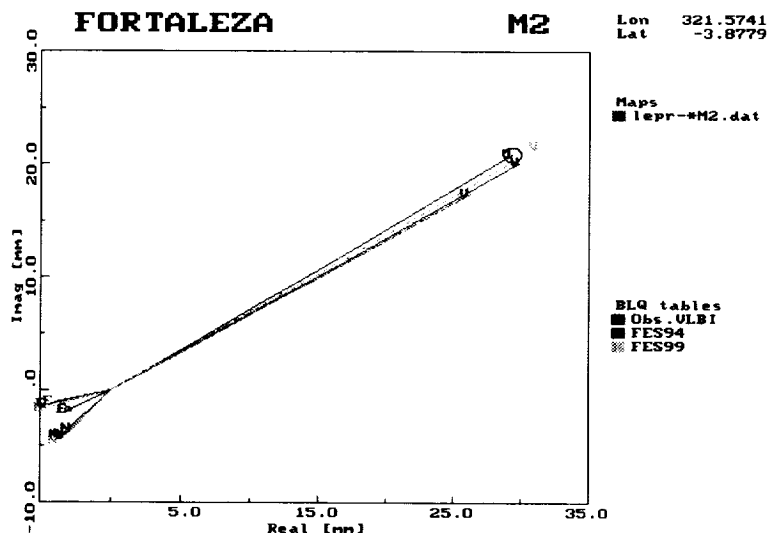


Figure 1. Loading phasors at Fortaleza, tide  $M_2$ . Vertical motion is indicated by symbol V, east and north by E and N, respectively. The FES94 model [13] has been used in the map mode of load computations, equation (7), shown in dark gray (purple), and using the point load method with refined coastlines, shown in lighter gray (blue). The difference in the vertical component is five millimeters. Agreement between the point load results based on [13], the more recent  $0.25^\circ$  model [11] (lightest gray (green)), and VLBI observations shown in black with one-sigma error ellipse (see section 4 for details) is much better, hinting at a lesser reliability of the map method.

## 2. Methods of Computation

The loading effect on a radially symmetric earth can be computed by convolution of the surface mass load with a kernel function, the Green's function of the normal stress surface loading problem on a self-gravitating planet. The property of radial symmetry of the structure and rheology renders the Green's function to depend only on the distance between the load point and the field point, not on the explicit location or on the azimuth.

The Green's functions are computed from solving the loading problem for each spherical harmonic degree at a time, giving three independent parameters at each degree  $n$ , the so-called load Love numbers (LLN). These three dimensionless numbers,  $h'_n$ ,  $l'_n$ , and  $k'_n$  characterize the vertical displacement  $u$ , the horizontal displacement  $\mathbf{v}$ , and the secondary gravity potential perturbation  $\Phi$ , respectively. All other loading effects (like surface gravity change  $\delta g$ , tilt, vertical deflection,

strain) can be represented by linear combinations of the LLN.

We thus have the point-load (PL) Green's functions and the relations between a loading mass element  $dm$  and the incremental effect it generates as follows

$$du = \frac{a}{M_E} \sum_{n=0}^{\infty} h'_n P_n(\cos \theta) dm \quad (1)$$

$$d\Psi = \frac{a^2}{M_E} \sum_{n=0}^{\infty} l'_n P_n(\cos \theta) dm \quad (2)$$

$$\mathbf{v} = -\nabla\Psi = \hat{\alpha} \sum_{n=0}^{\infty} l'_n \frac{dP_n(\cos \theta)}{d\theta} dm \quad (3)$$

$$d\Phi = \frac{ga}{M_E} \sum_{n=0}^{\infty} k'_n P_n(\cos \theta) dm \quad (4)$$

$$\delta g = \frac{2g}{a} u + \frac{g}{M_E} \sum_{n=0}^{\infty} (n - (n-1) k'_n) P_n(\cos \theta) dm \quad (5)$$

where  $a$ ,  $g$ , and  $M_E$  denote the radius, gravity and mass of the model earth, respectively (one uses the mean values of the ellipsoidal quantities). Note that  $\psi$  is a horizontal displacement potential, a scalar quantity. The Green's functions involve Legendre polynomials  $P_n$ . The distance  $\theta$  is measured as an angle along a great circle, and the azimuth is  $\hat{\alpha}$ . The sums can generally not be truncated; limiting values can be computed with the Kummer transform [8], [22].

An identity of the above using spherical harmonic development (SHD) provides

$$\left\{ \begin{array}{c} U_{nmk} \\ \Psi_{nmk} \end{array} \right\} = \frac{3}{2n+1} \frac{\rho}{\bar{\rho}} \left\{ \begin{array}{c} h'_n \\ l'_n \end{array} \right\} \zeta_{nmk} \quad (6)$$

for the displacement scalars, where, instead of the loading mass, we have developed the ocean tide amplitude  $\zeta$ , and multiplied with a constant ocean water density,  $\rho$ . The earth's mean density is denoted by  $\bar{\rho}$ .

The maximum degree of an SHD is limited in practice. Therefore, the following advantages and disadvantages are encountered in the PL method (equations (1) to (5)) and the SHD (equation (6)). The SHD would calculate an entire global map for each partial tide and component of the loading effect in one stage. This appears rather convenient contemplating the ever increasing number of stations demanding a continuing service for employing the PL integral method.

In practice, the PL integral is replaced by a sum over the grid elements of an ocean tide model. The ocean grid can be refined according to convergence criteria. The requirement for refinement occurs when a station is near a coast, since the Green's functions have a singularity at zero distance (the asymptote is one over the chord distance).

If crude accuracy is sufficient, the SHD method can be used. Experience shows that errors in excess of 1 mm result at many coasts, so the method is not an option for VLBI. The reason for the inaccuracy is related to the coarse resolution of the coasts, rather than to the truncation implied by the low maximum SH degree of the LLN included in (6). In an attempt to increase the accuracy by extending the degree range of the harmonic development, a semi-fast method can be used that utilizes the circular convolution theorem of Fourier series ( $\mathcal{F}$  denoting the discrete Fourier transform). It proceeds by taking all grid nodes along a pair of colatitude rings ( $\beta_k, \beta_l$ )

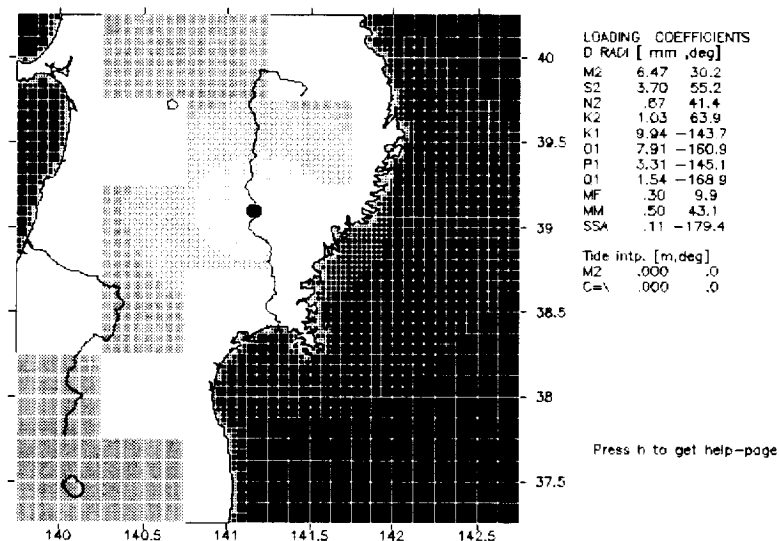


Figure 2. The refined loading grid. Inside a  $3^\circ \times 3^\circ$  area, the coastline is retrieved using a quad-tree algorithm. The basic box size for load integration is refined by an areal factor of four when the distance to the site is less than ten times the radius of a box or until it fits the coastline. The distance-dependent refinement is seen in the figure in the case of the land-boxes (gray). The example is for Mizusawa, Japan.

into account simultaneously

$$\mathcal{F}\{\mathbf{u}_k\} = \frac{a^3 \rho}{M_E} \mathcal{F}\{\tilde{\mathbf{G}}_{kl}\} \mathcal{F}\{\zeta_l\} \quad (7)$$

where we use a box-integrated Green's function

$$\tilde{\mathbf{G}}_{kl} = [\tilde{g}_{kl,0}, \tilde{g}_{kl,1}, \dots, \tilde{g}_{kl,M-1}]$$

$$\tilde{g}_{kl,r} = \int_{\beta_l - \Delta\beta/2}^{\beta_l + \Delta\beta/2} \int_{(\lambda_l - 1/2)\Delta\lambda}^{(\lambda_l + 1/2)\Delta\lambda} \mathcal{G}(\cos \beta_k \cos \beta + \sin \beta_k \sin \beta \cos \lambda) \cos \beta \, d\beta \, d\lambda$$

The formulas for the horizontal displacement potential follow analogously, and  $\mathcal{G}$ , the Green's function, is the infinite sum in (1) or (2), respectively.

Thus, this semi-fast map method with the integrated Green's function treats effectively the ocean tide on its original grid. It does the equivalent of distributing a tide value constantly over a grid box and convolving it with the point-load Green's function. This extension alleviates the LLN truncation; however the coastline cannot be refined without refining the grid everywhere globally. Going to the  $5' \times 5'$  grid of a standard topographic data base to retrieve a more accurate coastline would result in enormous computation times. Using the  $0.5^\circ \times 0.5^\circ$  of [13] we arrive at errors in excess of 1 mm for example at Fortaleza (Fig. 1). Thus we are doubtful about the fast or semi-fast methods that generate loading results on global maps.

We rather stay with a per-site PL computation. In the following section we describe an automatic service available over the Internet.

### 3. The Automatic Ocean Loading Provider

The automatic ocean loading provider is a web service available at <http://www.öso.chalmers.se/≈loading>. We employ the point-load method, one set of Green's functions for a continental earth structure, and eleven different ocean tide models. The different models reflect the most important source of uncertainty in the model computations at present.

#### 3.1. Ocean Tide Models

The ocean tide models can be divided into those which are purely hydrodynamic, purely based on altimetry data and those which are of a hybrid form. Nowadays, most published models are of the last type. All models described are barotropic (depth-averaged) and employ the Laplace tidal equations. Regularly, these models are self-gravitating and self-loading using a local coefficient [1], a procedure which, however, may yield significant systematic error [21].

One of the first accurate ocean tide models was the one of Schwiderski [27]. Its success was partly the result of forcing the model to fit almost all available tide gauge observations at the coast. For long-term continuity it has again been added to the ocean tide loading provider. A closely related model is NAO99 [16] but with the inclusion of altimetry data and an improved assimilation scheme. FES94.1 [13] is a purely hydrodynamic finite-element model with enhanced resolution on the shelves. FES95.2 [14] was an update of FES94.1 with the introduction of better Arctic tides and a longwave adjustment using TOPEX/Poseidon (T/P) altimetry data.

Other models which also employ a longwave T/P adjustment of and loading effects due to FES94.1 are CSR3.0, CSR4.0 [6] and GOT99.2b [20]. Since T/P does not exceed the  $\pm 66^\circ$  latitude bounds, these models are equal to FES94.1 in these polar regions. Furthermore, CSR3.0 and CSR4.0 have spurious wet nodes on land. These must be carefully excluded in loading calculations. Secondly, these two models do not extend under the Antarctic ice shelves. To amend this, the values of GOT00.2 have been added in these places. GOT00.2 is an update of GOT99.2b and has been extended by the assimilation of ERS1/2 altimetry data.

Recently, the models FES98 [11] and FES99 [12] have been published. They are both hydrodynamic models with assimilated tide gauge, while FES99 also incorporates T/P data. Finally, the model TPXO.5 [7] has been added because it is an independent model; it is a fully inverse, hydrodynamic model that uses the representer method to fit tide gauge and altimetry data.

All models are given on a  $0.5^\circ \times 0.5^\circ$  grid except for Schwiderski which has  $1^\circ \times 1^\circ$  and FES98/99 which are given on a  $0.25^\circ \times 0.25^\circ$  grid.

It must be noted that these models do not conserve the water mass during one tidal cycle. To remedy this defect it is common practice to subtract a uniform layer with a certain phase lag from the model. Fortunately this effect is small for the most recent ocean tide models.

#### 3.2. Implementation

For the computation of the loading using the PL method, the integral must be replaced by a summation. A natural choice of the discretization is to use the grid of the ocean tide model and sum each cell that has tidal values weighted with the Green's function. Thus:

$$du(\mathbf{r}) = \rho \sum_{i=1}^N \sum_{j=1}^M \mathcal{G}(|\mathbf{r} - \mathbf{r}'_{ij}|) \zeta_{ij} \Delta A_{ij} \quad (8)$$

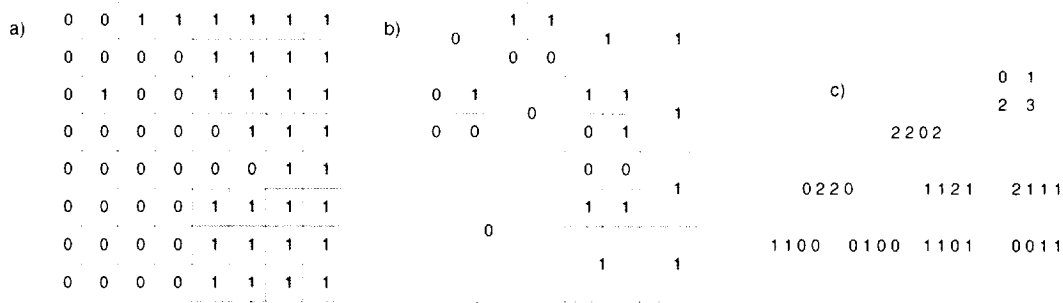


Figure 3. The schematic principle of the quad tree. First, the coastline data of GMT is digitized (a). Next, the data is decomposed into blocks (b) and finally these blocks are stored into a hierarchical tree (c). In this three, the highest level represent the whole area, one level down the leaves describe the status of the 4 smaller parts of the area. The number 2 indicates that the area contains land and water, the number 1 that it is totally land and 0 that it is totally filled with water. The nodes at each branch describe, from left to right, the upper-left, upper-right, bottom-left, bottom-right part of the cell.

with  $N$  and  $M$  the number of rows and columns of the grid. For the density of water we assume  $\rho=1030 \text{ kg/m}^3$ . The Green's function is available in tabular form [8], [9]. The use of point loads to represent the effect of an areal load  $\rho\zeta \Delta A$  is justified for large distances. For distances less than ten times a grid cell diameter, however, this is no longer valid. Furthermore, when fitting the model to the coastline it becomes important to represent the actual amount of water loading the Earth. The solution is to refine the grid, and this can be done gradually and locally around the station where it is needed. Inside the refinement area, the tide variation inside a gridbox can be interpolated or extrapolated into e.g. estuaries using the neighboring nodes. By doing the refinement automatically most of the arguments against this method [18] are removed.

The refinement is performed by dividing a grid cell recursively into 4 smaller blocks until two criteria for 1) approximating the cell load by a point load and 2) fit of the model to the coastline are satisfied. The tidal values for these smaller blocks are derived using bilinear interpolation of the original model.

Finally one has to define the water area  $A$ . For high coastline resolutions of less than  $1\text{km}$  the size of a global digitized land-water map becomes prohibitive. In cooperation with Simon Williams [*pers. communication, 2000*] a compression program was developed, again exploiting the algorithm of recursively divided blocks. First, the coastline data base of GMT [28] has been digitized (resolution= $0.00549^\circ \approx 600\text{m}$ ) after which the data has been decomposed into a quad tree [10], see Figure 3.

In practice Equation 8 is computed first with a program called `olfg` [23]. If necessary, a square of  $3^\circ \times 3^\circ$  is left out of the computation and post-processed with the program `olmpp`. A screenshot of such an area is given in Figure 2.

### 3.3. Comparison of Program Codes

Other programs that compute the ocean tide loading using the PL method are: `NLOADF` [2], `GOTIC2` [17], `conmodb` [Baker, *pers. comm. 2000*] and `LOADSDP` [19]. `NLOADF` differs from the others by projecting the ocean onto a template grid centered on the station, each ring having approximately constant loading sensitivity. The highest coastline resolution is  $1/64^\circ \approx 1.7\text{km}$ .

Table 1. The vertical ocean loading tide computed by different programs using CSR4.0, harmonic  $M_2$  [6]. LOADSDP uses FES95.2 [14] and a regional model for Canadian waters, however [19]. The displacement is positive upwards and the phase lags negative relative to the astronomical tide at Greenwich.

Station	NLOADF [2]		GOTIC2 [17]		conmodb [4]		LOADSDP [19]		olfg/olmpp [23]	
	mm	°	mm	°	mm	°	mm	°	mm	°
FD-VLBA	1.48	168.4	1.46	168.7	1.45	167.8	1.43	165.2	1.48	167.7
Fortaleza	35.84	34.1	36.20	34.0	35.56	33.8	35.55	34.0	35.70	34.0
GilCreek	8.97	99.5	9.08	99.4	8.95	99.2	8.99	97.4	9.05	99.2
HartRAO	16.53	-131.9	16.54	-131.9	16.47	-131.9	16.42	-131.3	16.66	-131.8
Kashima	8.87	46.2	8.91	46.1	8.87	46.5	8.80	44.5	8.80	46.2
Kokee	12.63	-120.3	12.79	-120.7	12.58	-120.2	12.55	-119.2	12.63	-120.0
DSS65	14.36	-89.0	14.51	-89.2	14.35	-89.2	14.64	-89.4	14.55	-89.2
Medicina	5.33	-70.9	5.31	-71.0	5.25	-70.4	5.49	-70.4	5.43	-71.3
Noto	5.93	-85.4	5.93	-85.2	5.93	-85.6	5.93	-85.3	6.03	-85.7
Ny-Alesund	8.14	174.0	8.39	174.5	8.22	173.7	7.86	-175.9	8.37	174.1
Onsala	3.48	-67.0	3.42	-66.1	3.47	-64.7	3.60	-69.2	3.51	-65.4
Richmond	7.74	162.7	7.80	162.7	7.63	162.3	8.27	170.0	7.81	162.0
Westford	7.45	-179.1	7.56	-179.2	7.49	-179.3	8.24	157.3	7.31	-179.2
Wetzell	5.08	-71.5	5.05	-72.0	5.02	-71.5	5.29	-71.7	5.08	-71.5

Table 2. Formal uncertainties of estimated load tide coefficients in this study. The unit is millimeters.

Station	vert.	horiz.	Station	vert.	horiz.	Station	vert.	horiz.
FD-VLBA	0.34	0.09	Fortaleza	0.65	0.20	Gilmore	0.24	0.08
HartRAO	1.05	0.32	Kashima	1.01	0.31	Kokee	0.34	0.12
DSS65	1.03	0.26	Medicina	0.77	0.18	Noto	1.30	0.29
Ny-Ålesund	0.48	0.14	Onsala	0.48	0.14	Richmond	0.56	0.13
Westford	0.24	0.08	Wetzell	0.27	0.10			

GOTIC2 uses integrated Green's function and has a manual high-resolution land masking feature. LOADSDP is also a direct implementation of Equation 8 using FES95.2 and several local ocean tide models.

As these independent programs use the same input (CSR4.0, in the Antarctic region augmented with GOT00.2) and the same Green's functions (Gutenberg-Bullen Earth), they can be employed to indicate the numerical accuracy of loading coefficients.

The results are listed in Table 1. One can see, excluding LOADSDP because it uses another model, that the differences are small and the numerical accuracy is seen to be near  $0.2mm$ . The effect of using another Green's function such as PREM [3] is around  $0.1mm$  and is therefore negligible.

#### 4. VLBI Observations and Discussion

We use estimated ocean loading coefficients from the VLBI solution reported in [26]. Table 2 shows the uncertainties for each station. The uncertainties vary as a result of signal power and number of experiments.

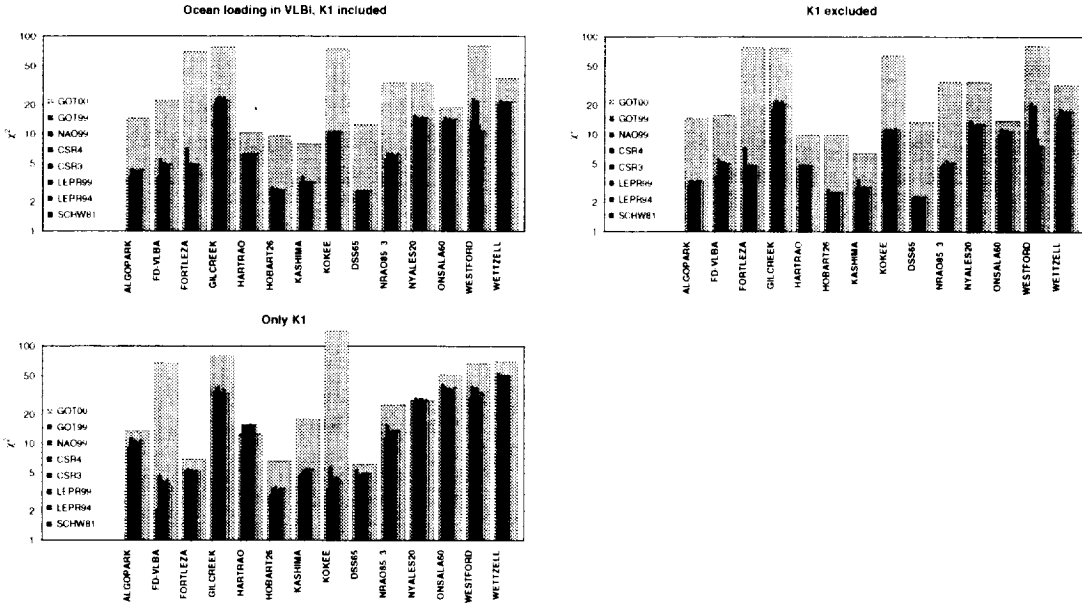


Figure 4. Comparison of observed ocean loading tide coefficients with models. Shown is the weighted Chi-square of the fit, including the eight diurnal tides and the three spatial components. The wide, gray bars show the observed signal in terms of multiples of the standard deviation, and the coloured bars show the remaining signal after subtracting one of the seven tide loading models. The problems with the K1 tide in the observations are exhibited by excluding this tide in the middle frame, and showing it separately in the lower frame.

In the comparison with models we show

$$\chi^2 = \frac{1}{3N} \sum_{n=1}^N \sum_{c=1}^3 \frac{|S_{nc}^{(o)} - S_{nc}^{(m)}|^2}{\sigma_{nc}^2}$$

where  $S_{nc}$  denotes a complex valued loading coefficient, superscript ( $o$ ) the VLBI observation,  $n$  steps through the tides ( $M_2, S_2, N_2, K_2, K_1, O_1, P_1, Q_1$ ), and  $c$  counts the three spatial components. The result is shown in Figure 3. The different tide models we have included, signified by superscript ( $m$ ), are the Naval Surface Weapons Center model, SCHW81 [27]; two versions of the Grenoble/CNES model, LEPR94 [13] and LEPR99 [11]; two versions of the University of Texas Center of Space Research model, CSR3 and CSR4 [6]; two versions of the Goddard Space Flight Center model, GOT99 and GOT00 [20]; and the model from the National Astronomical Observatory of Japan, NAO99 [16].

The most noticeable result of the comparison is that the internal agreement among the models is much greater than between any single model and our VLBI observations. The variation between the models at Westford is due to the Gulf of Maine, which is present in SCHW81, CSR4, LEPR99, GOT99-00, and NAO99, but excluded in the other models. The  $K_1$  tide is observed in good agreement with the ocean loading model only at two stations, Fort Davis (FD-VLBA) and Kokee Park. In all other cases the models do not explain more than 50 percent of the observed tide. Both Fort Davis and Kokee Park have considerable diurnal solid earth tides; problems with that tide would affect all stations except eventually one at the equator (where the vertical and east

components are zero) or at  $45^\circ$  (where the north component is zero). Closer inspection shows that errors at  $K_1$  exist likewise in the vertical and the horizontal components.

We know from [24] that the vertical component decouples almost perfectly from the Earth Orientation parameters. Supposing a common source for the defect, one has to look into station-dependent conditions. The question arises why the results seem to have much less systematic error at Fort Davis and Kokee.

Onsala shows the greatest disagreement. Problems with the modelling code or with ocean models are not very likely, however, since GPS solutions appear to be in quite good agreement with models [25]. From discussions with Leonid Petrov [*pers. comm., 2002*] we realize that our VLBI solution appears to contain more systematic error power than a recent GSFC solution. There is a lot more to explore here.

## 5. Conclusions

Ocean tide loading modelling appears to provide consistent results. We have compared different software products and a range of different ocean tide models. A predominant error source appears to exist at the  $K_1$  tide frequency. The perturbation could be an effect of solar radiation, which leaks into the  $K_1$  frequency band.

It appears advisable to recompute ocean loading estimates from VLBI, including the experiments after 1999 and take a careful look at possible sources of perturbations, in particular in the diurnal frequency band.

**Acknowledgments.** We thank Rüdiger Haas for making the VLBI results available to us. The contributors of ocean loading modelling code and the makers of global ocean tides are kindly acknowledged. This work is supported by grants from the Swedish Research Council and by the European Union program for Training and Mobility of Researchers.

## References

- [1] Accad, Y. and Pekeris, C. L., Solution of the tidal equations for the  $M_2$  and  $S_2$  tides in the world oceans from a knowledge of the tidal potential alone, *Phil. Trans. Roy. Soc. London, Ser. A*, Vol.290, 235–266, 1978.
- [2] Agnew, D.C., NLOADF: a program for computing ocean-tide loading, *J. Geophys. Res.*, Vol.102, 5109–5110, 1997.
- [3] Anderson, D.L., and Dziewonski, A., Preliminary Reference Earth Model, *Phys. Earth. Planet. Int.*, Vol. 25, 297–356, 1981.
- [4] Baker, T.F. Tidal gravity in Britain, tidal loading and the spatial distribution of the marine tide, *Geophys. J. R. astr. Soc.*, Vol. 62, 249–267, 1980.
- [5] Dach, R., R. Dietrich, Influence of the ocean loading effect on GPS derived precipitable water vapor, *Geophys. Res. Letters*, Vol. 27, 2953–2956, 2000.
- [6] Eanes, R. and S. Bettadpur, The CSR 3.0 global ocean tide model, Center for Space Research, Technical Memorandum, CSR-TM-96-05, 25pp., 1996.
- [7] Egbert, G. D., Bennett, A. F., and Foreman, M. G. G. TOPEX/POSEIDON tides estimated using a global inverse model. *J. Geophys. Res.*, Vol.99, 24,821–24,852, 1994.
- [8] Farrell, W.E., Deformation of the Earth by Surface Loads, *Rev. Geophys. Space Phys.*, Vol. 10, 761–797, 1972.

- [9] Francis, O. and P. Mazzega, Global charts of ocean tide loading effects. *J. Geophys. Res.*, Vol.95, 11,411–11,424, 1990.
- [10] Knuth, D. E., *Fundamental Algorithms: The art of computer programming*, Vol. 1. Addison-Wesley, second edition, 1973.
- [11] Lefvre, F., Lyard, F. H., and Le Provost, C. FES98: A new global tide finite element solution independent of altimetry. *Geophys. Res. Letters*, 27(17):2717–2720, 2000.
- [12] Lefèvre, F., Lyard, F. H., Le Provost, C. and Schrama, E. J. O., FES99: A tide finite element solution assimilating tide gauge and altimetric information. *J. Atm. Oceano. Tech.*, *submitted*, 2001.
- [13] Le Provost, C., M.L. Genco, F. Lyard, P. Vincent, and P. Canceil, Spectroscopy of the world ocean tides from a finite element hydrological model, *J. Geophys. Res.*, Vol.99, 24,777–24,798, 1994.
- [14] Le Provost, C. Lyard, F., Molines, J. M., Genco, M. L. and Rabilloud, F., A hydrodynamic ocean tide model improved by assimilating a satellite altimeter-derived data set, *J. Geophys. Res.*, Vol.103(C3), 5513–5529, 1998.
- [15] Mathers, E.L., and P.L. Woodworth, Departures from the local inverse barometer model observed in altimeter and tide gauge data and in a global barotropic numerical model, *J. Geophys. Res.*, Vol.106, 6957–6972, 2001.
- [16] Matsumoto, K., Takanezawa, T. and Ooe, M. Ocean Tide Models Developed by Assimilating TOPEX/POSEIDON Altimeter Data into Hydrodynamical Model: A Global Model and a Regional Model Around Japan. *J. of Oceanog.*, Vol.56, 567–581, 2000.
- [17] Matsumoto, K., T. Sato, T. Takanezawa, and M. Ooe, GOTIC2: A Program for Computation of Oceanic Tidal Loading Effect, *J. Geod. Soc. Japan*, Vol.47, 243–248, 2001.
- [18] Mitrovica, J. X., Davis, J. L., Shapiro, I. I., A spectral formalism for computing three-dimensional deformations due to surface loads. 1 Theory, *J. Geophys. Res.*, Vol.99, 7057–7073, 1998.
- [19] Pagiatakis, S.D.. Program LOADSDP for the calculation of ocean load effects. *Manuscripta Geodaetica*, Vol.17, 315–320, 1992.
- [20] Ray, R., A Global Ocean Tide Model From TOPEX/POSEIDON Altimetry: GOT99.2, NASA Technical Memorandum, NASA/TM-1999-209478, National Aeronautics and Space Administration, Goddard Space Flight Center, Greenbelt, MD, 1999.
- [21] Ray, R., Ocean Self-Attraction and Loading in Numerical Tidal Models. *Marine Geodesy*, Vol.21, 181–192, 1998.
- [22] Scherneck, H.-G., Loading Green's functions for a continental shield with a Q-structure for the mantle and density constraints from the geoid, *Bull. d'Inform. Mares Terr.*, Vol. 108, 7775–7792, 1990.
- [23] Scherneck, H.-G., A parametrized solid earth tide model and ocean tide loading effects for global geodetic baseline measurements, *Geophys. J. Int.*, Vol.106, 677–694, 1991.
- [24] Scherneck, H.-G., R. Haas, Effect of horizontal ocean tide loading on the determination of polar motion and UT1, *Geophys. Res. Let.*, Vol. 26, 501–504, 1999.
- [25] Scherneck, H.-G., J.M. Johansson, and F.H. Webb, Ocean Loading Tides in GPS and Rapid Variations of the Frame Origin, in K.-P. Schwarz (ed.): *Geodesy beyond 2000 The Challenges of the First Decade*, IAG General Assembly Birmingham, July 19-30, 1999, pp. 32–40, 2000.
- [26] Scherneck, H.-G., R. Haas, and A. Laudati, Ocean loading tides for, in, and from VLBI, in N.R. Vandenberg and K.D. Baver (eds.): *International VLBI Service for Geodesy and Astrometry, 2000 General Meeting Proceedings*, pp. 257-262, NASA/CP-2000-209893, NASA Center for Aerospace Information, Hanover, MD, 2000.
- [27] Schwiderski, E. W., On charting global ocean tides, *Rev. Geophys. Space Phys.*, Vol.18, 243–268., 1980.
- [28] Wessel, P., Smith, W. H. F., A global, self-consistent, hierarchical, high-resolution shoreline database, *J. Geophys. Res.*, Vol.101, 8741–8743, 1996.

# Gradient Mapping Functions for VLBI and GPS

Arthur Niell<sup>1</sup>, Jennifer Tang<sup>2</sup>

<sup>1</sup>) MIT Haystack Observatory

<sup>2</sup>) Rice University

Contact author: Arthur Niell, e-mail: [aniell@haystack.mit.edu](mailto:aniell@haystack.mit.edu)

## Abstract

A hydrostatic gradient mapping function based on *in situ* meteorological data has been developed to provide an *a priori* correction to the hydrostatic delay. In the same way that the symmetric atmosphere estimation is improved by first removing the hydrostatic delay, application of the *a priori* hydrostatic gradient delay correction allows the use of a more accurate partial derivative for the asymmetric wet component, to the extent that it can be described by the gradient formulation. Application of the *a priori* hydrostatic gradient delays prior to estimating a wet gradient improves the repeatability of baseline lengths for the twelve days of CONT94 compared to estimating a hydrostatic gradient.

## 1. Background

The Niell mapping function [3] (NMF) provides accuracy and precision comparable to mapping functions using surface meteorology as input, but without the need for external input. It has been clear for some time that, to improve the accuracy of the atmosphere delay estimation further, some form of *in situ* information is needed to follow the mapping function variations on daily and sub-daily time scales. Such data can be obtained from a numerical weather model (NWM). Niell (2000) [4] described one possible implementation: the 200 hPa geopotential heights provide input for the azimuthally symmetric hydrostatic mapping function, IMFh, and the vertical distribution of wet refractivity is used to calculate the azimuthally symmetric wet mapping function, IMFw. Comparison of baseline lengths among the seven antennas for the twelve days of CONT94 [5] demonstrated that the use of IMFh/IMFw for the atmosphere estimation reduced the RMS scatter compared to using NMF. The amount of reduction corresponds to removing  $\sim 4$  mm of vertical height error (Figure 1).

## 2. The *a priori* Hydrostatic Gradient

The estimation of gradients was included for both the NMF and IMFh/IMFw analyses by using the hydrostatic gradient model of [1] (CH). Although Chen and Herring showed, both analytically and by raytracing one year of data from a numerical weather model, that the hydrostatic and wet gradients have a slightly different elevation dependence, as would be expected for the difference in scale heights, up to now no *a priori* model has been proposed. However, it occurred to one of us (AEN) that the same isobaric surface that is used to provide the input for IMFh could represent the “tilt” of the hydrostatic atmosphere corresponding to the hydrostatic gradient. This would allow the separation of the hydrostatic and wet components contributing to the azimuthally asymmetric delay of the troposphere, analogous to separation of the symmetric mapping functions.

The “tilt” of the hydrostatic atmosphere is calculated as the normal to the surface defined by the 200 hPa geopotential heights at the four grid points surrounding the site of interest. The

NWM that has been used to determine the inputs for both IMF and the hydrostatic gradient is the re-analysis of the Data Assimilation Office of the Goddard Space Flight Center [6]. The grid spacing is  $2^\circ$  by  $2.5^\circ$  in latitude and longitude. The normal to the 200 hPa surface above the point of interest is estimated along with the geopotential height of the surface. The geopotential height is the input parameter for IMFh, and the gradient is accommodated by adjusting the zenith direction to coincide with the direction of the normal to the 200 hPa surface. Although the mapping function value at an elevation of  $90^\circ$  is no longer exactly one, the error in delay is less than 0.2 mm. As a check on the consistency with the gradient functions of Chen and Herring, the delay difference was confirmed to be less than one millimeter at all elevations down to  $5^\circ$  (the minimum elevation validated for Chen and Herring) for the tilt corresponding to 1 mm of gradient in the sense used by Chen and Herring.

The *a priori* hydrostatic gradient mapping function, designated GMFh, when multiplied by the *a priori* zenith hydrostatic delay, gives the hydrostatic delay at the observation elevation. The model values of the NWM from DAO are tabulated every six hours beginning at 0 UT, and the mapping function is obtained by interpolation to the time of the observation for each VLBI or GPS antenna. By using a global gridded NWM the mapping functions are available for a site anywhere on the surface of the Earth.

### 3. Evaluation of GMFh

The best evaluation of the “tilt” model would be comparison with raytracing of the three-dimensional distribution of refractivity of the NWM, but this has not been done yet. A second test is to compare the repeatability of estimated site position using the different atmosphere models. An improvement in the atmosphere model is likely to improve the repeatability (unless the poorer model has been compensating for the error in some other model component, such as a seasonal effect in antenna position). The data of CONT94 were again used, thus allowing comparison with NMF and IMFh/IMFw.

The positions of six antennas were estimated relative to a fixed position for the Fairbanks antenna using the *solvk* analysis package [2]. The *a priori* hydrostatic delay was calculated using GMFh, IMFw was used for the symmetric wet mapping function, and the residual gradient was estimated using the Chen and Herring (1997) wet gradient model. The baseline length repeatabilities for the NMF and the GMFh analyses are shown in Figure 2. The improvement in repeatability going from NMF with the CH hydrostatic gradient model, to GMFh as *a priori* and CH wet as the gradient model, is shown in Figure 3. Only one baseline is not improved. The greater improvement for longer baselines is consistent with a reduction in the error in the local vertical component of site position. For this set of data the reduction is approximately 4.5 mm.

### 4. Caveats and Future Plans

It is promising that baseline repeatability is improved when a better model is incorporated. However, there are other possible explanations that must be eliminated to strengthen the case that inclusion of the hydrostatic gradient model is responsible. In addition to the possibility mentioned above, the time scale for variability of the gradient must be explored. The time scale for the estimated gradient variability was set to roughly twelve hours, while the *a priori* hydrostatic gradient had significant change over the six hour separation between input values. The effect of

increasing the allowed variability of the estimated gradients must be investigated.

The other investigation that is important is the comparison of the hydrostatic delay change due to the tilted atmosphere with actual raytraced delays from the NWM. Higher horizontal resolution weather models will also allow improvement in the wet gradient mapping function and perhaps will provide evaluation whether the form assumed for the gradients is correct.

## References

- [1] Chen, G. and T. A. Herring, Effects of atmospheric azimuthal asymmetry on the analysis of space geodetic data, *J. Geophys. Res.*, 102, B9, 20,489-20,502, 1997.
- [2] Herring, T. A., J. L. Davis, and I. I. Shapiro, Geodesy by radio interferometry: The application of Kalman filtering to the analysis of very long baseline interferometry data, *J. Geophys. Res.*, 95, 12,561-12,581, 1990.
- [3] Niell, A.E., Global mapping functions for the atmosphere delay at radio wavelengths, *J. Geophys. Res.*, 101, B2, 3227-3246, 1996.
- [4] Niell, A.E., Improved atmospheric mapping functions for VLBI and GPS, *Earth, Planets, and Space*, 52, 699-702, 2000.
- [5] Niell, A. E., Preliminary evaluation of atmospheric mapping functions based on numerical weather models, *Phys. Chem. Earth*, 26, 475-480, 2001.
- [6] Schubert, S. D., J. Pjaendtner, and R. Rood, An assimilated data set for Earth science applications, *B. A. M. S.*, 74, 2331-2342, 1993.

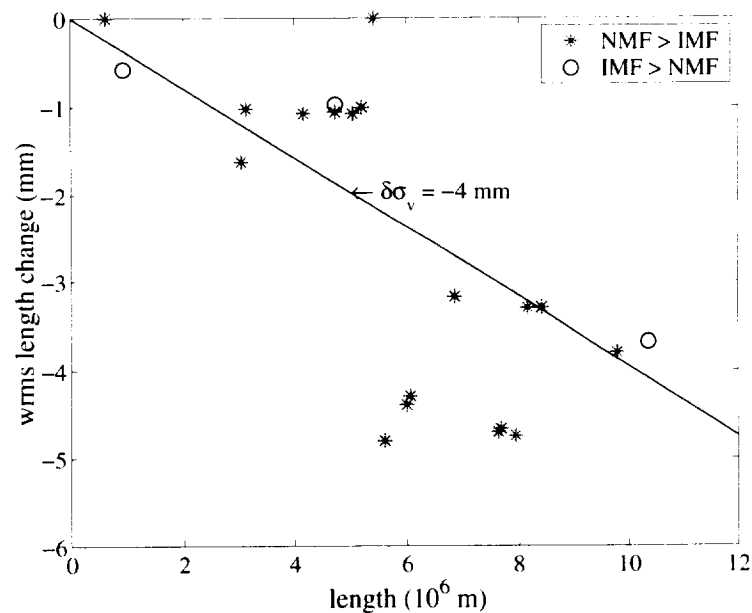


Figure 1. Reduction of baseline length scatter for the CONT94 campaign by using IMF instead of NMF. The line corresponds to removing 4 mm of vertical error at each site.

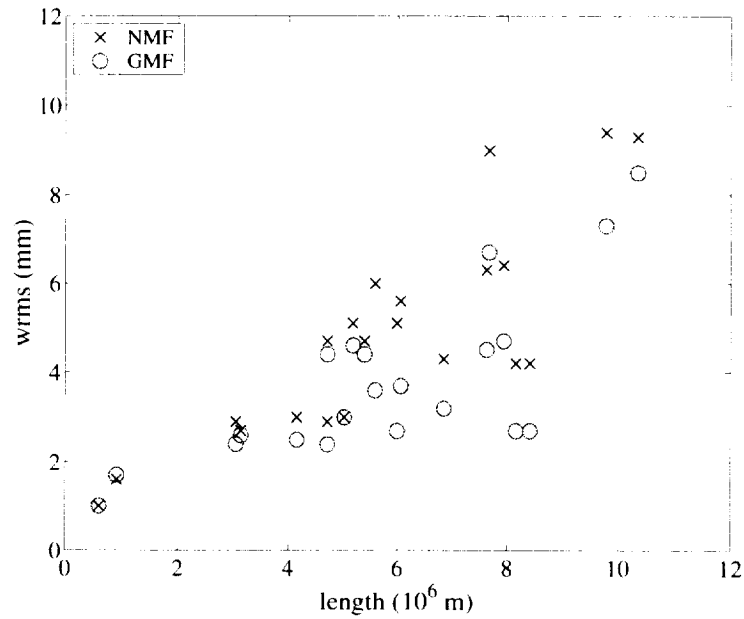


Figure 2. Baseline length repeatability for the CONT94 campaign showing the improvement using an *a priori* hydrostatic gradient and wet gradient mapping function instead of NMF and a hydrostatic gradient mapping function. The minimum elevation is  $5^\circ$ .

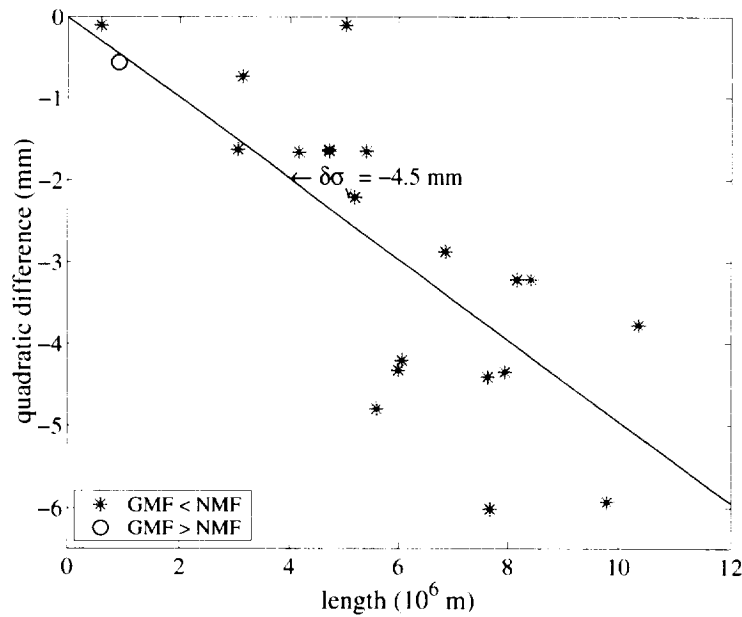


Figure 3. Reduction of baseline length scatter for the CONT94 campaign by using an *a priori* hydrostatic gradient and wet gradient mapping function instead of NMF. The line corresponds to removing 4.5 mm of vertical error at each site.

# Tropospheric Zenith Path Delays Derived from GPS Used for the Determination of VLBI Station Heights

Johannes Boehm, Harald Schuh, Robert Weber

*Institute of Geodesy and Geophysics IGG, University of Technology, Vienna*

*Contact author: Johannes Boehm, e-mail: [jboehm@luna.tuwien.ac.at](mailto:jboehm@luna.tuwien.ac.at)*

## Abstract

The variable tropospheric refraction is a major error source for the estimation of geodetic parameters by GPS and VLBI. As both techniques use microwave signals, tropospheric zenith delays derived by GPS are comparable to those obtained by VLBI. In the investigation presented here, zenith delays which were provided by the IGS (International GPS Service) at 2h time intervals were entered and constrained in the VLBI analyses. This procedure avoids the correlation between station height parameters and zenith delay parameters and reduces the number of unknowns in the VLBI least-squares fits. The formal errors and repeatabilities of several VLBI station heights were compared with results of standard VLBI analyses where no external information about the troposphere had been used. About 100 VLBI NEOS-A experiments in 1999 and 2000 were analyzed. The results show that the repeatability of VLBI station heights has significantly improved (up to 40%) when constraining the GPS zenith delays.

## 1. Introduction

Modeling the tropospheric refraction in VLBI and GPS is usually done by the equation

$$dL(e) = dL_h^z \cdot mf_h(e) + dL_w^z \cdot mf_w(e) \quad (1)$$

$dL(e)$  is the total delay at a certain elevation  $e$ ,  $dL_h^z$  and  $dL_w^z$  are the zenith path delays due to the hydrostatic and wet component of the troposphere, respectively, and  $mf_h$  and  $mf_w$  are the corresponding mapping functions. Correlation matrices of analyses of typical VLBI sessions show that station heights and zenith path delays are correlated by about -0.4. Equation 1 implies that station heights and zenith path delays can only be de-correlated if observations at low elevations are available. In terms of geometry, the determination of station heights is the better the lower elevation angles are used. On the other hand, the accuracy of the mapping function becomes worse for lower elevations. Based on these considerations, the introduction of independent information about the troposphere avoids the correlation between station heights and zenith path delays, and, as a result, the repeatability (scatter around the mean) of VLBI station heights is expected to improve if the external information is sufficiently good. In this project the official IGS (International GPS Service) total zenith path delays (Gendt, 1996 [2]) are introduced as external information into the VLBI analyses. They are provided in weekly files per station at 2h time intervals as a combined series of several solutions submitted by individual IGS Analysis Centers (AC). These ACs apply different analysis strategies (mapping functions, cutoff angles, ..). In most cases the ACs fix the station coordinates to the current ITRF, so that the IGS total zenith path delays are not directly affected by the correlation described above.

## 2. Constraining IGS Total Zenith Path Delays in the VLBI Solutions

About 100 VLBI NEOS-A experiments in 1999 and 2000 were analyzed. In a first step VLBI total zenith path delays were determined by the OCCAM 5.0 software package (Titov et al., 2001 [3]). All station coordinates were fixed to the ITRF2000. As can be seen from figures 1 and 2 top and centre plots, the VLBI and GPS total zenith path delays agree quite well except for an offset that is always negative over the two years (Boehm, 2002, this issue [1]). Thus, one mean offset per station between IGS and VLBI zenith path delays for the total time span (1999 and 2000) was calculated and removed from the IGS series. These corrected path delays, now also taking into account e.g. different estimation strategies or different heights of VLBI telescopes and GPS antennas, were entered and constrained in the VLBI analyses. One height parameter per station of the 24h session was estimated, all horizontal coordinates were fixed to the ITRF2000 and no tropospheric gradients were allowed. The cutoff angle was set to  $10^\circ$  elevation. The formal errors and repeatabilities of the station heights obtained by the approach described above were then compared to those obtained from standard VLBI analyses.

## 3. Results

A considerable improvement of up to 40% can be seen in the repeatability of the station heights of all VLBI stations (see figures 1 and 2, bottom plot, and tables 1 and 2, column 2). For example, the scatter of the individual height components around their mean at Fortaleza has decreased from  $\pm 1.88$  cm to  $\pm 1.48$  cm. There is also a significant decrease of the mean one-sigma formal errors of station heights when constraining external zenith delays from IGS (see tables 1 and 2, column 3). It can be explained by the fact that the correlation between zenith delay and station height parameters does not appear for this approach (because zenith delays are not estimated) and by the smaller number of unknowns in the least-squares fits. On the other hand, it is clear that the root-mean-square values of the residual delays get worse when constraining external information (see tables 1 and 2, column 4).

Table 1. Statistics for station Fortaleza, Brazil, without and with external tropospheric zenith delays from IGS for NEOS-A sessions in 1999 and 2000

<b>Fortaleza</b>	scatter around the mean station height [cm]	mean formal error of station heights [cm]	mean rms of fit [cm]
no external tropospheric zenith delays	1.88	1.43	1.61
with external tropospheric zenith delays	1.48	0.68	1.80

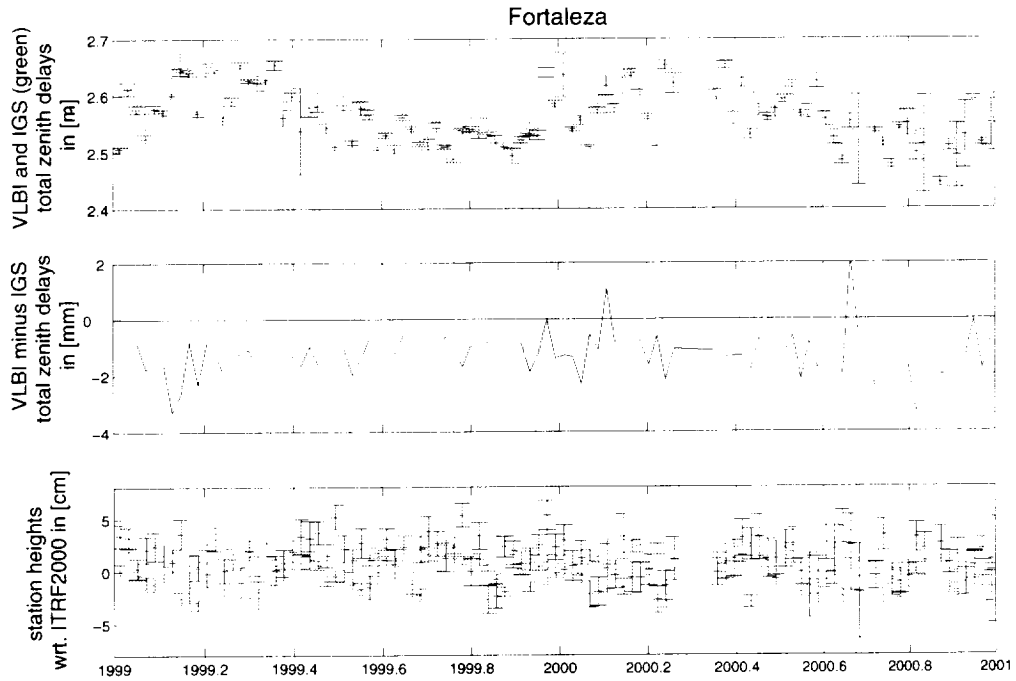


Figure 1. VLBI NEOS-A (blue) and IGS (green) total zenith path delays (top) and differences between the total zenith path delays (centre); station heights with (red) and without (blue) IGS zenith path delays at Fortaleza (bottom)

Table 2. Statistics for station Wettzell, Germany, without and with external information from IGS for NEOS-A sessions in 1999 and 2000

<b>Wettzell</b>	scatter around the mean station height [cm]	mean formal error of station heights [cm]	mean rms of fit [cm]
no external tropospheric zenith delays	1.07	0.93	1.61
with external tropospheric zenith delays	0.66	0.44	1.80

#### 4. Conclusions and Outlook

Once again, the mutual benefits between the different space geodetic techniques could be demonstrated. Introducing GPS total zenith path delays into VLBI analyses improves the repeatability of station heights, because the correlation with zenith path delays is avoided. The offsets between GPS and VLBI total zenith path delays are still an open question (see also Boehm et al., 2002, this issue [1]). They could be due to the systematic influences on the GPS measurements, e.g. by multipath effects or by phase center variations, or due to different elevation cutoff

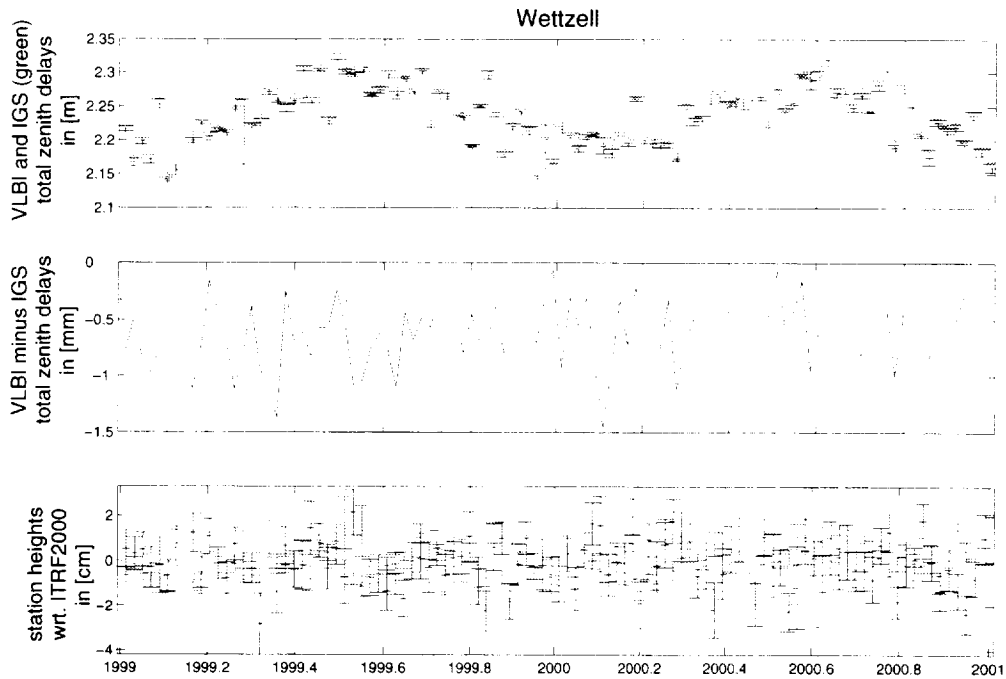


Figure 2. VLBI NEOS-A (blue) and IGS (green) total zenith path delays (top) and differences between the total zenith path delays (centre); station heights with (red) and without (blue) IGS zenith path delays at Wetzell (bottom)

angles. VLBI could support the investigation of these effects. Future investigations should deal with water vapour radiometer data and numerical weather models as means to complement VLBI and GPS analyses.

## References

- [1] Boehm, J., E. Messerer and H. Schuh, Comparison of tropospheric parameters submitted to the 2nd IVS Analysis Pilot Project, in: IVS 2002 General Meeting Proceedings, edited by N. R. Vandenberg and K. D. Baver, NASA/CP-2002-210002, 2002.
- [2] Gendt, G., Comparisons of IGS tropospheric estimates, Proceedings IGS Analysis Center Workshop, 19-21 March 1996 Silver Spring, Maryland USA, Eds. R E Neilan, P A Van Scoy, J F Zumberge, pp. 151-164, 1996.
- [3] Titov, O., V. Tesmer and J. Boehm, OCCAM Version 5.0 software. User Guide. AUSLIG Technical Reports 7, AUSLIG, Canberra, 2001.

## Comparison of Atmospheric Parameters from VLBI, GPS and WVR

Ryuichi Ichikawa<sup>1</sup>, Yasuhiro Koyama<sup>1</sup>, Junichi Nakajima<sup>1</sup>, Mamoru Sekido<sup>1</sup>, Eiji Kawai<sup>1</sup>, Hiroshi Ohkubo<sup>1</sup>, Hiro Ohsaki<sup>1</sup>, Tetsuro Kondo<sup>1</sup>, Jun Amagai<sup>2</sup>, Hitoshi Kiuchi<sup>2</sup>, Taizoh Yoshino<sup>2</sup>, Fujinobu Takahashi<sup>2</sup>, Kazumasa Aonashi<sup>3</sup>, Yoshinori Shoji<sup>3</sup>, Hiromu Seko<sup>3</sup>, Tetsuya Iwabuchi<sup>3</sup>, Ryu Ohtani<sup>4</sup>, Kazuhiro Takashima<sup>5</sup>, Shinobu Kurihara<sup>5</sup>, Yoshihiro Fukuzaki<sup>5</sup>, Yuki Hatanaka<sup>5</sup>

<sup>1)</sup> *Kashima Space Research Center, Communications Research Laboratory*

<sup>2)</sup> *Communications Research Laboratory*

<sup>3)</sup> *Meteorological Research Institute, Japan Meteorological Agency*

<sup>4)</sup> *Geological Survey of Japan, National Institute of Advanced Industrial Science and Technology*

<sup>5)</sup> *Geographical Survey Institute*

Contact author: Ryuichi Ichikawa, e-mail: [richi@crl.go.jp](mailto:richi@crl.go.jp)

### Abstract

The comparison of atmospheric parameters (equivalent zenith wet delay and linear horizontal delay gradients) derived from VLBI, GPS, and WVR has been carried out to reveal the limitation of the anisotropic mapping functions. The horizontal delay gradient components from all these techniques at Kashima and Shintotsugawa are not consistent with each other while the agreement for the zenith wet delay estimates are significant. Moreover, we perform a numerical simulation of the atmospheric parameters using a non-hydrostatic numerical weather model to assess the utility of the anisotropic model.

### 1. Introduction

Radio signal delay associated with the neutral atmosphere is one of the major error sources for space-based geodetic techniques such as the Global Positioning System (GPS) and Very Long Baseline Interferometry (VLBI). The comparison of atmospheric parameters (equivalent zenith wet delay and linear horizontal delay gradients) derived from VLBI, GPS, and WVR has been carried out to reveal the limitation of the anisotropic mapping functions. We are also evaluating those parameters by comparing with the ray-traced slant path delay through the two days data sets of the non-hydrostatic numerical weather prediction model with 1.5 km horizontal resolution. We describe our preliminary findings based on these comparisons.

### 2. Observations and Data Analysis

We carried out WVR observations nearby VLBI and GPS stations of the Kashima Space Research Center from June 1998 to October 2001 with several periods of interruption. Kashima station was one of the Key Stone Project (KSP) geodetic network. In addition another WVR observation was carried out at one VLBI station (Shintotsugawa) of Geographical Survey Institute (GSI). These stations are shown in Figure 1. For these observations, we use the Radiometrics<sup>TM</sup> WVR1100, which has an optional azimuth driver to point to any sky direction.

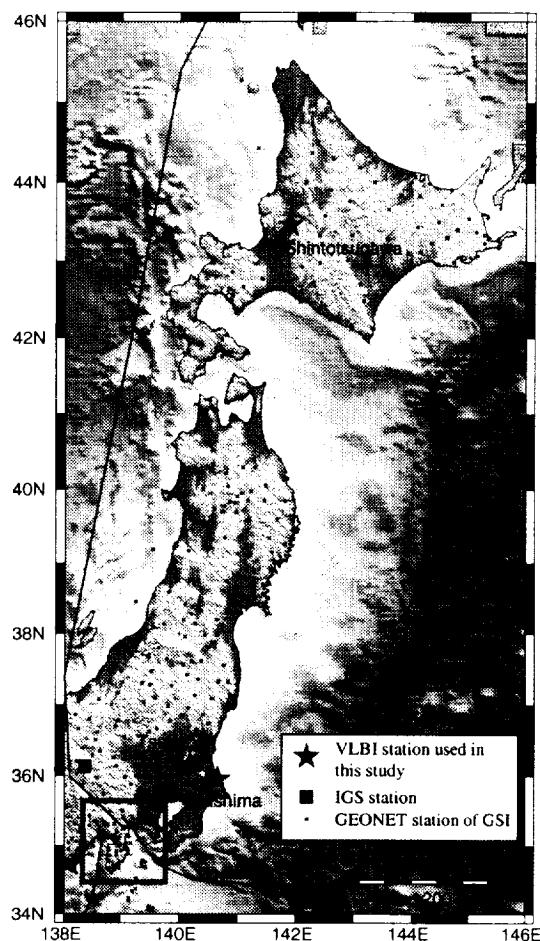


Figure 1. Map showing VLBI stations for the comparison of atmospheric parameters

We analyze atmospheric parameters obtained from all these techniques. The WVR-based gradient vector was estimated as a piecewise linear function with three-hour intervals by fitting the observed slant delays to the Chen and Herring gradient model [2]. The VLBI data were analyzed using the CALC/SOLVE software package [3], applying the Niell mapping functions [5] and the gradient model. The GPS data were analyzed using the Bernese software package [1] applying the same mapping functions as included in SOLVE.

We are also evaluating those parameters by comparing with the ray-traced slant path delay through the non-hydrostatic numerical weather prediction model (NHM) with 1.5 km horizontal resolution. This NHM provides temperature, humidity and geopotential height at the geosurface and at 38 surfaces of constant pressure (which vary between 1000 and 10 hPa), for each node in a 1.5 km by 1.5 km grid that covers the Izu Peninsula region which is indicated by a gray square as shown in Figure 1.

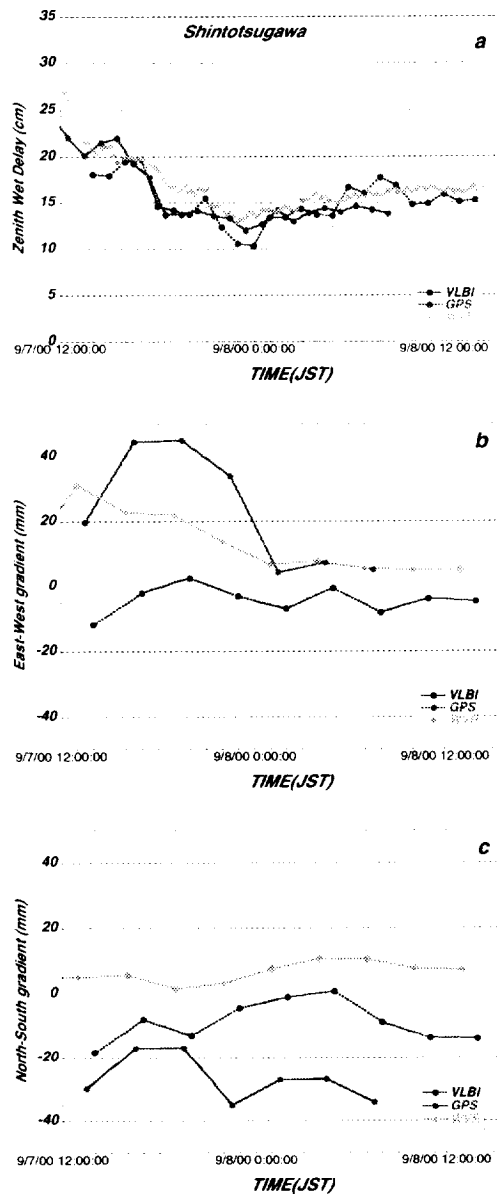


Figure 2. Time series of atmospheric parameters at Shintotsugawa: a), the zenith wet delays, b), the east delay gradients, c) the north delay gradients.

### 3. Results

#### 3.1. WVR Observations

We find estimated weighted RMS differences below the 10-millimeter level and correlation coefficients more than 0.8 for the zenith wet delays derived from GPS and WVR in Kashima. However, RMS differences between the zenith wet delays derived from VLBI and those from WVR

are more than 50 millimeters. In addition, the agreement for the estimated horizontal delay gradients from these three techniques is less clear. The discrepancy between the VLBI results and other techniques is caused by the difficulty to estimate the vertical position, the clock offset and tropospheric parameters independently due to the relatively short baselines (about 150 km at maximum) of the KSP network. The comparison at Kashima is described in more detail in Ichikawa et al.(2001) [4].

We performed other WVR observations at Kashima and Shintotsugawa in order to investigate atmospheric parameters for the longer baseline. The baseline length between them is about 850 km. Figure 2 shows the time series of the atmospheric delay parameters using WVR at Shintotsugawa. The zenith wet delays (ZWD) obtained by WVR are well consistent with the those estimated from VLBI from 1200JST of 7 September to 1400JST 8 September 2000 as shown in Figure 2(a). GPS-derived ZWDs are also consistent with the other measurements as shown in the same figure. Unfortunately, we could not observe ZWD using WVR at Kashima because it was raining in Kashima at that period.

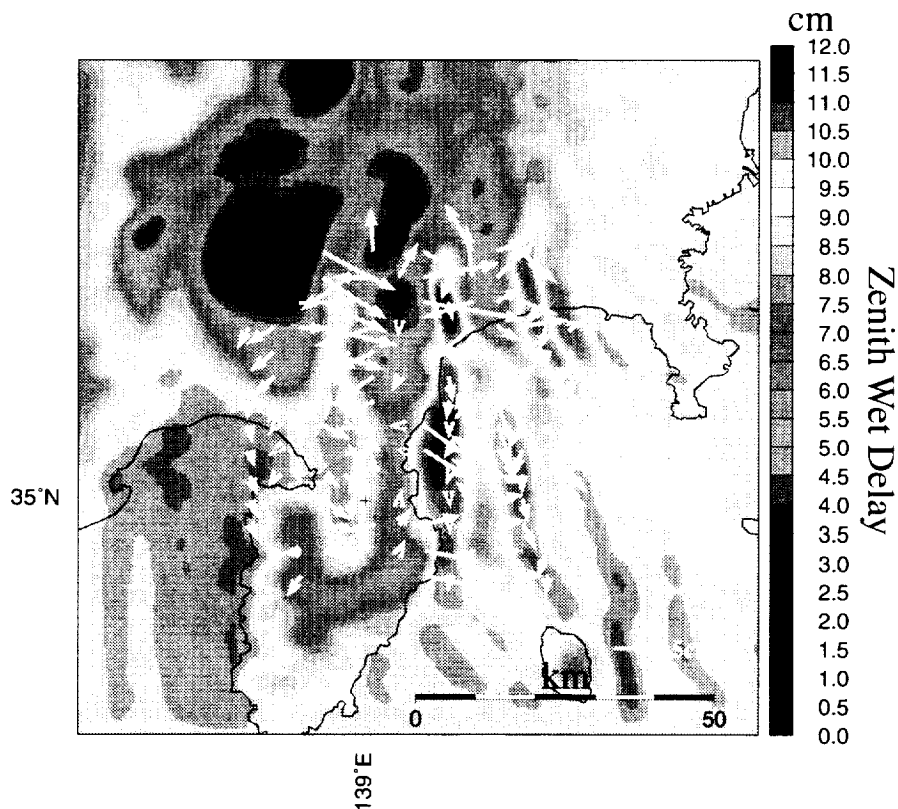


Figure 3. Zenith wet delay retrieved by the 1.5 km NHM at the 1200UT of March 7, 1997. Arrows indicate gradient vectors estimated by the best-fit anisotropic model to the ray-traced pointed delays through the 1.5 km model.

In the Figure 2 we show the estimates of the EW (b) and NS (c) gradient components. The agreement of the results for the gradient components is still less clear as same as the result from KSP network [4]. The WVR results indicate a positive contribution while the VLBI results tend

to a negative contribution for both east and north components. However, both time series have a similar pattern. The GPS results present quite different pattern from other results obtained by WVR and VLBI. This cannot be explained by the contamination of the hydrostatic delay gradient which is not sensed by the WVR. It might be caused by the multipath effect of the GPS and/or WVR observations since we use an elevation cut-off angle of 10 degrees which is chosen in the VLBI observation strategy. Further investigations and recomparisons based on the different analysis strategy are necessary.

### 3.2. Numerical Simulation Using NHM

We calculate the slant delay using ray-tracing technique through the one day data set of the 1.5 km NHM at 1200 UT March 7, 1997. At each station we traced about 100 rays to the station with roughly uniform density (count per unit solid angle) on the upper hemisphere, so as to approximate a sampling geometry similar to both GPS and VLBI. The ZWD field in Izu peninsula is illustrated in Figure 3 as an example. This figure demonstrates the significant ZWD gradient in the east of the peninsula. The sharp gradient is caused by a mountain wave. We also represent the gradient vectors retrieved from the best fit anisotropic model to the ray-traced delays in the same figure. Maximum gradient vectors are plotted in the high ZWD region. In addition the directions of the vectors in this region represent complex distribution corresponding with the local variability of the ZWD distribution. In order to assess the slant delay estimations and the utility of the anisotropic model we will perform a statistical analysis.

### References

- [1] Rothacher M., G. Beutler, E. Brockmann, S. Fankhauser, W. Gurtner, J. Johnson, L. Mervart, S. Schaer, T. A. Springer, R. Weber, The Bernese GPS Software Version 4.0, Astronomical Institute, University of Berne, Switzerland, 1996.
- [2] Chen, G. and T. A. Herring, "Effects of atmospheric azimuthal asymmetry on the analysis of space geodetic data", *J. Geophys. Res.*, 102, 20489-20502, 1997.
- [3] C. Ma, J. W. Ryan and D. S. Caprette, NASA Space Geodesy Program-GSFC Data Analysis-1993, VLBI Geodetic Results 1979-92, NASA TM-104605, Goddard Space Flight Center, 1994.
- [4] Ichikawa, R., Ohkubo H., Koyama Y., and Kondo T., An Evaluation of Atmospheric Gradient using Water vapor Radiometers in Kashima, Japan, *J. Comm. Res. Lab.*, 48, pp. 97-103, 2001.
- [5] Niell, A.: Global mapping functions for the atmosphere delay at radio wavelength, *J. Geophys. Res.*, 101(B2), 3227-3246, 1996.

# A Discussion on the Modeling of the Residual Clock Behavior and Atmosphere Effects in the Astrometric and Geodetic VLBI Data Analysis

*Jinling Li, Bo Zhang, Guangli Wang*

*Shanghai Astronomical Observatory*

*Contact author: Jinling Li, e-mail: jll@center.shao.ac.cn*

## Abstract

We checked the dependence of the estimation of scientific interest parameters on the choice of the time span of each piece in the continuous piecewise linear modeling of the residual clock behavior and atmosphere effects by single analysis of 27 randomly selected VLBI sessions in which Shanghai station (Seshan25) participated. Results show that (1) different choices of the time span of each piece lead to differences in the estimation of station coordinates up to *centimeters* and in the weighted root mean squares (*wrms*) of the delay residuals up to dozens of *picoseconds*; (2) since the conditions of clock and atmosphere are different from session to session and from site to site, the reasonable range of the time span of each piece should be tested and chosen for each session as well as for each site, which is really arduous work in routine data analysis.

We also checked the performance of this modeling by simulated data tests. By using the User Partial function of CALC/SOLVE we compared the delay residuals from the continuous piecewise linear modeling of the residual clock behavior with that from the periodic modeling.

## 1. Introduction

The clock behavior and the atmosphere effects are those of the principle errors in the astrometric and geodetic VLBI data analysis. A suitable modeling of these effects is accordingly important to the improvement in precision of estimations of scientific interest parameters such as site and source positions. While the ionosphere effects are computed from the differences in delay at two frequencies, the troposphere effects are relatively complicated and are usually modeled as the product of the surface meteorology dependent zenith delay and the observation elevation dependent mapping function [1]. There are residual atmosphere delays at each site and which exhibit as short-term variations. The modeling of the timing system also permits short, random clock variations while placing realistic physical constraints on the continuity and rates of change. The clock model is firstly a polynomial with parameters for offsets in clock epoch and rate and for frequency drift. Similar to the residual atmosphere effects there are residual short-term clock variations. Ma et al. [2] modeled these residual variations in clock behavior and atmosphere effects by continuous piecewise linear functions realized in CALC/SOLVE, Goddard's analysis software for astrometric and geodetic data. The estimated parameters are the initial residual zenith path delay and its rate of change in each linear section, the residual clock rates in each section with zero value at the first observation epoch. These parameters are considered as nuisance parameters to accommodate the residual variations and so are helpful to improve the estimation precision of scientific interest parameters.

We checked the dependence of the estimation of scientific interest parameters on the choice of the time span of each piece in the continuous piecewise linear modeling of the residual clock

behavior and atmosphere effects by single analysis of 27 randomly selected VLBI sessions related to Shanghai station (Seshan25). We also checked the performance of this modeling by simulated data tests. By using the User Partial function of CALC/SOLVE we compared the delay residuals from this modeling of the residual clock behavior with that by periodic modeling.

## 2. Data and Software

Seshan25 began to participate in regular astrometric and geodetic VLBI experiments from April of 1988. As of April of 2001 about 90 sessions are accumulated and the number of sessions each year is shown in Fig.1. From these sessions 27 are randomly selected and the single analysis of these sessions are performed by using CALC (9.12) and SOLVE (released on June 5 of 2000). The 1996 conventions of the International Earth Rotation Service [3] and the New Mapping Function [4] are adopted. The cut-off elevation angle is  $7^\circ$  and the type of data is group delay.

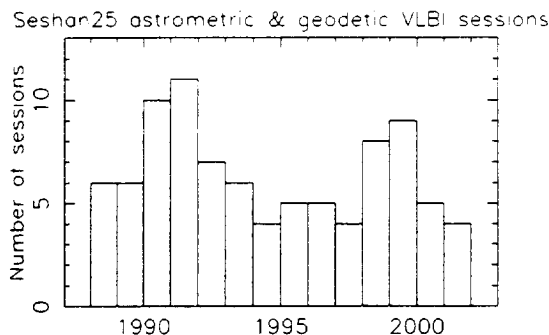


**Fig.1.** The distribution of the astrometric and geodetic VLBI sessions involving SESHAN25 during 1988 to 2001

## 3. Analysis and Discussion

We tested the performance of the continuous piecewise linear modeling of the residual clock behavior and atmosphere effects by setting the time span of each piece as  $391 - 4i$  (min,  $i = 1, \dots, 97$ ). The calculation stops when the observation equation becomes singular. When we check the modeling of the clock behavior the time span of each piece for the modeling of the atmosphere effects is 20 min. When we check the modeling of the atmosphere effects that for clock behavior is 60 min. We extracted from the results of the single analysis the delay residual *wrms*, the adjustment and its formal error ( $\sigma_x$ ) of the *x*-component of site coordinates in order to survey the effects of the (time span) length of each piece on the parameter estimation.

Take the session on July 29 of 1988 (\$98JUL29XA) as an example. Fig.2 and Fig.3 show respectively the distribution of the *x*-component adjustment, its formal error and the delay residual *wrms* versus the length of each piece in the modeling of the residual clock behavior and the atmosphere effects. Fig.4 shows the *x*-component adjustments of SESHAN25 in all the selected 27 sessions versus the piece length in the modeling of the clock behavior. Fig.5 is for the modeling of the atmosphere effects. The situations for *y* and *z*-components are similar to that for *x*. From these figures the following can be deduced. (1) Different choices of the piece length leave significant differences in the adjustments of coordinates and in the delay residual *wrms* up to *centimeters* and dozens of *picoseconds* respectively. (2) When the piece length is relatively short, the distribution of the adjustment of coordinates and the delay residual *wrms* are scattering, while as the piece length increasing the distribution exhibit some fluctuation. (3) The effects of different piece lengths on the adjustment of coordinates are different from session to session as well as from site to site and up to *centimeters* in difference. (4) Generally speaking, the parameter estimations are stable with relatively short piece lengths. But the length cannot be too short in order to provide enough

degrees of freedom. With the piece length for atmosphere effects at 20 min it is preferable to set the piece length between 20 min to 100 min for the clock behavior (refer to Fig.4). With the clock at 60 min it is preferable to set between 10 min to 40 min for the atmosphere (refer to Fig.5). However, even if these settings are chosen the coordinate adjustments in some sessions are fluctuated by several *centimeters*.

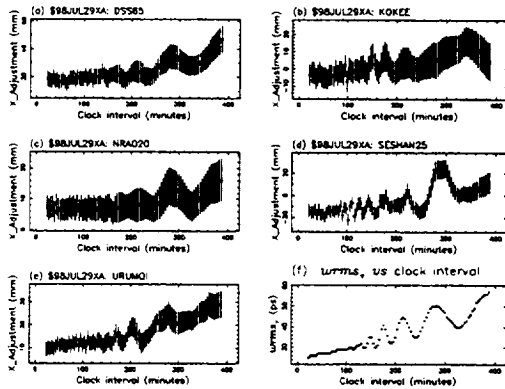


**Fig.2.** The distributions of the adjustment and formal error of *x*-component versus the piece length in the modeling of clock

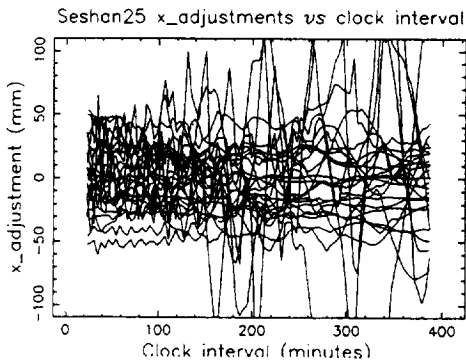


**Fig.4.** The adjustments of *x*-component of SESHAN25 versus the piece length in the modeling of clock for all the analyzed 27 sessions

With the continuous piecewise linear modeling of the residual clock behavior and atmosphere effects it is good to choose the suitable piece length for each session as well as for each site. This is arduous work and accordingly it is necessary to test other modeling ways.

#### 4. Simulated Data Tests

Let the simulated data be in the form  $\sum_i A_i \sin(2\pi t_j/T_i + \phi_i) + N(0, \sigma_n)$ , where  $i = 1, \dots, n$  denotes the sequence number of the periodic terms,  $t_j$  is the observation epoch,  $N(0, \sigma_n)$  is white noise with zero value mean and standard deviation  $\sigma_n$ . Here we take the periods in hours as 0.5, 1.0, 4.0, 5.0, 12.0 and 24.0, the corresponding amplitudes (in any default units) as 22.0, 20.0, 90.0, 999.0, 50.0 and 50.0, the phases in degrees as 10.0, 13.0, 34.0, 80.0, 80.0 and  $-80.0$  and  $\sigma_n$  as

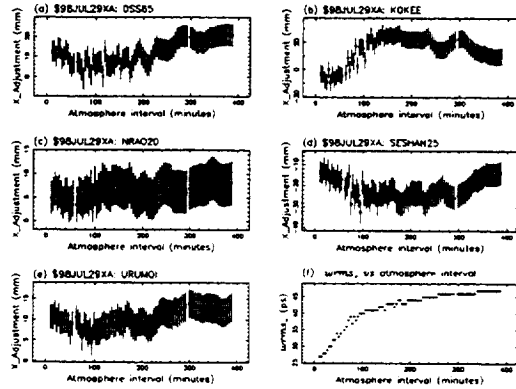


**Fig.3.** The distributions of the adjustment and formal error of *x*-component and the delay residual *wrms* versus the piece length in the modeling of atmosphere

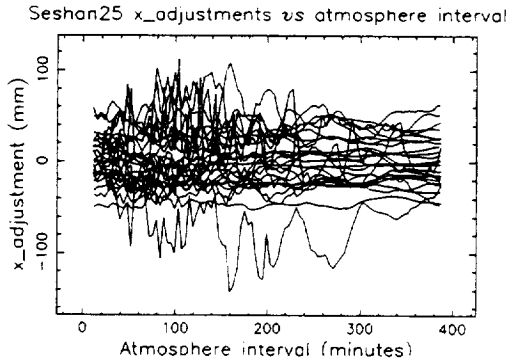


**Fig.5.** The adjustments of *x*-component of SESHAN25 versus the piece length in the modeling of atmosphere for all the analyzed 27 sessions

1999.0. The simulated data are generated with 90 s sampling interval and with the assumed first and last observation epoch at 0 h and 24 h.

Set the piece length in the continuous piecewise linear modeling in the form  $5.0 + 5.0k$  (min,  $k = 1, 2, \dots$ ). Fig.6 shows the simulated data (points) and their modeling with piece length as 20 min (short broken line) and 300 min (long broken line). It is clear that the short pieces can track the data better than the long pieces. Fig.7 shows the distribution of the residual *wrms* versus the piece length. When the pieces are very short the residual *wrms* (about 2000) is on the same level of  $\sigma_n$  (1999.0), which indicates that the periodic variations in the simulated data are well modeled. As the piece length increasing the *wrms* increases rapidly and exhibits some fluctuation around the standard deviation of the simulated data (note that within a whole period the standard deviation of a periodic signal is  $A/\sqrt{2}$ ,  $A$  is the amplitude), which indicates that the simulated data are not properly modeled. In conclusion, the piece length in the continuous piecewise linear modeling cannot be arbitrarily chosen. There should be some reasonable range and it should be determined by real case based on observation analysis.

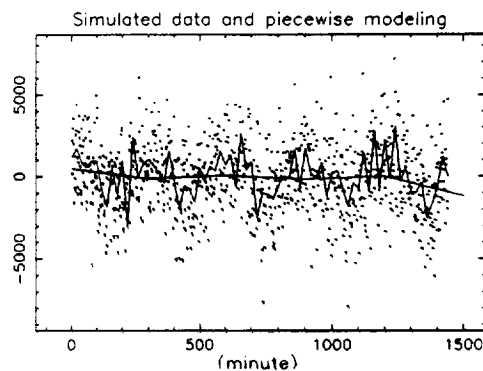


**Fig.6.** Simulated data and the continuous piecewise linear modeling

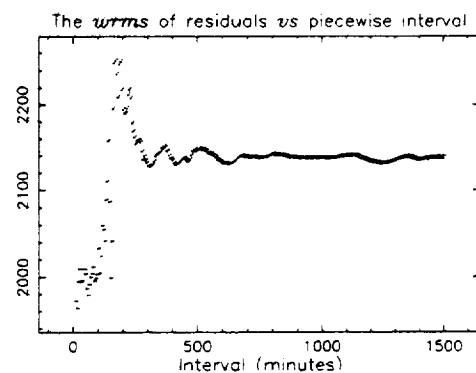


**Fig.7.** The residual *wrms* of the simulated data versus the piece length

Set the periods in hours of the periodic modeling as 0.5, 1.0, 2.0, 3.0, 4.0, 5.0, 6.0, 8.0, 12.0 and 24.0. Through a least squares fitting of the above mentioned simulated data the residual *wrms* is found to be 1981.9, which is very near to the standard deviation of the white noise and which demonstrates a good modeling of the simulated data. By comparing the situation with short piece length in the continuous piecewise linear modeling, the periodic modeling can track the variation of the data with rather small numbers of parameters.

We also tested the periodic modeling by using simulated broad frequency band noise as shown in Fig.8 (dots). The periodic and continuous piecewise linear modeling of the simulated noise are shown in Fig.8, Fig.9 and Fig.10. It is shown that the periodic function tracks the variation of data well.

## 5. Real Data Tests

By applying the User Partial function in CALC/SOLVE, we performed single analysis of the 90 sessions in Fig.1. Fig.11 shows the delay residual *wrms* from the periodic and from the piecewise modeling of the residual clock behavior. It is shown that the periodic modeling can reduce the delay residual *wrms* by 2 ps to 10 ps compared with that of the piecewise modeling.

## 6. Concluding Remarks

From the above analysis it is deduced that the choice of the piece length in the continuous piecewise linear modeling of the residual clock behavior and atmosphere effects leaves effects on the estimation of scientific interest parameters for instance up to *centimeters* in coordinates and up to several *picoseconds* in delay residual *wrms*. This effect can be different from session to session as well as from site to site. It is accordingly necessary to determine the suitable piece length in real data analysis. Simulated data tests and real data analysis show that the periodic modeling is preferable in modeling the residual short-term variations.

Our work is still in its preliminary stage. We will perform full tests of the periodic modeling of residual clock behavior and realize the periodic modeling of the residual atmosphere effects in data analysis software.

**Acknowledgements** This work is partly supported by the Chinese national projects (G1998040703, No.970231003), Chinese National Natural Science Foundation Committee (No.19833030, No.10173019), Chinese Academy of Sciences (No.KJ951-1-304), Science and Technology Foundation of Shanghai City (No.JC14012).

## References

- [1] Sovers, O. J. et al., 1998. Astrometry and geodesy with radio interferometry: experiments, models, results. *Review of Modern Physics*, 70: 1393-1454.
- [2] Ma, C., J. M. Sauber, L. J. Bell, T. A. Clark et al., 1990. Measurement of horizontal motions in Alaska using Very Long Baseline Interferometry. *J. Geophys. Res.*, 95: 21991-22011.
- [3] McCarthy, D. D., 1996. IERS Conventions (1996), IERS Technical Note 21, Observatoire de Paris, 1996.
- [4] Niell, A. E., 1996. Global mapping functions for the atmospheric delay of radio wavelengths. *J. Geophys. Res.*, 101: 3227-3246.

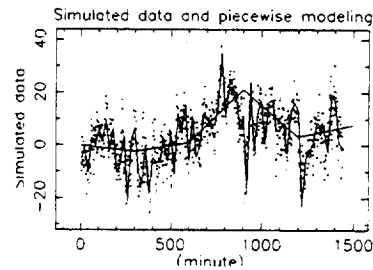


**Fig.8.** Simulated broad frequency band data and the piecewise modeling

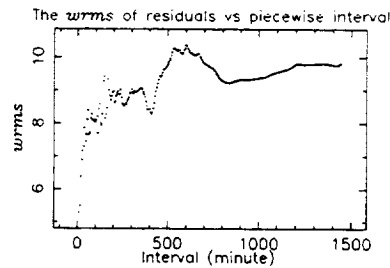


**Fig.9.** The residual *wrms* of the simulated broad frequency band data versus the piece length

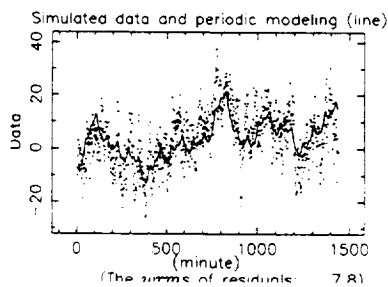


**Fig.10.** The periodic modeling of the simulated broad frequency band data

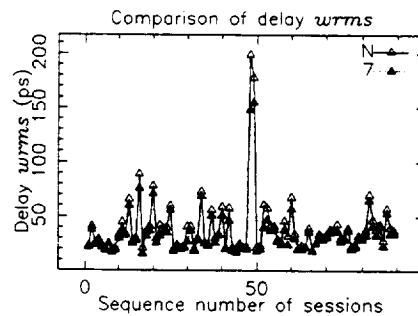


**Fig.11.** Comparison of the delay residual *wrms* from periodic ("7") and piecewise ("N") modeling of the residual clock behavior

# Modeling Radio Source Structure for Improved VLBI Data Analysis

Patrick Charlot

Observatoire de Bordeaux CNRS/UMR 5804

e-mail: charlot@observ.u-bordeaux.fr

## Abstract

At the milliarcsecond scale, most of the extragalactic radio sources exhibit spatially extended intrinsic structures which are variable in both time and frequency. Such radio structures may introduce sizeable effects in the VLBI measurements which must be corrected for improved VLBI data analysis. Modeling these effects requires identification of a truly kinematically stable morphological feature for each source and calculation of structure corrections for the VLBI delays based on images of the source brightness distribution. This paper presents the model for calculating source structure corrections, discusses the magnitude of these corrections, and reviews the results obtained so far, with emphasis on a detailed study of the structural effects caused by the source 2200+420 in the framework of the massive analysis reported by Sovers et al. in these proceedings.

## 1. Introduction

Current limitation of VLBI data analysis is caused predominantly by troposphere and instrumental errors, but also at some level by the extended brightness distribution of the observed radio sources, which are only imperfect fiducial points in the sky at the milliarcsecond (mas) scale [1, 2, 3]. Such radio structures give rise to structural VLBI delays which vary with the length and orientation of the VLBI baselines relative to the source brightness distribution, causing extra “noise” for the more extended sources. Temporal evolution of these structures may also result in apparent source position variations when observations are made at several epochs [4].

While structural effects may be considered as an intrinsic limitation of the extragalactic radio reference frame, it is worthwhile to try modeling them to further improve the accuracy of the celestial frame and reduce VLBI analysis errors. This requires that a true kinematically-stable feature be identified within each extended source, to serve as the source reference direction. The theoretical basis for such modeling is presented in Section 2, followed by comments about the selection of the source reference direction (Section 3). The magnitude of source structure effects is discussed in Section 4, with emphasis on the definition of the structure index, an indicator of the source quality. Finally, in Section 5, we review the results obtained so far when modeling structural delays in actual data, including a detailed report about recent work on the source 2200+420.

## 2. Theoretical Modeling

The complex visibility  $V$  of a spatially-extended source measured by an interferometer with baseline  $\mathbf{b}$  is given by

$$V(\mathbf{b}, \omega, t) = \int_{\Omega_s} I(\mathbf{s}, \omega, t) \exp\left(-\frac{i\omega}{c} \mathbf{b} \cdot \mathbf{s}\right) d\Omega, \quad (1)$$

where  $I(\mathbf{s}, \omega, t)$  is the source brightness distribution which depends on the direction  $\mathbf{s}$  on the sky, the frequency  $\omega = 2\pi c/\lambda$ , and time  $t$ , while the integration is over the extended source of solid angle  $\Omega_s$ . If we adopt a reference direction  $\mathbf{s}_0$  within the source,  $\mathbf{s}$  can be written as  $\mathbf{s} = \mathbf{s}_0 + \boldsymbol{\sigma}$ , where  $\boldsymbol{\sigma}$  is in the plane of the sky. The visibility function then can be written as

$$V(\mathbf{b}, \omega, t) = \exp\left(-\frac{i\omega}{c} \mathbf{b} \cdot \mathbf{s}_0\right) \int_{\Omega_s} I(\mathbf{s}_0 + \boldsymbol{\sigma}, \omega, t) \exp\left(-\frac{i\omega}{c} \mathbf{b} \cdot \boldsymbol{\sigma}\right) d\Omega, \quad (2)$$

which also can be written as

$$\begin{aligned} V &= A \exp[i(\phi_g + \phi_s)], \\ &= A \exp(i\phi_t), \end{aligned} \quad (3)$$

where the total phase  $\phi_t$  is the sum of the geometric phase for the reference direction  $\mathbf{s}_0$ ,

$$\phi_g = -\frac{\omega}{c} \mathbf{b} \cdot \mathbf{s}_0, \quad (4)$$

and the additional structure phase introduced by the source brightness distribution,

$$\phi_s = \arg \left[ \int_{\Omega_s} I(\mathbf{s}_0 + \boldsymbol{\sigma}, \omega, t) \exp\left(-\frac{i\omega}{c} \mathbf{b} \cdot \boldsymbol{\sigma}\right) d\Omega \right]. \quad (5)$$

The amplitude  $A$  observed by the interferometer is given by

$$A = \left| \int_{\Omega_s} I(\mathbf{s}_0 + \boldsymbol{\sigma}, \omega, t) \exp\left(-\frac{i\omega}{c} \mathbf{b} \cdot \boldsymbol{\sigma}\right) d\Omega \right|. \quad (6)$$

The VLBI delay observable used in astrometry is defined by the partial derivative of the total phase with respect to frequency. For an extended source, the delay can be written as

$$\begin{aligned} \tau &= \frac{\partial \phi_t}{\partial \omega} = \frac{\partial \phi_g}{\partial \omega} + \frac{\partial \phi_s}{\partial \omega}, \\ &= -\frac{1}{c} \mathbf{b} \cdot \mathbf{s}_0 + \tau_s, \end{aligned} \quad (7)$$

where the first term is the geometric delay corresponding to the reference direction  $\mathbf{s}_0$ , and the second term  $\tau_s$  is the additional delay introduced by the extended brightness distribution. Thus, the absolute source position determined in VLBI astrometry is the position of the adopted reference direction  $\mathbf{s}_0$  if delay structure corrections are modeled in this way. In practice, the delay structure corrections  $\tau_s$  are determined as the slope of a straight line fitted to the individual structure phases calculated for each frequency channel used during the observations, in order to match precisely the scheme used to build the bandwidth synthesis delay observable at the correlator (see [5]). The effect introduced by the extended source brightness distribution in the phase-delay rate, defined by the partial derivative of the total phase with respect to time, is obtained in a similar way, and must also be accounted for in a complete astrometric analysis. The interested reader is referred to [5] for a more thorough discussion of the phase-delay rate observable.

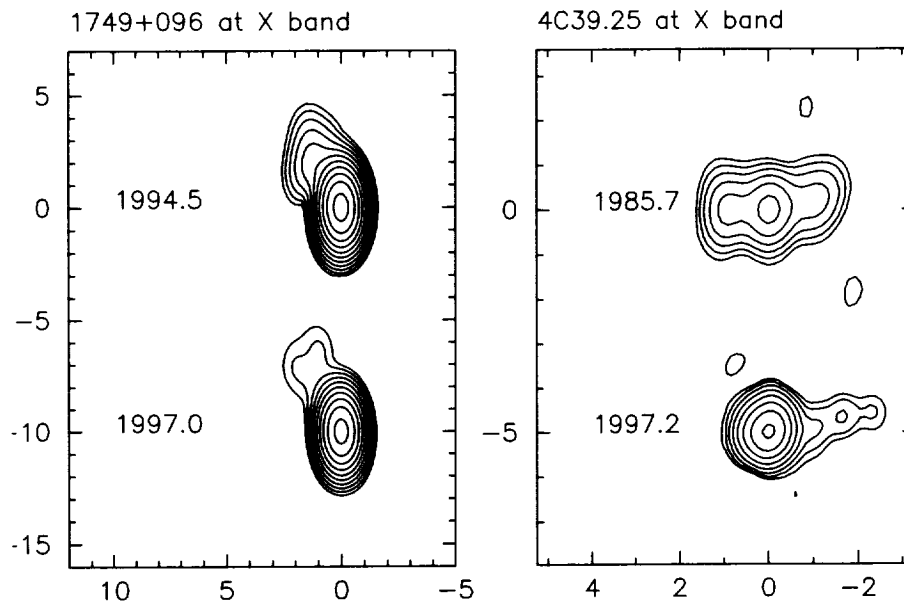


Figure 1. X-band VLBI maps at two epochs for the core-dominated source 1749+096 [1, 3] and the complex source 0923+392 (4C 39.25) [7]. The two maps in each panel are aligned vertically according to their peak brightness. The scale is in milliarcseconds.

In the case of dual-frequency S/X observations, the combined S/X structure correction is derived by combining the individual X- and S-band structure corrections with the same scale factors as those used to derive the dual-frequency-calibrated delay from the X- and S-band delay measurements. These factors are approximately 1.08 for the X-band delay and 0.08 for the S-band delay. The S-band structure corrections are therefore scaled by a factor of  $0.08/1.08 \sim 1/13$  relatively to the X-band corrections, which limits their overall impact in the combined S/X corrections. Such a combination implies indeed that the same reference direction is selected for the X and S bands.

### 3. Choice of the Reference Direction

Calculation of source structure corrections requires the choice of a reference direction  $\mathbf{s}_0$  within the source brightness distribution. As discussed previously, this reference direction is equivalent to the absolute position of the source in the extragalactic reference frame. An appropriate choice of the reference direction is critical for the source position stability since the absolute positions of the source brightness distributions are unknown with respect to the celestial frame. For sources with time-variable structure, it is important that this reference direction be set to a truly kinematically-stable morphological feature well identified over time. The identification of such a feature, however, is sometimes hard, for example in the case of core-jet sources with blended core and jet components, or for sources which change morphology over time.

Figure 1 illustrates the question of the reference direction for two different sources, 1749+096 and 0923+392 (4C 39.25). In the case of 1749+096, the peak brightness is a reasonable choice for the reference direction, as the brightness distribution is core-dominated and has evolved little between the two epochs. On the other hand, 0923+392 shows a totally different morphology at the

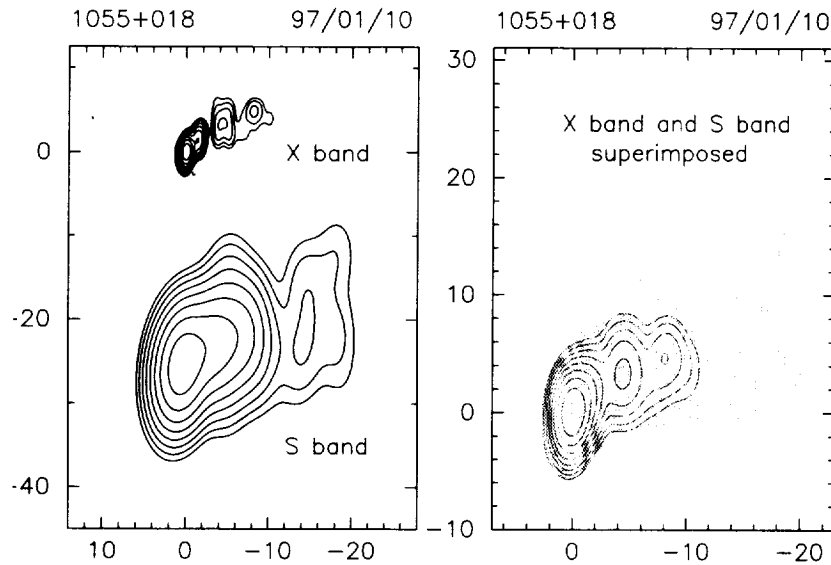


Figure 2. X- and S-band VLBI maps of the source 1055+018 [3]. The scale is in milliarcseconds. *Left:* Images convolved with a different beam at each frequency, reflecting the corresponding interferometer resolution. *Right:* Tentative superimposition of the two maps after convolution with the same beam (the S-band map, in blue/light grey was superresolved by a factor of 1.9, whereas the X-band map, in red/dark grey was underresolved by the same factor).

first epoch (triple structure) and at the second epoch (single component with a weak extension), making the cross-identification of the components largely impossible without information about the structure evolution at intermediate epochs. For this source, it turns out that the strongest component seen at the second epoch corresponds to the eastern (left-hand side) component of the earlier map [6, 7]. Registration of the two maps based on the peak brightness, as proposed in Fig. 1, is therefore not correct and would lead to inconsistent coordinates between the two epochs.

The calculation of dual-frequency S/X structure corrections similarly requires correct registration of the X- and S-band maps. This may even be harder than time registration, due to the difference in resolution, and because source structure is often significantly different at the two frequencies. Figure 2 illustrates such difficulty for the source 1055+018. On the left-hand side, the X- and S-band maps are plotted at the same scale, each convolved with a beam reflecting the intrinsic frequency-dependent interferometer resolution, while on the right-hand side, they are superimposed after convolution with an identical beam. It is evident from this figure that the peaks of the three detected components cannot be superimposed at once, as a consequence, most probably, of opacity variations within the structure. This makes registration errors inescapable, but fortunately these are attenuated in actual data analysis, as they are reduced by a factor of 13, like the S-band structure corrections, when deriving the combined S/X structure corrections (see Section 2).

The examples discussed above show that modeling radio source structure has two basic requirements: (i) regular VLBI monitoring to track source structure evolution, and (ii) a careful examination of each map to identify the proper reference direction for each source. The influence of the choice of the reference direction on actual VLBI results will be discussed further in Section 5.

#### 4. Magnitude of Source Structure Effects

The theoretical modeling developed in Section 2 shows that source structure corrections depend on the exact form of the spatial brightness distribution of the extended radio source  $I(\mathbf{s}, \omega, t)$  relative to the geometry of the VLBI baseline vector  $\mathbf{b}$  projected onto the plane of the sky (see Equations (5) and (7)). The overall source structure effect magnitude for a given source is then most easily estimated by calculating these corrections for a range of  $u, v$  coordinates (the coordinates  $u$  and  $v$  are the coordinates of the baseline vector  $\mathbf{b}$  projected onto the plane of the sky and are expressed in units of the observing wavelength). Along this direction, we defined a source “structure index” according to the median value of the structure delay corrections,  $\tau_{\text{median}}$ , calculated for all projected VLBI baselines that could be possibly observed with Earth-based VLBI (i.e. for all baselines with  $\sqrt{u^2 + v^2}$  less than the diameter of the Earth), separating the sources into four classes as follows:

$$\text{Structure Index} = \begin{cases} 1, & \text{if } 0 \text{ ps} \leq \tau_{\text{median}} < 3 \text{ ps}, \\ 2, & \text{if } 3 \text{ ps} \leq \tau_{\text{median}} < 10 \text{ ps}, \\ 3, & \text{if } 10 \text{ ps} \leq \tau_{\text{median}} < 30 \text{ ps}, \\ 4, & \text{if } 30 \text{ ps} \leq \tau_{\text{median}} < \infty. \end{cases} \quad [2]$$

Based on this definition, two structure indices are obtained for each source, one at X-band and one at S-band, each of which provides an indication of the source structure effect magnitude at the corresponding frequency band. For consistency with the procedure used to derive the dual-frequency structure corrections (see above), the structure corrections are scaled by 1.08 at X-band and by 0.08 at S-band, prior to the structure index assignment.

Shown in Fig. 3 are contour plots of the radio emission at X-band of four sources (0138–097, 0108+388, 0544+273 and 2201+315) representative of each structure index class. The corresponding structure-effect maps showing the magnitude of the corrections to the VLBI delay observable as a function of the interferometer resolution are also represented along with indication of the mean, rms, median and maximum values of these structure corrections. Figure 3 reflects the increase of the magnitude of the structure effects as the brightness distribution becomes more extended. For 0108+388, these effects are very large because the source structure is composed of two components of approximately equal strength, causing very low visibility regions in the  $u$ - $v$  plane and thus large structure corrections (see [5] for a detailed study of the case of a two-component model).

Figure 4 shows the overall structure index distribution at X- and S- bands for the 392 sources of the International Celestial Reference Frame (ICRF) [4] that have currently available structure indices. At X-band, it is shown that approximately 60% of the sources in this sample have a structure index of either 1 or 2, an indication of compact or very compact structures, while the remaining 40% of the sources with a structure index of either 3 or 4 have more extended emission structures. At S-band, source structure effects appear to be less significant, as reflected by the large number of sources with a S-band structure index of either 1 or 2 in Fig. 4 (about 90% of the sources). This is an indirect indication that the contribution of the S-band structure to the dual-frequency-calibrated delay is usually smaller as compared to the X-band structure contribution, a consequence of the fact that the S-band structure corrections have been scaled by a factor of 0.08.

In all, it is recommended that only sources with a structure index of either 1 or 2 be used for the most precise astrometric or geodetic work [2, 3]. Sources with a structure index of 3 should only be used with caution while those with a structure index of 4 should not be used at all.

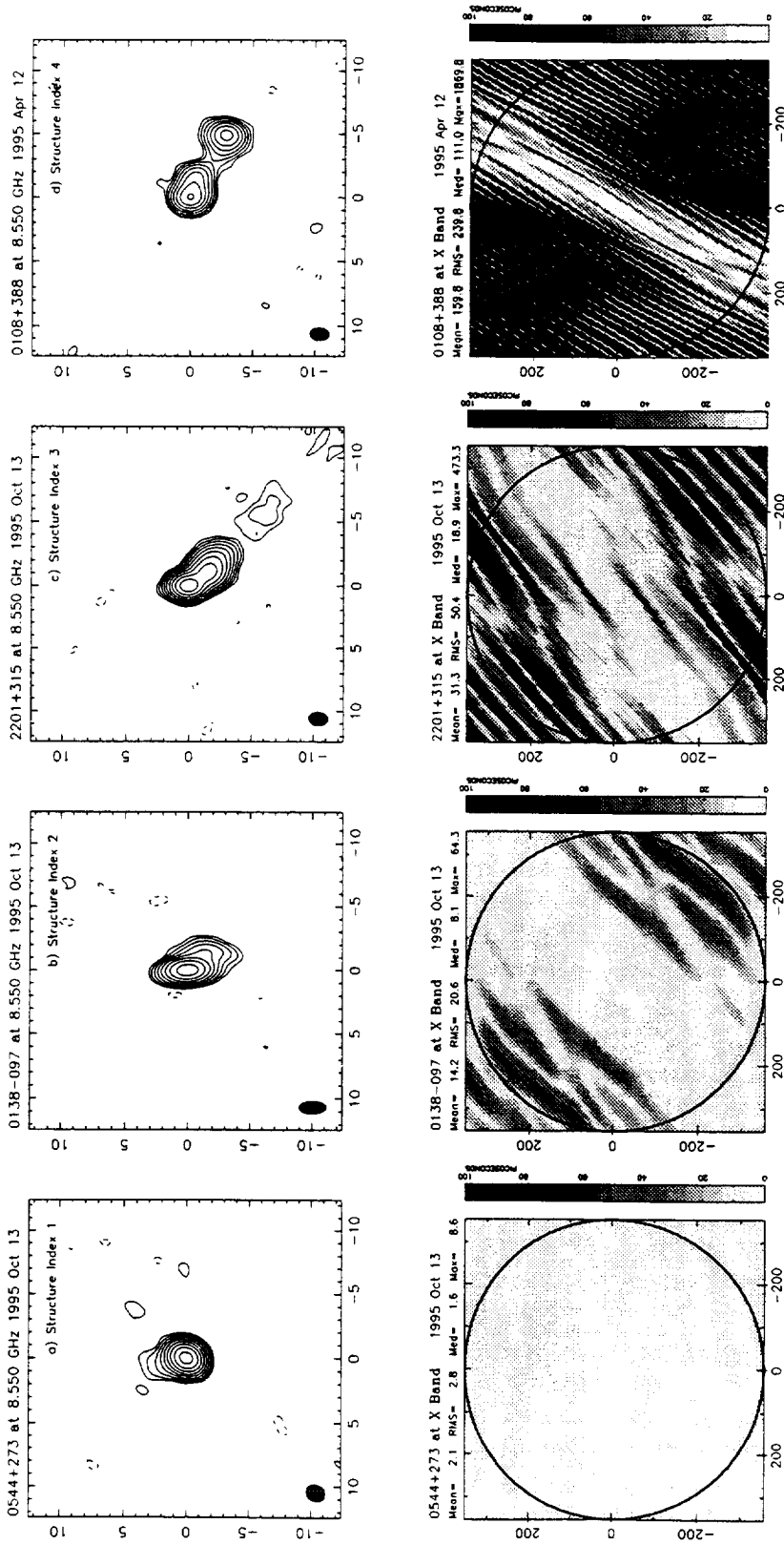


Figure 3. *Top*: Contour plots of the radio emission at X-band for the four sources a) 0544+273, b) 0138-097, c) 2201+315 and d) 0108+388, representative of each structure index class. The X-band structure index of these sources is indicated in each panel. *Bottom*: Gray-scale plots showing the magnitude of the structural delays (absolute value) induced by the extended radio emission at X-band for the same four sources. The structural delay is plotted as a function of the length and orientation of the VLB baseline projected onto the sky, expressed in millions of wavelengths ( $u, v$  coordinates). The gray scale is identical in each panel and ranges from 0 to 100 picoseconds (ps). All structure corrections larger than 100 ps are plotted as black. The circle drawn in these plots has a radius equal to one Earth diameter, corresponding to the longest baselines that can be theoretically observed with Earth-based VLB. The mean, rms, median and maximum values of the structure corrections for all baselines contained within this circle are indicated in each panel.

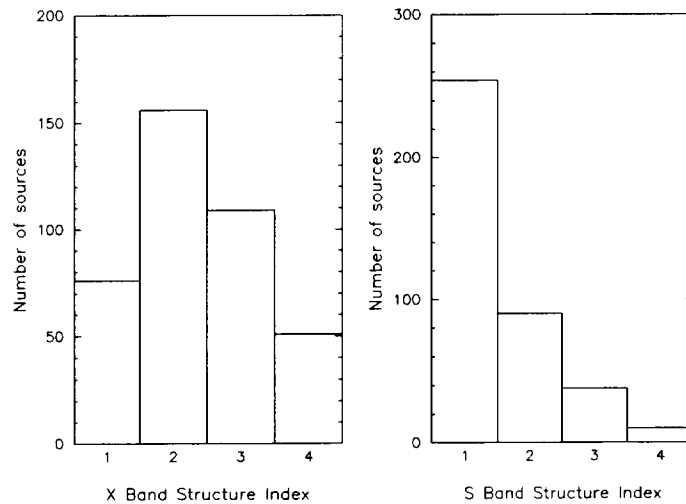


Figure 4. Distribution of the X- and S-band structure indices for 392 ICRF sources.

## 5. Modeling Structure Delays in Actual VLBI Observations

While the structure index is useful for planning experiments and estimating the extra noise caused by source structure in existing data, the ultimate goal is indeed to directly apply structure corrections to actual observations. A first step in this direction was made by using data from the mid-80s on the extended core-jet source 3C273 (1223+026), intensively observed in geodetic experiments at that time. The results of this initial study, based on two years of data, showed that modeling structure effects significantly improves the positional stability of 3C273 and reduces the rms delay residuals [8]. More recently, a similar analysis was carried out for the source 4C39.25 (0923+392) using a longer data span (12 years of observations) [7]. This source has been known for its peculiar systematic long term proper motion in right ascension with an average value of  $\sim 0.06$  mas/yr [9]. After incorporating source structure modeling, this proper motion was found to largely vanish, confirming that it is not real, but caused by source structure evolution [7].

Just recently, such exploratory studies have been extended to a much larger scale with a data set consisting of the first 10 RDV sessions, including 160 sources observed over up to all 10 epochs and a total of  $\sim 200,000$  observations [10]. This massive analysis made use of 800 maps from the Radio Reference Frame Image Data Base of the US Naval Observatory [11] produced from the same 10 RDV experiments. Overall, the weighted rms delay residuals ( $\sim 30$  ps) were found to decrease by 8 ps in quadrature upon introducing source maps to model the structure delays, with improvements as large as 40 ps for some sources with extended or fast-varying structures. Scatter of “arc positions” about a time-linear model were also found to decrease substantially for most sources. While a complete description of this analysis and overall statistical results are given in [10], we report here further details of our results for the source 2200+420.

The source 2200+420 was selected for this study because its data were found to be significantly affected by structural effects, thus providing a good case to test our software and illustrate specific questions like the impact of the choice of the reference direction on the results. Figure 5 shows the 10 successive X- and S-band VLBI maps of 2200+420 used in our analysis. At X-band, the source consists of two major components, whose relative position and strength apparently change

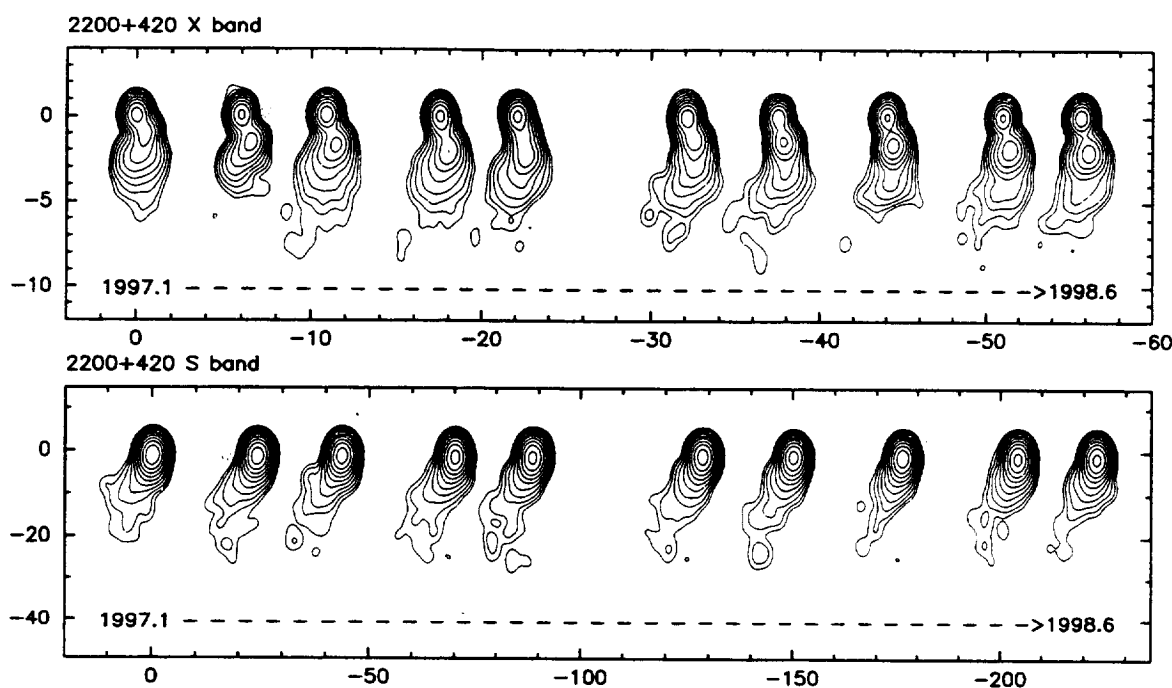


Figure 5. VLBI images of 2200+420 at X band (top) and S band (bottom) for 10 successive epochs, spanning the period 1997.1–1998.6, as available from [11]. The maps are aligned horizontally according to the northern structural component and are spaced linearly according to their observing epochs. The scale is in milliarcseconds.

over time. The northern component is generally stronger, except for the maps at epochs 7 and 8. At S-band, the source structure is similar, but the two major components are blended due to the weaker resolution at this frequency.

We have conducted four successive astrometric analyses estimating “arc positions” of 2200+420, one of which (solution **a**) did not incorporate structural delay modeling, while the three others (solutions **b**, **c** and **d**) had structural delays modeled via the source maps in Fig. 5. The difference between solutions **b**, **c** and **d** lies in the choice of the reference direction, which was either set on the peak brightness (solution **b**) or the brightness centroid (solution **c**) using an automatic procedure, or chosen *manually* after a careful examination of each map aimed at locating the most-likely stable fiducial feature within the source extended structure (solution **d**). This led us to select the northern map component (at both X- and S-bands) for the latter, under the assumption that this feature constitutes the source core.

The results of these four “arc positions” astrometric analyses are plotted in Fig. 6. Without structural delay modeling (solution **a**), the rms position scatter is 0.0080 mas for right ascension and 0.41 mas for declination. The larger scatter in declination is due mostly to the estimated positions at epochs 7 and 8, which are off by 0.5 to 1 mas from the other estimated positions. When modeling structure delays, source position scatter is either substantially worse (solution **b**) or largely improved with quasi-perfect correction of the shifts for epochs 7 and 8 (solutions **c** and **d**), indicating that these are really an effect of extended structure. Degraded scatter in solution **b** obviously originates in inconsistent choice of the reference direction, fixed to the southern

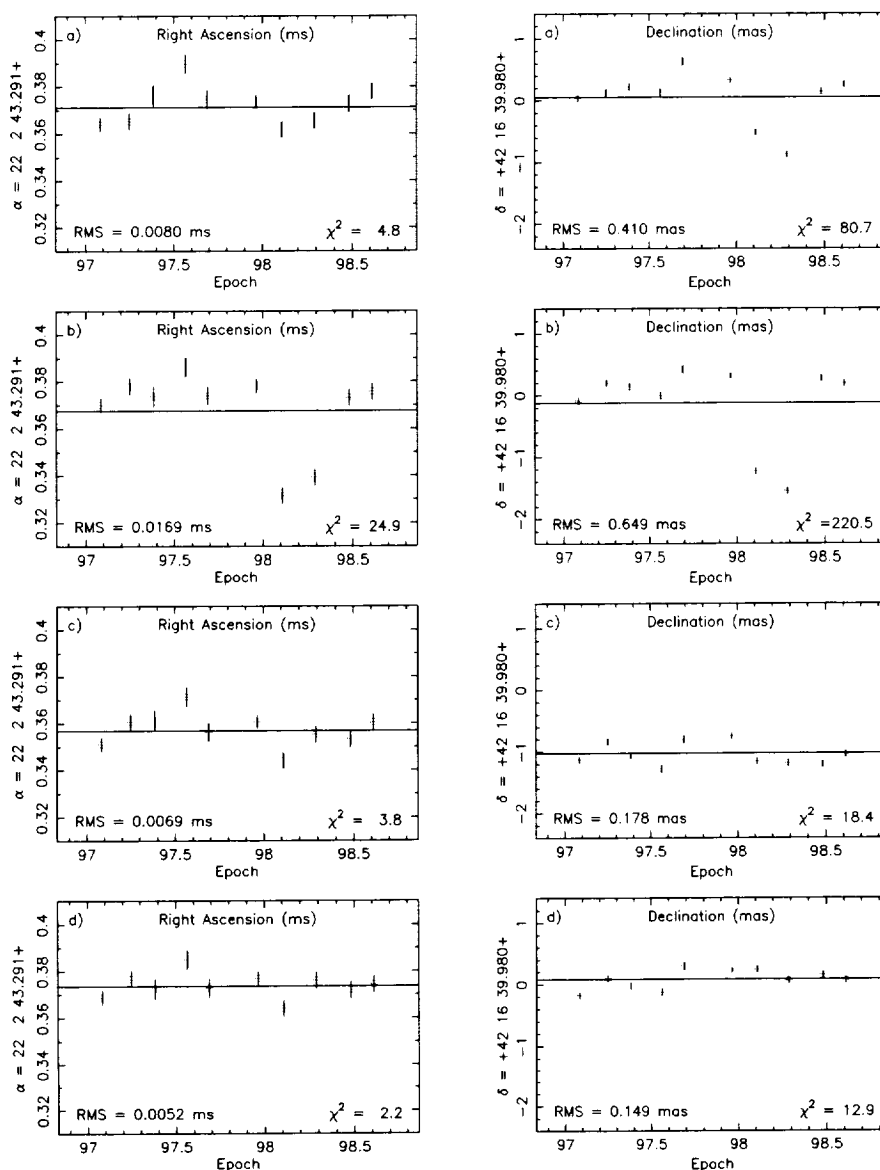


Figure 6. Estimated right ascension and declination of 2200+420 for 10 successive epochs, spanning the period 1997.1–1998.6. Source structure is modeled using the VLBI maps from Fig. 5 with the following specifications: a) no modeling, b) map peak as reference direction, c) brightness centroid as reference direction, d) northern structure component as reference direction.

structure component at epochs 7 and 8 and to the northern component at all other epochs, as a result of the peak brightness “blind” selection. Overall, the smallest position scatter is obtained for solution **d** when selecting the northern structural component as the source reference direction. In this case, scatter is reduced from 0.0080 to 0.0052 ms in right ascension and from 0.41 to 0.15 mas in declination (along with large decrease in  $\chi^2$  per degree of freedom values) upon modeling structural delays (Fig. 6), thus indicating that such modeling really improves the source position stability.

## 6. Conclusion

The analyses carried out so far to evaluate the magnitude of the source structure effects, based on the modeling described in Section 2, indicate that these effects are significant. Structural delays range from a few picoseconds for the most compact sources to several hundreds of picoseconds for the very extended sources. In this connection, the structure index defined in [2, 3] is a useful indicator to evaluate the source quality. About 60% of the ICRF sources evaluated in this way are found to have structure indices of either 1 or 2, making them suitable for high-precision astrometry.

Additionally, it has now been demonstrated that massive application of structure maps to correct for structural delays is possible and improves VLBI analysis, predominantly for sources with extended structures [10]. The specific case of 2200+420 discussed in Section 5 shows that identification of a true fiducial feature within each extended source is crucial to properly and accurately model structural delays, as otherwise the results may be worse than with no structure corrections. Future plans should especially focus on such identification so that analyses incorporating massive source structure modeling like that described in [10] can be further improved.

## References

- [1] Fey, A. L., Clegg, A. W., Fomalont, E. B., 1996, VLBA Observations of Radio Reference Frame Sources, *ApJS*, 105, 299–330.
- [2] Fey, A. L., Charlot, P., 1997, VLBA Observations of Radio Reference Frame Sources. II. Astrometric Suitability Based on Observed Structure, *ApJS*, 111, 95–142.
- [3] Fey, A. L., Charlot, P., 2000, VLBA Observations of Radio Reference Frame Sources. III. Astrometric Suitability of an Additional 225 Sources, *ApJS*, 128, 17–83.
- [4] Ma, C., Arias, E. F., Eubanks, T. M., Fey, A. L., Gontier, A.-M., Jacobs, C. S., Sovers, O. J., Archinal, B. A., Charlot, P., 1998, The International Celestial Reference Frame as Realized by Very Long Baseline Interferometry, *AJ*, 116, 516–546.
- [5] Charlot, P., 1990, Radio-Source Structure in Astrometric and Geodetic Very Long Baseline Interferometry, *AJ*, 99, 1309–1326.
- [6] Guirado, J. C., Marcaide, J. M., Alberdi, A., Elósegui, P., Ratner, M. I., Shapiro, I. I., Kilger, R., Mantovani, F., Venturi, T., Rius, A., Ros, E., Trigilio, C., Whitney, A. R., 1995, Proper Motion of Components in 4C 39.25, *AJ*, 110, 2586–2596.
- [7] Charlot, P., 2000, Models for Source Structure Corrections, in *Proceedings of IAU Colloquium 180, Towards Models and Constants for Sub-microarcsecond Astrometry*, Eds. K. J. Johnston, D. D. McCarthy, B. J. Luzum and G. H. Kaplan, U. S. Naval Observatory, Washington, D. C., p. 29–39.
- [8] Charlot, P., 1994, Evidence for Source Structure Effects Caused by the Quasar 3C273 in Geodetic VLBI Data, in *VLBI Technology – Progress and Future Observational Possibilities*, Eds. T. Sasao, S. Manabe, O. Kameya, and M. Inoue, Tokyo: Terra Scientific Publishing Company, p. 287–294.
- [9] Fey, A. L., Eubanks, T. M., Kingham, K. A., 1997, The Proper Motion of 4C 39.25, *AJ*, 114, 2284–2291.
- [10] Sovers, O. J., Charlot, P., Fey, A. L., Gordon, D., 2002, Structure Corrections in Modeling VLBI Delays for RDV data, these proceedings.
- [11] Fey, A. L., Boboltz, D., Gaume, R., Kingham, K. A., 2002, USNO Analysis Center for Source Structure Report, International VLBI Service for Geodesy and Astrometry 2001 Annual Report, Eds. N. R. Vandenberg and K. D. Baver, NASA/TP-2002-210001 (in press).

## Structure Corrections in Modeling VLBI Delays for RDV Data

Ojars J. Sovers<sup>1</sup>, Patrick Charlot<sup>2</sup>, Alan L. Fey<sup>3</sup>, David Gordon<sup>4</sup>

<sup>1)</sup> *RSA Systems/Jet Propulsion Laboratory*

<sup>2)</sup> *Observatoire de Bordeaux – CNRS/UMR 5804*

<sup>3)</sup> *U.S. Naval Observatory*

<sup>4)</sup> *Raytheon ITSS/NASA Goddard Space Flight Center*

Contact author: Ojars J. Sovers, e-mail: [ojars@rsasys.com](mailto:ojars@rsasys.com)

### Abstract

Since 1997, bimonthly S- and X-band observing sessions have been carried out employing the VLBA and as many as 10 additional antennas. Maps of the extended structures have been generated for the 160 sources observed in ten of these experiments ( $\approx 200,000$  observations) taking place during 1997 and 1998. This paper reports the results of the first massive application of such structure maps to correct the modeled VLBI delay in astrometric data analysis. For high-accuracy celestial reference frame work, proper choice of a reference point within each extended source is crucial. Here the reference point is taken at the point of maximum emitted flux. Overall, the weighted delay residuals ( $\approx 30$  ps) are reduced by 8 ps in quadrature upon introducing source maps to model the structure delays of the sources. Residuals of some sources with extended or fast-varying structures improve by as much as 40 ps. Scatter of “arc positions” about a time-linear model decreases substantially for most sources. Based on our results, it is also concluded that source structure is presently not the dominant error source in astrometric/geodetic VLBI.

### 1. Introduction

With the exception of some exploratory studies (*e.g.* [3]), analyses of VLBI data during the past 25 years have assumed that the compact extragalactic radio-emitting objects observed in geodetic and astrometric experiments are point sources. It has been known for some time [5] that most, and probably all, such sources have internal structures at the milliarcsecond level. Extended structures, when viewed from various baselines at varying times, can give rise to VLBI delay contributions of tens or even hundreds of picoseconds [6]. Since the current accuracy of the celestial reference frame (ICRF) is  $\approx 250 \mu\text{as}$  ( $\approx 20$  ps on a typical baseline) [7], correcting for these source structure contributions should be of some importance.

At this point in the development of the VLBI technique, when formal precisions have reached the  $10 \mu\text{as}$  level, it is important to assess the level at which source structure contributes to systematic mismodeling of the observables. Potential benefits of doing so include possible improvement of the ICRF accuracy, as well as a better characterization of the VLBI “error budget”. If source maps could be routinely introduced into analyses of astrometric experiments, it would be a start on the road to determining truly fiducial points in the sky.

### 2. Experimental Data and Analyses

Since 1997 GSFC, USNO, and NRAO have carried out bimonthly dual-frequency (S- and X-band) VLBI experiments employing the Very Long Baseline Array (VLBA). The observing sites

in these “RDV” experiments include all 10 VLBA antennas plus other stations in North America, Europe, Asia, and the Pacific. The first ten of these experiments (1997 Jan. to 1998 Aug.) were chosen for this study. They comprise 206,744 observation pairs (delay + delay rate) of 160 extragalactic radio sources. Mapping the source structures was done with the methods of [6]. The resulting data base of 800 pairs of maps serves as the basis for modeling structure corrections from the CLEAN components of the maps.

All subsequent analysis was done with the JPL software Modest [9]. The *a priori* terrestrial and celestial frames were ITRF 2000 and ICRF Ext.1, respectively [1] [7]. Source structure contributions to the observables were modeled following the work of Charlot [2]. OJ 287 served as the right ascension reference. Station clock parameters were estimated every 6 hours, zenith wet tropospheric delays every hour, and (E, N) tropospheric gradients daily. Earth orientation (UTPM and two nutation angles) were also estimated for every experiment, as well as station antenna axis offsets for each station. Observable weighting included additional elevation-dependent noise, whose scaling factor was adjusted for each baseline in each experiment in order to make  $\chi^2$  per degree of freedom  $\approx 1$ . Depending on the fit (see below), 6 to 7000 parameters were estimated from the observables.

Source structure effects were evaluated employing two sets of alternate approaches: on one hand, treating source coordinates as either universal or session-specific parameters, and on the other hand, omitting or applying delay and delay rate structure corrections to the modeled observables. In the session-specific case a new source position was estimated for each source in each experiment (with the exception of the adopted RA reference source). Only 47 of the 160 sources are observed in all 10 experiments, but these data comprise approximately 70% of the total observations in the data base. Comparison of the scatter of source positions of these 47 sources permits evaluation of the impact of source structure correction during the 1.5-year data span.

A crucial choice in correcting for source structure effects is the adoption of a reference point for each source. This is by no means trivial, and in fact may be more difficult than the process of generating the structure maps. Ideally, this fiducial point should be the center of the driving engine. As components are ejected and observed, the centroid or peak of the observed radio flux can vary substantially both with time and with frequency. Detailed studies of sequences of maps are required to try to approximate the true fiducial point within each extended source. For the experiments considered here, such studies are only in their initial stages [4]. In the present analyses the reference point of each source was taken at the maximum of the observed flux at each of the two frequencies (X- and S-bands).

### 3. Results

A broad-brush characterization of the results of fits to the ten RDV experiments includes overall weighted delay and delay rate residuals on the order of 30 ps and 90 fs/s. Formal uncertainties of source coordinates and other angular parameters (UTPM, nutation angles) are in the range of several tens of microarcseconds. Corresponding uncertainties of station coordinates and the antenna axis offsets are in the 1 mm range.

For the purposes of the present paper, two aspects of the VLBI parameter estimation are singled out. First, examination of the delay residuals should indicate whether modeling structural delays via source maps improves the overall fit between experiment and theory. Second, comparison of the variation of source coordinates from experiment to experiment with/without applied structure

corrections should show whether the structure delay corrections are indeed removing systematic errors introduced by variations in the appearance of the sources during 1997–98. These two aspects of the analysis are discussed in turn in the two following sections.

### 3.1. Delay Residuals

When source structure is not modeled, the weighted root-mean-square (WRMS) delay residuals for the 206,744 observations are 31.17 picoseconds with a single estimated position of each source, and 30.67 ps if a new set of source coordinates is estimated for each of the ten experiments. The RSS difference of these values (5.6 ps) may partly arise from source structural variations with time, and indicates the possible approximate scale of this effect during the 1.5-year data span.

Modeling additional structural delays by employing source maps reduces the above WRMS delay residuals to 30.17 and 29.75 ps, respectively. This indicates that accounting for the extended and time-varying appearance of each source improves the VLBI model by  $\approx 8$  ps (3 mm) in quadrature. The origin of this improvement can be probed more deeply by examining the behavior of weighted delay residuals for groups of sources. One relatively simple way of grouping them is by means of the “structure index” SI introduced in [6]. This integer ranges from 1 to 4 and increasing values indicate increasing average structural VLBI delay corrections. (A given source may have differing values of the structure index at S- and X-band, SSI and XSI respectively).

The improvement in delay residuals is defined as  $\Delta D$

$$(\Delta D)^2 = \sum_{i=1}^{N_{obs}} w_i (D_{i,uncor}^2 - D_{i,str}^2) / \sum_{i=1}^{N_{obs}} w_i, \quad (1)$$

where the summation extends over the  $N_{obs}$  observations  $i$  weighted by  $w_i$ , and  $D_{i,(uncor,str)}$  is the delay residual in a fit in which the source structure is respectively (uncorrected, corrected). Table 1 shows the weighted delay residual improvement for the four classes of structure index in both frequency bands. These results are from the “arc position” fits. Residual improvement

Table 1. Delay Residual Improvement (ps) *vs.* X- and S-band Structure Indices

XSI	$N_{obs}$	$\Delta D$	SSI	$N_{obs}$	$\Delta D$
1	76862	6.5	1	164151	6.4
2	76903	4.2	2	23483	8.2
3	32746	11.7	3	6912	13.8
4	8035	16.8	4	0	...

increases with increasing complexity of the source structure, with the biggest impact of structure modeling being evident for structure indices of 3 and 4.

### 3.2. Source Coordinates

In order to examine the impact of structure modeling on aspects of the fit other than the residuals, it is also prudent to examine the behavior of some of the estimated parameters. The logical choices for initial study are the source right ascension ( $\alpha$ ) and declination ( $\delta$ ). By analogy

with the delay residuals discussed in the previous section, measures of improvement can be defined for source coordinate scatter in an arc-position solution. Time-linear least squares fits were done for the ten pairs of source coordinates of each of the 47 sources that were observed in all 10 experiments. “Improvement” then means that the time variation of source coordinates is more stable when source structure is modeled. The definitions of scatter improvement are

$$(\Delta\alpha)^2 = \sum_{i=1}^{10} w_{\alpha_i} \left[ (\alpha_{i,uncor} - \bar{\alpha}_{i,uncor})^2 - (\alpha_{i,str} - \bar{\alpha}_{i,str})^2 \right] / \sum_{i=1}^{10} w_{\alpha_i} \quad (2)$$

$$(\Delta\delta)^2 = \sum_{i=1}^{10} w_{\delta_i} \left[ (\delta_{i,uncor} - \bar{\delta}_{i,uncor})^2 - (\delta_{i,str} - \bar{\delta}_{i,str})^2 \right] / \sum_{i=1}^{10} w_{\delta_i} \quad (3)$$

for right ascension and declination, respectively. Here the barred quantities represent the coordinates calculated from linear least-squares fits of the time dependence of the coordinates of each source,  $w_{(\alpha,\delta)_i}$  are weights, and as before, the subscripts (*uncor*, *str*) stand for coordinates from fits (uncorrected, corrected) for structure delay. Plus and minus signs of  $\Delta\alpha$  and  $\Delta\delta$  denote improvement and worsening, respectively (in the latter case, *e.g.*,  $\Delta\alpha^2$  is negative, and the metric  $\Delta\alpha$  is calculated as  $\Delta\alpha = -\sqrt{|\Delta\alpha^2|}$ ).

The average source coordinate scatter improvement values  $\langle\Delta\alpha\rangle$ ,  $\langle\Delta\delta\rangle$  are  $(-3, 24)$   $\mu\text{as}$  for the 47 sources if the averages are weighted by the number of observations of each source. Table 2 shows details of the scatter improvement resulting from introduction of source structure delay modeling for the 47 frequently observed sources. Here the sources are classified by their structure indices. It is seen that the overall  $(-3, 24)$   $\mu\text{as}$  improvements in RA and dec scatter are not

Table 2. Source Coordinate Scatter Improvement ( $\mu\text{as}$ ) *vs.* X- and S-band Structure Indices

XSI	$N_{obs}$	$\langle\Delta\alpha\rangle$	$\langle\Delta\delta\rangle$	SSI	$N_{obs}$	$\langle\Delta\alpha\rangle$	$\langle\Delta\delta\rangle$
1	62394	-8.4	4.3	1	124785	-2.8	22.7
2	54475	3.6	6.8	2	13097	-17.1	18.1
3	21013	6.5	115.4	3	0	...	...

uniformly distributed among sources with different structure indices. In particular, the right ascension results may be influenced by inappropriately fixing the RA orientation of the reference frame. This possibility will be investigated in the near future. Improvement in declination scatter can reach a substantial fraction of the current ICRF accuracy estimate of 250 microarcseconds.

### 3.3. VLBI Error Budget

The present fit to RDV data has implications for the astrometric/geodetic VLBI error budget. Source structure mismodeling was found to contribute  $\approx 8$  ps (3 mm) to the  $\approx 30$  ps (10 mm) WRMS residual delay. Assuming that the two other major contributors to unexplained discrepancies between theory and experiment are presently the instrumental and tropospheric delays, and that their mismodeling is of roughly equal magnitude, the conclusion is that each amounts to  $\approx 20$  ps or 6 mm. When the troposphere error is routinely reduced below 1 mm (3 ps) [8], the focus in reducing errors will have to be switched to instrumental systematics, and source structure corrections will need to play a larger role in VLBI analyses.

## 4. Conclusions

Modeling source structure with maps improves VLBI analysis, predominantly for sources with extended X-band structures. The improvement is larger for bad structures, and larger for declination than for right ascension. Impact of unmodeled source structure on the VLBI error budget is not overwhelming. It is estimated to be smaller than either the present unmodeled tropospheric or instrumental effects by at least a factor of 2. For sources that happen to be undergoing substantial activity during the VLBI observation period, modeling structural changes is extremely important.

Further exploratory work should be able to determine how effectively existing source maps can be used to correct observations in other experiments that are a few months removed from the mapping epochs. When troposphere errors can be reduced to 1–2 mm by improved WVRs, structure effects will become more prominent in the VLBI error budget. Detailed studies of time sequences of maps should permit location of the invariant (fiducial) points within sources. Future studies may show whether source structure produces an irreducible inherent uncertainty of the fiducial points on the sky. If so, the achievable accuracy of an inertial reference frame based on extragalactic radio sources would be ultimately limited by such fuzziness.

## References

- [1] Altamimi, Z., <http://lareg.ensg.ign.fr/ITRF/ITRF2000>
- [2] Charlot, P., Radio-Source Structure in Astrometric and Geodetic Very Long Baseline Interferometry, *Astron. J.* **99**, 1309, 1990.
- [3] Charlot, P., Evidence for Source Structure Effects Caused by the Quasar 3C273 in Geodetic VLBI Data, in *VLBI Technology – Progress and Future Observational Possibilities*, Proc. URSI/IAU Symp., ed. by T. Sasao, S. Manabe, O. Kameya and M. Inoue, Terra Scientific Publishing Company, Tokyo, Japan, 287–294, 1994.
- [4] Charlot, P., Modeling Radio Source Structure for Improved VLBI Data Analysis, these proceedings, 2002.
- [5] Fey, A.L., A.W. Clegg, and E.B. Fomalont, *Astrophys. J. Suppl. Ser.* **105**, 299, 1996.
- [6] Fey, A.L. and P. Charlot, VLBA Observations of Radio Reference Frame Sources. II. Astrometric Suitability Based on Observed Structure, *Astrophys. J. Suppl. Ser.* **111**, 95, 1997; Fey, A.L. and P. Charlot, VLBA Observations of Radio Reference Frame Sources. III. Astrometric Suitability of an Additional 225 Sources, *Astrophys. J. Suppl. Ser.* **128**, 17, 2000.
- [7] Ma, C., E.F. Arias, T.M. Eubanks, A.L. Fey, A.-M. Gontier, C.S. Jacobs, O.J. Sovers, B.A. Archinal, and P. Charlot, The International Celestial Reference Frame as Realized by Very Long Baseline Interferometry, *Astron. J.* **116**, 516, 1998; First Extension of the International Celestial Reference Frame – ICRF Ext. 1, In: *IERS Annual Report for 1998* (Observatoire de Paris, Paris), 83–128, 1999.
- [8] Naudet, C.J., S. Keihm, G. Lanyi, R. Linfield, G. Resch, L. Riley, H. Rosenbeger, A. Tanner, Media Calibration in The Deep Space Network – A Status Report, these proceedings, 2002.
- [9] Sovers, O.J. and Jacobs, C.S., Observation Model and Parameter Partialials for the JPL VLBI Parameter Estimation Software ‘MODEST’ - 1996, JPL Publication 83-39, Rev. 6, 151 pp., 1996.

# PIVEX: a Proposal for a Platform Independent VLBI Exchange Format

*Anne-Marie Gontier, Martine Feissel*

*Observatoire de Paris, SYRTE*

*Contact author: Anne-Marie Gontier, e-mail: [Anne-Marie.gontier@obspm.fr](mailto:Anne-Marie.gontier@obspm.fr)*

## Abstract

Following a recommendation of the 2nd IVS Analysis Workshop, a working group was set up to develop a VLBI exchange format independent of platforms and operating systems. The aim of this format is to ease the international extension of VLBI analysis for astrometry and geodesy. The working group members were selected in such a way that their knowledge should collectively encompass all data environments involved. We present, in this paper, the PIVEX format that was discussed and tested and the future insertion of the PIVEX files into the VLBI data flow.

## 1. The Working Group

The 2nd IVS Analysis Workshop (February 2001) created a Working Group to “organize the discussions and activities concerning the development of a new VLBI database structure independent of platform and operating system”. The membership of the WG was based on voluntary participation. It encompasses various data environments involved, namely:

- Correlators: MarkIV, Japanese, Canadian.
- Analysis software: CALC, ERA, GEOSAT, GLOBK, GLORIA, MODEST, OCCAM, STEELBREEZE.
- Data Centers.

The members list is as follows:

Martine Feissel (Chair),	Najat Essaifi,	Anne-Marie Gontier,
Calvin Klatt,	Chopo Ma,	Leonid Petrov,
Kazuhiro Takashima,	Oleg Titov.	

Ed Himwich and Dan McMillan were involved in the intensive discussions on the PIVEX file structure and information content, held during a three weeks stay of the first author in the VLBI group at GSFC. Further more, the following individuals were kept informed of the work progress:

P.H. Andersen,	J. Boehm,	S. Bolotin,	P. Charlot,	A. Fey,
Y. Koyama,	Z. Malkin,	A. Niell,	A. Nothnagel,	G. Elgered,
H. Schuh,	O. Sovers,	V. Tesmer,	N. Vandenberg.	

## 2. Environment

Historically, various data treatment levels downstream of the correlator were quite naturally implemented jointly in the Calc-Solve operation. The use of the VLBI data base files is currently integrated into the way GSFC does information transfer between programs, archiving and cataloging. The files consequently contain more than the raw fringe output and calibration data, the minimum information required for analysis. Today, with the multiplication of analysis software packages, it seems again natural to isolate a level of data exchange that will help newcomers to join, without the obligation to extract for themselves the information they need, out of informations dedicated to another software package, implying other modellings, other aprioris, etc. The minimum amount of information needed for analysis depends on what each analysis center wishes to do independently. Generally, for example, analysis centers using the current data base files have not redone the weather calibration from the station logs.

In the current scheme, a series of operations internal to Calc-Solve are performed prior to the posting of the databases on the IVS Data Centers. The external user must then select the part of information he needs (less than 1/3 of the total) to import the observations into his own computing environment. In the scheme the WG is aiming at, the Data Centers files contain only the useful information and can be imported by the analysts using a simple interface.

The current VLBI format consist of a database handler (called Mark3-dbh), two binary (CALC database) and two ascii (NGS) files. The database handler allow us to load in memory one experiment at one and the same time which does not make the global analyses easier. For the same experiment, both in binary and ascii format, the X- and S-band data are stored in two files independantly which leads to unnecessary redundancy. The binary and the ascii files differs by their content and structure. The binary file contains the observation informations as well as models and partial derivatives computed by the CALC software. The ascii format is fixed and documented but some observational informations, like the number of ambiguities, are missing. A proposed astro-geodetic VLBI format is described hereafter.

## 3. Astro-Geodetic VLBI Format

This project had already been treated in the two following instances, that served as a starting point for the WG discussions.

- Specifications for a “geo-VLBI format”, proposed by L. Petrov [1].
- The Gloria database structure, that was discussed internationally before its final adoption in 1999 [2].

The goals of the astro-geodetic VLBI format may be summarized as follow.

- Develop a flexible and efficient format for keeping and sharing astro-geodetic VLBI data. The criteria for optimization, in this context, are the minimization of the size of a database, the minimization of redundancy and the minimization of the time needed for reading/writing the database.
- Develop a share-ware library (Geo Vlbi Handler: GVH) which would support basic operations with datafiles. This library should run under several platforms (ideally under any platform).

The astro-geodetic VLBI format consists of a description of internal representation of the data in memory, a description of two external datafile formats on disk and a user interface (GVH).

In the future, two datafile formats will be available on disk.

- A binary format (bgv) which follows closely the internal structure of the data in memory and is oriented for processing experiments in automatic modes. This format could replace, one day, the actual CALC database.
- An ASCII format (PIVEX) more oriented for reading by a human being. It will replace, as soon as possible, the NGS files in IVS Data Centers.

The GVH procedures is a set of subroutines for the data manipulation. It provides the service of reading information from the input file(s) to the user program and writing information from a user program to the output file(s). User access to the information, at least for the binary files (bgv), will be through this standard interface. Generators of data for submission to IVS, essentially only the Operation Centers, will use the routines that pass information into PIVEX. Users doing analysis will only need to use the subroutines that retrieve information. Users may, of course, write their own code to access the PIVEX files.

The geo VLBI handler is able to load more than one experiment in memory and is an efficient tool to manipulate the data. The datafiles contain only observation informations like output of fringe fitting, parameters of observing session, correlator comments, calibration information or history records and is identical either in binary and ascii form. Some of the key structural points are that X and S band is merged with common access code for data item, all data are treated as two-dimensional although second dimension can be one and the format will be self-documenting and extensible by table of contents.

A description of the PIVEX file structure resulting from intensive discussions is given hereafter.

## 4. PIVEX Data Organisation

### 4.1. Supported Data

The data supported are of three kinds: text information, description of numerical data and numerical data themselves.

The text information is organized in one or more chapters. Each chapter has one line of title and a body consisting of one or more lines of variable length.

The numerical data consist of several arrays of access codes called **lcodes**. They could be of fixed or variable length and contain the data.

The description of numerical data is an array of fixed length which describe all access codes. It consists of a name, type, class, dimensions and a short explanation for each **lcode**. The following types are actually supported:

```
INTEGER*2      REAL*4      CHARACTER*1
INTEGER*4      REAL*8
```

The format can be easily extended to other types. In order to avoid data redundancy, as much as possible, all information is classified as session, scan, station or baseline.

### 4.2. File Structure

Each datafile has the following structure:

- one line of identification label which tells the name of the format and the revision date.  
*PVX format of 2001.11.25 32 bit address*

- one or several segments consisting of 5 sections (preamble, text, toc, data and heap).

Each section consists of a reserved keyword and a body. A brief description and a short example (in *italic*) of the different sections follows.

- Preamble: keyword **@PREA**

The body of this section consists of records of variable length, it contains general information on data type, class definition, generator ... For example:

```
@PREA section_length: 13 keywords
DEF_TYPE: 1 CHARACTER ASCII
DEF_TYPE: 2 INTEGER*2 IEEE-231
DEF_CLASS: 81 Session
DEF_CLASS: 84 Baseline
GENERATOR: ex1 GVH release of 2001.11.28
FILENAME: sample.bgv
CREATED_AT: 2002.02.26-15:22:07
```

- Text: keyword **@TEXT**

The section consists of records of variable length separated by terminator and organized in chapters and paragraphs. History of versions, correlation and post-correlation information are written in this section.

```
@TEXT section_length: 2 chapters
@@chapter 1 History of version 1
Dbedit: na444, NEOSA — geo_export
VLBI experiment NA444 ( NEOSA )
@@chapter 2 History of version 2. Created 2001-11-04T15:48:12 UTC
CALC 9.12 Ver. 2001.01.12 Tue Nov 20 10:48:02 2001 leo
```

- Tocs: keyword **@TOCS**

It consists of records of fixed length. It is the table of contents in the form lcode name, class, type, two dimensions and a short description.

```
@TOCS
NUMB_OBS SES I4 1 1 Number of observations in the session
SOURCE SCA C1 8 1 Source name
LO_FREQ STA I2 22 16 Local Oscillator frequencies per channel in MHz
GRIONFRQ BAS R8 2 1 Effective ionosphere frequency for group delay (MHz)
PHASE_AP BAS R4 -16 -512 Fringe phase per channel, per AP (rad)
```

- Data: keyword **@DATA**

The section consists of records of variable length. It contains the observations organized in four classes: session (**@@Session**), scan (**@@Scan**), station (**@@Station**), baseline (**@@Baseline**). It is value of lcodes of fixed length (dimensions are specified in the Toc section).

```
@DATA
@@Session
  NUMB_OBS 20
  CORPLACE HAYSTACK
@@Scan      1
  SEC_TAG 1.01
@@Station GILCREEK      1
  LO_FREQ 234 212 494 407 318 242 1093 463 511 349 1007 864 1129 750 850 554 887
441 731 221 822 641 564 843 605 959 1122 736 295 360 973 458
@@Station KAUAI      3
  LO_FREQ 1178 1048 368 684 417 320 1050 657 542 1167 582 550 828 887 1144 466 218
883 1132 709 1127 316 393 916 734 282 945 838 1120 692 901 598
@@Baseline GILCREEK KAUAI      1
  GROBSDEL .5040884613990784 .1870681047439575
@@Baseline GILCREEK NRAO85 3 2
  GROBSDEL .1870681047439575 4.285985231399536E-02
@@Scan      2
  SEC_TAG 2.02
```

- Heap: keyword **@HEAP**

It is one record of variable length. It contains the value of lcode of variable length. The maximum dimension is specified in the Toc section with negative value and the Data section contains the descriptors.

```
@HEAP
  PHASE_AP 0.123 0.456 1.3456
```

A summary of the PIVEX file structure is shown in figure 1.

## 5. PIVEX Prototype

### 5.1. Tested Experiments

In order to test the reading/writing code of the geo VLBI handler, we have written a small session prototype. The code to write informations from memory into either binary or ascii files is fully tested on a Unix HP computer. Moreover, the code to load informations in memory from a binary file is available and the same operation from the PIVEX file is in progress.

We also have tested the possibility to transform the actual CALC database to PIVEX format. Three different sessions were used for that purpose:

- one intensive experiment (01DEC31\_U, INT01-365), 2 stations, 18 observations;
- one NEOS experiment (01DEC11\_E, NEOS-A450), 6 stations, 1954 observations;
- one RDV experiment (01MAY09\_A, VLBA28), 18 stations, 24634 observations.

All the corresponding PIVEX files were created and even for the larger one, the ascii file is still manageable. The remaining programming work is to recode the GVH routines for multiple platforms.

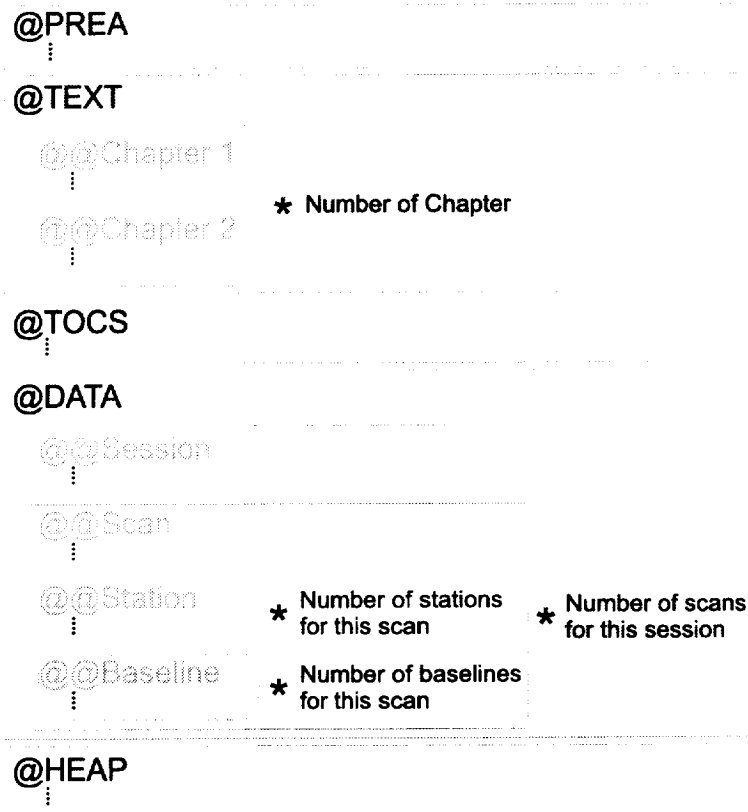


Figure 1. Schematic PIVEX structure

## 5.2. File Naming Convention

In order to avoid duplicate names and to recognize easily an experiment we proposed the following naming convention:

YYY\_MM\_DD\_CODIVS\_i.pvx

where YYY\_MM\_DD is the date, \_CODIVS is the IVS code for the experiment (available in master schedule file on IVS web site) and *i* is the file version (in case of re-fringing for example).

The resulting file names for the three tested experiments are:

2001\_12\_31\_I01365\_1.pvx

2001\_12\_11\_NA450\_1.pvx

2001\_05\_09\_RDV28\_1.pvx

They are available on the current PIVEX web site (<http://lareg.ensg.ign.fr/feissel/pivex.html>) and on IVS web site in the near future. For the binary file the extension will be .bgv with the same naming convention.

## 6. Future

The PIVEX proposal was accepted at the 3rd IVS analysis workshop (February 2002) in Tsukuba. A part of the remaining work is to complete the code to read the PIVEX format and to load it in memory. The next step, which consists of recoding and testing the geo VLBI handler on multiple platforms, will be realized by S. Bolotin, if he agrees.

In the same time, a full user documentation (interface and information contents) will be written and circulated for comments in IVS.

As soon as the PIVEX content is completely specified and the code to transform CALC database into PIVEX is fully tested, hopefully before the end of the year, next experiments will be available in this two formats (CALC database and PIVEX) on the IVS data centers.

After that step, the old experiments will also be transformed to PIVEX format on IVS Data Centers going back to the past.

In the future, any revision of the PIVEX format, extensible by table of contents, should be agreed upon by e.g. a PIVEX monitoring group under the responsibility of the IVS Analysis Coordinator.

## References

- [1] Petrov, L., In: Specifications of a proposed geo-VLBI data format, <http://gemini.gsfc.nasa.gov/development/gvf/gvf.html>, 1999.
- [2] Abdelkader, K., A.-M. Gontier, In: the GLORIA VLBI tables, [http://lareg.ensg.ign.fr/feissel/pivex/gloria\\_base.html](http://lareg.ensg.ign.fr/feissel/pivex/gloria_base.html), 1996.

# Integrating Analysis Goals for EOP, CRF and TRF

Chopo Ma <sup>1</sup>, Daniel MacMillan <sup>2</sup>, Leonid Petrov <sup>2</sup>

<sup>1</sup>) NASA Goddard Space Flight Center

<sup>2</sup>) NVI, Inc./NASA Goddard Space Flight Center

Contact author: Chopo Ma, e-mail: [cma@virgo.gsfc.nasa.gov](mailto:cma@virgo.gsfc.nasa.gov)

## Abstract

In a simplified, idealized way the TRF can be considered a set of positions at epoch and corresponding linear rates of change while the CRF is a set of fixed directions in space. VLBI analysis can be optimized for CRF and TRF separately while handling some of the complexity of geodetic and astrometric reality. For EOP time series both CRF and TRF should be accurate at the epoch of interest and well defined over time. The optimal integration of EOP, TRF and CRF in a single VLBI solution configuration requires a detailed consideration of the data set and the possibly conflicting nature of the reference frames. A possible approach for an integrated analysis is described.

## 1. Introduction

VLBI has features that give it unique capability in the area of fundamental reference frames and Earth orientation. These are summarized in Table 1.

Table 1. Features of VLBI

Sensitivity to all Earth orientation parameters: x-pole, y-pole, UT1, $\Delta\epsilon$ , $\Delta\psi$
Direct access to a quasi-inertial reference frame
Direct access to the terrestrial reference frame
Direct tie between celestial and terrestrial frames

In contrast, satellite space geodesy techniques lack direct access to a quasi-inertial reference frame and rely on VLBI measurements to make this connection. Routine generation of VLBI results for EOP and TRF implicitly assumes that the VLBI frames and EOP are derived from the same analysis. However for historical reasons and to achieve different optimization goals the analysis strategies for CRF, TRF, and EOP have been different in practice. In particular, the analysis strategy for the ICRF dispenses with the TRF. Consequently the various results are incompatible at some level. As even better accuracy and consistency are desired for scientific and operational uses the need for an integrated analysis optimized as well as possible for all these types of results has grown. The paper first describes ideal frames and data. Some problems of real data and possible analysis treatments are highlighted. Finally one possible strategy for an integrated analysis is given.

## 2. Ideal Frames and Data

The ideal TRF and CRF conditions along with the VLBI data required are summarized in parallel in Table 2.

Table 2. Ideal Frames

TRF	CRF
set of positions and linear velocities	set of positions
all stations rigidly connected by overlapping networks	all sources rigidly connected by overlapping source sets
sufficient time and data for velocity estimates	
all stations permanent	all sources permanent
even distribution of data over stations and time	even distribution of data over sources and time
even distribution over globe	even distribution over sky

From such data it would be straightforward to estimate a TRF from which a position and error for each station could be calculated at any past or future time. Since an ideal source has an unchanging position, its error would be constant in time. As new data were included in the analysis, the station positions at the reference epoch and the velocities would change only according to their statistical errors, and the statistical errors would decrease. A similar situation would apply for the CRF and EOP. Even with ideal VLBI data and station/source behavior, however, the real errors would need to take into account the imperfections of the geophysical modeling and of the estimation of non-TRF/CRF/EOP parameters, notably the troposphere and short-term station motions.

## 3. Some Real Data Conditions and Possible Analysis Options

Of course none of the actual stations and sources behaves exactly ideally, and the VLBI data set fails to meet the ideal conditions except for the rigid connection of sources. These shortcomings arise for historical and practical reasons. There has been a slow and continuing evolution of instrumentation, and the earlier data were limited by sensitivity, particularly in the choice of sources. The list of stations and sources used for the EOP monitoring programs, the dominant type of observing in terms of session count, is only a small part of the complete list of stations and sources. Stations and sources have been used and discontinued, some after only a few appearances but others after years. The quality of observing schedules has improved with experience and instrumentation. Certain conditions cannot be easily changed: the paucity of stations in the Southern Hemisphere and the number of stations that can be routinely correlated at the facilities supporting the geodetic observing programs. The deployment of TIGO in Chile will ameliorate the first problem in the near future, and the use of the VLBA correlator allows some large networks to be used occasionally.

Some non-ideal conditions affecting TRF, CRF and EOP results are listed in Table ?? along with ways to extract some useful information or to prevent undesirable distortion of the particular parameters.

Table 3. Real data and analysis options

	<b>condition</b>	<b>analysis</b>
<b>TRF</b>	nonlinear station motion	piecewise-linear continuous position parameters
	“loose” station	a priori EOP for session(s)
	short time span	a priori velocity error from model
	episodic motion	tie of velocity before and after event
<b>CRF</b>	unstable source	arc position parameters
	position drift	proper motion parameters
<b>EOP</b>	single baseline network	a priori EOP errors
	small network	exclude from time series after generation
	distorted CRF at epoch	arc position parameters
	distorted TRF at epoch	piecewise-linear continuous position parameters

A “loose” station is one that has only been observed with networks that do not overlap sufficiently with the rigidly connected stations. This situation occurs when the loose station’s networks do not have at least three, well-spaced stations in common with the set of rigidly connected stations. Some mobile VLBI stations (because of poor network design) and parts of the Japanese domestic network (because of incompatible equipment) fall into this category. A priori EOP information must be used to orient the poorly connected sessions. Episodic motion can be caused by seismic events or by major antenna repairs that move the VLBI reference point.

A data weakness for EOP time series is that some older sessions have only one baseline observing, so polar motion and UT1 cannot be separated. Values for these three parameters can be estimated if large a priori EOP errors are included, and the two orthogonal axes with real information can be obtained from the EOP covariance matrix. Another situation is that the networks for a few sessions are very small to provide relative positions of antennas at one or nearby sites. These sessions are valuable for the TRF but cannot generate useful EOP or source position results. A more pernicious situation is that for a particular session a station or source may not be located at the position projected from the TRF and CRF. The estimated EOP values will be affected at some level by using incorrect geometry.

What to do in any particular case is a matter of judgment or could be decided on the basis of objective criteria.

#### 4. A Possible Approach for Integrated Analysis

Table 4 shows a set of goals for the reference frames to be determined by an integrated solution and one important condition for each area. These conditions, and other reasonable choices, can conflict when optimizing an analysis for a single area. For example, using all the available data to maximize time span for TRF velocities would include data on non-ideal sources, which would affect the CRF. If only the sessions of the EOP observing programs were used, both the TRF and CRF would be very sparse since only a small portion of the total number of stations and sources

Table 4. Reference Frame Goals and Conditions

TRF	CRF	EOP
maximum number of site positions and velocities	highest accuracy for positions of best sources	accurate TRF/CRF at observing epoch
long time span for precise velocities	minimal effects from network geometry and unstable sources	subset of TRF/CRF used at each epoch

is used, in each session and in aggregate, in the EOP sessions.

Table 5 lists the steps in one possible strategy for an integrated analysis.

Table 5. Steps for an Integrated Analysis

1. Identify non-ideal stations and sources.
2. In a TRF-optimized solution, estimate TRF positions and velocities for ideal stations, treating non-ideal stations and sources as arc parameters.
3. In a CRF-optimized solution, estimate CRF positions for ideal sources, treating non-ideal sources as arc parameters.
4. Compute average positions and velocities of non-ideal stations from time series.
5. Compute average positions of non-ideal sources from time series.
6. Using the information from steps 2, 3, 4, and 5 examine each session to determine which station(s) and/or source(s) are not at their correct position at that epoch and flag these as arc parameters.
7. In a single solution, estimate TRF positions and velocities for all stations, CRF positions for all sources, and for each session five EOP values and the arc parameters found in step 6.
8. Discard EOP time series points derived from small networks.

The identification of non-ideal stations and sources in step 1 could be done from preliminary time series of station and source positions. The criteria for classifying as ideal or non-ideal would be developed from the actual range of behavior. In step 3, the station positions would be arc parameters. Steps 2 and 3 would generate time series for steps 4 and 5, respectively, and the process might be iterated. For all solutions the geophysical modeling and the estimation of non-TRF/CRF/EOP parameters would be identical, and the entire VLBI data set would be used. In step 6 the threshold for a station or source to be classified as “out of position” and therefore requiring arc parameters would be related to the criteria used in step 1. Step 8 recognizes the fact that some sessions have minuscule networks that are important for the TRF in locating nearby stations but provide no useful information for EOP.

The rationale for this type of approach is that data contribute to the TRF and CRF when the conditions of linear motion and constant source position are met. For ideal stations and sources,

all their data would be included. For non-ideal stations and sources, only data agreeing with their average velocity and position would contribute to the TRF and CRF, and the statistical errors would reflect only these points. For each session the subset of the TRF and CRF observed would be undistorted since the stations and sources with non-ideal behavior during that day would be treated as arc parameters. EOP values are thus determined from only the well-behaved elements of the TRF and CRF. Since no data points are eliminated, each observation can still provide information for non-TRF/CRF/EOP parameters. This approach is only suggestive, and the implementation of step 6 would be difficult.

## 5. Conclusion

To reach the full potential of VLBI in integrating CRF, EOP, and TRF the non-ideal nature of the sources and stations must be considered as well as limitations imposed by the heterogeneous nature of the VLBI data set. While one analysis strategy is described, others are conceivable. The choice of optimal strategy will depend on comparison of actual studies and the emphasis given to various desired outcomes.

# On Correlations Between Parameters in Geodetic VLBI Data Analysis

*Axel Nothnagel, Markus Vennebusch, James Campbell*

*Geodetic Institute of the University of Bonn*

*Contact author: Axel Nothnagel, e-mail: nothnagel@uni-bonn.de*

## Abstract

The study of correlations between parameters estimated in least squares adjustments helps to investigate observing geometries and permit a more thorough assessment of the parameters' formal errors. High correlations between atmospheric parameters represented as zenith atmospheric excess path lengths and the vertical component of the station coordinates have long been considered as established facts in geodetic and astrometric VLBI. In this paper we investigate this commonly held view on the basis of transforming the variance/covariance matrices from geocentric into local (topocentric) coordinates. We find that correlations between the estimated relative clock offsets and the local vertical components are much higher than those between the atmospheric parameters and the vertical components. This result may be used as an argument to invest more in the stability of atomic clocks for further improvements in geodetic and astrometric VLBI.

## 1. Introduction

In the statistical literature correlations are mainly treated in the context of correlations between observations and in cases where parameters from a first adjustment are used as inputs for a second one. In contrast to that the consequences of the existence of correlations between estimated parameters are seldom discussed or interpreted.

Correlations between parameters are expressed as correlation coefficients  $r_{xy}$  computed from the variance/covariance matrix, i.e. from the main diagonal elements (standard deviations  $\sigma_x = \sqrt{Q_{xx}}$  and  $\sigma_y = \sqrt{Q_{yy}}$ ) and the corresponding off-diagonal element, i.e. the covariance  $Q_{xy}$ :

$$r_{xy} = \frac{Q_{xy}}{\sigma_x \cdot \sigma_y}. \quad (1)$$

In the adjustment of VLBI observations a commonly held view is that the topocentric height component and the atmospheric excess zenith path parameter are highly correlated (e.g. [1], [2]). The reason given is that in both cases the delay observable is affected by the sine of the elevation ( $\epsilon$ ) at the observing site as expressed in (2) and (3):

$$\Delta\tau_{Atm} = -\frac{1}{c} \cdot \frac{1}{\sin \epsilon} \cdot \Delta L_{Atm}^Z \quad (2)$$

$$\Delta\tau_U = -\frac{1}{c} \cdot \sin \epsilon \cdot \Delta U \quad (3)$$

where  $\Delta L_{Atm}^Z$  is the change in atmospheric zenith path length,  $\Delta U$  the change in the vertical component of the station coordinates, and  $\Delta\tau$  are the resulting delay changes while  $c$  is the speed of light.

Generally, the vertical component  $\Delta U$  is not readily available in least squares adjustments of VLBI observing sessions since the model is normally represented in geocentric x,y,z coordinates. Hence, the variance/covariance matrix is also expressed geocentrically. In order to investigate correlations which are related to the topocentric station components, i.e. vertical (U), East (E) and North (N) components, the error propagation law has to be applied to the covariance matrix  $Q$  in the form (see [3]):

$$Q^{UEN} = \mathbf{B} \cdot Q^{XYZ} \cdot \mathbf{B}^T \quad (4)$$

$\mathbf{B}$  is the matrix of partial derivatives with respect to the individual parameters or the so-called design matrix (here we only display  $\mathbf{B}$  for a single site, for all other sites this pattern repeats):

$$\mathbf{B} = \begin{pmatrix} \frac{\partial U}{\partial X} & \frac{\partial U}{\partial Y} & \frac{\partial U}{\partial Z} & \frac{\partial U}{\partial CL0} & \frac{\partial U}{\partial CL1} & \frac{\partial U}{\partial CL2} & \frac{\partial U}{\partial AT1} & \dots & \frac{\partial U}{\partial ATn} & \frac{\partial U}{\partial NG} & \frac{\partial U}{\partial EG} \\ \frac{\partial E}{\partial X} & \frac{\partial E}{\partial Y} & \frac{\partial E}{\partial Z} & \frac{\partial E}{\partial CL0} & \frac{\partial E}{\partial CL1} & \frac{\partial E}{\partial CL2} & \frac{\partial E}{\partial AT1} & \dots & \frac{\partial E}{\partial ATn} & \frac{\partial E}{\partial NG} & \frac{\partial E}{\partial EG} \\ \frac{\partial N}{\partial X} & \frac{\partial N}{\partial Y} & \frac{\partial N}{\partial Z} & \frac{\partial N}{\partial CL0} & \frac{\partial N}{\partial CL1} & \frac{\partial N}{\partial CL2} & \frac{\partial N}{\partial AT1} & \dots & \frac{\partial N}{\partial ATn} & \frac{\partial N}{\partial NG} & \frac{\partial N}{\partial EG} \\ \frac{\partial CL0}{\partial X} & \frac{\partial CL0}{\partial Y} & \frac{\partial CL0}{\partial Z} & \frac{\partial CL0}{\partial CL0} & \frac{\partial CL0}{\partial CL1} & \frac{\partial CL0}{\partial CL2} & \frac{\partial CL0}{\partial AT1} & \dots & \frac{\partial CL0}{\partial ATn} & \frac{\partial CL0}{\partial NG} & \frac{\partial CL0}{\partial EG} \\ \frac{\partial CL1}{\partial X} & \frac{\partial CL1}{\partial Y} & \frac{\partial CL1}{\partial Z} & \frac{\partial CL1}{\partial CL0} & \frac{\partial CL1}{\partial CL1} & \frac{\partial CL1}{\partial CL2} & \frac{\partial CL1}{\partial AT1} & \dots & \frac{\partial CL1}{\partial ATn} & \frac{\partial CL1}{\partial NG} & \frac{\partial CL1}{\partial EG} \\ \frac{\partial CL2}{\partial X} & \frac{\partial CL2}{\partial Y} & \frac{\partial CL2}{\partial Z} & \frac{\partial CL2}{\partial CL0} & \frac{\partial CL2}{\partial CL1} & \frac{\partial CL2}{\partial CL2} & \frac{\partial CL2}{\partial AT1} & \dots & \frac{\partial CL2}{\partial ATn} & \frac{\partial CL2}{\partial NG} & \frac{\partial CL2}{\partial EG} \\ \frac{\partial AT1}{\partial X} & \frac{\partial AT1}{\partial Y} & \frac{\partial AT1}{\partial Z} & \frac{\partial AT1}{\partial CL0} & \frac{\partial AT1}{\partial CL1} & \frac{\partial AT1}{\partial CL2} & \frac{\partial AT1}{\partial AT1} & \dots & \frac{\partial AT1}{\partial ATn} & \frac{\partial AT1}{\partial NG} & \frac{\partial AT1}{\partial EG} \\ \vdots & \dots & \vdots & \vdots & \vdots \\ \frac{\partial ATn}{\partial X} & \frac{\partial ATn}{\partial Y} & \frac{\partial ATn}{\partial Z} & \frac{\partial ATn}{\partial CL0} & \frac{\partial ATn}{\partial CL1} & \frac{\partial ATn}{\partial CL2} & \frac{\partial ATn}{\partial AT1} & \dots & \frac{\partial ATn}{\partial ATn} & \frac{\partial ATn}{\partial NG} & \frac{\partial ATn}{\partial EG} \\ \frac{\partial NG}{\partial X} & \frac{\partial NG}{\partial Y} & \frac{\partial NG}{\partial Z} & \frac{\partial NG}{\partial CL0} & \frac{\partial NG}{\partial CL1} & \frac{\partial NG}{\partial CL2} & \frac{\partial NG}{\partial AT1} & \dots & \frac{\partial NG}{\partial ATn} & \frac{\partial NG}{\partial NG} & \frac{\partial NG}{\partial EG} \\ \frac{\partial EG}{\partial X} & \frac{\partial EG}{\partial Y} & \frac{\partial EG}{\partial Z} & \frac{\partial EG}{\partial CL0} & \frac{\partial EG}{\partial CL1} & \frac{\partial EG}{\partial CL2} & \frac{\partial EG}{\partial AT1} & \dots & \frac{\partial EG}{\partial ATn} & \frac{\partial EG}{\partial NG} & \frac{\partial EG}{\partial EG} \end{pmatrix} \quad (5)$$

Since in different coordinate systems there are only interdependencies in the coordinate components but not between other parameters, the design matrix can be simplified to read (again for one site only):

$$\mathbf{B} = \begin{pmatrix} \frac{\partial U}{\partial X} & \frac{\partial U}{\partial Y} & \frac{\partial U}{\partial Z} & 0 & \dots & 0 \\ \frac{\partial E}{\partial X} & \frac{\partial E}{\partial Y} & \frac{\partial E}{\partial Z} & 0 & \dots & 0 \\ \frac{\partial N}{\partial X} & \frac{\partial N}{\partial Y} & \frac{\partial N}{\partial Z} & 0 & \dots & 0 \\ \frac{\partial CL0}{\partial X} & \frac{\partial CL0}{\partial Y} & \frac{\partial CL0}{\partial Z} & 0 & \dots & 0 \\ \vdots & \vdots & \vdots & \vdots & \ddots & \vdots \\ 0 & 0 & 0 & 0 & \dots & 1 \end{pmatrix} \quad (6)$$

The correlation coefficients can then be computed according to (1) forming the matrix of correlation coefficients.

## 2. Results

For better insight we will display the correlation coefficients in a graphical form using shades of grey between black and white (correlation coefficient magnitude of 1 and 0, respectively) as displayed in a single baseline example in figure 1 (observations between Wettzell and Medicina carried out in a EUROPE session using a minimal parameterization). This consists of just the three topocentric station components (U,E,N) of Medicina, a second order clock polynomial ( $T_0, T_1, T_2$ ), and one atmosphere parameter for each station (A1, A2).

At first glance we see that the two atmosphere parameters are highly correlated due to the fact that the elevation angles for the two stations are very similar. The clock rate ( $T_1$ ) and acceleration ( $T_2$ ) parameters are correlated likewise due to the fact that  $T_2$  is always the square of  $T_1$ . What we do not see, however, is a high correlation between any of the atmosphere parameters and Medicina's vertical component. On the contrary, there is hardly any correlation between these parameters. More striking, the clock offset is highly correlated with the vertical component. In addition, a lesser degree of correlation with the East component is apparent leading to a prominent correlation between the East and the vertical component. The atmospheric parameters are correlated significantly only with the North component.

In order to study this phenomenon on a broader basis we transformed the covariances of a number of European and global 24-hour sessions in various configurations into the local systems. As an example, figure 2 displays the correlations of a five-station European session.

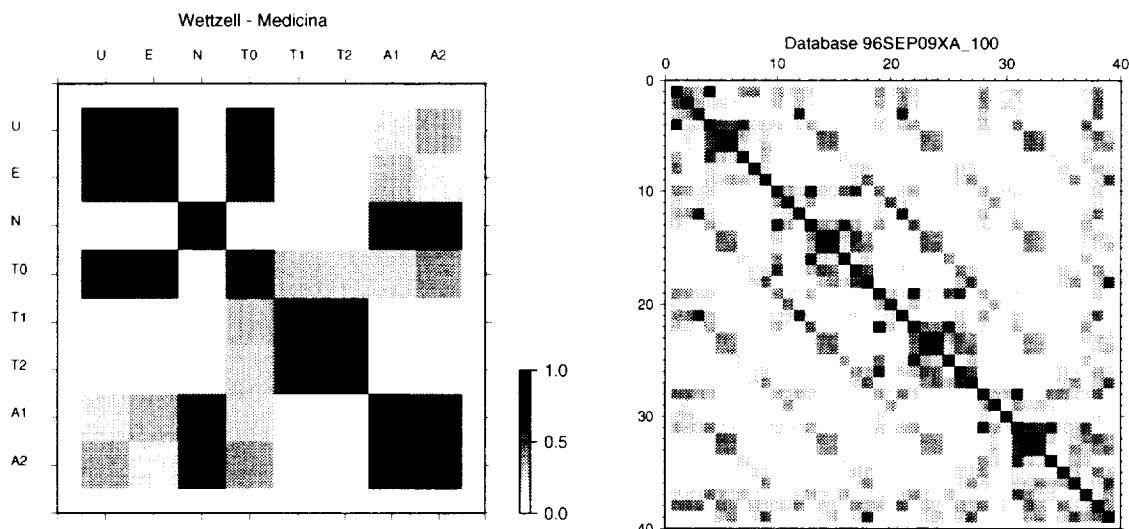


Figure 1 (left). Correlation coefficients. See text for explanation. Figure 2 (right). Correlation coefficients of 5-station EUROPE session. Parameter sequence: DSS65 (U,E,N,  $T_0$ ,  $T_1$ ,  $T_2$ ,  $Atm_1$ ,  $Atm_2$ ,  $Atm_3$ ), Matera (as DSS65), Noto (as DSS65), Onsala (as DSS65), Wetzell ( $T_0$ ,  $T_1$ ,  $T_2$ ,  $Atm_1$ ,  $Atm_2$ ,  $Atm_3$ )

Here, as in the single baseline example, the correlations between the clock offsets with the corresponding vertical components are clearly visible. Of course, there are the typical correlations between clock rate and acceleration or within the atmosphere gradients but they are of minor interest here.

A similar situation also prevails in a series of test computations we made with different parameterizations. In global networks we found the same trend in correlations between the vertical components and the clock offsets. However, here the magnitude of the individual correlation coefficients depended to a large extent on the observing schedule and the distribution and number of the observations on each baseline.

### 3. Discussion

The surprisingly low level of correlations between the atmosphere parameters and the vertical components we found in our study contradicts earlier investigations (e.g. [1], [2]). However, it is quite obvious to assume strong correlations between parameters for an observation at zenith where one can hardly distinguish between an error being caused by the atmosphere or by the local vertical.

In order to explain the phenomenon we return to the initial equations (2) and (3) which emphasize the importance of the elevation angles in this scenario. The estimation process is based on partial derivatives which in turn can easily be deduced from (2) and (3) resulting in

$$\frac{\partial \tau_{obs}}{\partial U} = -\frac{1}{c} \cdot \sin \epsilon \quad (7)$$

$$\frac{\partial \tau_{obs}}{\partial \text{Atm}^Z} = -\frac{1}{c} \cdot \frac{1}{\sin \epsilon}. \quad (8)$$

If we only had a few observations more or less near the zenith these would generate very similar coefficients close to 1 (ignoring the  $\frac{1}{c}$  here). The consequence would be that we would find a very high correlation coefficient between the vertical component and the atmosphere parameter in a least squares adjustment with only these observations.

But the observing schedules of VLBI sessions are constructed in a way that over the full 24-hour period the sky is sampled in as many different directions as possible generating a multitude of observing geometries with many different elevation angles. In recent years the elevation limits have been reduced to as low as 4°.

If we display the values of the partial derivatives w.r.t. the elevation (see figure 3) we see that at low elevations the values of the local vertical (U) and of the atmosphere parameter diverge considerably, a situation which leads to low correlation between atmosphere parameters and the vertical component. At the same time we see that the clock offset coefficient, which is a constant, always stays very close to the vertical or horizontal components (N,E). Hence, the observing geometry can never be varied in a way that the partial derivatives of coordinate components are very different from the clock offset and a high correlation has to be expected here.

In order to explain the high correlation between clock offset and vertical component we may also approach the problem from a geometrical perspective. Let's assume that we have only three different observations on a single short baseline (Fig. 4) where two observations are in opposite directions close to the horizon (elevation 0°, #1 and #2) and a third one is at zenith (#3).

The first two observations are necessary to determine the clock offset ( $T_0$ ) which, in the case of a low elevation observation, could otherwise not be distinguished from a horizontal shift of station B. The effect of the clock offset is identical in all directions (displayed as a semi circle about station B). If we now want to determine the height of station B we need the value of the clock offset as determined by the first two observations. If we had not determined the clock offset with the first two observations, the height of station B would be undetermined. Since the clock offset has an identical effect in all directions or elevations, its correlation with other parameters and particularly with the vertical coordinate component is much higher than that of the atmosphere which has a very strong elevation dependent signature.

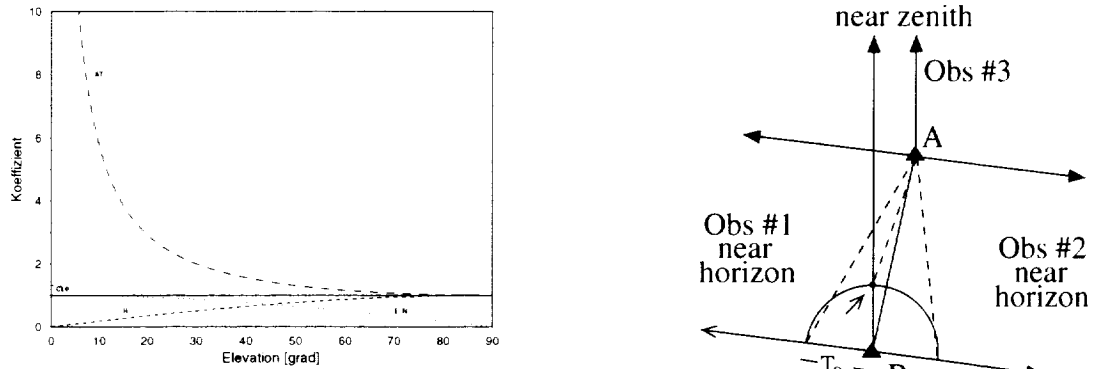


Figure 3 (left). Partial derivatives w.r.t. to elevation. Figure 4 (right). Three-dimensional geometry of 2 observations near horizon in opposite directions and one observation towards zenith with stations A and B. Clock offset  $T_0$  represented as distance from station.

#### 4. Conclusion

Although the high correlation coefficient between the clock offset and the topocentric vertical component comes as a surprise it can be explained from a geometric perspective as well as from a detailed analysis of the partial derivatives used in the least squares adjustment. At least from the standpoint of correlation, the atmosphere parameters do not seem to present the main problem for the accuracy of the vertical component. There does not appear to be a correlational mechanism by which the atmospheric errors are directly mapped into the vertical component. However, we should note the fact that the correlations increase when the elevation mask is lifted.

As a consequence of our investigations more attention should be paid to the stability of the atomic clocks used in VLBI observations. Our analysis shows that the clock errors are indeed mapped directly into the vertical components (correlation levels  $> 80\%$ ). As another test it would be interesting to investigate whether stations with stable hydrogen masers show a better repeatability in the height component than other stations. Nevertheless, we feel that clock stability aspects and clock parameterization in the least squares adjustments need further investigations in order to improve the overall accuracy of geodetic VLBI results.

#### References

- [1] Herring, T.A. (1986): Precision of vertical position estimates from Very Long Baseline Interferometry, *J. of. Geophysical Res.*, Vol. 91, B9 9177–9182
- [2] Kroger P.M., J.M. Davidson, E.C. Gardner (1986): Mobile Very Long Baseline Interferometry and Global Positioning System Measurement of Vertical Crustal Motion, *J. of. Geophysical Res.*, Vol. 91, B9, 9169–9176
- [3] Koch K.R. (1988): Parameter Estimation and Hypothesis Testing in Linear Models, *Springer Verlag*, Berlin

# Outlier Detection in the Combination of VLBI EOP

Christoph Steinforth, Axel Nothnagel

Geodetic Institute of the University of Bonn

Contact author: Christoph Steinforth, e-mail: steinforth@uni-bonn.de

## Abstract

On March 1, 2002, a new combined IVS EOP series has been established which is linked directly to the ITRF2000 reference frame. As compared to the input series submitted previously, the ITRF2000 based input series provided by the IVS Analysis Centers agree much better. In the process of automatic combination, the detection of outliers is of great importance in order to reduce human intervention to a minimum. The procedure used for outlier elimination responds to the level of the scatter in the residuals. As a consequence the new combination seems to be more robust against outliers.

## 1. Introduction

For almost 18 months now, the combined IVS Earth orientation parameter (EOP) series IVS01001 has been based on a number of different realizations of terrestrial reference systems and an alignment to the IERS C04 series [2] [3]. Depending on the quality of the nutation components of the input series, weighting factors have been assigned which are being updated from time to time. Current biases as subtracted before the combination and weight factors are summarized in table 1. A weight factor smaller than one means that the input of the respective series is downweighted correspondingly in the combination process.

Table 1. Biases and weight factors used in IVS01001 (determination period: 1.1.1999 - 31.9.2000); Weight factors greater than 1 increase the weight of the input series.

	$x_p$ [ $\mu$ as]	$y_p$ [ $\mu$ as]	$dUT1$ [ $\mu$ s]	w.f. [-]
AUS	-35.9	367.3	6.9	1.22
BKG	91.2	-8.0	-17.0	0.93
GSF	-43.0	281.7	8.4	0.90
IAA	-135.5	263.9	9.3	1.00
SPU	-46.3	155.1	16.6	1.11
USN	2.3	295.7	6.5	0.90

Comparing the formal errors of the input series as reported by the IVS Analysis Centers with the scatter of the post fit residuals as represented by the weighted RMS differences helps to assess the precision of the input series. In table 2 the mean formal errors of all input series and all EOP components show, on average, a fairly good level of agreement. As expected, some components have a higher post combination scatter than anticipated from the formal errors. However, most Analysis Centers show higher formal errors than post combination scatter except for the UT1-UTC component.

The mean formal precision of the combined series IVS01001 as reported in table 2 is reduced considerably as compared to the input series. Still lacking is the proper treatment of correlations between the input series which are expected to be as high as 70% due to the use of almost identical

observations, it seems quite natural that the formal precision of the combination series is so much better.

Table 2. Mean formal errors (MFE) of input and WRMS relative to combination IVS01001 (from 1.1.1999 to 31.12.2001)

	$x_p[\mu\text{as}]$		$y_p[\mu\text{as}]$		$dUT1[\mu\text{s}]$		$d\epsilon[\mu\text{as}]$		$d\psi \sin \epsilon_0[\mu\text{as}]$	
	MFE	WRMS	MFE	WRMS	MFE	WRMS	MFE	WRMS	MFE	WRMS
AUS	114.1	122.7	94.0	118.5	5.1	6.3	63.9	61.1	65.1	57.3
BKG	109.1	88.1	90.1	86.9	5.3	7.1	65.4	61.1	66.5	67.8
GSF	109.4	96.4	88.7	86.1	4.6	6.8	80.2	61.2	82.4	67.4
IAA	92.9	78.5	78.8	72.0	4.0	4.1	70.2	58.6	71.5	65.1
SPU	90.2	61.0	73.0	59.3	3.9	4.4	63.9	50.7	65.4	58.1
USN	109.2	98.3	88.4	70.6	4.6	3.5	80.4	73.1	82.3	76.1
mean formal precision of combination										
IVS	61.2		51.4		2.7		37.8		38.6	

A more realistic assessment of the errors can be carried out by comparing the IVS combined series with EOP series of other techniques or combination products where other techniques play an important role. For this reason, the combined IVS EOP series is regularly compared with the IERS C04 and the Bulletin B series [5]. Most important is the comparison of the combined VLBI EOP series with an EOP series derived from the results of an independent technique of similar quality, for example GPS. Weighted mean differences are  $-11.5 \mu\text{as}$ ,  $23.1 \mu\text{as}$  and  $-3.5 \mu\text{s}$  for x pole, y pole and UT1-UTC with weighted RMS differences of  $101.1 \mu\text{as}$ ,  $93.7 \mu\text{as}$  and  $5.6 \mu\text{s}$ . Figure 1 shows the weighted differences for the period from Jan. 1, 1999 to Dec. 31, 2001 for the y pole component. The rate of  $26.5 \mu\text{as}/\text{y}$  which can be seen is due to the use of different TRF.

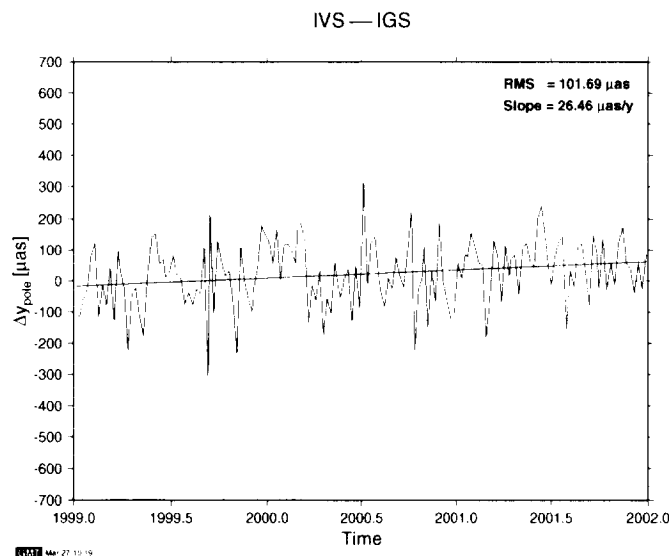


Figure 1. Differences between IVS01001 and IGS ( $y_p$ )

## 2. Outlier Detection

In order to increase the reliability of the combined EOP series, the input data is routinely being checked for outliers prior to the final combination. In a preliminary combination, residuals are computed for all input series relative to EOP from a provisional combination. As a test statistic the ratio of the combination residual  $v_k$  and its postfit standard deviation  $\sigma_{v_k}$  is then calculated for each component and each input series independently (eq. 1):

$$\tau_k = \frac{v_k}{\sigma_{v_k}} \quad (1)$$

$$|\tau_k| > \tau_{\alpha;n-u;n} \quad (2)$$

with  $\tau_{\alpha;n-u;n}$  = percentage point of  $\tau$ -distribution;  $n$  = number of observations;  $n - u$  = degree of freedom;  $1 - \alpha$  = significance level. An outlier at the significance level of  $1 - \alpha$ , for example 95%, is detected if the absolute value of the test statistic is greater than the respective percentage point of the central  $\tau$ -distribution [4]. Since all components are always combined rigorously, i.e. with the corresponding covariances, in this example  $n$  is 12 (3 components  $\times$  4 ACs) and  $n - u$  is 9. The outliers will be reported to the respective Analysis Centers with a request for further tests or for recomputation of the data point.

As a numerical example for the outlier detection, table 3 lists the  $dUT1$ -residuals for Jan. 5 2000 with, at that time, only four IVS Analysis Centers. The percentage point of the  $\tau$  distribution is 2.44. Looking at the values for all input series we find that the IAA data point has a value above the  $\tau$ -distribution limit. Hence this data point is marked as suspicious and is not included in the final combined data point.

Table 3. Numerical example for outlier detection; epoch Jan. 5, 2000; parameter  $dUT1$

AC	$v_k$ [ $\mu s$ ]	$\sigma_{v_k}$ [ $\mu s$ ]	$ \tau_k $ [-]	outlier ?
BKG	-5.1	3.3	1.55	-
GSF	1.1	3.7	0.30	-
IAA	14.7	5.7	2.57	yes
SPU	-3.2	5.7	0.56	-

## 3. New Combined Series IVS02001

The use of ITRF2000 station coordinates as the basis for the IVS combined series is the most recent step towards the generation of a consistent chain from the quasi-inertial frame of radio sources to a commonly accepted conventional terrestrial reference system. While the IVS01001 series was referred to the IERS C04 series through constant biases as described in 1 the new combined series IVS02001 is consistently linked to the ITRF2000. This has been made possible through the fact that almost all IVS Analysis Centers produce EOP series which either use ITRF2000 station coordinates as fixed input parameters or constrain their solutions to ITRF2000 on a no-net-translation and no-net-rotation basis.

The way the new combined series is computed differs only slightly from the way in which the series IVS01001 has been generated. The weight factors are computed in the same fashion as it is described in [2]. Although one would expect that all ITRF2000 based input series have a zero mean relative to the combined series, this is not the case at the level of several tens of microarcseconds. In order to eliminate the effects of these small scale systematics, we first generated a preliminary reference series for the period between January 1, 1999, and December 31, 2000. After extensive

tests an arithmetic mean of four input series from Geoscience Australia (OCCAM), Bundesamt für Kartographie und Geodäsie (CALC/SOLVE), Goddard Space Flight Center (CALC/SOLVE) and Institute for Applied Astronomy (OCCAM) has been computed. These series were chosen to give a good balance between the two different analysis software packages which are used at the IVS Analysis Centers. This preliminary reference series meets the consistency requirements as best as is possible under the current circumstances.

For all input series we then computed bias and rate terms with respect to the reference series in order to minimize possible AC-specific impacts on the combination (table 4). The bias terms are not really informative here since they depend on the reference epoch. Average magnitudes are  $-35.0 \mu\text{as}$  to  $30.0 \mu\text{as}$  at the center of the determination period.

Table 4. Rates and weight factors used in combination IVS02001 (determination period: 1.1.1999 - 31.12.2000)

	$x_p$ [ $\mu\text{as}/\text{y}$ ]	$y_p$ [ $\mu\text{as}/\text{y}$ ]	$dUT1$ [ $\mu\text{s}/\text{y}$ ]	w.f. [-]
AUS	-20.6	-11.1	0.3	1.22105
BKG	-24.2	10.2	0.0	0.94785
GSF	15.9	22.6	-0.2	1.13326
IAA	38.5	18.1	-1.0	1.08235
SPU	-45.6	-9.6	1.3	0.68767
USN	17.5	28.6	-0.2	1.15541

As compared to the IVS01001 series some of the weight factors had to be adjusted considerably. The validity of the reduction in the weight of the SPU series can easily be justified with the comparably large scatter of the nutation residuals (figure 2). It is quite understandable that a large scatter in the nutation residuals also has an impact on the other EOP components.

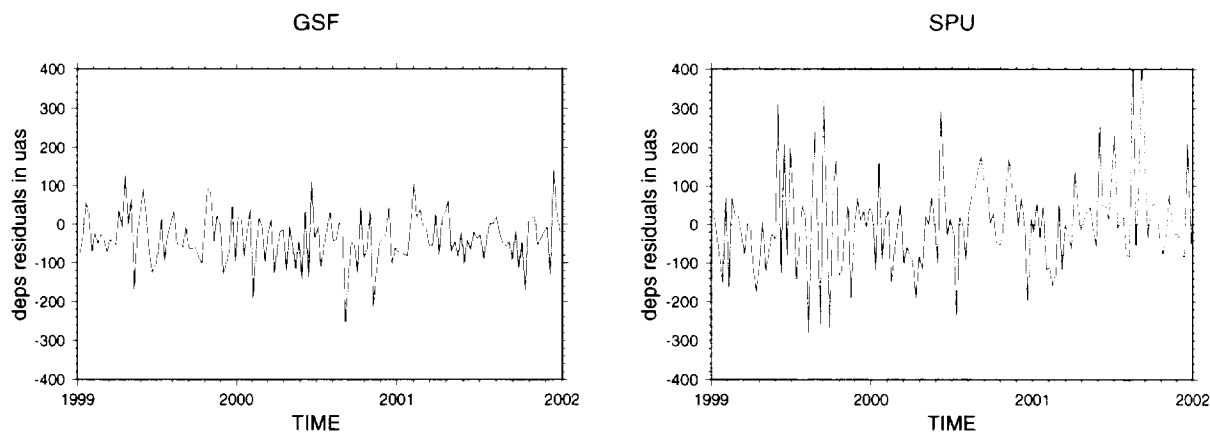


Figure 2. Comparison of  $d\epsilon$ -residuals relative to combination

Due to the fact that by now six IVS Analysis Centers regularly submit EOPs to the IVS Data Centers and due to the better agreement of the series (see below) outliers can be eliminated more reliably. As a numerical example for the outlier detection in the new combined series IVS02001 table 5 summarizes the  $y_p$ -residuals for July 2nd, 1999. In this example, the corresponding percentage point is  $\tau = 2.70$ . There is one data point in the series of the IAA which seems to be an outlier relative to the combination.

The final combination of polar motion and UT1-UTC is calculated using the full variance and

covariance information according to

$$x_{j,combi} = \frac{\sum_{i=1}^n f_i p_{x_{ij}} (x_{ij} - (rate_{i,x} \cdot MJD_j - b_{i,x}))}{\sum_{i=1}^n f_i p_{x_{ij}}} \quad (3)$$

with  $x_{ij}$  = observation;  $p_{x_{ij}}$  = input weight;  $f_i$  = weight factor;  $rate_{i,x}$  = rate relative to reference series (cf. table 4);  $b_{i,x}$  = y-axis intercept of straight line fit;  $j$  = epoch;  $n$  = number of Analysis Centers. For the combination of the nutation offsets no rates and biases are applied. The covariances are omitted in eq. 3 for clarity reasons.

Table 5. Numerical example for outlier detection in IVS02001; July 2, 1999; parameter  $y_p$

AC	$v_k$ [ $\mu as$ ]	$\sigma_{v_k}$ [ $\mu as$ ]	$ \tau_k $ [-]	outlier ?
AUS	-48.9	130.7	0.37	
BKG	-175.2	210.7	0.83	
GSF	-95.0	109.8	0.87	--
IAA	340.8	113.1	3.01	yes
SPU	-183.8	280.3	0.66	---
USN	-98.6	111.3	0.89	--

The averaged formal errors of the input series, the resulting WRMS relative to the combination and the mean internal precision of the combined series are listed in table 6. In some cases Analysis Centers used the change over from the IVS01001 to the IVS02001 solution for their transition to a different TRF realization. Station coordinates which were determined in pure VLBI solutions were replaced by fixed ITRF2000 coordinates. Other Analysis Centers map the VLBI coordinates onto ITRF2000 by using no-net-translation and no-net-rotation constraints. For this reason, the weighted RMS scatter of the post combination residuals also changed as a consequence of the new combination. In addition, the fixed ITRF2000 coordinates sometimes lead to slightly increased mean formal errors. The results of the new combination are, as usual, published on the IVS Analysis Coordinator's webpage both in graphical and in numerical representation.

Table 6. Mean formal errors (MFE) of input and WRMS relative to combination IVS02001 (from 1.1.1999 to 31.12.2001)

	$x_p[\mu as]$		$y_p[\mu as]$		$dUT1[\mu s]$		$de[\mu as]$		$d\psi \sin \epsilon_0[\mu as]$	
	MFE	WRMS	MFE	WRMS	MFE	WRMS	MFE	WRMS	MFE	WRMS
AUS	114.1	95.0	94.0	98.2	5.1	4.4	63.9	52.6	65.1	56.3
BKG	140.4	128.6	119.3	113.2	5.7	7.1	74.4	72.7	75.8	74.6
GSF	109.4	57.9	88.7	49.6	4.6	2.6	80.2	56.5	82.4	57.8
IAA	91.6	98.9	77.3	90.6	3.9	4.3	68.9	64.5	70.3	61.4
SPU	129.8	112.5	99.3	85.6	5.4	4.5	76.5	101.0	79.4	115.6
USN	109.2	61.3	88.4	51.6	4.6	2.9	80.4	56.0	82.3	57.6
mean formal precision of combination										
IVS	43.1		38.2		2.1		35.7		36.6	

Compared to the results listed in table 2 the IVS02001 series shows a better internal precision and a better consistency, but the formal precision seems to be even more optimistic than of the old

combined series. The reason for the better consistency is the more homogenous use of identical or very closely matching station coordinates. On March 1st, 20002, the new combined series IVS02001 has replaced the old series IVS01001.

The comparison of IVS02001 with the IGS series shows a much better agreement in terms of the WRMS differences. However, the bias in the y component of more than 300  $\mu\text{as}$  which is equivalent to almost 1 cm at one Earth radius is rather puzzling. Although the IGS only changed from ITRF97 to ITRF2000 station coordinates on December 2, 2001, the EOPs on the basis of ITRF97 should be fairly consistent with those after Decenber 2001 since both ITRFs are fairly consistent and since there is no obvious impact on the differences (see figure 3). The use of the ITRF97 coordinates by IGS in the first period of the comparison can, thus, not be the reason for the significant bias. Without a more detailed investigation there is no obvious explanation yet.

Table 7. Weighted mean differences and wrms IVS02001 - IGS (from 1.1.1999 to 31.12.2001)

	$x_p[\mu\text{as}]$	$y_p[\mu\text{as}]$	$dUT1[\mu\text{s}]$
WMEAN	-77.0	319.5	6.5
WRMS	95.4	85.4	5.9

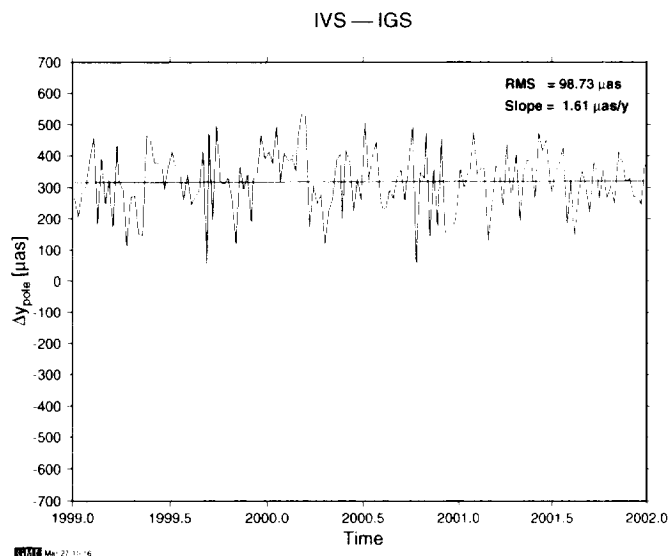


Figure 3. Differences between IVS02001 and IGS ( $y_p$ )

## References

- [1] Cannon, W. H., Comments on VLBI as a Fundamental Geodetic Positioning Technique and IVS Combined VLBI Products, Memo electronically available under <http://giub.geod.uni-bonn.de/vlbi/IVS-AC/divers/cannon.html>
- [2] Nothnagel, A., C. Steinforth, Analysis Coordinator Report 2000, In: International VLBI Service for Geodesy and Astrometry 2000 Annual Report, NASA/TP-2001-209979, N. R. Vandenberg and K. D. Baver (eds.), 55-64, 2001.
- [3] Nothnagel, A., C. Steinforth, Analysis Coordinator Report 2001, In: International VLBI Service for Geodesy and Astrometry 2001 Annual Report, N. R. Vandenberg and K. D. Baver (eds.), to be published

- [4] Koch, K.-R., Parameter Estimation and Hypothesis Testing in Linear Models, Springer, Berlin
- [5] <http://hpiers.obspm.fr/eop-pc>

# Statistical Assessment of Subdiurnal Earth Orientation Parameters from VLBI

*Hansjörg Kutterer, Volker Tesmer*

*Deutsches Geodätisches Forschungsinstitut (DGFI)*

*Contact author: Hansjörg Kutterer, e-mail: [kutterer@dgfi.badw.de](mailto:kutterer@dgfi.badw.de)*

## Abstract

Very Long Baseline Interferometry (VLBI) permits the direct determination of Earth orientation parameters (EOP) in subdiurnal resolution. For this reason, it enables monitoring of regular geophysical effects on this time scale such as EOP variations due to subdiurnal ocean tides. The question is if singular effects on the Earth rotation can also be detected which are, e.g., excited by earthquakes. Since the EOP are determined by means of a least-squares adjustment, the statistical properties of highly resolved EOP are of particular interest. Besides the analysis of VLBI session configurations, statistical hypothesis tests can be performed to assess the significance of the estimated EOP.

In this paper, eleven parallel NEOS-A and CORE-A sessions are considered. The data are processed using the software package OCCAM 5.0 LSM. The estimated EOP of each session and their variance-covariance matrices show a clear dependency of the precision and the correlations of the estimated EOP on the chosen temporal resolution. In addition, there is a strong relevance of the representation of the terrestrial and celestial reference frame by the VLBI antennas and the radio sources. The statistical significance of the highly resolved EOP decreases with increasing resolution. For this reason there is a limit for the magnitude of detectable geophysical causes.

## 1. Introduction

One expectation concerning the very high resolution of Earth orientation parameters (EOP) reads as: The signals in the EOP on the subdiurnal scale which are induced by geophysical processes are revealed more and more clearly with increasing resolution. This is true for regular events if the considered time span is sufficiently long to reduce the noise level and to separate neighbouring frequencies. However, in case of singular events this procedure can obviously not be applied. The noise which is caused by the observation and evaluation process as well as configuration weaknesses have to be considered in the quality assessment of highly resolved EOP (hr-EOP).

Therefore it is worthwhile to study the estimated hr-EOP series and their variance-covariance matrices (vcv) from an algebraic and statistical point of view regarding their ability to indicate effects caused by singular events. For this purpose a set of eleven parallel CORE-A and NEOS-A sessions is discussed in the following with respect to the particularities of the configurations and the significance of the estimated signals. Formal details are omitted; they can be found in [1].

## 2. Considered Sessions and Data Processing Specifications

The station-date matrices of the considered sessions are given in Figure 1, the numbers of observed sources in Figure 2 and the numbers of observations in Figure 3. The sessions were chosen representatively from the time interval between 1997 and 2000. In the CORE-A program the participating stations vary significantly whereas in the NEOS-A program the configuration is

stable. On average, the number of sources of NEOS-A is higher than of CORE-A but the number of observations is similar for both programs. Note that the average number of observations per station is higher for NEOS-A. CORE-A shows a typical geographical coverage of more or less the complete northern hemisphere including the South African HARTRAO and the Australian HOBART26. The NEOS-A stations represent only the northern quartersphere east of the Greenwich meridian.

CORE-A	25.03.97	08.04.97	09.09.97	22.09.98	20.10.98	01.12.98	13.07.99	21.09.99	14.12.99	21.03.00	18.04.00
GILCREEK											
ALGOPARK											
WESTFORD											
MATERA											
MEDICINA											
HARTRAO											
TSUKUB32											
HOBART26											

NEOS-A	25.03.97	08.04.97	09.09.97	22.09.98	20.10.98	01.12.98	13.07.99	21.09.99	14.12.99	21.03.00	18.04.00
KOKEE											
ALGOPARK											
NRAO20											
FOR TLEZA											
NYALES20											
WETTZEIL											

Figure 1. Station-date matrices for the considered CORE-A (left) and NEOS-A (right) sessions.

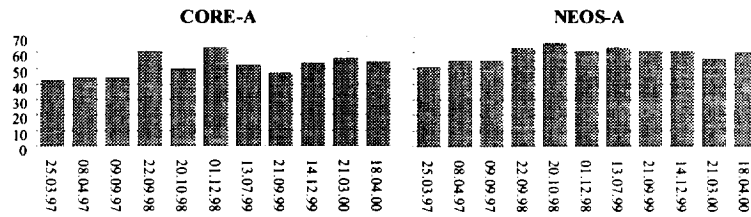


Figure 2. Numbers of sources in the considered sessions.

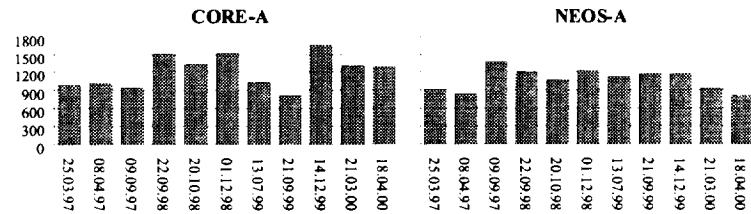


Figure 3. Numbers of observations in the considered sessions.

The offsets of the EOP with respect to the IERS C04 series were estimated for each network. Corrections due to diurnal and semidiurnal variations of the EOP were applied to the observations by means of the Ray model [2]. Different temporal resolutions were studied by halving the time intervals successively starting with a length of 24 hours and ending with 0.75 hours. The VLBI data were processed at the DGFI in Munich, Germany, using the OCCAM 5.0 LSM software. The positions of the VLBI antennas were fixed to their respective ITRF 2000 positions and the positions of the radio sources to the ICRF Ext. 1. The nutation parameters were fixed to the MHB 2000 model according to the IERS Conventions 2000 [3]. The coordinates of the pole as well as  $\Delta UT1$  were treated without constraints.

### 3. Average Precision of the hr-EOP

The average mean errors of the estimated  $\Delta UT1$  parameters are given in Figure 4 as precision measures session by session and resolution by resolution. Three results are important to mention. First of all, the precision of the CORE-A sessions is significantly better than the precision of the NEOS-A sessions. This holds for each temporal resolution. For a standard diurnal EOP resolution the obtained precision is in both cases better than  $5 \mu s$ . Second, in both programs the precision decreases with increasing resolution. Third, as a rule of thumb it holds that the higher the number of stations in the session and the more global their distribution, the better is the precision of the estimated EOP. However, exceptions from this rule are given: The CORE-A session of 08.04.97 shows considerably good results although there are only five participating stations and relatively few observations and sources (see Figures 1-3). On average, the precisions of the NEOS-A sessions of 01.12.98 and 14.12.99 are obviously better than the precisions of the NEOS-A sessions of 08.04.97 and 20.10.98 despite the homogeneity of the NEOS-A session configurations.

Some further results are briefly mentioned. The precisions of the hr-EOP within the same session are inhomogeneous which means that temporally successive EOP estimates have different standard deviations. The higher the temporal resolution the more dominant is the effect of the observation configuration (including the scheduling) on the precision. Actually, the available number of observations per time interval is of secondary importance. Please note that the results obtained for the position of the pole are similar to the ones presented here.

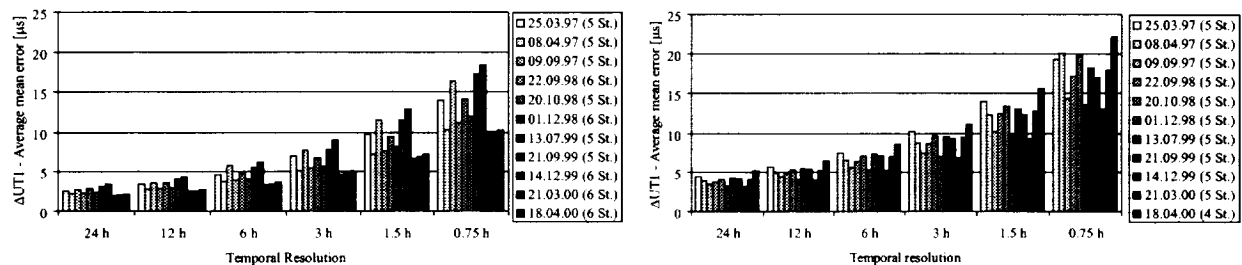


Figure 4. Average mean error of  $\Delta UT1$  for the considered CORE-A and NEOS-A sessions.

### 4. Correlation of the hr-EOP

Besides the mean errors, the correlations of the estimated hr-EOP reflect the quality of the configuration and scheduling. In Figure 5 two correlation scenarios are given representatively. The correlation coefficients are derived from the theoretical vcm of the estimated EOP. The CORE-A session of 21.03.00 yields nearly optimum results as there are neither significant inter-type nor intra-type (i.e. temporal) correlations of the estimated hr-EOP. This is in contrast to the results of the NEOS-A session of 09.09.97 with a negative inter-type correlation between  $x_{pole}$  and  $\Delta UT1$  and strong positive intra-type correlation, most prominent for  $x_{pole}$ , but also for  $y_{pole}$  and  $\Delta UT1$ . The analysis of the precision and of the correlation of the hr-EOP indicates that the common white-noise assumption for the estimated values (mainly equal variances and uncorrelatedness) does not hold from a theoretical point of view. As the inter-type correlation does not depend on the temporal resolution, it is probably caused by the geographical distribution of the participating stations.

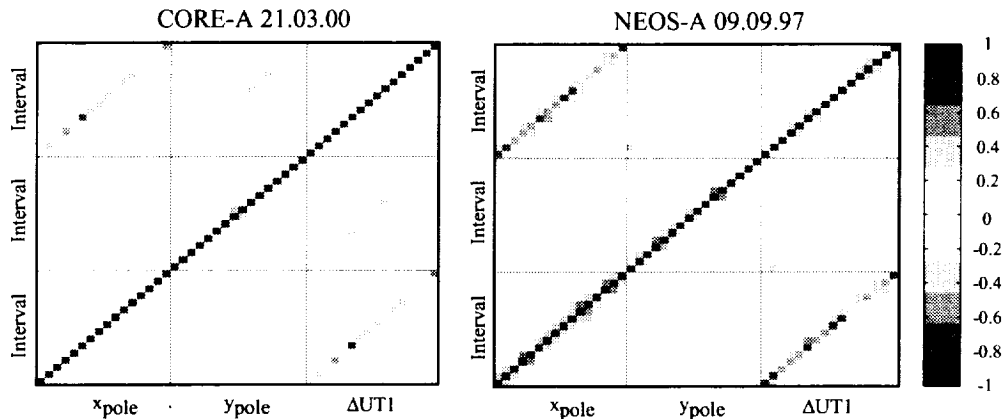


Figure 5. Correlation matrices of the estimated EOP in case of 1.5 h resolution. The main diagonals are plotted from bottom left to top right. The values are given type by type in chronological order.

### 5. Significance Test of the Higher Resolution

In order to check the benefit of an increased temporal resolution of the EOP, the corresponding reduction of the sum of squared residuals can be tested for significance by means of an F-test. The results are given in Figure 6 for the transitions between the different temporal resolutions both for the CORE-A and NEOS-A sessions. There is a weak significance in case of CORE-A sessions down to a temporal resolution of about 1.5 h. The significance is even weaker for the NEOS-A sessions. As the denominator of the test statistics is controlled by the variances of the observations, the significance would be reduced in its most parts if the observation variances were increased by a factor of 2. It would even vanish if a factor of 5 was applied.

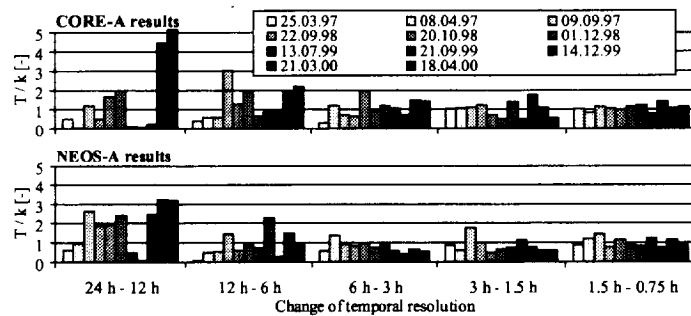


Figure 6. Significance of an increased temporal resolution of the EOP (pole coordinates and  $\Delta UT1$ ): The values of the test statistics  $T$  divided by the 0.99 fractile value  $k$  of the respective F-distribution are plotted; values greater than 1 are significant. Please note that diurnal and semidiurnal tidal signals according to the Ray model [2] were removed from the estimated EOP before the test.

### 6. Test of the Differences Between Parallel CORE-A and NEOS-A Sessions

A second significance test was performed to check the difference between the estimated hr-EOP from parallel CORE-A and NEOS-A sessions. The results are shown in Figure 7. Nearly all values

are less than 2. Thus, they are very weakly significant. As it was stated in the previous section, the increase of the observation variances by a certain factor would eliminate the significance. If one regards the difference between CORE-A and NEOS-A as accuracy measure, the application of the factor 2 would do the job. Note however that this argument is purely qualitative just to give an idea of the problems associated with the statistical significance of estimated hr-EOP. In addition, there is no dependency of the presented values on the temporal resolution.

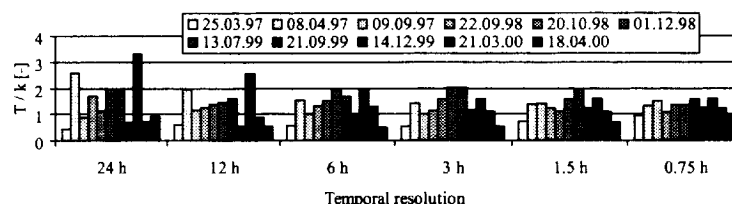


Figure 7. Significance of the differences of EOP from parallel CORE-A and NEOS-A sessions (pole coordinates and  $\Delta UT1$ ): The values of the test statistics  $T$  divided by the 0.99 fractile value  $k$  of the respective  $F$ -distribution are plotted; values greater than 1 are significant. Please note that diurnal and semidiurnal tidal signals according to the Ray model [2] were removed from the estimated EOP before the test.

## 7. Conclusions

The statistical quality of highly resolved EOP depends mostly on the particular configuration and scheduling of the sessions comprising the involved stations and sources as well as the number of observations. Inhomogeneities of the precision as well as considerable inter-type and intra-type correlations of the hr-EOP are found in the considered sessions. Taking the weak statistical significance of the estimated values and the surely too optimistic stochastic model of the VLBI observations into account, it is at present not likely to detect effects of singular geophysical events in the Earth rotation variations. For this reason it is recommended to develop and to apply a dedicated scheduling for the determination of hr-EOP to increase their precision and to decrease their correlation. As the present efforts of the International VLBI Service for Geodesy and Astrometry aim at globally distributed networks observing 24 hour sessions at short time intervals the situation will probably improve in the near future. Nevertheless it is recommended to study the new sessions as presented here. Further studies should also focus on the refinement of the stochastic model for the VLBI parameter estimation towards a more realistic formulation and on the benefit of VLBI-GPS combined determination of hr-EOP.

## References

- [1] Kutterer, H., V. Tesmer, Subdiurnal earth orientation parameters from VLBI-networks - determinability and significance, In: Proceedings of the IAG 2001 Scientific Assembly "Vistas for Geodesy in the New Millenium", Springer, Berlin (in print), 2002.
- [2] McCarthy, D.D., IERS Conventions (1996), IERS Technical Note 21, Obs. de Paris, 1996.
- [3] McCarthy, D.D., IERS Conventions (2000), Draft Version, 2001.

## RDV Analysis and Mark 4/VLBA Comparison Results

David Gordon

*Raytheon ITSS/NASA Goddard Space Flight Center*

*e-mail: [dgg@leo.gsfc.nasa.gov](mailto:dgg@leo.gsfc.nasa.gov)*

### Abstract

The processing of the RDV sessions and problems encountered in their analysis are briefly discussed. Results of a VLBA/Mark 4 correlator comparison are presented. Comparison of group delays in session RDV22 processed by two different correlating/fringing systems shows good agreement, with an RMS of  $\sim 12$  psec. Group delay formal errors may be underestimated in the RDV processing.

### 1. RDV Sessions

The RDVs, a joint VLBI program of NASA/GSFC, USNO, and NRAO scientists, use the 10 VLBA antennas and up to 10 additional Mark 4 antennas. Six RDVs experiments have been observed per year since 1997. Correlation is done on NRAO's VLBA correlator in Socorro, New Mexico, which produces cross-spectral visibility data. Further processing, to produce group delays, phases, and phase delay rates has been done at the GSFC Analysis Center using the NRAO analysis package AIPS. This processing involves phase calibration, fringing, computation of total delays and rates, conversion of observables from geocentric to reference station time tags, and reformatting the data into the Calc/Solve analysis system.

VLBA antennas are equipped with decoders which extract the phase calibration phases at two tones in each base band converter (BBC). These phases, interpolated to the middle frequency of each BBC, as well as a phase cal group delay for each BBC, have been used in the AIPS fringing and have been found to improve the results by a small amount ( $\sim 10$  psec in an RSS sense) compared to the use of manual phase (constant offset) calibration. The VLBA correlator itself cannot extract phase cal phases, therefore phase cal information at the Mark 4 stations is lost since they have no phase cal extraction capability. For this reason manual phase calibration has been applied for all the Mark 4 antennas in all the RDVs. Table 1 summarizes the major differences between the RDV sessions and Mark 4 sessions.

Some peculiarities were noticed early on in the analysis of the RDVs, although it was never fully understood what the problems were. The Solve solutions did not "look" the same as sessions processed through the Mark 3/4 correlators. There seemed to be a problem with excess noise for southern sources, and this phenomena came to be known as the "southern source" problem. The ratio of the square of a partial weighted sum of residuals for each source to its mathematical expectation exceeds 1 predominately for sources with southern declinations. This effect also shows a strong seasonal pattern, being greatest in the warm, humid (northern hemisphere) months, and almost non-existent in the colder, drier months. Such a pattern though is typical in geodetic VLBI.

The performance of the RDVs and the VLBA sites have been studied in several ways. Source positions obtained from the RDVs alone agree well with those obtained from Mark 3/4 sessions. Baselines with a VLBA site (coming primarily from the RDVs and earlier VLBA correlated sessions) show the best baseline length repeatability of all baselines (Figure 1). However, the chi-

Table 1. Differences in VLBA and Mark 4 Geodetic VLBI

VLBA	Mark 4
4 X, 4 S band channels, 8 MHz bandwidth	8 X, 6 S band channels, 2 to 8 MHz bandwidth
FX correlator, produces cross-spectral data	XF correlator, produces lag data
Correlated data processed by AIPS	Correlated data processed by Fourfit
Phase calcs extracted by a VLBA decoder at VLBA stations, lost for Mark 4 stations	Phase calcs extracted by Mark 4 correlator for all stations
Uses two phase cal tones at 10 and 7010 kHz and BBC single band delays	Uses one phase cal tone at 10kHz

square per degree of freedom of the residual baseline lengths show the largest values of all baselines (Figure 2), implying that the formal uncertainties of the baseline lengths derived from RDV experiments are systematically underestimated.

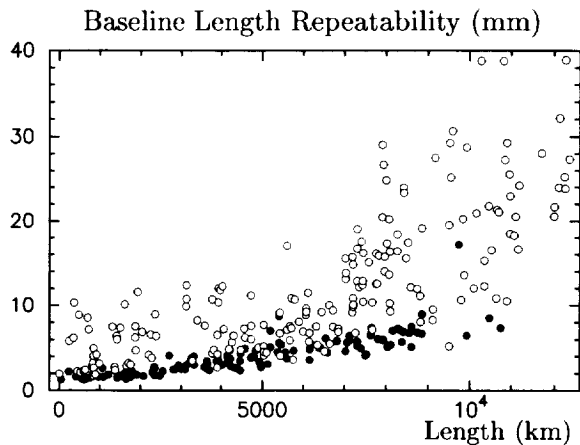


Fig. 1

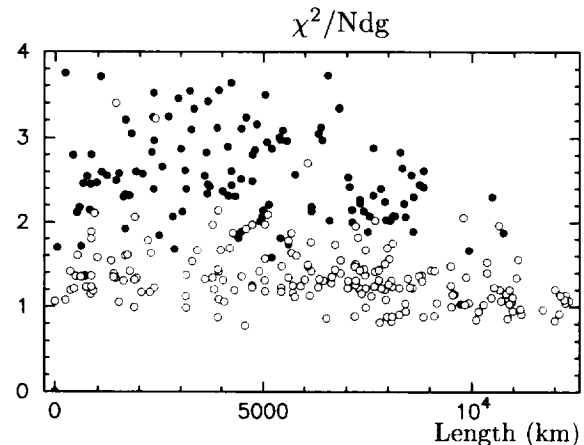


Fig. 2

Solid circles - baseline with a VLBA station at one or both ends.  
 Open circles - baselines with Mark3/Mark4 stations at both ends.

Baseline length evolution plots combining Mark 3/4 data with RDV data show no significant biases for the RDV points, except on Onsala baselines. The explanation for this seems to be a strong azimuthal dependence of the Onsala phase calcs and cable calcs, which introduces a bias when manual phase calcs are used. Modeling and correcting for this effect seems to be possible though.

In order to address the problems seen in the RDVs, a partial correlator comparison was planned for the RDV22 session (2000 July 6). Tapes from 8 stations (LA, PT, KP, BR, MK, OV, GC,

and KK) were forwarded to Haystack Observatory and, after considerable software enhancements, were correlated on the Mark 4 correlator and fringed with Fourfit. Two fringings were made, using extracted phase calcs and manual phase calcs. These were compared to AIPS fringings, both with manual and measured phase calcs. A third type of processing was also made, a hybrid of the Mark 4 and AIPS. The Mark 4 correlator output was input into AIPS using program MK4IN (recently developed by Walter Alef et al. at Bonn), which converts the Mark 4 lag data into cross-spectral data. The resulting AIPS file was fringed using manual phase calcs.

## 2. RDV22 Comparisons Using Measured Phase Calcs

The first Mark 4 fringing of RDV22 was made to match the standard AIPS processing. Extracted phase calcs at 10 kHz (plus additive phases as needed) were applied to the six VLBA sites, and manual phase calcs to the two Mark 4 sites. The same 8 stations in the VLBA/AIPS version were refringed, also using the measured phase calcs at the VLBA sites and manual phase calcs at the two Mark 4 sites. The two tones, at 10 and 7010 kHz, were linearly combined to give a value at the BBC mid-frequency (4000 kHz). Time tags were made to match those of the Mark 4/Fourfit version. Direct comparisons of the observed group delays were then made, after subtracting out average differences for each baseline. These comparisons show group delay differences that are systematic with elevation, at levels of typically 10-30 psec. These systematic effects were found to be the result of elevation dependent differences in the two sets of measured phase calcs. The 10 and 7010 kHz tones show group delay differences that are systematic with elevation, in patterns that vary by station, by up to 50 psec or so. Unless due to some spurious signals, this effect presumably represents an elevation dependence of the instrumental single band delays. As a test, the full RDV22 (18 stations) was reprocessed through AIPS using only the 10 kHz tone. This 10 kHz version was found to give a slightly noisier Solve solution, and the reprocessing had no effect on the scatter of residuals for southern sources. Thus, the indication is that this phase cal elevation dependence is real and should be calibrated for by using the two tones. But because of the uncertainty, a change, at least temporarily, has been made for future RDVs, to record the 10 and 5010 kHz tones instead. Another suggestion that may be tried is to increase the observing frequencies by 0.5 MHz and record the phase cal tones at 510 and 7510 kHz.

## 3. RDV22 Comparisons Using Manual Phase Calcs

Next, a set of comparisons were made in which the data were reprocessed using manual phase cal offsets at all 8 stations. Manual phase calibrations, being constant offsets, cannot impose any systematic differences on the delays. Three data sets were created for this study. The three versions were:

- 1) VLBA correlated/AIPS fringed (aips)
- 2) Mark 4 correlated/Fourfit fringed (mk4)
- 3) Mark 4 correlated/AIPS fringed (hy)

Version 3, as mentioned earlier, is a Mark 4/AIPS hybrid, made by fringing the Mark 4 correlated data with AIPS. Versions 2 and 3 (same correlator) used identical manual phase calcs, whereas

version 1 used a different set. Group delays and rates were differenced between pairs of these three versions, with average baseline differences subtracted out. The remaining delay differences appear completely random, i.e. no systematic dependence on time, elevation angle, or azimuth is apparent. The RMSs of the differences compare very well, if not better than, those of recent Mark 3/Mark 4 comparisons. In Table 2 we summarize the RMSs of the delay and rate differences, sorted by baseline length. Comparison of group delay formal errors also shows good agreement, with AIPS computed formal errors averaging  $\sim 1\%$  larger than those from Fourfit.

The numbered RMS columns in Table 2 can be described briefly as: (1) same correlator (Mark 4), different fringing software; (2) different correlators, same fringing software (AIPS); and (3) different correlators, different fringing software. It is not possible to determine how correlated the different processings are, or how much of the delay differences are due to random noise-like effects versus systematic effects. Comparison (1), which should have no contribution from correlating differences, shows the least scatter, as expected, with an average RMS of 8.7 psec, and with values as little as 3.1 psec on short baselines. Between comparison (2) and (3), the largest RMSs occur when the two correlations are both fringed through AIPS. While not absolutely conclusive, this is an indication that the data emerging from AIPS is noisier than the data emerging from Fourfit, and that this excess noise is unaccounted for in the AIPS delay formal errors.

There are additional reasons to suspect the accuracy of the delay formal errors computed by AIPS. AIPS fringing is spread between three different programs, and the computation of group delays and rates can be followed fairly clearly between these three programs. However, the computation of correlated fringe amplitudes and the accounting for total integrated observing time is computed separately from the delays and rates, and is very obscure in the AIPS code. As such, it is not clear whether the fringe amplitudes and coherence coefficients are defined and/or scaled similarly to those in Fourfit. Also, the number of bits used per observation may be maximum estimates, and thus may be overestimated in some cases. AIPS determines single band delays and phases, and then makes a least squares fit to the phases to determine group delays. The computation of formal errors does not account for uncertainties in the least squares fits, nor for differences in the number of bits used per channel. Thus, there are numerous reasons to suspect the AIPS delay formal errors of being underestimated.

#### 4. Conclusions

Though this study is not absolutely definitive, a few general conclusions can be made:

- Though there is some uncertainty about how phase calcs should be used for the VLBA sites, this uncertainty cannot explain the VLBA problem and appears to be unrelated to it.
- The AIPS determined group delays have no significant biases with respect to Mark 4 processed data, and there is no indication of any problem with the VLBA Correlator.
- The AIPS determined delay formal errors may be underestimated.

Table 2. Summary of RV22 Delay and Rate Differences

Baseline	Length (km)	RMS's of delay differences (psec)			RMS's of rate differences (fsec/sec)		
		mk4-hy (1)	aips-hy (2)	mk4-aips (3)	mk4-hy (1)	aips-hy (2)	mk4-aips (3)
LA-PT	236	5.4	5.2	6.4	10.4	20.6	41.0
KP-PT	417	4.7	8.1	6.3	12.2	37.0	44.3
KK-MK	508	11.1	15.8	13.8	35.1	76.4	73.2
KP-LA	652	3.2	6.9	6.6	12.7	35.4	38.3
KP-OV	845	4.7	8.1	7.6	10.7	34.6	37.1
OV-PT	973	4.7	7.4	7.2	19.5	34.7	45.9
LA-OV	1088	4.8	7.1	7.2	14.5	29.7	36.7
BR-OV	1215	5.9	13.8	9.6	18.9	39.9	73.9
BR-LA	1757	6.1	7.8	7.7	11.2	29.3	29.4
BR-PT	1806	6.5	11.3	11.0	28.6	51.9	69.5
BR-KP	1914	8.0	10.3	9.9	15.2	49.1	56.1
BR-GC	2482	9.1	14.9	11.5	16.6	47.6	51.8
GC-OV	3584	9.3	17.3	13.7	18.0	57.1	56.7
MK-OV	4015	8.8	16.1	13.5	26.2	33.6	40.2
KK-OV	4220	13.0	17.2	16.1	26.5	80.1	75.3
GC-PT	4225	10.0	12.5	10.8	17.1	49.1	50.7
GC-KP	4323	8.9	15.3	10.5	13.0	33.7	32.6
BR-MK	4399	13.8	22.6	28.2	18.3	38.6	61.0
KP-MK	4467	8.8	15.6	9.4	19.0	46.8	31.3
BR-KK	4469	13.1	18.4	16.9	41.5	83.4	77.1
GC-KK	4728	13.6	19.9	17.7	39.3	82.9	75.4
KK-KP	4736	11.4	16.0	12.1	34.1	65.4	65.0
GC-MK	4923	13.7	19.0	16.1	19.5	51.9	82.3
LA-MK	4970	7.3	11.0	10.8	22.2	43.3	38.2
KK-PT	5040	11.7	14.6	12.0	55.2	59.6	67.4
average:		8.7	13.3	11.7	20.0	48.5	54.0

# USNO Analysis of VLBA RDV Data

Alan L. Fey, David A. Boboltz

*U.S. Naval Observatory*

Contact author: Alan L. Fey, e-mail: [afey@usno.navy.mil](mailto:afey@usno.navy.mil)

## Abstract

Previous analyses have indicated that there may be a problem with the VLBA RDV data for sources south of the celestial equator. We present an analysis of the effects of including VLBA RDV data in global VLBI SOLVE solutions on astrometric position estimation and on Earth Orientation Parameter estimation.

## 1. Introduction

Previous analyses by various individuals have indicated that there may be an “anomaly” (formerly known as the “southern source problem”) with the VLBA RDV data. The primary manifestation of this anomaly was excess normalized residual delay (NRD) and/or excessive position variation for sources south of the celestial equator. We present an analysis of the effects of including VLBA RDV data in global SOLVE solutions on astrometric position and on Earth Orientation Parameter (EOP) estimation. *Note that this is a work in progress.* Additional details concerning this investigation and a complete description of the parameterization of the global SOLVE solutions can be found at

[http://rorf.usno.navy.mil/vlba\\_rdv/](http://rorf.usno.navy.mil/vlba_rdv/)

## 2. The Data

VLBA RDV data is defined as that data obtained under the auspices of the VLBA RDV proposals and correlated at the VLBA correlator in Socorro, NM. During each 24 hour VLBA RDV session, about 70 ICRF sources are observed at S/X band using the NRAO Very Long Baseline Array (VLBA) antennas together with up to 10 additional geodetic antennas. The VLBA RDV experiments are a joint collaboration between the USNO, Goddard Space Flight Center (GSFC) and the National Radio Astronomy Observatory (NRAO). The VLBA RDV data set used here is comprised of 527410 observations (delay/phase delay rate pairs) and covers the time range from 1997 to 2000 (RDV01 to RDV24 inclusive).

MkIII data is defined as VLBI data correlated with a Mark III/IV correlator. The full MkIII data set used in this analysis covers the time range from 1979 to 2001 and is comprised of 2489280 observations. The NEOS only data set used here is comprised of 210878 observations spanning the same time period as the VLBA RDV data (NA197 to NA397).

## 3. Excess Normalized Residual Delay

Previous analyses suggested that the primary manifestation of the VLBA RDV anomaly was excess normalized residual delay (NRD) for sources south of the celestial equator. Shown in

Figure 1 are plots of NRD as a function of declination for several VLBA RDV experiments. Note that there is larger than normal NRD, i.e. greater than 1.0, for some sources but these sources are not necessarily all southern hemisphere sources. Additionally, there appears to be a seasonal effect, i.e. winter experiments appear to have fewer sources with elevated NRD than do summer experiments.

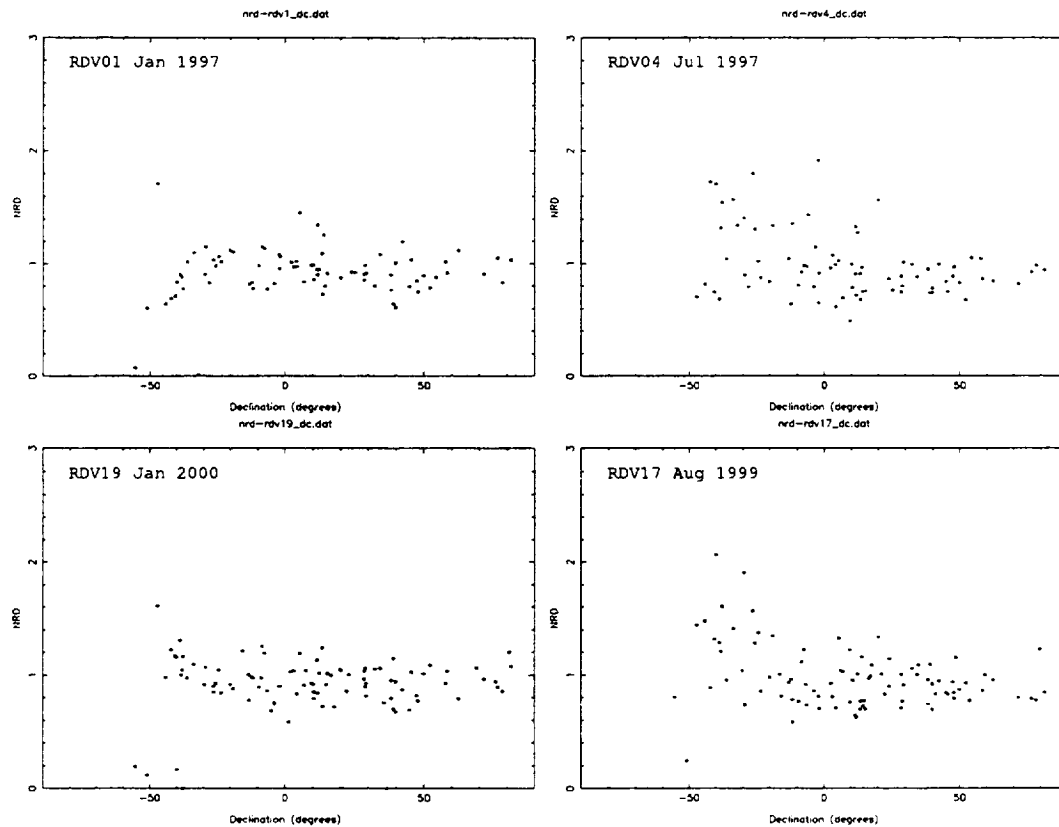


Figure 1. Normalized residual delay as a function of declination for four VLBA RDV experiments. The two panels on the left show values from winter experiments while the two panels on the right show values from experiments observed during the summer. Note the seasonal differences.

Shown in Figure 2 are results for combined solutions. With the exception of a few discrepant points, the NRD anomaly appears to almost completely disappear (or at least is extremely less well pronounced) when all the VLBA RDV data is combined into one global solution.

#### 4. Excess Position Variation

Another claimed manifestation of the VLBA RDV anomaly was excess position variation for sources south of the celestial equator. We compare statistics of “arc” positions for selected sources. Arc position time series were calculated in SOLVE global solutions using VLBA RDV data and NEOS data. Two sets of solutions were made: 1) using only VLBA RDV data (RDV01 to RDV24, inclusive); and 2) using only NEOS data from the same time period as the VLBA RDV data (NA197 to NA397). A total of 64 sources were observed with sufficient frequency in the VLBA

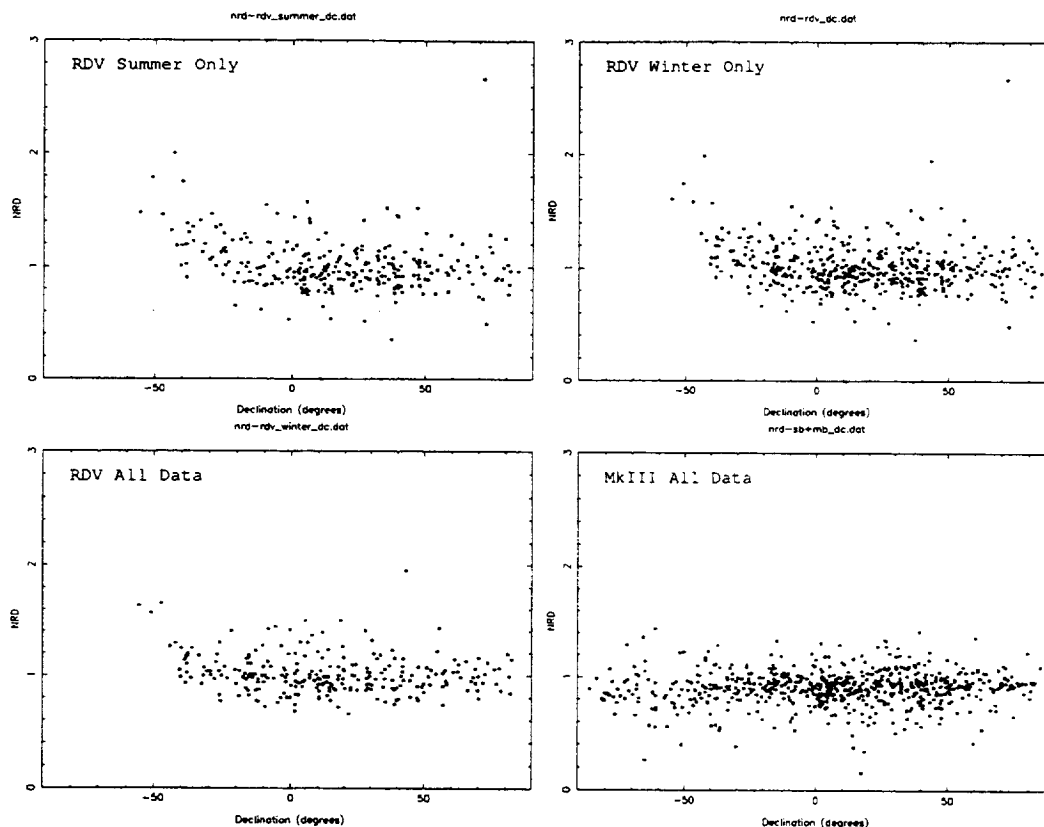


Figure 2. Normalized residual delay as a function of declination for combined VLBA RDV experiments. Note that the combined data show less seasonal differences than the individual experiments and when *all* VLBA RDV data are combined, the NRD “anomaly” almost completely disappears. The NRD for the MkIII data is shown for reference.

RDV data to estimate positions as arc parameters. Of these 64 sources, a total of 54 sources were observed with sufficient frequency in the NEOS data to estimate positions as arc parameters. Weighted root-mean-square (wrms) position residuals were calculated for each source using the GSFC program “ploser.” Results are shown in Figure 3 as a plot of wrms position residuals from the NEOS data vs. wrms position residuals from the VLBA RDV data. Sources with zero wrms are those 10 sources which had insufficient data in the NEOS experiments to calculate wrms position residuals. Note that the NEOS data has much larger wrms residuals than the VLBA RDV data for *all* sources in both right ascension and declination.

### 5. Effect on Position Estimation

A number of SOLVE global solutions were made for the specific purpose of position estimation. Source positions were estimated as global parameters in these solutions. The only differences between different solutions were the included data (eg. MkIII only, VLBA only, MkIII+VLBA, etc.). Source position global differences are listed in Table 1.

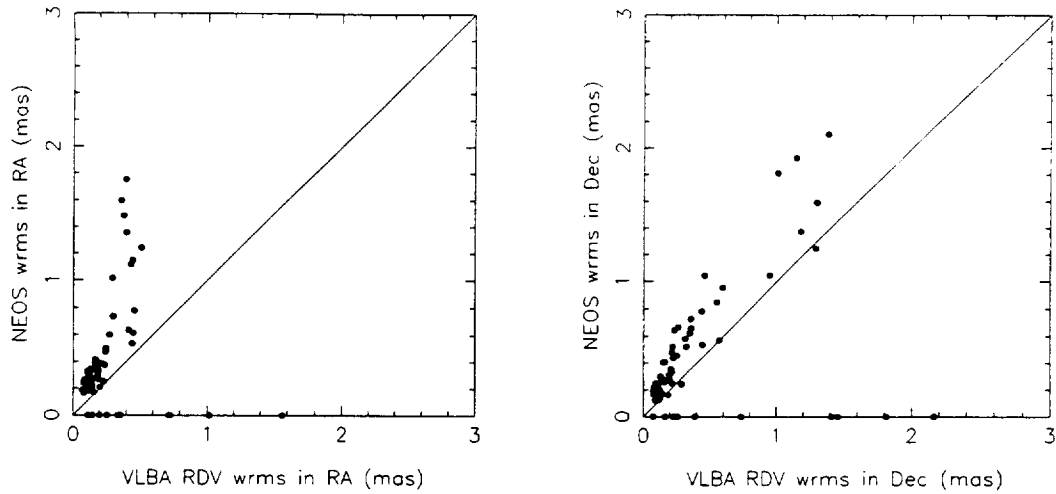


Figure 3. Weighted root-mean-square (wrms) position residuals derived using only NEOS data vs. wrms position residuals derived using only VLBA RDV data.

Solution Pair	RA mean (mas)	RA wrms (mas)	Dec mean (mas)	Dec wrms (mas)
MkIII/VLBA	-0.005	0.108	0.023	0.117
MkIII/VLBA Winter	0.003	0.102	0.030	0.114
MkIII/VLBA Summer	-0.015	0.123	0.014	0.137
VLBA Summer/Winter	0.016	0.085	0.019	0.104
<b>MkIII+VLBA/MkIII</b>	<b>0.000</b>	<b>0.031</b>	<b>-0.007</b>	<b>0.039</b>

Table 1. Weighted position differences for various solution pairs.

### 6. Effect on EOP

Two SOLVE global solutions were made for the specific purpose of EOP estimation. Wrms differences in X, Y, UT1,  $\Delta\Psi$  and  $\Delta\epsilon$  between different solutions are listed in Table 2. Comparison is made only for the time range 1997 to 2001. Solutions made at the USNO which include only the MkIII data are labeled USNO and solutions which include both the MkIII and the VLBA RDV data are labeled USNO+VLBA. Comparison is also made to the GSFC 2001c solution and to the IERS C04 series. These latter two comparisons are made for the time range 1996 to 2001. A slope and bias have been removed in all comparisons before calculation of the wrms.

Solution Pair	X ( $\mu\text{as}$ )	Y ( $\mu\text{as}$ )	UT1 ( $\mu\text{sec}$ )	$\Delta\Psi$ ( $\mu\text{as}$ )	$\Delta\epsilon$ ( $\mu\text{as}$ )
USNO+VLBA/USNO	76.7	72.9	3.33	143	51.6
USNO+VLBA/GSFC	77.0	94.6	3.85	160	54.5
USNO+VLBA/IERS	197	165	19.4	374	185

Table 2. Weighted EOP differences for various solution pairs.

## 7. Summary

Comparison of source positions between solutions with and without the VLBA RDV data show that differences are minimal (weighted mean and rms of  $0.0 \pm 31$  microarcsecond in right ascension and  $-7.4 \pm 39$  microarcsecond in declination). Plots of NRD (normalized residual delay) versus declination from solutions with individual VLBA RDV databases show that there is larger than normal NRD, i.e. greater than 1.0, for some sources but these sources are not necessarily all southern hemisphere sources. Additionally, there appears to be a seasonal effect, i.e. winter experiments have fewer sources with elevated NRD than summer experiments. However, in the combined solutions (i.e. solutions with all the VLBA RDV data), with the exception of a few discrepant points, the NRD “anomaly” appears to almost completely disappear (or at least is extremely less well pronounced). The NEOS data from the same time period as the VLBA RDV data have much larger weighted rms position residuals than those estimated from the VLBA RDV data. This is true for *all* sources, in both right ascension and declination. Differences in X, Y, UT1 and nutation between solutions with and without the VLBA RDV data show that the VLBA RDV data appears to have no negative effect on the global solution estimation of EOP.

# The New IERS Special Bureau for Loading (SBL)

*The SBL Team*

*For affiliation of team members, see Table 1.*

Contact author: Hans-Peter Plag, e-mail: [plag@statkart.no](mailto:plag@statkart.no)

## Abstract

Currently, the establishment of the International Earth Rotation Service (IERS) Special Bureau for Loading (SBL) is in progress as part of the IERS Global Geophysical Fluids Center (GGFC). The main purpose of the SBL is to provide reliable, consistent model predictions of loading signals that have been thoroughly tested and validated. The products will describe at least the surface deformation, gravity signal and geo-centre variations due to the various surface loading processes in reference frames relevant for direct comparison with existing geodetic observing techniques. To achieve these goals, major scientific advances are required with respect to the Earth model, the theory and algorithms used to model deformations of the Earth as well as improvements in the observational data related to surface loading.

## 1. Introduction

On 1 January 1998, the International Earth Rotation Service (IERS) established the Global Geophysical Fluids Center (GGFC) in an effort to expand IERS's services to the scientific community. Under the GGFC, seven Special Bureaus (SB) were established<sup>1</sup>. Each of these is responsible for research activities relating to a specific Earth component or aspect of the geophysical fluids of the Earth system. However, until recently, there was no specific focus on the interaction of the different components through gravitational and surface forces on the boundaries. In particular, consistent models of the deformation of the solid Earth due to loading of the atmosphere, ocean and terrestrial hydrosphere are presently not available. This is also reflected in the IERS Conventions [5], where standard models for solid Earth tides and ocean loading are discussed while no standard procedure is given for taking into account other surface loading effects.

In order to foster the development of consistent models for signals due to surface loading, the IERS on 31 October 2001 issued a Call for Proposals for a Special Bureau for Loading (SBL) with the task to promote, stimulate and coordinate the work and progress towards a service providing products related to surface mass loading. Eventually, the SBL is expected to provide in near real-time (NRT) a consistent global solution data set describing at least the surface deformation, gravity signal and geo-centre variations due to the various surface loading processes in reference frames relevant for direct comparison with existing geodetic observing techniques.

On 1 February 2002, the SBL<sup>2</sup> was formally established with a team of 10 members (see Table 1). These ten members represent expertise from all fields relevant for accurately modeling surface deformations, namely, theory of Earth deformation and Earth models, observations of surface loads, computation of tidal and non-tidal loading, space-geodetic and gravimetric observations. The team also includes the seven chairs of the already existing SBs. The chairs of the existing SBs

---

<sup>1</sup>see <http://bowie.gsfc.nasa.gov/ggfc/>

<sup>2</sup>see <http://www.gdiv.statkart.no/sbl/>

Table 1. Current Membership of the SBL

Note that the chairs of the existing SBs are members ex-officio. Currently, these are Ben Chao (Mantle), Veronique Dehant (Core), Richard Gross (Oceans), Richard Ray (Tides), David Salstein (Atmospheres), Michael Watkins (Geocenter), Clark Wilson (Hydrology).

Name	Affiliation or Function
Tonie van Dam	European Center for Geodynamics and Seismology (ECGS), Luxembourg (chair)
Hans-Peter Plag	Norwegian Mapping Authority (NMA), Norway (co-chair)
Geoffrey Blewitt	University of Nevada, Reno, U.S.A.
Jean-Paul Boy	Goddard Space Flight Center, U.S.A.
Olivier Francis	European Center for Geodynamics and Seismology, Luxembourg
Pascal Gegout	Ecole et Observatoire des Sciences de la Terre, Strasbourg, France
Halfdan Pascal Kierulf	Norwegian Mapping Authority, Norway
Tadahiro Sato	National Astronomical Observatory, Mizusawa, Japan
Hans-Georg Scherneck	Onsala Space Observatory, Sweden
John Wahr	University of Colorado, Boulder, U.S.A.

are ex-officio members of the SBL and participate in the SBL to insure close cooperation between their SBs and the SBL. Moreover, the combined membership provide the necessary links to other geodetic services and relevant projects, such as the IGS, IVS, ILRS, and the GGP.

The accuracy of the products provided through the SBL should, as much as model limitations allow, match the accuracy and precision of the space-geodetic and gravimetric observation techniques. Achieving this ambitious goal requires major scientific advances with respect to the Earth model, the theory and algorithms used to model deformations of the Earth and the observational data of surface loading. Consequently, a scientific agenda is required to perform the research necessary for the development of the models and algorithms and an operational agenda is directed towards the provision of validated products to potential users.

## 2. The Scientific and Operational Agendas

The workplan of the SBL is separated into a total of seven Work Packages. WP1 to WP4, which define the scientific agenda, address the research oriented tasks related to the different components for the computation of deformations due to surface loading, i.e. the Earth model, the theory used to compute the Earth's response to loading, and the observations of surface loads. WP5 to WP7, which define the operational agenda, will provide the product-oriented routines for the operational service and the production of research data sets. These WPs address the development of operational procedures, validation of products, and their distribution to the geodetic community.

### Work package 1: Earth model

Up to now, most loading calculations have been carried out for Spherically symmetric, Non-Rotating, Elastic and Isotropic (SNREI) Earth models. The standard model used for these calculations is the Preliminary Reference Earth Model (PREM) [2]. Computation of the Load Love Numbers (LLN) for the PREM is not straight-forward and inconsistencies have to be avoided. Moreover, it may be necessary to take into account rotation and ellipticity, viscoelasticity, the difference between continental and oceanic crusts, and eventually heterogeneous Earth models. The different options for Earth models will be evaluated and the sensitivity of the LLN and Body

Tide Love Numbers (BTLN) on computational algorithms and model differences will be studied. One SNREI and one 3-D model will be selected for the operational processing.

**Work package 2: Computation of Green's functions and convolution algorithms**

Using the LLNs, Green's functions describing the Earth's response to point loads can be computed in the space domain [3]. For SNREI models, the Green's function depends on the angular distance between load and observer only.

For ocean tidal loading, which is considered as an harmonic process, the loading signal is computed most economically in the frequency domain [3]. The resulting products are space-dependent harmonic loading coefficients, which can be determined for all harmonic tidal constituents, for which a sufficiently accurate ocean tidal model is available.

For non-tidal surface loads, the loading responses are normally computed in one of two ways: (1) Global convolution sum or point loading approach or (2) the spherical harmonic integration. It is expected that the spherical harmonic approach is considerably faster in the computation than the point loading approach. An analysis needs to be performed that weighs the benefits of reduced cpu-time offered by the spherical harmonic approach to the potential loss of accuracy.

In computing the load signals, special attention has to be devoted to the reference frame [1]. One possibility is to provide products in various frames, for example, center of mass of the entire Earth system (common in SLR), center of mass of the solid Earth (Farrell's assumption), center of figure frame (common in GPS).

The theory for rotating and elliptical models is available [11, 12, 6] and a perturbation method can be used to compute LLNs for viscoelastic, laterally heterogeneous and non-hydrostatically prestressed Earth models [6]. For the latter models, the Green's function becomes space-dependent and this complicates the computation of loading signals seriously.

**Work package 3: Surface loads**

It has been demonstrated that the effects of variations in atmospheric mass [7, 8], non-tidal ocean loading [9] and variations in continental water loading [10] can be observed in geodetic time series. As such, there are currently three global surface loads (atmospheric mass, continental water storage, and ocean bottom pressure) to be considered by the SBL. The accuracy of the available data sets needs to be evaluated before loading products can be generated.

**Work package 4: Integrated Earth system models**

Matching the accuracy expected for space-geodetic techniques within the next few years may require that we compute surface deformation, gravity changes and other relevant parameters in a consistent, integrated Earth system model. Initial considerations concerning a modular model have been published [4]. Though currently not of high priority, inclusion of WP4 signals that the development of integrated Earth system models may turn out to be unavoidable.

**Work package 5: Near-real time product generation**

It is likely that during the first year of the SBL, significant changes will take place in the algorithms and routines used for the computations. Moreover, more complete data sets for surface loads are likely to become available.

Initially, the SBL will concentrate on the computation of atmospheric loading products for the comparison with geodetic time series in the frame of a demonstration project. The initial NRT products will be flagged as a product under development made available for scientific research. Atmospherically driven loading effects will be made available for specific coordinates (e.g. all ITRF sites) and as global grids. The initial products will be computed on a SNREI model for both an oceanless and an inverted barometer ocean model. After a successful demonstration phase,

routines for the computation of Version 1 NRT products will be specified and implemented.

**Work package 6: Validation and reanalyses**

All products provided through the SBL will have to go through a thorough validation. For that, comparison of the modeled loading effects with geodetic time series will be crucial. GPS is the most globally distributed geodetic technique, and will play a central role in the validation. Additional validation through VLBI, SLR and DORIS observations will help to improve the assessment of the loading products. It is hoped that IERS will set up a coordinated validation project.

For a validation of the gravity loading corrections, observations from the approximately 30 globally distributed sites with superconducting gravimeters will be of key importance. Here, co-operation of the SBL with the Global Geodynamics Project (GGP) is a prerequisite.

Comparison of the predicted geocenter motion with those observed using low Earth orbiting satellites and made available by the SB Geocenter will provide validation for these products.

**Work package 7: Web-based distribution of products**

The main interface between the SBL and users will be through a web site providing access to all loading predictions as well as documentation of the data sets and the underlying algorithms used in the computations. The primary operational computations will be undertaken at and made available through the primary SBL web site maintained by NMA with identical mirror site at the ECGS in Luxembourg and at location to be selected in the United States.

The list of available products will eventually include but is not limited to NRT estimates of the radial and horizontal displacements, and gravity changes derived from the NCEP and ECMWF surface pressure fields; historical estimates of the deformation and gravity changes due to surface pressure, global water storage models, and ocean bottom pressure models.

In the case of the atmospheric loading estimates, results for both the case of no oceans and the inverted barometer ocean will be generated. Historical estimates will be made available as time series for at least all ITRF. Depending on the required cpu time, the historical estimates will also be made available as global grids. These grids will allow taking into account the loading signal at stations not included in one of the global networks (e.g. EUREF sites, GPS sites at tide gauges, or even campaign sites).

### 3. Outlook

It is planned that the newly established SBL eventually will provide an operational service for all geodetically and geophysically interesting signals due to surface loads. The list of relevant variables includes but is not limited to horizontal and vertical displacements, gravity changes, changes in the geoid, motion of the geocenter, and polar motion. Additionally, surface load induced relative sea level changes and changes in the length of day may become of interest. Global grided data sets with sufficient spatial and temporal resolution and time series for specific locations will be the basic means of providing these variables. All products will be computed consistently using the accepted IERS Conventions. The necessary spatial and temporal resolution of the products will depend on the accuracy requirements defined by the users and may change over time.

After validation, access to ocean tidal loading will be made available through links to existing web pages, which provide loading coefficients in agreement with the IERS Conventions.

Substantial progress is needed to provide the products with an accuracy matching the present accuracy and precision of the geodetic techniques. Moreover, the anticipated developments of these techniques over the next years will pose even higher demands on the models and algorithms used in

the computation of loading signals. It is expected that the initial version 1 products will be more of research value than being useful for e.g. corrections of station motion in real time positioning and meteorological applications of GPS.

Initially, we plan to set up a demonstration phase starting on 1 June 2001. The goal of the demonstration phase is to show that loading signals can be computed and made available in NRT. The minimum model for the demonstration phase is based on a SNREI model using the global atmospheric pressure field as input. The minimum product will be a global grid of radial surface displacement for both no ocean and inverse barometer ocean. A main contribution to the validation of the products hopefully will come from a coordinated IERS project involving all IERS techniques. It is planned to end the demonstration project by the end of 2002 and to start operational production of an extended list of products from 1 January 2003 according to standards developed by the different WPs.

## References

- [1] G. Blewitt, D. Lavallee, P. Clarke, and K. Nurutdinov. A new global mode of earth deformation: Seasonal cycle detected. *Science*, 294:2342–2345, 2001.
- [2] A. M. Dziewonski and D. L. Anderson. Preliminary reference Earth model. *Phys. Earth Planet. Int.*, 25:297–356, 1981.
- [3] W. E. Farrell. Deformation of the Earth by surface loads. *Rev. Geophys. Space Phys.*, 10:761–797, 1972.
- [4] H.-U. Jüttner and H.-P. Plag. On modelling of earth rotation variations in an integrated model and appropriate frame of reference. In M. Schneider, editor, 3. *DFG Rundgespräch zum Thema Bezugssysteme*, volume 5 of *Mitteilungen des Bundesamtes für Kartographie und Geodäsie*, pages 59–62. Bundesamtes für Kartographie und Geodäsie, 1999.
- [5] D. D. McCarthy. *IERS Conventions 1996*. IERS Technical Note 21. Observatoire de Paris, 1996. 95 pages.
- [6] H.-P. Plag, H.-U. Jüttner, and V. Rautenberg. On the possibility of global and regional inversion of exogenic deformations for mechanical properties of the Earth's interior. *J. Geodynamics*, 21:287–308, 1996.
- [7] T. M. van Dam, G. Blewitt, and M. B. Heflin. Atmospheric pressure loading effects on Global Positioning System coordinate determinations. *J. Geophys. Res.*, 99:23939–23950, 1994.
- [8] T. M. van Dam and T. A. Herring. Detection of atmospheric pressure loading using very long baseline interferometry measurements. *J. Geophys. Res.*, 99:4505–4517, 1994.
- [9] T. M. van Dam, J. Wahr, Y. Chao, and E. Leuliette. Predictions of crustal deformation and of geoid and sea-level variability caused by oceanic and atmospheric loading. *Geophys. J. Int.*, 99:507–515, 1997.
- [10] T. M. van Dam, J. Wahr, P. C. D. Milly, A. B. Shmakin, G. Blewitt, D. Lavallee, and K. M. Larson. Crustal displacements due to continental water loading. *Geophys. Res. Lett.*, 28:651–654, 2001.
- [11] John M. Wahr. A normal mode expansion for the forced response of a rotating earth. *Geophys. J. R. Astron. Soc.*, 64:651–675, 1981.
- [12] R. Wang. Effect of rotation and ellipticity on earth tides. *Geophys. J. Int.*, 117:562–565, 1994.



# Session 6. Analysis and Geodetic/Geophysical/ Astrometric Interpretation





# VLBI Solution DGF101R01 Based on Least-Squares Estimation Using OCCAM 5.0 and DOGS-CS

Volker Tesmer

*DGFI, Deutsches Geodätisches Forschungsinstitut*

*e-mail: tesmer@dgfi.badw.de*

## Abstract

The latest International Terrestrial Reference Frame realisation (ITRF2000) includes solutions of all space-geodetic techniques. All three VLBI solutions contributing to the ITRF2000 are computed using the CALC/SOLVE software package. Therefore a solution based on a different software should provide an insight in the reliability of VLBI results and could provide a higher reliability to a VLBI-determined terrestrial reference frame.

This paper presents the first DGFI VLBI solution computed with OCCAM 5.0 and DOGS-CS using the least-squares method (DGF101R01). It is based on observation data from 2067 VLBI sessions between 1984 and the end of 2000, available from the IVS and CDDISA. The solution strategy is discussed. Comparisons of the coordinates and velocities of the 47 stations of the DGF101R01 and other VLBI solutions with the ITRF2000 indicate that it is a competitive VLBI solution but needs still further improvement.

## 1. Solution Description

### 1.1. Observation Data

The observation data used for the solution was selected from 3400 sessions taken from NASA's CDDISA server as well as the IVS data servers. To reach a reasonable homogeneity of the data, we used only 24 h or longer sessions with at least three participating stations observing at least 250 times. Only non-mobile telescopes with sufficient observations during an adequate time span are included in order to obtain reliable velocities. If a telescope had less than 100 observations during a session, its observations were not used for this session. These strict criteria led to a basis of 2067 sessions between 1984 and the end of 2000 with 47 stations observing 1,933,748 group delays to 684 sources. The observation data is, in particular in its temporal evolution, quite inhomogeneous. This is due to varying objectives of geodetic VLBI as well as technological progress. For example, only 8 of the 47 stations in the solution have more than 400 sessions, 18 stations have between 400 and 50 sessions and 8 stations in the solution have less than 20 sessions. Further statistics concerning yearly averages of VLBI observation data used can be found in Figures 1 to 4.

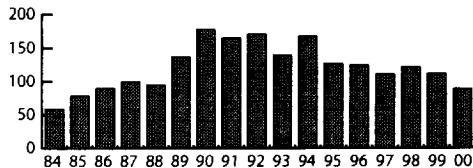


Figure 1. Number of sessions per year.

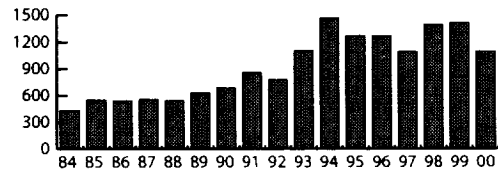


Figure 2. Yearly avg. # observations per session.

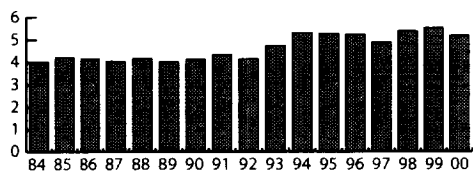


Figure 3. Yearly avg. # stations per session.

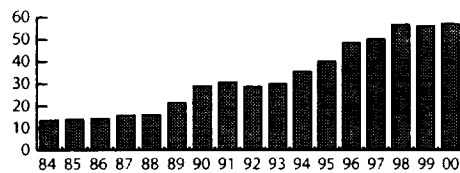


Figure 4. Yearly avg. # sources per session.

### 1.2. Solution Strategy

In a first step, datum-free normal equations for each single session were set up using OCCAM 5.0 LSM and transferred to the DOGS-CS software, which is being developed at the DGFI to accumulate and to solve normal equations. The normal equations included station coordinates at epoch 1997.0, velocities, EOP and auxiliary parameters such as clocks and troposphere. After the EOP and the auxiliary parameters were reduced from the original normal equations, they were accumulated to one datum-free normal equation system. To avoid distortion of the geometry of the solution and to provide a connection to existing terrestrial reference frames, the datum defect was removed by applying NNT and NNR conditions for coordinates and velocities to 10 well-determined stations w.r.t. ITRF2000 (see [1]) (Kauai, Kokee, Fairbanks, Westford, Fortaleza, Onsala, Wettzell, Hartbeesthoek, Kashima, Hobart).

### 1.3. Results

In the following section, illustrations and a short description of the velocities of DGFI01R01 together with the site velocities of ITRF2000 can be found (Figures 5, 6). Additionally, time series of residual coordinates of single session solutions w.r.t. DGFI01R01 (Figure 7) and EOP adjustments w.r.t. IERS C04 fixing stations to DGFI01R01 (Figure 8) are presented.

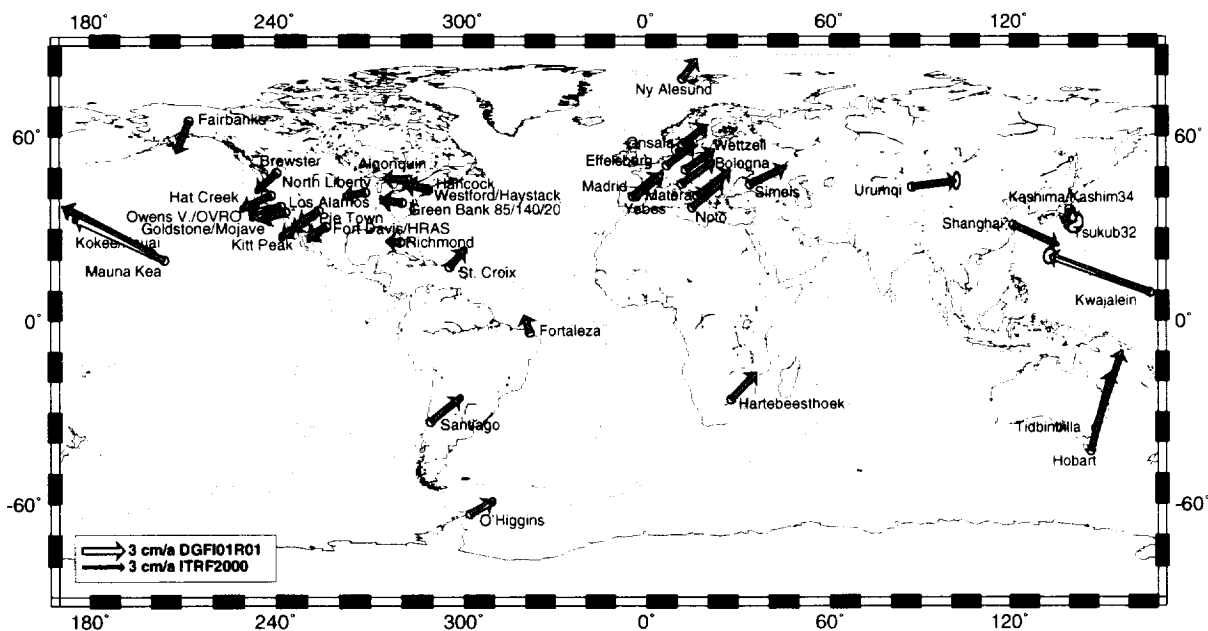


Figure 5. Comparison of horizontal site velocities from ITRF2000 and DGFI01R01.

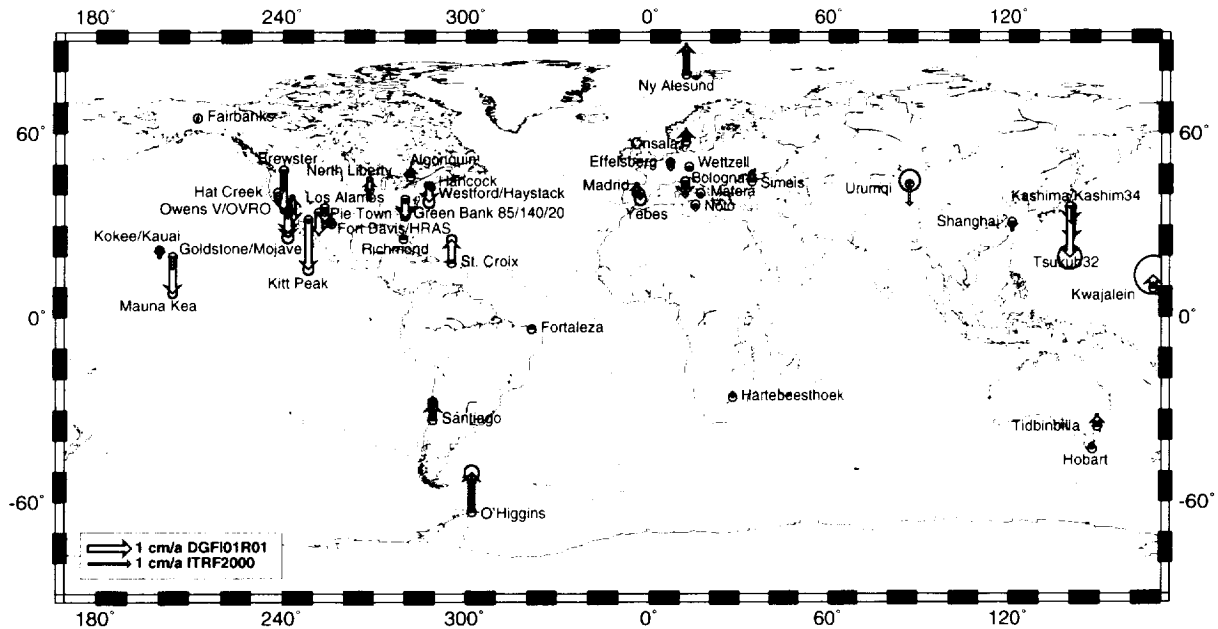


Figure 6. Comparison of vertical site velocities from ITRF2000 and DGFI01R01.

The comparison of the horizontal velocities of DGFI01R01 with the ITRF2000 (Figure 5) shows no significant differences regarding the error ellipses. The greatest differences are at the Tsukuba 32 m telescope, the Mauna Kea VLBA and O'Higgins. The problems are more obvious in the height velocities (Figure 6); they differ significantly for almost all VLBA and Tsukuba 32 m. This is supposed to be caused by the short time series of sessions for these telescopes in DGFI01R01 and an unclear modeling of a jump in height due to an antenna repair at Tsukuba in April 1999.

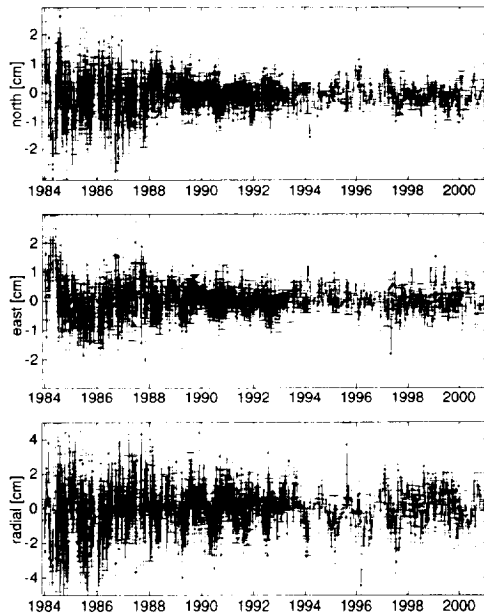


Figure 7. Residuals of WESTFORD session solutions w.r.t. DGFI01R01.

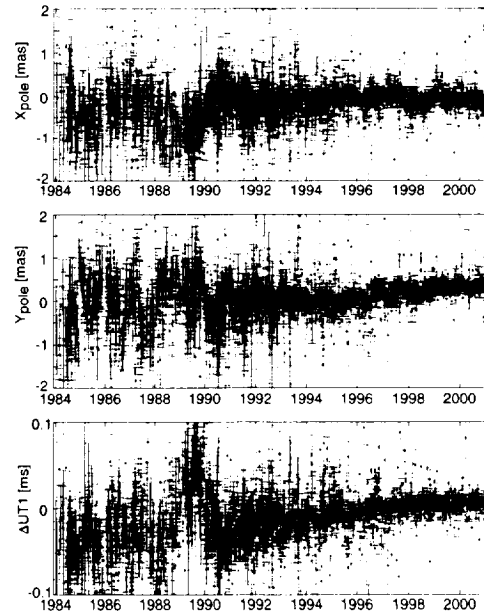


Figure 8. DGFIO1R01 EOP adjustment w.r.t. IERS C04.

Figure 7 shows a coordinate time series of DGFI01R01 for the Westford telescope. It is computed by minimizing the translation and rotation components of all stations in each single session w.r.t. DGFI01R01. Neither was the inner geometry distorted nor the single session scale affected. Three results are valid for almost all coordinate time series of all stations in the solution. Firstly, the results of sessions before 1989 are at least twice as noisy than after 1988, which is probably caused by technological reasons such as uncooled receivers. Secondly, the residual horizontal coordinates after 1988 are smaller than  $\pm 1$  cm, the vertical components smaller than  $\pm 2$  cm. Thirdly, many components show an annual signal with different orders of magnitude for each station and additionally for horizontal and vertical components.

In Figure 8, EOP adjustments w.r.t. to IERS C04 are presented. They were obtained from single session solutions fixing the DGFI01R01 coordinates and velocities. All sessions in the solution were used for their determination, including non-global networks like the EUROPE series, which are not sensitive for the Earth's orientation in space. Some systematic differences between the DGFI01R01 series and IERS C04 are obvious. Between 1996 and the end of 2000, the two series agree quite well at the order of magnitude of 0.5 mas for pole coordinates and 0.03 ms for  $\Delta$ UT1 respectively. More scatter is between 1991 and 1996, and the values of  $\Delta$ UT1 seem to have a linear trend w.r.t. IERS C04. The epoch before 1991 shows big systematic bumps with amplitudes comparable to bumps in other VLBI EOP series, but a with different pattern.

## 2. Comparisons of DGFI01R01 and other VLBI Solutions with ITRF2000

To get a closer insight in the qualities of DGFI01R01, it is reasonable to compare it together with other VLBI solutions to the actual terrestrial reference frame ITRF2000. More than 20 years of high-precision VLBI observables allow determination of very stable velocities for at least 40 telescopes. Therefore, deficiencies of DGFI01R01 as well as systematic differences between VLBI solutions and the ITRF2000 should easily be detected. Table 1 summarises some characteristics of the three compared VLBI solutions, the DGFI solution DGFI01R01, BKGTRA00 by the BKG, Leipzig, and GSFC's GLB2001cn (see [2]). They differ partially, e.g. in the modeling of the celestial reference frame. Please note that two independent software packages were used.

Table 1. Solution characteristics.

	<b>DGFI01R01</b>	<b>BKGTRA00</b>	<b>GLB2001cn</b>
<b>Software</b>	OCCAM5.0 LSM/DOGS-CS	CALC/SOLVE	CALC/SOLVE
<b># sessions</b>	2067	2376	3208
<b>data span</b>	1984 - 2000	1984 - 2000	1979 - May 2000
<b># stations</b>	47	51	137
<b>cel. frame</b>	fixed to ICRF-Ext1	NNR of 209 sources w.r.t. ICRF-Ext1	estimated
<b>EOP</b>	estimated	estimated	estimated
<b>datum, coordinates</b>	NNR+NNT of 10 stations w.r.t. ITRF2000	NNR+NNT of 12 stations w.r.t. ITRF97	NNR+NNT of 12 stations w.r.t. ITRF2000
<b>datum, velocities</b>	NNR+NNT of 10 stations w.r.t. ITRF2000	NNR+NNT of 5 stations w.r.t. ITRF97	NNR of 5 stations w.r.t. ITRF2000 + minimized hor. ajd. of 5 st. w.r.t. NUVEL-1A

All three VLBI solutions were subject to a 14 parameter Helmert transformation w.r.t. the ITRF2000, using almost the complete set of 47 stations of the DGFI solution as identical ones. As the twelve translation and rotation parameters are degrees of freedom, only the scale and its rate can be considered as objective information. The difference in scale is -1.05 ppb and -0.04 ppb/y for the DGFI solution corresponding to a 7 mm decrease of the radial component in DGFI01R01 compared to the ITRF2000, which is significant and not negligible. The parameters were -0.26 ppb and -0.04 ppb/y for BKGTRA00 and +0.29 ppb and -0.05 ppb/y for GLB2001cn, which are only marginally significant.

Most interesting are the residual coordinates and velocities of the three VLBI solutions w.r.t. the ITRF2000 after the transformation. The residual horizontal velocities of VLBI solutions are usually less than 1 mm/y, almost all are less than 2 mm/y. The vertical components differ by less than 1.5 mm/y for most stations, almost all differ by less than 3 mm/y. Comparing the residual coordinates, most horizontal components differ by less than 5 mm, almost all differ by less than 10 mm in all VLBI solutions. The residual vertical coordinates are usually less than 15 mm, almost all are less than 20 mm. The only stations with greater residuals are the very weakly determined Owens Valley 130, Green Bank 140, Urumqi and the Tsukuba 32m telescope.

Systematic differences of the VLBI solutions w.r.t. ITRF2000 appear for the height of the Green Bank 20 and 85 telescopes, whose velocities differ consistently and significantly by about 3 mm/y in all VLBI solutions, but were set equal in ITRF2000. The height coordinates of stations in the very south and north, O'Higgins and NyAlesund differ consistently and significantly by up to 20 mm from the ITRF2000, the Australian DSS 45 and Hobart by about 10 mm in all components.

Additionally, the DGFI solution shows great differences up to 25 mm and 10 mm/y, respectively, for almost all VLBA telescopes, which is supposed to be caused by a considerably smaller amount of RDV sessions in this solution.

### 3. Conclusions

DGFI01R01, the first VLBI solution of the DGFI is a competitive non-CALC/SOLVE solution, but obviously needs partial improvements. In particular, adding the observational data of the year 2001 and some RDV sessions should stabilise the results of the VLBA and the Tsukuba 32m telescopes. Further investigations must be carried out concerning the scale of DGFI01R01 and its EOP series, which show different "bumb-patterns" w.r.t. IERS C04 than other VLBI solutions.

The comparisons of three VLBI solutions with the ITRF2000 can be summarized as follows: VLBI solutions do not have explicit systematic differences w.r.t. each other. Considering only well-determined stations, VLBI solutions have very few non-systematic differences greater than 25 mm and 5 mm/y resp. Furthermore, VLBI solutions have some non-negligible systematic differences w.r.t. ITRF2000, which should be subject to extensive intra-VLBI investigations.

This research has made use of NASA Goddard Space Flight Center's VLBI terrestrial reference frame solution GLB2001cn, 2001 May. The author thanks the GSFC and the IVS for the observation data, the BKG and GSFC for their solutions BKGTRA00 and GLB2001cn, respectively.

### References

- [1] Webpage of the ITRF2000, <http://lareg.ensg.ign.fr/ITRF/ITRF2000>
- [2] NASA Goddard Space Flight Center VLBI Group, 2001 May. Data products available electronically at <http://lupus.gsfc.nasa.gov/global/glb.html>

## SLR-based TRF Contributing to the ITRF2000 project

*Toshimichi Otsubo, Tadahiro Gotoh*

*Communications Research Laboratory*

*Contact author: Toshimichi Otsubo, e-mail: [otsubo@crl.go.jp](mailto:otsubo@crl.go.jp)*

### Abstract

The 10-year TRF solution constructed by Communications Research Laboratory contributed to the ITRF2000 project as one of SLR solutions. Our solution used LAGEOS-1 and -2 data to derive the position and velocity vectors of 60 worldwide stations.

The ITRF2000 final solution released in March 2001 adopted the newly defined datum based on SLR and VLBI. The SLR-based TRFs had a great advantage in the precise determination of the origin (a few mm) and the scale ( $\sim 1$  ppb).

### 1. Introduction

Along with VLBI and GPS, satellite laser ranging (SLR) has contributed to space geodesy for decades. Currently, the instrument error in good SLR observatories has been reduced to a few millimetres. SLR has also benefited from the well-modelled tropospheric correction model of optical wavelength compared with microwave-based techniques. The greatest advantage of SLR is in the determination of the gravitational scale of the Earth (GM) and the origin and scale of the terrestrial reference frame (TRF) [1] [2].

The International Terrestrial Reference Frame (ITRF) is used worldwide as a standard set of TRF. It is a combination of solutions from multiple space geodetic techniques including VLBI, GPS, SLR, LLR and DORIS. The International Earth Rotation Service (IERS) has assembled the latest version, ITRF2000, from more than 30 contributions [3].

At CRL, we gained experience in analysing orbit determination from developing our own software package CONCERTO [4]. We constructed a TRF, SSC(CRL)00L02, from global satellite laser ranging data obtained over the last ten years, and made our first submission to the ITRF2000 project.

### 2. Construction of SSC(CRL)00L02

The following set of satellite laser ranging data was reduced in CONCERTO:

- LAGEOS-1 and LAGEOS-2
- ILRS 2-minute normal-point
- MJD 47000-51500 (roughly 1990.0 to 2000.0)
- 60 stations at 48 sites

Since it was impossible to solve all the parameters at once, we divided the whole sequence into two stages (Fig. 1). First, we prepared 73 observation data sets of 50-day spans so that the whole data covered ten years. In each of the 50-day spans, the satellite orbits, EOPs, range biases

and station coordinates were loosely solved for. The Java version of CONCERTO with models mostly compatible with IERS Conventions [5] was used. We obtained 73 sets of solutions of station positions. We then assembled the 73 sets and derived three-dimensional positions and velocities for the 60 stations, again applying loose constraints: 10 m for positions and 1 m/y for velocities. The solution, SSC(CRL)00L02, was submitted to the ITRF2000 project in April 2000.

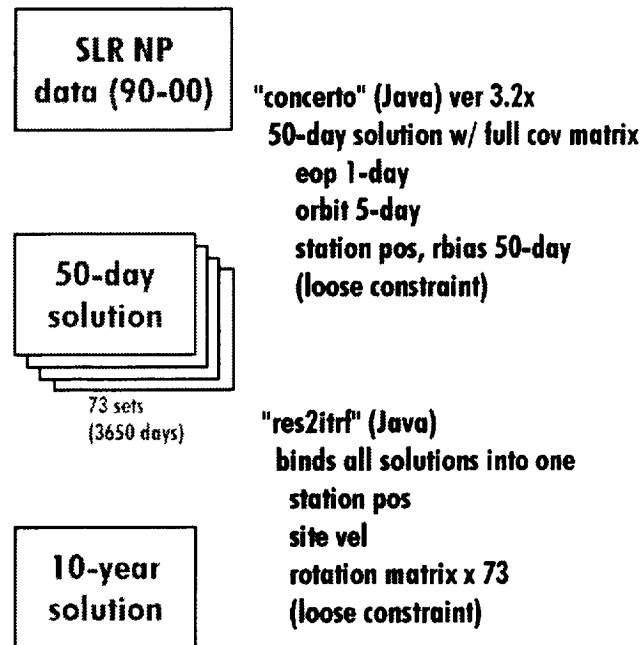


Figure 1. SSC(CRL)00L02 data flow.

### 3. Quality of SSC(CRL)00L02

A loosely estimated solution rotates freely and is not suitable for measuring the formal error or for direct comparison with other TRFs. We therefore constructed a tightly constrained TRF SSC(CRL)00L01.

For “good” laser ranging stations that have consistently yielded high quality data, the formal errors of the estimated positions were 0.5-0.8 mm for horizontal and 1.5-2.0 mm for vertical components. Velocity errors were 0.2-0.3 mm/y for horizontal and 0.3-0.8 mm/y for vertical components.

We compared the TRF SSC(CRL)00L01 with the former standard ITRF97 and the new standard ITRF2000. The horizontal and vertical velocity vectors of the major stations are shown in Fig. 2. For the “good” stations located at a collocation site, the average differences of position between ours and ITRF2000 were < 3 mm for horizontal and about 8 mm for vertical components, and those of velocity were 1.5 mm/y for horizontal and 2.5 mm/y for vertical components, which is not as good as VLBI and GPS solutions but comparable with other SLR solutions. Considering the estimated error, no significant vertical motion was detected in any of these laser ranging stations. Owing to the recent improvement in Chinese and Russian laser ranging stations, we got a more realistic assessment of their horizontal motion than that in ITRF97, which was reflected in

ITRF2000.

Of the nine SLR solutions submitted to the ITRF2000 project, seven were included in the final ITRF2000 solutions, and five (CGS, CRL, CSR, DGFI and JCET) were used to establish the newly defined datum. The CRL solution was one of the five. The scale of the Earth is defined by the three VLBI solutions (50%) and the five SLR solutions (50%), and the origin is defined by the five SLR solutions (100%). The CRL solution sits around the centre of the five solutions for both scale and origin (see IERS [6] for details).

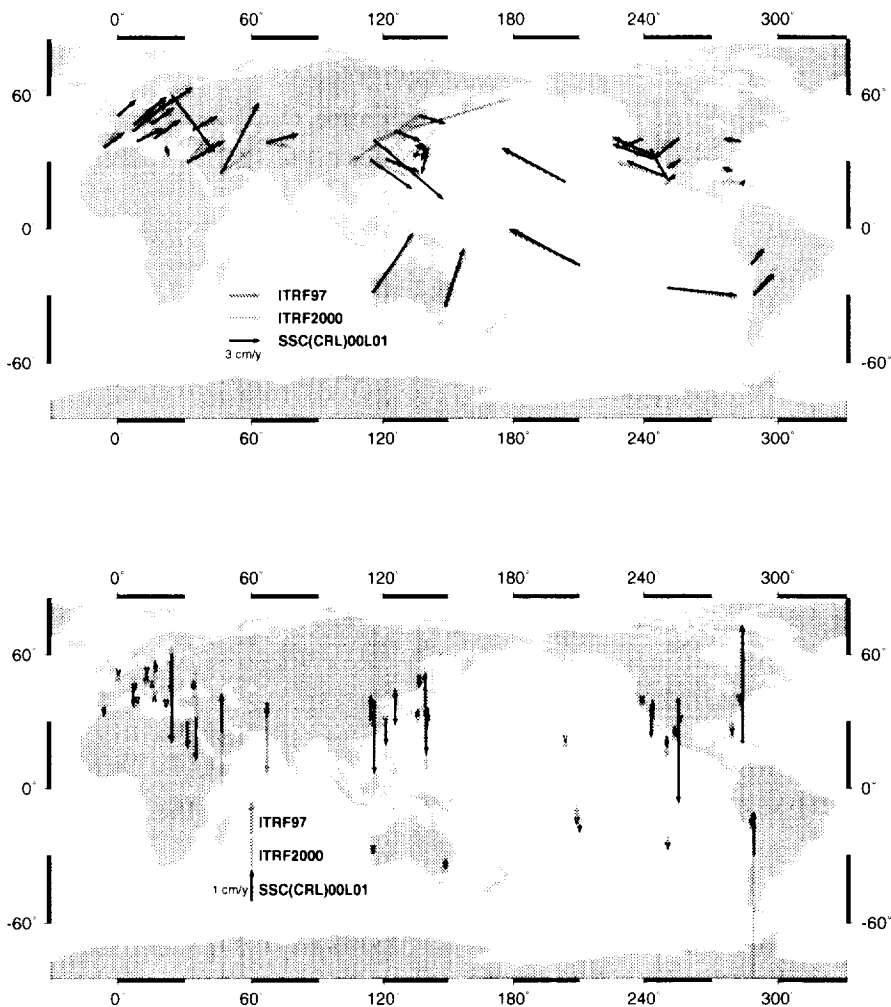


Figure 2. SSC(CRL)00L02 velocity field in comparison with ITRF97 and ITRF2000. Top: horizontal components. Bottom: vertical components.

#### 4. Conclusions

We contributed to the ITRF for the first time. The ITRF2000 project showed that CRL's ten-year solution was comparable to other good solutions and it was actually used to define the new datum (scale and origin). This suggests that our software CONCERTO is reliable for constructing long-term TRFs.

The Analysis Working Group of the International Laser Ranging Service (ILRS) is working hard to establish a scheme to routinely generate the best combined solution from several local solutions. CRL, as an associate analysis centre of ILRS, has contributed to all of the pilot projects.

SLR is expected to provide the most accurate scale of the Earth, but the SLR solutions are scattered by  $\pm 1$  ppb, which is larger than the scatter of VLBI solutions, in the ITRF2000 project. Analysts need to overcome the error sources currently degrading the scale of the Earth, such as the atmospheric correction model and the centre-of-mass correction of geodetic satellites.

#### References

- [1] Smith, D. E., R. Kolenkiewicz, P. J. Dunn, M. H. Torrence, Earth scale below a part per billion from satellite laser ranging, *Geodesy beyond 2000*, IAG General Assembly, Springer, 3-12, 1999.
- [2] Eanes, R., Corrections to the Marini-Murray refraction model that affect the scale of the SLR station solutions and GM, *Proceedings of 12th International Workshop on Laser Ranging, 2000* (in print).
- [3] Altamimi, Z., The accuracy of ITRF2000, *European Geophysical Society XXVI General Assembly, G6*, 2001.
- [4] Otsubo, T., H. Kunimori, B. Engelkemier, F. Takahashi, Error control of numerical integration in SLR analysis software CONCERTO, *Journal of the Geodetic Society of Japan*, 40, 4, 347-355, 1994.
- [5] IERS, *IERS Conventions (1996)*, IERS Technical Note 21, 1996.
- [6] IERS, ITRF2000 website, <http://lareg.ensg.ign.fr/ITRF/ITRF2000/>, 2001.

# Establishment of the New Geodetic Reference Frame of Japan (JGD2000)

*Tetsuro Imakiire, Masaki Murakami*

*Geographical Survey Institute*

*Contact author: Tetsuro Imakiire, e-mail: imq@gsi.go.jp*

## Abstract

The Geographical Survey Institute (GSI) has constructed a new geodetic reference frame of Japan. The Survey Act and the related government ordinances were revised to adopt the new geodetic frame as the national reference system. The new frame is a geocentric system based on the observation using space geodetic techniques. The current framework based on Tokyo Datum was established at the beginning of the twentieth century and has been used as a national reference for nearly one hundred years. However, it has a large internal distortion and a shift from a geocentric reference frame, which was revealed by space geodetic techniques. The new framework has been built by referring to ITRF94 (International Terrestrial Reference Frame 1994) at the epoch of 1997.0. The coordinates of the Kashima VLBI station are fixed in ITRF94 using the data from international VLBI observations. Positions of two other domestic VLBI stations (Shintotsugawa and Kainan) were determined referred to Kashima VLBI station. Using these three VLBI stations as anchor points, the coordinates of 950 stations of the nationwide permanent GPS array (GEONET) were determined. The coordinates of the first- through third-order triangulation points are calculated by referring to the GPS array. GSI resurveyed 6300 of first- to third-order triangulation points using EDM or GPS. For other 30,000 triangulation points, survey records, which have been obtained by theodolite since 1883, are used. The coordinates newly determined for VLBI stations, GPS stations, and triangulation points are the realization of Japan's new geodetic reference system. GSI named it "Japanese Geodetic Datum 2000" (JGD2000).

## 1. Introduction

Japanese government decided to adopt new geodetic reference frame as the legal system. The new reference frame is referred as the name of "World Geodetic System" generally. When it is defined as a unique system with certain parameter set, it would be called as "Japanese Geodetic Datum 2000 (JGD2000)".

## 2. Current Status of Tokyo Datum (horizontal)

"Tokyo Datum" is the name for the present legal geodetic system as defined by Survey Act before this revision. "Horizontal" means Tokyo Datum has vertical reference system also, however the vertical system was not changed this time. Survey Act, the law regulating survey and mapping, has been defining the ellipsoid. The equatorial radius and flattening of the reference ellipsoid were defined in the law (Bessel ellipsoid). Governmental ordinances have been defining geographical longitude, latitude and datum azimuth of the datum. According to these definitions, the whole geodetic network in Japan has been constructed. Those parameters were determined based on the astronomical survey in Meiji era (more than one hundred years ago, in nineteenth century). This geodetic reference system has been referred as "Japanese Geodetic System (Tokyo Datum)" or

shortly “Tokyo Datum” However, the space geodetic observations, such as GPS, SLR and VLBI, revealed that Tokyo Datum is not consistent with the newest global frame. Both longitude and latitude are different by 12” at the datum monument. Furthermore, the network is distorted because of the old survey limitation.

### 3. Process for the Adoption of World Geodetic System

GSI decided that geodetic reference frame should shift to a world geodetic system in 1997. GSI started the computation of coordinates using the observation data obtained by space geodetic techniques, such as the global and domestic VLBI, GPS. GSI started the preparation for the revision of the Survey Act, and relating governmental ordinances, too. GSI decided that reference frame should be International Terrestrial Reference Frame, and ellipsoid should be one defined in Geodetic Reference System 80 by IUGG. The process for the determination of control points were constructed under these definitions. The determination of coordinates was carried out in six steps (Murakami et al, 1999). First, the coordinates of Kashima VLBI station were determined globally by international VLBI observation. Second, domestic VLBI observation data was used for the computation of the coordinates of two other VLBI stations. Third, the coordinates of GPS-based control points (permanent GPS observation stations) were computed using the VLBI stations as the fixed points. Forth, the coordinates of higher order (first or second order) triangulation points, which have been surveyed recently by EDM or GPS, were computed by the network solution fixing GPS-based control points. Fifth, the coordinates of lesser order triangulation points, most of those are third order ones, were computed based on the angular observation data, because they have not been re-surveyed since Meiji era. Finally, the coordinates of fourth order triangulation points were computed by interpolation method with neighboring higher order points coordinates data. While GSI was carrying out these computations of the coordinates of control points, the bill for revising the Survey Act was submitted and the Diet passed it on June 12, 2001. Hydrological Survey Act, which regulates the hydrological survey on the sea, was also revised simultaneously to adopt a world geodetic system. Relating governmental ordinances were also revised in December 28, 2001. Those laws and ordinances come into effect after April 1, 2002. Official survey and mapping in Japan should be carried out based on the world geodetic system defined by laws and ordinances (JGD2000) after this date.

### 4. VLBI Observation

To replace the conventional datum, a start point that is precisely connected with the geocenter should be settled. GSI has been participating in the international VLBI experiments with Kashima VLBI Station. The ITRF94 coordinates of Kashima VLBI station are precisely determined through more than ten years of observations. The ITRF94 coordinates of Kashima are treated as a practical origin of the JGD2000. During 1986 to 1997, GSI carried out many domestic VLBI observations using mobile VLBI stations and Kashima VLBI station. After an assessment of the effect of crustal movements, two mobile VLBI stations (Shintotsukawa and Kainan) were selected as primary reference points and the three others (Chichijima, Mizusawa, Sagara and Shin-tomi) were selected as points for comparison. The baseline vectors in ITRF94 between mobile VLBI stations and Kashima VLBI station were used for the computation of coordinates of mobile VLBI stations at epoch 1997.0. From ITRF94 parameters of Kashima and baseline vector,

coordinates of mobile VLBI station can be calculated on an epoch of the observation. Using data set from the repeated observation, a regression line can be described on position vs. time chart. Coordinates of the epoch 1997.0 of the mobile VLBI station can be obtained from this regression line.

## 5. GEONET, the Permanent GPS Array

GEONET (GPS Earth Observation NETWORK) is the name of nationwide GPS permanent station array system of GSI. The system includes about one thousand GPS permanent stations covering all over Japanese islands and the analysis center in GSI office. The typical separation between two GPS stations is about 25 km. All stations equip a GPS receiver to obtain carrier phase and code data of GPS satellites with thirty seconds epoch. The data of all station are downloaded once per day to the analysis center (Miyazaki et al, 1998). This GPS array was first established to monitor the crustal deformation continuously. Actually GEONET revealed tectonic movement within Japanese islands as well as the co-seismic movement related to significant earthquakes since 1994. On the other hand, GEONET has been providing continuous GPS observation data usable for field GPS survey. Therefore the permanent stations are referred to as "GPS-based control points". The coordinates of GEONET stations were determined in ITRF94 (epoch 1997.0). We used the data obtained during the period from 27 December 1996 to 5 January 1997 for this computation. At that period the number of GEONET stations was 616 and 595 of them were available. The data was analyzed with GAMIT and adjusted with GLOBK. The three VLBI stations were tied to GEONET and their coordinates were held fixed in the network adjustment. Accuracy assessments have been done with the coordinates at VLBI stations for comparison. They show an agreement of about 3 cm in horizontal components while a formal error of the GPS net adjustment is 2 mm. Baseline analysis of GEONET stations was also carried out with BERNESE to check the results. Because the number of GPS stations has increased since January 1997, coordinates of 350 more stations are being calculated referenced to neighboring existing GPS stations. These VLBI and GPS stations consist of the backbone of JGD2000.

## 6. Triangulation Points

GSI computed the coordinates of all triangulation points, which are used for survey and mapping, in network adjustment with various observation data. Highly Precise Geodetic Network (HPGN), which consists of 493 first and second order triangulation points, were directly tied to GEONET at 164 points. The computation for HPGN points was carried out using three-dimensional adjustment program. The observation data for this step was totally GPS baseline data. Primary Precise Geodetic Network (PPGN), which consists of the first and second order triangulation points, was directly tied to GEONET at 522 points. Distance measurement data by EDM obtained during 1979-1997 were used for the adjustment by the projection method onto Bessel ellipsoid. Coordinates of 2465 points were derived with the above-mentioned 522 points being fixed. Positional errors relative to neighboring points are estimated to be 3 cm. Secondary Precise Geodetic Network (SPGN), which consists of second and third order triangulation points, was connected to directly GPS stations, HPGN or PPGN points. The coordinates of 3,069 points were computed using distance measurement data on Bessel ellipsoid. The rest of the second and third order triangulation points have not been re-surveyed since the establishment of Tokyo Datum.

We archived survey records of angular observation by theodolite since 1883 for these points. The coordinates of about 30,000 points were computed using archived data referenced to GEONET, HPGN, PPGN, or SPGN. Error of these coordinates was estimated by GPS direct tie survey for the evaluation of the adjustment. We found more than 90% of 856 points have coordinates consistent to the re-survey results within 20 cm. The number of the fourth order triangulation points is more than 60,000. A program that transforms the coordinates from Tokyo Datum to JGD2000 was developed for the determination of those points. This program has a parameter table which holds transformation vector on the grid points (30-second in latitude and 45-second in longitude) covering all over Japanese islands. The parameters were computed from the transformation vectors of superior order triangular points adjusted by the process described formerly. Then transformation vectors for respective fourth order triangulation points will be obtained by bilinear interpolation for this grid data set. This bilinear interpolation program, named "TKY2JGD", and grid data table set can be used for transformation of coordinates of public control points and cartographic products including digital maps in GIS (Geographic Information System) (Tobita, 2000). As GSI uploaded this program and parameter tables on our web site, users can use it freely for their purposes. Though we provide the program and relating documents only in Japanese, the source code by Microsoft Visual Basic, which is also uploaded on the same website, is available. (<http://vldb.gsi.go.jp/sokuchi/ky2jgd/download/agreement.html>)

## 7. Effect of New Geodetic Reference System

The shift of the geodetic system would affect not only surveyors but all citizens. For example maps should be changed. GSI is responsible to provide basic maps covering Japan. Therefore we started supply basic maps with the coordinates by JGD2000 from October 2001. GSI also provide a transformation table of the coordinates by JGD2000 for the four corners of the maps those are published by GSI. This table is also uploaded on our web site. ([http://www.gsi.go.jp/MAP/NEWOLDBL/New\\_OldBLindex.html](http://www.gsi.go.jp/MAP/NEWOLDBL/New_OldBLindex.html)) The coordinates of control points constructed by local governments should be transformed into JGD2000, too. GSI provides "Transformation Manual" to advise them how to transform the coordinates of control points and cartographic products. GSI held seminars to advise how to adopt new geodetic system.

## 8. Conclusion

GSI has constructed the new geocentric reference frame using space geodetic techniques. The positions of a thousand of GPS stations and a hundred thousand triangulation points have been calculated as a realization of the new datum. GSI is trying hard to ensure that the new system based on revised Survey Act would be accepted smoothly by civil society.

## References

- [1] Murakami, M., S. Ogi Realization of Japanese Geodetic Datum 2000(JGD2000) In: Bulletin of GSI, 45, 1-10, 1999.
- [2] Miyazaki, S., T. Saito, Y. Hatanaka, T. Sagiya, T. Tada The Nationwide GPS Array as an Earth Observation System In: Bulletin of GSI, 44, 11-22, 1998.
- [3] International VLBI Service for Geodesy and Astrometry 2000 Annual Report, NASA/TP-2001-209979, N. R. Vandenberg and K. D. Baver (eds.), 249-252, 2001.

- [4] Tobita, M. "TKY2JGD", Coordinate Transform Program for JGD2000 In: Technical Report of GSI, F-2, 2000.

## Variations of European Baseline Lengths from VLBI and GPS Data

*Zinovy Malkin, Natalia Panafidina, Elena Skurikhina*

*Institute of Applied Astronomy of Russian Academy of Sciences (IAA)*

*Contact author: Zinovy Malkin, e-mail: [malkin@quasar.ipa.nw.ru](mailto:malkin@quasar.ipa.nw.ru)*

### Abstract

Results of VLBI and GPS observations were analyzed with goal to investigate differences in observed baseline length derived from both techniques. VLBI coordinates for european stations were obtained from processing of all available observations collected on european and global VLBI network. Advanced model for antenna thermal deformation was applied to account for change of horizontal component of baseline length. GPS data were obtained from re-processing of the weekly EUREF solutions. Systematic differences between results obtained with two techniques including linear drift and seasonal effects are investigated.

## Influence of Antenna Thermal Deformations on Estimation of Seasonal Variations in Baseline Length

*Elena Skurikhina*

*Institute of Applied Astronomy of Russian Academy of Sciences (IAA)*

*e-mail: sea@quasar.ipa.nw.ru*

### Abstract

The results of analysis of baselines length variations calculated at the Institute of Applied Astronomy with the OCCAM package from all available VLBI sessions with and without modelling antenna thermal deformations are presented.

Some baseline variation time series show not only linear trend due to tectonic plates motion but seasonal variations too [2]. Antenna thermal deformations may be one of the possible reasons for this effect. The main aim of this work is to investigate what part of baseline length seasonal variations can be explained by this effect. All computation of station coordinates and baseline lengths was made with OCCAM package. Model of thermal deformations proposed in [1] was used for this computation. This model extends one recommended by IERS Conventions (2000) for all mount types.

Fig. 1 shows the differences of baseline lengths computed with and without modelling of antenna thermal deformations. Obviously thermal deformation influences baseline lengths as a combination of a bias and a periodic part with 1-year period. List of analyzed baselines is presented in Table 1. The name of a baseline consists of the first 4 letters of station names. First column of the Table 1 is values of biases and the last column is amplitudes of the year term.

As recommended in [2] baseline length time series was approximated as a combination of a linear trend and two periodic terms with annual and semiannual period. Baseline length rate was found to be practically independent of antenna thermal deformations.

Amplitudes of annual and semiannual terms are presented in Table 2 for two variants: the first column corresponds to calculation without thermal deformations modelling (Amp-1 — the amplitude of annual term), the second column contains the amplitude of the annual term for calculations with thermal deformations modelling, the third and fourth columns show the amplitudes of semiannual terms in the same order.

An unexpected consequence of this work is that seasonal variations of baseline lengths can be hardly explained by the effect of the VLBI antenna thermal deformations. Amplitude spectra of baseline length time series demonstrate that the 1-year period is not the largest period in these spectra. Some baseline lengths (HRASRICH, RICHWETT, GILCRICH, FORTNYAL, FORTWETT, FORTNYAL) have significant 2-year (or 2.25 year) periodic terms and also 1.25 and 1.7-year terms. Baseline lengths ALGOGILC, FORTNYAL, FORTWETT, NR20NYAL, NR20WETT have 1.5-, 1.7-, 2.25-year terms and baseline lengths NR20NYAL, NR20WETT have 0.75-year term. However, more detailed spectral analysis of baseline length time series and more careful approximation planned for the nearest future might specify the influence of antenna thermal deformations on estimation of seasonal variations in baseline length.

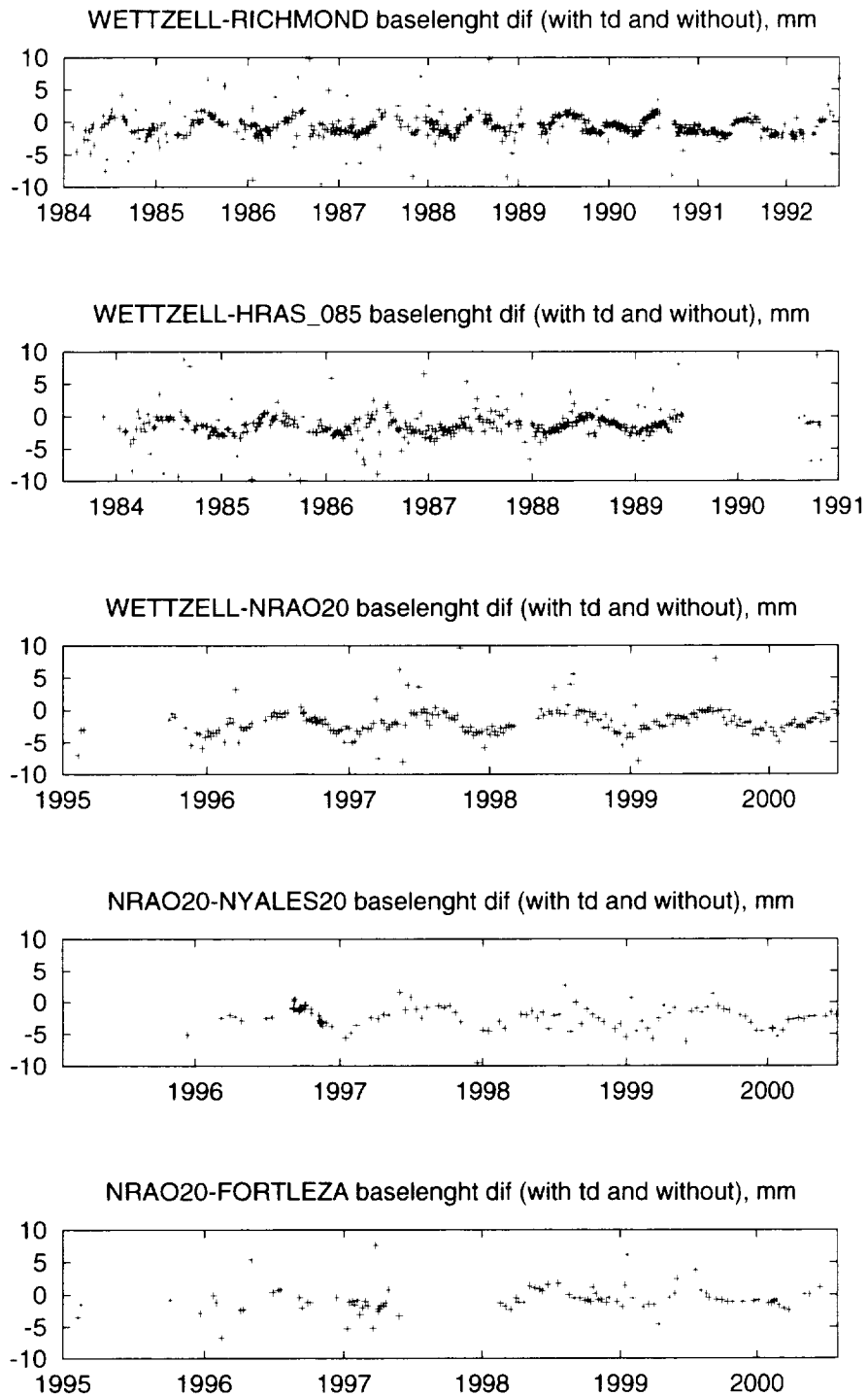


Figure 1. Influence of thermal deformation modelling on baseline length.

Table 1. Influence of thermal deformation modelling on baseline length.

Baseline	Nsess	Period	bias, mm/y	Ampl, mm
WESTWETT	872	1983.9 – 2001.7	-2.0 ± 0.09	0.8
RICHWEST	545	1984.0 – 1992.5	-0.39 ± 0.02	0.1
RICHWETT	506	1984.1 – 1992.2	-0.48 ± 0.02	0.3
KOKEWETT	496	1993.4 – 2002.0	-1.1 ± 0.07	0.4
GILCWETT	496	1984.7 – 2002.0	-1.7 ± 0.07	1.0
HRASWEST	483	1981.4 – 1990.7	-0.3 ± 0.02	0.4
GILCNR85	431	1989.1 – 1995.3	-1.7 ± 0.07	1.0
GILCKAUA	431	1984.5 – 1993.5	-0.5 ± 0.04	0.3
FORTWETT	436	1993.5 – 2002.0	-0.4 ± 0.04	0.2
FORTKOKE	411	1993.5 – 2001.9	-0.2 ± 0.05	0.2
HRASWETT	397	1983.9 – 1990.7	-0.4 ± 0.02	0.3
GILCWEST	398	1984.7 – 2001.7	-1.9 ± 0.11	1.4
MOJAWEST	378	1983.6 – 1992.5	-0.8 ± 0.05	0.9
GILCKOKE	367	1993.4 – 2001.9	-0.8 ± 0.04	1.5
HRASRICH	336	1984.0 – 1990.8	-0.1 ± 0.02	0.1
KAUANR85	267	1989.1 – 1993.2	-0.3 ± 0.04	0.6
KOKENR20	280	1995.1 – 2000.5	-1.5 ± 0.10	1.0
FORTGILC	258	1993.5 – 2002.0	-1.3 ± 0.12	0.8
NR20WETT	256	1995.1 – 2000.4	-1.7 ± 0.10	1.3
MOJAWETT	253	1984.7 – 1992.6	-0.9 ± 0.10	0.8
GILCMOJA	244	1984.5 – 1992.6	-0.8 ± 0.05	0.8
ONSAWETT	231	1983.9 – 2001.4	-0.2 ± 0.03	0.6
NYALWETT	231	1994.8 – 2002.0	-1.2 ± 0.04	0.4
KOKENYAL	226	1994.8 – 2001.9	-2.2 ± 0.08	0.8
ONSAWEST	216	1981.8 – 2001.2	-1.6 ± 0.15	0.6
ALGOGILC	219	1984.6 – 2001.9	-2.1 ± 0.13	1.9
MOJARICH	204	1984.0 – 1992.6	0.15 ± 0.08	0.3
FORTNR20	200	1995.1 – 2000.5	-0.7 ± 0.09	0.6
NR85WETT	187	1991.9 – 1996.6	-1.5 ± 0.06	0.6
ALGOWETT	185	1990.5 – 2002.0	-2.2 ± 0.15	1.7
GILCKASH	139	1984.6 – 1998.7	-1.3 ± 0.13	0.3
FORTNYAL	169	1994.8 – 2001.9	-1.4 ± 0.08	0.8

Table 2. Influence of thermal deformations on estimates of amplitudes of annual and semiannual terms in baseline length variations (cont.).

Baseline	Amp_1, mm	Amp_1th, mm	Amp0.5, mm	Amp0.5.th, mm
WESTWETT	1.8 ± 0.5	2.4 ± 0.6	1.5 ± 0.5	0.6 ± 0.4
RICHWEST	0.8 ± 0.5	1.0 ± 0.5	1.5 ± 0.5	1.6 ± 0.4
RICHWETT	1.4 ± 1.1	2.5 ± 1.0	1.6 ± 1.1	1.4 ± 1.0
KOKEWETT	0.6 ± 0.5	1.8 ± 0.8	2.5 ± 0.5	2.4 ± 0.5
GILCWETT	3.5 ± 0.9	4.1 ± 0.9	1.0 ± 0.9	1.1 ± 0.9
HRASWEST	1.9 ± 0.9	2.6 ± 1.0	1.0 ± 0.8	0.9 ± 0.8
GILCNR85	2.1 ± 0.8	2.7 ± 0.8	0.8 ± 0.8	1.2 ± 0.8
GILCKAUA	1.2 ± 0.7	2.3 ± 0.8	2.8 ± 0.7	1.5 ± 0.6
FORTWETT	2.7 ± 0.7	2.6 ± 0.8	0.6 ± 0.7	0.7 ± 0.8
FORTKOKE	2.8 ± 1.3	2.8 ± 1.4	1.6 ± 1.4	2.0 ± 1.3
HRASWETT	6.3 ± 1.8	8.2 ± 2.0	2.8 ± 1.8	2.6 ± 1.8
GILCWEST	2.8 ± 0.5	3.8 ± 0.5	0.5 ± 0.5	0.5 ± 0.4
MOJAWEST	3.2 ± 0.5	4.1 ± 0.6	1.4 ± 0.5	1.4 ± 0.5
GILCKOKE	4.7 ± 0.5	4.7 ± 0.5	0.7 ± 0.5	0.7 ± 0.5
HRASRICH	1.4 ± 1.0	1.6 ± 0.9	0.2 ± 1.1	0.5 ± 1.0
KAUANR85	4.4 ± 1.0	5.4 ± 1.1	1.0 ± 1.0	1.5 ± 1.0
KOKENR20	3.2 ± 1.7	2.4 ± 1.7	2.9 ± 1.6	2.0 ± 1.6
FORTGILC	2.8 ± 1.3	3.9 ± 1.3	2.0 ± 1.3	2.3 ± 1.3
NR20WETT	2.9 ± 0.9	4.5 ± 0.9	1.7 ± 0.8	1.4 ± 0.8
MOJAWETT	3.1 ± 1.2	3.9 ± 1.2	1.4 ± 1.2	1.2 ± 1.2
GILCMOJA	4.3 ± 0.7	5.1 ± 0.7	2.0 ± 0.7	2.3 ± 0.7
ONSAWETT	1.7 ± 0.4	2.0 ± 0.5	2.7 ± 0.4	2.7 ± 0.4
NYALWETT	0.4 ± 0.5	1.3 ± 0.5	1.2 ± 0.5	0.4 ± 0.4
KOKENYAL	1.5 ± 1.1	0.7 ± 1.2	2.4 ± 1.1	2.4 ± 1.1
ONSAWEST	1.1 ± 0.6	3.1 ± 0.6	1.8 ± 0.6	1.9 ± 0.5
ALGOGILC	9.5 ± 2.2	7.2 ± 1.8	0.9 ± 2.3	8.9 ± 1.9
HARTWEST	2.8 ± 0.9	3.3 ± 0.9	0.7 ± 0.9	0.8 ± 0.9
MOJARICH	5.3 ± 2.5	4.5 ± 3.1	3.9 ± 2.5	3.6 ± 3.1
FORTNR20	4.6 ± 1.1	4.9 ± 1.2	3.1 ± 1.1	3.2 ± 1.1
NR85WETT	3.8 ± 1.0	5.1 ± 1.0	1.5 ± 1.0	1.8 ± 1.0
ALGOWETT	2.8 ± 0.8	4.3 ± 0.9	1.5 ± 0.8	1.3 ± 0.8
GILCKASH	1.0 ± 1.4	0.9 ± 1.4	2.3 ± 1.4	2.8 ± 1.4
FORTNYAL	4.5 ± 1.2	5.4 ± 1.2	1.4 ± 1.2	1.5 ± 1.2

## References

- [1] Skurikhina E. On Computation of Antenna Thermal Deformation in VLBI Data Processing. In: D. Behrend and A. Rius (Eds.), Proc. 15th Working Meeting on European VLBI for Geodesy and Astrometry, Barcelona, Spain, September 07-08, 2001.
- [2] Titov O. A., Yakovleva H. G. Seasonal variations in radial components of VLBI stations. *Astron. Astrophys. Trans.*, 2000, No 4, 591–603.

# Spectral Analysis of the Baseline Length Time Series from VLBI Data

*Oleg Titov*

*Geoscience Australia*

*e-mail: olegtitov@auslig.gov.au*

## Abstract

In addition to a linear trend VLBI baseline lengths demonstrate seasonal variations. Spectral and wavelet analysis of the baseline time series having the longest history show that annual and semiannual variations are present at these frequencies. It appears that the baseline length variations arise from instability in the vertical component of one or both VLBI sites.

## 1. Introduction

In accordance with the conventional model of tectonic plate motion NNR-NUVEL1 the variations of baseline lengths should be fitted by a linear approximation [1]. But at the beginning of the 90s scientists found a seasonal signature in a few baselines time series [2]. Later, the various deviations from linear dependence were described by Zarraoa [3]. The problem becomes complicated due to the fact that the detected seasonal variations can be affected by incorrect modeling of other natural effects. For example, Niell [4] showed that the seasonal variations into both horizontal and vertical components arise from incompleteness of mapping function simulation.

Important results on seasonal variations of the Earth's surface were published in papers about atmospheric pressure loading effect on VLBI station components displacement [5,6,7,8]. In spite of different approaches for modelling, the authors obtained similar estimates for vertical components annual shift (1-2 cm).

Scientists are used to paying more attention to high-frequency (2 weeks) variations of atmospheric pressure and VLBI site position components rather than to seasonal effects [9,10]. Additionally, Manabe et al., [7] and vanDam et al., [9] have studied the presence of an annual signal.

Titov et al., [11] have made a spectral analysis of baseline length time series from GSFC global solution published in 1995 [12]. They obtained evidence of annual and semiannual signals in the variations of the time series. It was demonstrated that variations of vertical components are responsible for changes in baselines.

In the last few years much new evidence for the presence of seasonal signals in geodetic time series have been collected. For example, Becker et al., [13] detected a seasonal signal for the Wettzell site vertical component from GPS time series. The signal has an amplitude about 4 mm. New results on seasonal variations of VLBI baseline lengths are presented this paper. The research has been made using NASA GSFC terrestrial reference frame solution 2001, July 2001 [14].

## 2. Results

Fig.1-3 demonstrate the results of WETTZELL - GILCREEK spectral and wavelet analysis. The spectrum in fig.1 has at least three significant signals - 0.5 year, 1 year and about 1.2 year

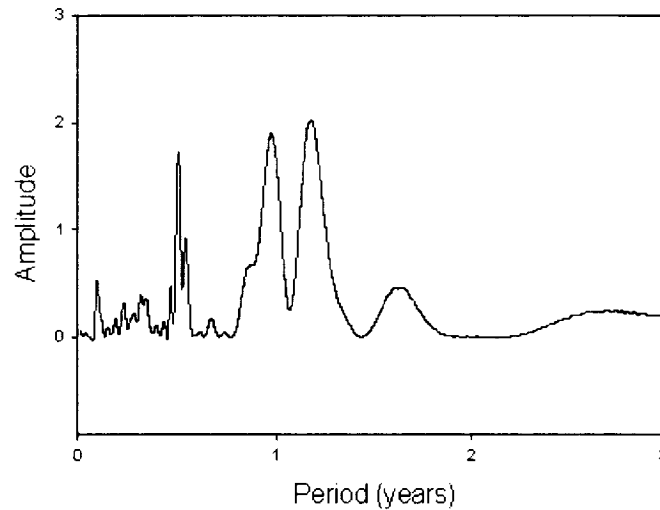


Figure 1. Spectrum of WETTZELL - GILCREEK baseline length time series. Significant semiannual, annual signals as well as signal with period about 1.2 year are visible.

which is close to the period of the Chandler wobble.

Detailed analysis showed that the periods and amplitudes of the signals are not constant, so it is impossible to use conventional procedures like least squares method for estimation of the parameters of the signals. Temporal behavior of the seasonal variations can be studied using wavelets. The method allows investigation of temporal variations of the periods and amplitudes if the signal is claimed as a process with variable parameters. To study unevenly spaced time series the special software by Foster [15] has been applied.

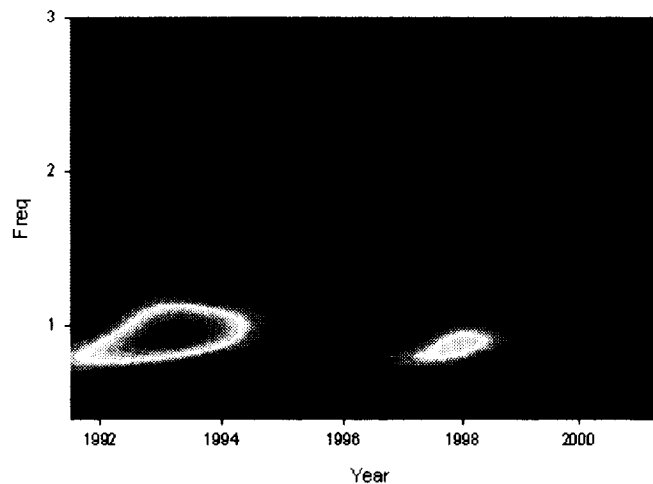


Figure 2. Wavelet of WETTZELL - GILCREEK baseline length variations (parameter 0.0125). Note increase in power near years 1993 and 1998.

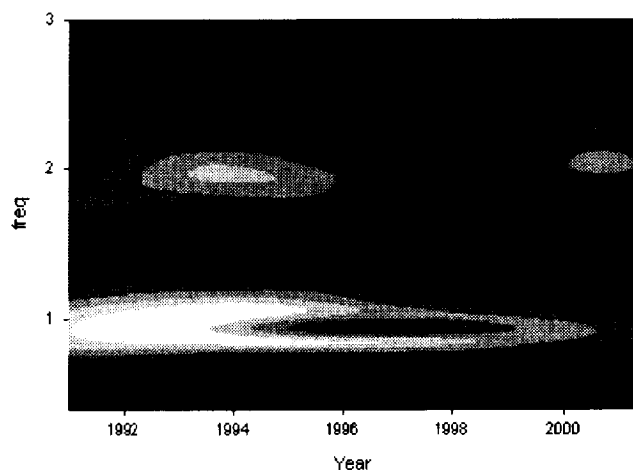


Figure 3. Wavelet of WETTZELL - GILCREEK baseline length variations (parameter 0.0030). The power is expanded across time interval, but now three signals are recognized (see fig.1).

In the wavelet technique a special parameter drives resolution in the time and frequency domains. The parameter 0.0125 provides an approximately equal resolution in both domains. Increasing the parameter results in increasing the resolution in time domain and decreasing in frequency domain. Decreasing the parameter has an opposite effect.

Results of the wavelet application to variations of baseline length WETTZELL - GILCREEK are shown on fig.2-3. In fig.2 the wide annual signal has maximum power near years 1993 and 1998. The semiannual signal has the only peak near year 1993. In fig.3 due to better resolution in the frequency domain the annual signal has been separated into two - properly annual signal and signal with period about 1.2 year. As to semiannual signal there are two wide maximums: in years 1993-1995 and in years 2000-2001.

Fig.4 demonstrates a spectrum of WETTZELL - WESTFORD baseline length variations between 1988 and 2001. Only an annual signal has been detected. Wavelets of the baseline length time series are shown in fig.5. The annual component in the baseline WETTZELL - WESTFORD has been fitted using least squares method to evaluate a range of seasonal signals (in spite of the variability of period). The estimate of the annual signal amplitude is  $4.5 \pm 0.7$  mm.

Similar estimation for baseline WETTZELL - GILCREEK (under assumption of constant periods and amplitudes) produced the following values: for period 0.5 year -  $2.4 \pm 0.7$  mm, for period 1 year -  $1.7 \pm 0.7$  mm, for period 1.2 year -  $2.1 \pm 0.7$  mm. It is obvious that for the period of maximum power the amplitudes are increasing and can reach a level of 4-5 mm.

### 3. Conclusion

Semiannual and annual signals have been found in spectra of baseline length time series. Additionally, a signal with period about 1.2 year has been found in the spectrum of baseline WETTZELL - GILCREEK. Meantime, detailed analysis of the time series using wavelets disclosed irregular behavior of the signals. Evaluation of the seasonal components under assumption of stability of the signals produced average estimates of the amplitude for all three components about  $2.0 \pm 0.7$

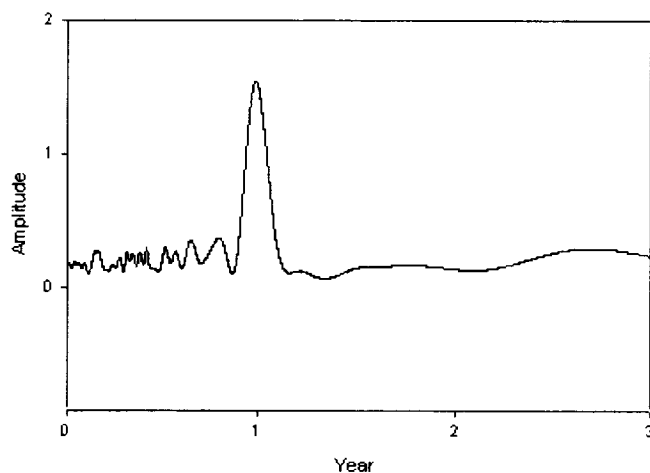


Figure 4. Spectrum of WETTZELL - WESTFORD baseline length variations has only one signal with period about 1 year.

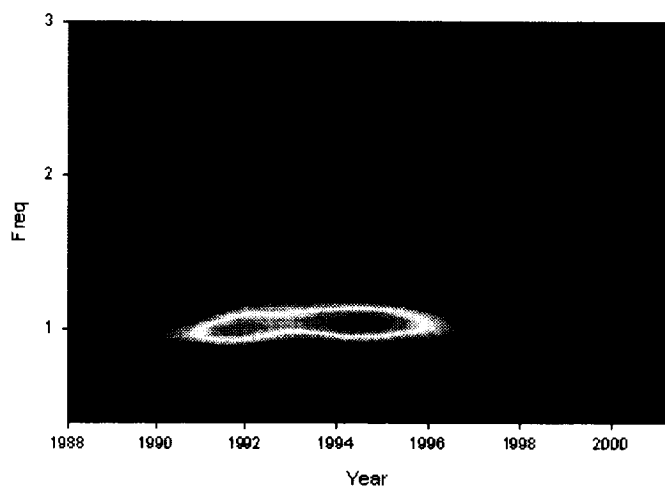


Figure 5. Wavelet of WETTZELL - WESTFORD baseline length variations (parameter 0.0125). The only annual signal has a maximum of power between years 1990 and 1997.

mm for baseline WETTZELL - GILCREEK and  $4.5 \pm 0.7$  mm for annual signal for baseline WETTZELL - WESTFORD.

#### 4. References

1. Argus, D.F., R.G. Gordon, No Net Rotation Model of Current Plate Velocities Incorporating Plate Model NUVEL-1, *Geophys. Res. Lett.*, 18, 2039-2042, 1991.
2. Herring, T.A., D. Dong, Current and future accuracy of Earth Orientation Measurements,

- in Proc. of AGU Chapman Conference on Geodetic VLBI: Monitoring and Global Change, 306-324, 1991.
3. Zarraoa, N., VLBI in the Far North. A Closer Look. in Proc. of 10-th Meeting on European VLBI for Geodesy and Astrometry, 103-108, 1995.
  4. Niell, A., Vertical Change and Atmospheric Correction in VLBI, in Proc. of AGU Chapman Conference on Geodetic VLBI: Monitoring and Global Change, 147-158, 1991.
  5. Stolz, A., D.E. Larden, Seasonal Displacement and Deformation of the Earth by the Atmosphere, *J. Geophys. Res.*, 84, 6185-6194, 1979.
  6. Rabbel, W., J. Zschau, Static Deformations and Gravity Changes at the Earth's Surface due to Atmospheric Loading, *J. Geophys. Res.*, 90, 80-99, 1985.
  7. Manabe, S., T. Sato, S. Saki, K. Yokoyama, Atmospheric loading effect on VLBI observations, in Proc. of AGU Chapman Conference on Geodetic VLBI: Monitoring and Global Change, 111-122, 1991.
  8. MacMillan, D. S., J. Gipson, Atmospheric Pressure Loading Parameters from Very Long Baseline Interferometry Observations, *J. Geophys. Res.*, 99, 18081-18087, 1994.
  9. vanDam, T. M, T.A. Herring, Detection of Atmospheric Pressure Loading using Very Long Baseline Interferometry, *J. Geophys. Res.*, 99, 4505-4517, 1994.
  10. MacMillan, D. S., C. Ma, Very Long Baseline Interferometry Atmospheric Modeling Improvement, *J. Geophys. Res.*, 99, 637-651, 1994.
  11. Titov, O., E. Yakovleva, Seasonal Variations in Radial Components of VLBI Stations, *Astron. Astroph. Transactions*, 18, 593-606, 1999.
  12. Ma C., J. Ryan, NASA Space Geodesy Program - GSFC Data Analysis, VLBI Geodetic Results, 1979-1995.5, Goddard Space Flight Center, Greenbelt, Maryland, 1995.
  13. Becker, M., J. Campbell, A. Nothnagel, Ch. Steinforth, Comparison and Combination of Recent European VLBI- and GPS-solutions, in Proc. of 14-th Working Meeting on European VLBI for Geodesy and Astrometry, 35-40, 2000.
  14. NASA Goddard Space Flight Center VLBI Group, Data products available electronically at <http://lupus.gsfc.nasa.gov/global>, 2001.
  15. Foster, G., Wavelets for Period Analysis of Unevenly Spaced Time Series, *Astrophysical Journal*, 112, 1789-1799, 1996.

## Comparison of the Baseline Length Between the Keystone Sites by Different Space Geodetic Techniques

Taizoh Yoshino<sup>1</sup>, Hiroo Kunimori<sup>2</sup>, Futaba Katsuo<sup>2</sup>, Jun Amagai<sup>2</sup>, Hitoshi Kiuchi<sup>2</sup>,  
Toshimichi Otsubo<sup>1</sup>, Tetsuro Kondo<sup>1</sup>, Yasuhiro Koyama<sup>1</sup>, Ryuichi Ichikawa<sup>1</sup>,  
Fujinobu Takahashi<sup>2</sup>

1) *Kashima Space Research Center/Communications Research Laboratory*

2) *Communications Research Laboratory*

Contact author: Taizoh Yoshino, e-mail: [yosh@crl.go.jp](mailto:yosh@crl.go.jp)

### Abstract

Three independent space geodetic systems, VLBI, SLR and GPS, are closely located at the Keystone sites maintained by the Communications Research Laboratory (CRL). The main purpose of the system is the study of the crustal deformation around Tokyo area. The other purpose is to contribute to improve the terrestrial reference frame. In the summer of 2000, extraordinary crustal deformation was observed in the Keystone network due to the seismic and volcanic event occurred at the Izu islands about 150 km south of Tokyo. Full process of the event was observed by the VLBI system. And a part of the process was also observed by the SLR and GPS of CRL. This kind of significant crustal deformation was firstly observed by the collocated space geodetic systems. Exploiting unique facilities, baseline length is compared between the different space geodetic systems which are tied by the precise surveying. The obtained geodetic results are contributed to the IERS to improve the ITRF.

### 1. Key Stone Project

The Keystone Project (KSP) was planned to observe the crustal deformation around Tokyo area using VLBI, SLR and GPS. For this purpose, precise geodetic observation systems are deployed at four sites (Koganei, Kashima, Miura and Tateyama) for regular observation. Since 1996, regular VLBI observation has been carried out with four stations. Since 1997, we performed quasi real-time VLBI observation for quick service. The other aspect of the project is to study the advanced geodetic observation by the collocation of independent geodetic observation system. We can study the error sources which are invisible by the single system observation. Moreover, we can contribute to the terrestrial reference frame by the collocated system.

### 2. Local Tie at the Key Stone Network

Three independent space geodetic systems, VLBI, SLR and GPS, are closely located at the Keystone sites as is seen in Figure 2. Precise survey was repeatedly performed to have precise eccentricity vectors between the observing systems. It is essential to show how the surveying data is obtained instead of showing only the results because we discuss the millimeter precision. Sharing the information of how to measure the precise position of reference point must be beneficial. Hence, the surveying data and method is opened. It is available from the following URL (<http://www2.crl.go.jp/t/team6/survey/contents.htm>).

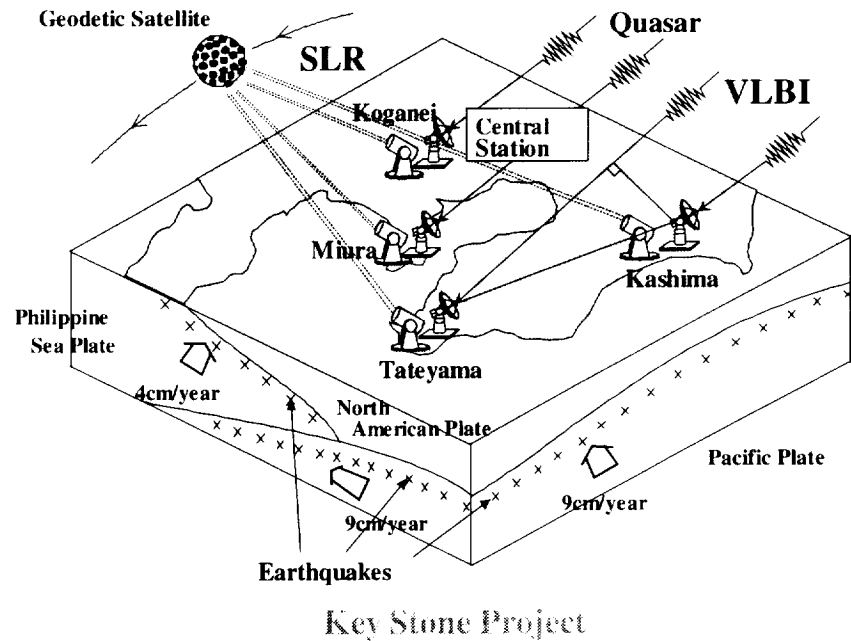


Figure 1. Network of the keystone project.

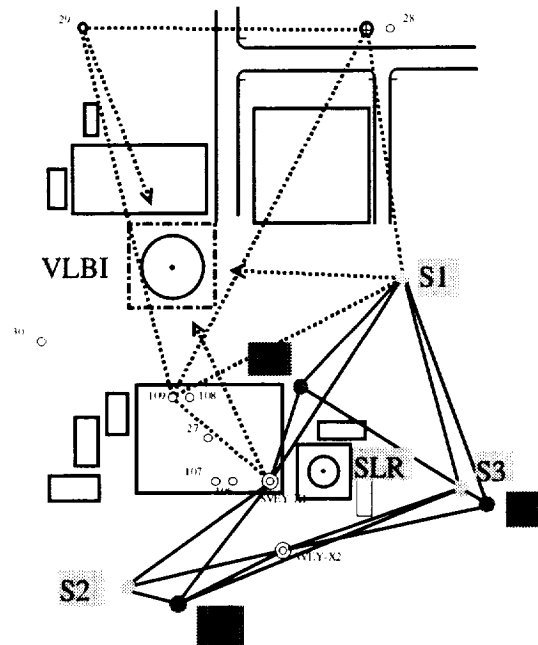


Figure 2. Koganei site and the surveying network

### 3. Extraordinary Crustal Deformation Observed in the Key Stone Network and the Comparison of the results from independent techniques

Extraordinary crustal deformation due to the seismic and volcanic activities at Izu islands was detected since the end of June, 2000 (Figure 3). The baseline length change over 2cm/month was

observed between Kashima and Tateyama, which is the largest in the Keystone network. It is one of the most significant crustal deformation detected by a space geodetic network of collocation sites. Full process of the event was observed by the VLBI system. And a part of the process was also observed by the SLR and GPS operated by CRL. Comparison of VLBI and SLR results is shown in Figure 4. Local tie data is applied to the plot. This is the first case to track the crustal deformation by both VLBI and GPS. Time resolution of SLR data is 15 days here. We see no bias between them within a formal error.

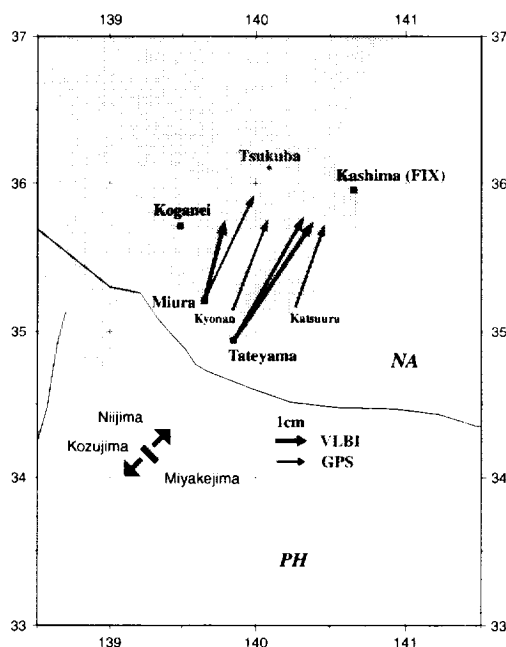


Figure 3. Site displacement in June 26 - Sept. 15, 2000.(GPS: GEONET).

#### 4. VLBI and GPS observation

At the event of the summer in 2000, significant crustal deformation was observed firstly by both VLBI and GPS. Full process of the event was observed. Baseline length change of Kashima-Tateyama is shown in Figure 5. Systematic error is not found.

#### 5. Contribution to the TRF

The obtained geodetic results and local tie data are contributed to the IERS to improve the ITRF. The data is to be included in the establishment of next ITRF.

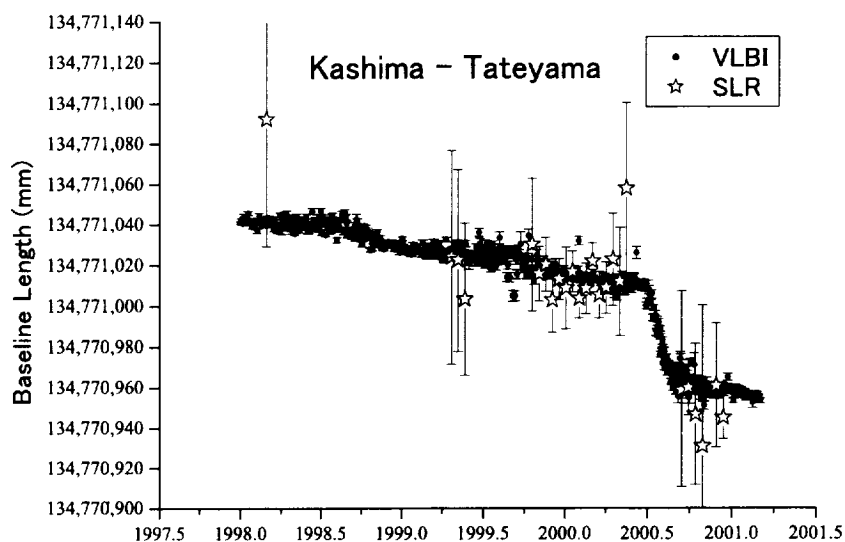


Figure 4. Comparison of the baseline length observed by VLBI and SLR using the local tie vector. (VLBI: 24hrs. solution, SLR: 15 days solution.).

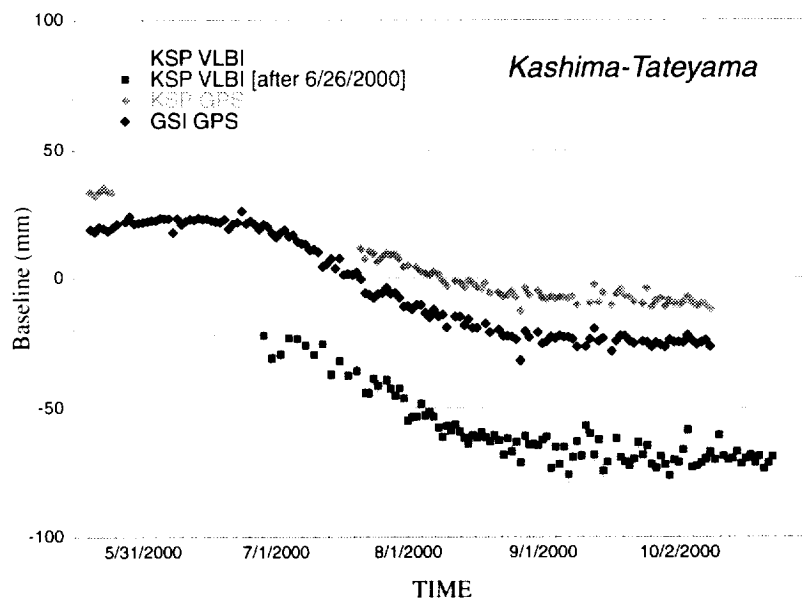


Figure 5. Network of the keystone project.

## The Antarctic VLBI Experiments During JARE39 and Geodetic Analysis by the Mitaka FX Correlator

Takaaki Jike<sup>1</sup>, Seiji Manabe<sup>1</sup>, Yoshiaki Tamura<sup>1</sup>, Kazuo Shibuya<sup>2</sup>, Koichiro Doi<sup>2</sup>, Teruhito Tanaka<sup>3</sup>, Peter McCulloch<sup>4</sup>, Marco Costa<sup>4</sup>, George Nicolson<sup>5</sup>, Jonathan F. H. Quick<sup>5</sup>, Katsuhisa Sato<sup>1</sup>, Katsunori M. Shibata<sup>6</sup>, Yoshihiro Fukuzaki<sup>7</sup>, David L. Jauncey<sup>8</sup>, John Reynolds<sup>8</sup>

<sup>1)</sup> National Astronomical Observatory Mizusawa, Japan

<sup>2)</sup> National Institute of Polar Research, Japan

<sup>3)</sup> NEC Corporation, Japan

<sup>4)</sup> University of Tasmania, Australia

<sup>5)</sup> Hartebeesthoek Radio Astronomy Observatory, South Africa

<sup>6)</sup> National Astronomical Observatory Mitaka, Japan

<sup>7)</sup> Geographical Survey Institute, Japan

<sup>8)</sup> Australia Telescope National Facility, CSIRO, Australia

Contact author: Takaaki Jike, e-mail: jike@miz.nao.ac.jp

### Abstract

JARE39 started the Antarctic VLBI project at Syowa station. In this project, four regular VLBI observations during the wintering were carried out and the VLBI raw data were correlated by the Mitaka FX correlator. We developed new software and applied it to the geodetic analysis of the Antarctic VLBI data. Main parts of development are the bandwidth synthesis and the time system transformation. By using this software, the position of Syowa VLBI reference point was estimated with standard deviations of 2.9 cm, 2.5 cm and 6.2 cm in x-, y- and z-components in the geocentric Cartesian system. These errors are larger than typical values of recent inter-continental VLBI experiments. To inspect the reliability of our analysis software, we compared performance of ours and GSI's analysis system by using observed delays which were determined from common VLBI data. Then, systematic delay differences with about 2 nanosecond were detected. Now, we are investigating its cause.

### 1. Introduction

Syowa station is one of the largest earth scientific observation complexes in the world. It is located on bedrock and has several geodetic observation instruments including space geodetic facilities. In 1998, a program for monitoring earth scientific phenomena occurring in the Antarctic plate by those instruments was advancing. As one of the main parts of this program, JARE39 (the Japanese Antarctic Research Expedition 39th, 1998) installed a standard VLBI observation system and started the Antarctic VLBI observation project [1]. In the project, regular VLBI observations throughout a year are planned and carried out during the wintering. Australian, South African and Japanese VLBI stations participated. Furthermore, this project has been continuing thereafter.

Two recording systems, K4 and S2, were used in the Antarctic VLBI project. The Mitaka FX correlator is able to handle both recording systems and, therefore, we adopted the Mitaka FX correlator to carry out correlation processing. However, necessary geodetic analysis tools were not fully implemented in the Mitaka FX correlator. Accordingly, we developed new geodetic analysis

tools for reducing the data of the Antarctic VLBI project. It is to be mentioned that the Mitaka FX correlator adopts the geocentric time system, which is different from other correlators used in geodesy previously. Therefore, we adopted and installed a function of time system transformation.

The position of Syowa VLBI reference point was determined from the JARE39 data with the newly developed geodetic analysis system mentioned above and agreed with the result of the observation in 1999 obtained with the use of a usual analysis system.

In this paper, we describe result of regular Antarctic VLBI observations in 1998, result of the correlation by Mitaka FX correlator, constitution of the newly developed geodetic software and result of the geodetic analysis by the software.

## 2. Result of the Observation and the Correlation

The VLBI experiments were carried out four times in 1998. Summary of the experiments is shown in Table 1. HartRAO, Hobart and Syowa formed a core network of the Antarctic VLBI project.

Table 1. Summary of the experiments conducted during JARE39.

Experiment Name	Start Epoch (UT)	End Epoch (UT)	Number of Obs.	Station ID
S98040,041	98/Feb/09 08:13	98/Feb/11 08:18	318	Hh,Ho,Sy,Ka
S98131,132	98/May/11 08:00	98/May/13 08:01	347	Hh,Ho,Sy,Ka
S98221	98/Aug/09 08:00	98/Aug/11 08:08	337	Hh,Ho,Sy
SYW984	98/Nov/09 08:00	98/Nov/11 08:12	398	Hh,Ho,Sy,Pk
Hh:HartRAO, Ho:Hobart, Sy:Syowa, Ka:Kashima, Pk:Parkes				

The Mitaka FX correlator started the correlation in April 1999. Various troubles specific to Syowa station that occurred in wintering gave big damage to our observation results. We could not detect fringes in the X-band in February observation. Quality of the data of the May and August experiments was not enough to perform analyses. In the November experiment, the trouble did not occur during observation, thus, good correlation results were obtained for all the baselines. Final result of correlation by the Mitaka FX correlator is shown in Table 2.

Table 2. Result of the correlation by the Mitaka FX correlator.

Exp. Name	Hh-Ho	Hh-Sy	Hh-Ka	Hh-Pk	Ho-Sy	Ho-Ka	Ho-Pk	Sy-Ka	Sy-Pk
S98040	○	S	○	-	S	○	-	S	-
S98041	○	S	-	-	S	-	-	-	-
S98131	-	○	-	-	-	-	-	-	-
S98132	○	×	○	-	×	○	-	×	-
S98221	×	×	-	-	×	-	-	-	-
SYW984	○	○	-	○	○	-	○	-	○
○:Fringes were detected in multiple scans. ×:No fringe was detected. S:Fringes were detected from only S band data.									

### 3. Outline of the Newly Developed Geodetic Analysis Software

Figure 1 shows the structure of the geodetic analysis system applied to the reduction of the Antarctic VLBI observations. The various steps are necessary before starting geodetic parameter estimation. In these tools, the bandwidth synthesis and time system transformation are mainly developed in this software.

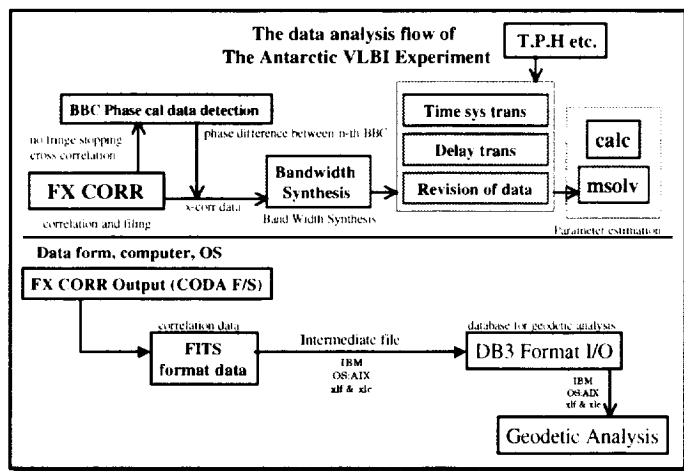


Figure 1. Structure of the geodetic analysis system for the Antarctic VLBI observations.

A standard algorithm is used in the bandwidth synthesis. However, the observed delay that the software outputs is expressed in geocentric time system that differs from the geodetic analysis specification. It is following the specification of the Mitaka FX correlator which adopts the geocenter as a time reference station common to all the ground stations. In processing of the Mitaka FX correlator, a delay is defined as a difference of epochs when the same wave-front from a celestial body passes the geocenter and a ground station, respectively, while observed delay is the difference in the time when this wave front passes two ground stations. The geometrical delay between two ground stations is computed as a difference of the delays between the geocenter and individual ground stations. On the other hand, the reference time of a priori delay used in geodetic analyses is the time when the wave-front from a celestial body reaches the time reference station on the ground. Figure 2 shows difference of two time system and delays. The magnitude of the delay due to the difference of the time systems is at most 1–10 nanoseconds and changes with time. Therefore the time system transformation is necessary to compensate the influence of the difference of time system between the observed and a priori delays. In figure 2, if the same wave front is observed with both time systems, the relation of two time systems is able to be expressed as  $t_x = t_0 + \tau_x$ .

In order to convert the delay following this transformation method, twice the atmosphere propagation delay must be added. By these processing, comparison of observed delay obtained

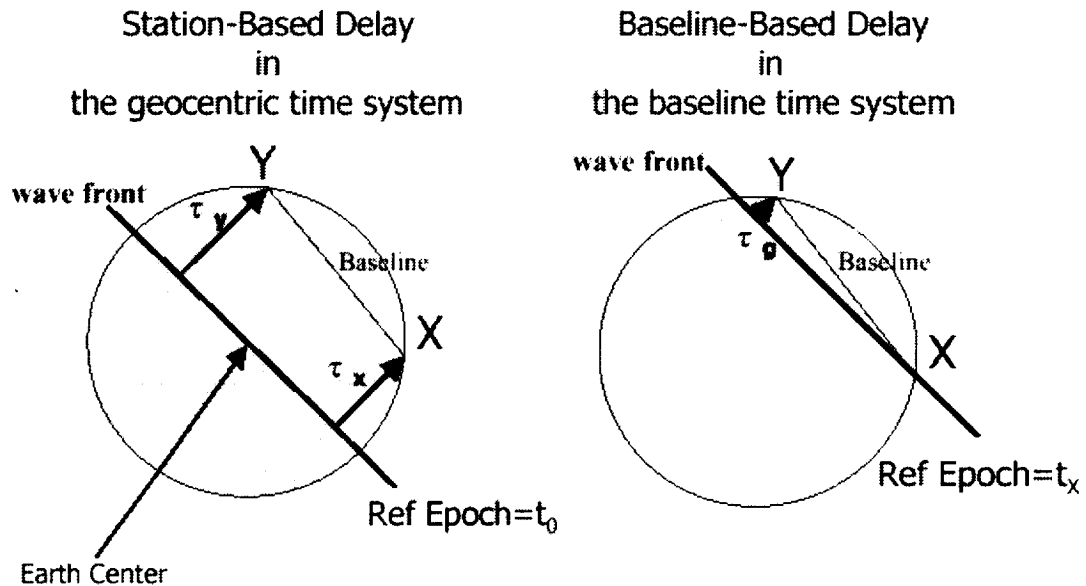


Figure 2. Delays in the geocentric time system and in the baseline time system.

from the Mitaka FX correlator and a priori delay computed with CALC3 became possible.

#### 4. Result of the Analysis

The parameter estimation was performed for the data in November, 1998 by using “msolv”. By the processing, the position of the Syowa VLBI point was estimated with differences in -0.3 cm, -1.6 cm and 2.1 cm to the position predicted from ITRF2000 and with standard deviations of 2.9 cm, 2.5 cm and 6.2 cm in x-, y- and z-components in the geocentric Cartesian system. An error ellipsoid is shown in figure 3. Form of this ellipsoid does not contradict the error estimation of the VLBI position measurement reported by Takahashi [2]. In addition, standard deviations of the post-fit residual delays for the individual baselines are about 300 picoseconds. These errors were larger than typical values of recent inter-continental VLBI experiments.

The causes of the large standard deviation must be researched to confirm the reliability of the newly developed analysis system and the analysis result. Thereupon, we compared the accuracy of delay determination with our newly developed analysis system and GSI’s analysis system. In the comparison, the differences were obtained in two observed delay sets which were individually determined with two systems mentioned above. Furthermore, the common VLBI data used in the comparison is SYW997, which was obtained with the Antarctic VLBI observation in 1999. As the result, the systematic delay differences of about 2 nanoseconds were detected, when the delays were discerned with the individual observed radio sources. Now, in order to resolve the problem, we are investigating the influences which are bases to the special processing of the Mitaka FX correlator.

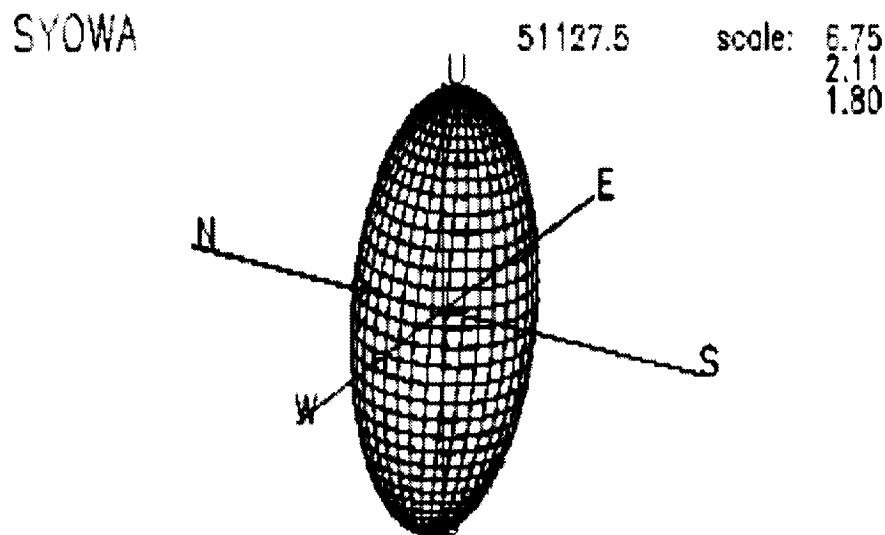


Figure 3. Error ellipsoid of the estimated position of Syowa.

#### 4.1. Future Plan of Software Development

The main part of the geodetic analysis system for the Mitaka FX correlator is considered to be usable as one of the core parts of a VERA analysis system and a large contribution is expected in the VERA project. Accordingly, the improvement of the reliability is indispensable. Furthermore, the reconstruction of the software will be continued along with the future activity of other VLBI analysis software and global models.

#### 5. Acknowledgements

The VLBI experiments at Syowa station are supported by many people and many institutes at various stages. The authors would like to express their thanks to K. Kashiwabara (Anritsu Corporation, JARE39), S. Kuji, N. Kawaguchi, T. Miyaji (NAO), M. Tobita, T. Kawahara, S. Ogi, K. Takashima (GSI), Y. Takahashi, N. Kurihara (CRL) and members of JARE39.

#### References

- [1] Jike, T., T. Tanaka, K. Shibuya, S. Manabe, Y. Tamura, K. Sato, P. McCulloch, M. Costa, G. Nicolson, J. F. H. Guick, K. M. Shibata, K. Doi, Y. Fukuzaki, D. L. Jauncey, J. Reynolds, VLBI Experiments at Syowa Station, Antarctica, In: Proceedings of the International Workshop on GEodetic Measurements by the collocation of Space Techniques ON Earth, Jan. 25-28, 1999, CRL, Koganei, Tokyo.
- [2] Takahashi, Y., Estimation of errors in VLBI data and position, In: J. Geod. Soc., Japan, 40, 309-332.

## VLBI Evidence for Glacial Rebound in Europe

*Kurt Lambeck*<sup>1</sup>, *Anthony Purcell*<sup>1</sup>, *Oleg Titov*<sup>2</sup>, *David Jauncey*<sup>3</sup>

<sup>1)</sup> *Research School of Earth Sciences, ANU*

<sup>2)</sup> *Geoscience Australia*

<sup>3)</sup> *ATNF, CSIRO*

*Contact author: Kurt Lambeck, e-mail: [kurt.lambeck@anu.edu.au](mailto:kurt.lambeck@anu.edu.au)*

### Abstract

The present-day glacial rebound of northern Europe is well recorded in tide gauge records. Less well recorded are the horizontal displacements of the crust associated with the rebound. Predicted rates of displacement are of the order of 1 mm/yr. Reasons for observing rebound include i) the evidence it presents for mantle rheology, and ii) the associated strain field is indicative of the changes in stress of the lithosphere. The VLBI baselines containing information on the horizontal displacements are complementary to the vertical displacements measured by geodetic and geological means, and lead to improved solutions for mantle rheology. Observed baselines between four selected VLBI sites are compared with predictions based on different combinations of earth and ice models to determine optimum rebound parameters. In addition, prediction of rebound displacements are made for potential future VLBI observations using the Crimean and Svetloe sites, as well as a possible mobile site on the Gulf of Bothnia.

## Comparative Study of the EOP Series Derived for the Second IVS Pilot Project

*D. Gambis, Ch. Bizouard, T. Carlucci, D. Jean-Alexis*

*IERS EOP-PC / Observatoire de Paris*

*Contact author: D. Gambis, e-mail: [daniel.gambis@obspm.fr](mailto:daniel.gambis@obspm.fr)*

### Abstract

Biases and rms of IVS 2001 Pilot series with respect to the IERS reference series C04 are presented and compared to those derived by the GPS operational series. Significant inconsistencies appear and are discussed.

### 1. Consistency of EOP Series

An important task of the IERS is to maintain reference series for Earth Orientation Parameters (EOP), providing users the rotation matrix between the International Celestial Reference Frame (ICRF) and the International Terrestrial Reference Frame (ITRF). The reference series, labelled as C04, is achieved from the combination of individual EOP series for a given space geodetic technique and are collected at the EOP Product Center at the Paris Observatory.

The Earth Orientation Parameters of the reference series C04 present significant biases and trend with respect to those of the individual series. The most common explanation is that they arise from the small rotation matrix between the ITRF, respectively the ICRF - to which is theoretically referred the C04 series, and the terrestrial, respectively the celestial, reference frame associated with the individual series.

Let  $\Delta x$ ,  $\Delta y$  be the observed biases for  $x$  and  $y$  pole coordinates,  $\Delta UT1$  the observed bias for  $UT1 - UTC$ ,  $\Delta\psi$ ,  $\Delta\varepsilon$  the observed biases for nutation offsets. The theoretical biases can be induced from infinitesimal rotation angles  $R_{i(i=1,2,3)}$  (respectively  $A_{i(i=1,2,3)}$ ) from the ITRF (respectively ICRF) to the terrestrial (respectively celestial) frame associated with the individual series. The closure relation between observed biases and theoretical ones are called consistencies, and have the following expressions :

$$\begin{aligned} C(x) &= \Delta x - R_2 \\ C(y) &= \Delta y - R_1 \\ C(kUT1) &= k\Delta UT1 - (-R_3 + A_3) \\ C(\delta\psi \sin \varepsilon_0) &= \Delta\psi - A_2 \\ C(\delta\varepsilon) &= \Delta\varepsilon + A_1 \end{aligned}$$

where  $k = 1.00273$  is the conversion factor from the mean solar day to the sidereal day and  $\varepsilon_0$  the obliquity of the ecliptic at the epoch J2000.0.

When considering all the available series, we can distinguish two cases :

- Consistencies of a given EOP parameter present small dispersion with respect to a significant average. In this case the C04 series present a shift with respect to international reference frames, and have to be corrected by adding offsets.
- Consistencies present large dispersion: we can conclude there are inconsistencies in the individual series.

For a better understanding of the origin of inconsistencies, IVS organized a campaign analysis in which EOP parameters are determined by constraining the radio source coordinates to those of the ICRF-Ext1 and the station source coordinates to those of the ITRF 2000. In this case angles  $R_{i(i=1,2,3)}$  and  $A_{i(i=1,2,3)}$  are equal to zero, and consistencies are directly equal to observed bias. In turn if C04 series be ideal, biases should be equal to zero.

In the following section, we present the bias of IVS Pilot series with respect to C04. Then we shall present similar analysis for GPS and SLR operational series collected at the EOP Product Center. Finally we discuss the “mean consistency” of all these series.

## 2. Bias of IVS Pilot Series

IVS Pilot series were derived from all available NEOS-A 24hr VLBI session. They range from 1999.0 to 2001.0. Estimated parameters include the pole components x-pole, y-pole, UT1-UTC and the nutation offsets  $d\psi$ ,  $d\epsilon$  with respect to IAU 1980 model. Eleven centers participated in this campaign. Actually some of the series considered here are operational ones, updated twice a week (IAA, BKG, AUS, SPBU, GSF).

We have computed the biases and rms of these series with respect to C04 series, and for each EOP parameter. They are displayed on Figures 1 for x-pole and y-pole.

For x-pole coordinate, the bias are not so homogeneous ranging from  $-0.016$  mas (BKG) to  $-0.22$  mas (JPL). The standard deviations are between 0.1 and 0.2, except for the JPL series which presents a suspect rms. The averaged bias, without considering JPL series, is about  $-0.060 \pm 0.076$  mas. For y-pole coordinate biases are much more homogeneous than for x-pole, and are centered around the mean value  $0.326 \pm 0.024$  mas. The JPL series and CAN series have anomalous bias and too large rms.

For UT1-UTC the biases range between 5 and 25 microseconds. Again the JPL series present anomalous rms.

For nutational offsets, the bias and rms are much less homogeneous than for the other parameters. For IGF and DGF series the observed large bias and rms, according to the authors of these series, do not reflect reality but some analysis problem linked to bad choice of unit. The mean value of the bias, except for anomalous values, is  $-0.012 \pm 0.058$  mas for  $d\psi \sin \epsilon_0$  and  $0.048 \pm 0.034$  mas for  $d\epsilon$ .

## 3. Biases of GPS Operational Series

The same kind of approach was done for the nine GPS operational series, covering the period 1999-2001, which we collect at Paris Observatory in the framework of the EOP Product Center of the IERS. We report bias and rms for x-pole and y-pole on Fig. 2. The biases are much more heterogeneous than in the case of VLBI pilot series. This could be expected from the fact that GPS series are referred to ITRF 2000 sub-network, which present significant small rotations with

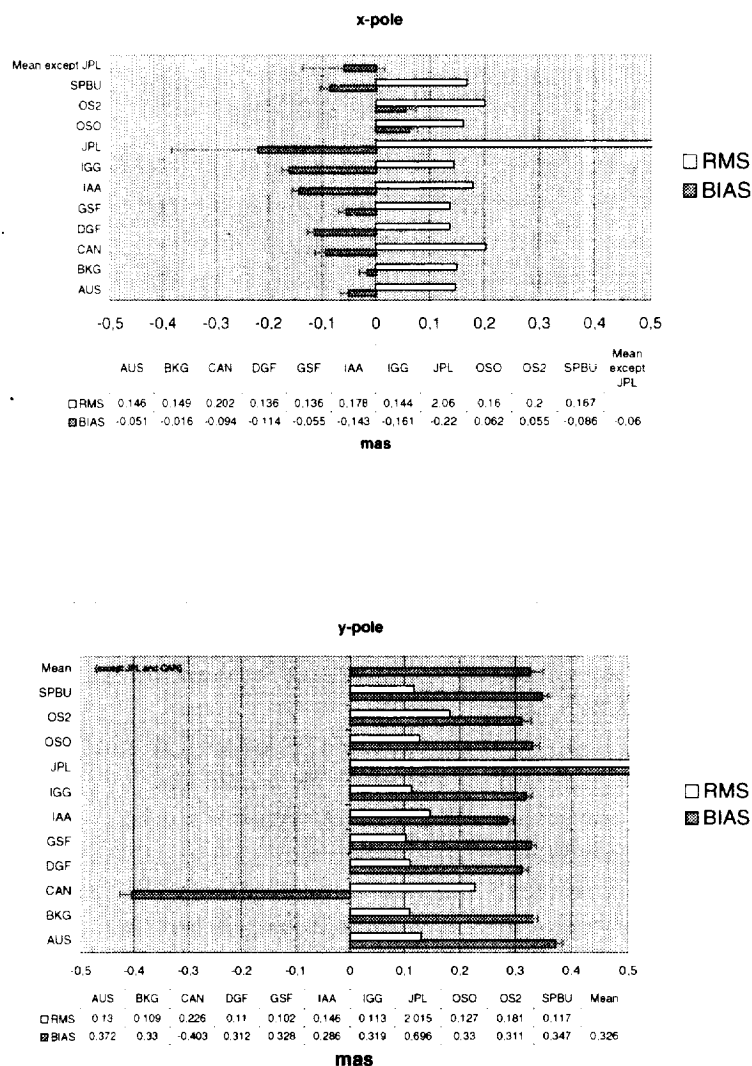


Figure 1. Biases and rms of VLBI Pilot series with respect to C04 : x-pole, y-pole.

respect to ITRF 2000.

The mean bias for x-pole is  $-0.024 \pm 0.024$  mas and for y-pole  $0.170 \pm 0.058$  mas.

The rms are about two times smaller than in the case of VLBI series. Actually this does not prove that GPS series are better, but this reflects the greater weighting of GPS operational series in the combined solutions C04.

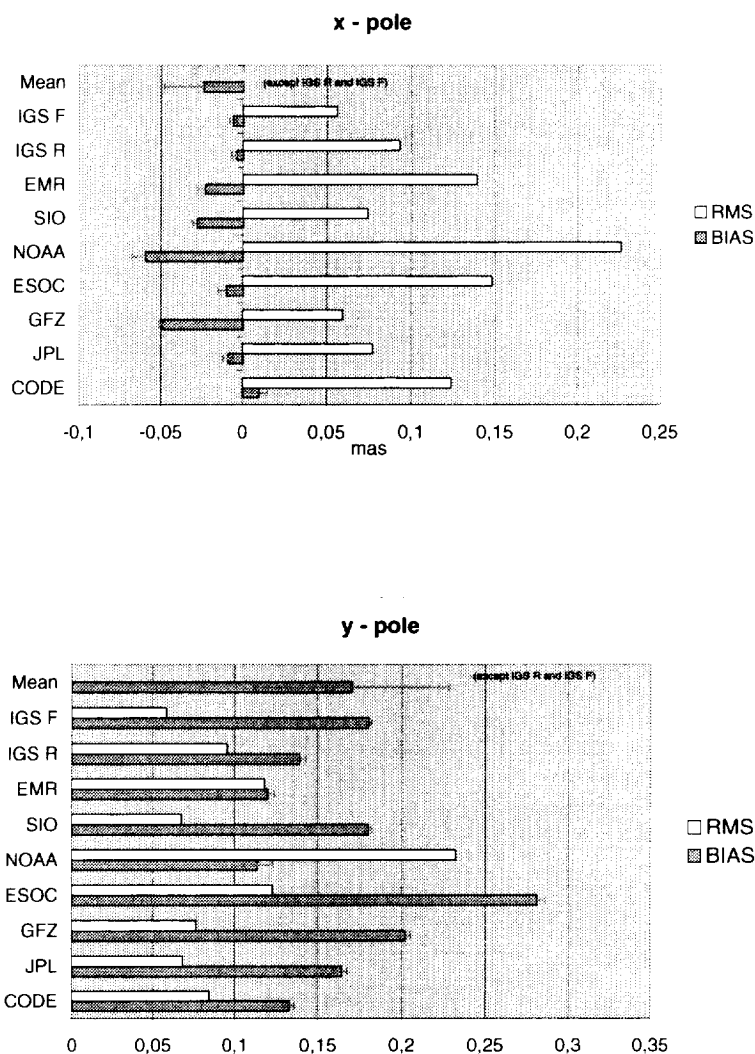


Figure 2. Biases and rms of GPS operational series with respect to C04 : x-pole, y-pole.

#### 4. Mean Consistencies

Considering that the series are in principle referred to ITRF and ICRF, their corresponding consistencies are directly given by their bias with respect to C04. We present here a comparison between the mean consistency for IVS Pilot series, GPS operational series, SLR operational series, and VLBI series analysed in the framework of the IERS 2000 annual report.

Fig. 3 shows that all consistency values have the same sign, except for SLR series. Notice that consistencies of polar motion derived from SLR is almost perfect.

For nutational pole offsets inconsistencies are at the level of 0.04 mas, but are smaller than the rms of the individual series (more than 0.1 mas).

A larger confidence can be attributed to the mean consistencies for polar motion. In the case of VLBI Pilot series they are about two times larger than in the case of GPS series. Comparison with the mean consistencies of VLBI series for IERS annual report 2000 cannot be done strictly, in the sense the consistency analysis has been for a much larger interval of data, in most of the cases 1988-2000.

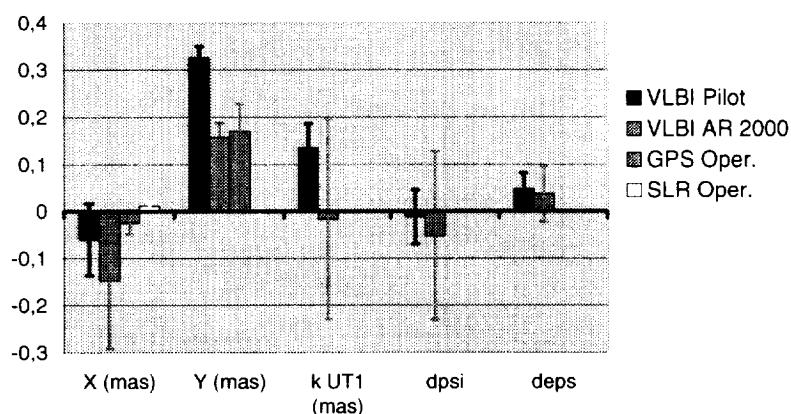


Figure 3. Mean consistencies of VLBI Pilot, GPS operational, VLBI Annual Report 2000, SLR operational series.

## 5. Conclusion

Systematic differences appear between the IVS Pilot series and C04 for the time span 1999-2001. The most significant ones concern polar motion, up to 0.3 mas for y-pole coordinate. GPS operational solutions for polar motion present also significant offset with respect to C04, on average two times smaller than the IVS Pilot series. Mean differences between VLBI and GPS Pilot solutions are  $-0.036$  mas for x-pole and  $0.156$  mas for y-pole.

Such discrepancies could be due to sub-network effects, insufficient modelling of the tropospheric correction. More investigations are needed at the level of the analysis centers, for instance the test of the influence of the network for GPS solutions.

These results show slight inconsistency of the C04 polar motion. It seems that C04 is a little bit shifted with respect to ITRF 2000, by  $-0.30$  mas in y-component according to Pilot series,  $-0.15$  mas according to GPS operational series, and that a jump of the opposite quantities (but which ones?) should be applied for setting it in agreement with ITRF 2000.

# A Comparison of the VLBI Nutation Series with IAU2000 Model

Zinovy Malkin

*Institute of Applied Astronomy of Russian Academy of Sciences (IAA)*

*e-mail:* malkin@quasar.ipa.nw.ru

## Abstract

This paper presents preliminary results of investigation of VLBI nutation series available in the IVS data base. It is shown that rather large systematic differences exist between these series, especially in 1984-1986. However, all series reveal common details in comparison with IAU2000A and MHB2000 nutation models. From analysis of the differences between VLBI and model nutation series preliminary values of corrections to precession parameters are estimated.

## 1. Introduction

This paper continues an analysis of investigation of the VLBI results of determination of nutation of the Earth's rotation axis in comparison with the latest nutation models ([4]). At the first step of this study we performed mutual comparison of the VLBI nutation series. Then they are compared with the MHB2000 model ([3]) and IAU2000 model available in the draft IERS Conventions (2000) distribution available at <ftp://maia.usno.navy.mil/conventions/>. The only difference between these models is that the latter does not include unpredictable, time-varying Free Core Nutation (FCN) contribution.

We used for comparison four long-time VLBI series available in the IVS data base and MHB2000 series available at <http://www-gpsg.mit.edu/~tah/>. The latest MHB2000 version used here is of the end of 2001 and provides FCN amplitudes determined from observations for period ended at epoch June 1, 2001. After this date FCN value is available only as prediction and one should keep this in mind during comparisons of the model with observations after this date.

## 2. Preliminary Investigation of the VLBI Series

We have used for our analysis four series: BKG00001, GSF2001C, USN2001D computed with CALC/SOLVE, and IAAO0106 computed with OCCAM. Only one of three BKG series available in the IVS was used after preliminary analysis which showed that systematic differences in nutation series between them is negligible for this study. No one reported data were excluded except several GN88 experiments present in the BKG solution.

Figure 1 shows formal errors reported in the compared series. Since formal errors and overall rms differences with MHB2000 differ for compared series at the level about 10% no weighting of input series was applied.

It was found [4] that differences between nutation series obtained with CALC/SOLVE and OCCAM packages contain an annual term with amplitude about 0.16-0.17 mas, whereas the differences between series obtained with the same software are very small (usually less than corresponding rms). Detailed investigation of this problem led us to the conclusion that the most probable reason for that systematic difference is the double account of the effect of geodesic precession in OCCAM.

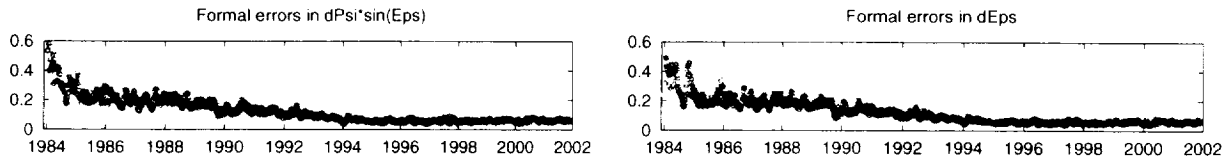


Figure 1. Formal errors in nutation series: BKG (circles), GSF (triangles), IAA (diamonds), USN (inverted triangles).

Table 1 shows comparison of nutation series before and after correction of OCCAM (IAA) data. One can see that after correction systematic differences between IAA and CALC/SOLVE-based series practically disappeared. Fortunately, this error can be easily corrected in submitted OCCAM series without re-processing.

Table 1. Annual term in differences between IAA and others  $\Delta\psi$  series before (on the left) and after (on the right) correction of the IAA series,  $\mu\text{as}$ .

	AUS	BKG	GSF	SPU	USN		AUS	BKG	GSF	SPU	USN
IAA	25	176	189	72	184	IAA	147	38	33	100	32
	$\pm 30$	$\pm 28$	$\pm 26$	$\pm 30$	$\pm 26$		$\pm 30$	$\pm 29$	$\pm 26$	$\pm 30$	$\pm 26$

Another possible reason of systematic differences between nutation series computed in various Analysis Centers is using different models of daily and subdaily EOP variations models. Judging by descriptions of VLBI EOP solutions present in the IVS data base four or five models of short-period tidal variations are used in various AC which lead to inconsistency of nutation series. For preliminary estimation of a possible effect we compared two series computed at the IAA with two models of daily and subdaily EOP variations. The result presented in Table 2 show small but visible influence of choice of model on estimates of nutation. Obviously, this problem should be investigated in more detail.

Table 2. Differences between series computed with two models of daily and subdaily EOP variations (Eanes's model – Ray's model): bias, rate/year, amplitude of annual term, amplitude of semiannual term,  $\mu\text{as}$ .

EOP	bias	rms	rate	rms	amp(a)	rms	amp(sa)	rms
$\Delta\psi$	-27	18	16.3	7.3	20	26	27	26
$\Delta\epsilon$	22	9	2.2	3.4	7	12	5	12

### 3. Comparison with the MHB2000 Model

The result of comparison of the VLBI series with the MHB2000 model is shown in Figure 2. One can see that differences are rather large for the period before about 1990.0, especially for 1984–1985 where, in addition, systematic difference between IAA and CALC/SOLVE-based series is clearly detected. Also, all series show the same discrepancy with the MHB2000 model during last several months which evidently can be explained by errors in FCN extrapolation after 2001.4.

Some analysts suppose that a reason for peculiarities in the EOP series in the 1980s is non-linear motion of HRAS station. However, in all the compared series its position is modelled with linear velocity, and a possible effect of irregular HRAS motion must be the same for all

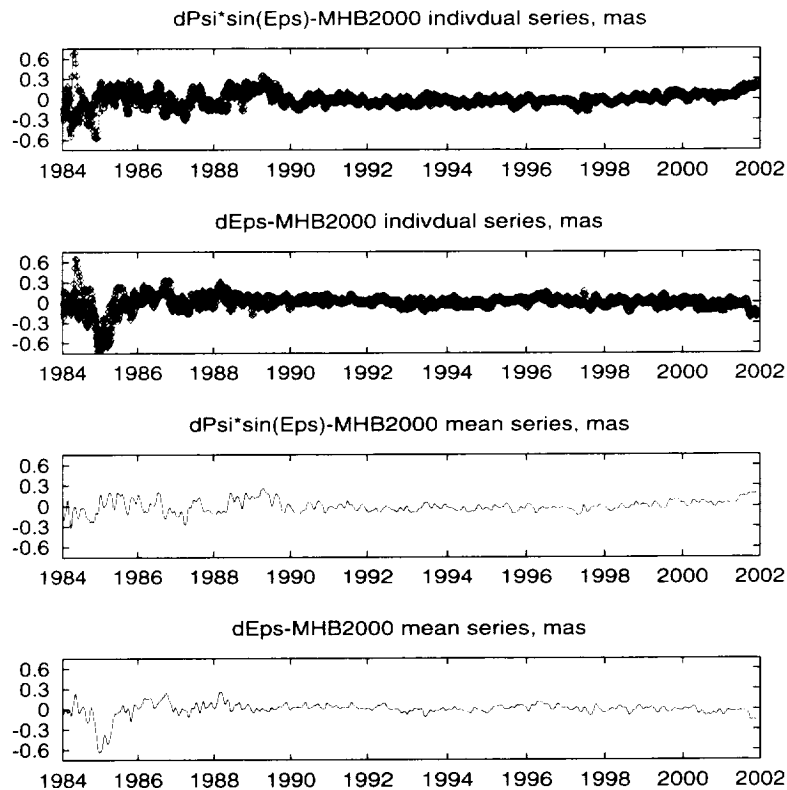


Figure 2. Comparison of the VLBI series with the MHB2000 model (smoothed). Two top plots show individual nutation series: BKG (circles), GSF (triangles), IAA (diamonds), USN (inverted triangles). Two bottom plots show unweighted average values.

compared series. Besides, analysis made by L. Petrov (GSFC) showed that differences between nutation series obtained with linear and more sophisticated model of HRAS motion are much lesser than found here ([http://gemini.gsfc.nasa.gov/pet/discussion/hras\\_eop/hras\\_eop.html](http://gemini.gsfc.nasa.gov/pet/discussion/hras_eop/hras_eop.html)). Evidently more detailed analysis is needed to explain these differences.

In any case, FCN model evidently requires substantial correction for the period 1984–1985. On the other hand, these differences can be a result of some common error in the VLBI results, indeed.

#### 4. Comparison with the IAU2000 Model

Figure 3 shows the results of comparison of the VLBI nutation series with the IAU2000 model which can be interpreted as FCN contribution. Again, all series show a good agreement except for the period 1984–1985.

It is of common interest to investigate how accurate the FCN contribution can be predicted. The first experiments with auto-regression algorithm show that it can be predicted with accuracy at least  $50 \mu\text{as}$  for a period of several months.

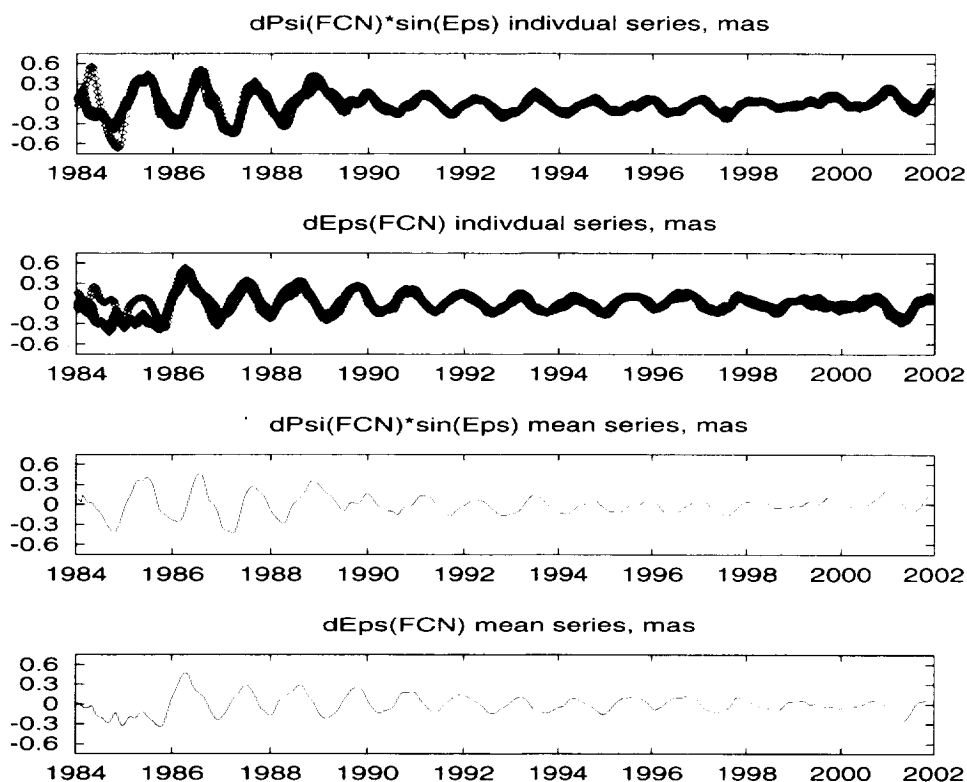


Figure 3. Comparison of the VLBI series with the IAU2000A model (FCN contribution, smoothed). Two top plots show individual nutation series: BKG (circles), GSF (triangles), IAA (diamonds), USN (inverted triangles). Two bottom plots show unweighted average values.

## 5. Corrections to Precession Parameters

Precession parameters were estimated as linear trend along with largest long-period terms  $6798.38^d$ ,  $3399.19^d$ ,  $365.26^d$ ,  $182.62^d$ ,  $121.75^d$ . One can see from Figures 1 and 2 that VLBI results show significant improvement beginning from epoch  $\sim 1990.0$ . So, we have computed the precession parameters both for the whole interval 1984.0–2001.9 and for 1990.0–2001.4. (In the latter case the term with period  $6798.38^d$  was not included in the adjustment procedure.)

The results of computation are presented in Table 3. For more detailed comparison we computed results both for individual series and for all their combinations. Table 3 contains results for individual series, averaged CALC/SOLVE series and averaged over all four compared series. One can see that there is no evident systematic differences between OCCAM and CALC/SOLVE results for  $\Delta\psi$ , however such a difference obviously exists for  $\Delta\epsilon$ .

Obtained corrections to precession parameters  $\Delta\psi$  and  $\Delta\epsilon$  rates averaged over all the series are in reasonable good agreement with those found in [1, 2].

## 6. Conclusions

The results of this study allow us to make some conclusions.

Table 3. Corrections to precession parameters.

Series	1984.0–2001.9				1990.0–2001.4			
	$\Delta\psi$		$\Delta\epsilon$		$\Delta\psi$		$\Delta\epsilon$	
	bias	rate	bias	rate	bias	rate	bias	rate
BKG	$-14\pm 9$	$+42\pm 4$	$-25\pm 4$	$+11\pm 2$	$-42\pm 5$	$+24\pm 2$	$-10\pm 2$	$-6\pm 1$
GSF	$+18\pm 9$	$+20\pm 4$	$-27\pm 3$	$+6\pm 2$	$-36\pm 5$	$+13\pm 2$	$-20\pm 2$	$-9\pm 1$
IAA	$+12\pm 9$	$+34\pm 4$	$+37\pm 3$	$-5\pm 2$	$-72\pm 5$	$+25\pm 2$	$+29\pm 2$	$-2\pm 1$
USN	$-23\pm 9$	$+27\pm 4$	$-34\pm 4$	$+8\pm 2$	$-71\pm 6$	$+14\pm 2$	$-14\pm 2$	$-8\pm 1$
BKG GSF USN	$-7\pm 8$	$+31\pm 4$	$-28\pm 3$	$+8\pm 2$	$-50\pm 5$	$+17\pm 2$	$-14\pm 2$	$-8\pm 1$
BKG GSF IAA USN	$-2\pm 8$	$+32\pm 4$	$-11\pm 3$	$+4\pm 1$	$-57\pm 5$	$+19\pm 2$	$-5\pm 2$	$-6\pm 1$

1. Results of determination of nutation angles with OCCAM and CALC/SOLVE differ substantially in the period 1984–1986 which must be investigated in more detail. All VLBI series indicate that MHB model (most probably FCN component) requires substantial correction for this period.

2. The analysis of differences between observed and theoretical nutation values along with comparison of formal errors of the VLBI nutation series give a hint that maybe only VLBI results obtained for observations made after 1989 are accurate enough for meaningful comparison with the modern models of Earth's rotation.

3. The influence of adopted model of short-period EOP variations should be investigated in more detail. It seems reasonable to use a unified model in all Analysis Centers for better consistency between EOP series.

## 7. Acknowledgement

Author is very grateful to the organizers of the Second IVS General Meeting for financial support of his trip to the meeting.

## References

- [1] Feissel, M., M. Yseboodt, V. Dehant, O. de Viron, C. Bizouard. How much can we cheat the non-rigid Earth nutation theory to make it match VLBI results? Journées 2001 "Influence of geophysics, time and space reference frames on Earth rotation studies", Brussels, Belgium, Sep 24–26, 2001.
- [2] Feissel, M., Ma, C. Radio Source Stability and the Observation of Precession-nutation. Second IVS General Meeting, Tsukuba, Japan, Feb 3–7, 2002.
- [3] Herring, T. A., Mathews, P. M., Buffet, B. A. Modelling of Nutation-Precession: Very long baseline interferometry results. JGR, in press.
- [4] Malkin, Z. A comparative analysis of the VLBI nutation series. Presented at the Journées 2001 Influence of geophysics, time and space reference frames on Earth rotation studies, Brussels, Belgium, 24–26 September 2001.

## Comparison of Tropospheric Parameters Submitted to the 2nd IVS Analysis Pilot Project

*Johannes Boehm, Eva Messerer, Harald Schuh*

*Institute of Geodesy and Geophysics IGG, University of Technology, Vienna*

*Contact author: Johannes Boehm, e-mail: [jboehm@luna.tuwien.ac.at](mailto:jboehm@luna.tuwien.ac.at)*

### Abstract

At the IVS Analysis Workshop at GSFC in February 2001, it was agreed that the 2nd IVS Analysis Pilot Project should also deal with a comparison of tropospheric parameters to be submitted by the Analysis Centers (AC) in addition to the Earth orientation parameters. Nine ACs provided ten series of tropospheric parameters, derived from all NEOS-A sessions in the years 1999 and 2000. These parameters included total (hydrostatic and wet) zenith path delays and horizontal gradients. First comparisons show that the VLBI and IGS (International GPS Service) total zenith path delays are of comparable accuracy with regard to 24 h mean values as well as hourly values. However there is a constant offset between the VLBI and GPS time series of the individual sites.

### 1. Introduction

At the 2nd IVS Analysis Workshop at Goddard Space Flight Center (GSFC) in February 2001, the 2nd IVS Analysis Pilot Project (PP) was initiated. The submission of tropospheric parameters derived from all (104) NEOS-A sessions in 1999 and 2000 was requested in addition to the Earth orientation parameters. The Institute of Geodesy and Geophysics (IGG) at the Vienna University of Technology, Austria, which is in charge of the tropospheric part of the 2nd PP, received ten different solutions from nine ACs with the Onsala Space Observatory (OSO) submitting two solutions (Table 1). Four ACs used OCCAM software packages, another four CALC/SOLVE and the AC at Jet Propulsion Laboratory (JPL) applied the MODEST software package. Apart from two ACs (AUS, IAA) which used the Kalman filter technique, all other ACs applied the "classical" least-squares fit with the Gauss-Markoff model for their analyses. The Niell

Table 1. Overview of the participating Analysis Centers (AC). Ten solutions were submitted by nine ACs.

AUS	AUSLIG, Australia	Occam
BKG	BKG, Germany	Calc/Solve
CAN	NRC, Canada	Calc/Solve
DGF	DGFI, Germany	Occam
GSF	NASA GSFC, U.S.A.	Calc/Solve
IAA	IAA, Russia	Occam
IGG	IGG, Austria	Occam
JPL	NASA JPL, U.S.A.	Modest
OSO	OSO, Sweden	Calc/Solve
OS2	OSO, Sweden	Calc/Solve

mapping functions (Niell, 1996 [2]) were used for all analyses. The cutoff elevation angles were always below eight degrees, mostly set to five degrees elevation. As requested for this Pilot Project, all station coordinates were fixed to the ITRF2000.

## 2. Comparison of Total Zenith Path Delays

After manual editing (removal of outliers, closing gaps by interpolation), the total zenith path delays submitted by the individual ACs were compared with regard to

- 24 h mean values, i.e. one value per session,
- hourly values.

Furthermore, the total zenith path delays of a combined VLBI solution were compared to GPS total zenith path delays released as official IGS (International GPS Service) products (Gendt, 1996 [1]).

### 2.1. 24 h Mean Values

As the zenith path delays from AUS, IAA and CAN deviated significantly from the other time series (Figure 1) and the remaining seven solutions agreed very well, a combined VLBI solution was determined from the latter. This combined solution is the arithmetical mean per session of all time series after referring them to a common mean per station for the total time span (1999 and 2000) (Figure 2). Finally the combined solution was compared to the IGS time series of total zenith path delays. It is of comparable accuracy but there remains an offset between the two series (Figure 3) almost constant over the two years, even after accounting for the additional hydrostatic and wet path delays that are due to the height differences between the VLBI telescopes and the GPS antennas (see Table 2 for a detailed description). The remaining offsets might be due to

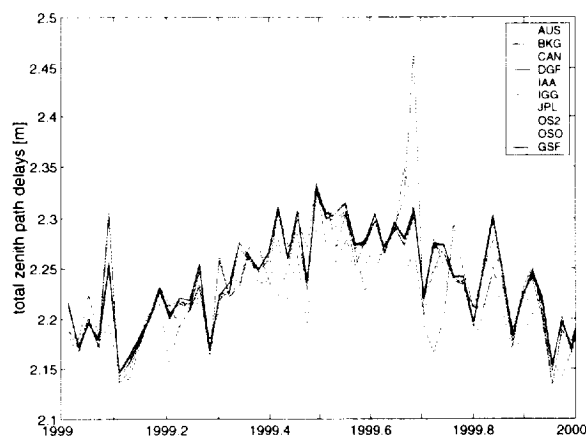


Figure 1. 24 h mean values of the total zenith path delays as submitted by the nine ACs for the station Wettzell. For clarity only the year 1999 is shown here.

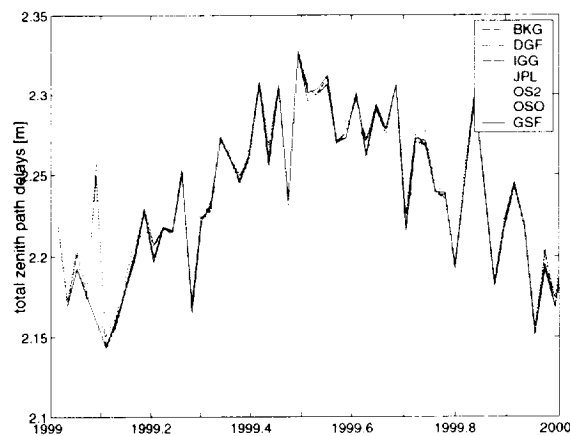


Figure 2. 24 h mean values after shifting them to a common mean for the total time span (1999 and 2000) for Wettzell. All time series except those from AUS, IAA and CAN were used for computing the common mean.

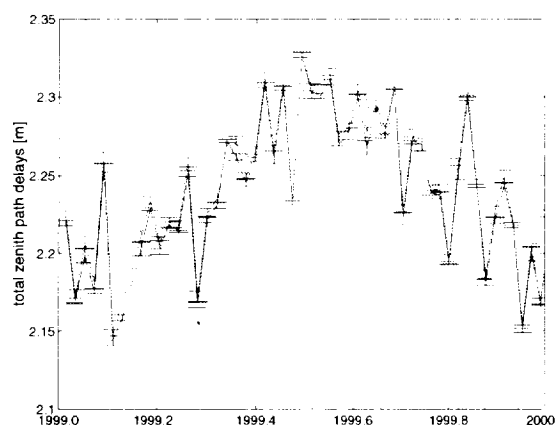


Figure 3. Combined VLBI solution of mean values per session of the total zenith path delays at Wettzell compared with the IGS 24 h mean time series. Again, only the year 1999 is shown here.

different estimation strategies (cutoff angles, mapping functions, ..), GPS phase center variations, VLBI subreflector bending, different ITRFs and geophysical models used for data analysis.

### 2.2. Hourly Values

The data submitted by AUS and IAA could not be used for the comparison of hourly values, because these ACs used the Kalman filter technique and provided only one value per session. In a first step the eight time series from the other ACs (Figure 4) were referred to a common mean (Figure 5). The total zenith path delays from CAN were not used for the calculation of the common mean because the CAN time series were always significantly shifted with respect to the others. Then a combined VLBI solution was calculated by simply determining the arithmetical mean of the time series for the hourly time epochs (Figure 6). Data were removed as outliers if the difference to the combined time series was larger than 2.5 times the standard deviation at a certain epoch. Finally the combined VLBI solution was compared to the IGS time series (Figure

Table 2. Mean offsets between the combined VLBI solution of 24 h mean total zenith path delays and the corresponding parameters from IGS. The second column shows the offsets and standard deviations resulting from a first comparison. The third column provides the height differences between the VLBI telescopes and the GPS antennas and the fourth column the corresponding hydrostatic and wet zenith path delays calculated for the mean temperatures, atmospheric pressures and relative humidities at each station. After applying these corrections there still remain offsets between the VLBI and GPS time series (fifth column) that are always negative.

Station	dZPD [mm]	dH [m]	dZPD h+w [mm]	dZPD res. [mm]
ALGO	-14.1 ± 2.9	23.1	7.1 + 2.1	-4.9
FORT	-14.1 ± 8.3	3.6	1.1 + 0.8	-12.2
GILC	-4.6 ± 2.6	13.1	3.9 + 0.5	-0.1
KOKE	-13.6 ± 2.9	9.2	2.5 + 1.5	-9.6
NYAL	-3.7 ± 2.7	8.8	2.7 + 0.3	-0.7
WETT	-3.6 ± 2.4	3.1	0.9 + 0.3	-2.4

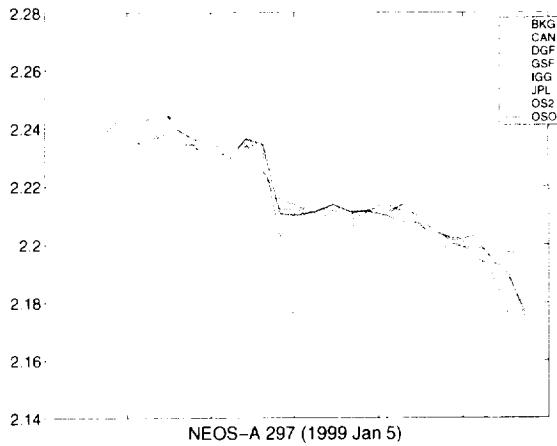


Figure 4. Hourly total zenith path delays at Wettzell for NEOS-A 297 as submitted by the ACs.

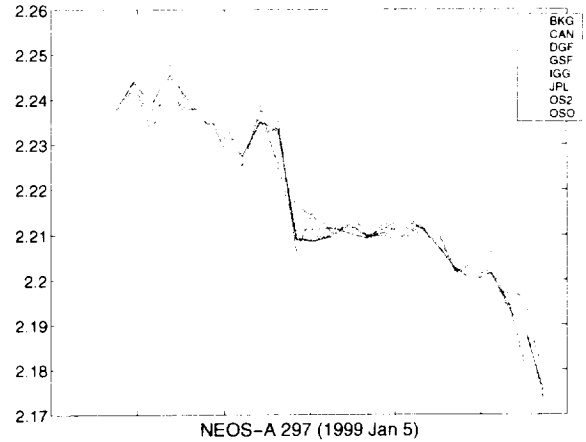


Figure 5. Hourly total zenith path delays at Wettzell for NEOS-A 297 referred to a common mean.

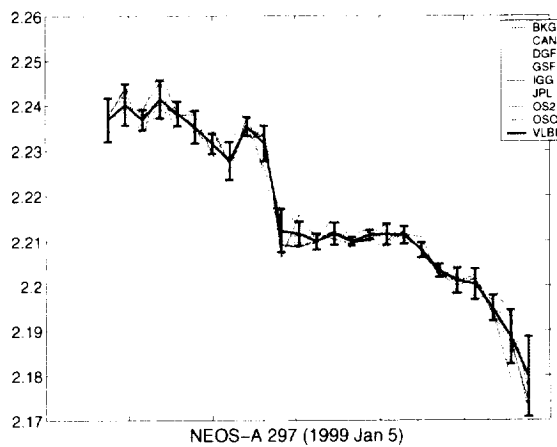


Figure 6. Individual submissions and combined VLBI solution (in blue, with one-sigma error bars) of hourly total zenith path delays at Wettzell for NEOS-A 297.

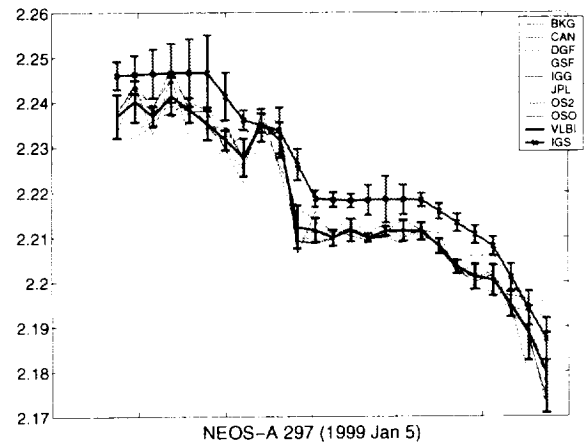


Figure 7. Combined VLBI solution of hourly total zenith path delays at Wettzell for NEOS-A 297 compared to the IGS time series (red). The latter are published in 2h time intervals and are interpolated in between.

7). The agreement is quite good, but again there is an offset between the VLBI and GPS results. The mean standard deviations of the hourly total zenith path delays per station for 1999 and 2000 can be found in Table 3; Figure 8 provides the mean standard deviations and offsets w.r.t. the common mean per session per AC at Wettzell.

### 3. Conclusions and Future Outlook

This preliminary comparison shows a good agreement between the zenith path delays submitted by most ACs. Weaknesses of individual AC solutions can be detected by the Pilot Project in

terms of offsets or outliers and useful feedback to the ACs can be given. First combined VLBI series yield standard deviations of about  $\pm 4.1$  mm for the total zenith path delays. This value will probably decrease if more rigorous outlier tests are applied. Further results including the comparison of horizontal gradients describing the azimuthal asymmetry of the refractivity at a site will be provided in a final report that will be accessible via the IVS homepage in spring 2002. Based on these results a new Pilot Project was approved at the 7th Directing Board Meeting in Tsukuba (Feb. 2002) in preparation of official IVS tropospheric products.

Table 3. Mean standard deviations of the hourly total zenith path delays per station for 1999 and 2000 in [mm].

Algo	Fort	Gilc	Koke	Nyal	Wett
4.1	5.6	3.4	4.1	3.8	3.9

### References

- [1] Gendt, G., Comparisons of IGS tropospheric estimates, Proceedings IGS Analysis Center Workshop, 19-21 March 1996 Silver Spring, Maryland USA, Eds. R E Neilan, P A Van Scoy, J F Zumberge, pp. 151-164, 1996.
- [2] Niell, A.E., Global Mapping Functions for the Atmospheric Delay at Radio Wavelengths, J. Geophys. Res., 101 (B2), pp. 3227-3246, 1996.

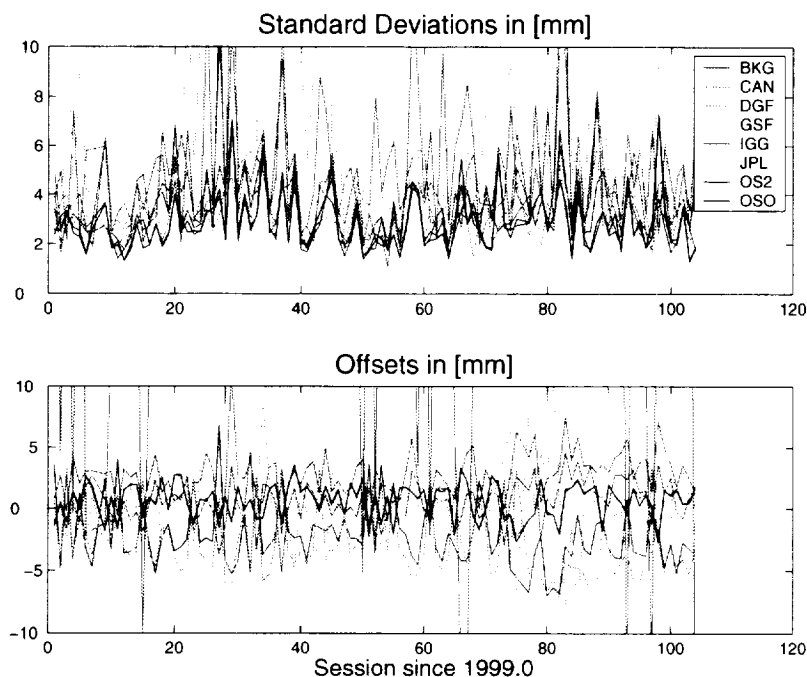


Figure 8. Mean standard deviations of the hourly total zenith path delays and offsets w.r.t. the common mean in 1999 and 2000 at Wettzell for all ACs.

# Determination of Ionospheric Parameters by Geodetic VLBI

Thomas Hobiger, Johannes Boehm, Harald Schuh

*Institute of Geodesy and Geophysics IGG, University of Technology, Vienna*

Contact author: Thomas Hobiger, e-mail: [thobiger@luna.tuwien.ac.at](mailto:thobiger@luna.tuwien.ac.at)

## Abstract

In geodetic VLBI the observations are performed at two frequencies (2.3 and 8.4 GHz) in order to determine ionospheric delay corrections. This also provides information about the total electron content (TEC) of the ionosphere from VLBI observables. Various VLBI sessions are used to determine TEC differences. The results are compared with TEC values obtained from GPS within IGS (IONEX). A very good agreement can be observed, in particular for baselines longer than 2000 km. By using external information for absolute calibration it is possible to calculate the unknown offset per baseline and to generate regional maps of TEC values, e.g. over Europe. Animated maps that represent the time dependency of the data are also produced and compared with GPS solutions.

## 1. Theory

The refraction of electromagnetic waves by the ionosphere was described e.g. by Brunini (1997) [1], Hartmann and Leitinger (1984) [2], Lohmar (1985) [3], and Schaer (1999) [4]. Adaption to VLBI yields for the slant total electron contents  $STEC_i$  observed at the two stations  $i = 1, 2$

$$\underbrace{STEC_2 - STEC_1}_{\Delta STEC} = \frac{\tau_X - \tau_S}{40.28 \left( \frac{1}{f_X^2} - \frac{1}{f_S^2} \right)} + offset \quad (1)$$

The left side of equation (1) can be derived from group delay measurements  $\tau_X$  and  $\tau_S$  in X- and S-band if the baseline-dependent offset is known. The equation is only valid for the effective ionospheric frequencies  $f_x$  and  $f_s$ , contained in the denominator on the right side. One total electron content unit (TECU) equals  $10^{16}$  electrons in a volume with a cross section of  $1 \text{ m}^2$  that reaches from the antenna along the ray path. STEC values observed at zenith distance  $z_i$  are transformed into vertical TEC (VTEC) values at station  $i$  by

$$VTEC_i = \frac{STEC_i}{\sqrt{1 - \left( \frac{R_e}{R_e + h} \sin z_i \right)^2}} \quad i = 1, 2 \quad (2)$$

$R_e$  represents the mean radius of the Earth and  $h$  is the assumed height of the ionospheric layer as plotted in figure 1. The intersection point of the ray path with the ionospheric shell is called the sub-ionospheric point and defines latitude and longitude of a VTEC value.

## 2. Comparison of $\Delta STEC$ Values from VLBI and GPS

$\Delta STEC$  values derived by VLBI and GPS were compared for various VLBI sessions of the CORE-A and EUROPE networks. There is a good agreement for medium length baselines (500 –

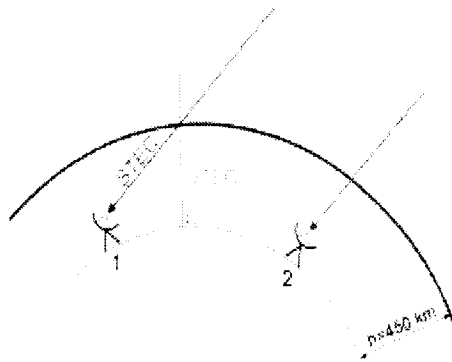
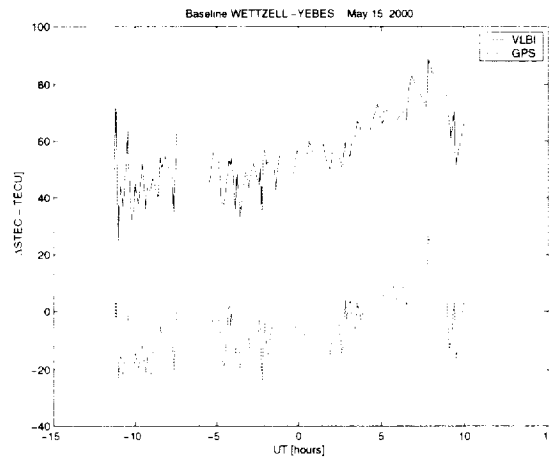


Figure 1. Single layer model

2000 km) with correlation coefficients  $r > 0.7$ . For baselines longer than 2000 km the correlation is even higher ( $r > 0.9$ ) which was also shown by Sekido et al. (2001) [6]. In figure 2  $\Delta STEC$  values of the baseline Wetzell-Yebes are plotted, obtained during the VLBI EUROPE session on May 15th, 2000. The values from both techniques are obviously highly correlated and the offset,


 Figure 2.  $\Delta STEC$  from VLBI and GPS

contained in equation (1), can be seen. If absolute STEC values of one station are known it is possible to derive STEC values of the other station (or of all other stations in a multi-station network). It has to be considered that the accuracy  $\sigma_{\Delta STEC}$  of absolute values mainly depends on the determination of the unknown offset per baseline (see equation 1) and can be expressed by

$$\sigma_{\Delta STEC} = \sqrt{\sigma_{meas}^2 + \sigma_{offset}^2} \quad (3)$$

with

$$\sigma_{meas}^2 = \frac{\sigma_{\tau_X}^2 + \sigma_{\tau_S}^2}{40.28 \left( \frac{1}{f_X^2} - \frac{1}{f_S^2} \right)} \quad (4)$$

$\sigma_{\tau_X}$ ,  $\sigma_{\tau_S}$  are the standard deviations of the observed group delays  $\tau_X$ ,  $\tau_S$ , and  $\sigma_{offset}$  the standard deviation of the offset obtained by the least-squares fit described in step 1 of section 3.

### 3. Determination of Absolute STEC Values from VLBI

As described in the previous section external information (from GPS, Ionosondes, Incoherent Scatter Radar, Faraday rotation measurements) is needed to calculate the unknown baseline-dependent offsets and to compute absolute STEC values. In this work GPS VTEC values provided by the International GPS Service (IGS), and given in ionospheric exchange format (IONEX, Schaer et al., 1998 [5]), were used. Based on this information STEC differences ( $\Delta STEC$ ) were calculated and compared with VLBI derived values. Under the assumption that the offset per baseline did not vary during an experiment the following procedure was applied (see flow chart, figure 3).

1. Once a day (when the mean elevation at all stations reaches a maximum) all offsets in a network were fixed by the use of the  $\Delta STEC$  values derived by GPS. This requires GPS receivers on every station or global models like IONEX. A least-squares fit under the condition that the sum of the offsets in a triangle equals zero, which can be written in the form

$$offset_{12} + offset_{23} + offset_{31} = 0 \quad (5)$$

was carried out to estimate the unknown offsets. The mean variances of the offsets are  $\pm 1$ -2 TEC units.

2. For the calculation of absolute values one site was chosen as reference station for which the IONEX data were fixed (VTEC values stored in a geographical grid for every 2 hours were transformed into STEC values).
3. By a shortest path Dijkstra algorithm the path from the reference station to every other station in the network was calculated. By adding the sum of  $\Delta STEC$  values along the path to the fixed value, absolute STEC values of each site were obtained.
4. These STEC values were transformed into VTEC numbers so that they can be compared with results from other techniques.
5. The TEC measurements allow derivation of ionospheric maps for areas with dense VLBI networks, e.g. over Europe. For that purpose the EUROPE VLBI sessions were used with seven to ten stations observing simultaneously. We have to assume that the temporal and spatial variations of the ionosphere are small to gain more data. Therefore data from a time span of  $T \pm 3$  hours were used for each time epoch T for producing high resolution maps. The geographic coordinates of the sub-ionospheric point related to a VTEC value were rotated around the geomagnetic north pole. The rotation angle needed for this step equals the time span between the time of observation and the reference time T.
6. In *static ionospheric mapping* the VTEC values are arranged by an interpolation algorithm on a rectangular grid that represents the status of the ionosphere for a certain time. As an example a regional VTEC map derived from the VLBI EUROPE session on December 13, 1999 is shown in figure 4, left. The results agree rather well with the VTEC map derived by GPS for the same epoch (figure 4, right).

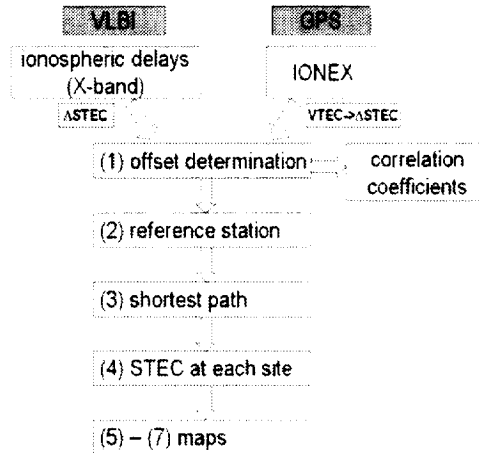


Figure 3. Flow chart of the determination of ionospheric parameters by VLBI

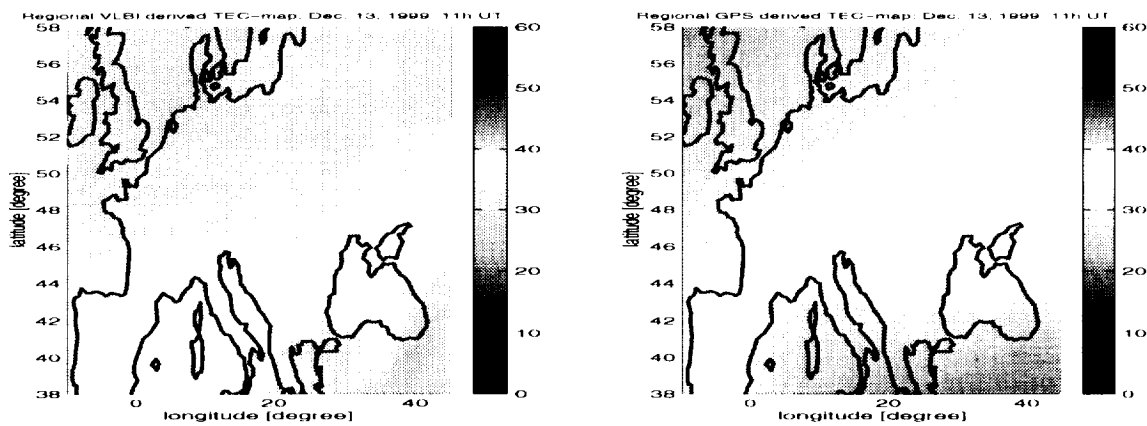


Figure 4. Regional VTEC maps from VLBI (left) and GPS (right)

7. In *dynamic ionospheric mapping* such maps dependent on time are produced. Animated maps are obtained that allow conclusions on temporal and spatial behaviour of the ionosphere over a certain region.

#### 4. Conclusions

First results show good agreement between VLBI and GPS relative STEC values. A method was developed to determine absolute VTEC values from VLBI with calibration by any external measurement or model. Static and dynamic VTEC maps can be computed from sufficiently dense VLBI networks and these maps can be compared with results from other techniques.

## References

- [1] Brunini, C., Global ionospheric models from GPS measurements, PhD-Thesis, Universidad Nacional de La Plata, 1997.
- [2] Hartmann, G. K., R. Leitinger, Ranger errors due to ionospheric and tropospheric effects for signal frequencies above 100 MHz, pp. 109-136, Bull. Geod. 58, 1984.
- [3] Lohmar, F.J., Zur Berechnung ionosphärischer Refraktionskorrekturen für VLBI-Beobachtungen aus simultanen Dopplermessungen nach Satelliten, Mitteilung a. d. Geodätischen Instituten der Rhein. Friedr.-Wilh.-Univ. Bonn, Nr. 67, Bonn, 1985.
- [4] Schaer, St., Mapping and Predicting the Earth's Ionosphere Using the Global Positioning System, PhD-Thesis, Bern, 1999.
- [5] Schaer St., W. Gurtner, J. Feltens, IONEX: The IONospheric Map EXchange Format Version 1, February 25, 1998, in Proceedings of the 1998 IGS Analysis Centers Workshop, ESOC, Darmstadt, Germany, February 9-11, 1998.
- [6] Sekido, M., T. Kondo, K. E. Kawai, M. Imae, Comparison of Ionospheric delay between GPS and VLBI (II), In: IVS CRL-TDC News No. 18, June 2001.

## Extending the ICRF to Higher Radio Frequencies

C. S. Jacobs<sup>1</sup>, D. L. Jones<sup>1</sup>, G. E. Lanyi<sup>1</sup>, S. T. Lowe<sup>1</sup>, C. J. Naudet<sup>1</sup>, G. M. Resch<sup>1</sup>, J. A. Steppe<sup>1</sup>, L. D. Zhang<sup>1</sup>, J. S. Ulvestad<sup>2</sup>, G. B. Taylor<sup>2</sup>, O. J. Sovers<sup>3</sup>, C. Ma<sup>4</sup>, D. Gordon<sup>5</sup>, A. L. Fey<sup>6</sup>, D. A. Boboltz<sup>6</sup>, P. Charlot<sup>7</sup>

<sup>1</sup>) *Jet Propulsion Laboratory, California Institute of Technology*

<sup>2</sup>) *National Radio Astronomy Observatory*

<sup>3</sup>) *RSA Systems Inc. / Jet Propulsion Laboratory*

<sup>4</sup>) *Goddard Space Flight Center*

<sup>5</sup>) *Raytheon ITSS / NASA Goddard Space Flight Center*

<sup>6</sup>) *U.S. Naval Observatory*

<sup>7</sup>) *Observatoire de Bordeaux - CNRS/UMR 5804*

Contact author: C. S. Jacobs, e-mail: [Chris.Jacobs@jpl.nasa.gov](mailto:Chris.Jacobs@jpl.nasa.gov)

### Abstract

The ICRF ([1]) forms the basis for all astrometry including use as the inertial coordinate system for navigating deep space missions. This frame was defined using S/X-band observations over the past 20+ years. In January 2002, the VLBA approved our proposal for observing time to extend the ICRF to K-band (24 GHz) and Q-band (43 GHz). The first step will be observations at K- and Q-bands on a subset of ICRF sources. Eventually, K- and Q-band multi-epoch observations will be used to estimate positions, flux density and source structure for a large fraction of the current S/X-band ICRF source list. This work will benefit the radio astronomy community by extending the VLBA calibrator list at these bands.

In the longer term, we would also like to extend the ICRF to Ka-band (32 GHz). A celestial reference frame will be needed at this frequency to support deep space navigation. A navigation demonstration is being considered for NASA's Mars '05 mission. The initial K- and Q-band work will serve to identify candidate sources at Ka-band for use with that mission.

### 1. Introduction

Early in the development of the VLBI technique, it was appreciated that VLBI observations of distant active galactic nuclei (AGNs) had the potential to form a quasi-inertial celestial reference frame with milli-arcsecond (mas) or better accuracy. In the 1990s the IAU working group on reference frames brought together workers from astrometric groups from around the world to produce a standard celestial reference frame that was to become known as the International Celestial Reference Frame (ICRF - [1]). This foundational work was done at S/X-band (2.3/8.4 GHz) with a parallel realization of the frame at optical frequencies based on HIPPARCOS satellite data. It was appreciated by many that extension of the ICRF to additional frequencies would further enhance the value of the work already done.

A number of developments have converged to make the first decade of the new millennium an opportune time to pursue the extension of the ICRF to radio frequencies in the 24–43 GHz range. First, the S-band environment is increasingly cluttered by radio frequency interference making continued observations at S/X ever more difficult. Second, high frequency radio amplifiers are now (K- and Q-band) or will shortly be (Ka-band) available for use by the VLBI technique. Third,

radio systems for planetary probes are moving to Ka-band (32 GHz) and are expected to require sub-mas tracking accuracy. This paper will describe a proposal to extend realizations of the ICRF to K-, Ka-, and Q-bands. Section 2 will describe the team that has been assembled to accomplish the task. Section 3 will highlight our motivations for pursuing this task. Section 4 will outline our observing and data analysis plan.

## 2. The Collaboration

Historically, the creation of accurate global reference frames has been a large undertaking. The effort described in this paper is expected to be no exception. Based on this expectation, a team of scientists from several institutions was organized in the fall of 2001. The current list of institutions and individuals involved in the collaboration are as follows:

- JPL: C.S. Jacobs, D.L. Jones, G.E. Lanyi, S.T. Lowe, C.J. Naudet, J.A. Steppe, L.D. Zhang
- NRAO: J.S. Ulvestad, G.B. Taylor
- RSA: O.J. Sovers
- GSFC: D. Gordon, C. Ma
- USNO: D.A. Boboltz, A.L. Fey
- Bordeaux Observatory: P. Charlot

Much of the initial impetus for this collaboration came from George Resch of JPL. As noted at the meeting, he died unexpectedly in November 2001. This collaboration is part of his legacy.

## 3. Motivation

What is our motivation for such a large undertaking as building a high accuracy reference frame at a new set of frequencies? At present there are three main motivations: improving the science of astrometry, enabling better VLBA phase referencing at high frequencies, and preparing for deep space navigation at higher frequencies. Let's briefly look at each of these in turn.

### 3.1. Astrometry

Current astrometric accuracy (*e.g.* [2] and [3]) is limited by instrumental phase stability, troposphere (*e.g.* [4] and [5]), and source structure (*e.g.* [6] & [7]). At this point, it is unknown whether instrumentation will be more or less stable at K-, Ka-, and Q-bands compared to S/X instrumentation. The troposphere is non-dispersive in the microwave region and thus is expected to contribute the same to the delay error budget. The last error type, source structure, is expected to change with frequency because extended emission in AGN is usually steep spectrum. Thus, there should be less of it at higher frequencies. Consequently, in addition to expecting the centroid of emission to be closer to the central engine and thus more positionally stable, the emission should be more localized (*i.e.* point like). This should enable more precise astrometry at frequencies higher than the current S/X-band standard.

### 3.2. VLBA Phase Referencing

The astrometry and fluxes that come from these observations will be useful in extending the VLBA calibrator list at K- and Q-bands. This would enhance high accuracy phase referencing observations, enabling weaker sources to be observed as well as providing the associated differential astrometry at these bands. This would be of direct scientific benefit and also would enhance the VLBA's infrastructure for the radio astronomy community at large.

### 3.3. Deep Space Navigation

Interplanetary spacecraft are navigated in the inertial reference frame defined by the ICRF. Increasing radio frequency interference at S-band (2.3 GHz) and the need for higher telemetry rates are both pushing spacecraft radio systems to higher frequencies. The next allocation for deep space communications is at Ka-band (32 GHz). The ability to have an accurate astrometric frame tied to the ICRF at Ka-band would enhance or enable a number of deep space missions by providing improved accuracy for landers, atmospheric entry/aerobraking, allowing tracking closer to the Sun, and greatly reducing the plasma error budget (which was the dominant error for the Mars 2001 Odyssey mission). The Mars 2005 mission is considering a Ka-band navigation demonstration, thus lending an air of urgency to this work. The proposed K- and Q-band work will bracket the Ka-band telemetry band until NASA's Deep Space Network is fully equipped to acquire Ka-band VLBI—currently expected in mid 2003.

## 4. Experimental Details

As indicated above, we plan to observe a subset of the sources from the S/X-band ICRF during our initial K- and Q-band experiments. Based on past experience, we expect that much of the early effort will be spent on learning to observe in a regime unfamiliar to many of us.

### 4.1. Observing Sequences

At the time of the second IVS General Meeting, our initial observing proposal had just been accepted by the VLBA. Detailed planning for the initial observing sequence is now underway. The source list for the first round included approximately 40 sources. For the most part, these sources were chosen to have  $> 0.7$  Jy of estimated flux density based on VLA multi-frequency observations. The early efforts will concentrate on stronger sources with some effort to favor sources near the Mars '05 trajectory. Once we gain more experience with observing at higher frequencies, we will venture into the weaker parts of the ICRF source list.

Our plan is to point to a given source, record a few minutes of data at K-band and then record a few minutes of data at Q-band before slewing to the next source. Our goal is to take three to five snapshot observations for each source on our observing list. Based on simulated uv coverage, we expect that the VLBA—even with this small number of snapshots—will provide enough data to make images (see fig. 1). We intend to take data roughly three times per year. This is necessary in order to observe a large fraction of the ICRF source list and also in order to sample the effects of intrinsic source variability and weather induced variability. The constancy of sources is of special concern in applications to spacecraft navigation where there is often only one calibrator source and often no chance to re-observe.

## 4.2. Data Analysis

After collecting the data, the long process of analysis will begin with the goal of extracting both astrometric positions and images from the data set. To achieve this goal, we plan to draw on the varied talents of our collaborators. In brief outline, the plan is to correlate at NRAO Socorro's VLBA correlator. The fringe fitting/phase tracking will use the AIPS software. The results will be archived in GSFC Calc/Solve database format for astrometric analysis at GSFC and USNO. Bordeaux Observatory will convert the group delay and delay rate data to JPL/MODEST database format. This will enable analysis using JPL's astrometric analysis software ([3]).

## 5. Conclusion

While it has long been understood that the value of the ICRF would be enhanced by extending its realization to many observing bands, the time has now come to wholeheartedly pursue such an effort. A collaboration of observers and analysts has been assembled. The motivations for the extension to three specific bands (K, Ka, Q) have been enumerated. An initial observing proposal has been written, submitted and accepted by the VLBA. We anticipate beginning to collect data within the next few months. We hope to realize high accuracy ICRFs at K-, Ka-, and Q-bands well before the end of the decade.

## 6. Acknowledgements

The authors would like to acknowledge Dr. George Resch of JPL for initiating the collaboration described in this paper.

## References

- [1] Ma, C., E.F. Arias, T.M. Eubanks, A.L. Fey, A.-M. Gontier, C.S. Jacobs, O.J. Sovers, B.A. Archinal, and P. Charlot, 'The International Celestial Reference Frame as Realized by Very Long Baseline Interferometry', *Radio Sources*, *Astronomical Journal*, Vol. 116 no 1, pp. 516-546, July 1998. <http://www.journals.uchicago.edu/AJ/journal/issues/v116n1/970504/970504.html>
- [2] Jacobs, C.S., O.J. Sovers, C.J. Naudet, R.F. Coker, and R.P. Branson, 'The JPL Extragalactic Radio Reference Frame: Astrometric Results of 1978-96 Deep Space Network VLBI', *NASA JPL TDA Progress Reports*, vol 133, pp. 1-55, 15 May 1998. [http://tmo.jpl.nasa.gov/tmo/progress\\_report/42-133/133E.pdf](http://tmo.jpl.nasa.gov/tmo/progress_report/42-133/133E.pdf)
- [3] Sovers, O.J., J.L. Fanselow, and C.S. Jacobs, 'Astrometry and Geodesy with Radio Interferometry: Experiments, Models, Results', *Reviews of Modern Physics*, vol. 70, no. 4, Oct. 1998. <http://xxx.lanl.gov/abs/astro-ph/9712238>
- [4] Resch, G.M., J.E. Clark, S.J. Keihm, G.E. Lanyi, C.J. Naudet, A.L. Riley, H.W. Rosenberger, and A.B. Tanner, 'The Media Calibration System for Cassini Radio Science: Part II', *TMO Prog. Rept.*, 42-145, pp. 1-20, Jan-Mar 2001. [http://tmo.jpl.nasa.gov/tmo/progress\\_report/42-145/145J.pdf](http://tmo.jpl.nasa.gov/tmo/progress_report/42-145/145J.pdf)
- [5] Naudet, C.J., S. Keihm, G.E. Lanyi, R.P. Linfield, G.M. Resch, L. Riley, H. Rosenberger, A. Tanner, 'Media Calibration in the Deep Space Network - A Status Report', this volume, 2002.
- [6] Sovers, O. J., Charlot, P., Fey, A. L., Gordon, D., 'Structure Corrections in Modeling VLBI Delays for RDV data', this volume, 2002.
- [7] Charlot, P., 'Modeling Radio Source Structure for Improved VLBI Data Analysis', this volume, 2002.

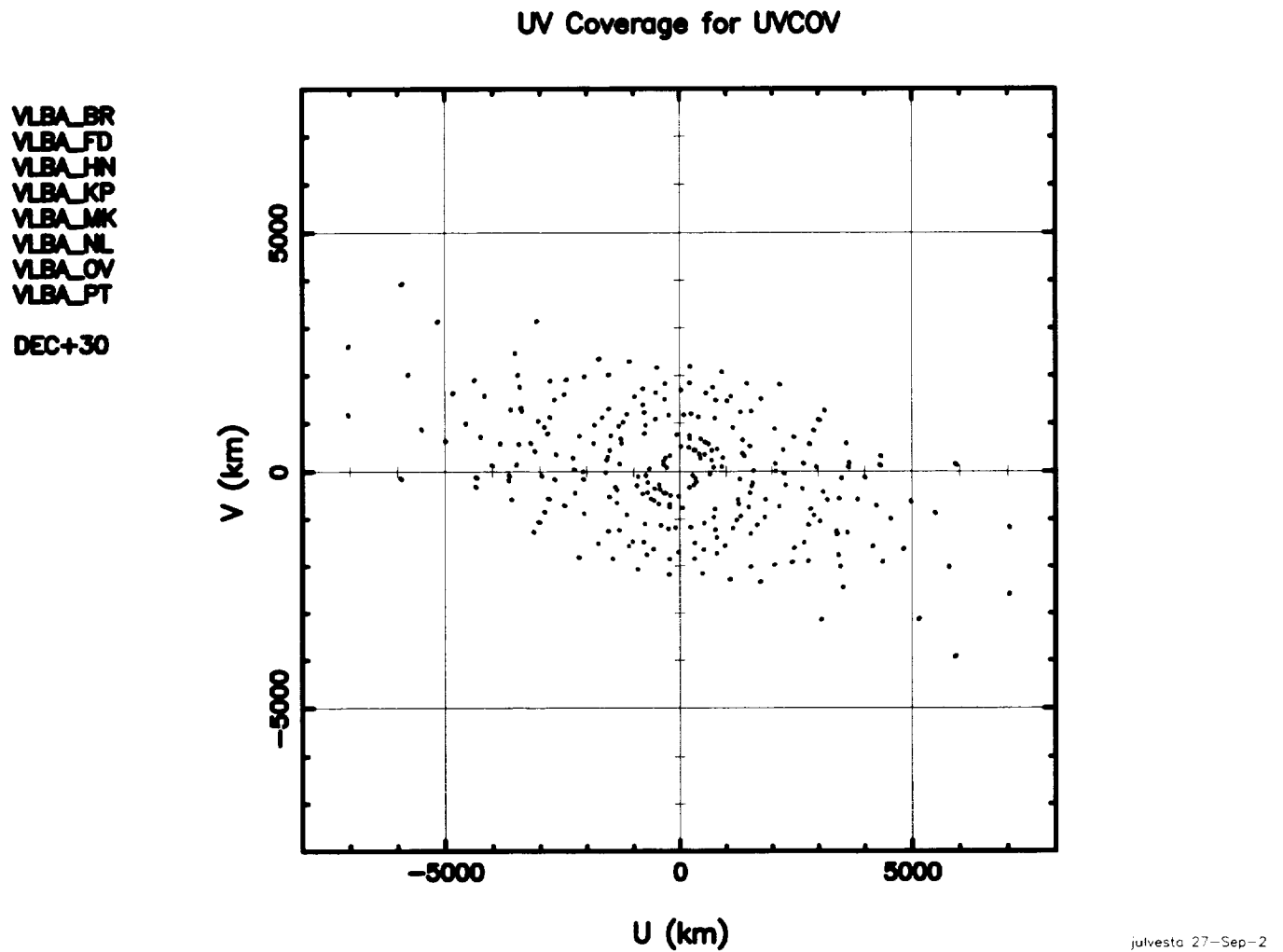


Figure 1. Simulated UV coverage based on five snapshots each 2 minutes in duration and separated by 1.5 hours. Horizontal axis, U, in km, vertical axis, V, in km, source declination 30 degrees. Eight VLBA antennas are included: BR, FD, HN, KP, MK, NL, OV, PT. Two antennas (LA, SC) were excluded to simulate imperfect (*i.e.* realistic) observing conditions. The consequences of the VLBA having a much greater East-West than North-South extent are apparent.

## Towards a Future ICRF Realization

Chopo Ma<sup>1</sup>, David Gordon<sup>2</sup>, Daniel MacMillan<sup>3</sup>, Leonid Petrov<sup>3</sup>

<sup>1</sup>) NASA Goddard Space Flight Center

<sup>2</sup>) Raytheon ITSS/NASA Goddard Space Flight Center

<sup>3</sup>) NVI, Inc./NASA Goddard Space Flight Center

Contact author: Chopo Ma, e-mail: [cma@virgo.gsfc.nasa.gov](mailto:cma@virgo.gsfc.nasa.gov)

### Abstract

The data and analysis for the ICRF were completed in 1995 to define a frame to which the Hipparcos optical catalog could be fixed. Additional observations on most of the 608 sources in the overall ICRF catalog have been acquired using a small portion of geodetic observing time as well as astrometric sessions concentrating on the Southern Hemisphere. Positions of new sources have been determined, including ~1200 from a VLBA phase calibrator survey. A future ICRF realization will require improved geophysical modeling, sophisticated treatment of position variations and/or source structure, optimized data selection and weighting, and re-identification of defining sources. The motivation for the next realization could be significant improvement in accuracy and density or preparation for optical extragalactic catalogs with microarcsecond precision.

### 1. Introduction

The ICRF (International Celestial Reference Frame), which became effective as the realization of the ICRS (International Celestial Reference System) on 1 January 1998, is a fundamental change from previous realizations. The most important characteristics are summarized in Table 1.

Table 1. Characteristics of the ICRF

Set of positions of 212 defining radio sources
Independent of equator, equinox, ecliptic
Independent of epoch
Position error floor 0.25 milliarcsec
Orientation stability ~20 microarcsec

Each characteristic is radically different from the earlier reference frames defined by the series of FK5 stellar catalogs. While the changes go in the direction of conceptual simplicity along with significantly better accuracy and stability, in two areas the ICRF is less accessible than FK5. The number of defining sources is an order of magnitude smaller, and the wavelength and mode of observation are quite different from usual astrometry.

The analysis of the VLBI data that resulted in the ICRF is summarized in Table 2. It should be emphasized that this analysis was developed to optimize the accuracy of the defining source positions and the positions of "candidate" sources that had no evidence of instability. Because the majority of sources had few observations, sufficient data to determine position instability was not the norm. The ICRF was isolated from problems in the terrestrial reference frame by estimating

Table 2. Characteristics of the ICRF analysis

Used all relevant data 1979-1995.6
Treated “unstable” sources as arc parameters
Treated stations as arc parameters
State of the art analysis for 1995

station positions independently for each session as arc parameters. The geophysical modeling, notably for the troposphere, was at the state of the art for 1995. ICRF-Ext.1 was completed in 1999 to make use of additional data to improve the errors of the candidate sources and to add 59 new sources. The VLBA Calibrator Survey (VCS) added ~1200 more sources north of -30 degrees to the overall astrometric list. A second extension is planned for 2002. A basic requirement for ICRF extensions is that they do not differ systematically from the ICRF. Consequently only small changes have been made in modeling and the analysis procedures.

## 2. Considerations for a New ICRF

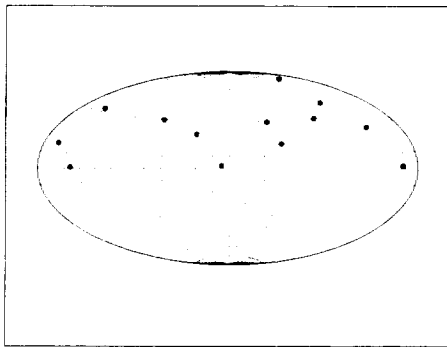
Since VLBI data and analysis both continue to progress, a new ICRF realization from VLBI is almost inevitable. A number of considerations are discussed below.

### 2.1. Rationale or Goal

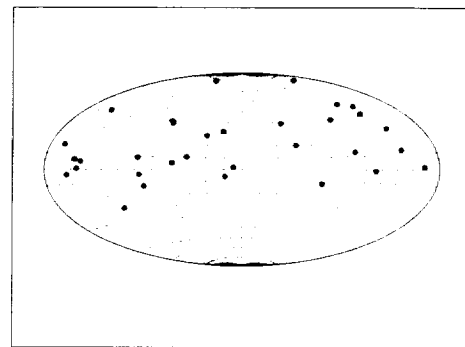
The rationale of the next ICRF may be derived from internal improvements or from external needs. Criteria for internal justification might be the ability to reach a significantly higher level of accuracy or to greatly expand the number or distribution of defining sources. The external need might be to provide a refined catalog for connection or comparison to a precise frame observed at another wavelength. The impetus for completion of the ICRF was, in fact, the requirement of the Hipparcos optical catalog for precise alignment with the ICRS. At present there is no catalog at another wavelength as good as the ICRF, but future satellites like GAIA and SIM have the potential to measure extragalactic objects in the optical with much better precision than the radio ICRF.

### 2.2. Data

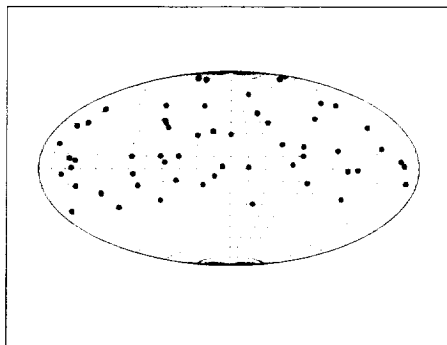
The data set of the ICRF was 95% from geodetic programs. The criteria for selecting sources for geodetic observing are rather different from what would be most desirable for an optimal astrometric data set. The geodetic sources are selected balancing source strength and source structure, with greater emphasis on the former. Especially in the early years of dual-frequency VLBI, lack of instrumental sensitivity required the use of the relatively few very strong compact objects whose structure resulted in positional instability. An astrometric observing program would distribute the observations over a large number of sources uniformly in time and on the sky. The geodetic source list is by comparison much smaller although it has grown and changed over time as shown in Figures 1A through 1E. Since the geodetic data will most likely be the dominant part of a new ICRF, these sources are the real skeleton of the frame. However, as there are significantly



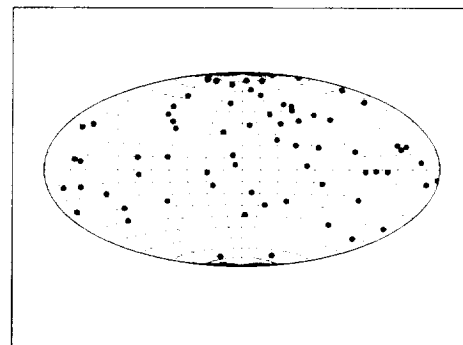
A. 13 sources, 1979-1983.



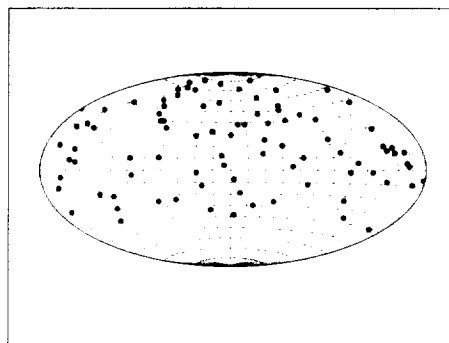
B. 32 sources, 1984-1988.



C. 57 sources, 1989-April 1993.



D. 70 sources, May 1993-1996.



E. 92 sources, 1997-2001.

Figure 1. Progression of most commonly observed sources, 1979-2001.

more data available now than in 1995, it might be advisable to discard the early data dominated by unstable sources. It would also be worthwhile to have a more extensive observing program for the astrometric sources. Because of limited resources, there have been few astrometric sessions in recent years but the astrometric sources are observed a few at a time in some of the geodetic programs. The current observing program for the celestial reference frame focuses on the Southern Hemisphere with different networks for astrometry and mapping.

### 2.3. Defining and Unstable Sources

The current ICRF has 212 defining sources with preponderance in the Northern Hemisphere. This is a consequence of the small number of VLBI stations in the south. An important consideration for the new ICRF is the expansion in numbers and spatial distribution of the defining sources. A second consideration is the proper identification of the unstable sources. Unless it can be shown conclusively that the positional stability of a source can be inferred from source structure information at one or only a few epochs, both aspects require sufficient data on a large set of sources to provide position time series for statistical analysis. At present generally only geodetic sources have sufficient data, and some of these have detectable instability or apparent motion over the time span of their observations. Providing such data would probably require a significantly greater commitment of VLBI resources to the ICRF than allotted recently.

### 2.4. Analysis Changes

There are several areas where analysis improvements may contribute to a new ICRF. In the ICRF analysis geophysical and geometric effects impinge on the celestial position results in two main ways: motions of the VLBI antenna reference points within one day (loading phenomena of various origins, thermal changes, antenna flexure, etc.) and propagation media delays. Models of such effects are better than in 1995 although modeling of antenna structure changes is still rudimentary. The troposphere delay probably can never be adequately modeled a priori, so accuracy of the mapping function and gradient estimation may be a limiting factor for the ICRF.

Astrophysical modeling using source maps is attractive in principle but may have limited application in the actual ICRF. It is not possible to have maps for all sources for all times, and it seems unlikely that it will be possible to have sufficient maps for both the north and south for the same times. In addition, assigning the correct reference point for a given source from map to map is as yet a rather time-consuming task. In concept, however, a new ICRF could be generated from a limited number of observing sessions that provide both astrometric and astrophysical information, perhaps observations from the extended VLBA along with the best southern hemisphere mapping and astrometric networks.

The modeling of unstable sources in the ICRF analysis could be refined. For the original ICRF all sources identified as unstable were treated as arc parameters. This method diluted the effect of a source's position instability on the relative positions of the other sources observed in the same session. If the position of a source fluctuates randomly significantly above the level expected from the observation errors, this procedure is probably the only possibility that still allows the use of the source's observations for other parameters like the clock and troposphere. However, a source position could change linearly or smoothly or could have periods of stability. The use of proper motion parameters, piecewise linear approximations, or arc parameters when the position is unstable could permit such sources to contribute to the strength of the daily and concatenated

reference frames.

The weighting of the data is an area that was insufficiently explored in the ICRF analysis because of software limitations. Other weighting algorithms should be examined carefully for the next ICRF. Besides reweighting by added station noise, reweighting by elevation and source might improve the analysis.

The error analysis of a new ICRF is critical to understand the real accuracy. This analysis requires detailed comparisons between results from different software, data sets, models, and plausible analysis strategies. Creating a catalog from the combination of results from different solutions should be explored but the data and analysis similarities may preclude a significant improvement.

Finally, the unique capability of VLBI is to tie the ICRF and ITRF directly, but the current ICRF analysis optimizes the first in a way that prevents the realization of the second. Analysis strategies must be developed that allow both frames to be derived from the same solution while reducing systematic errors from nonlinear motions or unstable positions.

## Searching for High Quality VLBI Calibrators

Edward Fomalont <sup>1</sup>, Tony Beasley <sup>2</sup>, Alison Peck <sup>3</sup>, Colleen Gino <sup>4</sup>

1) *National Radio Astronomy Observatory*

2) *Owens Valley Radio Observatory*

3) *Harvard-Smithsonian Center for Astrophysics*

4) *Union College*

Contact author: Edward Fomalont, e-mail: [efomalon@nrao.edu](mailto:efomalon@nrao.edu)

### Abstract

Phase referencing techniques are now commonly used with VLBI astronomical observations for the imaging of weak radio sources, and for the determination of relative positions with accuracies as small as tens of micro-arcseconds. This observing scheme alternates observations every few minutes between the target source and a suitable calibrator detectable in a few minutes, typically with correlated flux density  $> 50$  mJy, less than several degrees from the target source. Over the last seven years, a VLBA Calibrator Survey (VCS1) with dual-frequency S/X observations has been made for over 1800 radio sources. Most sources are suitable for phase referencing, and some of these sources are potential ICRF candidates. We are continuing the search for calibrators in regions of the sky with a low density of calibrators.

### 1. The VCS1 Calibrator Survey

The VCS1 observations were made with the VLBA in ten 24-hr sessions between August 1994 and August 1997; a full description of these observations and results are given elsewhere [1]. The observing scheme used a dual-frequency geodetic mode, observing simultaneously at 2.3 and 8.4 GHz, with a 100 MHz spanned bandwidth at 2.3 GHz and 400 MHz at 8.4 GHz to provide accurate group delays. Most of the sources were selected from the Jodrell Bank–VLA astrometric survey (JVAS) [2]. For all sessions, JVAS sources were selected from a limited range of declination, but were interspersed with 57 well-observed ICRF sources around the sky in order to determine the necessary geodetic/astrometric parameters needed for accurate position determination. For each source in a session, two or three scans, each of length 1.5 minutes, were made.

Using the AIPS calibration package, we applied the apriori amplitude calibration of the telescopes and then detected the source using fringe-fitting techniques. The data were then edited, imaged and self-calibrated using the Caltech Difmap package. The typical result for a source suitable as a phase reference is shown in Figure 1. Approximately 1300 of the sources had significant emission in a compact component with flux density  $> 100$  mJy and are suitable for phase referencing with a sensitive system such as the VLBA.

Astrometric processing of the sources was made using the NASA Goddard Space Flight Center Calc/Solve software package. Solve solutions were made for each session to determine large position offsets and to flag bad data. However, the final positions were generated from a solution made from all ten sessions. Over half of the sources have an estimated position error  $< 1$  mas, and those few sources with errors larger than 10 mas are very resolved. Some of the weaker but point-like sources have positions derived only from the 8.4 GHz data. Relevant information on the VCS1 sources can be found in [http://magnolia.nrao.edu/vlba\\_calib/index.html](http://magnolia.nrao.edu/vlba_calib/index.html).

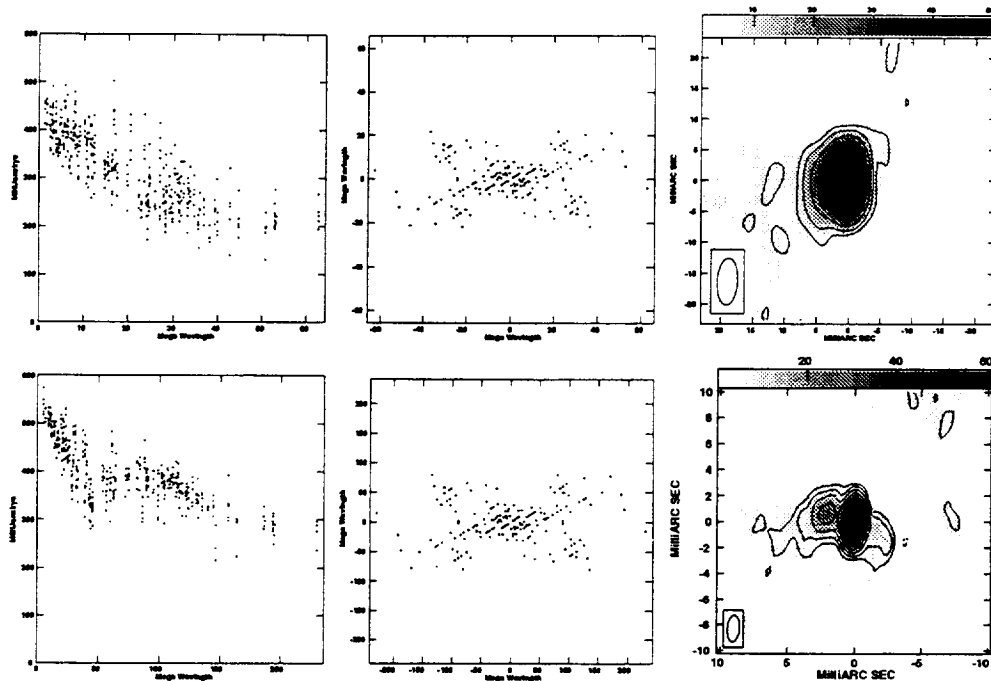


Figure 1. **Results for J0004–1148:** Top Line=2.3 GHz; Bottom Line=8.4 GHz. Left=visibility versus baseline length; Center=u-v coverage; Right=radio image. Bottom contour is 5 mJy at 2.3 GHz and 3 mJy at 8.4 GHz, with contour levels at -1,1,2,4,8,16,32,64. The resolution is shown by the ellipse in the bottom left of each contour plot.

## 2. The VCS2 Survey Extension

Two additional 24-hour sessions (VCS2) are scheduled for observations in Jan 2002 and April 2002 to fill existing holes in the present sky coverage of calibrators: in the declination range  $-20^\circ$  to  $-45^\circ$ ; near the galactic plane; and for ICRF sources with somewhat limited structural information. A total of about 500 additional potential calibrator sources will be checked, with emphasis on filling the obvious holes shown in the sky coverage in Figure 2, bottom.

The density of calibrator sources is becoming sufficiently large so that phase referencing calibrators within a few degrees of most targets will be available north of declination  $-40^\circ$ . In order to obtain a deeper net of calibrators, as weak as 20 mJy, target-specific observation will be necessary.

## 3. Acknowledgements

The authors thank the NRAO and GSFC staff members who assisted in the preparation of the VCS catalogs. The National Radio Astronomy Observatory is a facility of the National Science Foundation operated under cooperative agreement by Associated Universities, Inc.

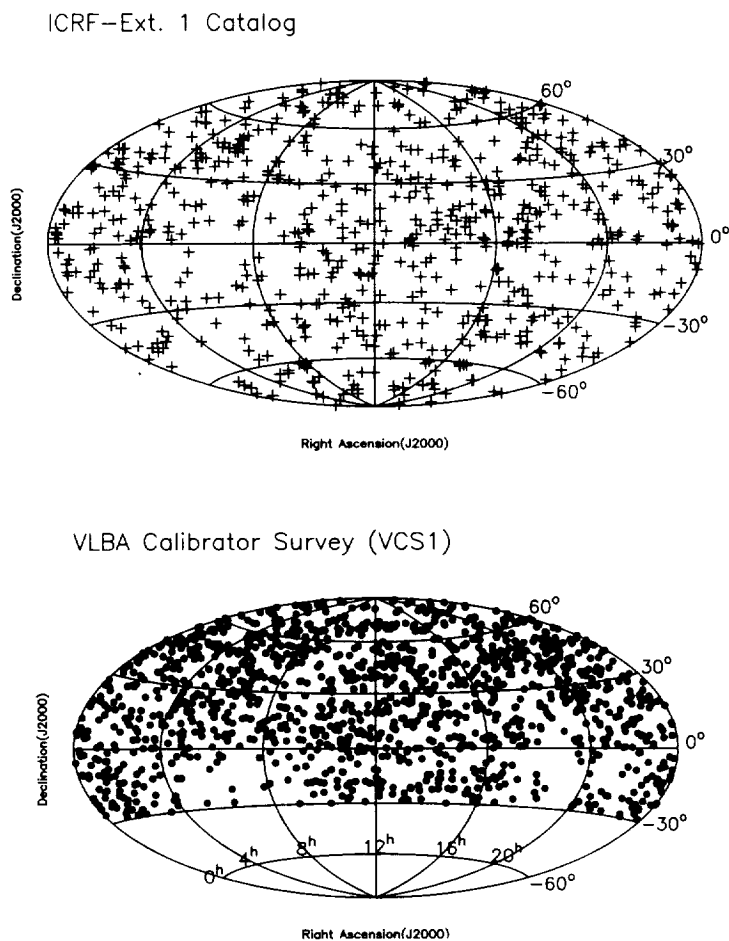


Figure 2. **Sky Coverage:** Top, ICRF-Ext 1 sources list; Bottom, VCS1 Catalog. The VCS2 observations will attempt to fill in the holes down to  $-40^\circ$ .

## References

- [1] Beasley, A. J, Gordon, D, Peck, A. B., Petrov, L., MacMillan, D. S., Fomalont, E. B., & Ma, C. 2002, ApJ, in press. (astro-ph/0201414)
- [2] Wilkinson, P. N., Browne, I., Patnaik, A. R., Wrobel, J. M. & Sorathia, B., 1998, MNRAS, 300, 790

## Extragalactic Radio Source Selection for Radio/Optical Frame Ties

*Alan L. Fey, David A. Boboltz, Ralph A. Gaume, T. Marshall Eubanks,  
Kenneth J. Johnston*

*U.S. Naval Observatory*

*Contact author: Alan L. Fey, e-mail: [afey@usno.navy.mil](mailto:afey@usno.navy.mil)*

### Abstract

Future space-based optical astrometric satellite missions present the possibility of directly linking the radio and optical reference frames at the micro-arcsecond level. We have evaluated the current database of radio observations of the extragalactic objects which make up the International Celestial Reference Frame to determine the optimum candidates, in terms of their radio properties, for use as radio/optical frame tie sources. We suggest that the radio astrometric quality as described in this paper can be applied to the next realization of the ICRF.

### 1. Introduction

In the next decade, there will be significant advances in the area of space-based optical astrometry. Current or planned missions will be able to determine the positions of stars with a precision approaching the micro-arcsecond level. Measurements at this level of precision will allow the determination of astronomical distances with unprecedented accuracy. To achieve these goals, these mission will need to construct their own precise reference frames, as no previous astrometric observations have ever achieved the planned level of accuracy. To maximize their utility to the entire astronomical community, these astrometric grids will also need to be anchored to the quasi-inertial celestial frame defined by extragalactic objects – currently the International Celestial Reference Frame (ICRF).

We use radio astrometric and ancillary data to evaluate ICRF objects in terms of their suitability for use as radio/optical frame tie sources. These data include radio source position uncertainties derived from least-squares astrometric analyses of VLBI observations taken from the USNO astrometric/geodetic database, radio source positional stability information also derived from least-squares astrometric analyses, and intrinsic radio source structure information obtained from Very Long Baseline Array observations. Using these data, each source is evaluated and graded (with respect to all other sources) to obtain an estimate of their radio astrometric quality and hence their suitability as possible frame tie objects. Optical information on the radio objects is currently limited to estimates of the redshift and visual magnitude of their optical counterparts.

Additional details concerning this investigation and a complete description of the analysis can be found in Fey et al. (2001, *AJ*, 121, 1741).

### 2. Criteria for Estimating Radio Astrometric Quality

Criteria for estimating radio astrometric quality are listed below along with their relative weight in the combination (see Section 3).

- (1.0) position uncertainty - the right ascension and declination formal uncertainties from least-squares global SOLVE solutions
- (1.0) position stability - weighted root-mean-square uncertainty estimates in right ascension and declination from “arc” position time series
- (0.5) compactness - source spatial extent as measured from X-band radio images
- (0.5) structure index - an estimate of the contribution of intrinsic structure to the measured group delay

### 3. Application of Criteria for Radio Astrometric Quality

Rather than defining categories and setting cutoffs for inclusion in a particular category (eg. in the construction of the ICRF, all sources with position uncertainties less than or equal to 1 mas were considered for inclusion in the defining category), each source is evaluated and graded individually for each selection criteria, usually on a scale from 1 to 10. The individual scores based on each selection criteria are then totaled for each source, resulting in an estimate of their radio astrometric quality.

For example, the distribution of position formal uncertainties in right ascension is divided into 10 approximately equal number bins, i.e., bins are defined such that each bin has an approximately equal number of sources. The sources in each bin are then given a score from one to ten, with the sources having the smallest formal uncertainties receiving the highest score and the sources with the largest formal uncertainties receiving the lowest score. The same procedure is repeated for the other criteria with the appropriate weighting as listed in Section 2.

The final step is to sum the score for each source. Because sources with no structure information (either radio compactness or structure index) are essentially not evaluated for these criteria (they receive no score so the maximum possible score is different than for those sources with structure information), they are consequently on an absolute scale different from those sources for which this information is available. Thus, we normalize the total score for each source to a scale ranging from zero (for the worst astrometric sources) to one hundred (for the best astrometric sources). The resulting score is our estimate of radio astrometric quality. The distribution of radio astrometric quality for 392 ICRF sources taken from Fey et al. (2001, AJ, 121, 1741) is shown in Figure 1.

### 4. Source Selection for Radio/Optical Frame Ties

Future space-based optical astrometric satellite missions present the possibility of *directly* linking the radio and optical reference frames through mutual observations of extragalactic objects. For the particular case of the Space Interferometry Mission (SIM), the limiting magnitude will be about  $m_v \approx 21$ . However, the optical counterparts of the extragalactic radio sources ideally should be brighter than about  $m_v \leq 18$  to minimize on-source integration time. The distribution of visual magnitudes for the potential ICRF link sources is shown in Figure 2. About half of the available sources are bright enough for SIM to observe efficiently. However, in addition to optical brightness, the candidate link sources should also have a high radio astrometric quality.

Shown in Figure 3 are the 50 optically brightest sources having the highest radio astrometric quality with the additional criterion that 25 sources are selected from the Southern Hemisphere independent of the 25 selected in the Northern Hemisphere. These objects represent our current

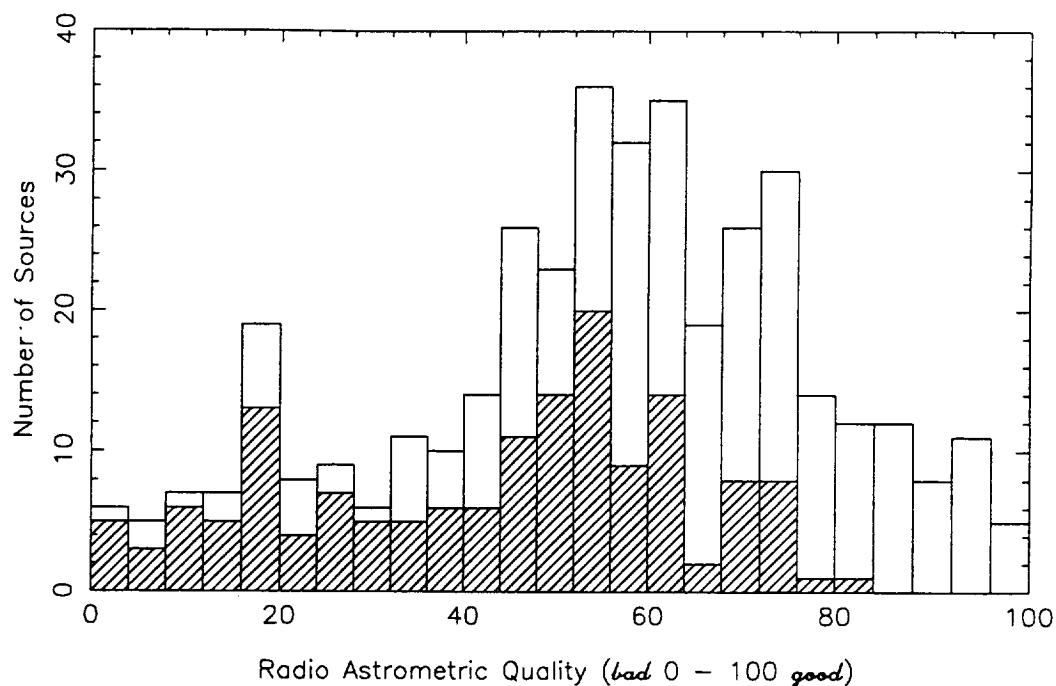


Figure 1. Distribution of radio astrometric quality for 392 ICRF sources taken from Fey et al. (2001, AJ, 121, 1741). The astrometric quality ranges from zero for the worst astrometric sources to 100 for the best astrometric sources. Sources with declinations south of the Celestial Equator are shown hatched. The median of the distribution is 57.

best attempt to construct the most suitable list of ICRF sources for a SIM radio/optical frame tie. Examination of this figure shows a fairly uniform distribution of sources on the sky, but at the cost of having significantly lower radio astrometric quality sources in the Southern Hemisphere (median 57) compared to those in the Northern Hemisphere (median 87).

## 5. Summary

The ideal situation for a radio/optical frame tie would be to observe as many extragalactic objects as possible to minimize systematic errors. However, with finite SIM mission time, the amount of observations dedicated to the frame link will be limited. Even with these limitations, a reasonably accurate frame link can still be achieved. For example, using 50 sources will result in a frame tie accuracy in one coordinate on the order of  $0.25 \text{ mas}/\sqrt{50} \approx 35 \mu\text{as}$  (assuming the SIM mission reaches the expected  $\mu\text{as}$  level for extragalactic objects).

We have attempted to construct a suitable set of frame tie sources but found a significant deficit of candidate sources in the Southern Hemisphere. More radio observations are required, particularly in the Southern Hemisphere. In addition, we conclude that the ICRF will limit the accuracy of any radio/optical frame tie based on future optical astrometric satellite observations if the projected accuracies for these missions are realized.

**Finally, we suggest that the radio astrometric quality as described in this paper can be applied to the next realization of the ICRF.**

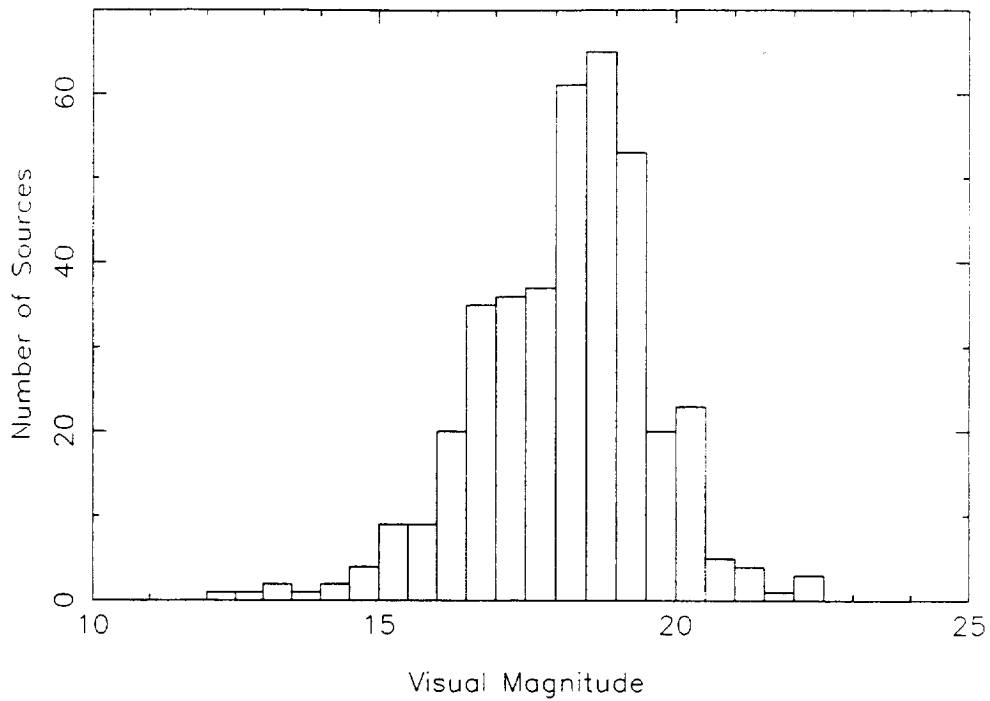


Figure 2. Distribution of visual magnitude for the optical counterparts of 392 ICRF sources listed in Fey et al. (2001, AJ, 121, 1741). The median of the distribution is  $m_v = 18.1$ .

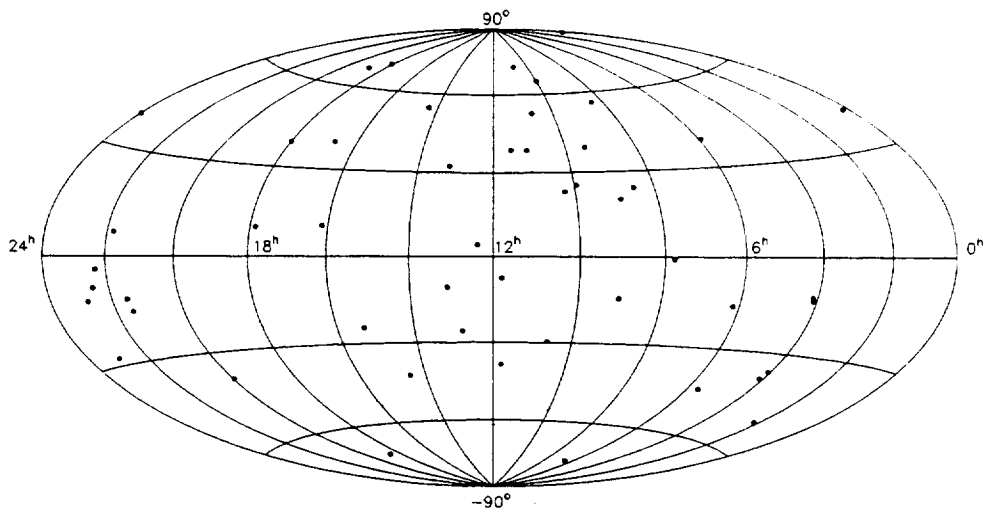


Figure 3. Distribution of the 25 Northern Hemisphere and the 25 Southern Hemisphere ICRF sources listed in Fey et al. (2001, AJ, 121, 1741) selected independently as having the highest astrometric quality and  $m_v \leq 18.0$ , plotted on an Aitoff equal area projection of the celestial sphere. The dotted line represents the Galactic equator.

# Radio Source Stability and the Observation of Precession-Nutation

Martine Feissel <sup>1</sup>, Chopo Ma <sup>2</sup>

<sup>1</sup>) *Observatoire de Paris and Institut Geographique National*

<sup>2</sup>) *NASA Goddard Space Flight Center*

Contact author: Martine Feissel, e-mail: [feissel@ensg.ign.fr](mailto:feissel@ensg.ign.fr)

## Abstract

Some of the radio sources used by VLBI to materialize the celestial reference frame are known to have apparent motions at the sub-milliarcsecond level, particularly those observed in the early years. On the other hand, state of the art precession-nutation models match the observations at this same level. We investigate to what extent the source instability may contaminate the VLBI determination of precession and nutation corrections in several frequency domains.

## 1. Introduction

Precise determination of precession and nutations is based on VLBI data analysis. The classical way to analyse the data is to consider that the celestial objects used to materialize the reference frame are fixed in space and to use this fixed reference frame to observe the fluctuations of the Earth orientation in space. Those VLBI-derived values are then compared with the output of theoretical precession/nutation models and the differences are analysed. In this paper, the reference nutation model is MHB2000 [1], which was adopted as the international conventional model by the International Astronomical Union in 2000. Two possible causes for the observed discrepancies may be considered ([2]): (1) the variations in the atmospheric forcing (and potentially the oceanic forcing) of the nutations derived from actual observations, and (2) the contamination of VLBI-derived nutation amplitudes by apparent motions of the extragalactic radio sources. This paper concentrates on the second effect.

## 2. Radio Sources Stability

While the classical precession-nutation VLBI analysis process is based on the assumption that the apparent direction of the observed radio sources is fixed in space, the emitting structure of radio sources is known to have variability. Figure 1 shows examples of time variability for four well observed sources (derived from [4]) and Figure 2 (reproduced from [3]) shows the envelopes of source variability for several hundred of the ICRF [5] sources. As the result of this variability, the effective celestial reference used in the VLBI analysis may be slightly changing with time, raising the question of contamination of the derived nutation amplitudes.

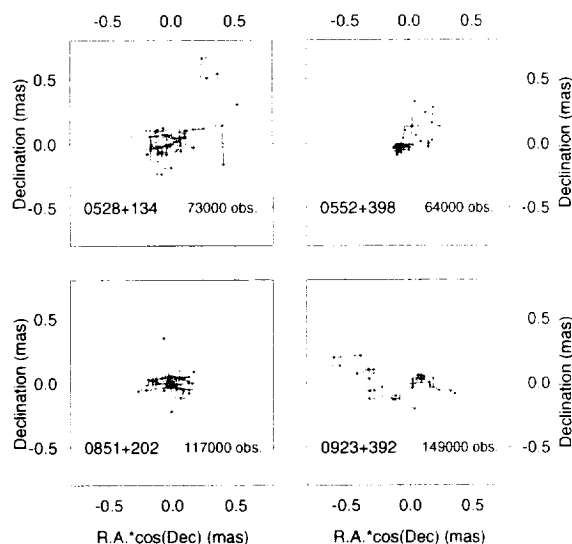


Figure 1. Source position time series at 0.5-year intervals, 1984-1999

### 3. VLBI Analysis of Precession and Nutation

In order to evaluate the stability of VLBI nutation observations, results obtained with two different approaches are considered. They are described hereafter.

1. The first set of VLBI results used here are time series of  $(d\psi, d\epsilon)$  derived from the analysis of the complete observations data set (over 1980.0 - 2001.4) in two parallel ways, (1) with all source coordinates held fixed, and (2) by restricting the analysis to the most stable sources. We label “ $\Delta$ VLBI” the difference of nutation results derived from the second series with those derived from the first one. The two series of celestial pole offsets are analysed, looking for differences in the low frequency terms (precession, obliquity rate and 18.6-year term) as well as variable medium-frequency terms (annual and semi-annual forced nutation, 430d Free Core Nutation).
2. The second set of VLBI results that we consider are time series of source coordinates, estimated for each session in which the source was observed [4]. The time variations of the right ascensions and declinations of 639 sources over 1980.0-1999.3 (150,000 individual coordinates) are analysed by the least-square method to detect a possible contamination of the apparent celestial pole direction, either linear or with the main nutation periods. Would such signatures be found, additive corrections “ $\Delta$ CRF” to the VLBI estimates of  $(d\psi, d\epsilon)$  for the corresponding components would have to be considered.

#### 3.1. Precession and the 18.6-year Nutation

Table 1 gives the value of the precession correction that is associated with the MHB2000 nutation model, the difference of the VLBI results with this reference value, and the two estimates of the effect of source instability on the precession and obliquity rates. The VLBI discrepancy with the MHB2000 precession correction is in statistical agreement with the MHB2000 residual.

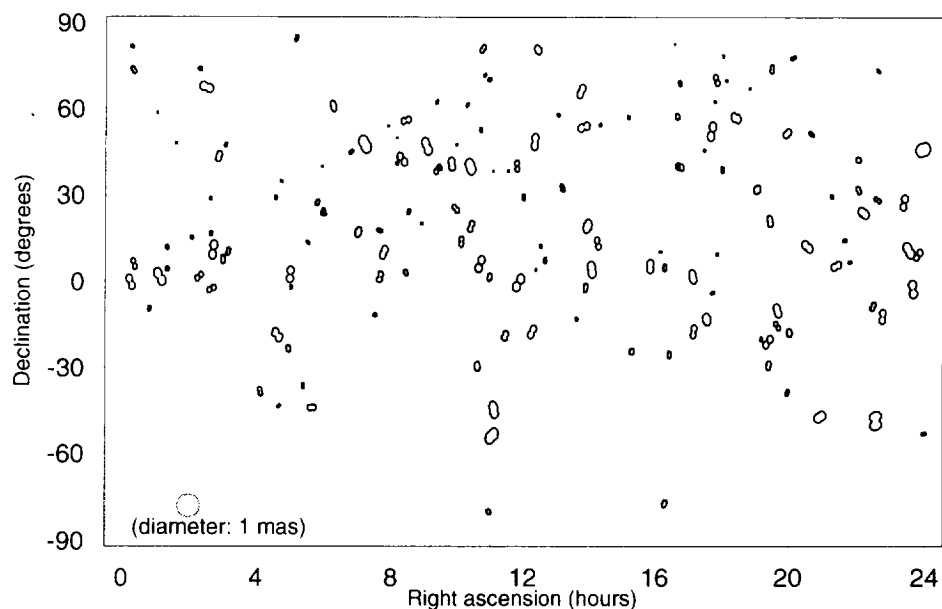


Figure 2. Extragalactic radio sources observed with VLBI, 1985.5-1999.3: envelopes of local variability at 0.5-year intervals.

The two estimates of the source instability effect are in weak agreement, but their similar order of magnitude, as well as their amplitudes relative to the MHB2000 residuals, are an indication of the relevance of considering this aspect.

Table 1. Modeled and estimated values of trends in the celestial pole motion

Data	Precession corr. 0.001"/year	Obliquity rate 0.001"/year
MHB2000	-2.997	
MHB residual	.036 ± .018	
VLBI-MHB	.018 ± .005	
Estimated perturbation due to source selection		
Arcs	-.001 ± .008	-.031 ± .003
CRF	.009 ± .002	-.008 ± .001

Figure 3 shows the two estimates of the impact of source instability on the determination of the 18.6-year nutation term. The point labelled "VLBI" is the estimate derived from the VLBI series based on all radio sources. The estimate of the atmospheric effect is taken from [2]. The "CRF" correction estimate is smaller than the "Arcs" one. The correction obtained by the two methods are somewhat in disagreement: "CRF" would better reconcile the observations with the model in the case of the prograde component, while "Arcs" works better in the retrograde component. Again, the similar orders of magnitude, both between the two estimates and with the discrepancy

with the MHB2000 model, give arguments for the relevance of the question asked.

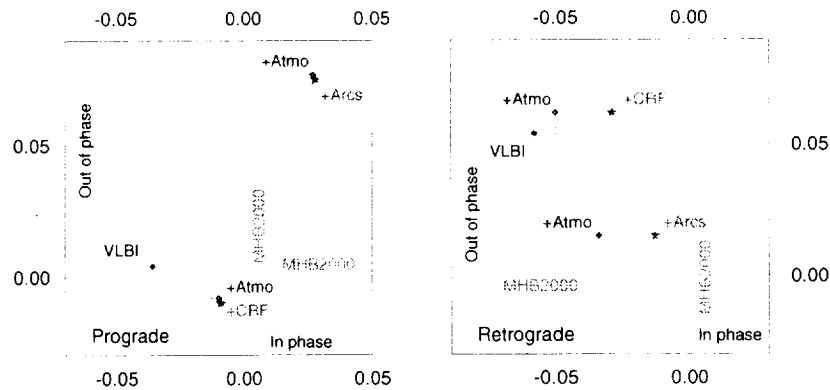


Figure 3. Corrections to the MHB2000 18.6-year nutation term, obtained from analysis of the VLBI series (VLBI) based on all sources, corrected for the effect of arc sources  $\Delta$ VLBI (+Arcs) or of celestial pole motion effect  $\Delta$ CRF (+CRF), and then for the atmospheric excitation (+Atmo). Unit:  $0.001''$ .

### 3.2. The forced Annual and Free Core Nutations

Figure 4 shows the Earth's transfer function for a core resonance period of 430 days, retrograde. Excitations near this frequency are expected to be enhanced.

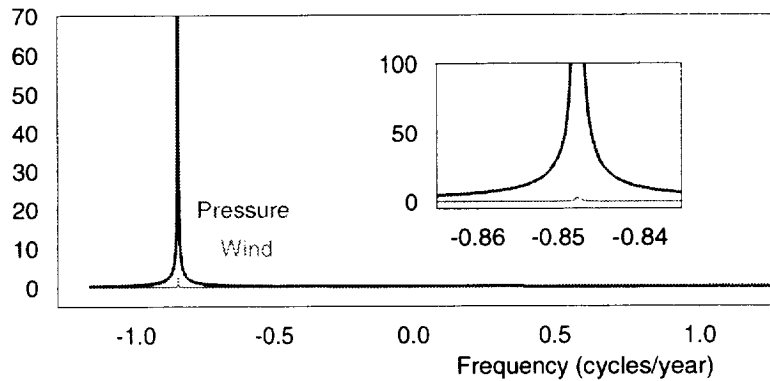
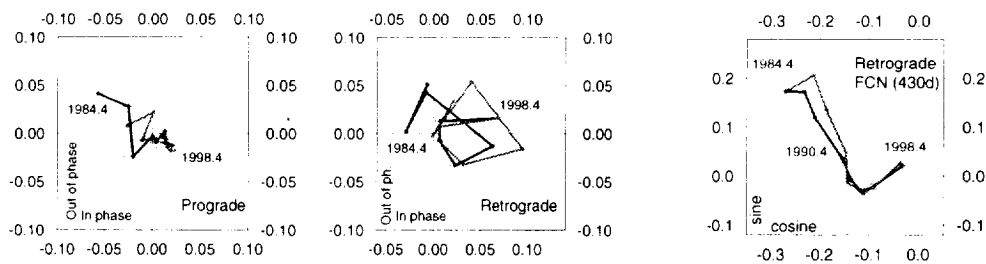


Figure 4. Transfer function for a non-rigid Earth, with a 430-day retrograde FCN. The relative influences of the pressure and wind terms (resp. red and brown/lighter) of atmospheric excitation are shown (arbitrary units).

The left part of figure 5 illustrates the influence the treatment of the source coordinates in the determination of the time-varying annual nutation. The atmospheric excitation in the seasonal frequency band is active mainly in the retrograde component and it varies with time [2]. One indeed hopes to observe these variations in the VLBI results. The observed prograde component shows negligible variations after about 1986, especially when only the stable sources are used. The retrograde component results show significant time variations, as expected. Note that the solution

based on the more stable sources is shifted toward positive in-phase values.

On the right part of figure 5, the influence of source coordinates treatment in the determination of the time-varying Free Core Nutation (retrograde 430-day) is shown to be non-negligible in the 1980s. However, it cannot be invoked as a cause for the change in phase and amplitude around 1990. Arguments in favor of an atmospheric origin for this change are given in [2].



Prograde and retrograde components of the annual nutation derived from VLBI observations. The MHB2000 model values are shown as the intersection of the straight lines. Unit: 0.001”

VLBI-derived retrograde component at the FCN frequency (430 days). The origin of phases is J2000.0. Unit: 0.001”

Figure 5. Influence of the modelling of radio source coordinates on the determination of the forced annual and free core nutation coefficients. The blue (darker) lines are for results based on all sources; the pink (lighter) lines are for results based on the stable sources only.

#### 4. Conclusion

While the precision of VLBI-derived precession and nutation amplitude results is at the level of  $\pm 10 \mu\text{s}$ , these results show clearly that the role of the celestial frame stability is worth analyzing in a rigorous way if further progress is to be made in the understanding of the Earth’s precession and nutations.

#### References

- [1] Mathews, P.M., Herring, T.A., and Buffett, B.A., 2001, “Modeling of nutation-precession: new nutation series for nonrigid Earth, and insights into the Earth’s interior, *J. Geophys. Res.*, in press.
- [2] V. Dehant, M. Feissel, O. de Viron, C. Ma, M. Yseboodt, C. Bizouard, 2002. Nutation at the sub-milliarcsecond level (submitted to *JGR*).
- [3] A.-M. Gontier, K. Le Bail, M. Feissel, T. M. Eubanks, 2001. Stability of the extragalactic VLBI reference frame. *AA* 376, 661.
- [4] Eubanks, T.M., 1999, private communication.
- [5] Ma, C., Arias, E.F., Eubanks, T.M., Fey, A.L., Gontier, A.-M., Jacobs, C.S., Sovers, O.J., Archinal, B.A., Charlot, P., 1998, “The international Celestial Reference Frame as realized by very long baseline interferometry”, *AJ* 116, 516.

# Astrometric and Geodetic Analysis System of VERA

Seiji Manabe, Hiroshi Imai, Takaaki Jike, VERA Group

National Astronomical Observatory of Japan

Contact author: Seiji Manabe, e-mail: manabe@miz.nao.ac.jp

## Abstract

VERA is a unique VLBI array both in scientific objectives and in innovative technologies. Its hardware is designed for accomplishing highest accuracy in determining relative positions of a pair of radio sources up to two degrees apart by phase-referencing VLBI. Each antenna is equipped with a dual-beam observation system. A system for calibrating difference in optical path length between the two beams is an indispensable component of the dual-beam observing system. The analysis software of VERA is required to handle properly the calibration data in order to remove instrumental errors as much as possible. Very high accuracy of antenna position determination and precise information on structures of reference sources are also required.

No existing software system meets all the requirements of VERA and a new one is under development. In the first step of the development, functions to meet VERA's requirements will be added to NRAO's AIPS. The reason to use AIPS as a platform is that phase-referencing observations will begin in this year and the reduction program must be ready before the observations. However, whether or not AIPS or AIPS++ is adopted as a platform of the VERA analysis software is still under investigation. A database for managing raw data from the Mitaka FX correlator is under development and will become available soon. Other databases that manage intermediate and final analysis results are in a designing phase. In this paper requirements to, design of and current status of the software are reviewed.

## 1. Requirements to the Software

VERA (VLBI Exploration of Radio Astrometry) is a VLBI array consisting of four dual-beam radio telescopes and the FX correlator at Mitaka. It aims at determining 3-dimensional positions and velocities of galactic maser sources associated with star forming regions and late-type stars. The accuracy goal in position determination is about  $10 \mu\text{as}$ . The major requirements to the analysis software are listed below.

1. **High accuracy in position determination.**  $10 \mu\text{as}$  is a target accuracy of a single determination of position of a maser source. Simulation results show that even higher accuracy can be expected in the determination of annual parallaxes. However, in order to realize this accuracy, accurate calibration data specific to VERA and their proper use are necessary.
2. **Establishment of a standard method and semi-automation of the analysis.** In order to accomplish the VERA's main scientific target, which is to reveal structure and dynamics of our galaxy, 150-200 days/year must be devoted to this project observation. This produces huge amount of data and the data analysis might be a bottleneck of VERA project unless fast and uniform reduction of data is operational. Thus, it is necessary to establish a standard method of reduction applicable to most of the *usual* radio sources.
3. **Construction of integrated data management system.** VERA's data consist of raw data from the correlator, intermediate results such as precise  $(u, v)$  and calibrated visibility, and right ascensions and declinations of individual maser features at individual observation

epochs. The raw data will be re-reduced with the improvement of adopted model parameters and analysis method. This may happen even 10 years after the observation. Therefore, a very stable, reliable and extendable data management system is indispensable.

- 4. Determination of proper motions and annual parallaxes of maser sources.** It is not always simple to determine proper motions and annual parallaxes, even if positions of maser features are given at individual observation epochs. This is because lifetimes of individual maser features are not always long enough to trace their motions over a year and distinguish annual parallaxes from proper motions. In addition identifying individual maser features between observations at different epochs is not trivial. Furthermore, asymmetric and/or random motions of individual maser features in a maser spot may cause incorrect determination of motion of the maser spot. This error is not serious as long as statistical properties of motions of maser spots are concerned and internal motions of maser features are small enough compare to random motions of maser spots in our galaxy. However, since typical speed of internal motions of maser features are of the same order of peculiar velocities of stars, this might be serious for some maser sources. A lot of experiences in treating real data are necessary for semi-automating this process.

## 2. Strategy of the Development and Current Status

### 2.1. Development Environment

The Mitaka FX correlator, which has been primarily used for the VSOP project, is also used for VERA. It produces raw visibility and related calibration data in a form called CODA F/S. The CODA F/S is a flexible and self-descriptive structure of directories and files. The CODA F/S is designed for efficient use at the Mitaka correlator. Therefore, the use of CODA F/S as a basic platform of data management is natural and almost mandatory. Other format such as FITS can be used for data exchange.

As for the geodetic analysis, the software that was developed at NAOJ and covers from the bandwidth synthesis to the final global parameter fitting has been used. This system is also used for VERA.

The VERA hardware is in the phase of system adjustment and performance check. The first phase-referencing VLBI observation with the dual-beam receiving system is expected to take place in this year. The first version of the analysis software to obtain astrometric results has to become available by early 2003. Geodetic analysis will be working before the astrometric analysis because precise positions of the antennas are required for precision astrometry.

The main computer system is IBM's RS6000/SP whose operating system is AIX. Since this operating system is not very popular in the field of astronomy and geodesy, some effort is necessary for porting widely used free software such as AIPS++.

### 2.2. Data Flow and General Structure of the Software

Fig.1 shows VERA databases and programs to process them. The main body of the databases is raw observed data and logs. The catalogues and constants are also important and indispensable components for later use. Typical example is the case where positions of the antennas are revised and the past data have to be re-reduced. Details of the structure of the database of astrometric

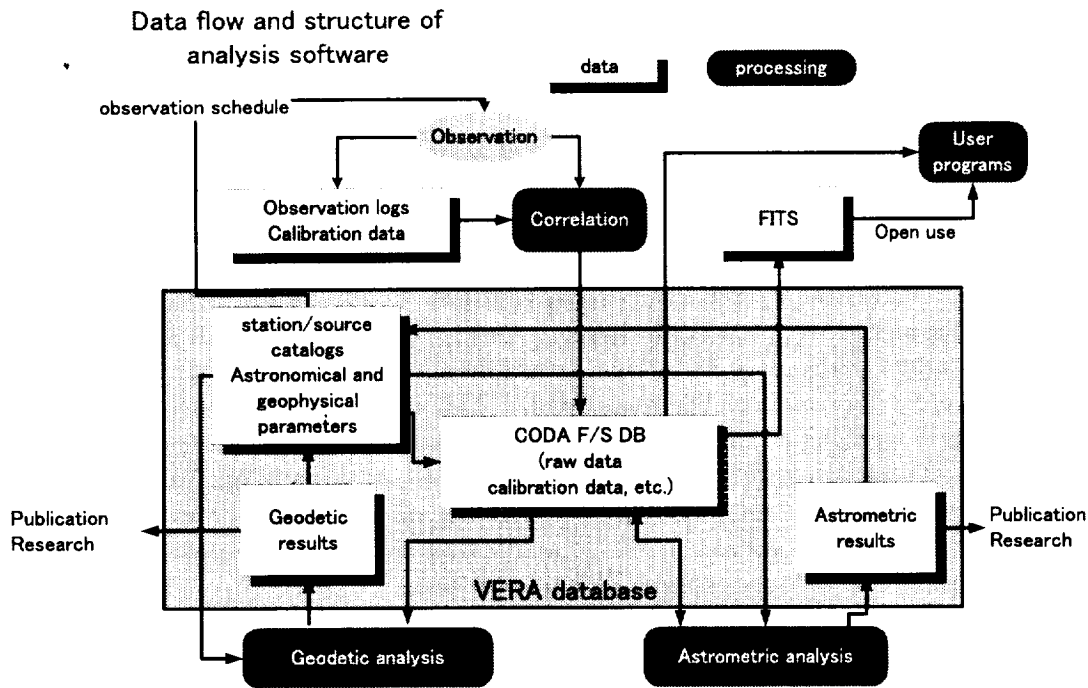


Figure 1. Data flow and processing program

results are shown in fig. 2.

### 2.3. Investigation of Applicability of Existing Software

There are some software packages for reduction of VLBI in the astrophysical field. Examples are NRAO's AIPS and CalTech's DIFMAP. If these packages are operationally usable for VERA, it is not necessary to add a new software. We are evaluating the astrometric accuracy of AIPS by using real and simulated data. The accuracy here concerns with algorithms of data processing and their implementation as program codes.

Capability of the existing software to handle VERA data is also investigated. Easiness of adding new functions specific to VERA such as the CODA F/S interface is important target of the investigation.

We have obtained an impression that AIPS can be used at least in experimental phase of data reduction. However, a lot more must be added for operational use.

### 2.4. Development of a Simulator

We are developing a program that produces simulated visibility. This program is used for checking accuracy of existing software, clarifying necessary performance of the system such as the calibration of the phase difference between the dual beams and mechanical stability of the antenna and necessary accuracy of geophysical and other parameters such as instantaneous positions of antennas and atmospheric propagation model, etc. A block diagram of the simulation program is

## Structure of a database of astrometric results

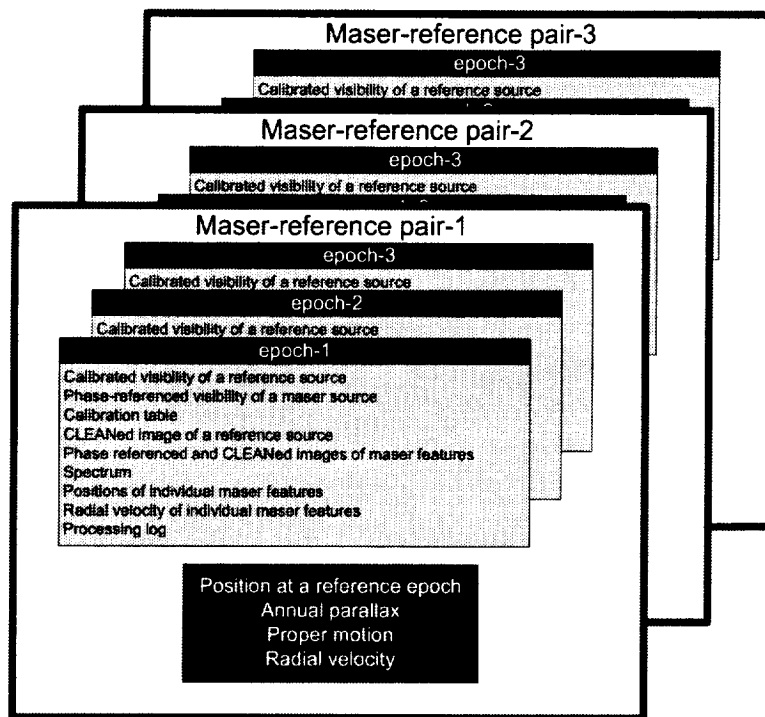


Figure 2. Structure of the database of analysis results

shown in fig. 3.

### 2.5. Catalogue of the CODA F/S

In order to efficiently manage huge amount of data from various kinds observations, a catalogue system for CODA F/S is being made. The major functions and specifications of the catalogue are as follows.

- **Retrieval** Project name, source name, station name, date of processing, processing status
- **Display** Retrieval condition, start and end epochs of observation, location of data including dissemination record, data amount, revision history, comments
- **Graphical data display** Data flagging status, fringe pattern
- **File system manipulation** Registration to the catalogue and deletion, migration from disk to tape library and vice-versa, FITS transformation and exportation,
- **Consistency check between datasets and catalogue**
- **User interface** Browsing and manipulating data through web browser. Program interfaces with Fortran, c, c++ and Java.
- **DBMS** PostgreSQL

This catalogue will become available in March, 2002.

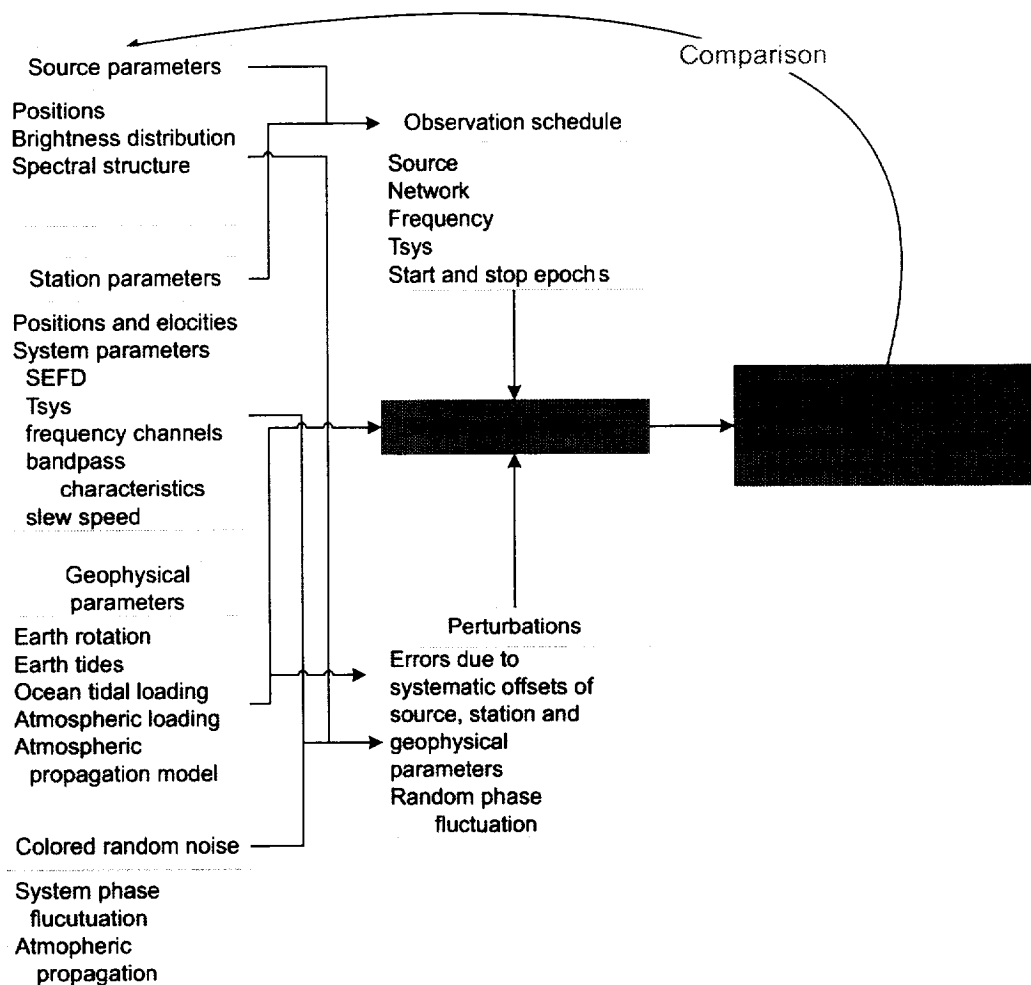


Figure 3. Block diagram of the simulation

## 2.6. Geodetic Analysis Software

Jike *et al.* (2002, [1]) has established a geodetic analysis system which derives geodetic parameters from FITS output of the Mitaka FX correlator. It is almost ready to analyze data of geodetic observations with VERA for determining positions of VERA antennas, although some discrepancies have been found in bandwidth-synthesized delays between the Mitaka FX correlator and the XF correlator of the Geographic Survey Institute. This problem has to be solved as soon as possible. In addition, capability of direct handling of CODA F/S in place of FITS is still needed to be implemented.

## References

- [1] Jike, T., S. Manabe, Y. Tamura, K. Shibuya, K. Doi, and the Antarctic VLBI Group, The Antarctic VLBI Experiments During JARE39 and Geodetic Analyses by the Mitaka FX Correlator, IVS 2002 General Meeting Proceedings, edited by N. R. Vandenberg and K. D. Baver, NASA/CP-2002-210002.

## Results of the Critical Design for the Selenodetic Mission using Differential VLBI Methods by SELENE

Takahiro Iwata<sup>1</sup>, Takeshi Sasaki<sup>1</sup>, Yusuke Kono<sup>2</sup>, Hideo Hanada<sup>2</sup>, Nobuyuki Kawano<sup>2</sup>, Noriyuki Namiki<sup>3</sup>

<sup>1</sup>) National Space Development Agency of Japan, Tsukuba Space Center

<sup>2</sup>) National Astronomical Observatory, Mizusawa Astrodynamics Observatory

<sup>3</sup>) Kyushu University, Department of Earth Planet Science

Contact author: Takahiro Iwata, e-mail: [tiwata@rd.tksc.nasda.go.jp](mailto:tiwata@rd.tksc.nasda.go.jp)

### Abstract

Global mapping of the lunar gravity field will be conducted using two micro sub-satellites of SELENE; the Relay Satellite (Rstar) and the VLBI Radio Satellite (Vstar). Differential VLBI observations will be conducted for three pairs of S-band and one pair of X-band carriers emitted from "The Differential VLBI Radio Sources (VRAD)" on Rstar and Vstar. Four-way Doppler measurements toward the SELENE Main Orbiter above the lunar far side will be conducted by "The Relay Satellite Transponder (RSAT)" on Rstar. These sub-satellites are requested to have long arcs of orbit without maneuver to detect orbit turbulence perturbed by lunar gravity, and to be simple design, therefore, there is no orbital and attitude control except spin stabilization. We have designed the simple structured and light weighted release mechanism, and confirmed the release properties by ground tests. Attitude analysis shows that the nutation caused by the tip off by the release mechanism is dominant for the attitude inclination.

### 1. Introduction

The spatial distributions of the lunar gravity field have been investigated from the orbit perturbations which had been observed by two-way range and range rate (RARR) measurements for spacecraft in lunar orbits. The orbital determination data till Lunar Prospector have produced and improved the models of the lunar gravity field [1]. The gravity data above the lunar far side were, however, less accurate than those above the near side, because they were observed from higher orbits or estimated from the near side data which were affected with accumulated acceleration by the far side gravity.

SELENE, the SELEnological and ENgineering Explorer, is under development by National Space Development Agency of Japan (NASDA) and Institute of Space and Astronautical Science (ISAS), and will be launched in 2005 to elucidate lunar origin and evolution. SELENE is composed of Main Orbiter, and two micro sub-satellites: the Relay Satellite (Rstar) and the VLBI Radio Satellite (Vstar) which will be used for selenodesy experiments [2]. Rstar and Vstar will be injected into the initial elliptical orbit of 2,400-100 km and 800-100 km in altitude, respectively. Main Orbiter will be controlled to keep the circular orbit of 100 km in altitude. These satellites will be used to obtain selenodetic data of higher accuracy by differential VLBI observations and four-way Doppler measurements. We report results of the critical design of the SELENE sub-satellites in the following sections.

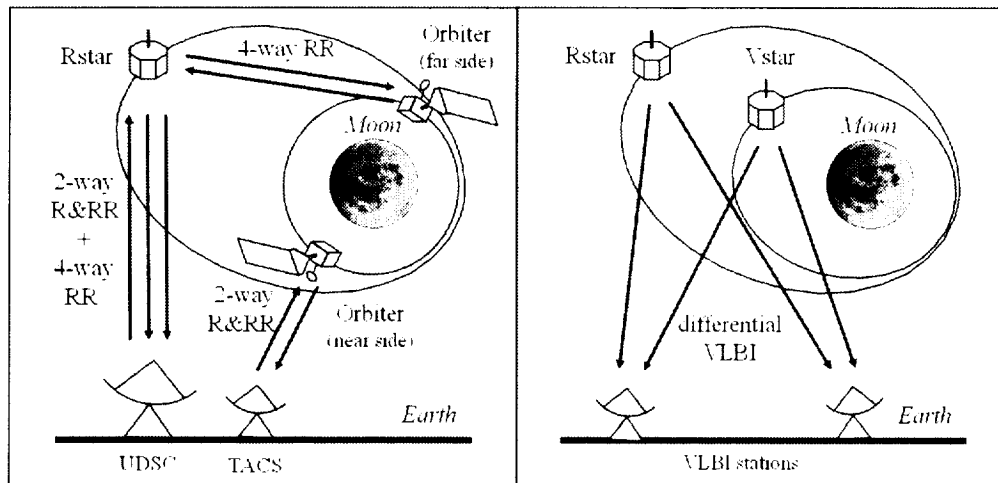


Figure 1. , The concept of the gravity field measurements using SELENE. Left is range (R) and range rate (RR), and right is differential VLBI.

## 2. Outline of the Mission

### 2.1. VRAD: Differential VLBI Radio Sources

Orbits of Rstar and Vstar will be determined with the highest accuracy by differential VLBI observation methods toward S- and X-band radio sources on Rstar and Vstar [3]. Figure 1 (right) shows the mission concept of the differential VLBI observations using VRAD, the Differential VLBI Radio Sources. VRAD-1 and VRAD-2 will be installed on Rstar and Vstar, respectively.

Each radio sources has three S-band carrier signals and one X-band carrier signal to calibrate the delay by the terrestrial ionosphere and to solve uncertainties over one wave length. Narrow bandwidth VLBI terminals for this mission have been developed and are planned to be established at three stations of VERA and four stations in China (Shanghai and Urumqi), Australia, and Europe. The accuracy of the satellite positions determined by VRAD are estimated to be about 20 cm [4], which are more precise by three orders than those obtained by hitherto two-way RARR methods. Because neither Rstar nor Vstar have orbit and active attitude control, the longest arc of orbits are analyzed to produce the highest sensitivity for the lower degrees of lunar gravity coefficients [3].

### 2.2. RSAT: Relay Satellite Transponder

The orbit of SELENE Main Orbiter above the lunar far side will be directly determined by the four-way Doppler measurements relayed by Rstar [2]. The orbit of Rstar will be simultaneously measured by two-way RARR method. Figure 1 (left) shows the mission concept of the four-way Doppler measurements using RSAT, the Relay Satellite Transponder. RSAT-1 and RSAT-2 will be installed on Rstar and Main Orbiter, respectively.

RSAT-1 receives ranging signals of S-band from 64-m antenna at Usuda Deep Space Center (UDSC) and returns the signals to UDSC to produce two-way RARR measurements. RSAT-1 relays the carrier signals to RSAT-2 at Main Orbiter above the lunar far side simultaneously.

RSAT-2 receives carriers and returns to RSAT-1. RSAT-1 receives those, converts the frequency to X-band, and transmits the carrier signals to UDSC to produce four-way Doppler measurements. Signal frequencies of these loops will be coherently converted. Four-way Doppler measurements derive the first direct orbit determination of low lunar orbiter above the lunar far side, which produce the first global gravity map of the moon. Analysis of the coverage considering the four-way links shows that our method derives fully covered gravity map [5].

### **3. Design of the System**

#### **3.1. Outline of Rstar and Vstar System Design**

Communications toward ground stations will be linked by an S/X-band coaxial vertical dipole antenna with a toroidal beam of about 40 degrees width at Rstar and Vstar. Communications toward Main Orbiter will be linked by two pairs of S-band patch omni-directional antennas with a conical beam of about 140 degrees width at Rstar.

Rstar and Vstar are designed to be light-weight enough and cost-effective to conduct selenodesy experiments. Size of each main body is 1m x 1m x 0.65m which is determined by the size of the highly efficient silicone cell solar array to supply the demanded electric power of 70W. There are no orbital and attitude control except spin stabilization on these satellites to lighten the mass. The separation velocity and the spin will be injected by the simple structure and light weight release mechanism which has been developed for Rstar and Vstar [6]. The mass distribution of both Rstar and Vstar are adjusted to be the same, and the total masses of these satellites are designed to be 45 kg.

#### **3.2. Spin and Attitude Properties of Rstar and Vstar**

Spin stabilization without orbital and attitude control maneuver is useful to obtain longer arcs of orbit, which is effective to detect orbit turbulence perturbed by lunar gravity. The spin and attitude properties are, however, affected by the characteristics of the separation of Rstar and Vstar from Main Orbiter. These properties were measured by ground tests of the release mechanism using the terrestrial gravity cancel mechanism. The full width of the nutation caused by the tip off at the separation is reported to be 11.4 deg in the maximum [7]. The nutation is also caused by the slant of the inertia axis against the mechanical axis of Rstar and Vstar. The measurement of the momentum of inertia and the product of inertia using the mechanical test model of Rstar and Vstar reported that the full width of the nutation caused by the slant is less than 6 deg [7]. The allocated values of each attitude fluctuation factor derived by the attitude analysis suggest that the nutation caused by the tip off at the separation and the slant of the inertia axis is larger than the inclination caused by the torque of the solar radiation pressure and the gravity field inclination.

### **4. Summary**

SELENE Relay Satellite (Rstar) and VLBI Radio Satellite (Vstar), which will be used for the differential VLBI observations and the four-way Doppler measurements for selenodesy, have been designed. These sub-satellites are requested to have long arcs of orbit without maneuver, therefore, spin stabilization is adopted to avoid active attitude control. We have designed the simple structure

and light weight release mechanism, and measured the release properties by ground tests to estimate the nutation angle caused by the tip off at the separation. We also measured the momentum and product of inertia of Rstar and Vstar mechanical test model to estimate the nutation angle caused by the slant of the inertia axis.

## References

- [1] Konopliv, A. S., Asmar, S. W. Carranza, E., Sjogren, W. L., and Yuan, D. N.: Recent Gravity Models as a Result of the Lunar Prospector, *Icarus*, 150, 1-18, 2001.
- [2] Iwata, T., Takahashi, M., Namiki, N., Hanada, H., Kawano, N., Heki, K., Matsumoto, K., and Takano, T. : Mission Instruments for Lunar Gravity Measurements using SELENE Sub-satellites, *J. Geod. Soc. Japan.*, 47, 558-563, 2001.
- [3] Hanada, H., Iwata, T., Kono, Y., and Matsumoto, K.: VRAD Mission: Precise Observation of Orbits of Sub-satellites in SELENE, Proc. International VLBI Service for Geodesy and Astrometry 2002 General Meeting, 3-02P, 2002.
- [4] Kono, Y., Hanada, H., Kawano, N., Iwadate, K., Koyama, Y., and Fukuzaki, Y.: Precise Positioning of Spacecrafts by Multi-frequency VLBI, Proc. International VLBI Service for Geodesy and Astrometry 2002 General Meeting, 4-07P, 2002.
- [5] Matsumoto, K., Heki, K., and Hanada, H.: Global Lunar Gravity Field Recovery from SELENE, Proc. International VLBI Service for Geodesy and Astrometry 2002 General Meeting, 6-14P, 2002.
- [6] Iwata, T., Nagae, Y., Takahashi, M., Namiki, N., and Hanada, H.: System Design of SELENE Relay Satellite for Selenodesy Mission, in Proc. 22nd International Symposium on Space Technology and Science, eds. Y. Arakawa et al. (Sanbi Insatsu: Tokyo), pp.1582-1587, 2000.
- [7] Iwata, T., Sasaki, T., Izumi, T., Kono, Y., Hanada, H., Kawano, N., and Takano, T.: Properties of the Release Mechanism of SELENE Relay Satellite and their Influences for the Lunar Gravity Observation, in Proc. 23rd International Symposium on Space Technology and Science, in press, 2002.

# Global Lunar Gravity Field Recovery from SELENE

*Koji Matsumoto, Kosuke Heki, Hideo Hanada*

*Division of Earth Rotation, National Astronomical Observatory*

*Contact author: Koji Matsumoto, e-mail: matumoto@miz.nao.ac.jp*

## Abstract

Results of numerical simulation are presented to examine the global gravity field recovery capability of the Japanese lunar exploration project SELENE (SELEnological and ENgineering Explorer) which will be launched in 2005. New characteristics of the SELENE lunar gravimetry include 4-way satellite-to-satellite Doppler tracking of main orbiter and differential VLBI tracking of two small free-flier satellites. It is shown that planned satellites configuration will improve lunar gravity field in wide range of wavelength as well as far-side selenoid.

## 1. Introduction

Many gravity potential models of the Moon have been developed mainly from 2-way Doppler tracking data of spacecraft orbiting the Moon, in which the lunar gravity potential is usually modelled in terms of spherical harmonics as follows,

$$V(\phi, \lambda, r) = \frac{GM}{r} \sum_{n=0}^N \left(\frac{R}{r}\right)^n \sum_{m=0}^n (\bar{C}_{nm} \cos m\lambda + \bar{S}_{nm} \sin m\lambda) \bar{P}_{nm}(\sin \phi) \quad (1)$$

where the expansion is given in spherical coordinates with latitude  $\phi$ , longitude  $\lambda$ , radius  $r$ ;  $G$  is the universal constant of gravitation;  $M$  is the lunar mass;  $R$  is some reference radius;  $\bar{C}_{nm}$  and  $\bar{S}_{nm}$  are the normalized selenopotential coefficients to be determined, and  $\bar{P}_{nm}$  are the normalized associated Legendre functions of degree  $n$  and order  $m$ . The state of the art lunar gravity models of LP series [1] are completed to degree and order over 100, and have revealed many new masscons. In determining the gravity coefficients in a least-squares sense, however, a kind of constraint taken from Kaula's [2] rule of thumb has been imposed in order to avoid numerical instabilities stemming from spatial data coverage limited to almost near-side. The Kaula-type signal constraint acts as a gravity field smoother and results in good data fit over near-side, but the far-side gravity field is almost meaningless as is clearly shown by Floberghagen [3].

In the Japanese lunar exploration project SELENE (SELEnological and ENgineering Explorer) to be launched in 2005, far-side data coverage will be greatly improved by means of high-low 4-way satellite-to-satellite Doppler tracking. The differential VLBI tracking of two sub-satellites [4] is also a new technique applied to the lunar gravimetry. In this article, basing on computer simulation, we discuss the anticipated accuracy of recovered lunar gravity field from SELENE with these new tracking methods.

## 2. SELENE Gravimetry

SELENE consists of three satellites; the main lunar orbiter (hereinafter referred to as orbiter), the relay sub-satellite (Rstar), and the VLBI sub-satellite (Vstar). The orbiter is a low-altitude

(100 km above the Moon) satellite in a circular orbit with inclination of  $90^\circ$ . The Rstar is a high-altitude (perilune height of 100 km and apolune height of 2400 km) spin-stabilized small satellite in an eccentric orbit with the same inclination as the orbiter. The Rstar is equipped with a communication instrument which relays Doppler signal to/from orbiter, which realizes direct tracking of the orbiter in the far-side (RSAT mission) [5]. The perilune height of the Vstar orbit is 100 km and the apolune height is 800 km. Two radio sources VRAD-1 and VRAD-2 on board the Rstar and the Vstar continuously emit four carrier waves with different frequencies in S and X bands for differential VLBI (VRAD mission) [4].

The orbit of the main orbiter will be perturbed by attitude control maneuver about every 18 hours, while no artificial disturbance will be made to the Rstar and the Vstar orbit. Since gravity acceleration is inversely proportional to  $r^{n+2}$ , the orbiter at 100 km altitude is more sensitive to high-degree gravity fields than the Rstar or the Vstar. The Rstar and the Vstar are, on the other hand, more appropriate than the orbiter to determine low-degree gravity fields because of attenuation of high-degree gravity signal on their relatively high mean altitude. Unperturbed long arc-length of the Rstar and the Vstar orbit is also preferable to determine long-wavelength gravity potentials. Consequently, the combination of gravity solutions from the three satellites will result in a fine lunar gravity field model over a wide range of wavelengths.

### 3. Simulation Setting and Results of Covariance Analysis

GEODYN II [6] and SOLVE [7] programs are used for the simulation and the covariance analysis. GEODYN II has been modified so that it can handle interplanetary 4-way Doppler measurement. The simulation is conducted for the nominal mission period of one year. Table 1 summarizes the tracking data assumed in the simulation in terms of measurement type, accuracy, and data rate. The measurement accuracy depends on the performance of the tracking stations.

Table 1. Tracking data assumed in the simulation

Target satellite	measurement type	accuracy	data rate
Main orbiter	2-way Doppler	2.0 mm/s	10 s
	4-way Doppler	1.0 mm/s	10 s
Rstar	2-way Doppler	0.2 mm/s	10 s
	Differential VLBI with Vstar	1 mm	120 s

The differential VLBI is treated as doubly differenced 1-way range.

Various restrictions to the tracking data acquisition have been taken into account to get realistic simulation results, which are (1) the antenna sharing plan with other space missions, (2) the engineering requirement for the Rstar that the satellite must be in full sunlight during the whole revolution to obtain 4-way Doppler data, (3) the condition that the 2-way and 4-way Doppler data of the orbiter cannot be obtained synchronously, (4) the antenna pattern angle limiting the 4-way link establishment, and (5) the ground station condition restricting the VLBI observation to be 3 days/week and 8 hours/day. Three stations among VERA stations [8] are selected to form over 1000km-long baselines as shown in Figure 1. It is under way to establish an international VLBI network to realize longer baselines [4]. We used LP75G as the true lunar gravity field to simulate observation data as well as a priori gravity field model for the estimation of the gravity potential

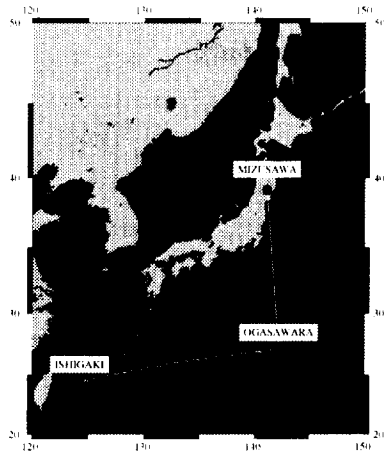


Figure 1. Japanese domestic VLBI stations and baselines used in the simulation.

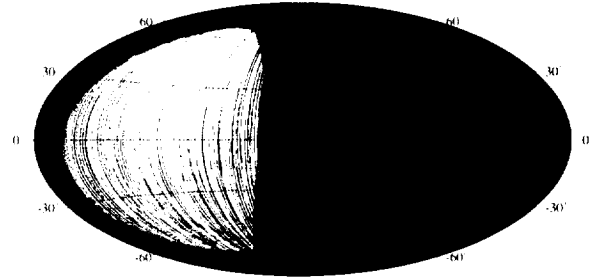


Figure 2. 1-year data coverage of the main orbiter. The map is centered on 270° E longitude, with the far-side of the Moon to the left of the center, and the near-side to the right.

up to degree and order 30. The arc length is set to 1 day for the orbiter and 15 days for the Rstar and the Vstar. Shown in Figure 2 is the date coverage of the orbiter based on the orbit configuration and the analysis conditions described above. A better far-side data coverage in the southern hemisphere is due to the placement of the Rstar apoapsis on the southern hemisphere, which makes the link between the orbiter and the Rstar easier when the orbiter is in the southern hemisphere. Although some data blank areas appear in the northern hemisphere, we can expect generally good far-side coverage from 1 year mission period.

In order to see error spectrum of the recovered gravity field we calculate coefficient sigma degree variance  $\sigma_n$  which is defined as

$$\sigma_n = \left[ (2n + 1)^{-1} \sum_{m=0}^n \left\{ \sigma^2(\bar{C}_{nm}) + \sigma^2(\bar{S}_{nm}) \right\} \right]^{1/2} \quad (2)$$

where  $\sigma(\bar{C}_{nm})$  and  $\sigma(\bar{S}_{nm})$  are the error of the gravity potential coefficients. Plotted in Figure 3 is the coefficient sigma degree variances for the four cases summarized in Table 2. In case A, the gravity coefficients higher than degree 10 are strongly affected by the constraint. Case B suggests that the 4-way Doppler data on the far-side significantly improves gravity coefficients for all degrees up to degree 30, which is compared with LP100J. This implies the importance of

Table 2. Case setting for covariance analysis

Case name	Measurement type				A priori constraint
	orbiter 2-way	orbiter 4-way	Rstar 2-way	$\Delta$ VLBI	
A	Yes	No	No	No	Yes
B	Yes	Yes	No	No	No
C	Yes	Yes	Yes	No	No
D	Yes	Yes	Yes	Yes	No

far-side data coverage on spherical harmonic approach to lunar gravity field recovery. From case C we see that the Rstar contribution is significant for low-degree fields ( $n \leq 10$ ), as expected in section 2. The differential VLBI data further improves low-degree coefficients as seen in the result for case D. Since the accuracy of the lunar moments of inertia is currently dependent on the

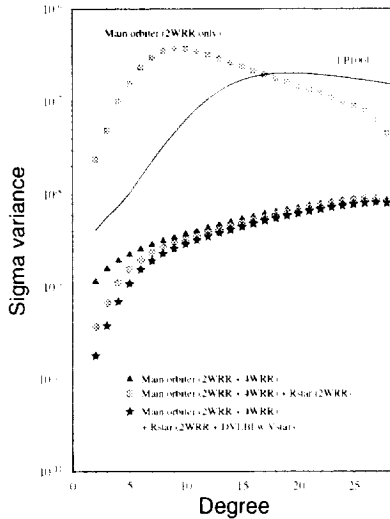


Figure 3. Anticipated coefficient sigma degree variances. The solid line shows LP100J error variances.

errors in  $J_2$  and  $C_{22}$  [9], the contribution from the Rstar and the Vstar will be of particular importance to constrain the radius or density of the lunar core which can be deduced from the lunar moment of inertia.

Selenoid height errors are calculated by propagating a full error variance-covariance matrix of the gravity coefficients [10]. Figure 4 shows the selenoid height error which is anticipated for case A and Figure 5 is the same but for case D. Large selenoid error exceeding 25 m in Figure 4 indicates that even if a Kaula-type signal constraint is applied to the solution, the lunar far-side gravity field is poorly determined from conventional near-side 2-way Doppler observation only. However, the selenoid height errors in the far-side are significantly reduced down to below a few meters in case D, much of which is contributed from far-side 4-way Doppler data. Even though relatively larger error is seen in 4-way data blank area, Figure 5 again shows the importance of the far-side data coverage.

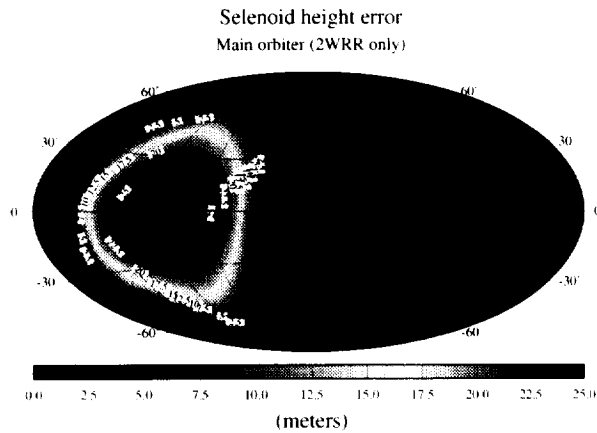


Figure 4. Anticipated selenoid height error for case A. A Kaula-type constraint is applied to the solution in order to avoid numerical instability.

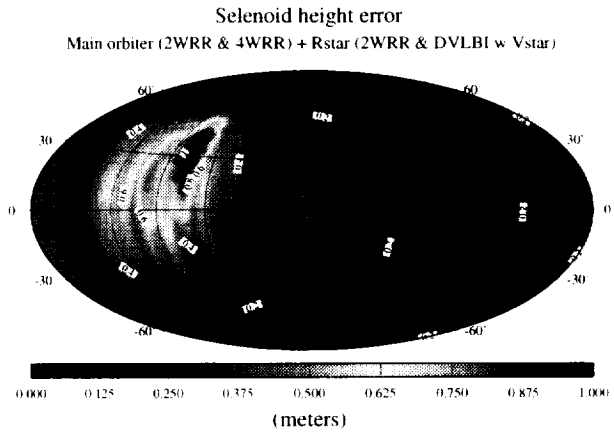


Figure 5. Same as Figure 4, but for case D. No constraint is applied to the solution. Note that the scale is different from that of Figure 4.

#### 4. Summary

We have presented preliminary simulation results with regard to the lunar gravimetry in the coming SELENE project. It is shown that sufficient data coverage over the lunar far-side will be realized by high-low satellite-to-satellite 4-way Doppler measurement with planned satellites configuration. The far-side data result in significant improvement of lunar gravity field over a wide range of wavelengths as well as improvement of the far-side selenoid. The orbiter contribution and the Rstar contribution to the gravity field solution are complementary and the Rstar is expected to contribute to the improvement in low degree gravity coefficients such as  $J_2$  and  $C_{22}$ . We can expect further improvement in the low degree coefficients by the differential VLBI measurement between the Rstar and the Vstar. This feature will be enhanced by an international VLBI network with longer baselines.

#### 5. Acknowledgements

GEODYN II/SOLVE programs were introduced to NAO under a joint research contract with NASA/GSFC and we thank Prof. B. Chao and Dr. D.D. Rowlands for their continuous help.

#### References

- [1] Konopliv, A. S., S. W. Asmar, E. Carranza, W. L. Sjogren, D. N. Yuan, Recent Gravity Models as a Result of the Lunar Prospector Mission, *Icarus*, 150, 1–18, 2001.
- [2] Kaula, W. M., Theory of satellite geodesy, Blaisdell Pub. Co., Waltham, Mass., 1966.
- [3] Floberghagen, R., J. Bouman, R. Koop, P. Visser, On The Information Contents and Regularisation of lunar gravity field solutions, *Adv. Space Res.*, 23, 1801–1807, 1999.
- [4] Hanada, H, T. Iwata, Y. Kono, K. Matsumoto, S. Tsuruta, T. Ishikawa, K. Asari, J. Ping, K. Heki, N. Kawano, VRAD Mission: Precise Observation of Orbits of Sub-Satellites in SELENE with International VLBI Network, *Proc. IVS2002*, this issue.
- [5] Iwata, T., T. Sasaki, Y. Kono, H. Hanada, N. Kawano, N. Namiki, Results of the critical design for the selenodetic mission using differential VLBI methods by SELENE, *Proc. IVS2002*, this issue.
- [6] Pavlis, D. E., D. Moore, S. Luo, J. J. McCarthy, S. B. Luthcke, GEODYN Operations Manual, 5 Volumes, Hughes/STX, prepared for NASA Goddard Space Flight Center, Greenbelt, Maryland, 1997.
- [7] Ullman, R. E., SOLVE Program: Mathematical formulation and guide to user input, Hughes/STX contractor report, contract NAS5-31760, NASA Goddard Space Flight Center, Greenbelt, Maryland, 1994.
- [8] Sasao, T., VERA Project Team, Scientific objective and present status of VERA Project, *Proc. IVS2002*, this issue.
- [9] Williams, J. G., X X Newhall, J. O. Dickey, Lunar moments, tides, orientation, and coordinate frames, *Planet. Space Sci.*, 44, 1077–1080, 1996.
- [10] Haagmans, R. H. N., M. Gelderen, Error variances-covariances of GEM-T1: Their characteristics and implications in geoid computation, *J. Geophys. Res.*, 96, 20011–20022, 1991.



# Splinter Meeting Reports





## Mini-TOW (Technical Operations Workshop)

Rich Strand<sup>1</sup>, Brian Corey<sup>2</sup>

<sup>1)</sup> *Gilmore Creek Geophysical Observatory*

<sup>2)</sup> *MIT Haystack Observatory*

Contact author: Rich Strand, e-mail: [oper@blizzard.gcgo.nasa.gov](mailto:oper@blizzard.gcgo.nasa.gov)

### Abstract

This paper summarizes discussions and activities at the Mini-TOW (Technical Operations Workshop) held during the 2002 IVS General Meeting. Specific topics include roundtable discussions, a GSI correlator tour, a tape recorder session, an RFI session and a final panel discussion.

### 1. Introduction

The Mini-TOW (Technical Operations Workshop) was held during the 2002 IVS General Meeting on Wednesday, February 6, 2002 from 14:30 to 18:00 at the Geographical Survey Institute, Tsukuba, Japan.

Present were the host Kazuhiro Takashima, GSI, and Network Coordinator Ed Himwich, NVI. VLBI experts Brian Corey and Dan Smythe from MIT Haystack were available for group discussions and technical sessions. Kerry Kingham, USNO, represented the correlator during roundtable discussions. See Appendix A for Kerry's comments on Mark 4 correlator operations and the new IVS observing schedule. Rich Strand, GCGO, was discussion chairman representing IVS network stations. See table 1 for a full list of the participants.

### 2. Roundtable Discussions

Kerry Kingham discussed the need for operators to make complete remarks in e-mail for any possible data loss. Comments in the data log are still useful but the post-session briefing e-mail is required. The new Mark 4 correlator operation for the rapid-return "R" sessions requires advance setup and these data loss comments are now necessary so that the setup can be completed before the tapes arrive. The USNO is still seeing data loss or problems that have not been described or mentioned. These data "hits" often cost the correlator an investment in time and resources to research and correct.

Matt Harms, Honeywell-TSI operator at Kokee Park, raised the issue of observing with a warm receiver. Jay Redmond, Honeywell-TSI, who repairs dewars, said that the moving parts in the dewar refrigerators are the cause of most failures. Helium leaks and compressor filters are also problems. Rich Strand, GCGO, mentioned two different scenarios for a failure during a session. One occurs when the session is running and the receiver starts to warm, and the other occurs when the receiver is already at ambient before the session starts. The least amount of time to cool is nine hours, and fully warming up a receiver prior to recooling adds several more hours. If the decision is made not to recool, the warm-up can be deliberately slowed by keeping the compressor running. Data are lost when observing is halted to recool, or some data are effectively lost when

Table 1. Participants Mini-TOW IVS GM 2002 Japan

Name	Affiliation	Country
Mario Bérubé	NRC	Canada
Brian Corey	MIT Haystack	USA
Yoshihiro Fukuzaki	GSI	Japan
Ray Gonzalez	NVI, Inc./GSFC	USA
Matt Harms	Honeywell-TSI/Kokee Park	USA
Ed Himwich	NVI, Inc./GSFC	USA
Kerry Kingham	USNO	USA
Charles Naudet	JPL/DSN	USA
Hiro Osaki	CRL	Japan
Matti Paunonen	FGI	Finland
Jay Redmond	Honeywell-TSI/GGAO	USA
Duk-Gyoo Roh	KAO	Korea
Dan Smythe	MIT Haystack	USA
Rich Strand	GCGO	USA
Hiroshi Takaba	Gifu University	Japan
Kazuhiro Takashima	GSI	Japan
Gino Tuccari	CNR	Italy
Alex Volvach	CAO	Ukraine

observing warm due to degraded system sensitivity. Brian Corey explained data loss from warm receivers. The schedules are generated to achieve a minimum SNR for each scan. If the target SNR is low, weak sources may fall below the sensitivity of the network as the receiver warms and the SEFD goes up [1]. Quality code summaries in correlator reports are a poor indicator of the impact on the VLBI data of observing warm, as the quality code is not adversely affected by low sensitivity unless fringes are too weak to be detected. These summaries therefore are not useful as guidelines for when to observe warm. The final VLBI geodetic solution is the most important indicator of the effect of observing warm.

Final resolution of the discussion was stated by Ed Himwich. Stations should continue to observe warm but refer the problem to IVS. A decision would be made to have the station continue to observe or halt for re-cooling. This would depend on SNR requirements for the network, total number of warm receivers, and the possibility of a successful cool-down.

### 3. GSI Correlator Tour

Kazuhiro Takashima gave a tour of the GSI K4 Correlator [2]. This system uses the HP 9000 to process three stations, three baselines at 512 Mbps. The GSI VLBI correlator runs unattended using an automatic correlation process and tape changers.

#### 4. Tape Recorder Session

The tape recorder session was held in the GSI Tsukuba VLBI operations building by Dan Smythe. The discussion included basic recorder pretests for checking recorder performance. Also included was a detailed discussion of thin tape and the special recorder alignments needed to prevent damage [3]. Vacuum shift tests and head calibration demonstrations were held. This workshop was conducted in two sessions due to class size. The reference files used in the class can be found in table 2.

Table 2. Additional reference material for the Haystack-Metrum recorder

<ftp://web.haystack.mit.edu/pub/mark4/memos/267.pdf> (pdf file)  
<ftp://web.haystack.mit.edu/pub/mark4/DAS/reccheck.text> (plain text)

<ftp://web.haystack.mit.edu/pub/mark4/DAS/RecFund.pdf>

<ftp://web.haystack.mit.edu/pub/mark4/DAS/RecFundV.pdf>

<ftp://web.haystack.mit.edu/pub/mark4/recorder/RecFund/TrackLayout.pdf>

<ftp://web.haystack.mit.edu/pub/mark4/recorder/RecFund/headloypasses.pdf>

<ftp://web.haystack.mit.edu/pub/mark4/recorder/RecFund/headstackdef.pdf>

#### 5. RFI Session

The RFI session was led by Brian Corey at the GSI Tsukuba 32m radio telescope. The discussion included finding and analyzing a strong S-band interfering signal coming from Tsukuba City. Even though a signal may appear to be very strong on a spectrum analyzer, its total power may be less than the total noise power in the RF or IF band if the signal has a narrow bandwidth. Such a signal that is outside the observing passband does not affect the VLBI data directly. If an out-of-band signal is strong enough that it raises the overall power level significantly, however, it can cause front-end overload and thereby affect the in-band VLBI data indirectly through amplifier compression. (In order to avoid saturation effects, the general recommendation is that the receiver output 1-dB compression point be at least 10 dB higher than the signal level. In an X-band receiver, the phase cal pulse is typically ~10 dB stronger than the average system noise level when the pulse is on. The X-band 1-dB point should therefore be >20 dB higher than the average system noise level, in order to avoid phase cal intermodulation effects caused by amplifier saturation.) In-band RFI is normally more of a concern than out-of-band because it decreases the system sensitivity and it can bias the group delays measured at the correlators [4]. In-band RFI that raises the system power by >10% in one or more frequency channels should be identified at the stations. This is most easily done by a combination of Tsys measurements, spectrum measurements with an analyzer, and observation of variable power levels in channels due to intermittent RFI. Site specific RFI sources were discussed by the participants. This workshop was conducted in two sessions due

to class size.

## 6. Final Panel Discussion

The final panel discussion was chaired by the IVS Network Coordinator Ed Himwich. After a brief feedback on the day's activities a discussion started on the new IVS observing schedule that includes the rapid-return sessions. Kerry Kingman remarked that the new NEOS, now R4, do not work because the tapes are one week behind. The R1 tapes are on the same plane as the R4 from Ny-Ålesund and that causes a problem. The Ny-Ålesund observing schedule doesn't allow days off. The new IVS sessions have new names, start times, etc. Dan Smythe and Ed Himwich discussed observing strategy but no useful ideas emerged. Ed said he would continue this panel discussion with the IVS Board.

The Mini-TOW ended at 18:00 and the participants were bused back to the Epochal Conference Center.

## 7. Appendix A

Kerry Kingham, USNO correlator notes:

1. All experiments designated "IVS-R" (i.e., R1s and R4s) are "RAPID" experiments. The tapes should be shipped immediately by express paths.
2. The correlators are setting these experiments up before the tapes arrive and they use the network station's e-mail messages as the primary source of information about the experiment operations at the network station. Please be complete, and note any missed scans or other problems during the experiment. Logs are the secondary source of information.
3. The Mark 4 correlators are more log-dependent than the old Mark IIIs. Please get the logs to cddisa in a timely and complete manner.
4. At the Washington Correlator, we stop everything to do the Intensives (Kokee and Wettzell daily 1 hour experiments) as soon as the last tape (typically Wettzell) arrives. The "R" experiments are next in importance and also start processing within an hour of the arrival of the last tape. This is why it is important that we get all of the appropriate information (particularly e-mails and logs) from the stations as soon as possible, so we can be ready when the tapes arrive.
5. The correlators can be of some help in diagnosing problems at your station. We can look at a spectrum of the passband for RFI or spurious signals; we can check playback quality of the recordings; and we can do a limited amount of phase-cal analysis which can indicate spurious phase-cal signals, reflections, etc., although tracking down the source is up to the station. We can do what we can, but we are, typically, thousands of kilometers away!
6. The correlators are trying to improve our feedback to the stations, and changes are being made to the experiment reports to try and deliver more information from the correlators to both the Network Stations and Analysis Centers. Comments are welcome.

## References

- [1] Dave Shaffer RadioMetrics: Calibration, Field System Manual, April, 1984. For IVS workshop version with notes, 1998 VLBI TOW Haystack Proceedings, Amplitude Calibration, pages 5-9.
- [2] Misao Ishihara, et al.: Tsukuba VLBI Center, 1999 IVS Annual Report.
- [3] Don Sousa, MIT Haystack and Bruce Thornton, NVI: 1998 VLBI TOW Haystack Proceedings, THIN TAPE
- [4] Dave Shaffer, "RFI: Effects on Bandwidth Synthesis," in IVS 2000 General Meeting Proceedings, available at <http://ivscc.gsfc.nasa.gov/publications/gm2000/shaffer/>.

## Summary of the Third IVS Analysis Workshop

*Axel Nothnagel*

*Geodetic Institute of the University of Bonn*

*e-mail:* nothnagel@uni-bonn.de

### Abstract

On February 8, 2002, the Third IVS Analysis Workshop was held at the Epochal Conference Center, Tsukuba, Japan. The one-day meeting was attended by about 40 participants. Here, a short summary of the discussion topics and the most important results is given.

### 1. Preliminary Results of the Second IVS Analysis Pilot Project

C. Steinforth showed the first preliminary plots of residuals. Combining the results of the Pilot Project submissions and comparing the combined series with the regular IVS series IVS01001 yielded an agreement at the level of 100 microarcseconds in all components. This preliminary result indicates that the EOP series are more consistent throughout the IVS Analysis Centers with ITRF2000 station coordinates and ICRF Ext. 1 source positions. It was questioned whether the rates in these comparisons were significant.

The Analysis Coordinator regretted that only seven solutions had been submitted by the IVS Analysis Centers for this Analysis Pilot Project limiting the input series to only three different software packages.

It was mentioned that in the future the term "Pilot Project" should only be used if the activity is carried out in preparation of a routine product. In this respect, the term "IVS Analysis Research Project" seems to be more appropriate.

### 2. Comparison of EOP Series Derived for the Second IVS Analysis Pilot Project

C. Bizouard and co-workers presented their results of initial comparisons. In the y pole component there appears to be a systematic disagreement between VLBI and GPS of 156 microarcseconds. Between VLBI and SLR it is even larger (331 microarcsec). At the x pole component there is no significant disagreement.

### 3. Discussion of the Second IVS Analysis Pilot Project - Troposphere

J. Boehm presented the first results of the comparisons of troposphere parameters estimated in the Second Analysis Pilot Project. The results are very satisfactory and a proposal was being announced to make troposphere parameters a regular product of the IVS. The IVS Directing Board had already discussed this proposal by the Vienna Institute for Geodesy and Geophysics and had decided to set up an IVS Pilot Project which will help to prepare making atmosphere parameters a routine IVS product. Analysis Centers will be asked for participation. The format of the submissions will be discussed in due course but will closely resemble the IGS SINEX format for

troposphere parameters. For more details see paper by Boehm et al. in the IVS GM Proceedings and the corresponding proposal text.

It was noted that packages using Kalman Filters may have difficulties to produce the atmosphere parameters for specific time intervals.

#### **4. Extension of the SINEX Format for VLBI**

On the basis of a proposal of the IVS Analysis Coordinator and of inputs from the other space geodetic techniques, the IERS Analysis Coordinator had compiled a proposal for SINEX Version 2.0 which now includes all current VLBI related parameters. The LOD parameter is inconsistent within the group of rate parameters due to its inverse sign. SINEX 2.0 also permits the submission of normal equations (or reduced normal equations) with their right hand side column for easy combination with other solutions, both VLBI and other space techniques.

Reduced normal equations for further combinations are ideally singular and are, thus, not solutions in a general sense. The pros and cons of reduced normal equations versus submission of solutions with covariance and constraint matrices were discussed extensively.

As a result it was decided by the participants that in the future there will be two types of SINEX submissions on the basis of SINEX 2.0:

- a) solutions which are described in full by their covariance and constraint matrices and
- b) reduced normal equations with their complete right hand side column for the sole purpose of further combination with other solutions.

In the context of solutions with covariance and constraint matrices, a proposal by L. Petrov to include a data block for singular constraints as well as an extension of the permitted nutation reference models was also accepted. Concerning atmosphere gradient parameters, it was emphasized that it has to be stated to which part of the atmosphere (hydrostatic or wet) the gradient is referred.

The IERS Analysis Coordinator who attended the workshop will use this information to extend the SINEX V2.0 proposal and bring it forward for further discussions with representatives of the other space techniques.

#### **5. PIVEX: Platform Independent VLBI Exchange Format**

Following the presentation of A.-M. Gontier during the IVS General Meeting, more details were discussed. Chopo Ma will follow as chairperson of the working group after Martine Feissel had carried out the initial phase of the project. A.M. Gontier is prepared to develop the programs for writing PIVEX files from Mark III/IV databases. She will put out the so-called LCODES (i.e. codes of the data fields) which will be transferred from the databases to the PIVEX files for a period of about 6 weeks for comments. After this, programming will be started.

S. Bolotin volunteered to develop special readers for PIVEX but colleagues who may be able to help are very welcome. Although the readers should be platform independent, it would be helpful to know which computers are currently in use for this type of work. All analysts are asked to send their requests for specific computers to the chairperson.

PIVEX files will be generated by the IVS Operation Centers when the conversion programs have been tested (in parallel to NGS card files). As soon as the readers are available there will be

a grace period for NGS card files for a maximum of six months. After this, NGS card files will not be produced any more.

## 6. Scheduling Considerations in High Data Rate VLBI

C. Klatt raised the question of how to optimize scheduling when high data rates, i.e.  $> 56$  Mb/s, are used. Since so far no experience exists, it was decided that a call will be made soliciting participants for an Email discussion group.

## 7. Analysis of EOP Rate Results

Z. Malkin presented a comparison of the first BKG solution which also solved for pole rates as well as for UT1-UTC rates with IGS results. In the discussion it was stated that one series alone is not really conclusive but that the rate parameters weaken the VLBI solutions. Larger networks may improve the stability.

The Analysis Coordinator emphasized that users are very keen to use EOP rates from VLBI analyses for their investigations of geophysical excitations. More solutions with EOP rates are very valuable and should be submitted in parallel to the regular series.

## 8. Implementation of IAU2000 Resolutions

N. Capitaine gave an overview of the IAU2000 resolutions and their impact on VLBI data analysis. Since VLBI observations are not sensitive to the equinox but to the Geocentric Celestial Reference System (GCRS), the long term consistency of the EOP will improve. A special IERS workshop will be held on this topic in Paris on April 18 - 19, 2002.

## 9. Reference Temperatures used in VLBI Analyses

Z. Malkin presented a list of long term mean temperatures of regularly used VLBI telescopes for correction of thermal expansion effects. After extensive discussion it was decided that an official list of reference temperatures will be published on the Web on the basis of this list. One of the reasons for this list is that there cannot be a single reference temperature for all sites and that this list represents the mean temperatures on which the ITRF2000 is based.

Reference temperatures will be the open area air temperatures and will be rounded to the next full degree Celsius. For sites with radomes, stations will be asked to provide their long term average temperatures within the radome. For new sites, reference temperatures will be taken from meteorological history of the respective area.

The discussion of reference atmospheric pressure values for pressure loading effects was abandoned since more investigations are necessary.

## 10. The Use of the ICRF in EOP Determinations

Chopo Ma reminded the participants of the evolution of the ICRF now often serving as the basis for EOP determination. The CRF observed during EOP monitoring sessions is a small subset of the ICRF and has evolved, beginning with a small number of very strong sources, many

with significant structure, to a much larger number, some of which still have detectable positional variation. With the current and future levels of accuracy for the EOP, the instability of part of the CRF should be considered in EOP analysis, which could be derived from source position time series.

## 11. Abandoned Problems of Operative Data Analysis

L. Petrov presented a list of problem areas which need a closer look. A number of hardware induced error sources should be investigated and be reported to the stations for elimination. Some of these error sources can only be addressed if the data which is used to determine the delay observables is looked at in more detail.

The Analysis Coordinator stressed the importance of these investigations and asked all participants to contribute to these efforts. There are still a number of items which have to be solved for further improvements in the geodetic VLBI technique.

## 12. Differences in Results between Mark III and Mark IV Observations

D. Macmillan presented results of recent Mark IV observations which showed significant differences compared to Mark III style sampling rates. Since these differences are most dominant on baselines with Onsala, it was suggested to look at the effects of Onsala cable cal which had been found to compensate this type of error already in the early nineties.

## 13. Miscellaneous

- The IVS data structure will be prepared for baseline length results as a separate IVS product.
- On the basis of the discussion concerning the SINEX 2.0 extension, IVS Analysis Centers are asked to submit SINEX 2.0 files with reduced normal equations for all site coordinates and EOP including EOP rates for each session.
- Next IVS Analysis Research Project: EOP and EOP rates on the basis of fixed ITRF2000 station coordinates and fixed ICRF source positions for a period of 2 years, to be announced in late spring.
- Next meeting: The Fourth IVS Analysis Workshop has been invited to take place at Paris Observatory, France, in cooperation with the Institute Geographique National (IGN) in early 2003. Although February 2003 would keep the sequence of workshops at 12 month intervals, it may be advisable to shift the Fourth IVS Analysis Workshop to early April 2003, the week prior to the EGS/AGU General Assembly. More details will be announced on the IVS Analysis Coordinator's web page in the next few months.

## 14. Acknowledgements

The IVS Analysis Coordinator is very grateful to the members of the Geographical Survey Institute and the Communications Research Laboratory for hosting the Third IVS Analysis Workshop at the Tsukuba Epochal Conference Center.

# IVS Analysis Working Group for Geophysical Models in VLBI Software: Splinter Meeting

*Hans-Georg Scherneck*

*Chalmers University of Technology, Onsala Space Observatory*

*e-mail: [hgs@oso.chalmers.se](mailto:hgs@oso.chalmers.se)*

## Abstract

The IVS Analysis Working Group for Geophysical Models in VLBI Software arranged a splinter meeting during the Second General Meeting at Tsukuba. A detailed memorandum and list of participants is available at <http://www.oso.chalmers.se/~hgs/IVS-WGGM/pm-tsukuba.html>

## 1. Short Summary of the Meeting

The IVS Analysis Working Group for Geophysical Models in VLBI Software (WGGM) was created at the First General Meeting in Kötzing 2000 as a component under the IVS Analysis Coordinator. At Tsukuba the WGGM held its second meeting.

### 1.1. Terms of Reference

The group approved its Terms of Reference, see Appendix. The group will issue Notes of attention, Suggestions, and Recommendations. Its main purpose is the continuing development of VLBI software. The scope covered by geophysical models includes effects due to atmosphere, ocean, solid earth, core, and tidal forces on estimated positions, earth orientation parameters, troposphere, and estimatable fundamental parameters

### 1.2. Regular Session

The following items were discussed:

**Nutation model** The eventual future need of a variable NDFW-frequency was discussed.

**Atmosphere.** The influence of estimating troposphere gradients on earth orientation parameters and source positions was discussed. The adoption of a standard gradient model for each site and the dissemination of atmosphere parameters to serve in the Niell mapping functions was discussed.

**Loading.** A strategy for atmospheric loading implementation was recommended, in particular emphasizing that reference loading displacements are to be applied such that position estimates are not affected in ITRF2000 (subtract the mean of the loading series). Future ITRFs will probably include a pressure loading model. Then, a long-term pressure loading reference field has to be maintained. This is a task for the future Sub-Bureau for Loading of the Geophysical Fluid Center.

We further discussed tides computed from harmonic development, the postglacial rebound model in the IERS Conventions, and whether the group would endorse ionosphere measurements to support single-frequency VLBI. .

### 1.3. The Determinations of the WGGM in Summary

- **Recommendation:** Nota Bene: Estimation of source position and Earth orientation parameters require that atmospheric gradients are taken into account (e.g. estimated simultaneously).
- **Recommendation:** The IERS WG on TRF is to be contacted to initiate and supervise jointly with the GFC-SBL the definitions of a reference field of atmospheric loading effects as a component of the International Terrestrial Reference System.
- **Suggestion:** Experimenters should drop the idea of single-frequency VLBI observations! or else augment the missing ionosphere information by local GPS measurements. No concerted effort is suggested.

A complete memorandum of the meeting is available at <http://www.oso.chalmers.se/~hgs-IVS-WGGM/pm-tsukuba.html>.

## 2. Contact Points

A home page is planned at <http://www.oso.chalmers.se/~hgs/IVS-WGGM/index.html>.

The mail exploder [ivs-awgmodel@ivscc.gsfc.nasa.gov](mailto:ivs-awgmodel@ivscc.gsfc.nasa.gov) includes currently the addresses of 30 colleagues.

The chairmanship is shared by Hans-Georg Scherneck and Rüdiger Haas, both at Chalmers, Onsala Space Observatory. Electronic mail addresses [hgs@oso.chalmers.se](mailto:hgs@oso.chalmers.se) and [haas@oso.chalmers.se](mailto:haas@oso.chalmers.se).

## Appendix

### Terms of Reference

Working group for Geophysical Models in VLBI Software

IVS-WGGMVS TERMS OF REFERENCE

Thematic scope

The working group considers:

- \* The representation and implementation, the coding and the parameterization of geophysical effects in software packages that process geodetic VLBI data.
- \* Effects due to atmosphere, ocean, solid earth, core, and tidal forces on estimated positions, earth orientation parameters, troposphere, and estimatable fundamental parameters.
- \* Systematic comparison of software.

- \* Assessment of ancillary parameters.
- \* The working group's taboo is The permanent tide.

#### Members

- \* Regular members are scientists and engineers who are involved in the development of the VLBI software packages.
- \* Guests are welcome with contributions that point out shortcomings in the representation of geophysical effects in the VLBI analysis stream. 1)

#### Temporal scope

- \* To be determined.

#### Delivers

- \* Software.
- \* Documents with Notes of attention, Suggestions, and Recommendations on the basis of practical experience with the performance of the software (in the form of e.g. written abstracts to be posted on a web area).
- \* Contributions to the development of IERS Conventions.
- \* Reports of their activities, plans of their studies and a summary of results to the IVS Analysis Coordinator, the IVS Directing Board and all IVS associate members, and to the IERS Analysis Coordinator.

#### Needs

- \* The collaboration of modelers, e.g. when documentation of geophysical effects is scarce or contradictory.
- \* Cooperation with analysis and combination groups and centers.

#### Meetings

- \* Annual working group meetings

1) By this membership definition the present chairperson is not a regular member---the group accepted a chairmanship with assistance of a regular member (Scherneck and Haas)

# Registered Participants





## Registered Participants

Name	Institution	Country	E-mail
Akahori, Junichi	Japan Communication Equipment Co., Ltd.	Japan	akahori@nitsuki.com
Amagai, Jun	Communications Research Laboratory	Japan	amagai@crl.go.jp
Andersen, Per Helge	Forsvarets forskningsinstitutt	Norway	per-helge.andersen@ffi.no
Arimura, Shinobu	Communications Research Laboratory	Japan	arimura@crl.go.jp
Berube, Mario	Natural Resources Canada	Canada	mario@geod.nrcan.gc.ca
Bizouard, Christian	Observatoire de Paris (Paris Observatory)	France	bizouard@danof.obspm.fr
Boboltz, David	U.S. Naval Observatory	USA	dboboltz@usno.navy.mil
Boehm, Johannes	IGG, University of Technology, Vienna	Austria	Jboehm@luna.tuwien.ac.at
Cannon, Wayne	York University	Canada	wayne@sgl.crestech.ca
Capitaine, Nicole	Observatoire de Paris	France	capitaine@obspm.fr
Cappallo, Roger	MIT Haystack Observatory	USA	rjc@haystack.mit.edu
Charlot, Patrick	Observatoire de Bordeaux	France	charlot@observ.u-bordeaux.fr
Corey, Brian	MIT Haystack Observatory	USA	bcorey@haystack.mit.edu
Cox, Clyde	Honeywell-TSI	USA	clyde.cox@honeywell-tsi.com
Demura, Hirohide	National Space Development Agency of Japan	Japan	demura.hirohide@nasda.go.jp
Drewes, Hermann	Deutsches Geodaetisches Forschungsinstitut	Germany	drewes@dgfi.badw.de
Edwards, Philip	The Institute of Space and Astronautical Science	Japan	pge@vsop.isas.ac.jp
Engelhardt, Gerald	Bundesamt fuer Kartographie und Geodaesie (BKG)	Germany	engelhardt@leipzig.ifag.de
Fey, Alan	U.S. Naval Observatory	USA	afey@usno.navy.mil
Fomalont, Ed	NRAO	USA	efomalon@nrao.edu
Fujisawa, Kenta	National Astronomical Observatory of Japan	Japan	kenta@hotaka.mtk.nao.ac.jp
Fukuzaki, Yoshihiro	Geographical Survey Institute	Japan	fukuzaki@gsi.go.jp
Gontier, Anne-Marie	Paris Observatory	France	Anne-Marie.Gontier@obspm.fr
Gonzalez, Raymond	NVI, Inc./NASA GSFC	USA	rgonzale@gemini.gsfc.nasa.gov
Gordon, David	Raytheon ITSS, NASA/GSFC	USA	dgg@leo.gsfc.nasa.gov

## Registered Participants

Name	Institution	Country	E-mail
Hakoishi, Takahisa	Sony Corporation	Japan	hakoishi@sys1.cpg.sony.co.jp
Hanada, Hideo	National Astronomical Observatory	Japan	hanada@miz.nao.ac.jp
Harms, Matthew	Honeywell-TSI	USA	matthew.harms@honeywell-tsi.com
Hatanaka, Yuki	Geographical Survey Institute	Japan	hata@gsi.go.jp
Himwich, Ed	NVI Inc./NASA GSFC	USA	weh@vega.gsfc.nasa.gov
Hirabayashi, Hisashi	ISAS	Japan	hirax@vsop.isas.ac.jp
Hirasawa, Eri	Communications Research Laboratory	Japan	hirasawa@ss.crl.go.jp
Hobiger, Thomas	IGG, University of Technology, Vienna	Austria	thobiger@luna.tuwien.ac.at
Hoshino, Yoshihisa	Geographical Survey Institute	Japan	hoshino@gsi.go.jp
Ichikawa, Ryuichi	Communications Research Laboratory	Japan	richi@crl.go.jp
Ichikawa, Yuichi	Japan Communication Equipment Co., Ltd.	Japan	ichikawa@nitsuki.com
Iida, Takashi	Communications Research Laboratory	Japan	iida@crl.go.jp
Imakiire, Tetsuro	Geographical Survey Institute	Japan	imq@gsi.go.jp
Inoue, Makoto	National Astronomical Observatory	Japan	inoue@nro.nao.ac.jp
Ito, Takeshi	Cosmo Research Corp.	Japan	ito@cosmoresearch.co.jp
Iwamura, Sotetsu	NTT Information Sharing Platform Laboratories	Japan	iwamura.sotetsu@lab.ntt.co.jp
Iwata, Takahiro	National Space Development Agency of Japan	Japan	tiwata@rd.tksc.nasda.go.jp
Jike, Takaaki	National Astronomical Observatory, Japan	Japan	jike@miz.nao.ac.jp
Kaidzu, Masaru	Geographical Survey Institute	Japan	kaizu@gsi.go.jp
Kameno, Seiji	National Astronomical Observatory of Japan	Japan	kameno@hotaka.mtk.nao.ac.jp
Kawaguchi, Noriyuki	National Astronomical Observatory of Japan	Japan	kawagu@hotaka.mtk.nao.ac.jp
Kawai, Eiji	Communications Research Laboratory	Japan	kawa@crl.go.jp
Kawano, Nobuyuki	National Astronomical Observatory of Japan	Japan	kawano@miz.nao.ac.jp
Kim, Tu-Hwan	Ajou University	Korea	thkim@madang.ajou.ac.kr
Kimura, Moritaka	Communications Research Laboratory	Japan	mkimura@crl.go.jp

## Registered Participants

Name	Institution	Country	E-mail
Kingham, Kerry	U.S. Naval Observatory	USA	kak@cygx3.usno.navy.mil
Kiuchi, Hitoshi	Communications Research Laboratory	Japan	kiuchi@crl.go.jp
Kizu, Shigeo	Toshiba Corporation	Japan	shigeo.kizu@toshiba.co.jp
Klatt, Calvin	Natural Resources Canada	Canada	cklatt@nrcan.gc.ca
Kobayashi, Hideyuki	National Astronomical Observatory of Japan	Japan	hkobaya@hotaka.mtk.nao.ac.jp
Kobayashi, Kyoko	Geographical Survey Institute	Japan	k_kyoko@gsi.go.jp
Kodak, Charles	GSFC Code 920/Honeywell Technology Solutions Inc.	USA	Charles.kodak@honeywell-tsi.com
Komaki, Kazuo	Geographical Survey Institute	Japan	komaki@gsi.go.jp
Kondo, Tetsuro	Communications Research Laboratory	Japan	kondo@crl.go.jp
Kono, Yusuke	National Astronomical Observatory	Japan	kono@miz.nao.ac.jp
Koyama, Yasuhiro	Communications Research Laboratory	Japan	koyama@crl.go.jp
Kudryashova, Maria	Astronomical Institute of Saint Petersburg University	Russia	manyasha_vk@mail.ru
Kurihara, Shinobu	Geographical Survey Institute	Japan	skuri@gsi.go.jp
Kutterer, Hansjoerg	Deutsches Geodaetisches Forschungsinstitut	Germany	kutterer@dgfi.badw.de
Lanotte, Roberto	CGS Matera - Telespazio	Italy	lanotte@asi.it
Li, Jinling	Shanghai Astronomical Observatory	P.R. China	jll@center.shao.ac.cn
Liu, Qinghui	Kagoshima University	Japan	eem0338@elib.eee.kagoshima-u.ac.jp
Ma, Chopo	NASA Goddard Space Flight Center	USA	cma@virgo.gsfc.nasa.gov
MacMillan, Daniel	NVI, Inc. and Goddard Space Flight Center	USA	dsm@leo.gsfc.nasa.gov
Machida, Morito	Geographical Survey Institute	Japan	machida@gsi.go.jp
Malkin, Zinovy	Institute of Applied Astronomy	Russia	malkin@quasar.ipa.nw.ru
Manabe, Seiji	National Astronomical Observatory of Japan	Japan	manabe@miz.nao.ac.jp
Masuko, Harunobu	Communications Research Laboratory	Japan	masuko@crl.go.jp
Matsumoto, Koji	National Astronomical Observatory, Japan	Japan	matumoto@miz.nao.ac.jp
Matsuzaka, Shigeru	Geographical Survey Institute	Japan	shigeru@gsi.go.jp

## Registered Participants

Name	Institution	Country	E-mail
Minh, Young Chol	Korea Astronomy Observatory	Korea	minh@trao.re.kr
Miyagawa, Kohei	Geographical Survey Institute	Japan	miyagawa@gsi.go.jp
Miyoshi, Makoto	NAOJ	Japan	miyoshi@miz.nao.ac.jp
Mizutani, Atsushi	A.E.S.(Advanced Engineering Services Co., Ltd.)	Japan	a_mizutani@aes.co.jp
Morikawa, Takao	Communications Research Laboratory	Japan	tak@crl.go.jp
Mueskens, Arno	Geodetic Institute of the University of Bonn	Germany	mueskens@mpifr-bonn.mpg.de
Munekane, Hiroshi	Geographical Survey Institute	Japan	munekane@gsi.go.jp
Murakami, Makoto	Geographical Survey Institute	Japan	mccopy@gsi.go.jp
Murata, Yasuhiro	The Institute of Space and Astronautical Science	Japan	murata@vsop.isas.ac.jp
Nagata, Katsuhiro	Geographical Survey Institute	Japan	nagata@gsi.go.jp
Nakagawa, Hiroyuki	Geographical Survey Institute	Japan	hnakagaw@gsi.go.jp
Nakahori, Yoshiro	Geographical Survey Institute	Japan	nakahori@gsi.go.jp
Nakajima, Junichi	Communications Research Laboratory	Japan	nakaji@crl.go.jp
Naudet, Charles	Jet Propulsion Laboratory	USA	Charles.J.Naudet@jpl.nasa.gov
Niell, Arthur	MIT Haystack Observatory	USA	aniell@haystack.mit.edu
Nishi, Shujiro	Geographical Survey Institute	Japan	nishi@gsi.go.jp
Noguchi, Wataru	Digitallink Co., LTD	Japan	noguchi@venetex.co.jp
Nothnagel, Axel	Geodetic Institute of the University of Bonn	Germany	nothnagel@uni-bonn.de
Ohishi, Tadanao	Chiba Institute of Technology	Japan	oohishi@pf.it-chiba.ac.jp
Okubo, Hiroshi	Communications Research Laboratory	Japan	okubo@crl.go.jp
Osaki, Hiro	Communications Research Laboratory	Japan	osaki@crl.go.jp
Otsubo, Toshimichi	Communications Research Laboratory	Japan	otsubo@crl.go.jp
Oyama, Tomoaki	Tokyo University	Japan	oyamatm@cc.nao.ac.jp
Paunonen, Matti	Finnish Geodetic Institute	Finland	Matti.Paunonen@fgi.fi

## Registered Participants

Name	Institution	Country	E-mail
Petrachenko, Bill	Natural Resources Canada (NRCan)	Canada	billp@drao.nrc.ca
Petrov, Leonid	NVI, Inc./NASA Goddard Space Flight Center	USA	pet@leo.gsfc.nasa.gov
Plag, Hans-Peter	Norwegian Mapping Authority	Norway	plag@statkart.no
Redmond, Jay	Honeywell	USA	jay.redmond@honeywell-tsi.com
Ritakari, Jouko	Metsahovi Radio Observatory	Finland	Jouko.Ritakari@hut.fi
Rizwan, Mamat	Kitami Institute of Technology	Japan	reziwan@infmd2.cs.kitami-it.ac.jp
Roh, Duk-Gyoo	Korean Astronomy Observatory	Korea	dgroh@trao.re.kr
Romney, Jonathan	National Radio Astronomy Observatory	USA	jromney@aoc.nrao.edu
Rothacher, Markus	Forschungseinrichtung Satellitengeodaesie	Germany	rothacher@bv.tum.de
Sakai, Yasuyoshi	Communications Research Laboratory	Japan	sakai@crl.go.jp
Sasanuma, Tony	Sony Corporation	Japan	Tony.Sasanuma@jp.sony.com
Sasao, Tetsuo	National Astronomical Observatory, Japan	Japan	sasao@miz.nao.ac.jp
Scherneck, Hans-Georg	Chalmers University of Technology	Sweden	hgs@oso.chalmers.se
Schlueter, Wolfgang	Bundesamt fuer Kartographie und Geodaesie	Germany	schlueter@wettzell.ifag.de
Schuh, Harald	Vienna University of Technology	Austria	hschuh@luna.tuwien.ac.at
Schupler, Bruce	Honeywell Technology Solutions Inc	USA	Bruce.Schupler@Honeywell-tsi.com
Shibuya, Kazuo	National Institute of Polar Research	Japan	shibuya@nipr.ac.jp
Smythe, Dan	MIT Haystack Observatory	USA	dsmythe@haystack.mit.edu
Sovers, Ojars	RSA Systems/JPL	USA	ojars@rsasys.com
Sovers, Zinta	RSA Systems	USA	ojars@rsasys.com
Steinforth, Christoph	Geodetic Institute of the University of Bonn	Germany	steinforth@uni-bonn.de
Strand, Richard	Gilmore Creek Geophysical Observatory	USA	kl7ra@blizzard.gcgo.nasa.gov
Sunakawa, Takashi	Geographical Survey Institute	Japan	sunakawa@gsi.go.jp
Suzuki, Katsumi	Cosmo Research Corp.	Japan	ito@cosmoresearch.co.jp
Takaba, Hiroshi	Gifu University, Faculty of Engineering	Japan	takaba@cc.gifu-u.ac.jp
Takahashi, Fujinobu	Communications Research Laboratory	Japan	fuji@crl.go.jp
Takahei, Kenichiro	Anritsu Corporation	Japan	takahei.kenichiro@jj.anritsu.co.jp

## Registered Participants

Name	Institution	Country	E-mail
Takashima, Kazuhiro	Geographical Survey Institute	Japan	takasima@gsi.go.jp
Takayama, Jun	Sony Corporation	Japan	
Tamura, Yoshiaki	National Astronomical Observatory, Mizusawa	Japan	tamura@miz.nao.ac.jp
Tanaka, Eiichi	Sony Marketing(Japan) Inc	Japan	eiichi.tanaka@smoj.sony.co.jp
Tesmer, Volker	DGFI, Munich	Germany	tesmer@dgfi.badw.de
Thomas, Cynthia	NVI, Inc./GSFC	USA	cct@gemini.gsfc.nasa.gov
Thorandt, Volkmar	Bundesamt fuer Kartographie und Geodaesie (BKG)	Germany	thorandt@leipzig.ifag.de
Thornton, Bruce	NVI, Inc./USNO	USA	blt@casa.usno.navy.mil
Titov, Oleg	Geoscience Australia	Australia	olegtitov@auslig.gov.au
Tobita, Mikio	Geographical Survey Institute	Japan	tobita@gsi.go.jp
Tomita, Koichiro	A.E.S.(Advanced Engineering Services Co., Ltd.)	Japan	tm-perse@me.catv.ne.jp
Tsuji, Hiromichi	Geographical Survey Institute	Japan	tsuji@gsi.go.jp
Tuccari, Gino	IRA CNR	Italy	tuccari@ira.oto.cnr.it
Ujihara, Hideki	National Astronomical Observatory in Japan	Japan	ujihara@hal.mtk.nao.ac.jp
Uose, Hisao	NTT Laboratories	Japan	uose.hisao@lab.ntt.co.jp
Vandenberg, Nancy	NVI, Inc./GSFC	USA	nrv@gemini.gsfc.nasa.gov
Volvach, Alexandr	Crimean Astrophysical Observatory	Ukraine	volvach@crao.crimea.ua
Whitney, Alan	MIT Haystack Observatory	USA	awhitney@haystack.mit.edu
Wildes, William	GSFC NASA	USA	WTW@wildbill.gsfc.nasa.gov
Yaguchi, Akira	Geographical Survey Institute	Japan	a-yagu@gsi.go.jp
Yamashita, Ayumi	YEM Inc.	Japan	ayumi@yem.co.jp
Yonezawa, Ikuto	Ibaraki University	Japan	yonezawa@orion.sci.ibaraki.ac.jp
Yoshino, Taizoh	Communications Research Laboratory	Japan	yosh@crl.go.jp
Zheng, Weimin	Shanghai Astronomical Observatory, Chinese Academy of Sciences	P.R.China	zhwm@center.shao.ac.cn

# Program





# Second IVS General Meeting Program Tsukuba, Japan

Monday, February 4, 2002

## Opening Ceremony (09:40-10:00)

Toshiki Aoyama (Vice-Minister for Engineering Affairs, Ministry of Land, Infrastructure and Transport)  
Takashi Iida (President, Communications Research Laboratory)

10:00 **BREAK**

## Session 1. VLBI: Precise and Consistent for Decades Chair: Fuji Takahashi

- 10:10 1-01. **Welcome by IVS Chair and Chair's Report**  
Wolfgang Schlüter, Bundesamt für Kartographie und Geodäsie (BKG)
- 10:20 1-02. **Coordinating Center Report**  
Nancy Vandenberg, NVI, Inc./GSFC
- 10:30 1-03. **The Essential Contribution of VLBI to Fundamental Astronomy** (*invited*)  
Nicole Capitaine, Observatoire de Paris
- 11:00 1-04. **Challenges for VLBI Within a Global Geodetic Observing System** (*invited*)  
Hermann Drewes, Deutsches Geodätisches Forschungsinstitut (DGFI)
- 11:30 1-05. **Combination of the Space-Geodetic Techniques** (*invited*)  
Markus Rothacher, Technical University of Munich
- 12:00 **LUNCH**

## Session 2. Improving the Performance and Products of IVS Chair: Bill Petrachenko

- 13:30 2-01. **IVS Working Group 2 for Product Specification and Observing Programs** (*invited*)  
Harald Schuh, Institute of Geodesy and Geophysics, Vienna University of Technology
- 14:00 2-02. **IVS Observing Programs 2002–2005** (*invited*)  
Nancy Vandenberg, NVI, Inc./GSFC

## Monday, February 4, 2002 (continued)

- 14:20 2-03. **Recent Developments in IVS Analysis Coordination**  
Axel Nothnagel, Geodetic Institute of the University of Bonn
- 14:35 2-04. **Geodetic Results from Mark 4 VLBI**  
Daniel MacMillan (1), Leonid Petrov (1), Chopo Ma (2), (1) NVI, Inc./GSFC,  
(2) Goddard Space Flight Center
- 14:50 2-05. **Expected Contributions of the K4 and its Next-generation Systems**  
Yasuhiro Koyama, Communications Research Laboratory
- 15:05 2-06. **Geodetic S2 VLBI: International Plans**  
Calvin Klatt (1), Mario Berube (1), Wayne Cannon (2), Bill Petrachenko (1), Anthony  
Searle (1), (1) Geodetic Survey Division, Natural Resources Canada, (2) York University
- 15:20 **BREAK**

### **Session 3, Part 1. Network Stations, Operation Centers, Correlators** **Chair: Ed Himwich**

- 15:50 3-01. **Network Coordinator Report**  
Ed Himwich, NVI Inc./NASA GSFC
- 16:05 3-02. **Fundamentals of Phase Calibration in Geodetic VLBI** (*invited*)  
Brian Corey, MIT Haystack Observatory
- 16:20 3-03. **Mark 4 Correlator Software: Status and Plans**  
Roger Cappallo, MIT Haystack Observatory
- 16:35 3-04. **Status Report on the Washington VLBI Correlator**  
Kerry Kingham, U.S. Naval Observatory
- 16:50 3-05. **The Mark IV Correlator - Faster, Better, Optimal??**  
Arno Müskens, Iza bela Rottmann, Ingrid Benndorf, University of Bonn
- 17:05 3-06. **Comparisons of the Output of Repeated Mark III/IV Correlations**  
Axel Nothnagel, Olaf Bromorzki, James Campbell, Arno Müskens, Helge Rottmann,  
Izabela Rottmann, Geodetic Institute of the University of Bonn
- 17:20 3-07. **The Medicina Station and the Sardinia 64-m Radio Telescope: Geodetic  
Activities and Status Report**<sup>†</sup>  
Franco Mantovani, Istituto di Radioastronomia, CNR
- 17:35 3-08. **Status of SYW geodetic VLBI experiments and collocated observations  
at Syowa Station, Antarctica**  
Kazuo Shibuya, Koichiro Doi, Shigeru Aoki, National Institute of Polar Research

---

<sup>†</sup> presented as a poster paper (3-23P)

**Monday, February 4, 2002 (continued)**

17:50 **3-09 Foot-Print of the Space-Geodetic Observatory, Ny-Ålesund, Svalbard**  
Halfdan P. Kierulf, Lars Bockmann, Oddgeir Kristiansen, Hans-Peter Plag, Norwegian  
Mapping Authority

18:05 **BREAK**

**Poster Session (18:30-21:00)**

**Core Time for the Poster Session (Room 201)**

**Tuesday, February 5, 2002**

**Session 3, Part 2. Network Stations, Operation Centers, Correlators**  
**Chair: Arno Müskens**

08:30 **3-10. TIGO in the Southern Hemisphere** (*invited*)  
Hayo Hase, BKG Wettzell

08:45 **3-11. Korea's New VLBI Project: KVN** (*invited*)  
Young Chol Minh, Korea Astronomy Observatory

**Session 4. New Technology Developments in VLBI**  
**Chair: Wayne Cannon**

09:00 **4-01. A VSI-H Compatible Recording System for VLBI and e-VLBI**  
Jouko Ritakari, Ari Mujunen, Metsähovi Radio Observatory

09:15 **4-02. IP Data Transfer System for Real-time VLBI**  
Sotetsu Iwamura (1), Hisao Uose (1), Tetsuro Kondo (2), Shin-ichi Nakagawa (2),  
Kenta Fujisawa (3), (1) NTT Information Sharing Platform Labs, (2) Communications  
Research Laboratory, (3) National Astronomical Observatory of Japan

09:30 **4-03. VSI Interface Implementation, Performance Enhancement of Gbps-VLBI  
Instruments**  
Junichi Nakajima, CRL, Kashima Space Research Center

09:45 **4-04. Mark 5 Disc-Based VLBI Data System**  
Alan Whitney, Haystack Observatory

10:00 **BREAK**

## Tuesday, February 5, 2002 (continued)

- 10:30 **4-05. Real-time Gigabit VLBI System and Internet VLBI System**  
T. Kondo (1), Y. Koyama (1), J. Nakajima (1), M. Sekido (1), R. Ichikawa (1),  
E. Kawai (1), H. Okubo (1), H. Osaki (1), M. Kimura (1), and GALAXY Team (1,2,3,4),  
(1) Kashima Space Research Center/CRL, (2) NAOJ, (3) ISAS, (4) NTT
- 10:45 **4-06. High-Speed e-VLBI Demonstration: Haystack Observatory to NASA/GSFC**  
Alan Whitney, Haystack Observatory
- 11:00 **4-07. Multi-Beam VLBI**  
Bill Petrachenko, Calvin Klatt, Vincent Ward, Geodetic Survey Division, Natural  
Resources Canada
- 11:15 **4-08. 10 micro-arcsecond Astrometry with Two Beam System of VERA**  
Noriyuki Kawaguchi, Testuo Sasao, Seiji Manabe, Hideyuki Kobayashi, Osamu Kameya,  
National Astronomical Observatory of Japan
- 11:30 **4-09. The VSOP-2 Mission**  
Hisashi Hirabayashi, VSOP-2 working group, The Institute of Space and Astronautical  
Science
- 11:45 **4-10. A Proposal for Constructing a New VLBI Array, "Horizon Telescope"**  
Makoto Miyoshi, Seiji Kamenno, NAOJ
- 12:00 **LUNCH**

## Session 5, Part 1. Data, Models, and Software Chair: Axel Nothnagel

- 13:30 **5-01. Displacements Due to Ocean Tide and Atmospheric Loading** (*invited*)  
Hans-Georg Scherneck (1), Machiel S. Bos (2), (1) Chalmers/Onsala Space Observatory,  
(2) TU Delft/Dept. Geodetic Engineering
- 14:00 **5-02. Gradient mapping functions for VLBI and GPS** (*invited*)  
Arthur Niell, Haystack Observatory
- 14:20 **5-03. Modeling Radio Source Structure for Improved VLBI Data Analysis** (*invited*)  
Patrick Charlot, Observatoire de Bordeaux
- 14:40 **5-04. Structure Corrections in Modeling VLBI Delays**  
O. Sovers (1), P. Charlot (2), A.L. Fey (3), D. Gordon (4), (1) RSA Systems/JPL,  
(2) Observatoire de Bordeaux, (3) USNO, (4) Raytheon/GSFC
- 14:55 **5-05. Integrating Analysis Goals for EOP, CRF and TRF**  
Chopo Ma (1), Daniel MacMillan (2), Leonid Petrov (2), (1) Goddard Space Flight  
Center, (2) NVI, Inc./GSFC

**Tuesday, February 5, 2002 (continued)**

15:10 5-06. **PIVEX: A Proposal for a Platform-Independent VLBI Exchange Format**  
*(invited)*  
Anne-Marie Gontier (1), Martine Feissel, (1, 2), (1) Observatoire de Paris/UMR 8630, (2)  
Institut Géographique National

15:30 **BREAK**

**Session 5, Part 2. Data, Models, and Software**  
**Chair: Taizoh Yoshino**

16:00 5-07. **VLBI Error Analysis**  
Leonid Petrov, NVI, Inc./GSFC

16:15 5-08. **On Correlations Between Parameters in VLBI Data Analysis**  
Axel Nothnagel, James Campbell, Markus Vennebusch, Geodetic Institute of the  
University of Bonn

16:30 5-09. **Statistical Assessment of Subdiurnal Earth Orientation Parameters  
from VLBI**  
Hansjoerg Kutterer, Volker Tesmer, Deutsches Geodätisches Forschungsinstitut

16:45 5-10. **RDV Analysis and MK4/VLBA Comparison Results**  
David Gordon (1), Leonid Petrov (2), (1) Raytheon/GSFC, (2) NVI, Inc./GSFC

17:00 5-11. **Outlier Detection in the Combination of VLBI EOP**  
Christoph Steinforth, Axel Nothnagel, Geodetic Institute of the University of Bonn

17:15 5-12. **Technological Processes at BKG Data and Analysis Center**  
Volkmar Thorandt, Dieter Ullrich, Reiner Wojdziak, BKG, Federal Agency for  
Cartography and Geodesy

17:30 5-13. **Special Bureau for Loading (SBL)**  
Tonie van Dam (1), Hans-Peter Plag (2), (1) European Center for Geodynamics and  
Seismology, (2) Norwegian Mapping Authority

17:45 **END OF SESSION**

**BANQUET (19:00-21:00)**

**SANSUITEI restaurant**

Wednesday, February 6, 2002

**Session 6, Part 1. Analysis and Geodetic/Geophysical/Astrometric Interpretation**

**Chair: Dan MacMillan**

- 08:30 6-01. **VLBI Solution DGFI01R01 Based on Least Squares Estimation Using OCCAM 5.0 and DOGSCS**  
Volker Tesmer, Deutsches Geodätisches Forschungsinstitut
- 08:45 6-02. **Establishment of the New Geodetic Reference Frame of Japan (JGD2000)**  
Tetsuro Imakiire, Masaki Murakami, GSI
- 09:00 6-03. **Variations of European Baseline Lengths from VLBI and GPS Data**  
Zinovy Malkin, Natalia Panafidina, Elena Skurikhina, Institute of Applied Astronomy
- 09:15 6-04. **Combination of Space Geodetic Data for the Realization of Terrestrial and Celestial Reference Frames**  
Per Helge Andersen, Forsvarets forskningsinstitutt, FFI
- 09:30 6-05. **Can VLBI Help to Verify Seasonality Found in Nationwide Continuous GPS data: A Signal From Crust or Artifacts?**  
Makoto Murakami, Crustal Deformation Laboratory, Geographical Survey Institute
- 09:45 6-06. **Results of the Critical Design for the Selenodetic Mission Using Differential VLBI Methods by SELENE**  
Takahiro Iwata (1), Takeshi Sasaki, (1), Yusuki Kono (2), Hideo Hanada (2), Nobuyuki Kawano (2), Noriyuki Namiki (3), (1) National Space Development Agency of Japan, (2) Mizusawa, NAO, (3) Kyushu University
- 10:00 **BREAK**

**Session 6, Part 2. Analysis and Geodetic/Geophysical/Astrometric Interpretation**

**Chair: Seiji Manabe**

- 10:30 6-07. **Analysis of the EOPs from Independent Parallel VLBI Sessions**  
Oleg Titov, Geoscience, Australia
- 10:45 6-08. **Comparison of the VLBI Nutation Series with IAU2000**  
Zinovy Malkin, Institute of Applied Astronomy
- 11:00 6-09. **Comparison of Tropospheric Parameters Submitted to the 2nd IVS Analysis Pilot Project**  
Johannes Boehm, Eva Messerer, Harald Schuh, Institute of Geodesy and Geophysics, Vienna University of Technology

**Wednesday, February 6, 2002 (continued)**

- 11:15 **6-10. Determination of Ionospheric Parameters by Geodetic VLBI**  
Thomas Hobiger, Johannes Boehm, Harald Schuh, Institute of Geodesy and Geophysics,  
Vienna University of Technology
- 11:30 **6-11. A Proposal to Extend the ICRF to Higher Frequencies<sup>†</sup>**  
Chris Jacobs (1) and 24 co-authors(1,2,3,4,5,6,7), (1) JPL, (2) NRAO, (3) RSA Systems,  
(4) GSFC, (5) USNO, (6) Bordeaux Observatory, (7) Communications Research  
Laboratory
- 11:45 **6-12. Towards a Future ICRF Realization**  
Chopo Ma (1), David Gordon (2), Daniel MacMillan (3), Leonid Petrov (3), (1) Goddard  
Space Flight Center, (2) Raytheon/GSFC, (3) NVI, Inc./GSFC
- 12:00 **END OF SESSION**

**Closing Session**

- 12:00 **Closing Remarks**  
Wolfgang Schlüter, Bundesamt für Kartographie und Geodäsie (BKG)
- 12:30 **ADJOURN**

---

<sup>†</sup> presented as a poster paper (6-15P)

# Posters

## Session 3. Network Stations, Operation Centers, Correlators

- 3-01P. **VLBI Field System**  
Raymond Gonzalez, Ed Himwich, NVI, Inc./GSFC
- 3-02P. **VRAD Mission: Precise Observation of Orbits of Sub-satellites in SELENE with International VLBI Network**  
Hideo Hanada (1), Takahiro Iwata (2), Yusuke Kono(3), Koji Matsumoto (1), Seiitsu Tsuruta (1), Toshiaki Ishikawa (1), Kazuyoshi Asari (1), Jinsong Ping (1), Kosuke Heki (1), Nobuyuki Kawano (1), (1) National Astronomical Observatory, (2) National Space Development Agency of Japan, (3) Graduate University for Advanced Studies
- 3-03P. **A Next Generation Geodetic Experiment Scheduling Tool? (SKED++)**  
Calvin Klatt, Mario Berube, Anthony Searle, Jason Silliker, Geodetic Survey Division, Natural Resources Canada
- 3-04P. **Geodesy VLBI by Using the World Smallest 3-m VLBI Antenna**  
Hiroshi Takaba (1), Yoshida Minoru (1), Wakamatsu Ken-ichi (1), CRL VLBI team (2) and GSI VLBI team (3), (1) Gifu University, (2) Communications Research Laboratory, (3) Geographical Survey Institute
- 3-05P. **Local Ties of the Space Geodetic Techniques at the Onsala Space Observatory**  
Martin Lidberg, Sten Bergstrand, Rüdiger Haas, Jan M. Johansson, Gunnar Elgered, Onsala Space Observatory
- 3-06P. **VLBI-GPS Collocation Method at Geographical Survey Institute**  
S. Matsuzaka, Y. Hatanaka, K. Nemoto, Y. Fukuzaki, K. Kobayashi, K. Abe, T. Akiyama, Geographical Survey Institute
- 3-07P. **The Mark IV Correlator - Faster, Better, Optimal??**  
Arno Müskens, Izabela Rottmann, Ingrid Benndorf, University of Bonn
- 3-08P. **Comparison of the VLBI Observables from MkIII and MkIV Correlation of a 24-hour Geodetic Experiment**  
Brian Corey, Michael Titus, Haystack Observatory
- 3-09P. **VLBI Activities at GSI**  
Kazuhiro Takashima, Yoshihiro Fukuzaki, and the members of the GSI VLBI group, Geographical Survey Institute
- 3-10P. **Status of the KSP VLBI Stations and IMT-2000 Interference**  
Jun Amagai, Hitoshi Kiuchi, Yasuhiro Koyama, Mamoru Sekido, Ryuichi Ichikawa, Tetsuro Kondo, Taizoh Yoshino, Koichi Sebata, Communications Research Laboratory
- 3-11P. **The Canadian Transportable VLBI Antenna**  
Mario Berube, Geodetic Survey Division, Natural Resources Canada

## Posters (continued)

- 3-12P. **Yellowknife Geophysical Observatory**  
Mario Berube, Geodetic Survey Division, Natural Resources Canada
- 3-13P. **Algonquin Radio Observatory**  
Mario Berube, Geodetic Survey Division, Natural Resources Canada
- 3-14P. **The Geodetic Observatory O'Higgins - an IVS Network Station in Antarctica**  
Gerhard Kronschnabl, Andreas Reinhold, Walter Schwarz, Reiner Wojdziak, Bundesamt für Kartographie und Geodäsie (BKG)
- 3-15P. **Seshan VLBI Station Status**<sup>†</sup>  
Shiguang Liang, Shanghai Observatory
- 3-16P. **Geodetic Study at the Simeiz IVS Station**  
N. Nesterov, A. Volvach, Lab of Radio Astronomy of Crimean Astrophysical Observatory
- 3-17P. **Kashima 34-m Radio Telescope Improvement and Future: Status Report**  
Hiroshi Okubo (1), Eiji Kawai(1), Junichi Nakajima (1), Hiro Osaki (1), Tetsuro Kondo (1), Toshihiro Omodaka (2), Satoru Morisaki(2), (1) Communications Research Laboratory(CRL), (2) Kagoshima University
- 3-18P. **Metsähovi Geodetic VLBI: Status Report**  
Matti Paunonen, Finnish Geodetic Institute
- 3-19P. **MV-3 Operations**  
Jay Redmond, Honeywell VLBI Group
- 3-20P. **Gilmore Creek Geophysical Observatory**  
Richard Strand, GCGO
- 3-21P. **A Multiband Primary Focus Receiver for Noto Antenna**  
Gino Tuccari, Radioastronomy Institute of the Italian Research National Council
- 3-22P. **Noto Station: Status Report on the Geodetic Activity**  
Gino Tuccari, Carlo Stanghellini, Franco Mantovani, Istituto di Radioastronomia CNR

## Session 4. New Technology Developments in VLBI

- 4-01P. **Observation of Atmospheric Disturbances Using a Real-Time VLBI System**  
Qinghui Liu, Masanori Nishio, Tomoyuki Miyazaki, Kunihiro Yamamura, Faculty of Eng. Kagoshima University

---

<sup>†</sup> withdrawn

## Posters (continued)

- 4-02P. **The Roles of Real-time VLBI for the R&D of Network Technology**  
Fujinobu Takahashi, Tetsuro Kondo, Yasuhiro Koyama, Hiro Osaki, Communications Research Laboratory
- 4-03P. **High-sensitivity VLBI observation with GALAXY**  
Kenta Fujisawa (1), Noriyuki Kawaguchi (1), Tetsuro Kondo(2), Junichi Nakajima (2), Yasuhiro Murata (3), Hisashi Hirabayashi (3), Hisao Uose (4), Sotetsu Iwamura(4), (1) National Astronomical Observatory of Japan, (2) Communications Research Laboratory, (3) The Institute of Space and Astronautical Science, (4) NTT Information Sharing Platform Labs
- 4-04P. **Parallel Data Processing System**  
Hitoshi Kiuchi, Communications Research Laboratory
- 4-05P. **Geodetic Observation System in VERA**  
Yoshiaki Tamura, VERA Group, National Astronomical Observatory, Japan
- 4-06P. **Wide-band Data Transmission System Expected in the Next Generation Space VLBI Mission: VSOP-2**  
Yasuhiro Murata (1), Hisashi Hirabayashi (1), Jim Springett (2), Joel Smith(2), Hideyuki Kobayashi(3), Noriyuki Kawaguchi (3), David Murphy (2), (1) The Institute of Space and Astronautical Science, (2) Jet Propulsion Laboratory, (3) National Astronomical Observatory, Japan
- 4-07P. **Precise Positioning of Spacecrafts by Multi-frequency VLBI**  
Yusuke Kono (1), Hideo Hanada (1), Nobuyuki Kawano (1), Kenzaburo Iwadate (1), Yasuhiro Koyama (2), Yoshihiro Fukuzaki(3), (1) NAOJ, (2) CRL, (3) GSI
- 4-08P. **Processing of the Data of Syowa VLBI Experiment by Copying Between the Different Recording Systems and the Result**  
Yoshihiro Fukuzaki(1), Kazuo Shibuya (2), Koichiro Doi(2), Takaaki Jike (3), (1) Geographical Survey Institute, (2) National Institute of Polar Research, (3) National Astronomical Observatory, Japan
- 4-09P. **Laser-pumped Cs Gas-cell Type Atomic Clock for VLBI**  
K. Takahei (1), H. Suga (1), Y. Ohuchi (1), H. Sutoh (1), M. Uchino (1), S. Mattori (1), M. Tsuda (1), Y. Saburi (1), Y. Koga (2), K. Hagimoto (2), T. Ikegami (2), (1) Anritsu Corporation, (2) National Institute of Advanced Industrial Science and Technology
- 4-10P. **Media Calibration in The Deep Space Network- A Status Report**  
G.M. Resch, S.J. Keihm, G.E. Lanyi, R.P. Linfield, C.J. Naudet, A.L. Riley, H.W. Rosenberger, A.B. Tanner, Jet Propulsion Laboratory
- 4-11P. **The S3 Wide Bandwidth VLBI Data Record-Playback System**  
W. H. Cannon (1), P. Newby (2), G. Feil (2), A. Novikov (2), B. Feir (2), J. Eriksen(3), (1) Department of Physics and Astronomy, York University, (2) Space Geodynamics Laboratory, CRESTech, (3) Crossbow Electronics Inc.

Posters (continued)

**Session 5. Data, Models, and Software**

- 5-01P. **Tropospheric Zenith Path Delays Derived from GPS Used for the Determination of VLBI Station Heights**  
Johannes Boehm, Harald Schuh, Robert Weber, Institute of Geodesy and Geophysics, Vienna University of Technology
- 5-02P. **Evaluation of Atmospheric Slant Path Delay from GPS and VLBI Measurements**  
Ryuichi Ichikawa (1) and 11 co-authors (1,2,3,4), (1) Kashima Space Research Center, Communications Research Laboratory, (2) MRI, (3) AIST, (4) GSI
- 5-03P. **Piecewise Linear Modeling of Residual Atmospheric Variations and Clock Rates in Analysis of VLBI Geodetic Data**  
Jinling Li, Guangli Wang, Bo Zhang, Shanghai Astronomical Observatory
- 5-04P. **Reweighting Techniques for Use in VLBI Parameter Estimation**  
Hansjoerg Kutterer, Volker Tesmer, Robert Heinkelmann, Deutsches Geodätisches Forschungsinstitut
- 5-05P. **Global Collocation of the IRIS and NEOS VLBI Sessions<sup>†</sup>**  
V. S. Gubanov, I. F. Surkis, Yu. L. Rusinov, Institute of Applied Astronomy
- 5-06P. **USNO Analysis of VLBA RDV Data on Source Position and EOP Estimation**  
Alan Fey, David Boboltz, U.S. Naval Observatory
- 5-07P. **Data Flow and Analysis Processes at BKG Data and Analysis Center**  
Volkmar Thorandt, Dieter Ullrich, Reiner Wojdziak, BKG, Federal Agency for Cartography and Geodesy
- 5-08P. **Deformation of VLBI Antenna Due to Temperature Change Detected by GPS**  
Kyoko Kobayashi, Yoshihiro Fukuzaki, Katsuhiko Nagata, Geographical Survey Institute
- 5-09P. **VLBI Analysis at the U.S. Naval Observatory**  
David Boboltz, Alan Fey, David Hall, U.S. Naval Observatory
- 5-10P. **Current Works of the IVS Analysis Center at BKG**  
Gerald Engelhardt, Volkmar Thorandt, Dieter Ullrich, Bundesamt für Kartographie und Geodäsie
- 5-11P. **USNO Analysis Center for Source Structure**  
Alan Fey, David Boboltz, Ralph Gaume, Kerry Kingham, U.S. Naval Observatory
- 5-12P. **GSFC VLBI Analysis Center**  
David Gordon (1), Chopo Ma (2), Dan MacMillan (3), Leonid Petrov (3), Karen Baver (1), Cindy Lonigro (1), (1)Raytheon/GSFC, (2) NASA/GSFC, (3) NVI, Inc./GSFC

---

<sup>†</sup> withdrawn

## Posters (continued)

- 5-13P. **IVS Analysis Center of Saint-Petersburg University**  
Maria Kudryashova, Oleg Titov, Veniamin Vityazev, Astronomical Institute of Saint Petersburg University
- 5-14P. **IAA VLBI Analysis Center Activity in 2001**  
Zinovy Malkin (with co-authors), Institute of Applied Astronomy
- 5-15P. **AUSLIG International VLBI Service Analysis Centre**  
Oleg Titov, Geoscience, Australia

## Session 6. Analysis and Geodetic/Geophysical/Astrometric Interpretation

- 6-01P. **Searching for High Quality VLBI Calibrators**  
Edward B. Fomalont, National Radio Astronomy Observatory
- 6-02P. **Extragalactic Radio Source Selection for Radio/Optical Frame Ties**  
Alan Fey, David Boboltz, Ralph Gaume, T. Marshall Eubanks, Kenneth Johnston, U.S. Naval Observatory
- 6-03P. **Radio Source Stability and the Observation of Precession-nutation**  
M. Feissel (1), C. Ma (2), (1) Observatoire de Paris and Institut Géographique National, (2) Goddard Space Flight Center
- 6-04P. **Scientific Objective and Present Status of VERA Project**  
Tetsuo Sasao and VERA Project Team, National Astronomical Observatory, Japan
- 6-05P. **Astrometric and Geodetic Analysis System of VERA**  
Seiji Manabe, Hioshi Imai, Takaaki Jike, National Astronomical Observatory of Japan
- 6-06P. **Comparative study of the EOP series derived for the second IVS Pilot Project**  
Daniel Gambis, Christian Bizouard, Jean-Alexis Didier, Teddy Carlucci, IERS, Observatoire de Paris
- 6-07P. **Comparison of the Baseline Length Between the Keystone Sites by Different Space Geodetic Techniques**  
Taizoh Yoshino and the members of Keystone Project, Communications Research Laboratory
- 6-08P. **Spectral Analyses of Baseline Length Time Series from VLBI Data Analysis**  
Oleg Titov, Geoscience Australia
- 6-09P. **Seasonal Variations in Baseline Lengths and Station Positions**  
Elena Skurikhina, Institute of Applied Astronomy

## Posters (continued)

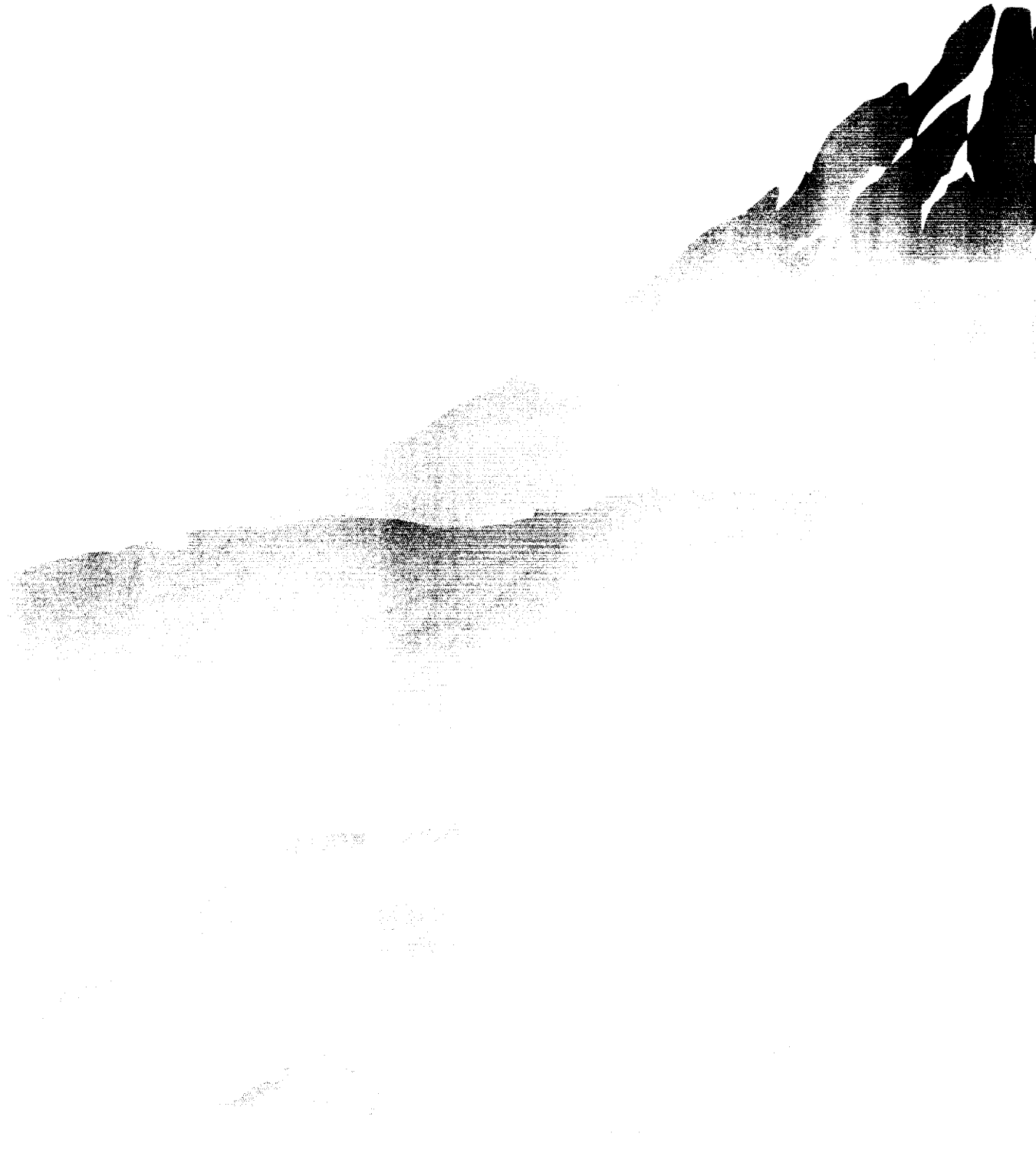
- 6-10P. **VLBI Evidence for Glacial Rebound in Europe**  
Kurt Lambeck (1), Anthony Purcell (1), Oleg Titov (2), David Jauncey (3), (1) Research School of Earth Sciences, ANU, (2) Geoscience Australia, (3) ATNF, CSIRO
- 6-11P. **The Antarctic VLBI Experiments During JARE39 and Geodetic Analyses by the Mitaka FX Correlator**  
Takaaki Jike (1), Seiji Manabe (1), Yoshiaki Tamura (1), Kazuo Shibuya (2), Koichiro Doi (2), and the Antarctic VLBI Group (1,2), (1) National Astronomical Observatory, Japan, (2) National Institute of Polar Research
- 6-12P. **Combined GPS and VLBI Analysis Processing**<sup>†</sup>  
Marcelo Santos (1), Clavin Klatt (2), (1)University of New Brunswick, (2) Geodetic Survey Division, Natural Resources Canada
- 6-13P. **SLR-based TRF Contributing to the ITRF2000 Project**  
Toshimichi Otsubo, Tadahiro Gotoh, Communications Research Laboratory
- 6-14P. **Global Lunar Gravity Field Recovery from SELENE**  
Koji Matsumoto, Kosuki Heki, Hideo Hanada, National Astronomical Observatory, Japan

---

<sup>†</sup> withdrawn



# Index of Authors





## Author Index

(First authors are designated by (1) at the end of the title.)

- Abe, Kaoru*: p. 96, VLBI-GPS Collocation Method at Geographical Survey Institute  
*Akiyama, Noriyuki*: p. 81, Geodesy with the World's Smallest (3-m) VLBI Telescope  
*Akiyama, Tadayuki*: p. 96, VLBI-GPS Collocation Method at Geographical Survey Institute  
*Amagai, Jun*: p. 81, Geodesy with the World's Smallest (3-m) VLBI Telescope  
*Amagai, Jun*: p. 117, Status of the KSP VLBI Stations and IMT-2000 Interference (1)  
*Amagai, Jun*: p. 223, Comparison of Atmospheric Parameters from VLBI, GPS and WVR  
*Amagai, Jun*: p. 320, Comparison of the Baseline Length Between the Keystone Sites by Different Space Geodetic Techniques  
*Aonashi, Kazumasa*: p. 223, Comparison of Atmospheric Parameters from VLBI, GPS and WVR  
*Aoyama, Toshiki*: p. 4, Welcome Address of Geographical Survey Institute (1)  
*Asari, Kazuyoshi*: p. 72, VRAD Mission: Precise Observation of Orbits of Sub-Satellites in SELENE with International VLBI Network  
*Beasley, Tony*: p. 360, Searching for High Quality VLBI Calibrators  
*Benndorf, I.*: p. 102, The Mark IV Correlator - Faster, Better, Optimal??  
*Bergstrand, Sten*: p. 91, Local Ties Between the Space Geodetic Techniques at the Onsala Space Observatory  
*Bérubé, Mario*: p. 60, Geodetic S2 VLBI: International Plans  
*Bérubé, Mario*: p. 77, A Next Generation Geodetic Experiment Scheduling Tool? (SKED++)  
*Beutler, Gerhard*: p. 24, Challenges for VLBI Within an Integrated Global Geodetic Observing System  
*Bizouard, Ch.*: p. 330, Comparative Study of the EOP Series Derived for the Second IVS Pilot Project  
*Boboltz, David A.*: p. 282, USNO Analysis of VLBA RDV Data  
*Boboltz, David A.*: p. 350, Extending the ICRF to Higher Radio Frequencies  
*Boboltz, David A.*: p. 363, Extragalactic Radio Source Selection for Radio/Optical Frame Ties  
*Bockmann, Lars*: p. 86, Foot-Print of the Space-Geodetic Observatory, Ny-Ålesund, Svalbard  
*Boehm, Johannes*: p. 219, Tropospheric Zenith Path Delays Derived from GPS Used for the Determination of VLBI Station Heights (1)  
*Boehm, Johannes*: p. 340, Comparison of Tropospheric Parameters Submitted to the 2nd IVS Analysis Pilot Project (1)  
*Boehm, Johannes*: p. 345, Determination of Ionospheric Parameters by Geodetic VLBI  
*Bos, Machiel S.*: p. 205, Ocean Tide and Atmospheric Loading  
*Bromorzki, O.*: p. 107, Comparison of the Output of Repeated Mark III and Mark IV Correlation Results  
*Campbell, J.*: p. 107, Comparison of the Output of Repeated Mark III and Mark IV Correlation Results  
*Campbell, James*: p. 260, On Correlations Between Parameters in Geodetic VLBI Data Analysis  
*Cannon, Wayne*: p. 60, Geodetic S2 VLBI: International Plans  
*Capitaine, Nicole*: p. 14, The Essential Contribution of VLBI to Fundamental Astronomy (1)  
*Cappallo, Roger*: p. 101, Mark 4 Correlator Software: Status and Plans (1)  
*Carlucci, T.*: p. 330, Comparative Study of the EOP Series Derived for the Second IVS Pilot Project  
*Charlot, Patrick*: p. 233, Modeling Radio Source Structure for Improved VLBI Data Analysis (1)  
*Charlot, Patrick*: p. 243, Structure Corrections in Modeling VLBI Delays for RDV Data  
*Charlot, Patrick*: p. 350, Extending the ICRF to Higher Radio Frequencies

- Corey, Brian*: p. 67, **Fundamentals of Phase Calibration in Geodetic VLBI** (1)
- Corey, Brian*: p. 112, **Comparison of the VLBI Observables from Mk3 and Mk4 Correlation of a 24-hour Geodetic Experiment** (1)
- Corey, Brian*: p. 389, **Mini-TOW (Technical Operations Workshop)**
- Costa, Marco*: p. 324, **The Antarctic VLBI Experiments During JARE39 and Geodetic Analysis by the Mitaka FX Correlator**
- Doi, Koichiro*: p. 184, **Processing of the Data of Syowa VLBI Experiment by Copying Between the Different Recording Systems and the Result of the Analysis**
- Doi, Koichiro*: p. 324, **The Antarctic VLBI Experiments During JARE39 and Geodetic Analysis by the Mitaka FX Correlator**
- Drewes, Hermann*: p. 24, **Challenges for VLBI Within an Integrated Global Geodetic Observing System** (1)
- Elgered, Gunnar*: p. 91, **Local Ties Between the Space Geodetic Techniques at the Onsala Space Observatory**
- Eubanks, T. Marshall*: p. 363, **Extragalactic Radio Source Selection for Radio/Optical Frame Ties**
- Feissel, Martine*: p. 248, **PIVEX: a Proposal for a Platform Independent VLBI Exchange Format**
- Feissel, Martine*: p. 367, **Radio Source Stability and the Observation of Precession-Nutation** (1)
- Fey, Alan L.*: p. 243, **Structure Corrections in Modeling VLBI Delays for RDV Data**
- Fey, Alan L.*: p. 282, **USNO Analysis of VLBA RDV Data** (1)
- Fey, Alan L.*: p. 350, **Extending the ICRF to Higher Radio Frequencies**
- Fey, Alan L.*: p. 363, **Extragalactic Radio Source Selection for Radio/Optical Frame Ties** (1)
- Fomalont, Edward*: p. 360, **Searching for High Quality VLBI Calibrators** (1)
- Fujisawa, Kenta*: p. 152, **IP Data Transfer System for Real-time VLBI**
- Fukuzaki, Yoshihiro*: p. 81, **Geodesy with the World's Smallest (3-m) VLBI Telescope**
- Fukuzaki, Yoshihiro*: p. 96, **VLBI-GPS Collocation Method at Geographical Survey Institute**
- Fukuzaki, Yoshihiro*: p. 179, **Precise Positioning of Spacecrafts by Multi-frequency VLBI**
- Fukuzaki, Yoshihiro*: p. 184, **Processing of the Data of Syowa VLBI Experiment by Copying Between the Different Recording Systems and the Result of the Analysis** (1)
- Fukuzaki, Yoshihiro*: p. 223, **Comparison of Atmospheric Parameters from VLBI, GPS and WVR**
- Fukuzaki, Yoshihiro*: p. 324, **The Antarctic VLBI Experiments During JARE39 and Geodetic Analysis by the Mitaka FX Correlator**
- GALAXY Team*: p. 142, **Real-time Gigabit VLBI System and Internet VLBI System**
- Gambis, D.*: p. 330, **Comparative Study of the EOP Series Derived for the Second IVS Pilot Project** (1)
- Gaume, Ralph A.*: p. 363, **Extragalactic Radio Source Selection for Radio/Optical Frame Ties**
- Gino, Colleen*: p. 360, **Searching for High Quality VLBI Calibrators**
- Gontier, Anne-Marie*: p. 248, **PIVEX: a Proposal for a Platform Independent VLBI Exchange Format** (1)
- Gordon, David*: p. 243, **Structure Corrections in Modeling VLBI Delays for RDV Data**
- Gordon, David*: p. 277, **RDV Analysis and Mark 4/VLBA Comparison Results** (1)
- Gordon, David*: p. 350, **Extending the ICRF to Higher Radio Frequencies**
- Gordon, David*: p. 355, **Towards a Future ICRF Realization**
- Gotoh, Tadahiro*: p. 300, **SLR-based TRF Contributing to the ITRF2000 project**
- Haas, Rüdiger*: p. 91, **Local Ties Between the Space Geodetic Techniques at the Onsala Space Observatory**
- Hagimoto, Ken*: p. 189, **Laser-Pumped Cs Gas-Cell Type Atomic Clock for VLBI**
- Hanada, Hideo*: p. 72, **VRAD Mission: Precise Observation of Orbits of Sub-Satellites in SELENE with International VLBI Network** (1)
- Hanada, Hideo*: p. 179, **Precise Positioning of Spacecrafts by Multi-frequency VLBI**
- Hanada, Hideo*: p. 377, **Results of the Critical Design for the Selenodetic Mission using Differ-**

**ential VLBI Methods by SELENE**

- Hanada, Hideo*: p. 381, **Global Lunar Gravity Field Recovery from SELENE**
- Hatanaka, Yuki*: p. 96, **VLBI-GPS Collocation Method at Geographical Survey Institute**
- Hatanaka, Yuki*: p. 223, **Comparison of Atmospheric Parameters from VLBI, GPS and WVR**
- Heki, Kosuke*: p. 72, **VRAD Mission: Precise Observation of Orbits of Sub-Satellites in SELENE with International VLBI Network**
- Heki, Kosuke*: p. 381, **Global Lunar Gravity Field Recovery from SELENE**
- Hirabayashi, Hisashi*: p. 171, **The VSOP-2 Space VLBI Mission (1)**
- Hirabayashi, Hisashi*: p. 175, **Wide-band Data Transmission System Expected in the Next Generation Space VLBI Mission: VSOP-2**
- Hobiger, Thomas*: p. 345, **Determination of Ionospheric Parameters by Geodetic VLBI (1)**
- Höfer, A.*: p. 102, **The Mark IV Correlator - Faster, Better, Optimal??**
- Hori, Hiroshi*: p. 81, **Geodesy with the World's Smallest (3-m) VLBI Telescope**
- Ichikawa, Ryuichi*: p. 81, **Geodesy with the World's Smallest (3-m) VLBI Telescope**
- Ichikawa, Ryuichi*: p. 117, **Status of the KSP VLBI Stations and IMT-2000 Interference**
- Ichikawa, Ryuichi*: p. 142, **Real-time Gigabit VLBI System and Internet VLBI System**
- Ichikawa, Ryuichi*: p. 223, **Comparison of Atmospheric Parameters from VLBI, GPS and WVR (1)**
- Ichikawa, Ryuichi*: p. 320, **Comparison of the Baseline Length Between the Keystone Sites by Different Space Geodetic Techniques**
- Ichikawa, Yuichi*: p. 142, **Real-time Gigabit VLBI System and Internet VLBI System**
- Iida, Takashi*: p. 5, **Welcome Address of Communications Research Laboratory (1)**
- Ikegami, Takashi*: p. 189, **Laser-Pumped Cs Gas-Cell Type Atomic Clock for VLBI**
- Imai, Hiroshi*: p. 372, **Astrometric and Geodetic Analysis System of VERA**
- Imakiire, Tetsuro*: p. 304, **Establishment of the New Geodetic Reference Frame of Japan (JGD2000) (1)**
- Ishikawa, Toshiaki*: p. 72, **VRAD Mission: Precise Observation of Orbits of Sub-Satellites in SELENE with International VLBI Network**
- Iwabuchi, Tetsuya*: p. 223, **Comparison of Atmospheric Parameters from VLBI, GPS and WVR**
- Iwadate, Kenzaburo*: p. 179, **Precise Positioning of Spacecrafts by Multi-frequency VLBI**
- Iwamura, Sotetsu*: p. 152, **IP Data Transfer System for Real-time VLBI (1)**
- Iwata, Takahiro*: p. 72, **VRAD Mission: Precise Observation of Orbits of Sub-Satellites in SELENE with International VLBI Network**
- Iwata, Takahiro*: p. 377, **Results of the Critical Design for the Selenodetic Mission using Differential VLBI Methods by SELENE (1)**
- Jacobs, C. S.*: p. 350, **Extending the ICRF to Higher Radio Frequencies (1)**
- Jauncey, David L.*: p. 184, **Processing of the Data of Syowa VLBI Experiment by Copying Between the Different Recording Systems and the Result of the Analysis**
- Jauncey, David L.*: p. 324, **The Antarctic VLBI Experiments During JARE39 and Geodetic Analysis by the Mitaka FX Correlator**
- Jauncey, David L.*: p. 329, **VLBI Evidence for Glacial Rebound in Europe**
- Jean-Alexis, D.*: p. 330, **Comparative Study of the EOP Series Derived for the Second IVS Pilot Project**
- Jike, Takaaki*: p. 184, **Processing of the Data of Syowa VLBI Experiment by Copying Between the Different Recording Systems and the Result of the Analysis**
- Jike, Takaaki*: p. 324, **The Antarctic VLBI Experiments During JARE39 and Geodetic Analysis by the Mitaka FX Correlator (1)**
- Jike, Takaaki*: p. 372, **Astrometric and Geodetic Analysis System of VERA**
- Johansson, Jan*: p. 91, **Local Ties Between the Space Geodetic Techniques at the Onsala Space Observatory**
- Johnston, Kenneth J.*: p. 363, **Extragalactic Radio Source Selection for Radio/Optical Frame**

## Ties

- Jones, D. L.:* p. 350, **Extending the ICRF to Higher Radio Frequencies**
- Kameno, Seiji:* p. 199, **A Proposal for Constructing a New Sub-mm VLBI Array, Horizon Telescope – Imaging Black Hole Vicinity**
- Katsuo, Futaba:* p. 320, **Comparison of the Baseline Length Between the Keystone Sites by Different Space Geodetic Techniques**
- Kawai, Eiji:* p. 81, **Geodesy with the World's Smallest (3-m) VLBI Telescope**
- Kawai, Eiji:* p. 142, **Real-time Gigabit VLBI System and Internet VLBI System**
- Kawai, Eiji:* p. 223, **Comparison of Atmospheric Parameters from VLBI, GPS and WVR**
- Kawano, Nobuyuki:* p. 72, **VRAD Mission: Precise Observation of Orbits of Sub-Satellites in SELENE with International VLBI Network**
- Kawano, Nobuyuki:* p. 179, **Precise Positioning of Spacecrafts by Multi-frequency VLBI**
- Kawano, Nobuyuki:* p. 377, **Results of the Critical Design for the Selenodetic Mission using Differential VLBI Methods by SELENE**
- Keihm, Steve:* p. 194, **Media Calibration in The Deep Space Network - A Status Report**
- Kierulf, Halfdan P.:* p. 86, **Foot-Print of the Space-Geodetic Observatory, Ny-Ålesund, Svalbard**  
(1)
- Kimura, Moritaka:* p. 123, **VSI Interface Implementation, Performance Enhancement of Gbps VLBI Instruments**
- Kimura, Moritaka:* p. 142, **Real-time Gigabit VLBI System and Internet VLBI System**
- Kiuchi, Hitoshi:* p. 117, **Status of the KSP VLBI Stations and IMT-2000 Interference**
- Kiuchi, Hitoshi:* p. 157, **Parallel Data Processing System** (1)
- Kiuchi, Hitoshi:* p. 223, **Comparison of Atmospheric Parameters from VLBI, GPS and WVR**
- Kiuchi, Hitoshi:* p. 320, **Comparison of the Baseline Length Between the Keystone Sites by Different Space Geodetic Techniques**
- Klatt, Calvin:* p. 60, **Geodetic S2 VLBI: International Plans** (1)
- Klatt, Calvin:* p. 77, **A Next Generation Geodetic Experiment Scheduling Tool? (SKED++)**  
(1)
- Klatt, Calvin:* p. 162, **Multi-Beam VLBI**
- Kobayashi, Kyoko:* p. 81, **Geodesy with the World's Smallest (3-m) VLBI Telescope**
- Kobayashi, Kyoko:* p. 96, **VLBI-GPS Collocation Method at Geographical Survey Institute**
- Koga, Yasuki:* p. 189, **Laser-Pumped Cs Gas-Cell Type Atomic Clock for VLBI**
- Kondo, Tetsuro:* p. 81, **Geodesy with the World's Smallest (3-m) VLBI Telescope**
- Kondo, Tetsuro:* p. 117, **Status of the KSP VLBI Stations and IMT-2000 Interference**
- Kondo, Tetsuro:* p. 123, **VSI Interface Implementation, Performance Enhancement of Gbps VLBI Instruments**
- Kondo, Tetsuro:* p. 142, **Real-time Gigabit VLBI System and Internet VLBI System** (1)
- Kondo, Tetsuro:* p. 152, **IP Data Transfer System for Real-time VLBI**
- Kondo, Tetsuro:* p. 223, **Comparison of Atmospheric Parameters from VLBI, GPS and WVR**
- Kondo, Tetsuro:* p. 320, **Comparison of the Baseline Length Between the Keystone Sites by Different Space Geodetic Techniques**
- Kono, Yusuke:* p. 72, **VRAD Mission: Precise Observation of Orbits of Sub-Satellites in SELENE with International VLBI Network**
- Kono, Yusuke:* p. 179, **Precise Positioning of Spacecrafts by Multi-frequency VLBI** (1)
- Kono, Yusuke:* p. 377, **Results of the Critical Design for the Selenodetic Mission using Differential VLBI Methods by SELENE**
- Koyama, Yasuhiro:* p. 55, **Expected Contributions of the K-4 and its Next-Generation Systems**  
(1)
- Koyama, Yasuhiro:* p. 81, **Geodesy with the World's Smallest (3-m) VLBI Telescope**
- Koyama, Yasuhiro:* p. 117, **Status of the KSP VLBI Stations and IMT-2000 Interference**
- Koyama, Yasuhiro:* p. 123, **VSI Interface Implementation, Performance Enhancement of Gbps**

**VLBI Instruments**

- Koyama, Yasuhiro*: p. 142, Real-time Gigabit VLBI System and Internet VLBI System  
*Koyama, Yasuhiro*: p. 179, Precise Positioning of Spacecrafts by Multi-frequency VLBI  
*Koyama, Yasuhiro*: p. 223, Comparison of Atmospheric Parameters from VLBI, GPS and WVR  
*Koyama, Yasuhiro*: p. 320, Comparison of the Baseline Length Between the Keystone Sites by  
**Different Space Geodetic Techniques**  
*Kristiansen, Oddgeir*: p. 86, Foot-Print of the Space-Geodetic Observatory, Ny-Ålesund, Sval-  
 bard  
*Kunimori, Hiroo*: p. 320, Comparison of the Baseline Length Between the Keystone Sites by  
**Different Space Geodetic Techniques**  
*Kurihara, Noriyuki*: p. 81, Geodesy with the World's Smallest (3-m) VLBI Telescope  
*Kurihara, Shinobu*: p. 81, Geodesy with the World's Smallest (3-m) VLBI Telescope  
*Kurihara, Shinobu*: p. 223, Comparison of Atmospheric Parameters from VLBI, GPS and WVR  
*Kutterer, Hansjörg*: p. 272, Statistical Assessment of Subdiurnal Earth Orientation Parameters  
**from VLBI (1)**  
*Lambeck, Kurt*: p. 329, VLBI Evidence for Glacial Rebound in Europe (1)  
*Lanyi, Gabor*: p. 194, Media Calibration in The Deep Space Network - A Status Report  
*Lanyi, G. E.*: p. 350, Extending the ICRF to Higher Radio Frequencies  
*Li, Jinling*: p. 228, A Discussion on the Modeling of the Residual Clock Behavior and Atmo-  
 sphere Effects in the Astrometric and Geodetic VLBI Data Analysis (1)  
*Lidberg, Martin*: p. 91, Local Ties Between the Space Geodetic Techniques at the Onsala Space  
 Observatory (1)  
*Linfield, Roger*: p. 194, Media Calibration in The Deep Space Network - A Status Report  
*Liu, Qinghui*: p. 147, Observation of Atmospheric Disturbances Using a Real-Time VLBI Sys-  
 tem (1)  
*Lowe, S. T.*: p. 350, Extending the ICRF to Higher Radio Frequencies  
*Ma, Chopo*: p. 50, Geodetic Results from Mark 4 VLBI  
*Ma, Chopo*: p. 255, Integrating Analysis Goals for EOP, CRF and TRF (1)  
*Ma, Chopo*: p. 350, Extending the ICRF to Higher Radio Frequencies  
*Ma, Chopo*: p. 355, Towards a Future ICRF Realization (1)  
*Ma, Chopo*: p. 367, Radio Source Stability and the Observation of Precession-Nutation  
*MacMillan, Daniel*: p. 50, Geodetic Results from Mark 4 VLBI (1)  
*MacMillan, Daniel*: p. 255, Integrating Analysis Goals for EOP, CRF and TRF  
*MacMillan, Daniel*: p. 355, Towards a Future ICRF Realization  
*Malkin, Zinovy*: p. 309, Variations of European Baseline Lengths from VLBI and GPS Data (1)  
*Malkin, Zinovy*: p. 335, A Comparison of the VLBI Nutation Series with IAU2000 Model (1)  
*Manabe, Seiji*: p. 324, The Antarctic VLBI Experiments During JARE39 and Geodetic Analysis  
 by the Mitaka FX Correlator  
*Manabe, Seiji*: p. 372, Astrometric and Geodetic Analysis System of VERA (1)  
*Matsumoto, Koji*: p. 72, VRAD Mission: Precise Observation of Orbits of Sub-Satellites in  
 SELENE with International VLBI Network  
*Matsumoto, Koji*: p. 381, Global Lunar Gravity Field Recovery from SELENE (1)  
*Matsuzaka, Shigeru*: p. 81, Geodesy with the World's Smallest (3-m) VLBI Telescope  
*Matsuzaka, Shigeru*: p. 96, VLBI-GPS Collocation Method at Geographical Survey Institute (1)  
*Mattori, Shigenori*: p. 189, Laser-Pumped Cs Gas-Cell Type Atomic Clock for VLBI  
*McCulloch, Peter*: p. 324, The Antarctic VLBI Experiments During JARE39 and Geodetic Anal-  
 ysis by the Mitaka FX Correlator  
*Messerer, Eva*: p. 340, Comparison of Tropospheric Parameters Submitted to the 2nd IVS  
 Analysis Pilot Project  
*Minh, Y. C.*: p. 68, Construction of the Korean VLBI Network (KVN) (1)  
*Miyagawa, Kohhei*: p. 81, Geodesy with the World's Smallest (3-m) VLBI Telescope

- Miyazaki, Tomoyuki*: p. 147, **Observation of Atmospheric Disturbances Using a Real-Time VLBI System**
- Miyoshi, Makoto*: p. 199, **A Proposal for Constructing a New Sub-mm VLBI Array, Horizon Telescope – Imaging Black Hole Vicinity (1)**
- Mujunen, Ari*: p. 128, **A VSI-H Compatible Recording System for VLBI and e-VLBI**
- Murakami, Masaki*: p. 304, **Establishment of the New Geodetic Reference Frame of Japan (JGD2000)**
- Murata, Yasuhiro*: p. 171, **The VSOP-2 Space VLBI Mission**
- Murata, Yasuhiro*: p. 175, **Wide-band Data Transmission System Expected in the Next Generation Space VLBI Mission: VSOP-2 (1)**
- Murphy, David W.*: p. 171, **The VSOP-2 Space VLBI Mission**
- Müskens, A.*: p. 102, **The Mark IV Correlator - Faster, Better, Optimal?? (1)**
- Müskens, A.*: p. 107, **Comparison of the Output of Repeated Mark III and Mark IV Correlation Results**
- Nakagawa, Shin-ichi*: p. 152, **IP Data Transfer System for Real-time VLBI**
- Nakajima, Jun-ichi*: p. 81, **Geodesy with the World's Smallest (3-m) VLBI Telescope**
- Nakajima, Junichi*: p. 123, **VSI Interface Implementation, Performance Enhancement of Gbps VLBI Instruments (1)**
- Nakajima, Junichi*: p. 142, **Real-time Gigabit VLBI System and Internet VLBI System**
- Nakajima, Junichi*: p. 223, **Comparison of Atmospheric Parameters from VLBI, GPS and WVR**
- Namiki, Noriyuki*: p. 377, **Results of the Critical Design for the Selenodetic Mission using Differential VLBI Methods by SELENE**
- Naudet, Charles J.*: p. 194, **Media Calibration in The Deep Space Network - A Status Report (1)**
- Naudet, Charles J.*: p. 350, **Extending the ICRF to Higher Radio Frequencies**
- Nemoto, Keizo*: p. 96, **VLBI-GPS Collocation Method at Geographical Survey Institute**
- Nicolson, George D.*: p. 184, **Processing of the Data of Syowa VLBI Experiment by Copying Between the Different Recording Systems and the Result of the Analysis**
- Nicolson, George*: p. 324, **The Antarctic VLBI Experiments During JARE39 and Geodetic Analysis by the Mitaka FX Correlator**
- Niell, Arthur*: p. 215, **Gradient Mapping Functions for VLBI and GPS (1)**
- Nishio, Masanori*: p. 147, **Observation of Atmospheric Disturbances Using a Real-Time VLBI System**
- Nothnagel, A.*: p. 107, **Comparison of the Output of Repeated Mark III and Mark IV Correlation Results (1)**
- Nothnagel, Axel*: p. 260, **On Correlations Between Parameters in Geodetic VLBI Data Analysis (1)**
- Nothnagel, Axel*: p. 265, **Outlier Detection in the Combination of VLBI EOP**
- Nothnagel, Axel*: p. 394, **Summary of the Third IVS Analysis Workshop (1)**
- Ohkubo, Hiroshi*: p. 223, **Comparison of Atmospheric Parameters from VLBI, GPS and WVR**
- Ohsaki, Hiro*: p. 223, **Comparison of Atmospheric Parameters from VLBI, GPS and WVR**
- Ohtani, Ryu*: p. 223, **Comparison of Atmospheric Parameters from VLBI, GPS and WVR**
- Ohuchi, Yuji*: p. 189, **Laser-Pumped Cs Gas-Cell Type Atomic Clock for VLBI**
- Okubo, Hiroshi*: p. 81, **Geodesy with the World's Smallest (3-m) VLBI Telescope**
- Okubo, Hiroshi*: p. 123, **VSI Interface Implementation, Performance Enhancement of Gbps VLBI Instruments**
- Okubo, Hiroshi*: p. 142, **Real-time Gigabit VLBI System and Internet VLBI System**
- Onogaki, Michiko*: p. 81, **Geodesy with the World's Smallest (3-m) VLBI Telescope**
- Osaki, Hiro*: p. 81, **Geodesy with the World's Smallest (3-m) VLBI Telescope**
- Osaki, Hiro*: p. 123, **VSI Interface Implementation, Performance Enhancement of Gbps VLBI Instruments**
- Osaki, Hiro*: p. 142, **Real-time Gigabit VLBI System and Internet VLBI System**

- Otsubo, Toshimichi*: p. 300, SLR-based TRF Contributing to the ITRF2000 project (1)
- Otsubo, Toshimichi*: p. 320, Comparison of the Baseline Length Between the Keystone Sites by Different Space Geodetic Techniques
- Panafidina, Natalia*: p. 309, Variations of European Baseline Lengths from VLBI and GPS Data
- Paunonen, Matti*: p. 120, Metsähovi Geodetic VLBI Station: Status Report (1)
- Peck, Alison*: p. 360, Searching for High Quality VLBI Calibrators
- Petrachenko, W.T.*: p. 60, Geodetic S2 VLBI: International Plans
- Petrachenko, W.T.*: p. 162, Multi-Beam VLBI (1)
- Petrov, Leonid*: p. 50, Geodetic Results from Mark 4 VLBI
- Petrov, Leonid*: p. 255, Integrating Analysis Goals for EOP, CRF and TRF
- Petrov, Leonid*: p. 355, Towards a Future ICRF Realization
- Ping, Jinsong*: p. 72, VRAD Mission: Precise Observation of Orbits of Sub-Satellites in SELENE with International VLBI Network
- Plag, Hans-Peter*: p. 86, Foot-Print of the Space-Geodetic Observatory, Ny-Ålesund, Svalbard
- Purcell, Anthony*: p. 329, VLBI Evidence for Glacial Rebound in Europe
- Quick, Jonathan F. H.*: p. 324, The Antarctic VLBI Experiments During JARE39 and Geodetic Analysis by the Mitaka FX Correlator
- Resch, George*: p. 194, Media Calibration in The Deep Space Network - A Status Report
- Resch, George*: p. 350, Extending the ICRF to Higher Radio Frequencies
- Reynolds, John*: p. 324, The Antarctic VLBI Experiments During JARE39 and Geodetic Analysis by the Mitaka FX Correlator
- Riley, Lance*: p. 194, Media Calibration in The Deep Space Network - A Status Report
- Ritakari, Jouko*: p. 128, A VSI-H Compatible Recording System for VLBI and e-VLBI (1)
- Roh, D. -G.*: p. 68, Construction of the Korean VLBI Network (KVN)
- Rosenberger, Hans*: p. 194, Media Calibration in The Deep Space Network - A Status Report
- Rothacher, Markus*: p. 33, Combination of Space-Geodetic Techniques (1)
- Rottmann, H.*: p. 102, The Mark IV Correlator - Faster, Better, Optimal??
- Rottmann, H.*: p. 107, Comparison of the Output of Repeated Mark III and Mark IV Correlation Results
- Rottmann, I.*: p. 102, The Mark IV Correlator - Faster, Better, Optimal??
- Rottmann, I.*: p. 107, Comparison of the Output of Repeated Mark III and Mark IV Correlation Results
- Rummel, Reiner*: p. 24, Challenges for VLBI Within an Integrated Global Geodetic Observing System
- Saburi, Yoshikazu*: p. 189, Laser-Pumped Cs Gas-Cell Type Atomic Clock for VLBI
- Sasaki, Takeshi*: p. 377, Results of the Critical Design for the Selenodetic Mission using Differential VLBI Methods by SELENE
- Sato, Katsuhisa*: p. 324, The Antarctic VLBI Experiments During JARE39 and Geodetic Analysis by the Mitaka FX Correlator
- SBL Team*: p. 287, The New IERS Special Bureau for Loading (SBL) (1)
- Scherneck, Hans-Georg*: p. 205, Ocean Tide and Atmospheric Loading (1)
- Scherneck, Hans-Georg*: p. 398, IVS Analysis Working Group for Geophysical Models in VLBI Software: Splinter Meeting (1)
- Schlüter, Wolfgang*: p. 9, Chair's Report at 2nd IVS General Meeting (1)
- Schuh, Harald*: p. 47, IVS Working Group 2 for Product Specification and Observing Programs (1)
- Schuh, Harald*: p. 219, Tropospheric Zenith Path Delays Derived from GPS Used for the Determination of VLBI Station Heights
- Schuh, Harald*: p. 340, Comparison of Tropospheric Parameters Submitted to the 2nd IVS Analysis Pilot Project
- Schuh, Harald*: p. 345, Determination of Ionospheric Parameters by Geodetic VLBI

- Searle, Anthony*: p. 60, Geodetic S2 VLBI: International Plans
- Searle, Anthony*: p. 77, A Next Generation Geodetic Experiment Scheduling Tool? (SKED++)
- Sebata, Koichi*: p. 117, Status of the KSP VLBI Stations and IMT-2000 Interference
- Sekido, Mamoru*: p. 81, Geodesy with the World's Smallest (3-m) VLBI Telescope
- Sekido, Mamoru*: p. 117, Status of the KSP VLBI Stations and IMT-2000 Interference
- Sekido, Mamoru*: p. 123, VSI Interface Implementation, Performance Enhancement of Gbps VLBI Instruments
- Sekido, Mamoru*: p. 142, Real-time Gigabit VLBI System and Internet VLBI System
- Sekido, Mamoru*: p. 223, Comparison of Atmospheric Parameters from VLBI, GPS and WVR
- Seko, Hiromu*: p. 223, Comparison of Atmospheric Parameters from VLBI, GPS and WVR
- Shiba, Kouhei*: p. 81, Geodesy with the World's Smallest (3-m) VLBI Telescope
- Shibata, Katsunori M.*: p. 324, The Antarctic VLBI Experiments During JARE39 and Geodetic Analysis by the Mitaka FX Correlator
- Shibuya, Kazuo*: p. 184, Processing of the Data of Syowa VLBI Experiment by Copying Between the Different Recording Systems and the Result of the Analysis
- Shibuya, Kazuo*: p. 324, The Antarctic VLBI Experiments During JARE39 and Geodetic Analysis by the Mitaka FX Correlator
- Shoji, Yoshinori*: p. 223, Comparison of Atmospheric Parameters from VLBI, GPS and WVR
- Silliker, Jason*: p. 77, A Next Generation Geodetic Experiment Scheduling Tool? (SKED++)
- Skurikhina, Elena*: p. 309, Variations of European Baseline Lengths from VLBI and GPS Data
- Skurikhina, Elena*: p. 310, Influence of Antenna Thermal Deformations on Estimation of Seasonal Variations in Baseline Length (1)
- Sovers, Ojars J.*: p. 243, Structure Corrections in Modeling VLBI Delays for RDV Data (1)
- Sovers, O. J.*: p. 350, Extending the ICRF to Higher Radio Frequencies
- Steinforth, Christoph*: p. 265, Outlier Detection in the Combination of VLBI EOP (1)
- Steppe, J. A.*: p. 350, Extending the ICRF to Higher Radio Frequencies
- Strand, Rich*: p. 389, Mini-TOW (Technical Operations Workshop) (1)
- Suga, Hirohiko*: p. 189, Laser-Pumped Cs Gas-Cell Type Atomic Clock for VLBI
- Sutoh, Hiroshi*: p. 189, Laser-Pumped Cs Gas-Cell Type Atomic Clock for VLBI
- Takaba, Hiroshi*: p. 81, Geodesy with the World's Smallest (3-m) VLBI Telescope (1)
- Takahashi, Fujinobu*: p. 223, Comparison of Atmospheric Parameters from VLBI, GPS and WVR
- Takahashi, Fujinobu*: p. 320, Comparison of the Baseline Length Between the Keystone Sites by Different Space Geodetic Techniques
- Takahashi, Yukio*: p. 81, Geodesy with the World's Smallest (3-m) VLBI Telescope
- Takahei, Kenichiro*: p. 189, Laser-Pumped Cs Gas-Cell Type Atomic Clock for VLBI (1)
- Takashima, Kazuhiro*: p. 81, Geodesy with the World's Smallest (3-m) VLBI Telescope
- Takashima, Kazuhiro*: p. 223, Comparison of Atmospheric Parameters from VLBI, GPS and WVR
- Tamura, Yoshiaki*: p. 167, Geodetic Observation System in VERA (1)
- Tamura, Yoshiaki*: p. 324, The Antarctic VLBI Experiments During JARE39 and Geodetic Analysis by the Mitaka FX Correlator
- Tanaka, Teruhito*: p. 324, The Antarctic VLBI Experiments During JARE39 and Geodetic Analysis by the Mitaka FX Correlator
- Tang, Jennifer*: p. 215, Gradient Mapping Functions for VLBI and GPS
- Tanner, Alan*: p. 194, Media Calibration in The Deep Space Network - A Status Report
- Taylor, G. B.*: p. 350, Extending the ICRF to Higher Radio Frequencies
- Tesmer, Volker*: p. 272, Statistical Assessment of Subdiurnal Earth Orientation Parameters from VLBI
- Tesmer, Volker*: p. 295, VLBI Solution DGF101R01 Based on Least-Squares Estimation Using OCCAM 5.0 and DOGS-CS (1)
- Titov, Oleg*: p. 315, Spectral Analysis of the Baseline Length Time Series from VLBI Data (1)

- Titov, Oleg*: p. 329, VLBI Evidence for Glacial Rebound in Europe
- Titus, Michael*: p. 112, Comparison of the VLBI Observables from Mk3 and Mk4 Correlation of a 24-hour Geodetic Experiment
- Tsuda, Masahiro*: p. 189, Laser-Pumped Cs Gas-Cell Type Atomic Clock for VLBI
- Tsuruta, Seiitsu*: p. 72, VRAD Mission: Precise Observation of Orbits of Sub-Satellites in SELENE with International VLBI Network
- Tuccari, Gino*: p. 84, A Multiband Primary Focus Receiver for Noto Antenna (1)
- Uchino, Masaharu*: p. 189, Laser-Pumped Cs Gas-Cell Type Atomic Clock for VLBI
- Uvestad, J. S.*: p. 350, Extending the ICRF to Higher Radio Frequencies
- Uose, Hisao*: p. 152, IP Data Transfer System for Real-time VLBI
- Vandenberg, Nancy R.*: p. 49, IVS Observing Programs 2002–2005 (1)
- Vennebusch, Markus*: p. 260, On Correlations Between Parameters in Geodetic VLBI Data Analysis
- VERA Group*: p. 167, Geodetic Observation System in VERA
- VERA Group*: p. 372, Astrometric and Geodetic Analysis System of VERA
- Wakamatsu, Ken-ichi*: p. 81, Geodesy with the World's Smallest (3-m) VLBI Telescope
- Wang, Guangli*: p. 228, A Discussion on the Modeling of the Residual Clock Behavior and Atmosphere Effects in the Astrometric and Geodetic VLBI Data Analysis
- Ward, Vincent*: p. 162, Multi-Beam VLBI
- Weber, Robert*: p. 219, Tropospheric Zenith Path Delays Derived from GPS Used for the Determination of VLBI Station Heights
- Whitney, Alan R.*: p. 132, Mark 5 Disc-Based Gbps VLBI Data System (1)
- Whitney, Alan R.*: p. 137, High-Speed e-VLBI Demonstration: Haystack Observatory to NASA/GSFC (1)
- Yamamura, Kunihiro*: p. 147, Observation of Atmospheric Disturbances Using a Real-Time VLBI System
- Yoshida, Minoru*: p. 81, Geodesy with the World's Smallest (3-m) VLBI Telescope
- Yoshino, Taizoh*: p. 117, Status of the KSP VLBI Stations and IMT-2000 Interference
- Yoshino, Taizoh*: p. 223, Comparison of Atmospheric Parameters from VLBI, GPS and WVR
- Yoshino, Taizoh*: p. 320, Comparison of the Baseline Length Between the Keystone Sites by Different Space Geodetic Techniques (1)
- Zhang, Bo*: p. 228, A Discussion on the Modeling of the Residual Clock Behavior and Atmosphere Effects in the Astrometric and Geodetic VLBI Data Analysis
- Zhang, L. D.*: p. 350, Extending the ICRF to Higher Radio Frequencies





# REPORT DOCUMENTATION PAGE

*Form Approved*  
OMB No. 0704-0188

Public reporting burden for this collection of information is estimated to average 1 hour per response, including the time for reviewing instructions, searching existing data sources, gathering and maintaining the data needed, and completing and reviewing the collection of information. Send comments regarding this burden estimate or any other aspect of this collection of information, including suggestions for reducing this burden, to Washington Headquarters Services, Directorate for Information Operations and Reports, 1215 Jefferson Davis Highway, Suite 1204, Arlington, VA 22202-4302, and to the Office of Management and Budget, Paperwork Reduction Project (0704-0188), Washington, DC 20503.

<b>1. AGENCY USE ONLY</b> <i>(Leave blank)</i>		<b>2. REPORT DATE</b> May 2002	<b>3. REPORT TYPE AND DATES COVERED</b> Conference Publication	
<b>4. TITLE AND SUBTITLE</b> International VLBI Service for Geodesy and Astrometry General Meeting Proceedings			<b>5. FUNDING NUMBERS</b> 920.1	
<b>6. AUTHOR(S)</b> Nancy R. Vandenberg and Karen D. Bayer, Editors				
<b>7. PERFORMING ORGANIZATION NAME(S) AND ADDRESS (ES)</b> Goddard Space Flight Center Greenbelt, Maryland 20771			<b>8. PERFORMING ORGANIZATION REPORT NUMBER</b> 2002-02213-0	
<b>9. SPONSORING / MONITORING AGENCY NAME(S) AND ADDRESS (ES)</b> National Aeronautics and Space Administration Washington, DC 20546-0001			<b>10. SPONSORING / MONITORING AGENCY REPORT NUMBER</b> CP—2002—210002	
<b>11. SUPPLEMENTARY NOTES</b> N. Vandenberg, NVI, Inc.; K. Bayer, Raytheon.				
<b>12a. DISTRIBUTION / AVAILABILITY STATEMENT</b> Unclassified—Unlimited Subject Category: 42 Report available from the NASA Center for AeroSpace Information, 7121 Standard Drive, Hanover, MD 21076-1320. (301) 621-0390.			<b>12b. DISTRIBUTION CODE</b>	
<b>13. ABSTRACT</b> <i>(Maximum 200 words)</i>  This volume is the proceedings of the second General Meeting of the International VLBI Service for Geodesy and Astrometry (IVS), held in Tsukuba, Japan, February 4–7, 2002. The contents of this volume also appear on the IVS Web site at <a href="http://ivscc.gsfc.nasa.gov/publications/gm2002">http://ivscc.gsfc.nasa.gov/publications/gm2002</a> . The key-note of the second GM was prospectives for the future, in keeping with the re-organization of the IAG around the motivation of geodesy as “an old science with a dynamic future” and noting that providing reference frames for Earth system science that are consistent over decades on the highest accuracy level will provide a challenging role for IVS. The goal of the meeting was to provide an interesting and informative program for a wide cross section of IVS members, including station operators, program managers, and analysts. This volume contains 72 papers and five abstracts of papers presented at the GM. The volume also includes reports about three splinter meetings held in conjunction with the GM: a mini-TOW (Technical Operations Workshop), the third IVS Analysis Workshop and a meeting of the analysis working group on geophysical modeling.				
<b>14. SUBJECT TERMS</b> Geodesy, astrometry, VLBI, geophysics, Earth orientation, very long baseline interferometry, interferometry, radio astronomy, geodynamics, reference frames, terrestrial reference frame, celestial reference frame, length of day, Earth system science, Earth rotation.			<b>15. NUMBER OF PAGES</b> 435	
			<b>16. PRICE CODE</b>	
<b>17. SECURITY CLASSIFICATION OF REPORT</b> Unclassified	<b>18. SECURITY CLASSIFICATION OF THIS PAGE</b> Unclassified	<b>19. SECURITY CLASSIFICATION OF ABSTRACT</b> Unclassified	<b>20. LIMITATION OF ABSTRACT</b> UL	